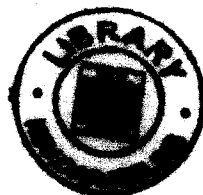


**SYNTHETIC, PHYSICO-CHEMICAL AND REACTIVITY ASPECTS  
OF CO-ORDINATION COMPOUNDS OF MOLYBDENUM AND  
DIOXOURANIUM (VI) WITH PTERIN AND ALDIMINE LIGANDS**

***THESIS***

2008

**SUBMITTED FOR THE DEGREE OF  
DOCTOR OF PHILOSOPHY (SCIENCE)  
OF  
THE UNIVERSITY OF NORTH BENGAL**



**Md. Afsar Ali, *M.Sc. (Chem.)*  
DEPARTMENT OF CHEMISTRY  
UNIVERSITY OF NORTH BENGAL**

**2008**

STOCK TAKING - 2011

Ref  
546.5342  
A 398s

**THIS WORK IS DEDICATED TO -**

My elder brother

**Matiur Rahaman,**

*Bhabi*

**218462**

02 DEC 2009

**Safika Banu (Sulekha)**

and

to the memory of  
my late parents.



## ACKNOWLEDGEMENT

I express my deep gratitude to Dr. Parag S. Roy, Professor of Chemistry, University of North Bengal, for his constant advice and guide throughout the research period. I am also grateful to all the teachers of the Department of Chemistry, University of North Bengal, for their encouragement and persistent interest in this work. During my whole research period, I have received constant assistance from the staff of this department. I also acknowledge the help of my colleagues in day – to – day research work. I am also expressing my thanks to the Staffs, Officers and others, particularly the USIC, University of North Bengal for the co-operation and services they have extended to me during my research tenure.

I would like to thank the CSIR, New Delhi for a research fellowship to me (JRF & SRF), the Department of Science and Technology and University Grants Commission, New Delhi for financial support to my research guide (Professor P.S.Roy), Indian Association for the Cultivation of Science, Kolkata for microanalytical data; RSIC, CDRI, Lucknow for ESIMS, NMR spectra and for some microanalytical data. Some of the NMR spectra were recorded by FTIR, Mumbai; IISc, Bangalore and IICB, Kolkata. CD spectra were recorded by the IICB, Kolkata. The EPR spectra were recorded by the IIT, Mumbai. DPV spectra were obtained from CSMCRI, Bhavnagar. Some of the microanalytical data and IR spectra were provided by the RSIC, NEHU, Shilong. Atomic

Absorption Spectra (molybdenum) were provided by Dr. M.C. Saha, G.S.I. Kolkata. X-ray diffraction data for one compound were obtained from the SAIF, Madras as a paid technical service. All the above services are heartily acknowledged. My earnest thanks to Prof. Reijo Hämäläinen, University of Helsinki, Finland for determining the X-ray crystal structure of one of my complexes.

I am lacking words to express my gratitude to my elder brother, Matiur Rahaman, without who's support and help this thesis could not have been completed. I also take the privilege to acknowledge the contributions of my beloved parents ; the support and services provided by my wife, Waresin Ara Begom Amin and other members of my family and friends who have played important role in my career building and have constantly stimulated my interest in research works.

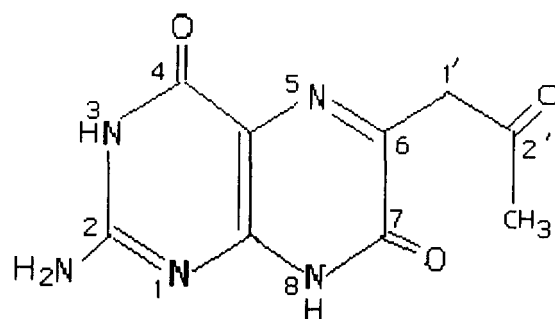
Department of Chemistry,  
University of North Bengal,  
P.O. – North Bengal University,  
Dist. – Darjeeling,  
Siliguri – 734013,  
INDIA.

Md. Afsar Ali  
19.8.2008  
(MD. AFSAR ALI)

## PREFACE

The research work embodied in this thesis entitled, “ *Synthetic, Physico-chemical and Reactivity Aspects of Co-ordination Compounds of Molybdenum and dioxouranium (VI) with Pterin and Aldimine Ligands*”, has been carried out in the laboratory of Professor Parag S. Roy, Department of Chemistry, University of North Bengal. The thesis consists of five chapters. In Chapter I, a general introduction stresses the importance of the works reported here, along with the highlights of the available knowledge in these fields and the necessary references (indicated by superscript numbers), which are grouped together at the end of this treatise. The aims and objectives of this work as described in Chapter I (Introduction), points out the scope of the present work, research goals to be achieved and the outlines of the experimental techniques used for realizing them. Chapter II, III and the first Section of Chapter IV are concerned with the investigation on coordination compounds of molybdenum with the following pterin ligands (schematic structures of both keto and enol forms, IUPAC and trivial nomenclatures, together with their abbreviations used here, are indicated below).

---

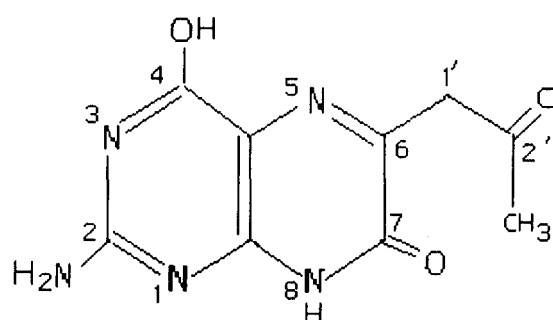


(keto – form)

**Scheme – (P-1)**

2 – amino – 6 – (2' - oxopropyl) pteridin – 4,7(3H, 8H) – dione

(IUPAC)



(enol – form)

**Scheme – (P-2)**

2 – amino – 4 – hydroxy – 6 – (2' - oxopropyl) pteridin – 7(8H) – one

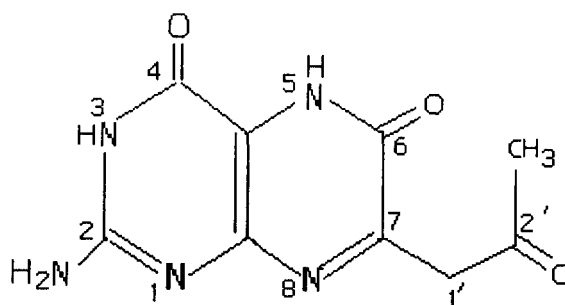
(IUPAC)

6 – acetyl – isoxanthopterin

(Trivial)

[H<sub>2</sub>(pte<sub>1</sub>)]

(abbreviation)

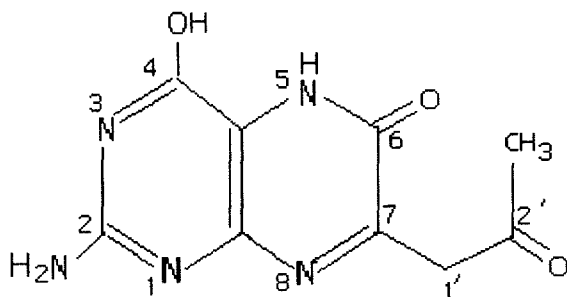


(keto – form)

**Scheme – (P-3)**

2 – amino – 7 – (2' - oxopropyl) pteridin – 4,6(3H,5H) – dione

(IUPAC)



(enol – form)

**Scheme – (P-4)**

2 – amino – 4 – hydroxy – 7 – (2' - oxopropyl) pteridin – 6(5H) – one

(IUPAC)

7 – acetyl – xanthopterin

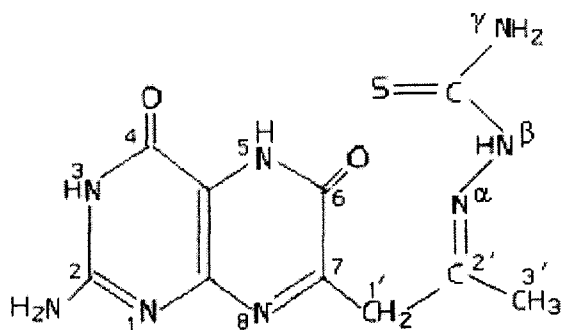
(Trivial)

[H<sub>2</sub>(pte<sub>2</sub>)]

(abbreviation)

*2 – pivaloylamino derivative of this compound has been crystallized and its crystal as well as molecular structures have been determined through single crystal X-ray diffraction study.*

A new Schiff base ligand has been synthesized by condensing 7 – acetyl – xanthopterin [H<sub>2</sub>(pte<sub>2</sub>)] with thiosemicarbazide [NH<sub>2</sub>C(=S)NHNH<sub>2</sub>, H(tsc)]:



**Scheme – (P-5)**

$\alpha$  – N (7 – acetylidene – xanthopterin) thiosemicarbazide

[H<sub>3</sub>(pte<sub>2</sub>-tsc)]

(abbreviation)

Studies on  $\mu$  - oxo binuclear molybdenum (V) complexes [possessing the  $(\text{Mo}^{\text{V}}_2\text{O}_3)^{4+}$  core] of aldimine derivatives of L - / D - amino acids, constitute the subject matter of Section - II of Chapter IV. In Chapter V dioxouranium (VI) complexes of chiral aldimine ligands derived from asparagines, arginine and glutamine are discussed.

In each Chapter Tables, Figures and Schemes have been numbered using a combination of Roman and Arabic numbers; for example, the first Table of Chapter I is numbered (I - 1), the second Table is numbered (I - 2), whereas the first Table of Chapter II is numbered (II - 1), the second Table as (II - 2) and so on. For Chapters containing two sections, the same procedure is followed without any break. In each Chapter (and for each Section of Chapters containing two Sections), the compounds have been assigned serial numbers (in bold letters within first bracket) and referred to them by these numbers during discussion.

The multiplicities of NMR spectral signals are indicated by the usual abbreviations, e.g., 's' for singlet ; 'bs' for broad singlet, 'd' for doublet, 'dd' for doublet of doublet, 't' for triplet and 'm' for multiplet.

The pterin ring numbering system has been used for the Schemes related to the Schematic structures as well and utilized in discussion part. The optimized (lowest steric energy) computational model (CHEM3D) of the pertinent ligands and complex compounds obtained here through molecular mechanics calculations (MM2) are numbered as per the program used [Chem3D ultra, version 8.0 (2004) and the higher version, Cambridge Soft Corporation, U.S.A.]. A correspondence between the two above-mentioned sets of numbering systems has been indicated in the text. The same applies for the ORTEP diagram obtained through X-ray crystallography for the 2 - pivaloylamino derivative of 7 - acetyl - xanthopterin [ $\text{H}_2(\text{pte}_2)$ ]. The CHEM3D model of this compound has also been obtained in order to compare the two sets of bond length ( $\text{\AA}$ ) and bond angle (deg.) data obtained through the MM2 calculations and single crystal X-ray diffraction study respectively; good agreement (discussed later) between the two sets of data, stresses the reliability of the MM2 method, which has been used here extensively.

For most of the compounds discussed here, the optimized (MM2) bond length (Å) and bond angle (deg.) data, have been compared with the available literature X-ray structural data of related systems, for checking the efficacy of the MM2 method in obtaining the CHED3D models of the present molybdenum – pterin systems as well as the molybdenum – aldimine systems. The following colour code has been used for labeling the different atoms of CHEM3D models:

- red coloured ball represents the oxygen atom;
- blue coloured ball represents the nitrogen atom;
- ash coloured ball represents the carbon atom;
- green coloured ball represents the chlorine atom;
- yellow coloured ball represents the sulphur atom;
- dark-ash coloured ball (larger size) represents the molybdenum atom;
- pink coloured ball (small size) represents the lone electron pair.

References are mentioned at the end of this thesis following standard international conventions. In spite of taking utmost care, very few number of references are repeated and the author expresses regret for this.

Preliminary reports involving part of this work have been submitted to CSIR, New Delhi as annual progress reports as well as final technical report. Two papers have already been published out of the subject matter of Chapter II<sup>34</sup>. Materials of other Chapters are presently in the process of publication in different journals. Several publications on coordination compounds of pterin ligands reflect continuing interest of this laboratory on this subject<sup>48, 178, 179</sup>. Parts of this work have been presented in a couple of reference proceedings, e.g., National Seminar on current Trends in Chemistry – II, 4<sup>th</sup> March, 2008.

August, 2008

Md. Afsar Ali; 19.8.2008  
(MD. AFSAR ALI)

# CONTENTS

	<b>Page No.</b>
<b>Dedication</b>	ii
<b>Acknowledgement</b>	iii - iv
<b>Preface</b>	v - ix
<b>Chapter I :</b> General introduction, Aims and objectives of the work.	1 – 15
<b>Chapter II</b>	
<b>Section - I :</b> A di - $\mu$ - oxomolybdenum(V) complex of 6-acetyl- isoxanthopterin, undergoing oxygen atom transfer with dimethyl sulphoxide.	16 – 39
<b>Section - II :</b> Synthesis and characterization of a molybdenum complex with sulphur and pterin ligands exhibiting saturation kinetics with pyridine N - oxide.	40 – 60
<b>Chapter III :</b> Studies on a new Schiff base ligand [H <sub>3</sub> (pte <sub>2</sub> -tsc)] synthesized by condensing 7 - acetyl - xanthopterin [H <sub>2</sub> (pte <sub>2</sub> )] with thiosemicarbazide [H(tsc)] and its molybdenum complexes exhibiting reactivity towards Me <sub>3</sub> N→O, PyN→O and PPh <sub>3</sub> ; crystal structure of 2 - pivaloylamino - 7 - acetyl-xanthopterin - water (1/1).	61 - 133
<b>Chapter IV</b>	
<b>Section - I :</b> Synthesis, characterization and reactivity studies on mixed ligand molybdenum (IV,V,VI) complexes with 6-acetyl-isoxanthopterin [H <sub>2</sub> (pte <sub>1</sub> )] and a sulphur containing ligand (cysteine or 2 - amino thiophenol or dihapto disulphide).	134 – 189

<b>Section - II :</b>	Kinetics of oxygen atom transfer reactions of pyridine N – oxide substrate with mono $\mu$ – oxo – bridged molybdenum(V) complexes of aldimine derivatives of L-/ D-amino acids : Conformational control of reactivity.	190 – 225
<b>Chapter V :</b>	Kinetic studies on redox reactions between $\text{Na}_2\text{SO}_3$ and dioxouranium (VI) complexes with chiral aldimine ligands derived from L-/ D – asparagine, arginine and glutamine; crystal structure of (2,2' – bipyridyl) dioxo (N – salicylidene – L – asparaginato) uranium (VI) – methanol (1/1).	226 – 266
	Summary and Concluding Remarks.	267 – 270
	References	271 – 284

## **CHAPTER I**

General introduction.

Aims and objectives of the work

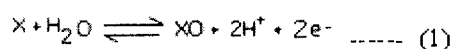
This treatise is concerned with the coordination Chemistry of molybdenum and dioxouranium (VI) [i.e., the uranyl ion,  $\text{UO}_2^{2+}$ ] with pterin and aldimine ligands containing a few selected  $\alpha$  – amino acids.

For molybdenum, the study involves both the pterin and aldimine ligands whereas for the uranyl ion, only the aldimine ligands have been used. Coordination Chemistry of molybdenum with pterin ligands constitutes the subject matter of the initial part of this work. The relevant new compounds involve the commonly accessible oxidation states of molybdenum, i.e., VI, V and IV ; several of them possess the attribute of an oxometal entity, i.e., a multiply bonded oxygen atom stabilizing the high charge (VI, V) on the molybdenum atom. In the higher oxidation states, different types of oxomolybdenum entities have been characterized structurally<sup>19, 55</sup>.

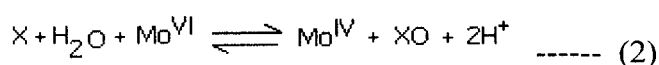
In the last two Chapters of this thesis, coordination Chemistry of  $(\text{Mo}^{\text{V}}_2\text{O}_3)^{4+}$  and  $\text{UO}_2^{2+}$  entities with aldimine ligands are discussed, especially their reactivity aspects and analyzing the relevant data in the light of stereochemical influences. In fact studies on coordination compounds of aldimine derivatives of amino acids constitute an important area of bioinorganic chemistry, due to their relevance to a diverse series of reactions in amino acid metabolism<sup>22, 74</sup>. The salicylideneamino chirality rule is helpful for assigning the absolute configuration / conformation of an entire set of chiral primary amines including  $\alpha$  – amino acids, by CD spectroscopy<sup>79</sup>. Necessary attention has also been paid to the NMR studies on conformation analysis of pyridoxal Schiff bases of  $\alpha$  – amino acids<sup>93</sup>. As delineated here in the relevant Chapters, the present aldimine ligands containing  $\alpha$  – amino acids help to elicit valuable inferences regarding structure – reactivity / property correlation of the pertinent  $(\text{Mo}^{\text{V}}_2\text{O}_3)^{4+}$  - and  $\text{UO}_2^{2+}$  - complexes.

In the introductory part of each of the subsequent chapters (e.g., Chapters II to V) the aims and objectives of that particular chapter are stated. In this Chapter the overall background about different aspects of this work is outlined.

Molybdenum containing enzymes catalyze a wide range of reactions in carbon, sulphur and nitrogen metabolism. Apart from nitrogenase (with a multinuclear active site), the other class of enzymes (nearly 50 such enzymes contain molybdenum in their active sites) generally function catalytically to transfer an oxygen atom either to or from a physiological acceptor / donor molecule<sup>1, 2, 26, 187, 189</sup>. In general, these enzymes utilize water as the ultimate source or sink of oxygen in the overall catalytic reaction (equation 1) and the reaction is coupled to electron transfer between substrate X / XO, on Fe – S centre, heme or flavin.



Considering the metal centre the overall reaction can be represented by equation 2.

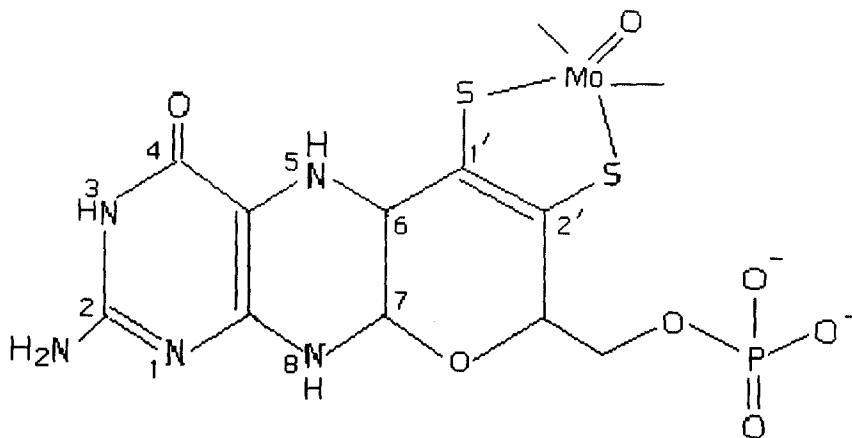


The enzymes are referred to as oxotransferases when the substrate is transformed by primary oxygen atom transfer and as hydroxylases when bound or unbound water or hydroxide is directly involved in the substrate transformation reaction. Among others, the oxidation of sulphite to sulphate and the reduction of DMSO to DMS (dimethyl sulphide) can be viewed as oxygen atom (= O, oxo group) transfer reaction. Members of the xanthine oxidase family catalyze the oxidative hydroxylation of a diverse range of aldehydes and aromatic heterocycles in reactions that necessarily involve the cleavage of a C – H bond, e.g., conversion of xanthine to uric acid.

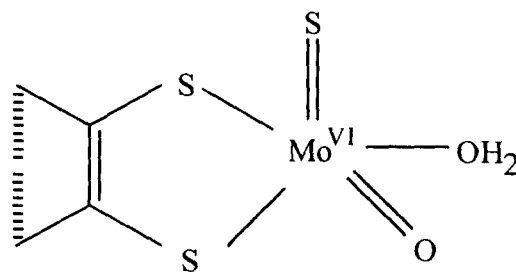
The term “oxotransferase” is not universally accepted and the nomenclature remains an active area of discussion<sup>187</sup>. Majority of these enzymes possess a Mo = O unit in their active sites ; however, some of them do not catalyze oxygen atom transfer (e.g., polysulphide reductase and possibly formate dehydrogenase) and others do not possess a Mo = O unit.

Hill<sup>187</sup> has classified molybdenum enzymes into three families based upon their protein sequences and the structures of their oxidized active sites ; each family is named as per its most prominent member, e.g., xanthine oxidase, sulphite oxidase and DMSO reductase families. Scheme (I – 2) shows outlines of their active sites in the oxidized (Mo<sup>VI</sup>) and reduced (Mo<sup>IV</sup>) sites. For the DMSO reductase family of enzymes, the Mo(IV) centre in the reduced form is devoid<sup>189</sup> of any terminal oxo (=O) group. In all

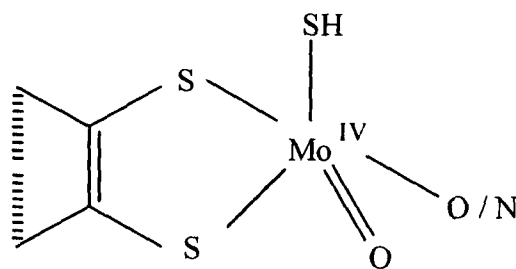
three families, additional ligands<sup>2, 189</sup> are present in the molybdenum coordination sphere which make the metal, minimally, five coordinate. In spite of the above differences with respect to their active sites, enzymes of this type are characterized by a pterin cofactor having a basic structure as per Scheme (I – 1).



**Scheme (I – 1):** Pyranopterin dithiolate – molybdenum coordination<sup>189</sup>



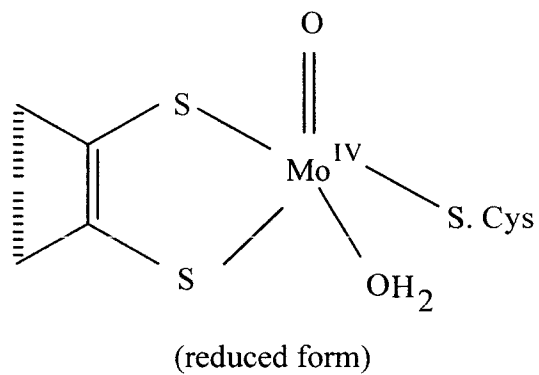
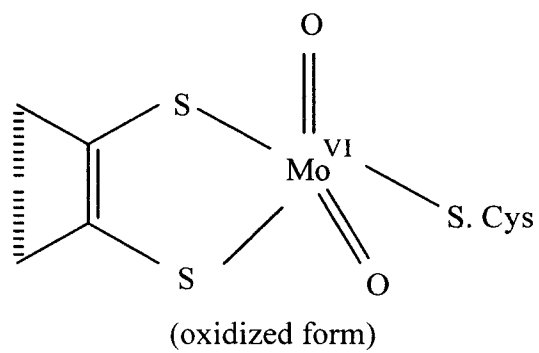
(oxidized form)



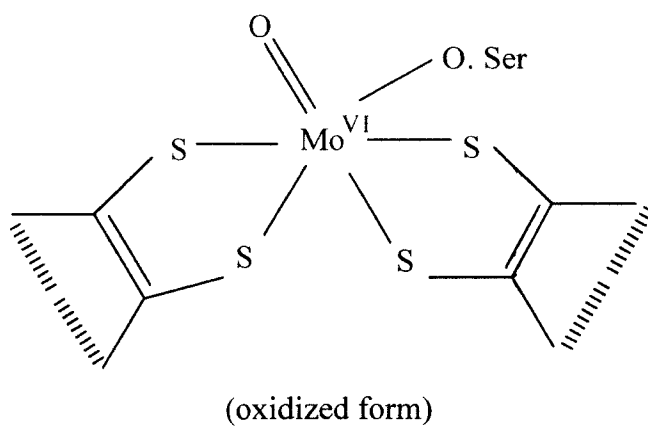
(reduced form)

The xanthine oxidase family (true hydroxylase)

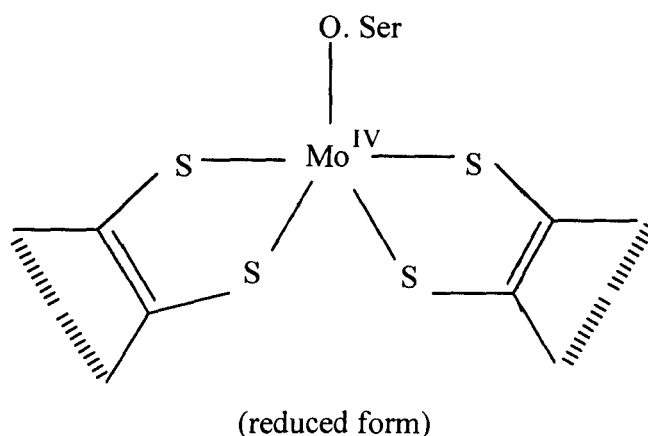
**Scheme (I – 2) ; continued below**



The sulphite oxidase family



**Scheme (I – 2)** ; continued below



The DMSO reductase family

**Scheme (I – 2)** <sup>187, 189</sup>

This pyranopterin structure has been established crystallographically in several cases <sup>1, 2, 187 – 189</sup>. The basic pterin ring structure and dithiolene side chain had been elucidated earlier by chemical analysis of the cofactor extracted from purified enzymes <sup>187</sup>. Presence of the pyran ring was established crystallographically <sup>187 – 189</sup>. According to a proposal put forward by Enemark and Garner <sup>1(b)</sup>, scission / condensation of the pyran ring of pyranopterin is needed for a change in oxidation level of the pterin nucleus by two unit, which can be synchronized with the reaction scheme represented by equation (2).

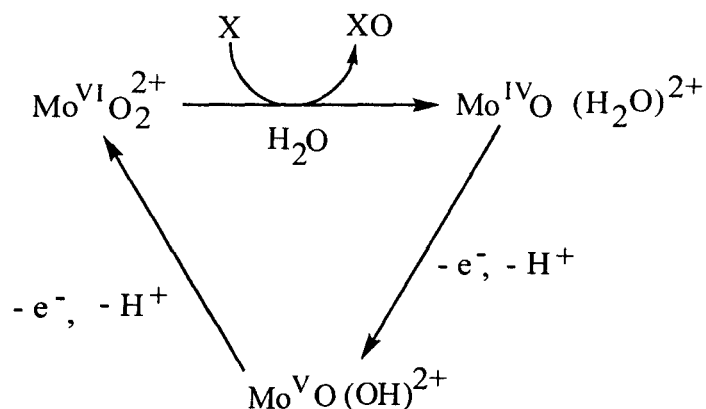
The choice of molybdenum by Nature for oxygen atom transfer activity of oxomolybdo-enzymes, is guided by several chemical reasons <sup>19, 41, 52(b), 187, 189</sup>. Molybdenum is widely available to biological systems due to the solubility of its high – valent oxides. Molybdenum is not as “oxophilic” as the early transition metals of groups IV and V. Its strong tendency to bind an oxo group is balanced by a capacity to lose a single oxygen atom easily. The redox potentials available to biological systems closely overlap with those of molybdenum that makes it the most preferred one among the group VI metals (Cr, Mo, W). Usually organisms find chromium too difficult to oxidize from the trivalent state and tungsten is not easily reduced from the hexavalent state. Perhaps it is one of the reasons that enzymes containing molybdenum at their active sites appear to be present in all forms of life, whereas well – characterized tungstoenzymes cover the

thermophilic bacteria and hyperthermophilic archaea<sup>81</sup>. Of course, the emergence of molybdenum and tungsten isoenzymes<sup>189</sup> adds a new dimension to this area of Chemistry / bioinorganic Chemistry. Available data shows that oxo transfer from substrate to metal ( $M^{IV} \rightarrow MO^{VI}$ ) is faster with tungsten and that to substrate from metal ( $MO^{VI} \rightarrow M^{IV}$ ) is faster with molybdenum. The results indicate a kinetic metal effect on direct oxo transfer for isoenzymes, provided the catalytic sites are isostructural.

The biochemical transformation involving the above enzymes are redox reactions and many involve at least formal oxygen atom transfer process. The one – and two – electron transfer capability associated with Mo / W (in the oxidation states VI, V, IV) and the ability to couple ion ( $H^+$  or  $O^{2-}$ ) transfer with electron transfer may be crucial to the chemical role played by these metals in enzymes.

Apart from the oxygen atom transfer formulation, the alternative mechanistic possibility involving electron / proton transfer process with a water molecule added or subtracted, depends on the possibility that incorporates the known effect of metal oxidation state on the  $pK_a$  of coordinated ligands<sup>19, 41</sup>. Oxidation of a metal ion makes it electron poor resulting in a pull of electron density from any coordinated heteroatom, A. If A is protonated, this flow of electron density increases the proton acidity of the AH group (i.e., lowers the  $pK_a$ ). Conversely, reduction of the metal pushes electron density back onto A and increases its basicity (raises the  $pK_a$ ). As the magnitude of this dependence may be as great as 8  $pK_a$  units per unit oxidation state change, a  $Mo^{VI} / Mo^{IV}$  redox cycle could vary ligand acidity by 16  $pK_a$  units or approximately the difference between a strong acid and water<sup>41</sup>. Thus the electron transfer at molybdenum cofactor may be intimately coupled to proton transfer in the same direction. A proposal for a coupled proton / electron transfer mechanism for the oxidation of xanthine by xanthine oxidase [with oxosulphido core at the metal centre, Scheme (I – 2)] involves two electron transfer to the metal ( $Mo^{VI} \rightarrow Mo^{IV}$ ); the increase in  $pK_a$  at the sulphido ligands (= S) causing proton transfer to sulphur to be coupled to the electron transfer process.

Two unit change of oxidation state at the metal centre [in case of xanthine oxidase, the cis – dioxo core is replaced by a oxosulphido core] is associated with the gain or loss of an oxygen atom (or, oxo group, = O) as shown below<sup>26</sup>.



Now the reactivity aspect of other metal – oxygen cores in Nature may be compared with that of molybdenum, e.g., oxygen evolution capability versus oxygen atom transfer activity respectively, in terms of their redox potential values.

The production of molecular oxygen in photosynthesis is assisted by a manganese enzyme, probably containing four atoms of manganese<sup>193</sup>. During the redox reactions the manganese centres shuttle between two oxidation states with each manganese atom increasing (and subsequently decreasing) its oxidation state by one unit, but it is not known with absolute certainty what these oxidation states are. In the reduced form the oxidation states may be as low as three Mn (II) and one Mn (III), but they are more likely to be three Mn (III) and one Mn (IV). In the lower oxidation states [e.g., Mn (II)], the affinity for oxygen is quite low.

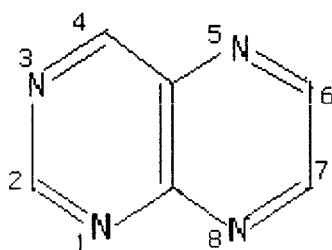
Oxygen evolution by catalase takes place due to high potential of the  $[\text{Fe}^{\text{V}}\text{O} + \text{H}_2\text{O}_2]$  system.

The biochemical significance of the above statements may be summarized as follows : the oxo groups of manganese and iron are strongly oxidizing and can take part in oxygen evolution ; the oxomolybdenum systems operate at low redox potential and cannot evolve oxygen, but can take part in oxo (= O) group transfer Chemistry<sup>52 (b)</sup>. Vanadium can hold one oxo – group in  $(\text{V}^{\text{IV}}\text{O})^{2+}$  at low potential, but it is then only a one – electron reactant and cannot carry out the molybdenum type reactions. The tungstoenzymes function at a lower potential range (under anaerobic conditions at ~ 100 °C) as compared to oxomolybdoenzymes operating in a wider potential range at lower

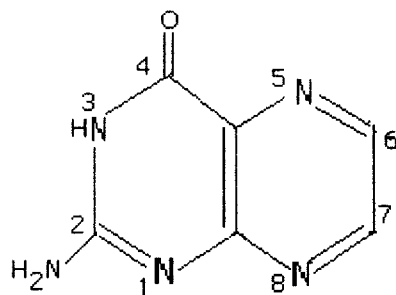
temperature. Most likely stronger  $\pi$  – interactions confer greater thermal stability on the tungsten centres in the corresponding class of enzymes ; besides this, greater stability of the higher oxidation states make the tungsten centre more air – sensitive and hence the need of anaerobic conditions for their operation.

### Aims and objectives of the work :

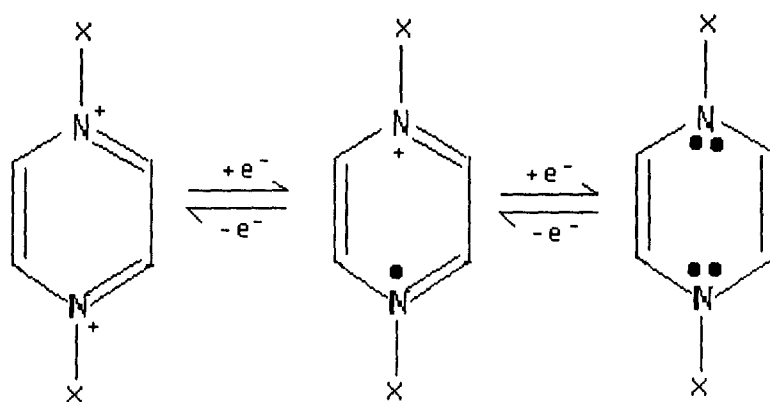
The term “pteridine” was introduced by Wieland for the fused ring system of pyrimidine and pyrazine rings and is related to the first isolation of such compounds from



natural sources like the pigments of butterfly wings <sup>84 (b)</sup>. Pterins (2-amino-4-oxopteridines) represent a system of heterocycles with unique structure and Nature has



selected them (especially, the 6-substituted variety) for a wide range of biological functions including the essential components of a large number of metal (e.g., Fe, Mo, W) containing enzymes <sup>26, 82, 187, 189, 194</sup>. The well – known ability of pterins to act as redox partners in biological redox systems is intimately connected with the ability of the



pyrazine moiety (of the pterin ring) to exist in different oxidation states <sup>4</sup>, thereby exhibiting multiple redox activity like the redox capabilities of the transition metal counterparts in the metalloenzymes stated above.

These facts have inspired symbiotic developments in the coordination Chemistry of pterin ligands and the assignment of oxidation states of both the metal and ligand centres in the new complexes along with their electronic structures is an involved task <sup>3, 20, 119</sup>.

The above facts have motivated the present synthetic work on new coordination compounds of molybdenum with the pterin ligands stated in the preface. Out of them the 2-pivaloylamino derivative of 7-acetyl-xanthopterin has been characterized using X-ray crystal structure determination. A new Schiff base ligand, [H<sub>3</sub>(pte<sub>2</sub> - tsc)] has been synthesized by condensing 7-acetyl-xanthopterin with thiosemicarbazide.

In many cases the complex formation process between the molybdenum starting material and the pterin ligand is accompanied by a redox reaction and due attention has been given in assigning the oxidation states of the metal centres in the resulting complexes. The results are expected to serve as bench mark data for understanding the roles of different components of pterin – containing biological systems and possible cooperativity between formally metal – based and pterin – based redox systems <sup>119</sup>. Furthermore, this effort will help to correlate the information obtained from chemical and electrochemical studies with the inferences derived from different spectroscopic methods <sup>34, 110, 127, 179, 180</sup>. It has been pointed out in the subsequent Chapters

that some of the new Mo(IV) – pterin complexes are devoid of terminal oxo (= O) group, just like the Mo(IV) centres of the DMSO reductase family in the reduced state<sup>187, 189</sup>. Some parallel examples exist with dithiolenes and a few NS ligands<sup>19, 191</sup>. The reason for this must lie in the ability of these ligands to act as strong  $\sigma$  – and  $\pi$  – donors while keeping sufficient  $\pi$  – acceptor quality to prevent complete charge transfer from ligand to metal. Some of the present physicochemical and spectroscopic data support this flexible redox property of the present ligands.

The new compounds have been characterized through physicochemical, spectroscopic data and their reactivities towards suitable substrates have been studied. Purity of the ligands and the new complex compounds reported here have been checked through TLC and their chemical compositions have been established through elemental analysis, mass spectral data (as well as the assignment of characteristic fragment through computer simulation) and different spectroscopic data. In several cases, the CHEM3D models have been obtained through molecular mechanics (MM2) calculations ; the optimized bond lengths (Å) and bond angles (deg) data so obtained, show good agreement with the literature X-ray structural data of related systems. The spectroscopic data are consistent with the CHEM3D models. Reactivity studies (both kinetic and stoichiometric aspects) of these compounds represent an important facet of this work.

Tables A & B below compare the bond angles and bond lengths data of [H<sub>2</sub>(2-piv-pte<sub>2</sub>)] derived from CHEM3D optimized computational model (MM2) and from single crystal X – ray diffraction method (shown in Chapter – III). The data derived from optimized computational model showing agreement with the X – ray structural data verifies the applicability of such an approach to molybdenum – pterin system or to the systems closely related to this, and provides with a suitable frame work for discussion on their spectroscopic, reactivity and other relevant aspects<sup>85, 111</sup>. This view is further substantiated by a comparative study of some vital optimized bond lengths (Å) of the CHEM3D model of some molybdenum – pterin complexes, showing good agreement with the corresponding X – ray structural data of several pterin compounds reported by different authors<sup>88(a)</sup>.

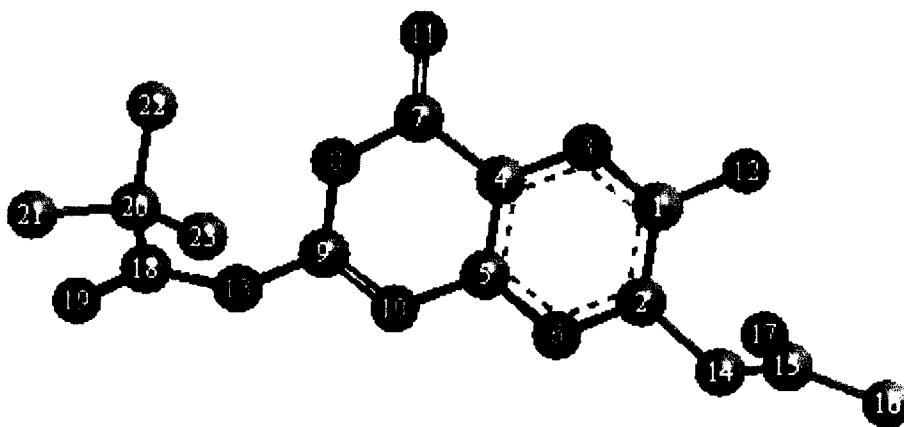


**Fig.(I – 1):** The optimized geometry (CHEM3D model obtained through MM2 calculations) of  $[H_2(2\text{-piv-pte}_2)]$  with a steric energy of  $-2.35 \text{ Kcal mol}^{-1}$ . Its numbering system is set by the software used<sup>87</sup> and is different from that in different Schemes.

**Table A :** Comparison of CHEM3D bond lengths & single crystal X – ray bond lengths of 2 – pivaloylamino – 7 – acetonylxanthopterin  $[H_2(2\text{-piv-pte}_2)]$  :

Atoms	CHEM3D Bond Distances(Å)	X – ray Bond Distances(Å)	Atoms	CHEM3D Bond Distances(Å)	X – ray Bond Distances(Å)
C(4)-N(3)	1.35	1.38	C(1)-O(12)	1.31	1.22
C(7)-O(11)	1.22	1.22	C(2)-C(14)	1.32	1.37
C(5)-N(10)	1.42	1.34	N(6)-C(2)	1.32	1.35
C(5)-N(6)	1.35	1.39	C(20)-C(22)	1.52	1.48
C(1)-C(2)	1.42	1.48	C(20)-C(23)	1.52	1.51
C(4)-C(7)	1.48	1.44	C(20)-C(18)	1.52	1.48
C(4)-C(5)	1.40	1.37	N(13)-C(18)	1.37	1.40
C(7)-N(8)	1.37	1.39	C(15)-O(17)	1.21	1.23
C(9)-N(13)	1.35	1.36	C(15)-C(16)	1.51	1.53
C(9)-N(10)	1.28	1.33	C(14)-C(15)	1.51	1.42
N(8)-C(9)	1.45	1.36	C(20)-C(21)	1.53	1.50
N(3)-C(1)	1.44	1.36	C(18)-O(19)	1.21	1.21

**Table B :** Comparison of CHEM3D bond angles & single crystal X – ray bond angles of 2 – pivaloylamino – 7 – acetylpterin [ $H_2(2\text{-piv-pte}_2)$ ] :

Angle Atoms	CHEM3D Bond Angles (degree)	X – ray Bond Angles (degree)
C(14)-C(2)-N(6)	120.3	123.5
N(6)-C(2)-C(1)	122.4	119.5
C(9)-N(8)-C(7)	126.6	123.4
N(13)-C(9)-N(10)	120.7	116.9
N(8)-C(9)-N(10)	119.3	123.2
C(5)-N(6)-C(2)	119.9	122.9
C(9)-N(10)-C(5)	118.1	115.2
C(1)-N(3)-C(4)	117.2	122.6
N(8)-C(7)-C(4)	114.4	113.5
N(6)-C(5)-C(4)	120.3	117.2
N(3)-C(4)-C(7)	121.7	119.6
N(3)-C(4)-C(5)	121.2	121.9
C(5)-C(4)-C(7)	119.1	118.5

Just as X – ray structural data of a compound correspond to its thermodynamically most stable form, the optimized geometries (obtained through MM2 calculations) of the present compounds correspond to their lowest steric energies. However, in solution intrinsic relative stability of different forms (e.g., tautomers, conformers, etc.,) of a compound are determined by different factors, e.g., hydrogen bonding and other intermolecular interactions, which can easily outweigh the small intrinsic energy barriers, leading to their labile equilibrium in solution <sup>4, 117</sup>. As far as the pterin compounds are concerned the roles of hydrogen bonding and tautomerism are well – documented <sup>6(c), 20(a), 84, 118</sup>.

A perusal of the tables comparing optimized bond lengths and bond angles of the free ligands and that of the complexes derived from these (presented in the successive Chapters) reveals that the pterin ring is attached to the Mo atom through the O(4) and N(5) atoms [Scheme (II – 1) / Scheme (III – 1)] resulting from the anion formation involving the amide function in positions 3, 4 and the vinylogous amide in position 5 including the adjacent side – chain [i.e., the proton from C(1') is located at N(5)]<sup>89, 123</sup>. The amide function in position 7, 8 is not involved in complex formation, as reflected by the bond length data (Å) of the ligands and complexes, for the C(6) – C(7) – N(8) region<sup>3(b), 20(a)</sup>.

The overall bond lengths of the free ligand [Tables (II – 2), (II – 6), (III – 8) & (IV – 2) and Scheme (II -1) & (III – 1)] are in good agreement with the existing literature<sup>88(a)</sup>. The only exception to this reasonable agreement between the computed bond length data (Å) and the literature X – ray data, is the N(8) – C(7) distance ; this is due to the presence of vinylogous amide in position 5 including the adjacent side – chain<sup>89, 121</sup>.

<sup>1</sup>H NMR data (1D and 2D) of ribavirin in DMSO – d<sub>6</sub> show that restricted rotation around a C – N bond can make even the two primary amide NH protons non – equivalent on the NMR time – scale<sup>14, 115, 116</sup>. <sup>1</sup>H NMR data (both 1D and 2D) of the compounds, in DMSO – d<sub>6</sub> (δ in ppm versus TMS) reflect this aspect. <sup>1</sup>H NMR spectra of the OH(4), NH(5) and NH(8) protons [Scheme (II – 1) or Scheme (III – 1)] of the pterin ligand in DMSO – d<sub>6</sub> appeared in the range of δ, (10 – 13.5) as broad singlets but they disappear when the NMR spectrum is recorded afresh in CD<sub>3</sub>OD indicating their exchangeable nature<sup>16, 118</sup>.

Due to interplay of the foregoing factors determining intrinsic relative stabilities of the different forms in solution, of the pterin compounds also exhibits more than one type of NMR signal for most of its ligand protons.

Importance of the study on coordination Chemistry of the two oxocations [e.g., (Mo<sup>V</sup><sub>2</sub>O<sub>3</sub>)<sup>4+</sup> and (U<sup>VI</sup>O<sub>2</sub>)<sup>2+</sup>] with aldimine ligands may be stated here briefly. While the importance of aldimine derivatives of α – amino acids as ligands, has been stated at the outset, details regarding them (i.e., their schematic structures, methods of preparation, etc.) have been given in appropriate chapters.

There are different possibilities of Mo = O<sub>t</sub> distortional isomers of the (Mo<sup>V</sup><sub>2</sub>O<sub>3</sub>)<sup>4+</sup> core by rotations around the linear Mo – O<sub>b</sub> – Mo bridge<sup>19, 165</sup>; structurally characterized species of this type usually possess cis – or trans – terminal oxygens and are diamagnetic due to coupling of the Mo<sup>V</sup>, d<sup>1</sup> – electrons through the three centre bond. For a skew arrangement of the two Mo = O bonds these two d – electrons are unlikely to overlap significantly, leading to a triplet (S = 1) ground state<sup>19, 164</sup>. It will be worthwhile to study the physicochemical property and reactivity aspects of (Mo<sup>V</sup><sub>2</sub>O<sub>3</sub>)<sup>4+</sup> – complexes with aldimine ligands with possibilities of distortional isomers / rotamers involving different arrangements of Mo = O<sub>t</sub> bonds with respect to the Mo – O<sub>b</sub> – Mo bridge.

The UO<sub>2</sub><sup>2+</sup> ion is one of the most stable dioxo cations known, being able to maintain its identity over a wide range of chemical situations. The metal centre of this linear entity, can accommodate 4 to 6 ligand donor atoms in its equatorial plane<sup>165</sup>. Its versatile complex forming ability is reflected in its rich coordination Chemistry with a wide variety of ligands as well as rapid growth of literature on different facets of its Chemistry / coordination Chemistry till date with a promise for interesting future developments<sup>105, 166 – 174, 177 – 179, 182 – 187</sup>.

They cover wide areas ranging from synthesis of novel coordination compounds to the interesting reactivity aspects as well as studies on different physicochemical, spectroscopic properties and electronic structure.

Here the attention is focused on the redox activity of several uranyl complexes towards Na<sub>2</sub>SO<sub>3</sub>. The chiral aldimine ligands help to follow the effect of stereochemical factors on the electron transfer process. One of the pertinent uranyl complexes has been characterized through X-ray crystallography.

## **CHAPTER II**

### **SECTION – I**

A di -  $\mu$  – oxomolybdenum(V) complex of 6-acetyl-isoanthopterin, undergoing oxygen atom transfer with dimethyl sulphoxide.

## Abstract

The new compound,  $\text{Na}[(\text{Mo}^{\text{V}}_2\text{O}_4)(\text{pte}_1)(\text{OCH}_3)(\text{CH}_3\text{OH})_2]$  ( $\text{pte}_1$  = anion of 6-acetyl-isoanthopterin), has been prepared using the redox 'non-innocent' title ligand in  $\text{CH}_3\text{OH} - \text{H}_2\text{O}$ , and characterized by elemental analysis and physico-chemical methods including, ESIMS, IR, UV-VIS,  $^1\text{H-NMR}$  spectra and CHEM3D representations. Rate constant data for its oxygen atom transfer (OAT) reaction with dimethyl sulphoxide (DMSO) tally with those of synthetic analogue systems reported earlier by different authors. The negative activation entropy ( $\Delta S^\ddagger = -206.3 \text{ J mol}^{-1} \text{ deg}^{-1}$ ) is consistent with an associative mechanism for this reaction.

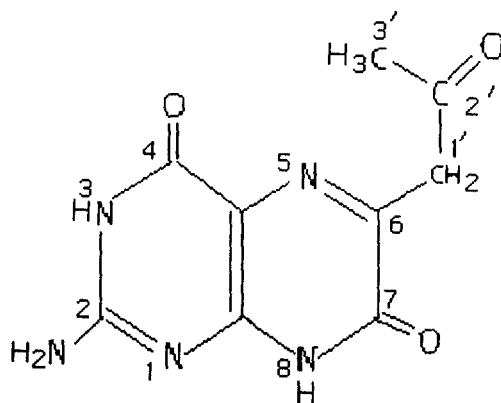


218462

## Introduction

Pterin derivatives, specially those with different types of 6-substituent, have been found in many metalloenzymes, where the metal atom may be Mo for molybdoenzymes, W for tungstopterin enzymes, and Fe or Cu for aromatic amino acid hydroxylases<sup>1,2,81,82</sup>. The well-known ability of the pterin ring to act as a redox partner in biological redox systems, is intimately connected with the ability of the pyrazine moiety (pterin ring) to exist in different oxidation states<sup>4</sup>. These facts have inspired symbiotic developments in the coordination Chemistry of pterin ligands<sup>3(a,b),20</sup>. In view of the multi-electron redox capability of both the molybdenum atom (VI, V, IV) and the pterin ligand, the redox aspect of molybdenum – pterin interaction and the reactivity of the resulting compounds still need careful study<sup>3(a,b)</sup>.

This work is connected with the synthesis, characterization and reactivity study towards DMSO, of a new di-nuclear molybdenum (V) complex of 6-acetyl-isoanthopterin [ $H_2(pte_1)$ , Scheme (II - 1)], whose 7-oxo group corresponds to the pyran ring oxygen atom of Mo-centered Functional Unit (McFU)<sup>1,2</sup> [Scheme (I-1)]. As delineated here,  $H_2(pte_1)$  acts as a reducing agent towards  $Na_2MoO_4$  in a  $CH_3OH - H_2O$  medium during the synthesis of the above mentioned complex.



Scheme (II - 1)

## Experimental

**Materials:** Reagent grade chemicals were used as received. Solvents were purified, prior to use, following literature procedure <sup>9</sup>. Na<sub>2</sub>MoO<sub>4</sub> · 2H<sub>2</sub>O was obtained from BDH, E. Merck, Mumbai. Et<sub>4</sub>NBr was obtained from Fluka Chemica. Kinetic and electrochemical measurements were performed in spectroscopic grade DMSO (SRL, Mumbai). Bu<sub>4</sub>NClO<sub>4</sub> (TBAP) for CV measurements, was obtained by published methods <sup>11</sup>.

**Method:** Elemental analysis (C,H,N) data were obtained from the IACS, Kolkata. Molybdenum was estimated by atomic absorption spectroscopy. <sup>1</sup>H-NMR data in DMSO-d<sub>6</sub> were obtained from the IISc, Bangalore (Bruker, DRX 500 MHz), RSIC, Lucknow (Bruker, DRX 300 MHz) and TIFR, Mumbai (Bruker, AMX 500 MHz). The electrospray mass spectra in CH<sub>3</sub>OH were obtained from RSIC, Lucknow (Micromass Quattro II triple quadrupole mass spectrometer). IR spectra (nujol mull) were recorded on a Philip Analytical SP3 – 300 spectrometer. Electrical conductivity data in DMF and DMSO (0.8 mmol dm<sup>-3</sup> solution) were measured using a digital conductivity meter (Systronics, model 304). Cyclic voltammetry data (vs. SCE, uncorrected for the junction contribution) were recorded under a N<sub>2</sub>- atmosphere on a BAS (CV-27), USA instrument. Electronic spectra and kinetic data (under N<sub>2</sub>- atmosphere) were recorded on a Shimadzu (UV-240) spectrophotometer, with thermostatic conditions (± 0.5 K) being maintained using a Shimadzu (TB-85) thermostat. Pseudo-first-order rate constants (k<sub>obs</sub>, s<sup>-1</sup>) were determined by the least square method from the plots of log(A<sub>∞</sub> – A<sub>t</sub>) vs. time, which were linear for at least three half-lives. These rate constants were used to determine activation parameters by means of an Eyring plot [ln (k<sub>obs</sub>/T) vs. (1/T)]; relevant data are collected in Table (II – 4). Magnetic susceptibility measurement were done with a Gouy balance, using Hg[Co(SCN)<sub>4</sub>] as calibrant.

## Synthesis of the complexes

### 6-acetyl-isoxanthopterin, $\text{H}_2\text{pte}_1 \cdot 0.5 \text{H}_2\text{O}$ (1)

The pterin ligand (1) was prepared in 75 % yield by modifying the original method of synthesis in the light of later developments (e.g., darkness,  $\text{N}_2$  – atmosphere,  $\text{pH} = 6.8$ )<sup>6</sup>. Purity of the product was checked through TLC [silica-gel GF<sub>254</sub>, UV – lamp], using  $\text{CH}_3\text{OH} - \text{H}_2\text{O}$  (4 : 1, v/v) solution and  $\text{Me}_2\text{CO} - \text{Et}_2\text{O}$  (1 : 1, v/v) as eluant.  $R_f$  : 0.65. The product gave positive 2,4 – DNP test and decomposed without melting above 573 K. Its solubility is ca. 5% in DMF (warming and stirring). Found : C, 44.0; H, 4.4; N, 28.4 %. Calc. for  $\text{C}_9\text{H}_9\text{N}_5\text{O}_3 \cdot 0.5 \text{H}_2\text{O}$  : C, 44.3; H, 4.1; N, 28.7 %. UV – VIS absorption bands [DMF,  $\lambda_{\text{max}}^{\text{nm}}(\log \epsilon)$ ]: 293 (3.68), 341 (3.86), 400 (3.28), 422 (3.27), 456 sh (3.00).

### $\text{Na}[(\text{Mo}^{\text{V}}_2\text{O}_4)(\text{pte}_1)(\text{OCH}_3)(\text{CH}_3\text{OH})_2]$ (2)

A purged ( $\text{N}_2$ ) aqueous solution (10 ml) of  $\text{Na}_2\text{MoO}_4 \cdot 2\text{H}_2\text{O}$  (0.242 g, 1 mmol) was treated with a stirred suspension of 6-acetyl-isoxanthopterin hemihydrate (0.244 g, 1 mmol) in  $\text{CH}_3\text{OH}$  (100 ml) under  $\text{N}_2$  in dark,  $\text{pH}$  adjusted to 4.8 (AcOH); finally a  $\text{CH}_3\text{OH}$  solution (10 ml) of  $\text{Et}_4\text{NBr}$  (0.525 g, 2.5 mmol) was added and stirring was continued for 25 h (301 K). The light yellow compound was recovered by filtration (fritte) under  $\text{N}_2$  in dark, washed with purged solvents [e.g.,  $\text{CH}_3\text{OH} - \text{H}_2\text{O}$  (1 : 1, v/v),  $\text{CH}_3\text{OH}$ ,  $\text{Et}_2\text{O}$ ], dried in vacuo over silica gel for 48 h. Yield : 60 %. Its purity was checked through TLC [silica-gel GF<sub>254</sub>, UV–lamp], using diluted (with 50 times  $\text{CH}_3\text{OH}$ ) DMSO solution and  $\text{CH}_2\text{Cl}_2 - \text{benzene}$  (1 : 1, v/v) as eluant.  $R_f$  : 0.54. Its solubility is ca. 4% in DMF. Found : C, 24.1; H, 3.1; N, 11.7; Mo, 31.9 %. Calc. for  $\text{NaMo}_2\text{O}_{10}\text{C}_{12}\text{H}_{18}\text{N}_5$  : C, 23.7; H, 3.0; N, 11.5; Mo, 31.6 %. UV-VIS absorption bands [DMF,  $\lambda_{\text{max}}^{\text{nm}}(\log \epsilon)$ ]: 291 (4.03), 342 (4.25), 400 (3.56), 422 sh (3.53), 458 sh (3.23)<sup>1,2</sup>. The compound is found to be diamagnetic in nature.

## Results and Discussion

The ligand (1) [Scheme (II-1)] used in this work is a 6 – substituted pterin compound and the reason behind its choice is to explore its participation in the redox activity at the Mo centre of the pertinent molybdenum complex (2) [Fig.(II-9a)]<sup>4, 119</sup>. Low solubility associated with hydrogen bonding (involving hydrophilic group like amino, hydroxo, etc.) is a characteristic feature of pterin Chemistry<sup>84(b)</sup>. But there is a good agreement between the experimental analytical data and the expected values for (1) and (2).

Electrospray Ionization Mass Spectroscopy (ESIMS) involving soft ionization technique, has proved to be a valuable tool for characterizing wide variety of compounds including inorganic and coordination sphere<sup>12, 110, 121</sup>. This technique helps in assigning the molecular mass of this type of synthetic compounds<sup>12, 85, 107</sup>. As true for different types of mass spectrometry, the assignment of molecular formula (or any definite fragment originating from it) is confirmed by the experimental value of  $m/z$  (most abundant isotopic mass) as well as matching between the experimental and calculated (simulated) isotopic distribution profile<sup>14, 85, 107, 117, 118</sup>. As far as organic compounds containing O, F, P and I are concerned, the relative intensities of  $M$ ,  $M+1$  and  $M+2$  isotope peaks are of great value in recognizing the molecular ion ( $M^+$ ) peak or any well – defined fragment containing it<sup>85</sup>. For (1), the ESIMS spectrum contains its molecular ion peak without  $0.5H_2O$ , at  $m/z = 235.9$  (relative abundance = 63 %). All the other fragmentation and fragment association peaks are also assigned as per the proposed molecular formula. In case of (2), the molecular ion peak appeared at  $m/z = 609.1$ ,  $[M + 2H]^+$  (relative abundance = 38.1 %), where ‘M’ corresponds to the molecular formula of (2)<sup>85, 107</sup>; it is associated with the characteristic distribution of molybdenum isotopes<sup>7(a), 14, 15</sup>. The ligand  $[H_2pte_1]^+$  peak is observed at  $m/z = 235.9$  (relative abundance = 89.2 %). Breaking up of (2) to some extent during recording of ESIMS data along with cluster formation ( $m/z = 825.0$ , relative abundance = 16.2 %) is indicated<sup>12(a)</sup>.

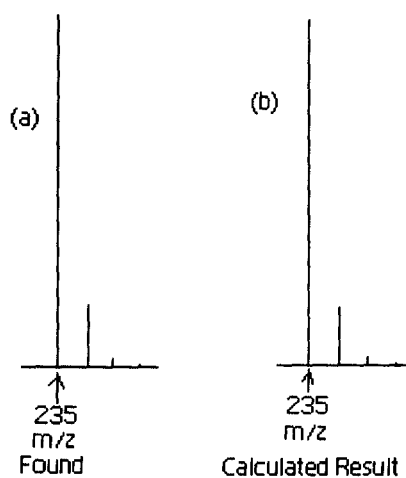


**Fig.(II-1):** (a) ESIMS data of (1) at  $m/z$  (= 235) region corresponding to  $[H_2pte_1]^+$  ;  
 (b) the calculated isotope pattern<sup>46</sup>. Formula:  $C_9H_9N_5O_3$ .

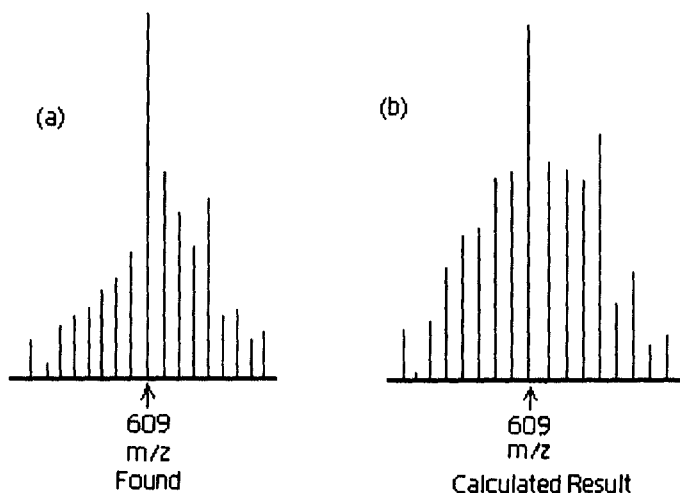


**Fig.(II-2):** (a) ESIMS data of (2) at  $m/z$  (= 609) region corresponding to  $[M + 2H]^+$  ;  
 (b) the calculated isotope pattern<sup>46</sup>. Formula:  $C_{12}H_{20}N_5O_{10}Mo_2Na$ .

The molecular ion peak of (1) at  $m/z = 235$  and that of (2) at  $m/z = 609.1$ , mentioned above, is simulated with the help of a computer program, 'Isotope Pattern Calculator' (IPC)<sup>46</sup> and found to be in good agreement with the experimentally obtained data [Fig.s(II-1) & (I-1) respectively] suggesting the accuracy of molecular mass prediction of these compounds.

The  $\Lambda_M$  values of (2) ( $\text{ohm}^{-1}\text{cm}^2 \text{mol}^{-1}$ , 301 K) = 27 (DMSO) and 73 (DMF) are consistent with its 1 : 1 electrolytic formulation<sup>13</sup>.

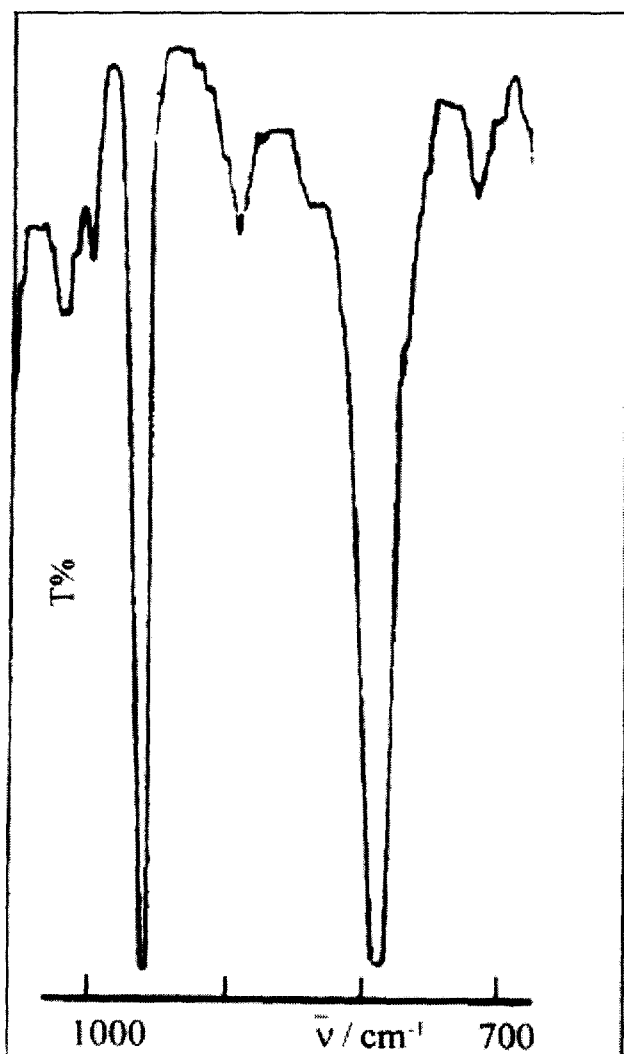
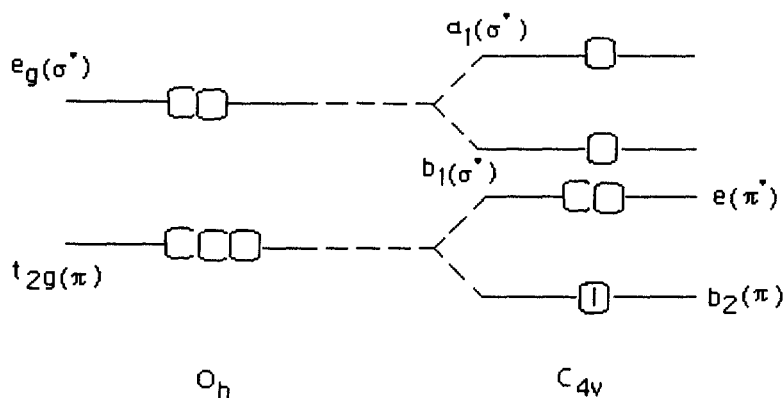


Fig.(II - 3): IR spectrum (nujol) of (2).

Comparison of the IR spectra of (1 & 2), shows that the three ligand bands in the  $1600 - 1700 \text{ cm}^{-1}$  region undergo considerable modification due to deprotonation of NH(3) and NH(8) groups [Scheme (II-1)] through enolisation involving the 4 - and 7 - oxo groups respectively, followed by coordination through O(4) and N(5) atoms<sup>3(a,b), 20(a,d), 27</sup> [Fig.(II-9a)]. For (2) the  $\nu(\text{C}=\text{O})$  mode of the 2' - oxo group appears as a strong band at  $1645 \text{ cm}^{-1}$ ; the  $\nu(\text{C}=\text{C})$ ,  $\nu(\text{C}=\text{N})$  vibrations of the pterin ring are associated with this band<sup>5, 6, 15, 16, 48</sup>. The characteristic IR bands of the  $(\text{Mo}^{\text{V}}_2\text{O}_4)^{2+}$  core in (2) appear at their expected positions [Fig.(II-3)]; as (2) has been obtained from a  $\text{CH}_3\text{OH} - \text{H}_2\text{O}$  reaction medium (pH = 4.5), presence of a di- $\mu$ -oxo core is quite likely<sup>29</sup>.

In  $C_{4v}$  symmetry the d orbitals transform according to  $a_1$  ( $d_{z^2}$ ),  $b_1$  ( $d_{x^2 - y^2}$ ),  $b_2$  ( $d_{xy}$ ) and  $e$  ( $d_{xz}$ ,  $d_{yz}$ ) representations, and the d – orbital (ligand field) portion of the MO diagram is shown in Fig.(II–4). The  $a_1$  level is strongly sigma anti-bonding due to interaction with a  $p\sigma$  orbital on O atom and (a weaker interaction) with a  $p\sigma$  orbital on the trans group. The  $d_{xz}$  and  $d_{yz}$  orbitals are involved in strong pi bonding with O  $p_x$  and  $p_y$  orbitals and as a result the e level is significantly raised in energy above the  $b_2$  ( $d_{xy}$ ) level.



**Fig.(II – 4):** Ligand – field splitting Diagram for  $C_{4v}$  complexes.

The distorted octahedral geometry of **(2)** [as bond angles data in Table(II–3)] leads to further ligand field splitting of d – orbitals (as compared to the usual  $e_g$  and  $t_{2g}$  level of  $O_h$  symmetry) and favours spin pairing in the  $d_{xy}$  ( $b_2$ ) level<sup>19</sup>. Of the three chemically relevant oxidation states of molybdenum (e.g.,  $Mo^{IV}$ ,  $Mo^V$  and  $Mo^{VI}$ ), during catalysis only the  $Mo^V$  ( $d^1$ ) state could be detected as a transient species by EPR spectroscopy in oxomolybdoenzymes ; the  $Mo^{IV}$  ( $d^2$ ) state is consistently diamagnetic in such cases<sup>26</sup>. Almost all the synthetic molybdenum pterin complexes reported so far are diamagnetic, including one formulated as containing a  $Mo^V$  centre; diamagnetic behaviour of the latter system is explained by invoking a strong antiferromagnetic coupling between the  $d^1$  ( $Mo^V$ ) electron and the delocalized electron system of the redox “noninnocent” pterin ligand<sup>20(a,d)</sup>. This unique nature of the pterin ligand is responsible for the observed diamagnetism of **(2)** and its high resolution  $^1H$  NMR data. The diamagnetic nature of **(2)** is also consistent with the observations on well – characterized dinuclear  $\mu$  – oxomolybdenum (V) complexes where the spins of the two  $d^1$  centres are antiferromagnetically coupled involving the 2p orbital of the bridging oxygen atom<sup>19</sup>.

For (1) [Table (II – 1)]  $^1\text{H-NMR}$  signals of the  $\text{CH}_3(3')$  and  $\text{CH}_2(1')$  groups [Scheme (II – 1)] appear as singlets at  $\delta$ , 2.18 and  $\delta$ , 3.74 respectively; these spectral assignments have been carried out on the basis of  $^1\text{H-}^1\text{H}$  COSY data [Fig.(II-6)], supported by proton integration values. In view of the oxo-transfer reaction of (2) with DMSO, several of its high resolution  $^1\text{H-NMR}$  spectra were recorded for unambiguous spectral assignments. One such spectrum [Fig.(II-5)] shows the  $\text{CH}_3(3')$  and  $\text{CH}_2(1')$  signals at  $\delta$ , 1.16 and  $\delta$ , 3.21 respectively.  $^1\text{H-}^1\text{H}$  COSY data (500 MHz, 280 K) help to identify the  $\text{CH}_3(3')$  ( $\delta$  1.18, triplet,  $J = 7.5$  Hz) and  $\text{CH}_2(1')$  ( $\delta$  3.22, quartet,  $J = 7.7$  Hz) signals; the  $J$  – values were estimated from the corresponding 2D –  $J$  resolved spectrum [Fig.(II-7)]. In Fig.(II-5) the  $\text{CH}_3$  signal of the two  $\text{CH}_3\text{OH}$  molecules and  $\text{CH}_3\text{O}$  – group appear together with the residual proton signal ( $\text{H}_2\text{O}$ ) at  $\delta$ , 3.38.

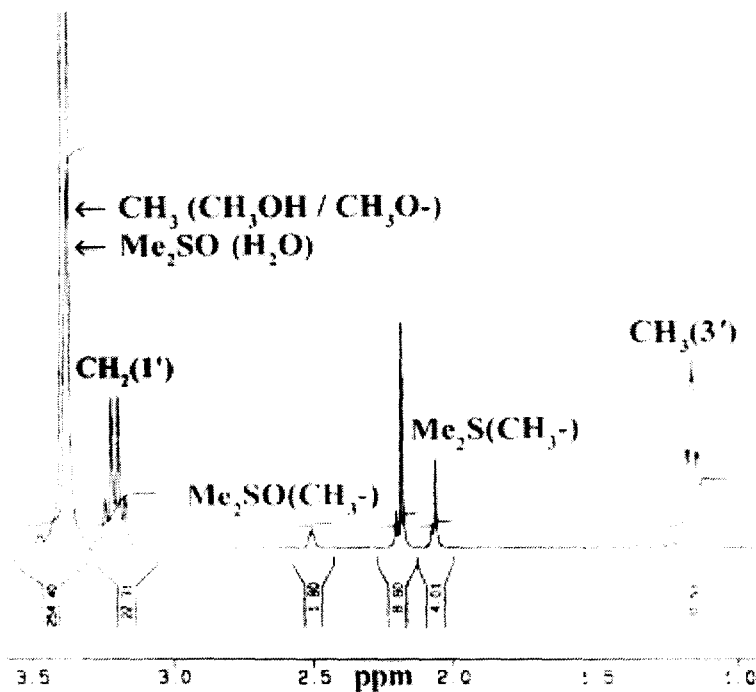


**Fig.(II-5):**300 MHz (298 K)  $^1\text{H NMR}$  spectrum in  $\text{DMSO} - d_6$  ( $\delta$ , ppm vs. TMS) of (2).

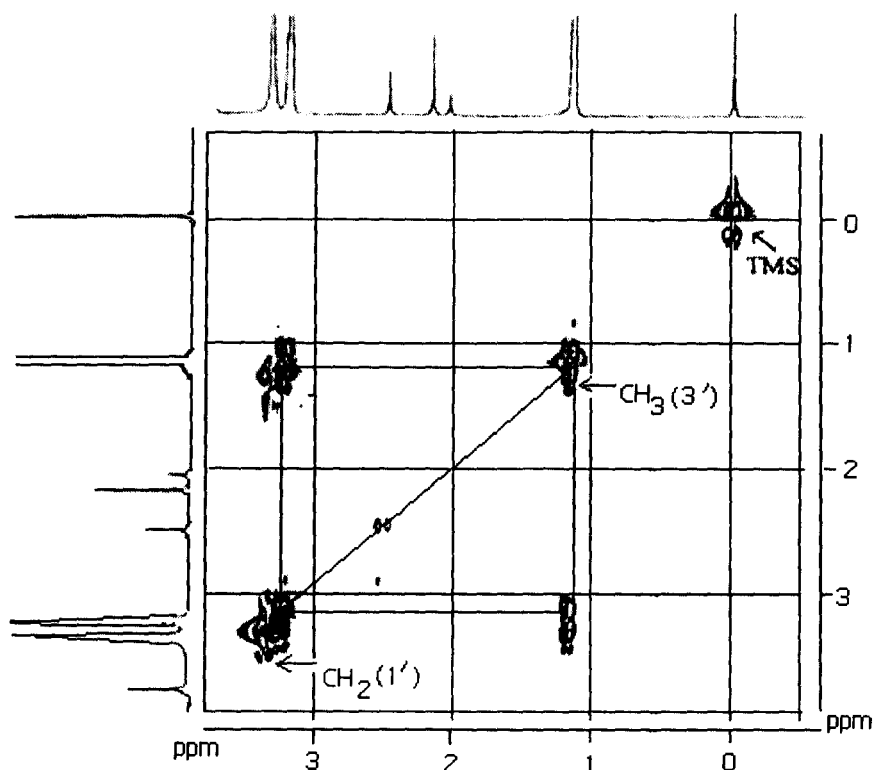


**Fig. (II-6)** : 500 MHz (280 K)  $^1\text{H} - ^1\text{H}$  COSY data of (2) in  $\text{DMSO} - d_6$ .

**Table (II-1)**: Relevant  $^1\text{H}$ -NMR signals in  $\text{DMSO} - d_6$  ( $\delta$  ppm, internal TMS) of (1) & (2), and  $\Delta$  ( $= \delta_{\text{compound}} - \delta_{\text{ligand}}$ ) values.

Compound <sup>a</sup>	$\text{CH}_3(3')$	$\text{CH}_2(1')$
(1) <sup>b</sup>	2.18 (s)	3.74 (s)
(2) <sup>c</sup>	1.16 (t)	3.21 (q)
$\Delta$	-1.02	-0.53

<sup>a</sup> Vide Scheme (II-1) for proton numbering system; <sup>b</sup> data at 500 MHz, 300 K; <sup>c</sup> data at 300 MHz, 298 K.

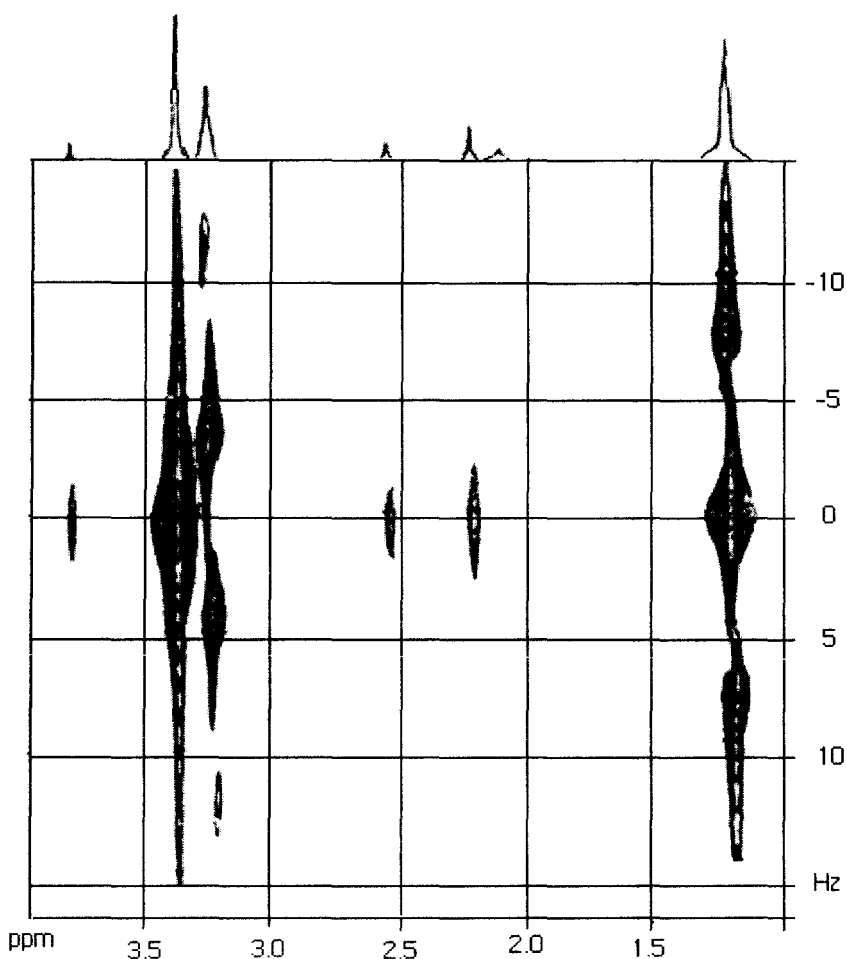


**Fig. (II-7) :** 500 MHz (280 K) 2D J resolved spectrum in DMSO -  $d_6$  of (2).

For (2), the -NH<sub>2</sub> (2) signal (500 MHz, 280 K) consists of a broad prominent signal at  $\delta$  7.0, associated with two weaker ones at  $\delta$  6.75 and 6.50 due to the two additional forms =N<sup>+</sup>H<sub>2</sub> and =NH [Fig.(II-9c) & (II-9a)] respectively. The proton integration data for the two protons of the -NH<sub>2</sub> (2) group (involving the three above mentioned signals) tally with those of the two -OH signals of the two CH<sub>3</sub>OH molecules in (2). As suggested by different authors, such transformations involving the -NH<sub>2</sub> (2) group are quite likely and help the pterin ring to play an active part essential for enzyme reactions<sup>3(a,b), 5, 35</sup>. Although the -OH signal of CH<sub>3</sub>OH (neat) usually appears at ca.  $\delta$  5.0, in (2), the two CH<sub>3</sub>OH molecules exhibit two separate -OH signals [due to the overall unsymmetrical nature of (2), Fig.(II-9a)] at  $\delta$ , 12.35 and  $\delta$  10.96. Depletion of

electron density associated with strong coordination to the Mo<sup>V</sup> – atoms<sup>29</sup>, is responsible for the substantial deshielding of these – OH signals of CH<sub>3</sub>OH in (2). Coordination of the CH<sub>3</sub>OH molecule to the molybdenum atom in different types of compound, sometimes leading to deprotonation / methoxide coordination, has been proposed by various workers and has been characterized by X-ray crystallographic data<sup>3(a,b), 20(a,d), 18, 27</sup>. The electronic effects associated with the possible existence of the – NH<sub>2</sub> (2) group in two additional forms [Fig.(II–9a) & (II–9c)] as stated above, are transmitted (via the pterin ring) even upto the two coordinated CH<sub>3</sub>OH molecules in (2); this is evident from the fact that each major methanolic – OH signal is accompanied by two minor ones. A comparative study [Table (II–1)] of the splitting patterns of the CH<sub>3</sub>(3′) and CH<sub>2</sub>(1′) signals in (1) and (2) also throws light on the above-mentioned electronic circulation effect. In (1), these two signals appear as singlets, whereas in (2) they are split up into a triplet and a quartet respectively. Although <sup>1</sup>H-<sup>1</sup>H COSY data indicate spin – spin interaction between these two signals in both these cases, most likely the increased electronic circulation due to coordination in (2) is responsible for the observed splitting of the CH<sub>3</sub>(3′) and CH<sub>2</sub>(1′) signals in this case. Besides this, contrary to expectation the proton signals [Table (II - 1)] of (2) exhibit varying degree of shielding effects (negative Δ values)<sup>83</sup>. The +2 charge on the (Mo<sup>V</sup><sub>2</sub>O<sub>4</sub>)<sup>2+</sup> core is satisfied by the deprotonated O(4) atom and methoxide group; the additional electron density released through deprotonation of – NH(8) [Na<sup>+</sup> salt formation with O(7), consistent with Λ<sub>M</sub> values] is transmitted via the redox ‘non-innocent’ pterin ligand to the region around the O(2′) atom of the 6-substituent [Scheme (II–1) & Fig.(II–9a) to (II–9c)], causing the observed shielding effect<sup>3(a,b), 4, 20(a,d), 27</sup>. This extra electron density around the (Mo<sup>V</sup><sub>2</sub>O<sub>4</sub>)<sup>2+</sup> core in (2), makes it a good reducing agent towards a typical enzyme substrate like DMSO, as revealed by following kinetic data; this process also indicates oxidation state less than VI for the Mo – atoms in (2). The proposed CHEM3D Representations of (2) involving a bridging pterin ligand is consistent with different types of structurally characterized binuclear molybdenum (V) complexes including triply bridged ones as well as structurally characterized metal – pterin complexes where the N(5) atom (pterin residue) [Scheme (II–1)] plays a pivotal role<sup>3(a,b), 5, 20(a,d), 29, 27, 39</sup>.

From the considerations of elemental analysis and ESIMS data (experimental and simulated) as well as other physicochemical data, the chemical compositions of the new compounds (ligand, complex and recovered complex) were established. Then their possible schematic structures were optimized by molecular mechanics calculations (MM2), giving the lowest steric energy [for **(1)** – 2.52 Kcal mol<sup>-1</sup> and for **(2)** 13.95 Kcal mol<sup>-1</sup>] CHEM3D model [e.g., Fig.(II-8) and Fig.(II-9a)], thereby throwing light on both stability and geometry of these compounds<sup>87</sup>. The molecular modelling force fields in use for molecular systems can be interpreted in terms of the four key contributions, e.g., bond stretching, angle bending, torsional terms and non-bonded interactions<sup>86</sup>; apart from the lowest steric energies of the molecules. Here, two basic parameters were evaluated, e.g., bond distances (Å) and bond angles (deg.). The most relevant of which are shown in Table (II-2) and Table (II-3), together with the available literature data on X-ray structural studies in the relevant fields<sup>3, 5, 20(a-c), 27, 29, 114 - 116</sup> and the data are in conformity with the recent trends of structure elucidation using optimized computational models<sup>108</sup>.

Concentrating on the chelating aspect of the pterin ligand towards molybdenum, the Mo-N(5) bond plays a pivotal role here [atom numbering as per Scheme (II-1)] and this bond distance shows a fair agreement between the computed and experimental data<sup>3, 5, 20(a-c), 27, 29, 114 - 116</sup> [Table (II-2)].

The most stable CHEM3D representation for **(1)** [Fig.(II-8)] shows nothing but the same structure as proposed in Scheme (II-1) above. In case of **(2)**, the most stable form [Fig.(II-9a)] (Steric energy = 13.95 Kcal mol<sup>-1</sup>) shows the participation of N(12) lone pairs towards the formation of  $\pi$  – bond with the adjacent C(5) atom having neutral N(12) and N(6) atoms but retaining aromaticity in the pyrazine ring.

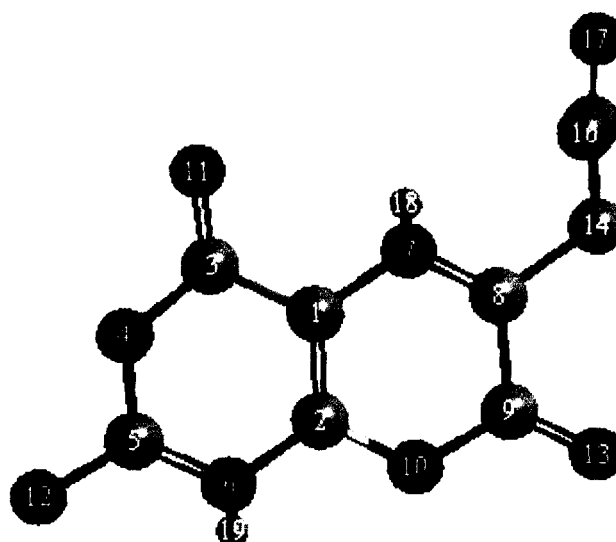


**Fig. (II- 8):** The optimized geometry (CHEM 3D model obtained through MM2 calculations) of (1) with a steric energy of  $-2.52 \text{ Kcal mol}^{-1}$ . Its numbering system is set by the software used<sup>87</sup> and is different from that in Scheme (II - 1).

**Table (II - 2):** Comparison of selected optimized bond lengths (Å) and bond angles (deg.) in the free ligand (1) and its molybdenum complex (2)

Atoms	Bond Distances(Å) <sup>+</sup>	Atoms	Bond Distances(Å) <sup>+</sup>
C(1)-N(7)	1.41 [1.40]	C(1)-C(3)	1.48 [1.44]
C(3)-O(11)	1.22 [1.36]	C(1)-C(2)	1.37 [1.41]
C(9)-O(13)	1.22 [1.36]	C(3)-N(4)	1.37 [1.32]
C(2)-N(6)	1.40 [1.41]	C(9)-N(10)	1.36 [1.37]
C(15)-C(16)	1.51 [1.51]	C(5)-N(12)	1.37 [1.31]
C(2)-N(10)	1.35 [1.36]	C(5)-N(6)	1.31 [1.45]
N(7)-C(8)	1.28 [1.33]	C(14)-C(15)	1.51 [1.52]
C(8)-C(9)	1.49 [1.48]	N(4)-C(5)	1.35 [1.44]
C(15)-O(17)	1.21 [1.22]	C(8)-C(14)	1.50 [1.51]

Angle Atoms	Bond Angle(deg.) <sup>†</sup>	Angle Atoms	Bond Angle(deg.) <sup>†</sup>
N(6)-C(5)-N(4)	120.9 [118.0]	C(1)-N(7)-C(8)	118.7 [103.6]
C(3)-N(4)-C(5)	124.8 [121.5]	C(1)-C(3)-N(4)	114.8 [121.4]
C(8)-C(9)-N(10)	114.9 [122.8]	N(6)-C(2)-C(1)	121.6 [121.0]
N(7)-C(8)-C(9)	123.0 [123.1]	N(10)-C(2)-C(1)	119.8 [118.9]
C(2)-N(10)-C(9)	122.7 [111.7]	N(7)-C(1)-C(2)	121.0 [129.1]
C(2)-N(6)-C(5)	119.7 [117.0]	C(3)-C(1)-C(2)	118.2 [118.6]

<sup>†</sup> Free ligand data are mentioned outside third bracket and the data derived from its molybdenum complex, (2), are mentioned within third bracket.

Comparing these two sets of data it is clear that both bond lengths and bond angles of the ligand residue have undergone a recognizable change in its complex (2) suggesting definite complexation of the [H<sub>2</sub>pte<sub>1</sub>] ligand with molybdenum metal. In comparison to the free ligand (1), the following bond lengths are increased in the complex: C(3) – O(11) from 1.22Å to 1.36Å, N(7) – C(8) from 1.28 Å to 1.33Å and C(15) – O(17) from 1.21 Å to 1.22 Å. This observation is consistent with the O(11), N(7) and O(17) [Fig.(II-8)] atoms' bonding with the molybdenum atom [compare with Fig.(II-9a)] leading to depletion of electron density from the bonds immediate to the bonds between metal and these atoms (i.e., the bonds mentioned above) and hence the observed increase in bond lengths in the complex. The C(5) – N(12) bond length has undergone a decrease from (1.37 – 1.31)Å on complexation indicating the N(12) [N(2) as per Scheme – (II-1)] lone pairs' participation in metal coordination via the pterin rings <sup>3(a,b), 5, 34, 35</sup>, as mentioned above. Some other bond lengths such as C(9) – O(13), C(1) – C(2), C(5) – N(6) etc. have also suffered visible change due to redistribution of overall electron density on metal coordination

In all the probable forms of (2) [Fig.(II-9a) to (II-9c)], one Na<sup>+</sup> ion is held by ionic force by the uni-negative O(13) atom. Another probable form containing N(12) – C(5)  $\pi$  bond, formed through the N(12) lone pairs' participation in this  $\pi$  bonding and acquiring positive and negative charges on N(12) and N(6) respectively [Fig.(II-9c)] found to be of moderately stable (Steric energy = 15.26 Kcal mol<sup>-1</sup>).

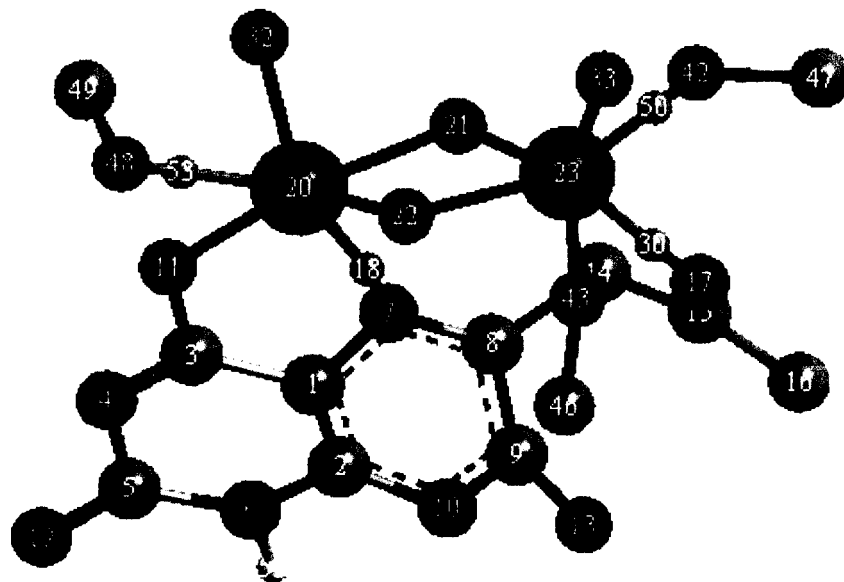


**Fig.(II-9a):** The optimized geometry (CHEM3D model obtained through MM2 calculations) of (2) with a steric energy of 13.95 Kcal mol<sup>-1</sup>. Its numbering system is set by the software used<sup>87</sup> and is different from that in Scheme (II - 1).

**Table (II-3):** Comparison of selected computed bond lengths(Å) and bond angles (deg.) involving Mo – atom in (2) from the optimized geometry [Fig.(II-9a), MM2 calculations] with the available literature data (in parenthesis) from X-ray structural studies\*

Atoms	Bond Distances(Å) <sup>+</sup>	Atoms	Bond Distances(Å) <sup>+</sup>
O(11)-Mo(20)	1.98(1.95–2.23) <sup>3(c), 20a</sup>	N(7)-Mo(20)	2.20(2.02) <sup>3(c)</sup>
O(42)-Mo(23)	2.14(2.32) <sup>109</sup>	Mo(20)-O(22)	1.97(1.93) <sup>19</sup>
O(21)-Mo(23)	1.97(1.93) <sup>19</sup>	O(48)-Mo(20)	2.24(2.32) <sup>109</sup>
Mo(23)-O(17)	2.18(2.01) <sup>109</sup>	Mo(23)-O(43)	1.97
Mo(20)-O(32)	1.98(1.66) <sup>3(c)</sup>	Mo(23)-O(33)	1.94(1.66) <sup>108</sup>

Angle Atoms	Bond Angle(deg.) <sup>+</sup>	Angle Atoms	Bond Angle(deg.) <sup>+</sup>
Mo(20)-N(7)-C(1)	120.8(119.3) <sup>3(c)</sup>	Mo(20)-O(11)-C(3)	119.1(112.1) <sup>3(c)</sup>
O(11)-Mo(20)-N(7)	80.6(74.1) <sup>3(c)</sup>	O(21)-Mo(23)-O(17)	109.0(105.9) <sup>109</sup>
Mo(20)-O(22)-Mo(23)	115.6	O(11)-Mo(20)-O(22)	137.9
O(33)-Mo(23)-O(22)	103.2	O(22)-Mo(20)-O(32)	90.3
O(21)-Mo(23)-O(22)	64.4	O(22)-Mo(20)-O(21)	64.0
O(17)-Mo(23)-O(33)	120.8	O(17)-Mo(23)-O(22)	125.3
Mo(20)-O(22)-Mo(23)	115.6	Mo(23)-O(21)-Mo(20)	114.9
O(22)-Mo(20)-N(7)	89.7	N(7)-Mo(20)-O(21)	72.3

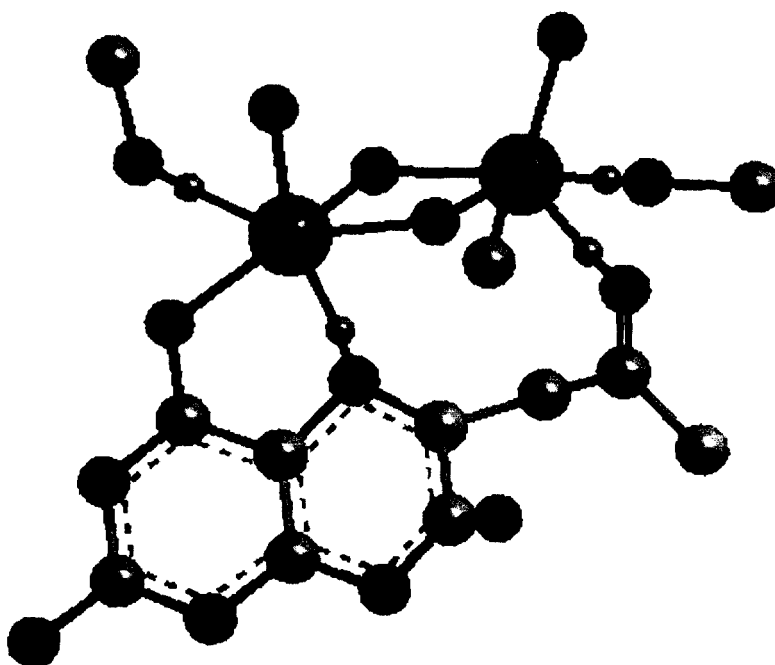
<sup>+</sup> Here O(11), N(7) and O(17) correspond to O(4), N(5) and O(2') donor atoms respectively, of the pterin ring as per Scheme (II – 1), while N(12) and N(6) correspond to the 2-substituent N and N(1) respectively.

\* X-ray structural data have been collected from references mentioned as superscript on the data within parenthesis.

Table (II-3) shows few relevant bond length and bond angle data of (2), together with the X-ray structural data on molybdenum complexes of pterin ligand obtained from the available literature<sup>3(c), 108, 109</sup>. This approach of rationalizing optimized structural data, is in line with the recent trends in structure (and property) elucidation<sup>48, 86, 108, 179</sup>. The agreement between the computed bond lengths and the literature X-ray structural data is good, especially for O(11) – Mo(20) and N(7) – Mo(20), O(21)-Mo(23), O(48)-Mo(20) etc. [Table (II-3)]. Of the different donor atoms from the pterin ligand, the O(4) and N(5) atoms [this numbering system corresponds to Scheme (II-1)] play a major role in the metal-ligand bonding process which has been verified through X-ray crystallography<sup>20(a,d), 27, 114 – 116</sup>. From chemical and X-ray structural studies on 6-substituted pterins, it has been inferred that sufficiently greater basicity / nucleophilicity resides at N(5) than at N(8) of the pterin ring [Scheme (II-1)], thereby influencing its above-mentioned coordinating ability<sup>88(a), 119</sup>. Another important aspect is the close tally of Mo(23) – O(17) bond length from CHEM3D data with available X-ray data is noteworthy. Considering the length of 6 – substituted chain [numbering as per Scheme

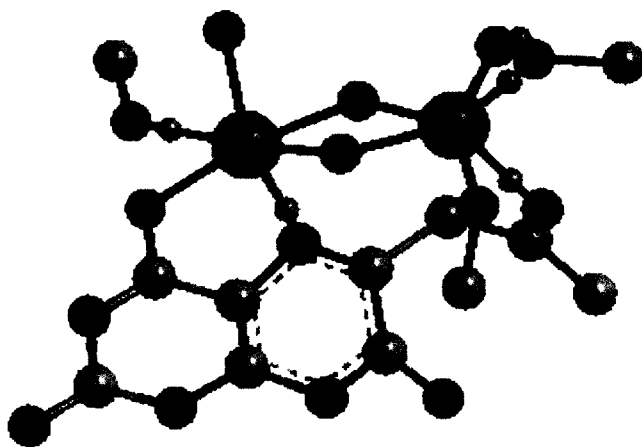
(II-1)] of the ligand, the O(17) atom's coordination to the other molybdenum atom [Fig. (II-9a)] is possible and can be understood in the light of the peptide chain's coordination in oxomolybdoenzymes<sup>2</sup>.

Table (II-2) shows the bond lengths and bond angles of the free ligand and that of the pterin ligand residue in the complex (2). Comparing these two sets of data it is clear that both bond lengths and bond angles of the pterin rings have undergone a visible change in its complex suggesting definite complexation of the pterin ligand with molybdenum metal.



**Fig.(II-9b):**The optimized geometry (CHEM3D model obtained through MM2 calculations) of another tautomeric form of (2) with a steric energy of  $65.54 \text{ Kcal mol}^{-1}$ . Its numbering system is set by the software used<sup>87</sup> and is different from that in Scheme (II - 1).

The another form [Fig.(II-9b)] retaining aromaticity in both the pterin rings was found to be the least stable (Steric energy =  $65.54 \text{ Kcal mol}^{-1}$ ). This form contains a single bond between N(12) and C(5). Here the planar nature of the aromatic rings hinders its stability in three dimensional space.



**Fig.(II-9c):** The optimized geometry (CHEM3D model obtained through MM2 calculations) of another tautomeric form of (2) with a steric energy of 15.26 Kcal mol<sup>-1</sup>. Its numbering system is set by the software used<sup>87</sup> and is different from that in Scheme (II - 1).

In all the CHEM3D optimized geometries of three tautomeric forms of (2), presented above, contain an octahedral (slightly distorted) environment around both the molybdenum atoms, and the (Mo<sup>V</sup><sub>2</sub>O<sub>4</sub>)<sup>2+</sup> core has cis disposition of its terminal oxygen atoms. That the (Mo<sup>V</sup><sub>2</sub>O<sub>4</sub>)<sup>2+</sup> core is essentially in cis form is supported by the magnitude of O(33)-Mo(23)-O(22) and O(22)-Mo(20)-O(32) bond angles [Table(II-3)]. On the other hand, the trans form, which ought to be more stable in general, was found to possess higher amount of steric energy. This is due to the very nature of bonding in this molecule; here one side of the bridged oxo-molybdenum core is occupied by the bulky pterin ligand via its three coordination sites [Fig.(II-9a) to (II-9c)] leaving more space to the other side. So, the cis disposition of the terminal oxygen atoms provides less steric repulsion to the structure than the trans arrangement in this case.

Table(II-3) shows some important bond angles of (2) essentially belonging to four types of computed bond angles, in complete agreement with the four types of bond angles (62 ° - 77 °, 83 ° - 90°, 103 ° - 109 ° and 115 ° - 155 °) found from X-ray structural studies on different molybdenum - pterin systems with distorted octahedral geometry around the Mo - atoms (both mono and binuclear types)<sup>3, 5, 20(a-c), 27, 114 - 116</sup>.

The above discussion on the geometrical aspect of optimized computational model (MM2) of a new complex compound, sharing agreement with available X-ray structural data (e.g., bond length, bond angle and overall geometry) verifies the applicability of such an approach to molybdenum – pterin systems and provides the frame work for discussion on their spectroscopic, reactivity and other relevant aspects <sup>86</sup>.  
108, 113.

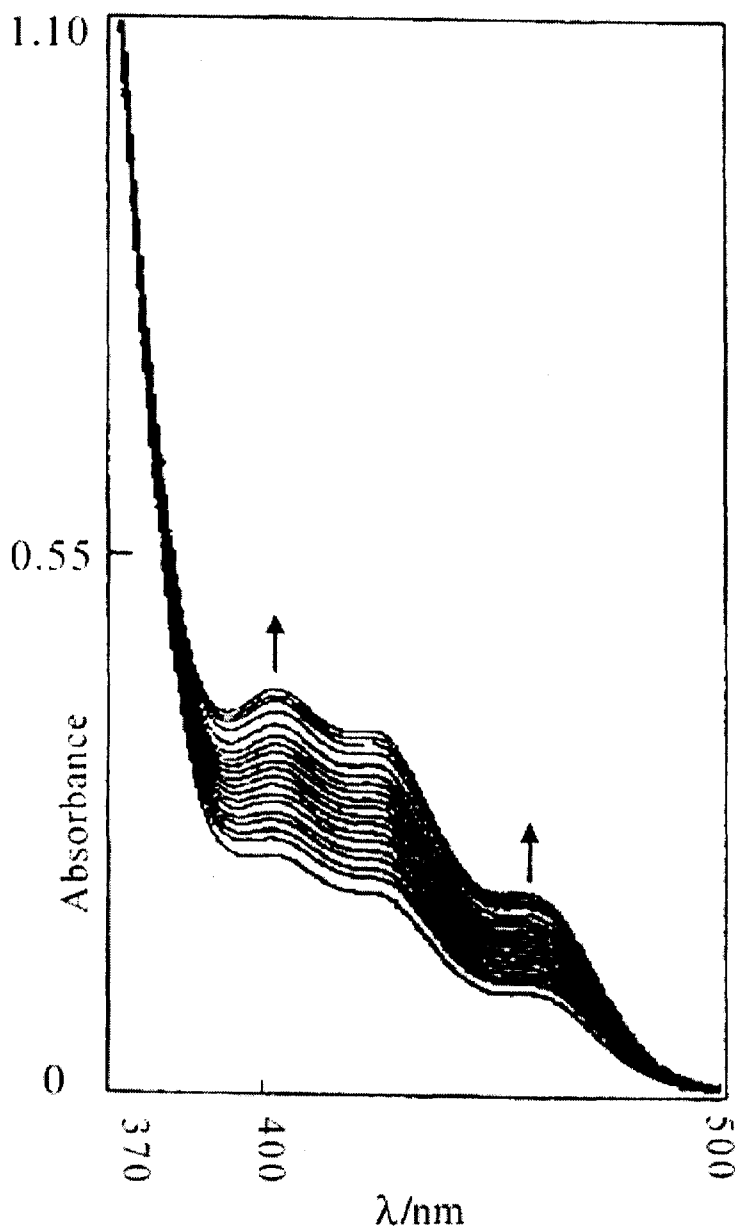


**Fig.(II-10):** UV – VIS absorption spectral changes recorded every 8 min. during the reaction of (2) [ $8.0 \times 10^{-4}$ (M)] with DMSO at 299.5 K.

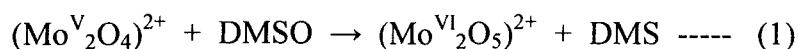
UV –VIS absorption bands of (2) contain all the pterin ligand's bands in (1) but in a slightly shifted position and with more intensity (higher log $\epsilon$  values) (essentially  $\pi \rightarrow \pi^*$  type), indicating more  $\pi$  – electron density in the ligand residue. This again can be explained by considering deprotonation from the pterin ligand during the complex formation reaction where the Mo<sup>VI</sup> was reduced to Mo<sup>V</sup>, and in this way pterin ligand acted as a reducing agent and subsequently itself got oxidized to more aromatic system [vide Fig.(II–8) to Fig.(II–9c)]. This argument is already substantiated by the NMR discussion and the kinetic studies discussed below.

The characteristic transitions of pterins in the 220 – 500 nm region depend to a large extent on the oxidation state and the tautomeric form of this ring system<sup>3(a,b), 20(a,d), 23, 27</sup>. The electronic spectral band of (2) above 400 nm are essentially of metal centered CT type [Fig.(II–10)] and their intensities grow with the progress of the oxygen atom transfer reaction with DMSO<sup>8(a,b)</sup>. The reaction of (2) with DMSO was followed at 401 nm and at four different temperatures in the range 300 – 325 K range. Additional time-dependent spectral studies indicated that (1) did not react with DMSO. The reaction (equation 1) is initiated through inner sphere electron transfer [e.g., concomitant with breaking of one of the bridges of the (Mo<sup>V</sup><sub>2</sub>O<sub>4</sub>)<sup>2+</sup> core], followed by relatively slow oxygen atom transfer reaction from the substrate, DMSO<sup>19</sup>.

**Table (II – 4):** Kinetic data for DMSO reduction by (2) through oxygen atom transfer:

T (K)	k <sub>obs</sub> x 10 <sup>3</sup> (s <sup>-1</sup> )	$\Delta H^\ddagger$ <sup>a</sup> (KJ mol <sup>-1</sup> )	$\Delta S^\ddagger$ <sup>a</sup> (J mol <sup>-1</sup> deg <sup>-1</sup> )	$\Delta G^\ddagger$ <sup>b</sup> (KJ mol <sup>-1</sup> )
300	1.4	25.5	- 206.3	91.2
309	1.9			
318	2.7			
325	3.4			

<sup>a</sup> Values obtained from the Eyring plot; <sup>b</sup> values obtained from  $\Delta G^\ddagger = \Delta H^\ddagger - T\Delta S^\ddagger$  at 318 K.



The IR spectrum of the isolated oxidation product (Equation 1) shows two strong, broad bands at 936 and 902 cm<sup>-1</sup> and a weaker band at 833 cm<sup>-1</sup>, which can be correlated with the presence of (Mo<sup>VI</sup><sub>2</sub>O<sub>5</sub>)<sup>2+</sup> core in this case.

Kinetic data for DMSO reduction [Fig.(II-10)] by (2) are summarized in Table (II-4). The large negative activation entropy ( $\Delta S^\ddagger$ ) is consistent with an associative reaction mechanism. Rate constants for molybdenum centered oxygen atom transfer reactions determined by different authors on a variety of analogue reaction systems, are in line with the present data <sup>8(a,b)</sup>. To establish reaction stoichiometry, the reaction of (2) ( $0.3 \text{ mmol dm}^{-3}$ ) with DMSO was followed for 70 h (333 K, darkness) under continuous flow of  $\text{N}_2$  and the emergin gas was passed into an aqueous solution of  $\text{HgCl}_2$ ; the resulting precipitate of the known compound  $(\text{HgCl}_2)_3(\text{DMS})_2$  was estimated <sup>8(d)</sup>. Ca. 0.9 mol of DMS (b.p. 309 – 310 K) was recovered per mol of (2) added, according to equation (1) below.

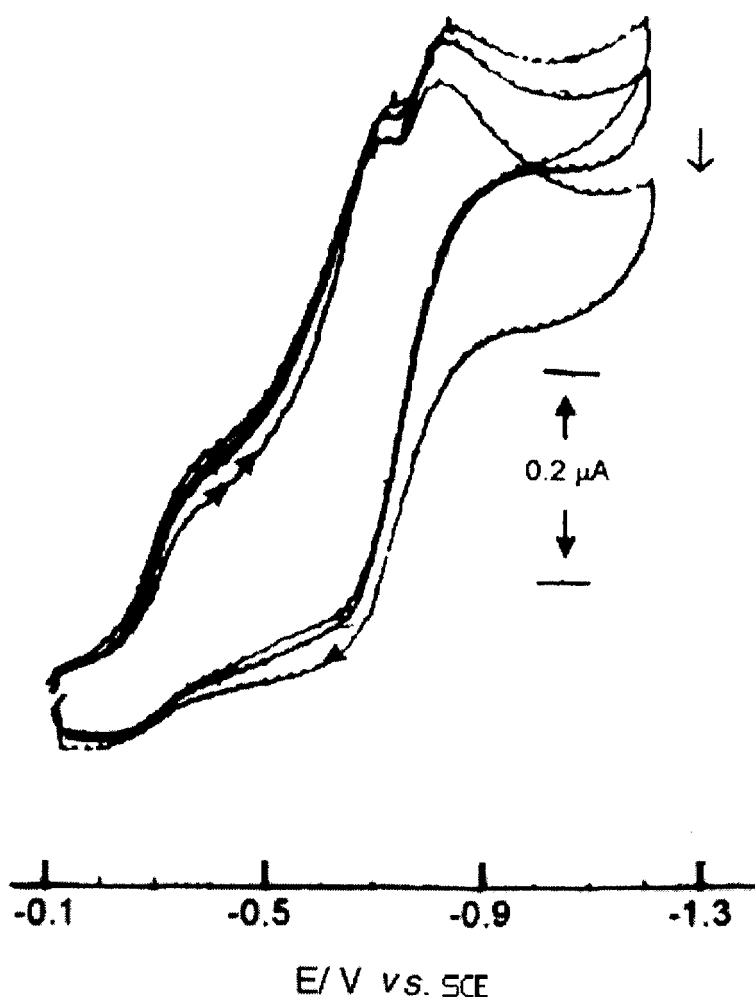


**Fig.(II-11):** CV scans during the progress of the reaction between (2) [ $0.8 \times 10^{-3} \text{ (M)}$ ] and DMSO. Data were recorded at 5 min. intervals using a Pt working electrode,  $\text{Bu}_4\text{NClO}_4$  [ $0.1 \text{ (M)}$ ], scan rate  $15 \text{ mVs}^{-1}$ .

Reactions of  $(\text{Mo}^{\text{V}}_2\text{O}_4)^{2+}$  species involving breaking of one or both of the bridges, even conversion to mononuclear molybdenum (V) complexes could be achieved through careful choice of reagents / ligands <sup>19</sup>. Progress of the reaction between **(2)** and DMSO can also be monitored using cyclic voltammetry (CV) [Fig.(II-11)] indicating a gradual fall in concentration of the electro-active species. The cathodic reduction peak ( $E_{pc}$ ) at  $-0.84\text{V}$  and the two shoulders at  $-0.74$  and  $-0.42\text{V}$  reflect reduction of the two molybdenum atoms  $[\text{Mo}^{\text{V}} \rightarrow \text{Mo}^{\text{IV}}]$ , associated with rearrangement.

## Conclusion

In concluding this discussion it can be said that the synthetic compound **(2)** bears functional resemblance to an appreciable extent to the oxomolybdoenzymes (particularly DMSO reductase here). The pterin ligand **(1)** here acts as a reducing agent and has reduced the  $\text{Mo}^{\text{VI}}$  starting material to  $\text{Mo}^{\text{V}}$  complex **(2)**, which has been characterized through all possible physico-chemical means. This molybdenum – pterin complex undergoes oxygen atom transfer reaction with a typical enzyme substrate, DMSO and the kinetic parameters [Table (II-4)] of this reaction are at par with the available literature on this line <sup>8(a,b)</sup>. So, this new synthetic molybdenum – pterin compound **(2)** can be considered as a functional model to the DMSO reductase, an oxomolybdoenzyme.

---

## **CHAPTER II**

### **SECTION – II**

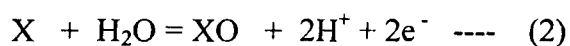
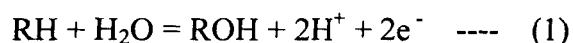
Synthesis and characterization of a molybdenum complex with sulphur and pterin ligands exhibiting saturation kinetics with pyridine N – oxide.

## Abstract

Redox reaction between 6 – acetyl-isoanthopterin [ $H_2(pte_1)$ ] and  $[Mo^{VI}O_2(ssp)]$  [ $ssp =$  anion of 2 – (salicylideneamino) benzenethiol] in  $CH_3OH - C_2H_5OH$  medium produces a new mixed ligand compound  $[Mo^{IV}(ssp)(Hpte_1)(OCH_3)]$ . It has been characterized by elemental analysis,  $\Lambda_M$ , ESIMS, UV–VIS, IR,  $^1H$  NMR (1D & 2D), CHEM3D, fluorescence & CV data. Kinetics of formation of this compound as well as that of its reaction with pyridine N–oxide (PyN→O) have been followed spectrophotometrically. Both the reactions follow substrate saturation kinetics and involve metal centered oxygen atom transfer (OAT) process. Large negative values of entropy of activation ( $\Delta S^\ddagger = -200.3 \text{ J mol}^{-1} \text{ deg}^{-1}$ ) indicate the operation of associative mechanism.

## Introduction

Recent X – ray structural characterization of several oxomolybdoenzymes reveal that a special pyranopterin [molybdopterin, Scheme (I – 1)] is coordinated to the molybdenum atom through a dithiolene group<sup>1</sup>. It has been proposed that the Mo(O) (molybdopterin) moiety is the Metal – centered Functional Unit (McFU) for such enzymes and variations in properties of the metal centre occur with the binding of other ligands, e.g., a terminal oxo or sulphido group, OH and / or H<sub>2</sub>O group(s), a second pterin, and /or a serine, a cysteine or selenocysteine group from the polypeptide backbone of the pterin<sup>1,2</sup>. Such enzymes catalyse formal hydroxylation (equation 1) and neat OAT reaction (equation 2), to and from a variety of biologically important substrates and the oxygen atom is ultimately derived from water<sup>1</sup>.



Alternatively, (1) and (2) may be regarded as Coupled Electron Proton Transfer (CEPT) reactions. Intimate catalytic mechanisms proposed in (1) and (2) involve the coordination of water to the molybdenum atom to give Mo – OH<sub>2</sub>, Mo – OH or Mo = O species which cycle between Mo(VI) and Mo(IV) oxidation states<sup>1(a)</sup>. The resolution of the X- ray crystal structures is insufficient for unambiguously resolving oxo, hydroxo and water ligands from one another, which leads to uncertainty in the oxidation state of the metal. Other limitations include uncertainty about the state of oxidation at the pyrazine ring carbon atoms or at the side-chain sulphur – bearing carbon atoms. Hence, the need for complementing the protein crystallographic results with spectroscopic data about the metal centers of these enzymes. In this context, the role of synthetic molybdenum – pterin compounds is vital for recording bench – mark data; development of such coordination Chemistry will also enable accomplishment of chemical and electrochemical studies that are relevant and complementary for the study of the functional aspects of the enzyme catalytic centers<sup>1(b,c)</sup>. Besides these, considerable challenge lies ahead to achieve a clear

description of how the nature of each of these metal centers changes during the operation of the enzyme's catalytic cycle as well as that of the corresponding molybdenum moiety. For explaining the DMSO reduction capability of a synthetic Mo<sup>IV</sup> – pterin complex, Viscontini and co-workers<sup>3(b), 4, 5(a)</sup> proposed a model reaction cycle, which involves participation of the NH<sub>2</sub>(2) and NH(5) protons of the pterin ring [Scheme (II – 1)] associated with electronic redistribution in the later as well as in the oxo groups attached to the molybdenum centre.

In view of the above perspectives, the present work embodies the redox reaction of [H<sub>2</sub>(pte<sub>1</sub>)]<sup>6</sup> [whose 7 – oxo group corresponds to the pyran ring oxygen atom of molybdopterin, Scheme (II – 1)] with a well – established dioxomolybdenum (VI) compound, [Mo<sup>VI</sup>O<sub>2</sub>(ssp)], leading to the isolation of a new mixed ligand Mo<sup>IV</sup> compound in the solid state. Its reactivity towards PyN→O, a typical enzyme substrate, has also been studied for corroborating the assignment of oxidation state of the metal centre<sup>8</sup>.

## Experimental

**Materials:** Reagent grade chemicals were used as received. Solvents were purified prior to use following the literature procedures<sup>9</sup>. Kinetic and electrochemical measurements were performed in spectroscopy grade DMF (SRL, Mumbai). 2-(salicylideneamino) benzenethiol (H<sub>2</sub>ssp), [Mo<sup>VI</sup>O<sub>2</sub>(ssp)], PyN→O and tetrabutyl ammonium perchlorate (TBAP) were obtained by published methods<sup>7, 10, 11</sup>. 6-acetonyl-isoxanthopterin [H<sub>2</sub>(pte<sub>1</sub>)] was prepared by modifying its original method of synthesis in the light of subsequent developments (e.g., darkness, N<sub>2</sub> – atmosphere, pH 6.8)<sup>6</sup> and characterized through different physico-chemical methods including elemental analysis, ESIMS, and <sup>1</sup>H NMR spectra.

**Method:** Dinitrogen atmosphere was maintained by applying Schlenk technique in the synthesis and handling steps of the complex. Most of the physico-chemical methods were same as mentioned in Chapter II, Section I. Fig.(II-17) demonstrates the absorption spectral changes associated with the reaction of  $[\text{Mo}^{\text{VI}}\text{O}_2(\text{ssp})]$  with  $\text{H}_2(\text{pte}_1)$  in DMF medium at 309 K. Kinetics of this reaction was followed at 400 nm and at four different temperatures in the range 299 – 324 K under pseudo – first – order conditions (maintaining 9 – 109 times excess of the pterin ligand). Observed rate constants ( $k_{\text{obs}}$ ) were determined by least square method from the plots of  $\log(A_t - A_\infty)$  vs. time, which were linear for at least three half – lives<sup>8</sup>. Fig.(II-18) shows the course of the change in absorption spectra (DMF, 298 K) over time resulting from the reaction of (1) with a typical enzyme substrate like, pyridine N-oxide ( $\text{PyN} \rightarrow \text{O}$ )<sup>8</sup>. This reaction was monitored under similar conditions as above (at 400 nm, keeping about 13 – 130 fold excess of  $\text{PyN} \rightarrow \text{O}$ ).

## Synthesis of the complex

### $[\text{Mo}^{\text{IV}}(\text{ssp})(\text{Hpte}_1)(\text{OCH}_3)]$ (1)

Complex (1) was synthesized by charging  $\text{H}_2(\text{pte}_1).0.5\text{H}_2\text{O}$  (0.244 g, 1 mmol) in  $\text{CH}_3\text{OH}$  (100 ml) to a suspension of  $[\text{Mo}^{\text{VI}}\text{O}_2(\text{ssp})]$  (0.355 g, 1 mmol) in  $\text{EtOH}$  (50 ml), and stirred for 30 h at RT (301 K), in darkness under dinitrogen atmosphere. The resulting chocolate – brown compound was filtered under  $\text{N}_2$  using glass- fritte, washed with purged solvents ( $\text{CH}_3\text{OH}$ ,  $\text{Et}_2\text{O}$ ) and dried in vacuo over silica-gel. Yield : 50 %. Solubility ca. 6.5 % in DMSO. Its purity was checked through TLC (Silica – gel GF<sub>254</sub> ; UV-lamp) using diluted (with 50 times  $\text{CH}_3\text{OH}$ ) DMSO solution (ca. 0.5 %) and benzene as eluant.  $R_f$ : 0.54. Found : C, 47.1 ; H, 3.2 ; N, 14.5 ; S, 5.2; Mo, 16.5 %. Calc. for  $\text{C}_{23}\text{H}_{19}\text{N}_6\text{O}_5\text{SMo}$  : C, 47.0 ; H, 3.2 ; N, 14.3 ; S, 5.4; Mo, 16.4 %. UV-VIS absorption bands [ $\text{DMF}$ ,  $\lambda_{\text{max}}^{\text{nm}}(\log\epsilon)$ ]: 285 (4.23); 320 (4.16); 338 sh (4.13); 398 (3.85); 424 sh (3.70); 458 sh (3.46). The compound is found to be diamagnetic in nature.

## Results and Discussion

As stated above, ESIMS has proved to be a valuable method to establish molecular formula and assigning the fragmentation or fragment association peaks formed during ESIMS life- time <sup>12</sup>. This technique can be applied to characterize wide variety of compounds including inorganic and coordination compounds <sup>110, 121</sup>. Similar to different types of mass spectrometry, the assignment of molecular formula (or any definite fragment originating from it) is confirmed by the experimental value of  $m/z$  (most abundant isotopic mass) as well as matching between the experimental and calculated (simulated) isotopic distribution profile <sup>14, 85, 107, 117, 118</sup>. As far as organic compounds containing O, F, P and I are concerned, the relative intensities of  $M$ ,  $M+1$  and  $M+2$  isotope peaks are of great value in recognizing the molecular ion ( $M^+$ ) peak or any well – defined fragment confirming it <sup>85</sup>. An  $M-1$  peak is common and occasionally an  $M-2$  peak (loss of  $H_2$ ) or even a rare  $M-3$  peak (from alcohols) is reasonable <sup>85</sup>. Absence of molecular ion (or an extremely weak  $M^+$  peak) is characteristic of highly branched molecule <sup>85, 107</sup>. For **(1)**, the peak at  $m/z = 525.0$  (relative abundance 100 %), associated with the characteristic distribution of molybdenum isotopes (seven) for mononuclear species, corresponds to the fragment  $[M-2CH_3O$  (1  $CH_3O$  from the coordination sphere and another from 6 – acetyl substituent)]<sup>+</sup>, where ‘ $M$ ’ is the molecular formula of **(1)** (F.W. = 588)<sup>7(a), 14, 15</sup>. The molecular ion peak appeared at  $m/z = 584.8$   $[M - 3H]^+$ . A couple of peaks arising out of deprotonation of the **(1)**, isotopic distribution of Mo atom in **(1)** are centered around the molecular ion peak. These peaks are simulated by IPC <sup>46</sup> [Fig.(II-12)] and found to be in good matching between the calculation result and that of the experimentally found one. From the above discussion it can be inferred that **(1)** is a mononuclear species [Fig.(II-16)], comparable to a related characterized complex through X- ray crystallography <sup>3(a)</sup>.

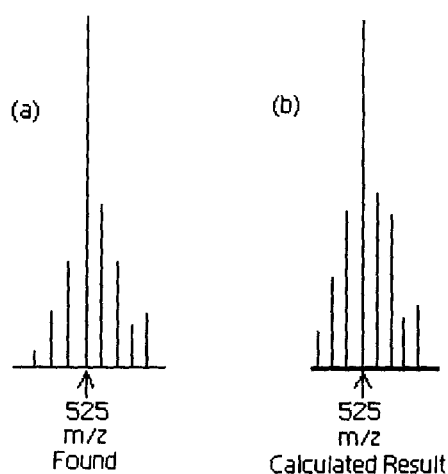


**Fig.(II-12):** (a) ESIMS data of (1) at  $m/z$  (= 525) region corresponding to  $[M - 2CH_3O]^+$ ; (b) the calculated isotope pattern<sup>46</sup>. Formula:  $C_{21}H_{11}N_6O_3MoS$ .

The  $\Lambda_M$  value ( $20 \text{ ohm}^{-1} \text{cm}^2 \text{mol}^{-1}$ , 303 K, DMF) is consistent with its non-electrolytic nature<sup>13</sup>.

A comparative study of the IR spectra ( $\text{nujol}$ ,  $\text{cm}^{-1}$ ) of (1) and that of the ligand,  $H_2(\text{pte}_1)$  throws light on the nature of donor sites in the ligand residue ( $H\text{pte}_1^-$ ) as well on the Mo – centered oxygen atom transfer occurring during its formation. IR absorptions typical of terminal  $\nu(\text{Mo}=\text{O})$  at  $930 \text{ cm}^{-1}$  and bridging  $\nu(\text{Mo}=\text{O} \rightarrow \text{Mo})$  at  $780 \text{ cm}^{-1}$  of  $[\text{Mo}^{\text{VI}}\text{O}_2(\text{ssp})]$  are absent in the IR spectrum of (1)<sup>7(b), 17</sup>, indicating the removal of such oxygen entities through reaction with the redox “non- innocent” pterin ligand. The residual IR band at 780 can be correlated with the IR absorption of the  $(\text{ssp}^{2-})$  residue, as verified through recording of IR spectrum of  $H_2\text{ssp}^{7(a)}$ . The intense IR bands in the region  $1700 - 1600 \text{ cm}^{-1}$  of the free ligand are modified significantly on coordination to the molybdenum atom in (1), reflecting enolisation of the 4 – oxo group followed by coordination of the ( $H\text{pte}_1^-$ ) residue involving the O(4), N(5) atoms, where the Mo – N(5) bond plays a pivotal role<sup>3(b), 5, 19</sup>. The  $\nu(\text{C}=\text{O})$  modes of the 2' and 7 – oxo groups appear together at  $1625 \text{ cm}^{-1}$  as a strong broad band in (1); the  $\nu(\text{CH}=\text{N})$  mode of the azomethine group (observed at  $1598 \text{ cm}^{-1}$ ) in (1) and the  $\nu(\text{C}=\text{C})$ ,  $\nu(\text{C}=\text{N})$  vibrations of the pterin ring lie hidden under this band<sup>5</sup>. Now, considering the tridentate ONS donating  $(\text{ssp}^{2-})$  residue and the  $(\text{CH}_3\text{O})$  group, a coordination number of six can be inferred for the  $\text{Mo}^{\text{IV}}$  atom in (1) [Fig.(II-16)]<sup>7(a), 18(a)</sup>.

Of the three chemically relevant oxidation states of molybdenum (e.g., Mo<sup>IV</sup>, Mo<sup>V</sup> and Mo<sup>VI</sup>), during catalysis in oxomolybdoenzymes, the Mo<sup>IV</sup> (d<sup>2</sup>) state is consistently diamagnetic<sup>26</sup>. Almost all the synthetic molybdenum pterin complexes reported so far are diamagnetic; their diamagnetic behaviour is explained by invoking a strong antiferromagnetic coupling between the d – electrons of the Mo – atom and the delocalized electron system of the redox “non-innocent” pterin ligand<sup>20(a,d)</sup>. This unique nature of pterin ligand is responsible for the observed diamagnetism of (1) and its high resolution <sup>1</sup>H NMR data [Fig.s(II-13) to (II-15)].

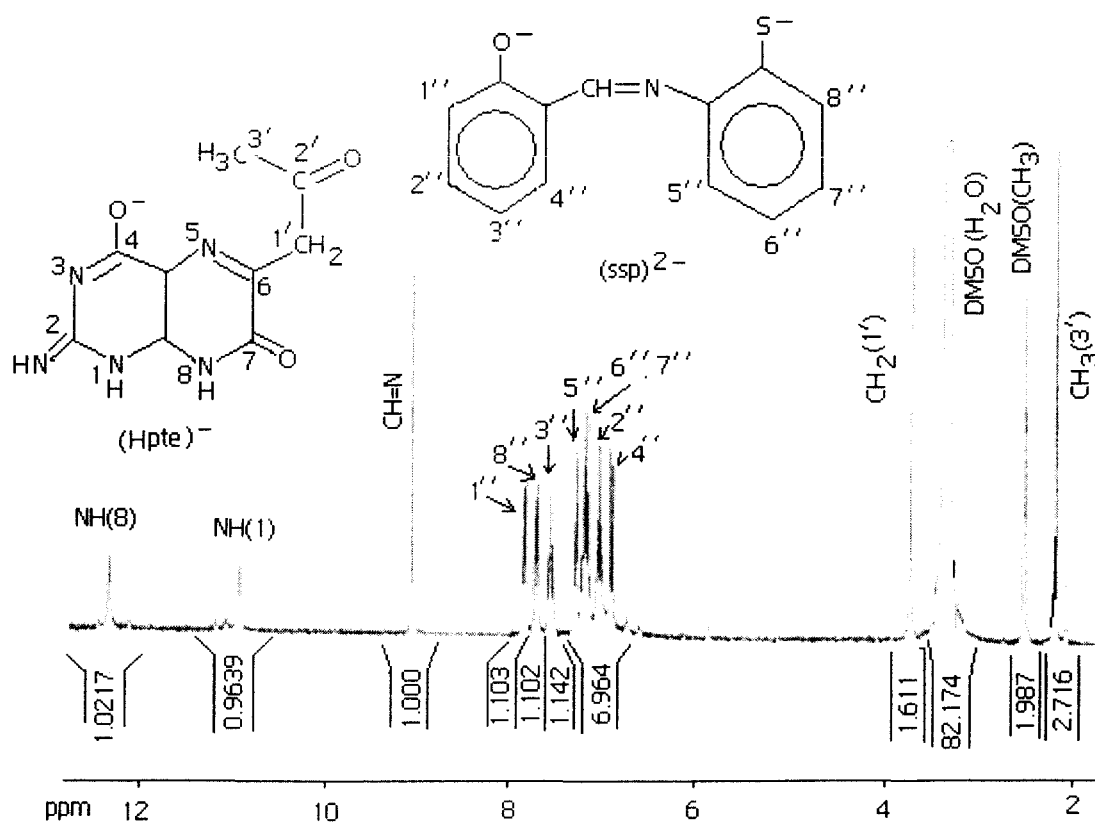


**Fig.(II -13):** 300 MHz <sup>1</sup>H NMR spectrum in DMSO – d<sub>6</sub> (δ, ppm vs. TMS) of (1).

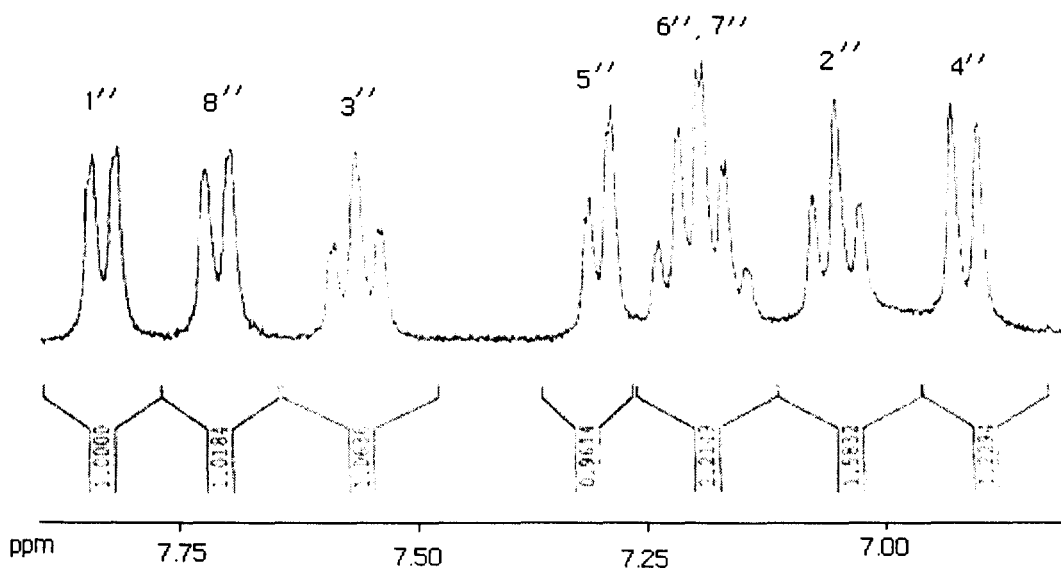


**Fig.(II-14):** 300 MHz  $^1\text{H}$  NMR spectrum (expanded) in  $\text{DMSO} - d_6$  ( $\delta$ , ppm vs. TMS) of (1).

$^1\text{H}$  NMR data of (1) have been assigned on the basis of the expanded spectrum ( $\delta$ , 8.0 – 6.5) [Fig.(II-14)], the corresponding  $^1\text{H} - ^1\text{H}$  COSY data [Fig.(II-15)], protonic integration values and  $^1\text{H}$  NMR data of  $\text{H}_2(\text{pte}_1)$ . A tautomeric form of  $(\text{Hpte}_1^-)$  residue involving protons of the N(1) and N(2) atoms<sup>90</sup> [Scheme (II-1)], is consistent with these data.  $\text{CH}_3(3')$ ,  $\text{CH}_2(1')$ ,  $\text{NH}(1)$  and  $\text{NH}(8)$  signals of the  $(\text{Hpte}_1^-)$  residue appear as singlets at  $\delta$ , 2.18;  $\delta$ , 3.74;  $\delta$ , 10.96 and  $\delta$ , 12.34 respectively<sup>16</sup>. The characteristic azomethine ( $\text{CH} = \text{N}$ ) signal at  $\delta$ , 9.06 (singlet) of the  $(\text{ssp}^{2-})$  residue is consistent with the observed data for closely related chelated ligand residues (ONO/ONS donors) in well-characterized coordination compounds of molybdenum<sup>7(a), 17</sup>. The protonic integration values of these signals [e.g.,  $\text{NH}(8)$  and  $\text{CH} = \text{N}$  – protons] indicate a 1 : 1 ratio of  $(\text{ssp}^{2-})$  :  $(\text{Hpte}_1^-)$  in (1). The proton signal of the  $(\text{CH}_3\text{O})$  residue is covered by the residual  $\text{H}_2\text{O}$  signal (of  $\text{DMSO} - d_6$ ) at  $\delta$ , 3.55. Importance of the molybdenum – methoxide interaction has been pointed out by several authors and established through X – ray crystal structure determination in one case<sup>18</sup>. For  $\text{H}_2(\text{pte}_1)$ , the  $\text{CH}_3(3')$ , and  $\text{CH}_2(1')$  proton signals (s)

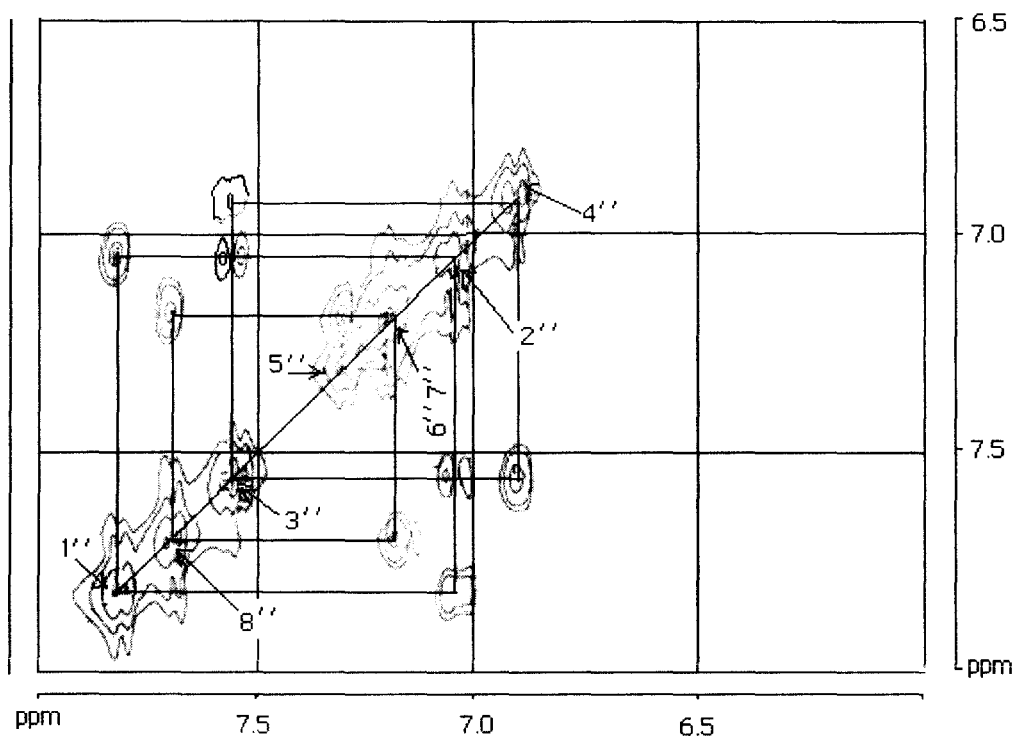


**Fig.(II – 15):** 300 MHz  $^1\text{H} - ^1\text{H}$  COSY data of (1) in DMSO –  $d_6$ .

appear at  $\delta$ , 2.18 and  $\delta$ , 3.74 respectively [vide Table(II-1)]; in (1)  $\delta$  values of these proton signals for the ( $\text{Hpte}_1^-$ ) residue remain essentially unchanged, thereby indicating that the  $\text{O}(2')$  atom [Scheme (II-1)] remains uncoordinated. Besides this,  $^1\text{H}$  NMR data of (1) also indicate that the  $\text{NH}_2(2)$  group exists here as shown in Scheme (II-1), with its two protons appearing essentially as a broad signal at  $\delta$ , 7.0. However, during the complex formation redox reaction a tautomeric change takes place and the  $\text{NH}(1)$  signal appears at  $\delta$ , 10.96 in (1) ; this supports participation of the pterin ring during oxygen atom transfer reaction occurring at the molybdenum centre  $^{3(b)}$ . The  $=\text{NH}(2)$  proton signal of (1) lies hidden under proton signal of the ( $\text{ssp}^{2-}$ ) residue, as evident from protonic integration data of the expanded spectrum.

From consideration of elemental analysis and ESIMS data (experimental and simulated) as well as other physicochemical data, the chemical compositions of the new compound was established. Then its possible schematic structure was optimized by molecular mechanics calculation (MM2), giving the lowest steric energy ( $= 13.2 \text{ Kcal mol}^{-1}$ ) CHEM3D model [Fig.(II-16)], thereby throwing light on both stability and geometry of this compound<sup>87</sup>. The molecular modeling force fields in use for molecular systems can be interpreted in terms of the four key contributions, e.g., bond stretching, angle bending, torsional terms and non-bonded interactions<sup>86</sup>; apart from the lowest steric energy of the molecule, two basic parameters were evaluated, e.g., bond distances (Å) and bond angles (deg.), the most relevant of which are shown in Table(II-5) together with the literature data obtained through X-ray structural studies on molybdenum complexes with different pterin ligands and relevant compounds<sup>3, 5, 20(a-c), 27, 29, 114 - 116</sup>; this is in conformity with the recent trends of structure elucidation using optimized computational models<sup>48, 86, 108, 179</sup>.

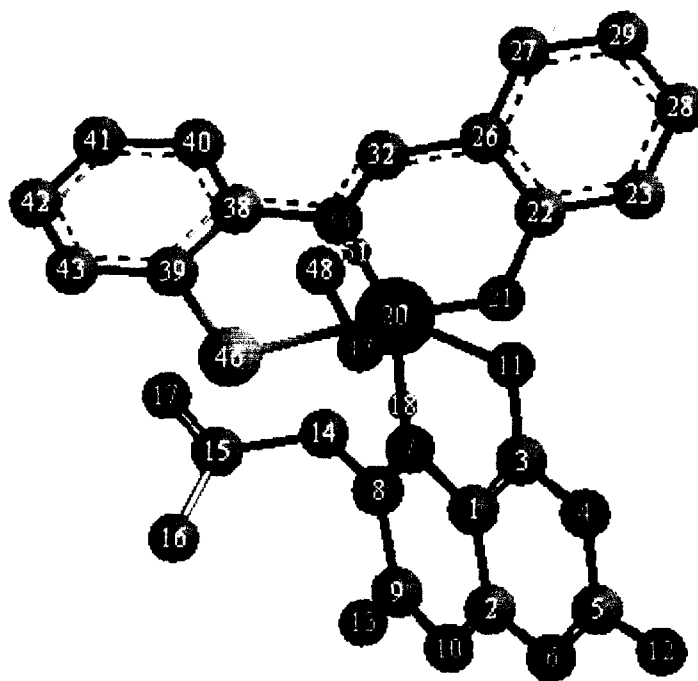


**Fig.(II-16):** The optimized geometry (CHEM3D model obtained through MM2 calculations) of (1) with a steric energy of  $13.2 \text{ Kcal mol}^{-1}$ . Its numbering system is set by the software used<sup>87</sup> and is different from that in Scheme (II - 1).

**Table (II-5):** Comparison of selected computed bond lengths(Å) and bond angles (deg.) involving Mo – atom in (1) from the optimized geometry [Fig.(II-16), MM2 calculations] with the available literature data (in parenthesis) from X-ray structural studies\*

Atoms	Bond Distances(Å) <sup>+</sup>	Atoms	Bond Distances(Å) <sup>+</sup>
N(33)-Mo(20)	2.12(2.16) <sup>108</sup>	S(46)-Mo(20)	2.37(2.37) <sup>109, 110</sup>
N(7)-Mo(20)	2.10(2.02) <sup>3(c)</sup>	Mo(20)-O(21)	1.98(1.70) <sup>109</sup>
O(47)-Mo(20)	1.98(2.32) <sup>109</sup>	O(11)-Mo(20)	1.10(2.23) <sup>3(c)</sup>

Angle Atoms	Bond Angle(deg.) <sup>+</sup>	Angle Atoms	Bond Angle(deg.) <sup>+</sup>
N(33)-Mo(20)-S(46)	76.7(77.5) <sup>109</sup>	N(7)-Mo(20)-O(11)	82.8(74.1) <sup>3(c)</sup>
O(21)-Mo(20)-O(11)	74.2(78.1) <sup>109</sup>	Mo(20)-N(7)-C(1)	118.2(119.3) <sup>3(c)</sup>
C(3)-O(11)-Mo(20)	112.9(112.1) <sup>3(c)</sup>	O(47)-Mo(20)-N(7)	103.2(103.3) <sup>109</sup>
N(33)-Mo(20)-O(21)	78.1(82.9) <sup>109</sup>	Mo(20)-N(33)-C(38)	127.0
N(33)-Mo(20)-N(7)	106.9	N(7)-Mo(20)-O(21)	74.8
N(7)-Mo(20)-S(46)	80.6	S(46)-Mo(20)-O(11)	136.2
S(46)-Mo(20)-O(21)	137.5	S(46)-Mo(20)-O(11)	136.2

<sup>+</sup> Here O(11), N(7) and O(17) correspond to O(4), N(5) and O(2') donor atoms respectively, of the pterin ring as per Scheme (II – 1), while N(12) and N(6) correspond to the 2-substituent N and N(1) respectively.

\* X-ray structural data have been collected from references mentioned as superscript on the data within parenthesis.

Concentrating on the chelating aspect of the pterin ligand towards molybdenum, the Mo-N(5) bond plays a pivotal role here [Scheme (II – 1) indicates the O(4), N(5) etc, numbering system] and this bond distance shows a fair agreement between the computed and experimental data<sup>3, 5, 20(a-c), 27, 29, 114 – 116</sup>. The calculated Mo-O(4) bond distance is slightly shorter than the available X – ray structural data, but this value is close to the Mo – O<sub>b</sub> bond distance (1.88 – 1.97 Å) of Mo – O<sub>b</sub> – Mo bridges ( of binuclear complex ) and is much longer than the terminal Mo=O<sub>t</sub> bond distance (1.66 – 1.67 Å).

Fig.(II-16) represents the most stable CHEM3D form of (1). In this form, the pterin ligand acts as an uni-negative ( $\text{Hpte}_1^-$ ) O(4), N(5) donor; where O(4) made a covalent bond and N(5) a coordinate bond with the  $\text{Mo}^{\text{IV}}$  atom. The ( $\text{ssp}^{2-}$ ) residue, which acts as a bi- negative ONS donor, coordinates to the metal atom through Mo – O & Mo – S covalent bond formation and one Mo – N coordinate bond formation (through the lone pair of N). One  $\text{CH}_3\text{O}$  group is also coordinated to the  $\text{Mo}^{\text{IV}}$  atom. The bond between the N(5) and  $\text{Mo}^{\text{IV}}$  forms the apex position of the pentagonal pyramidal geometry and other five bonds form the plane of this geometry in the molecule. Other possible structures of the complex originated by changing the positions of  $\pi$  – bonds in the pterin part also have almost similar stability. In all the cases the Mo – centre retained its pentagonal pyramidal geometry, but the variation is in the position of  $\pi$  – bonds. It is clear from these structures that a double bond at C(6) – C(1') position brings some instability to the molecule. The CHEM3D representations containing aromatic pterin ligand residue were less stable than the non – aromatic one.

**Table (II – 6):** Comparison of selected optimized bond lengths (Å) and bond angles (deg.) in the free ligand,  $\text{H}_2(\text{pte}_1)$  and its molybdenum complex (1).

Atoms	Bond Distances(Å) <sup>+</sup>	Atoms	Bond Distances(Å) <sup>+</sup>
C(1)-N(7)	1.41 [1.44]	C(1)-C(3)	1.48 [1.36]
C(3)-O(11)	1.22 [1.37]	C(1)-C(2)	1.37 [1.45]
C(9)-O(13)	1.22 [1.23]	C(3)-N(4)	1.37 [1.40]
C(2)-N(6)	1.40 [1.39]	C(9)-N(10)	1.36 [1.37]
C(15)-C(16)	1.51 [1.51]	C(5)-N(12)	1.37 [1.38]
C(2)-N(10)	1.35 [1.32]	C(5)-N(6)	1.31 [1.33]
N(7)-C(8)	1.28 [1.30]	C(14)-C(15)	1.51 [1.51]
C(8)-C(9)	1.49 [1.50]	N(4)-C(5)	1.35 [1.38]
C(15)-O(17)	1.21 [1.21]	C(8)-C(14)	1.50 [1.51]

Angle Atoms	Bond Angle(deg.) <sup>†</sup>	Angle Atoms	Bond Angle(deg.) <sup>†</sup>
N(6)-C(5)-N(4)	120.87 [122.84]	C(1)-N(7)-C(8)	118.67 [110.91]
C(3)-N(4)-C(5)	124.83 [122.34]	C(1)-C(3)-N(4)	114.84 [115.11]
C(8)-C(9)-N(10)	114.90 [121.42]	N(6)-C(2)-C(1)	121.60 [119.16]
N(7)-C(8)-C(9)	122.95 [123.34]	N(10)-C(2)-C(1)	119.78 [117.95]
C(2)-N(10)-C(9)	122.73 [118.50]	N(7)-C(1)-C(2)	120.97 [127.01]
C(2)-N(6)-C(5)	119.69 [117.92]	C(3)-C(1)-C(2)	118.17 [122.45]

<sup>†</sup> Free ligand data are mentioned outside third bracket and the data derived from its molybdenum complex, (1), are mentioned within third bracket.

Tables (II-6) shows the bond lengths and bond angles of the free ligand and that of the pterin ligand residue in the complex (1). Comparing these two sets of data it is clear that both bond lengths and bond angles of the pterin rings have undergone a visible change in it's complex suggesting definite complexation of the pterin ligand with molybdenum metal. The above discussion on the geometrical aspect of optimized computational model (MM2) of a new complex compound, having agreement with available X-ray structural data (e.g., bond length, bond angle and overall geometry) verifies the applicability of such an approach to molybdenum – pterin systems and provides the frame work for discussion on their spectroscopic, reactivity and other relevant aspects <sup>88(a), 108, 120</sup>.

UV – VIS absorption spectrum of the complex contains all the characteristic bands of pterin ligand including a peak at 320 nm characteristic of the (ssp<sup>2-</sup>) residue. Comparison of the UV – VIS spectral data of pterin ligand and that of (1) indicates that there are considerable increase in intensity (log $\epsilon$  – value) of the ligand bands (essentially  $\pi \rightarrow \pi^*$  type) through complex formation. This is in conformity with the – NH<sub>2</sub>(2) lone pair electrons' flow towards the metal atom through the pterin ring during complex formation.

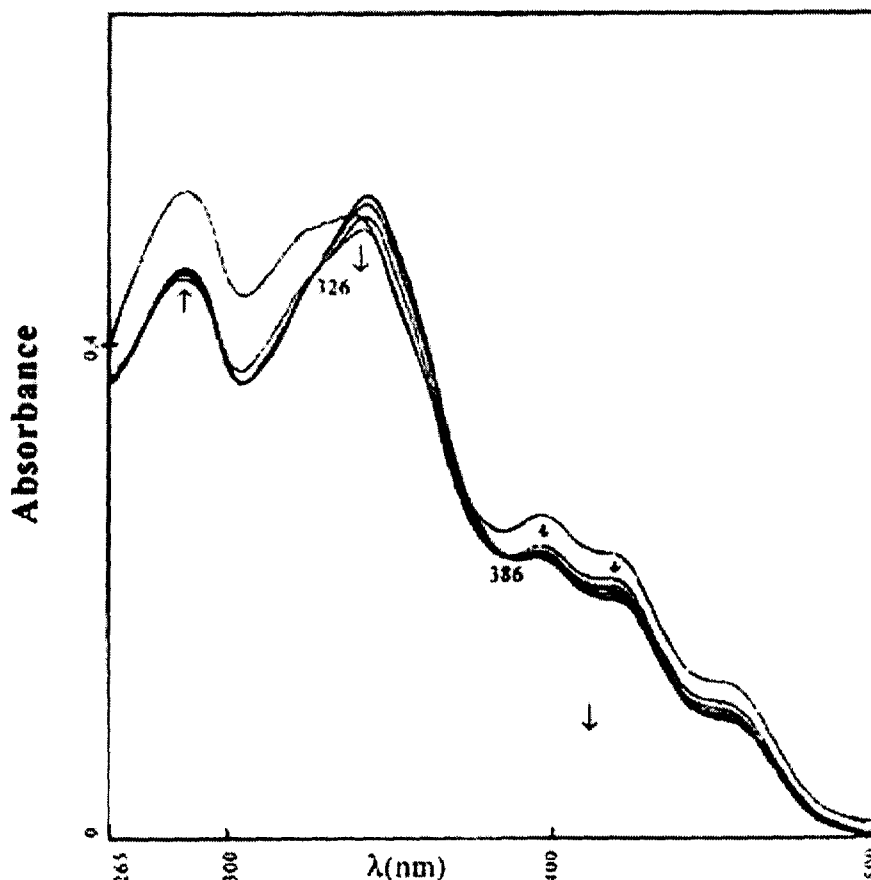


**Fig.(II-17):** Absorption spectral changes recorded every 8 min. during the reaction of  $[\text{Mo}^{\text{VI}}\text{O}_2(\text{ssp})]$   $[3.0 \times 10^{-6} \text{ (M)}]$  and  $\text{H}_2\text{pte}_1$   $[7.0 \times 10^{-5} \text{ (M)}]$  in DMF solution at 309 K.

Reactivity of (1) towards  $\text{PyN} \rightarrow \text{O}$  indicates that the molybdenum atom here exists in a lower oxidation state, e.g.,  $\text{Mo}^{\text{IV}}$ . The relevant oxidation product was isolated by reacting (1) (328 K, darkness, 5 h, DMF) with  $\text{PyN} \rightarrow \text{O}$  (in 1 : 3 molar ratio), followed by evaporation in a rotary evaporator, treatment of the residue with  $\text{CH}_3\text{OH}$ , filtration and washing with ether; elemental analysis indicated the composition  $[(\text{Mo}^{\text{VI}}_2\text{O}_5)(\text{Hssp})(\text{Hpte}_1)] \cdot 0.5\text{DMF}$ . The  $\nu(\text{Mo} = \text{O})$  and  $\nu(\text{Mo} - \text{O} - \text{Mo})$  modes characteristic of the  $(\text{Mo}^{\text{VI}}_2\text{O}_5)^{2+}$  core are observed at 925, 888 and  $825 \text{ cm}^{-1}$  respectively<sup>20</sup>. Most likely the initial product [e.g., possessing the  $(\text{Mo}^{\text{VI}}\text{O})^{4+}$  core] of  $\text{PyN} \rightarrow \text{O}$  oxidation undergoes hydrolysis with the moisture present in the solvents and  $\mu$ -oxo dimerization reaction, giving ultimately the  $(\text{Mo}^{\text{VI}}_2\text{O}_5)^{2+}$  core [Equations: 5(a) – 5(c), below]<sup>19, 20(c,d)</sup>.

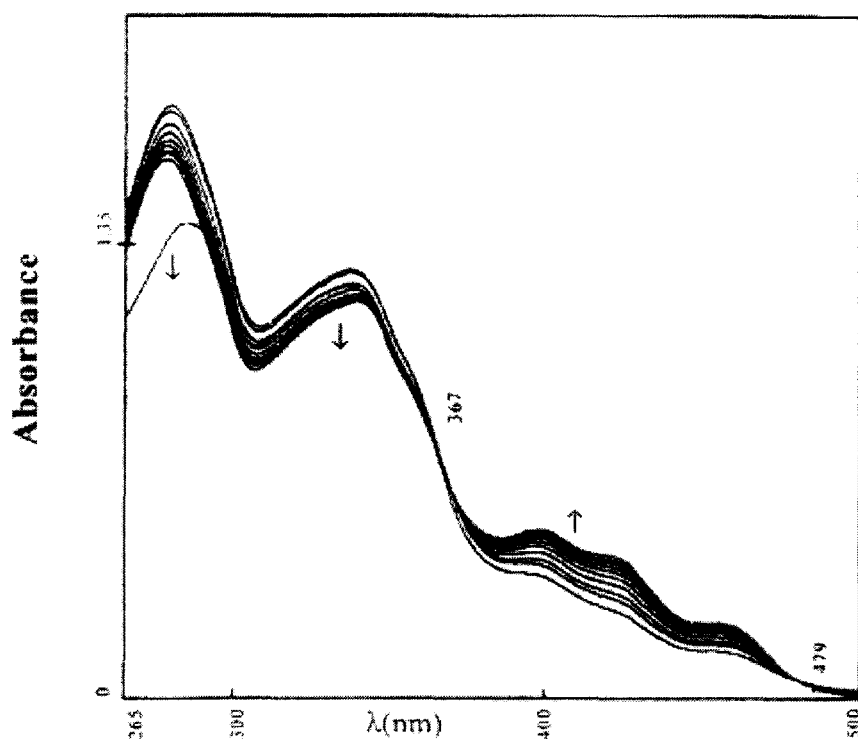


**Fig.(II-18):** Absorption spectral changes recorded every 3 min. during the reaction of (1) [ $3.4 \times 10^{-4}$ (M)] and PyN→O [ $2.5 \times 10^{-2}$ (M)] in DMF solution at 298 K.

Fig.s (II-17) & (II-18) represent the spectrophotometric monitoring of the reaction of  $[\text{Mo}^{\text{VI}}\text{O}_2(\text{ssp})]$  with  $[\text{H}_2(\text{pte}_1)]$  and that of (1) with PyN→O respectively<sup>21(a,b)</sup>. In the first figure isosbestic points are observed at 326 and 386 nm, while two isosbestic points can be identified at 367 and 479 nm in the second figure. Both the reaction systems exhibit substrate saturation kinetics at sufficiently high substrate concentration [Fig.s(II-19) & (II-20)]<sup>21</sup>. Under these conditions, the reactions are first order in  $[\text{Mo}^{\text{VI}}\text{O}_2(\text{ssp})]$  and (1) respectively, as shown by linear plots of  $\log(A_t - A_\infty)$  vs. time, from which the observed rate constants were obtained<sup>8(a,c), 17, 23</sup>.

The reaction [Scheme (II-3)] leading to the formation of (1), i.e., the mixed ligand  $\text{Mo}^{\text{IV}}$  compound, is initiated through reversible substrate [S], i.e.,  $[\text{H}_2(\text{pte}_1)]$  binding followed by oxo transfer (along with coupled electron proton transfer) with rate constant  $k_2$ . During isolation of the product on preparative scale in presence of methanol, further reactions occur with loss of both the oxo groups of  $[\text{Mo}^{\text{VI}}\text{O}_2(\text{ssp})]$ , giving (1) as the ultimate product. Loss of oxo ligands, during complex formation involving  $(\text{Mo}^{\text{VI}}\text{O}_2)^{2+}$  starting materials, is rare with conventional ligands unless an oxo abstractor

like  $\text{PPh}_3 / \text{Ph}_2\text{MeP}$  is present <sup>7(a,c), 17, 23(a)</sup>. In terms of Scheme (II-3), below, the  $k_{\text{obs}}$  can be represented as follows <sup>22</sup> :

$$k_{\text{obs}} = k_2[\text{S}]/(\text{K}_M + [\text{S}]) \quad \text{---- (3)}$$

Where,  $\text{K}_M = (k_2 + k_{-1})/k_1$ ,

Or,

$$1/k_{\text{obs}} = 1/k_2 + \text{K}_M/k_2[\text{S}] \quad \text{---- (4)}$$

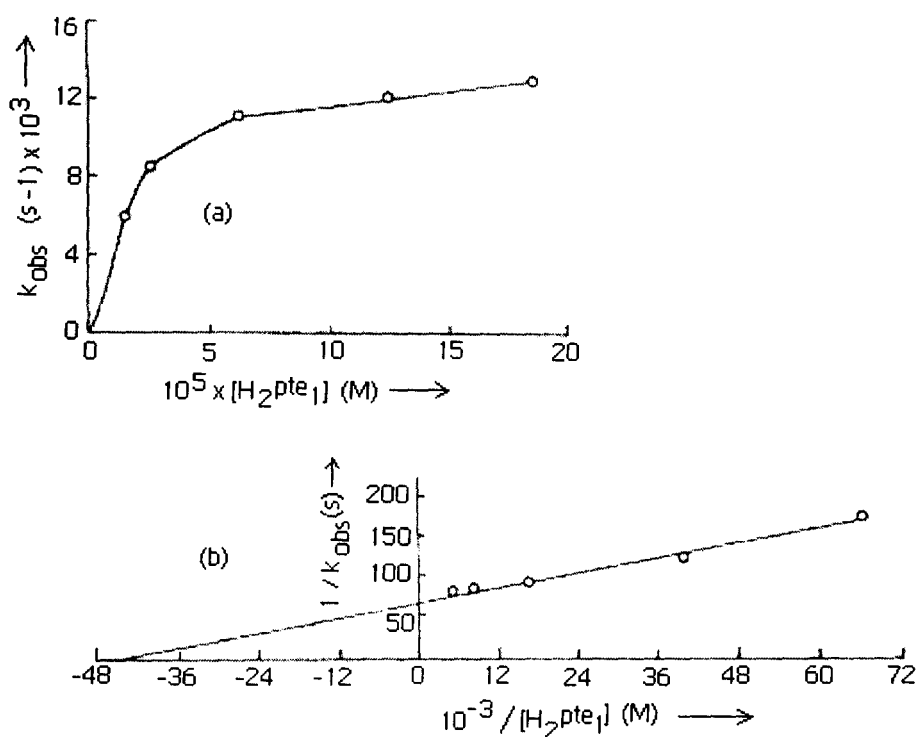
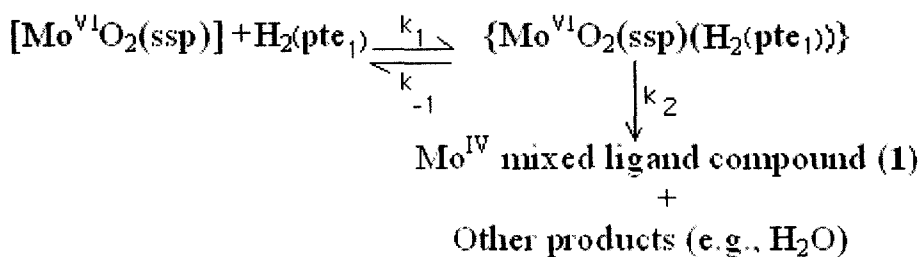
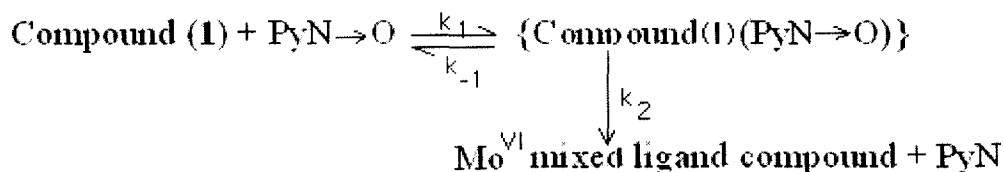


**Fig.(II-19):** (a)Dependence of the rate of reaction of  $[\text{Mo}^{\text{VI}}\text{O}_2(\text{ssp})]$   $[1.7 \times 10^{-6} \text{ (M)}]$  with  $\text{H}_2(\text{pte}_1)$  in DMF at 299 K;(b) the corresponding double reciprocal plot.

A plot of the  $k_{\text{obs}}$  vs.  $[\text{H}_2(\text{pte}_1)]$  in shown in Fig.(II-19a). The plot of  $1/k_{\text{obs}}$  vs.  $1/[\text{H}_2(\text{pte}_1)]$  should give a straight line with  $1/k_2$  as the intercept and  $\text{K}_M/k_2$  as the slop. The x – axis intercept equals  $1/\text{K}_M$ . From the double reciprocal plot of  $1/k_{\text{obs}}$  vs.  $1/[\text{H}_2(\text{pte}_1)]$  [Fig.(II-19b)],  $k_2$  and  $\text{K}_M$  were calculated as  $1.5 \times 10^{-2} \text{ s}^{-1}$  and  $2.2 \times 10^{-5} \text{ mol dm}^{-3}$  respectively at 299 K. The value of  $k_2$  is comparable in magnitude to those of molybdenum mediated oxygen atom transfer reactions obtained using a wide variety of model compounds and substrates <sup>8, 17, 23</sup>.



[Scheme (II - 3)]



[Scheme (II - 4)]

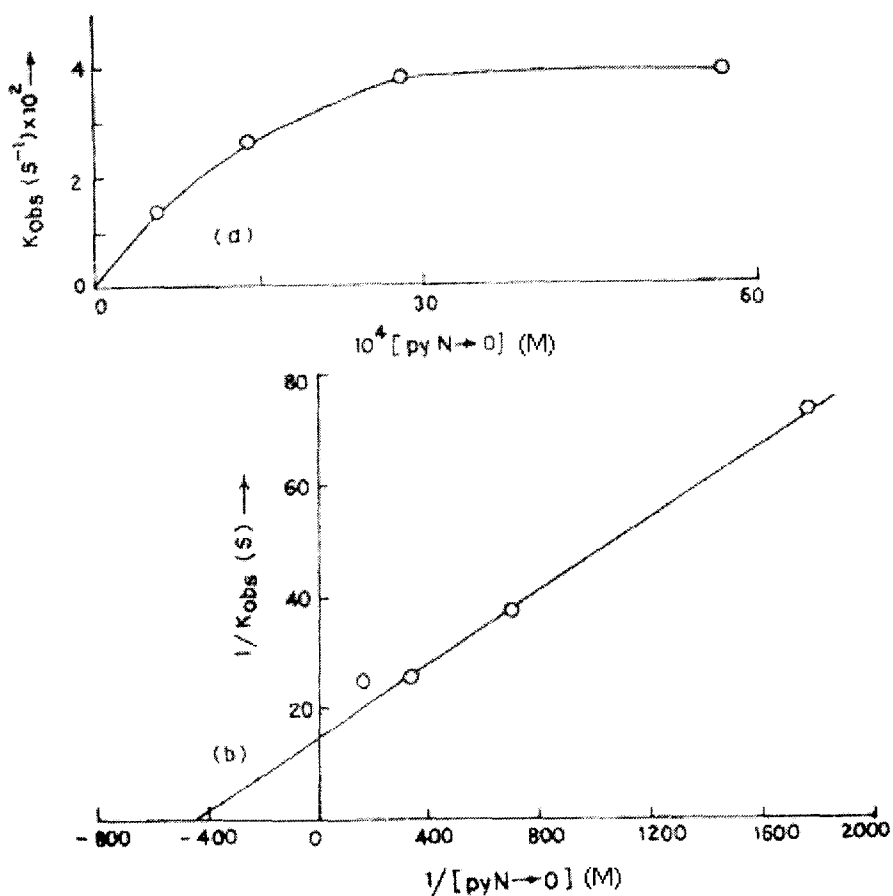
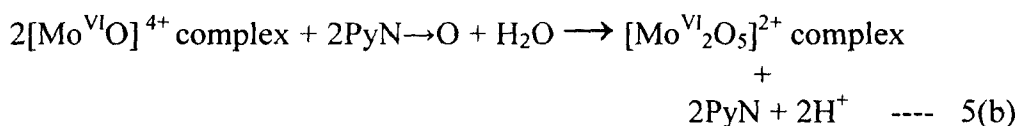
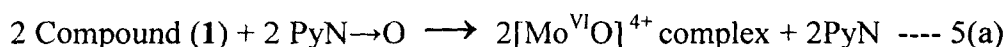


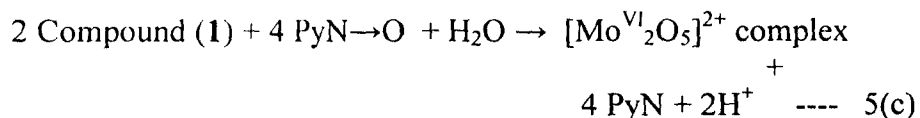
**Fig.(II-20):** (a) Dependence of the rate of reaction of (1) [ $4.4 \times 10^{-5}$  (M)] with PyN→O in DMF at 299 K; (b) the corresponding double reciprocal plot.

Activation parameters [ $\Delta H^\ddagger = 11.3 \text{ KJ mol}^{-1}$ ;  $\Delta S^\ddagger = -200.8 \text{ JK}^{-1} \text{ mol}^{-1}$ ] were obtained from the Eyring plot [ $\ln(k/T)$  vs.  $1/T$ ] using pseudo – first order rate constant data determined [keeping a 90 fold excess of  $\text{H}_2(\text{pte}_1)$ ] at different temperatures. The negative activation entropy is consistent with the proposed associative mechanism [Scheme (II–3)]<sup>24</sup>.

Scheme (II–4) represents the possible pathway of the reaction between (1) and  $\text{PyN}\rightarrow\text{O}$  in DMF medium, which involves the reversible formation of an intermediate containing both the reactants, followed by its transformation to the products. Reaction stoichiometry was established by estimating the amount of pyridine released through the reaction (328 K, 50 h,  $\text{N}_2$  atm., darkness) of a known weight of (1) with 10 equivalents of  $\text{PyN}\rightarrow\text{O}$ ; pyridine was estimated gravimetrically as the known compound  $[\text{Zn}(\text{C}_5\text{H}_5\text{N})_2](\text{SCN})_2$  from the petroleum ether extract of the reaction medium<sup>25</sup>. About 2 moles of pyridine were recovered per mol of (1) added as per the following equations :



**Overall reaction :**



The plot of ( $k_{\text{obs}}$ ) vs.  $[\text{PyN}\rightarrow\text{O}]$  is shown in Fig.(II–20a). Assuming the validity of equations (3) and (4), above, in this case as well, the double reciprocal plot of  $1/k_{\text{obs}}$  vs.  $1/[\text{PyN}\rightarrow\text{O}]$  [Fig.(II–20b)] was utilized for the calculation of  $k_2 = 6.7 \times 10^{-2} \text{ s}^{-1}$  and  $K_M = 2.3 \times 10^{-3} \text{ mol dm}^{-3}$  at 299 K. Variable temperature pseudo – first order rate constant data (determined using 80 fold excess of  $\text{PyN}\rightarrow\text{O}$ ) were used for calculating the activation parameters ( $\Delta H^\ddagger = 3.8 \text{ KJ mol}^{-1}$ ;  $\Delta S^\ddagger = -200.3 \text{ JK}^{-1} \text{ mol}^{-1}$ ) from the Eyring plot. The negative  $\Delta S^\ddagger$  value supports the formation of an intermediate as shown in Scheme (II– 4) above. The  $k_2$  – value is in line with the existing rate constant data for oxo transfer reactions of various  $\text{Mo}^{\text{IV}}$  complexes with  $\text{PyN}\rightarrow\text{O}$  and other similar substrates 8(c), 23(b).

The voltammogram of (**1**) is characterized by single irreversible reduction peak [ $\text{Mo}^{\text{IV}} \rightarrow \text{Mo}^{\text{III}}$ ] at  $-0.82\text{V}$  ( $50\text{ mV s}^{-1}$ ), is in conformity with the presence of only one Mo – atom in its formula. The pterin ligand itself undergoes reduction beyond  $-1.8\text{ V}$ <sup>12</sup>.

## Conclusion

ESIMS data in conjunction with elemental analysis data and supported by IR and <sup>1</sup>H NMR spectral studies, verify the **formulations / chemical compositions** of the new complex (**1**). Molecular modeling studies [CHEM3D models obtained through MM2 calculations] provide with its optimized molecular geometry as well as bond length and bond angle data. The later type of parameters are in agreement with the published X-ray structural data on different molybdenum – pterin coordination compounds in related systems. This aspect verifies their **molecular structures**.

<sup>1</sup>H NMR and IR spectral data point out that  $\text{H}_2(\text{pte}_1)$  exhibits redox “non-innocent” behaviour during its reaction with [ $\text{Mo}^{\text{VI}}\text{O}_2(\text{ssp})$ ]; the loss of oxygen atoms of the latter [leading to the formation of (**1**)] is accompanied by a tautomeric change involving the  $\text{NH}_2(2)$  group and related electronic redistribution in the pterin ring. The process is characterized by substrate saturation kinetics and may be regarded as a coupled electron proton transfer reaction. On the other hand, the reaction between (**1**) and  $\text{PyN} \rightarrow \text{O}$  is essentially an oxygen atom transfer process, conforming to substrate saturation kinetics as well and throwing light on the **oxidation state of the molybdenum atom** in (**1**). The final product in 5(c) reflects the role of hydrolysis and  $\mu$  – oxo dimerization reaction. The reductive half reaction of xanthine oxidase with sub - stoichiometric amounts of xanthine exhibits substrate saturation kinetics with faster  $k_2$  values<sup>21(c)</sup>.

Finally, the role of the solvent used for the preparative purpose here (e.g., CH<sub>3</sub>OH) is to be assessed vis-à-vis that of H<sub>2</sub>O in the catalytic cycle of oxo molybdoenzymes. Loss of an oxo group from the Mo<sup>VI</sup> species during enzyme turnover is made up by the H<sub>2</sub>O molecule giving Mo–OH<sub>2</sub> and undergoes facile deprotonation to Mo–OH or Mo = O species accompanied by changes in the oxidation state of the metal centre <sup>1(a), 26</sup>. During formation of (**1**), loss of oxo groups from [Mo<sup>VI</sup>O<sub>2</sub>(ssp)] is made up partly by the pterin ligand residue (Hpte<sub>1</sub>) <sup>20(a)</sup> and partly by the solvent molecule (CH<sub>3</sub>OH); through the formation of CH<sub>3</sub>O<sup>-</sup> group <sup>18</sup> and charge balance is achieved.

---

### CHAPTER III

Studies on a new Schiff base ligand  $H_3(pte_2-tsc)$  synthesized by condensing 7 – acetyl – xanthopterin [ $H_2(pte_2)$ ] with thiosemicarbazide [ $H(tsc)$ ] and its molybdenum complexes exhibiting reactivity towards  $Me_3N \rightarrow O$ ,  $PyN \rightarrow O$  and  $PPh_3$  ; crystal structure of 2 – pivaloylamino – 7 – acetyl – xanthopterin – water (1/1).

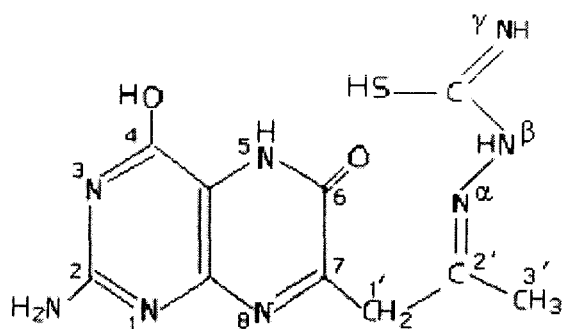
## Abstract

A new Schiff base ligand  $H_3(pte_2-tsc)$  (**1**) was synthesized by the condensation of 7-acetyl-xanthopterin [ $H_2(pte_2)$ ] and thiosemicarbazide [ $H(tsc)$ ]. The pterin starting material obtained by modifying a published method, was characterized through single crystal X-ray diffraction analysis of its 2-pivaloylamino derivative and other data; they are consistent with its 7-substituted-xanthopterin representation. Six new Mo(IV,V,VI) complexes have been synthesized using this Schiff base ligand and characterized by different physico-chemical methods including elemental analysis, ESIMS,  $\Lambda_M$  data,  $^1H$  NMR, IR, UV-VIS, fluorescence spectroscopy, CV data and supported by CHEM3D representations with lowest steric energy MM2 calculation. Here the  $H_3(pte_2-tsc)$  ligand acts as a reducing agent, reducing the metal centre of the molybdenum starting materials to some lower oxidation states ( $Mo^{IV/V}$ ) during synthesis in most cases. These complexes show reactivity towards oxygen atom donor agents, e.g.,  $Me_3N \rightarrow O$  or  $PyN \rightarrow O$  and kinetics of these reactions have been studied. For compound (**4**), which was obtained as oxidized product ( $Mo^{VI}$  center) by the aerial oxidation of (**3**), shows reactivity towards a typical oxygen atom abstractor, like  $PPh_3$ . All these reactions have negative values for entropy of activation [ $\Delta S^\ddagger = (-198 \text{ to } -208) \text{ J mol}^{-1} \text{ deg}^{-1}$ ], suggesting associative type reaction mechanism, like the enzyme-substrate reactions. These kinetic data [e.g.,  $k_{obs} = (3.82 \times 10^{-3} - 80.00 \times 10^{-3}) \text{ s}^{-1}$ ] are at par with the available literature in the related fields.

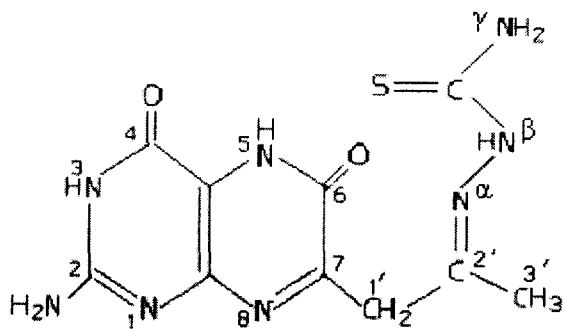
In several cases the reactivity aspects have been substantiated by kinetic data as well as reaction stoichiometry studies. They throw light on the oxidation state of the molybdenum centre in the pertinent compounds. Fluorescence spectral data give information on the changes in electron density on the complex during reaction with oxygen donor ( $Me_3N \rightarrow O$ ) or oxygen abstractor ( $PPh_3$ ) reagents. CV data indicate that the ligand centred redox process is considerably modified through coordination to the molybdenum centre.

## Introduction

Considering the composition of the metal centered functional unit (McFU) of oxomolybdoenzymes<sup>1,2</sup>, this Chapter embodies the synthesis of a new ligand, H<sub>3</sub>(pte<sub>2</sub>-tsc), its corresponding molybdenum complexes as well as their reactivity, especially towards the relevant enzyme substrates. This new ligand [Scheme (III-1A)] was synthesized by condensing a 7-substituted pterin [7-acetyl-xanthopterin, H<sub>2</sub>(pte<sub>2</sub>)] with thiosemicarbazide [H(tsc)]. Scheme (III-1B) reflects another tautomeric form of this ligand involving the thiocarbonyl group (S = C <) and NH<sub>2</sub> (γ) as well as the NH(3) and O(4) amide functions :



Scheme (III - 1A)



Scheme (III - 1B)

**Scheme (III - 1)**

All attempts for obtaining a similar Schiff base derivative with thiosemicarbazide through condensation with 6-acetyl-isoxanthopterin [ $H_2(pte_1)$ ] led to a cyclised product with no free metal coordination site. Distinct chemical difference between the two pterin starting materials, is responsible for the failure of  $H_2(pte_1)$  in furnishing a suitable Schiff base ligand. Most likely the higher basicity of the NH(5) site, along with tautomerism with the 6 – substituent, [Scheme (II-1)] is responsible for the above observation i.e., formation of a cyclised product with thiosemicarbazide in case of  $H_2(pte_1)$ .

As far as this Schiff base ligand [ $H_3(pte_2-tsc)$ ] is concerned there are three possible deprotonation sites e.g., OH(4), NH(5) and the thiol group [Scheme (III-1A) & Scheme (III-1B)]. Actual state of protonation of the ligand residue in complex compounds depends on several factors e.g., reaction conditions, oxidation state of the metal centre, presence of secondary ligands etc. This has been ascertained here through different physico-chemical and spectroscopic methods including IR and  $^1H$  NMR spectra as well as molecular modeling studies (e.g., the CHEM3D model giving the lowest steric energy through MM2 calculations, among different alternatives). As stated at the outset (Chapter I), the optimized bond length and bond angle data of the present systems have been compared with the literature X – ray structural data of related systems for authentication.

For confirming the structure of 7-acetyl-xanthopterin, its 2-pivaloylamino substituted derivative was obtained through reaction with pivalic anhydride and it could be crystallized out [ $CH_3OH - CH_2Cl_2$  (1:1,v/v)] for obtaining single crystals suitable for X-ray structure determination. It has distinctly higher solubility in the crystallizing solvent [ $CH_3OH - CH_2Cl_2$  (1:1,v/v)] as compared to the unpivalated ligand due to hydrogen bonding involving its  $NH_2(2)$  group [Scheme (P-1)]<sup>125</sup>. The notable aspect of the stability of the hydrogen bond between the pterin ligand and its constituent water molecule in (**a**)  $\{[H_2(2-piv-pte_2)].H_2O\}$  is verified through single crystal X-ray structure determination of 2-pivaloylamino-7-acetyl-xanthopterin monohydrate. Here the  $H_2O$  molecule is bonded to the NH(2) group [as per Fig.(III – 1A) the N(2) – H --- O hydrogen

bonding distance is 2.945 Å]. This strongly hydrogen bonded H<sub>2</sub>O molecule is not removed even during the reaction of 7-acetyl-xanthopterin with pivalic anhydride. This pivalated pterin [H<sub>2</sub>(2-piv-pte<sub>2</sub>)]·H<sub>2</sub>O was characterized by other physico-chemical methods (e.g., elemental analysis, ESIMS data, IR, UV-VIS, <sup>1</sup>H NMR spectra etc.), in addition to its single crystal X-ray structure determination.

In the next part of this chapter, chelating property of this N,O,S – donor Schiff base ligand [Scheme (III-1A) & Scheme (III-1B)] towards different molybdenum starting materials, characterization of the resulting complexes isolated in the solid state as well as their reactivity aspects are delineated.

## Experimental

**Materials:** Reagent grade chemicals were used as received. Solvents were purified before use following literature procedures <sup>9</sup>. Kinetic and electrochemical studies were performed in spectroscopy grade DMF(SRL, Mumbai). Bu<sub>4</sub>NClO<sub>4</sub> (TBAP) and PyN→O were prepared following literature procedures <sup>7, 10, 11</sup>. Me<sub>3</sub>N→O was obtained from Aldrich, Mumbai. 7-acetyl-xanthopterin monohydrate [H<sub>2</sub>(pte<sub>2</sub>)]·H<sub>2</sub>O was prepared in this laboratory and characterized through X-ray crystallography using a single crystal of its pivalated derivative. It was obtained by a similar method as that for 6-acetyl-isoxanthopterin [H<sub>2</sub>(pte<sub>1</sub>)] discussed in Chapter II except maintaining the pH at lower range (pH 4 – 4.5)<sup>6</sup>. Thiosemicarbazide and PPh<sub>3</sub> were obtained from SRL, Mumbai. MoO<sub>2</sub>(acac)<sub>2</sub>, (Et<sub>4</sub>N)<sub>2</sub>[MoOCl<sub>5</sub>], MoOCl<sub>3</sub>(bipy), (Et<sub>4</sub>N)<sub>2</sub>[MoS<sub>4</sub>] and (Bu<sub>4</sub>N)<sub>4</sub>[Mo<sub>8</sub>O<sub>26</sub>] were prepared in this laboratory following published methods <sup>40</sup>.

**Method:** All synthetic steps were carried out under dinitrogen atmosphere by applying Schlenk technique, except compound (4). For maintaining the desired reaction temperature, a silicon oil bath was used. Most of the physico-chemical methods are stated in Chapter II, Section – I. <sup>1</sup>H NMR data were obtained from R.S.I.C., Lucknow (300 MHz, DRX). IR data (KBr) were recorded in Shimadzu FTIR 8300. Steric energy

calculation of the CHEM3D representations were performed in CHEM3D Ultra, Version 8.0 (2004), Cambridge Soft Corporation, USA and the relevant structures were drawn in the higher versions. The UV-VIS absorption spectral monitoring of the reactions of the compounds with typical enzyme substrates like  $\text{PyN}\rightarrow\text{O}$ ,  $\text{Me}_3\text{N}\rightarrow\text{O}$  or  $\text{PPh}_3$  were carried out for throwing light on the oxidation state of the metal centre in these compounds. Kinetics of these reactions in DMF were followed under pseudo-first order condition (maintaining 35-70 times excess of the substrate,  $\text{PyN}\rightarrow\text{O}$ ,  $\text{Me}_3\text{N}\rightarrow\text{O}$  /  $\text{PPh}_3$ ). Rate constants ( $k_{\text{obs}}$ ) were calculated from the plots of  $\log(A_t - A_\infty)$  or  $\log(A_\infty - A_t)$  vs. time, which were linear for at least three half-lives<sup>8(a,c), 17, 23</sup>.

### **X – ray data collection and reduction**

A red coloured monoclinic crystal of  $\text{H}_2(2\text{-piv-pte}_2)\cdot\text{H}_2\text{O}$  (**a**) was obtained by slow evaporation of  $\text{CH}_3\text{OH} - \text{CH}_2\text{Cl}_2$  (1:1,v/v) solution of (**a**) over silica-gel in a desiccator for 10 days in darkness. This crystal was used for single crystal X-ray diffraction study at the SAIF, Madras as a paid technical service; an Enraf Nonius CAD 4 automatic diffractometer was used for this purpose and the basic conditions are stated in Table (III-1). The ORTEP diagram is shown in Fig.[III-1(A)] and the unit cell structure showing hydrogen bonding in different layers are presented in Fig.[III-1(B)] and Table (III – 3). Table (III – 4) shows the atomic coordinates ( $\times 10^4$ ) and equivalent isotropic displacement parameters ( $\text{A}^2 \times 10^3$ ) for (**a**). Table (III – 5) displays the anisotropic displacement parameters ( $\text{A}^2 \times 10^3$ ). Hydrogen coordinates ( $\times 10^4$ ) and isotropic displacement parameters ( $\text{A}^2 \times 10^3$ ) are presented in Table (III – 6) and the torsion angles [deg.] are given in Table (III – 7).

## Synthesis of compounds

### **H<sub>2</sub>(2-piv-pte<sub>2</sub>).H<sub>2</sub>O (a)**

7 - acetyl-xanthopterin [H<sub>2</sub>(pte<sub>2</sub>)].H<sub>2</sub>O (2.0 g, 7.9 mmol) and pivalic anhydride [(Me<sub>3</sub>CCO)<sub>2</sub>O] (3.213 g, 10.072 mmol, 3.5 ml) was taken in a 25 ml round bottomed flask and fitted with a micro condenser. The mass was subjected to reflux in an oil bath under dinitrogen atmosphere and darkness for 3 h. A deep brown solution was formed which on concentration in a rotary evaporator at 343 K a brown residue was obtained. This was subjected to high pressure column chromatography (silica-gel, 400 mesh). The fraction in CH<sub>2</sub>Cl<sub>2</sub> was collected as a dark brown solution and concentrated in rotary evaporator to get a dirty - brown solid which was dried in vacuo over silica-gel for 48 h. Yield: 70%. This compound has high solubility in CH<sub>2</sub>Cl<sub>2</sub>, CHCl<sub>3</sub>, CH<sub>3</sub>OH etc. Purity of the product was checked through TLC [ Silica-gel GF<sub>254</sub> ; I<sub>2</sub> - chamber], using CH<sub>2</sub>Cl<sub>2</sub> solution and diethyl ether as eluant. R<sub>f</sub>: 0.62. Found : C, 53.7; H, 6.4; N, 19.9 %. Calc. for C<sub>14</sub>H<sub>19</sub>N<sub>5</sub>O<sub>5</sub> : C, 49.9; H, 5.6; N, 20.8 %. UV-VIS absorption bands [CH<sub>3</sub>OH, λ<sub>max</sub><sup>nm</sup>(logε)]: 221 (4.06); 239 sh(3.89); 293 (3.74); 307 (3.72); 321 sh(3.73); 338 sh(3.80); 353 (3.82); 413 (3.62); 441 sh(3.37).

### **H<sub>3</sub>(pte<sub>2</sub> -tsc). DMF (1)**

A DMF solution (110 ml) of 7-acetyl-xanthopterin monohydrate, [H<sub>2</sub>(pte<sub>2</sub>)].H<sub>2</sub>O (0.253 g, 1 mmol) and a methanolic solution (10 ml) of sodium acetate (anhydrous) (0.123 g, 1.5 mmol) was mixed together in a flask and stirred for 5 min. A solution of thiosemicarbazide H(tsc) (0.091 g, 1 mmol) in DMF (40 ml) was added to the above reaction mixture. Within 10 min. the solution turned greenish-yellow with a flocculant precipitate; stirring at 343-353K under dinitrogen atmosphere and darkness, was continued for 1 h. After settling for 10 min., the reaction mixture was evaporated in rotary evaporator at 343K. The reddish-yellow residue was triturated with CH<sub>3</sub>OH (5 ml) and then diethyl ether was added. The reddish-brown crystalline precipitate so obtained was filtered using a glass-fritte, washed with CH<sub>3</sub>OH, ether and dried in vacuo over

silica-gel. Yield: 85%. Its solubility is ca. 4% in DMSO (warming and stirring) and slightly lower in DMF. Purity of the product was checked through TLC [ Silica-gel GF<sub>254</sub>; UV-chamber], using DMSO solution (diluted with 100 times CH<sub>3</sub>OH) and CH<sub>2</sub>Cl<sub>2</sub>-CHCl<sub>3</sub> (1:1, v/v) as eluant. R<sub>f</sub>: 0.44. Found : C, 40.5; H, 5.0; N, 32.7; S, 8.2 %. Calc. for C<sub>13</sub>H<sub>19</sub>N<sub>9</sub>O<sub>3</sub>S : C, 40.9; H, 4.9; N, 33.1; S, 8.4 %. UV-VIS. absorption bands [DMF, λ<sub>max</sub><sup>nm</sup>(logε)]: 310 (2.12); 355.5 sh (1.90); 408 br (2.02).

### **[Mo<sup>IV</sup>(pte<sub>2</sub>-tsc)(OCH<sub>3</sub>)(CH<sub>3</sub>OH)].0.5CH<sub>3</sub>OH (2)**

To a DMF solution (100 ml) of [Mo<sup>VI</sup>O<sub>2</sub>(acac)<sub>2</sub>] (0.326 g, 1 mmol), another solution (in DMF, 100 ml) of the ligand, H<sub>3</sub>(pte<sub>2</sub>-tsc).DMF, (0.381 g, 1 mmol) was mixed in a Schlenk flask. Heating and stirring at 313-323K under dinitrogen atmosphere and darkness was continued for 3 h. The yellow solution formed was allowed to settle for 1 h. The solvent was removed in rotary evaporator at 343K. The red oily residue formed was triturated with CH<sub>3</sub>OH (15 ml); diethyl ether (10 ml) was added when a red crystalline precipitate was obtained. It was filtered under dinitrogen, in a glass-fritte, washed with CH<sub>3</sub>OH, diethyl ether and dried in vacuo over silica - gel. Yield: 65%. Its solubility is ca. 5.5% in DMF. Purity of the product was checked through TLC [Silica-gel GF<sub>254</sub> ; UV-lamp], using DMSO solution (diluted with 100 times CH<sub>3</sub>OH) and CH<sub>2</sub>Cl<sub>2</sub> as eluant. R<sub>f</sub> : 0.46. Found : C, 29.0; H, 3.6; N, 23.0; S, 6.9; Mo, 20.1 %. Calc. for MoC<sub>12.5</sub>H<sub>18</sub>N<sub>8</sub>O<sub>4.5</sub>S : C, 31.2; H, 3.8; N, 23.3; S, 6.7; Mo, 20.0 %. UV-VIS absorption bands [DMF, λ<sub>max</sub><sup>nm</sup>(logε)]: 285(3.95); 341(4.02); 398(3.69); 420(3.68); 453sh (3.47). The compound is found to be diamagnetic in nature.

### **[Mo<sup>IV</sup>{H(pte<sub>2</sub>-tsc)}Cl<sub>2</sub>.DMF]. 2DMF (3)**

A DMF solution (20 ml) of (Et<sub>4</sub>N)<sub>2</sub>[Mo<sup>V</sup>OCl<sub>5</sub>] (0.55 g, 1 mmol) was mixed with a solution of H<sub>3</sub>(pte<sub>2</sub>-tsc).DMF (0.381 g, 1 mmol) in DMF (100 ml) in a Schlenk flask. The solvent and solutions were initially purged thoroughly with dinitrogen before mixing. Heating and stirring at 333K under dinitrogen atmosphere, darkness, was continued for 3h. A dark-red solution so obtained was concentrated to a red oil in rotary evaporator at

343K. This on trituration with CH<sub>3</sub>OH (10 ml) yielded a red crystalline precipitate, filtered in a glass-fritte, washed with CH<sub>3</sub>OH, diethyl ether and dried in vacuo over silica-gel. Yield: 60 %. Its solubility is ca. 5% in DMF. It's purity was checked through TLC [Silica-gel GF<sub>254</sub>; UV-lamp], using DMSO solution (diluted with 100 times CH<sub>3</sub>OH) and diethyl ether as eluant. R<sub>f</sub> : 0.25. Found : C, 33.5; H, 4.1; N, 22.2; S, 4.6; Mo, 14.1%. Calc. for MoC<sub>19</sub>H<sub>31</sub>N<sub>11</sub>O<sub>5</sub>SCl<sub>2</sub> : C, 33.0; H, 4.5; N, 22.2; S, 4.6; Mo, 13.9 %. UV-VIS absorption bands [DMF, λ<sub>max</sub><sup>nm</sup>(logε)]: 291(4.37); 346(4.45); 396(4.26); 420 sh(4.19); 453 sh(3.93). The compound is found to be diamagnetic in nature.

**(Et<sub>4</sub>N)[(Mo<sub>2</sub><sup>V</sup>O<sub>3</sub>) {H(pte<sub>2</sub>-tsc)}Cl<sub>5</sub>]. 0.5CH<sub>3</sub>OH (4)**

This compound was prepared from (3) stated above in the following way : after removing solvent (DMF) in rotary evaporator from the reaction mixture of (3) at 343K, a red oily mass so obtained was allowed to attain room temperature (301K); sufficient amount of CH<sub>3</sub>OH was added to have a clear solution. This solution was left in contact of air at 301K for 50h, during which the initial red colour changed slowly to green, concentrated to a minimum volume (5 ml) in a rotary evaporator when a green coloured precipitate settled down, filtered in a glass-fritte, washed with CH<sub>3</sub>OH, diethyl ether and dried in vacuo over silica-gel. Yield: 62%. Its solubility is ca. 5% in DMF. Purity of the product was checked through TLC [Silica-gel GF<sub>254</sub> ; UV-lamp], using diluted (with 100 times CH<sub>3</sub>OH) DMSO solution and CH<sub>2</sub>Cl<sub>2</sub> as eluant. R<sub>f</sub> : 0.35. Found : C, 25.5; H, 3.6; N, 14.3; S, 4.0; Mo, 22.0 %. Calc. for Mo<sub>2</sub>C<sub>18.5</sub>H<sub>32</sub>N<sub>9</sub>O<sub>5.5</sub>Cl<sub>5</sub>S : C, 25.5; H, 3.7; N, 14.5; S, 3.7; Mo, 22.1%. UV-VIS absorption bands [DMF, λ<sub>max</sub><sup>nm</sup>(logε)]: 291(4.00); 341(4.05); 396 sh(3.75); 419 sh(3.68); 453(3.44). The compound is diamagnetic in nature.

**[(Mo<sub>2</sub><sup>V</sup>O)<sub>2</sub> {H(pte<sub>2</sub>-tsc)}<sub>2</sub>(bipy)Cl<sub>12</sub>]. 8CH<sub>3</sub>OH (5)**

A DMF solution (80 ml) of [Mo<sup>V</sup>OCl<sub>3</sub>(bipy)] (0.374 g, 1 mmol) was charged with another DMF (100 ml) solution of H<sub>3</sub>(pte<sub>2</sub>-tsc).DMF (0.381 g, 1 mmol) and subjected to heating (at 333K) and stirring under dinitrogen atmosphere, darkness, for 3h. A clear red solution was obtained, concentrated in rotary evaporator at 343K when a red oil was

formed. On trituration with CH<sub>3</sub>OH (10 ml) gave a brick-red coloured, air stable precipitate which was filtered in a glass-fritte and dried in vacuo over silica-gel. Yield: 65%. Solubility of the complex is ca. 5.5 % in DMF. Purity of this compound was checked through TLC [Silica-gel GF<sub>254</sub> ;I<sub>2</sub>-chamber], using DMSO solution (diluted with 100 times CH<sub>3</sub>OH) and CH<sub>2</sub>Cl<sub>2</sub> as eluant. R<sub>f</sub> : 0.40. Found : C, 23.2; H, 2.8; N, 12.5; S, 4.0; 20.7 %. Calc. for Mo<sub>4</sub>C<sub>38</sub>H<sub>60</sub>N<sub>18</sub>O<sub>14</sub>Cl<sub>12</sub>S<sub>2</sub> : C, 24.4; H, 3.2; N, 13.5; S, 3.4; Mo, 20.6 %. UV-VIS absorption bands [DMF, λ<sub>max</sub><sup>nm</sup>(logε)]: 281.7(4.74); 343.6(4.52); 398 br(4.18); 422(4.18); 453(4.08); 491 sh(3.84). The compound is found to be diamagnetic in nature.

### **[(Mo<sub>2</sub><sup>V</sup>O<sub>4</sub>) {H(pte<sub>2</sub>-tsc)} (DMF)<sub>3</sub>].DMF.CH<sub>3</sub>OH (6)**

To a DMF solution (80 ml) of (Bu<sub>4</sub>N)<sub>4</sub>[Mo<sub>8</sub><sup>VI</sup>O<sub>26</sub>] (269 g, 1/8 mmol) in a Schlenk flask, H<sub>3</sub>(pte<sub>2</sub>-tsc).DMF (0.381 g, 1 mmol) in DMF (100 ml) was added under dinitrogen atmosphere. Heating and stirring of the reaction mixture at 338K under dinitrogen atmosphere and darkness was continued for 2h. The reaction mixture turned deep greenish-yellow. The solvent was removed in rotary evaporator at 343K when a brownish, oily residue was formed which on trituration with CH<sub>3</sub>OH (10 ml) a green precipitate formed. This was filtered in a glass-fritte and washed with CH<sub>3</sub>OH, diethyl ether; dried in vacuo over silica-gel. Yield: 60%. Its solubility is ca. 5% in DMF. Purity of the compound was checked through TLC [Silica-gel GF<sub>254</sub> ;UV-chamber], using DMSO solution (diluted with 100 times CH<sub>3</sub>OH) and CH<sub>2</sub>Cl<sub>2</sub> as eluant. R<sub>f</sub> : 0.50. Found : C, 32.1; H, 4.2; N, 18.5; S, 3.7; Mo, 21.8 %. Calc. for Mo<sub>2</sub>C<sub>23</sub>H<sub>42</sub>N<sub>12</sub>O<sub>11</sub>S : C, 31.1; H, 4.7; N, 18.9; S, 3.6; Mo, 21.7%. UV-VIS absorption bands [DMF, λ<sub>max</sub><sup>nm</sup>(logε)]: 279(4.28); 339(4.26); 422(3.86); 453 sh(3.77); 486 sh(3.49). The compound is diamagnetic in nature.

**$[(\text{Mo}_2^{\text{VI}}\text{S}_5) \{\text{H}(\text{pte}_2 - \text{tsc})\} (\text{CH}_3\text{OH})_3] \cdot \text{CH}_3\text{OH}$  (7)**

To a methanolic solution (30 ml) of  $(\text{Et}_4\text{N})_2[\text{MoS}_4]$  (0.484 g, 1 mmol), taken in a three necked Schlenk flask, a DMF solution (100 ml) of  $\text{H}_3(\text{pte}_2 - \text{tsc}) \cdot \text{DMF}$  (0.381 g, 1 mmol) was charged slowly through an addition funnel under stirring at 301K. The pH of the reaction mixture was adjusted to 6.0 with HCl in dioxane. The resulted solution was stirred at 333K under dinitrogen atmosphere, darkness, for 2 h when a dark red coloured solution was formed. This was concentrated to an oily residue in a rotary evaporator at 343K and subsequently triturated with  $\text{CH}_3\text{OH}$  (5 ml) to get a pink-brown precipitate which was filtered in a glass-fritte, washed with  $\text{CH}_3\text{OH}$ , diethyl ether and dried in vacuo over silica-gel. Yield: 45%. Its solubility is ca. 4.5% in DMF. Purity of the product was checked through TLC [Silica-gel GF<sub>254</sub> ;UV-chamber], using DMSO solution (diluted with 100 times  $\text{CH}_3\text{OH}$ ) and  $\text{CH}_2\text{Cl}_2$ - $\text{CHCl}_3$  (2:1,v/v) solvent mixture as eluant.  $R_f$  : 0.33. Found : C, 21.9; H, 3.4; N, 13.7; S, 25.0; Mo, 24.3 %. Calc. for  $\text{Mo}_2\text{C}_{14}\text{H}_{27}\text{N}_8\text{O}_6\text{S}_6$  : C, 21.35; H, 3.43; N, 14.23; S, 24.4; Mo, 24.4 %. UV-VIS absorption bands [DMF,  $\lambda_{\text{max}}^{\text{nm}}(\log\epsilon)$ ]: 280.5(4.33); 340(4.30); 398 br(3.97); 420(3.97); 453 sh(3.82). The compound is found to be diamagnetic in nature.

## Results and Discussion

The molecular structure of  $H_2(2\text{-piv-pte}_2)\cdot H_2O$  along with its numbering scheme is shown in Fig.[III-1(A)]. The data clearly shows the xanthopterin structure (7-oxo) of this Ligand <sup>28</sup>. Table (III-2) contains different bond lengths and bond angles information. The crystal contains one water molecule hydrogen bonded to the N(1) atom of the pterin as well as O(4) and N(5), as evident from Table (III - 3). The unit cell structure along with inter - layer hydrogen bonding is shown in Fig.[III - 1(B)].

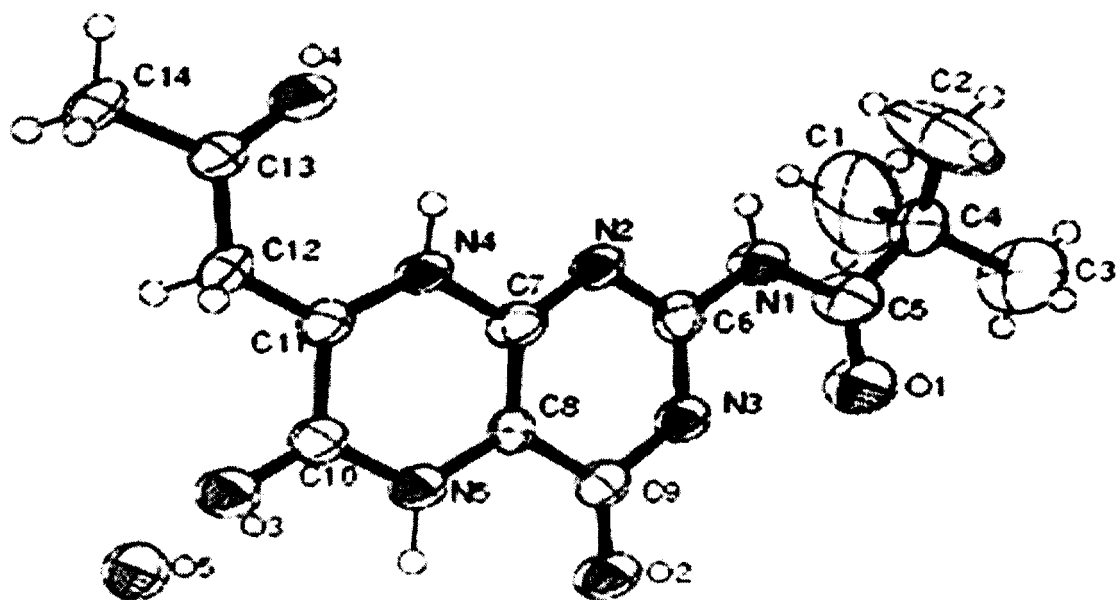
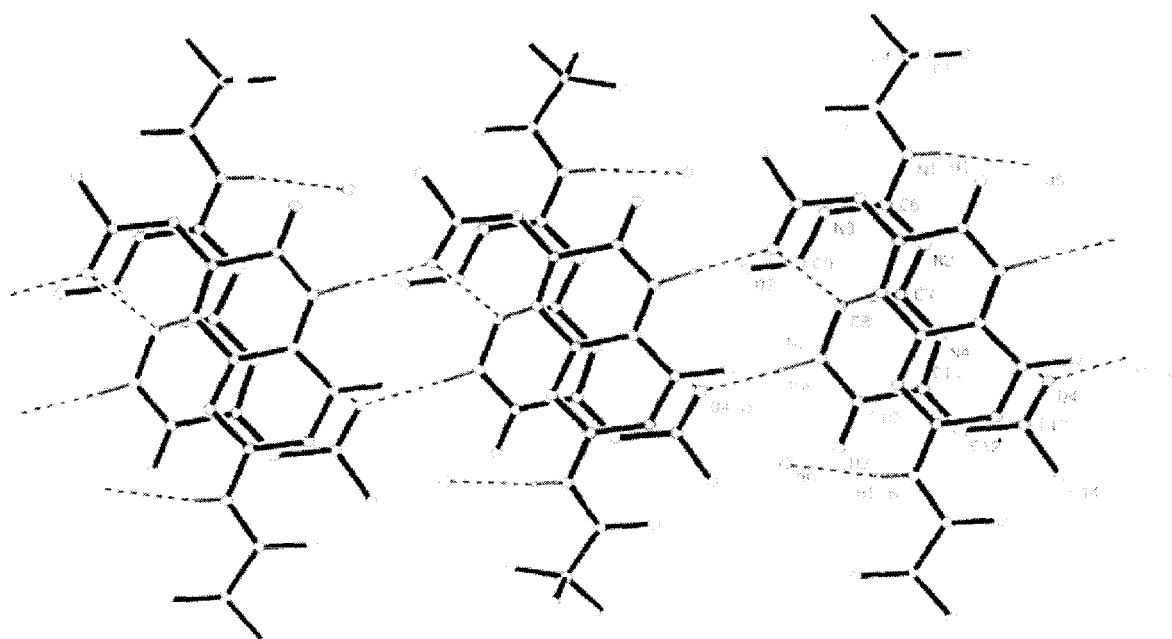


Fig. (III-1A)



**Fig. (III-1B)**

**Fig.(III-1):** (A) represents the single crystal X-ray structure of  $H_2(2-piv-pte_2).H_2O$  molecule and (B) the unit cell structure of  $H_2(2-piv-pte_2).H_2O$  crystal.

**Table (III – 1):** Crystal data and structure refinement for  $H_2(2-piv-pte_2).H_2O$ :

Empirical formula	$C_{14}H_{19}N_5O_5$
Formula weight	337.34
Temperature	293(2) K
Wave length	0.71073 Å
Crystal system	Monoclinic
Space group	P21/a
Unit cell dimensions	a = 15.722(5) Å alpha = 90 deg. b = 6.598(4) Å beta = 104.76(3) deg. c = 16.382(6) Å gamma = 90 deg.
Volume	1643.4(14) Å <sup>3</sup>
z	4
Calculated density	1.363 mg/ m <sup>3</sup>

Absorption coefficient	0.105 mm <sup>-1</sup>
F(000)	712
Crystal size	0.3 x 0.2 x 0.2 mm
Theta range for data collection	2.57 to 24.96 deg.
Limiting indices	0 ≤ h ≤ 18, 0 ≤ k ≤ 7, -19 ≤ l ≤ 18
Reflections collected / unique	2980 / 2860 [R(int) = 0.0279]
Completeness to theta = 24.96	99.3 %
Absorption correction	Psi- scan
Max. and min. transmission	0.9972 and 0.9032
Refinement method	Full- matrix least- squares on F <sup>2</sup>
Data / restraints / parameters	2860 / 0 / 230
Goodness- of- fit on F <sup>2</sup>	0.847
Final R indices [I > 2 sigma(I)]	RI = 0.0572, wR2 = 0.1269
R indices (all data)	RI = 0.1869, wR2 = 0.1664
Extinction coefficient	0.0007(9)
Largest diff. peak and hole	0.250 and -0.211 e. Å <sup>-3</sup>

**Table (III – 2):** Bond lengths [Å] and angles [deg.] for H<sub>2</sub>(2-piv-pte<sub>2</sub>) .H<sub>2</sub>O<sup>#</sup> :

C(1) – C(4)	1.508 (9)	O(1)–C(5)– N(1)	118.8 (4)
C(2) – C(4)	1.477 (6)	O(1)–C(5)– C(4)	124.1 (4)
C(3) – C(4)	1.495 (6)	N(1)–C(5)– C(4)	117.0 (4)
C(4) – C(5)	1.485 (6)	N(2)–C(6)– N(1)	116.9 (3)
C(5) – O(1)	1.213 (4)	N(2)–C(6)– N(3)	123.2 (3)
C(5) – N(1)	1.397 (5)	N(1)–C(6)– N(3)	119.9 (3)
C(6) – N(2)	1.331 (4)	N(2)–C(7)– C(8)	126.3 (3)
C(6) – N(1)	1.365 (4)	N(2)–C(7)– N(4)	116.5 (3)
C(6) – N(3)	1.365 (4)	C(8)–C(7)– N(4)	117.2 (3)
C(7) – N(2)	1.344 (4)	C(7)–C(8)– N(5)	121.9 (3)
C(7) – C(8)	1.369 (5)	C(7)–C(8)– C(9)	118.5 (3)
C(7) – N(4)	1.393 (4)	N(5)–C(8)– C(9)	119.6 (3)

C(8) – N(5)	1.383 (4)	O(2)–C(9)– N(3)	122.2 (3)
C(8) – C(9)	1.443 (5)	O(2)–C(9)– C(8)	124.3 (4)
C(9) – O(2)	1.225 (4)	N(3)–C(9)– C(8)	113.5 (3)
C(9) – N(3)	1.389 (4)	O(3)–C(10) – N(5)	121.4 (3)
C(10) – O(3)	1.218 (4)	O(3) – C(10) – C(11)	122.8 (4)
C(10) – N(5)	1.360 (5)	N(5)–C(10)– C(11)	115.7 (3)
C(10) – C(11)	1.482 (5)	N(4)–C(11)– C(12)	123.5 (3)
C(11) – N(4)	1.352 (4)	N(4)–C(11)– C(10)	119.5 (3)
C(11) – C(12)	1.374 (5)	C(12)–C(11)– C(10)	117.0 (3)
C(12) – C(13)	1.417 (5)	C(11)–C(12)– C(13)	123.8 (4)
C(13) – O(4)	1.228 (4)	O(4)–C(13)– C(12)	122.5 (4)
C(13) – C(14)	1.529 (5)	O(4)–C(13)– C(14)	120.7 (3)
C(2)–C(4)– C(5)	114.6 (4)	C(12)–C(13)– C(14)	116.8 (3)
C(2)–C(4)– C(3)	111.4 (5)	C(6)–N(1)– C(5)	126.7 (3)
C(5)–C(4)– C(3)	107.6 (4)	C(6)–N(2)– C(7)	115.2 (3)
C(2)–C(4)– C(1)	109.0 (6)	C(6)–N(3)– C(9)	123.4 (3)
C(5)–C(4)– C(1)	106.3 (4)	C(11)–N(4)– C(7)	122.9 (3)
C(3)–C(4)– C(1)	107.6 (5)	C(10)–N(5)– C(8)	122.6 (3)

# Symmetry transformations used to generate equivalent atoms.

**Table (III – 3):** Hydrogen bonds for (**a**) [A and deg.] :

D – H . . . A	d (D – H)	d (H . . . A)	d (D . . . A)	< (DHA)
N(1) – H(1) . . . O(5) # 1	0.80 (3)	2.16 (3)	2.945 (4)	168 (3)
N(4) – H(4) . . . O(4)	0.89 (3)	2.13 (3)	2.687 (4)	120 (2)
N(5) – H(5) . . . O(4) # 2	0.95 (4)	1.92 (4)	2.870 (4)	178 (4)

Symmetry transformations used to generate equivalent atoms :

# 1 - x, - y + 1, - z + 1    # 2 x + 1/2, - y + 1/2, z

**Table (III-4):** Atomic coordinates ( $\times 10^4$ ) and equivalent isotropic displacement parameters ( $\text{\AA}^2 \times 10^3$ ) for (a).  $U(\text{eq})$  is defined as one third of the trace of the orthogonalized  $U_{ij}$  tensor.

	x	y	z	$U(\text{eq})$
C(1)	751(6)	3866(13)	9080(4)	168(3)
C(2)	69(4)	552(14)	8780(3)	164(4)
C(3)	1624(3)	857(13)	9544(3)	150(3)
C(4)	893(3)	1696(9)	8857(3)	61(1)
C(5)	1204(3)	1768(7)	8074(3)	59(1)
C(6)	704(2)	2114(7)	6525(2)	43(1)
C(7)	161(2)	2447(7)	5116(2)	41(1)
C(8)	973(2)	2446(6)	4954(2)	40(1)
C(9)	1740(2)	2267(7)	5655(2)	47(1)
C(10)	383(2)	2927(7)	3461(3)	48(1)
C(11)	-500(2)	2839(7)	3626(2)	41(1)
C(12)	-1213(2)	3018(6)	2942(2)	40(1)
C(13)	-2098(2)	2956(7)	2996(3)	50(1)
C(14)	-2809(2)	3236(8)	2172(2)	73(2)
N(1)	563(2)	1974(6)	7311(2)	52(1)
N(2)	-5(2)	2276(5)	5879(2)	43(1)
N(3)	1542(2)	2090(5)	6431(2)	44(1)

N(4)	-568(2)	2594(6)	4427(2)	42(1)
N(5)	1075(2)	2644(6)	4144(2)	48(1)
O(1)	1970(2)	1672(6)	8061(2)	81(1)
O(2)	2499(2)	2270(5)	5588(2)	64(1)
O(3)	493(2)	3230(5)	2761(2)	64(1)
O(4)	-2297(2)	2696(5)	3666(2)	59(1)
O(5)	1307(2)	7106(5)	2859(2)	78(1)

**Table (III-5) :** Anisotropic displacement parameters ( $\text{Å}^2 \times 10^3$ ) for (a). The anisotropic displacement factor exponent takes the form :-  $2 \pi^2 [ h^2 a^{*2} U11 + \dots + 2 h k a^* b^* U12 ]$

	U11	U22	U33	U23	U13	U12
C(1)	262(10)	195(10)	64(4)	5(5)	71(5)	53(8)
C(2)	116(5)	316(12)	59(4)	2(5)	22(4)	-109(6)
C(3)	92(4)	299(10)	43(3)	42(5)	-13(3)	30(6)
C(4)	49(2)	92(5)	31(3)	4(3)	-8(2)	3(3)
C(5)	43(2)	84(4)	45(3)	-10(3)	0(2)	-16(3)
C(6)	42(2)	54(3)	28(2)	1(2)	3(2)	5(2)
C(7)	30(2)	52(3)	37(2)	-7(2)	3(2)	-1(2)
C(8)	31(2)	61(3)	24(2)	6(2)	2(2)	3(2)
C(9)	31(2)	63(3)	41(3)	3(2)	1(2)	-4(2)

C(10)	32(2)	72(4)	37(2)	2(3)	5(2)	-1(2)
C(11)	31(2)	57(3)	32(2)	0(2)	3(2)	1(2)
C(12)	31(2)	44(3)	40(2)	3(2)	-1(2)	4(2)
C(13)	29(2)	79(4)	38(2)	8(3)	4(2)	0(2)
C(14)	28(2)	135(5)	45(3)	18(3)	-10(2)	4(3)
N(1)	28(2)	93(3)	29(2)	-1(2)	-1(2)	-3(2)
N(2)	28(2)	64(3)	35(2)	3(2)	2(2)	5(2)
N(3)	30(2)	58(3)	38(2)	1(2)	1(1)	1(2)
N(4)	21(2)	70(3)	32(2)	0(2)	-1(1)	0(2)
N(5)	27(2)	74(3)	40(2)	6(2)	4(2)	0(2)
O(1)	44(2)	143(4)	45(2)	13(2)	-6(2)	-5(2)
O(2)	26(1)	107(3)	52(2)	6(2)	1(1)	2(2)
O(3)	36(2)	113(3)	41(2)	10(2)	8(1)	1(2)
O(4)	28(1)	99(3)	49(2)	7(2)	6(1)	1(2)
O(5)	48(2)	133(3)	48(2)	8(2)	4(1)	-1(2)

---

**Table (III – 6) :** Hydrogen coordinates ( $\times 10^4$ ) and isotropic displacement parameters ( $\text{\AA}^2 \times 10^3$ ) for (**a**).

	x	y	z	U(eq)
H(1A)	561	3902	9593	252
H(1B)	310	4473	8632	252
H(1C)	1292	4604	9158	252
H(2A)	- 80	555	9312	246
H(2B)	148	- 819	8617	246
H(2C)	- 396	1176	8359	246
H(3A)	1441	794	10060	226
H(3B)	2131	1718	9621	226
H(3C)	1770	- 480	9392	226
H(12A)	-1153	1958	2550	48
H(12B)	-1142	4294	2673	48
H(14A)	-3379	3161	2284	109
H(14B)	-2756	2189	1781	109
H(14C)	-2739	4536	1933	109
H(1)	60(20)	2090(50)	7314(19)	27(11)
H(4)	-1070(20)	2620(60)	4591(19)	39(10)
H(5)	1610(30)	2530(70)	3970(30)	72(13)

**Table (III – 7) : Torsion angles [deg.] for (a) #.**

---

C(2) – C(4) – C(5) – (1)	- 141.9(6)
C(3) – C(4) – C(5) – O(1)	- 17.4(8)
C(1) – C(4) – C(5) – O(1)	97.6(6)
C(2) – C(4) – C(5) – N(1)	38.6(7)
C(3) – C(4) – C(5) – N(1)	163.1(5)
C(1) – C(4) – C(5) – N(1)	- 81.9(6)
N(2) – C(7) – C(8) – N(5)	- 179.6(4)
N(4) – C(7) – C(8) – N(5)	1.9(6)
N(2) – C(7) – C(8) – C(9)	- 0.6(7)
N(4) – C(7) – C(8) – C(9)	- 179.2(4)
C(7) – C(8) – C(9) – O(2)	- 179.2(5)
N(5) – C(8) – C(9) – O(2)	- 0.3(7)
C(7) – C(8) – C(9) – N(3)	0.7(6)
N(5) – C(8) – C(9) – N(3)	179.7(4)
O(3) – C(10) – C(11) – N(4)	- 176.8(4)
N(5) – C(10) – C(11) – N(4)	3.3(6)
O(3) – C(10) – C(11) – C(12)	3.1(7)
N(5) – C(10) – C(11) – C(12)	- 176.9(4)
N(4) – C(11) – C(12) – C(13)	- 0.4(7)
C(10) – C(11) – C(12) – C(13)	179.7(4)
C(11) – C(12) – C(13) – O(4)	-1.4(7)
C(11) – C(12) – C(13) – C(14)	178.5(4)
N(2) – C(6) – N(1) – C(5)	179.1(4)
N(3) – C(6) – N(1) – C(5)	-1.1(7)

O(1) – C(5) – N(1) – C(6)	-1.0(7)
C(4) – C(5) – N(1) – C(6)	178.5(5)
N(1) – C(6) – N(2) – C(7)	178.9(4)
N(3) – C(6) – N(2) – C(7)	- 0.9(6)
C(8) – C(7) – N(2) – C(6)	0.7(7)
N(4) – C(7) – N(2) – C(6)	179.2(4)
N(2) – C(6) – N(3) – C(9)	1.2(7)
N(1) – C(6) – N(3) – C(9)	-178.6(4)
O(2) – C(9) – N(3) – C(6)	179.0(4)
C(8) – C(9) – N(3) – C(6)	-1.0(6)
C(12) – C(11) – N(4) – C(7)	-178.9(4)
C(10) – C(11) – N(4) – C(7)	1.0(6)
N(2) – C(7) – N(4) – C(11)	177.8(4)
C(8) – C(7) – N(4) – C(11)	-3.5(6)
O(3) – C(10) – N(5) – C(8)	175.1(4)
C(11) – C(10) – N(5) – C(8)	- 4.9(6)
C(7) – C(8) – N(5) – C(10)	2.5(7)
C(9) – C(8) – N(5) – C(10)	- 176.4(4)

---

# Symmetry transformations used to generate equivalent atoms.

Fast Atomic Bombardment (FAB) / ESIMS technique, has proved to be a valuable tool for characterizing many compounds including the inorganic coordination ones<sup>110, 121</sup>. As is the case for different types of mass spectroscopy, the assignment of molecular formula (or any definite fragment originating from it) is confirmed by the experimental value of m/z (the most abundant isotopic mass) as well as matching

between the experimental and calculated (simulated) isotopic distribution profile <sup>14, 85, 107, 117, 118</sup>. As far as organic compounds containing O, F, P and I are concerned, the relative intensities of M, M+1 and M+2 isotope peaks are of great value in recognizing the molecular ion ( $M^+$ ) peak or any well defined fragment confirming it <sup>85</sup>. Sometimes, isotope peaks may be more intense than the calculated values because of ion – molecule interactions that vary with the sample concentration or with the class of compound involved, e.g., the transfer of a hydrogen atom from the excess of the compound to the molecular ion in some case <sup>85</sup>. An M – 1 peak is common and occasionally an M – 2 peak (loss of H<sub>2</sub>) or even a rare M – 3 peak (from alcohol) is reasonable <sup>85</sup>. Absence of molecular ion (or an extremely weak  $M^+$  peak) is characteristic of highly branched molecules, alcohols, molecules with long alkyl chain, aryl ketones and benzyl compounds <sup>85, 107</sup>.

FAB mass spectrum of (1) [Fig.(III-2)] contains the molecular ion peak without solvent molecule (DMF) of crystallization at  $m/z = 307$ ,  $[M-DMF-H]^+$  (relative intensity 100%), where 'M' is the molecular formula of (1)<sup>7(a), 14, 15, 85, 107</sup> (F.W.= 381). This peak was simulated by IPC <sup>46</sup> [Fig.(III-3)]. The experimentally found peak and the simulated one show good agreement between them which supports the proposed molecular formula.

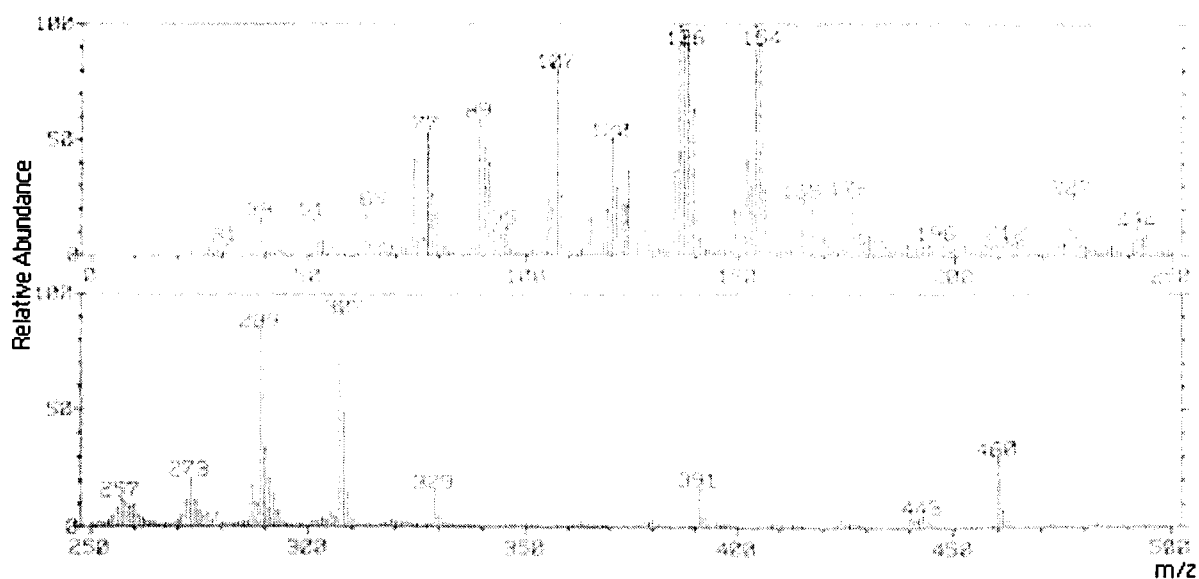


**Fig.(III – 2):** FAB Mass spectrum of (1) in CH<sub>3</sub>OH.

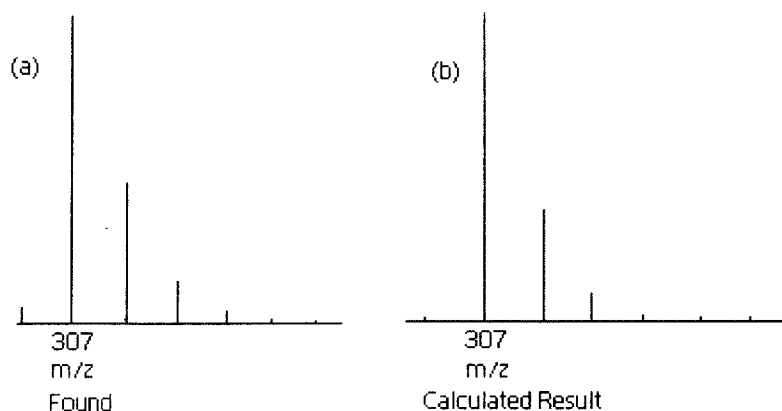


**Fig.(III-3):** (a) ESIMS data of (1) at the  $m/z$  (= 307) region corresponding to  $[M- DMF-H]^+$ ; (b) the calculated isotope pattern<sup>46</sup>. Formula :  $C_{10}H_{11}N_8O_2S$ .

The desolvated molecular ion peak in the ESIMS spectrum of (2) appeared at  $m/z = 464$ ,  $[M - 0.5CH_3OH]^+$ ; where 'M' is the molecular formula of (2) (F.W.= 479.94)<sup>7(a), 14, 15</sup>. The molecular ion peak without 0.5CH<sub>3</sub>OH is simulated [Fig.(III - 4)] by using the IPC program mentioned above<sup>46</sup>. Good agreement between the calculated and the experimentally found peaks suggests the correctness of the proposed molecular formula of (2).

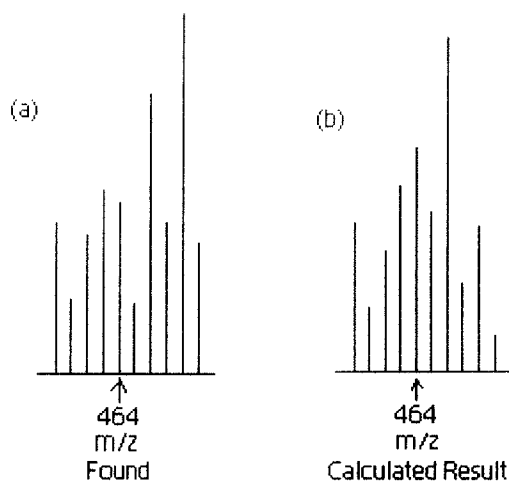


**Fig.(III-4):** (a) ESIMS data of (2) at the  $m/z$  (= 464) region corresponding to  $[M - 0.5CH_3OH]^+$ ; (b) the calculated isotope pattern<sup>46</sup>. Formula :  $C_{12}H_{16}N_8O_4MoS$ .

In the ESIMS data of (3) the peak at  $m/z = 656$  could be assigned to the characteristic fragment  $[M - Cl - 2H]^+$ <sup>85</sup>, where 'M' is the molecular formula of the complex (F.W.=692)<sup>7(a), 14, 15</sup>. The simulated and the experimentally obtained peaks

[Fig.(III – 5)]<sup>14, 46</sup> are consistent to each other and with the molecular formula of (3)<sup>7(a), 14, 15, 85, 107</sup>.

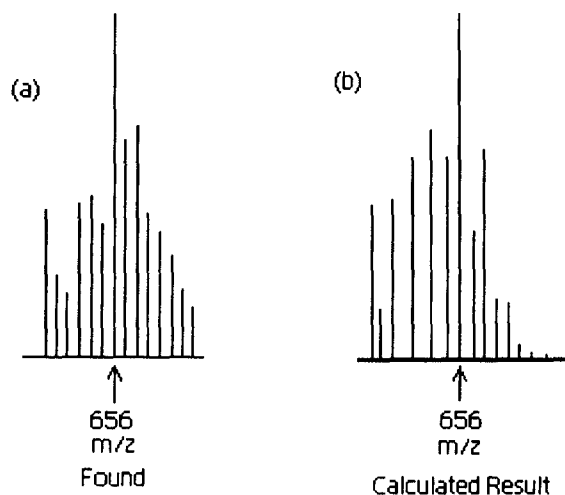


**Fig.(III – 5):** (a) ESIMS data of (3) at the  $m/z$  (= 656) region corresponding to  $[M - Cl - 2H]^+$ ; (b) the calculated isotope pattern<sup>46</sup>. Formula :  $C_{19}H_{29}N_{11}O_5MoSCl$ .

The essentially desolvated ESIMS peak of (4)  $[M - 0.5CH_3OH - H]^+$  is visible at  $m/z = 854$ , where 'M' is the molecular formula of the complex (F.W. = 869.38)<sup>7(a), 14, 15, 85, 107</sup>. This peak is simulated by using the IPC program<sup>46</sup> [Fig.(III – 6)] and found that both are in good match. The total number of peaks in this spectrum confirms the presence of a binuclear molybdenum species<sup>14</sup>.

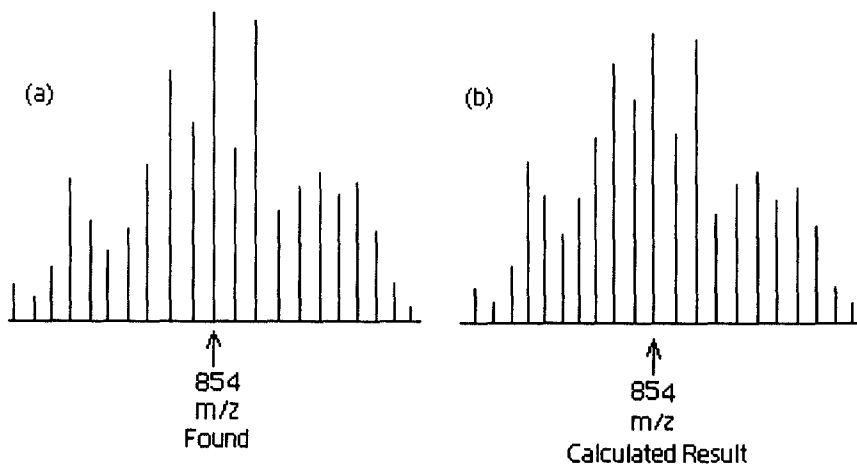


**Fig.(III-6):** (a) ESIMS data of (4) at the  $m/z$  (= 854) region corresponding to  $[M - 0.5CH_3OH - H]^+$ ; (b) the calculated isotope pattern<sup>46</sup>. Formula :  $C_{18}H_{29}N_9O_5Mo_2Cl_5S$ .

In case of (5) the ESIMS spectrum contains a peak at  $m/z = 894.3$  which can be assigned to the fragment  $[M/2 - Cl - 3H]^+$ , where 'M' is the molecular formula of the compound (F.W.=1865.76.)<sup>7(a), 14, 15</sup>. [Fig.(III-7)]<sup>46</sup> reflecting the matching of experimental and simulated ESIMS data confirms the binuclear nature of the fragment i.e., this in turn shows that the original tetranuclear species undergoes fragmentation process through a definite pathway leading to the above binuclear fragment<sup>85, 107</sup>.

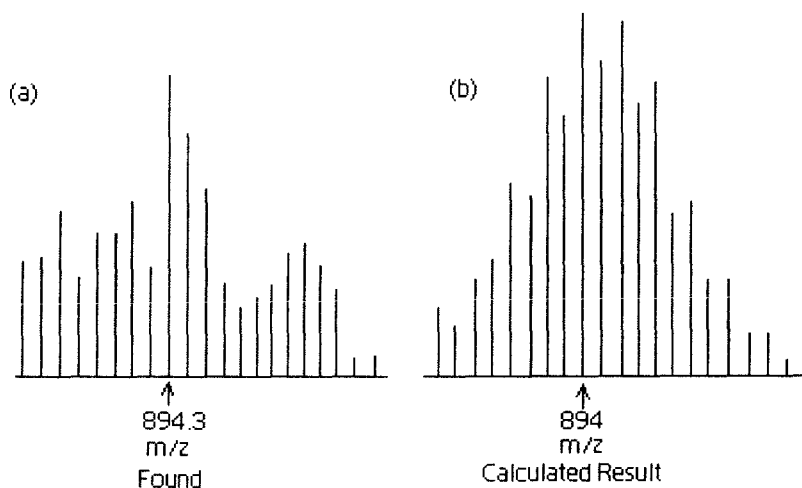


**Fig.(III-7):** (a) ESIMS data of (5) at the  $m/z$  ( $= 894.3$ ) region corresponding to  $[M/2 - Cl - 3H]^+$ ; (b) the calculated isotope pattern<sup>46</sup>. Formula :  $C_{19}H_{27}N_9O_7Mo_2Cl_5S$ .

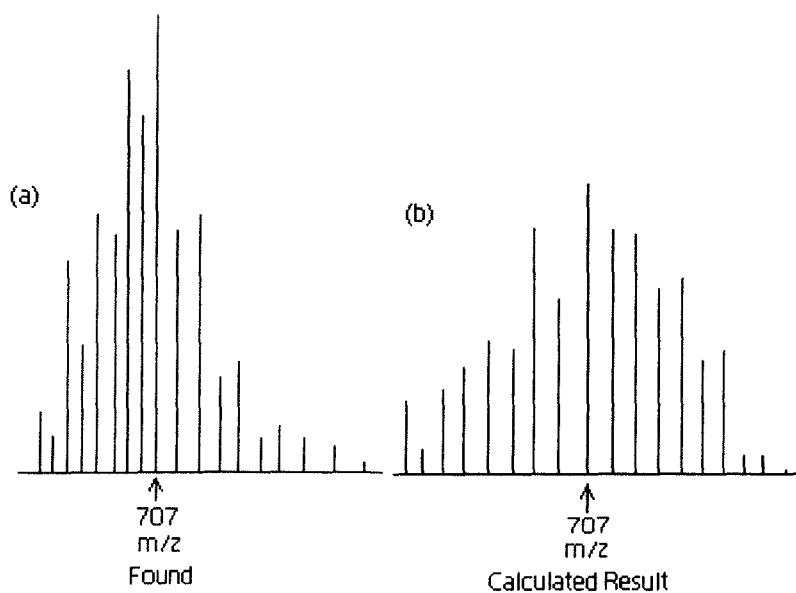


**Fig.(III-8):** (a) ESIMS data of (6) at the  $m/z$  ( $= 707.4$ ) region corresponding to  $[M - CH_3OH - 2DMF + H]^+$ ; (b) the calculated isotope pattern<sup>46</sup>. Formula :  $C_{16}H_{23}N_{10}O_8Mo_2S$ .

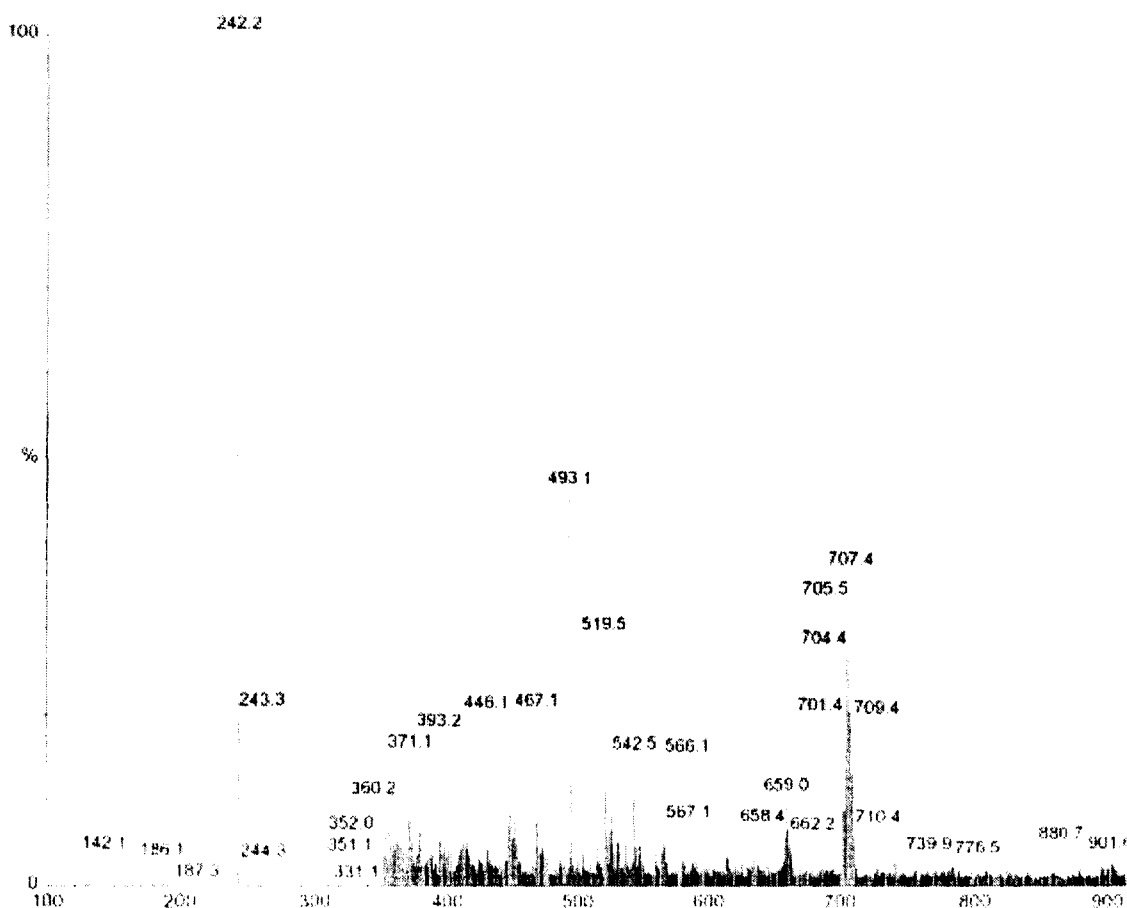


**Fig.(III – 9):** ESIMS spectrum of (6) in CH<sub>3</sub>OH.

Compound (6) shows the ESIMS peak for the partly desolvated species  $[M - \text{CH}_3\text{OH} - 2\text{DMF} - \text{H}]^+$  at  $m/z = 707.4$ , where 'M' is the relevant molecular formula (F.W. = 885.88)<sup>7(a), 14, 15</sup>. [Fig.(III – 9)] shows the ESIMS spectrum of (6), whereas [Fig.(III-8)] shows the simulated and experimental patterns for the above mentioned peak<sup>46</sup>. It is consistent with the binuclear formula of the complex<sup>14</sup>.

In case of (7) the ESIMS data shows a fragment  $[M - CO + H]^+$  at  $m/z = 760$ . It matches with its simulated pattern<sup>14, 46</sup> [Fig.(III-10)] thereby verifying the chemical composition of this compound.

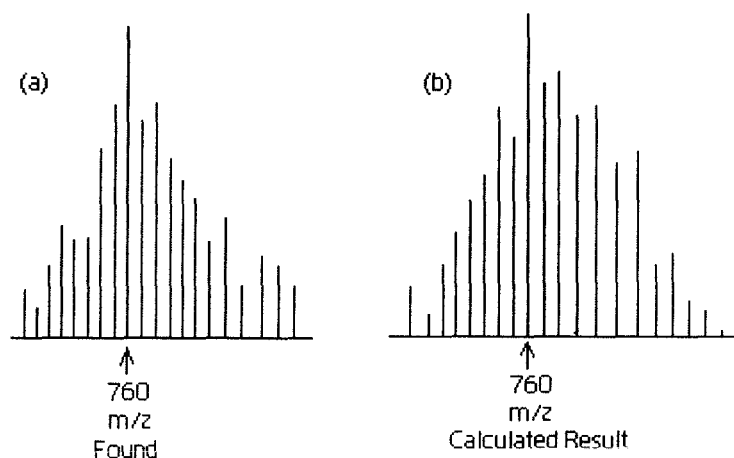


**Fig.(III-10):** (a) Computer simulation and (b) experimentally found ESIMS peaks of (7) corresponding to  $m/z = 760, [M - CO + H]^+$ . Formula :  $C_{13}H_{28}N_8O_5Mo_2S_6$ .

ESIMS method plays an important role in characterizing and identifying the novel products formed during its recording time<sup>12</sup>. In most of the cases discussed above, either the essentially almost intact molecular ion or the desolvated species could be assigned through matching of the relevant experimental and calculated isotopic distribution patterns. In a number of cases, definite fragments like a chlorine atom or a CO molecule is lost during the mass spectral process. These ESIMS data together with the elemental analysis data are adequate in establishing the chemical compositions of these new complexes described in the earlier part of this Chapter. The following peaks are found to be common in almost all the complexes discussed above:  $m/z = 331.1$   $[Mo\{H_2(pte_2)\}]^+$ ;  $m/z = 307.1$ ,  $[H_2(pte_2-tsc)]^+$ .

From the above discussion it is evident that the new Schiff base ligand, H<sub>3</sub>(pte<sub>2</sub>-tsc) is a stable one and is able to retain its identity throughout its reactions with a variety of molybdenum starting materials, leading to pure products.

The  $\Lambda_M$  [(9.12 – 32.2) ohm<sup>-1</sup> cm<sup>2</sup> mol<sup>-1</sup>, 301K, CH<sub>3</sub>OH] values for complexes (2), (3), (5), (6) & (7) support the non-electrolytic formulation of these complexes<sup>43</sup>. In case of (4),  $\Lambda_M$  (80.9 ohm<sup>-1</sup> cm<sup>2</sup> mol<sup>-1</sup>, 301K, CH<sub>3</sub>OH) is consistent with the 1:1 electrolytic nature of this complex<sup>43</sup>.

Some useful inferences regarding the ligand coordination sites could be drawn from a comparison of IR spectra of [H<sub>2</sub>(pte<sub>2</sub>)], H<sub>3</sub>(pte<sub>2</sub>-tsc) and the different complexes (2 – 7). Two intense bands with fine structure at 1690 cm<sup>-1</sup> and 1650 cm<sup>-1</sup> of H<sub>2</sub>(pte<sub>2</sub>) corresponding to different types of  $\nu$  (C=O) modes, are replaced by a band at 1647 cm<sup>-1</sup> in (1) corresponding to  $\nu$  (C=O) of O(6) and  $\nu$  (C=N) of C(2') [Scheme (III - 1)]. These two bands are present in slightly modified form in most of these complexes. As per X – ray structural data on different metal – pterin complexes<sup>3, 18, 20, 39</sup>, the M – N(5) bond plays a pivotal role in the pterin ligand chelation process. Again in the free ligand (1), [Scheme (III – 1)] the  $\nu$ (C – O) and  $\nu$ (C– O) +  $\delta$ (OH) modes of the OH(4) group could be located at 1458 cm<sup>-1</sup> and 1236 cm<sup>-1</sup> respectively, indicating its existence in the enol form e.g., involving the amide function in positions 3, 4 [Scheme–(III – 1A)], in some amount. On coordination with the Mo – atom in different complexes (3, 4, 5), the above two IR bands disappear along with the appearance of a new band at around 1238 – 1275 cm<sup>-1</sup> due to  $\nu$ (C – O) mode of the corresponding phenoxide groups [Fig.(III – 11)]<sup>85</sup> involving deprotonation of OH(4).

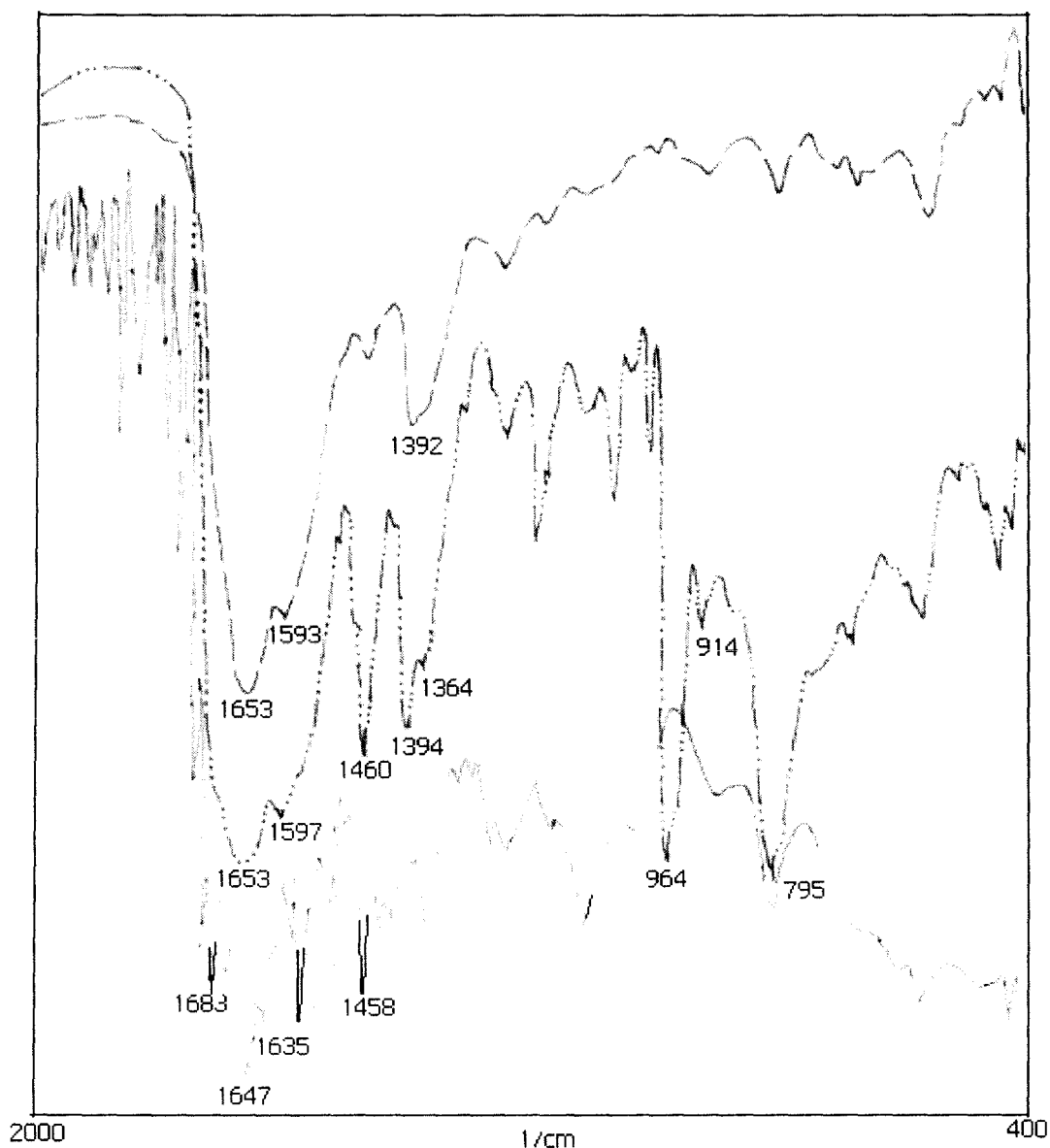


**Fig.(III - 11):** IR spectra (KBr) of (1)[—], (3) [— — —] and (4) [●●● — ●●●]

Besides these, molecular modeling studies (CHEM3D, MM2 calculations corresponding to the lowest energy structure) as stated later indicate involvement of the S – atom (thiosemicarbazide residue) in the complexation process. The frequency of the IR band corresponding to  $\nu(\text{C}=\text{O})$  and  $\nu(\text{C}=\text{N})$  mode has increased from  $1647 \text{ cm}^{-1}$  in free ligand to  $1653 \text{ cm}^{-1}$  in the complexes [Fig.(III - 11)] corroborating the decrease in length of bond; such as C(3)-N(4) bond length has decreased from  $1.3657$  to  $1.3038 \text{ \AA}$  and C(19)-N(17) bond from  $1.3730$  to  $1.2830 \text{ \AA}$  etc. which are presented in Table (III-8)

[atom numbering as per Fig.(III-12)]. Thus, it could be inferred that the Schiff base ligand (1) coordinates to the metal atom involving the three donor atoms e.g., O(4), N(5) and the S – atom. Usually tridentate bi-negative ligand coordination is observed except for one case where it is tri-negative.

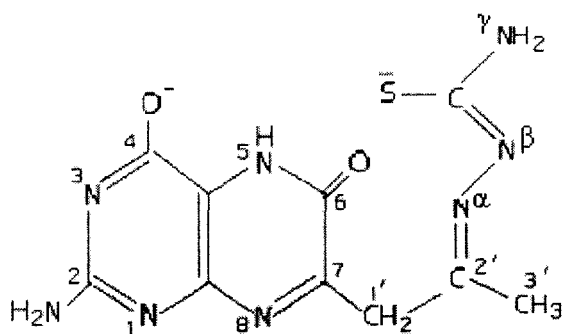
As evident from Fig.(III – 11), some interesting inferences could be drawn regarding the presence or absence of oxomolybdenum core in these cases. In case of (2) there is no  $\nu(\text{Mo} = \text{O}_t)$  or  $\nu(\text{Mo} - \text{O}_b - \text{Mo})$  band in the region  $800 - 1000 \text{ cm}^{-1}$  corresponding to its formulation here as devoid of any oxomolybdenum core. The same is true for complex (3). In complex (4) a pair of IR bands at  $965 \text{ cm}^{-1}$  [ $\nu(\text{Mo} = \text{O}_t)$ ] and another at  $795 \text{ cm}^{-1}$  [ $\nu(\text{Mo} - \text{O}_b - \text{Mo})$ ] characteristic of  $(\text{Mo}_2^{\text{VI}}\text{O}_3)^{6+}$  core could be identified<sup>36</sup>. This core has been identified structurally<sup>55</sup>. Appearance of these new bands in (4) verifies the oxygen atom transfer aspect of the conversion (3)→ (4) [Scheme-(III-3)]. In compound (5) a new band appears at  $790 \text{ cm}^{-1}$  corresponding to the  $(\text{Mo} - \text{O}_b - \text{Mo})$  mode. In (6) two new peaks characteristic of the  $(\text{Mo}_2^{\text{V}}\text{O}_4)^{2+}$  core appear at  $945 \text{ cm}^{-1}$ , [ $\nu(\text{Mo} = \text{O}_t)$ ] and  $790 \text{ cm}^{-1}$ , [ $\nu(\text{Mo} - \text{O}_b - \text{Mo})$ ] respectively. In (7) no IR band is observed in the region  $800 - 1000 \text{ cm}^{-1}$ , but a peak at  $503 \text{ cm}^{-1}$  [ $\nu(\text{Mo} = \text{S}_t)$ ] and another at  $470 \text{ cm}^{-1}$  [ $\nu(\text{Mo} - \text{S}_b - \text{Mo})$ ] assignable to  $(\text{Mo}_2^{\text{VI}}\text{S}_5)^{2+}$  core are observed<sup>38</sup>.

<sup>1</sup>H NMR data (DMSO-*d*<sub>6</sub>) of (1 – 7) have been assigned on the basis of protonic integration data, multiplicity, <sup>1</sup>H-<sup>1</sup>H COSY data and literature value<sup>16(b), 85</sup>. For (1) [Scheme (III – 1)] the –OH(4), NH(5) and NH(3) signals are observed at  $\delta$  12.49 (bs),  $\delta$  11.63 (bs), and  $\delta$  10.04 (bs) respectively indicating the presence of two tautomers [Scheme (III – 1A) and Scheme (III – 1B)] in DMSO solution. The NH<sub>2</sub> ( $\gamma$ ), NH ( $\beta$ ) and NH<sub>2</sub>(2) signals are observed at  $\delta$  7.46 (bs),  $\delta$  7.30 (bs) and  $\delta$  7.11 (bs) respectively. Besides these, the CH<sub>2</sub>(1') and CH<sub>3</sub>(3') signals are observed at  $\delta$  3.57(d, br) and  $\delta$  2.22(t) respectively.

In the pertinent complexes (2 – 7) the –OH(4) signal is absent indicating its deprotonation. The NH(5) signal appears at downfield ( $\delta$  11.10 – 10.98, bs) as compared to the free ligand value in most cases indicating involvement of the NH(5) group in metal coordination process<sup>3, 18, 20, 39</sup>. Both the CH<sub>2</sub>(1') and CH<sub>3</sub>(3') signals are shielded in the

complexes and appear in the region  $\delta$  3.21 – 3.19 (q) and  $\delta$  1.20 – 1.18 (t) respectively. The  $\text{NH}_2$  ( $\gamma$ ) and  $\text{NH}_2(2)$  signals appear in the region  $\delta$  7.06 – 6.75 (bs) and  $\delta$  6.99 – 6.65 (bs) respectively, i.e., shielding is observed for these signals as well.

A comparison of the two Schemes [(III - 1) & (III - 2)] shows the basic change over in electronic structure of the Schiff base ligand (1) during the coordination process, as evident from IR and  $^1\text{H}$  NMR spectral data, including attainment of aromatic character for the pyrimidine ring system of the pterin residue, it involves release of electron density through deprotonation of OH(4) and SH group. This imparts a reducing character to the ligand, leading to the reduction of the molybdenum (VI / V) starting materials during complex formation process. This change in electronic structure involving the entire ligand molecule is responsible for the above mentioned shielding process of the  $\text{CH}_2(1')$ ,  $\text{CH}_3(3')$ ,  $\text{NH}_2(2)$  and  $\text{NH}_2(\gamma)$  protons.



**Scheme (III - 2)**

The  $\text{CH}_3$  – proton signal of  $\text{CH}_3\text{OH}$  and DMF in different complexes are partially buried under the residual solvent peak around  $\delta$  3.3 (absorbed water in  $\text{DMSO-d}_6$ ); the proton signal of the  $\text{H-C(=O)N<}$  residue in DMF appears around  $\delta$  7.95. Although the  $-\text{OH}$  signal of  $\text{CH}_3\text{OH}$  appears around  $\delta$  5.0, in complexes (2) and (7) it appears at  $\delta$  12.34 (bs) indicating strong coordination of the  $-\text{OH}$  group of  $\text{CH}_3\text{OH}$  to the Mo – atom. Coordination of the  $\text{CH}_3\text{OH}$  molecule to the molybdenum atom in different types of compounds, sometimes leading to deprotonation / methoxide coordination, has been proposed by various workers and has been characterized by X-ray crystallographic data<sup>3, 18, 20, 27</sup>.

Now the possible schematic structures of the new compounds were optimized by molecular mechanics calculation (MM2), giving the lowest steric energy ( $\text{Kcal mol}^{-1}$ ) CHEM3D model <sup>87</sup> [e.g., Fig.(III –12) to Fig.(III – 18)], thereby throwing light on both stability and geometry of these compound. The molecular modelling force fields in use for molecular systems can be interpreted in terms of the four key contributions, e.g., bond stretching, angle bending, torsional terms and non-bonded interactions <sup>86, 111, 112</sup>; apart from the lowest steric energy of the molecule, two basic parameters were evaluated, e.g., bond distances ( $\text{\AA}$ ) and bond angles (deg.), the most relevant of which are shown in Table (III – 8) to Table (III – 14), together with the literature data obtained through X-ray structural studies on molybdenum complexes with different pterin ligands and other relevant compounds <sup>3, 5, 20(a-c), 27, 29, 114, 115, 116</sup>; this is in conformity with the recent trends of structure elucidation using optimized computational models <sup>108, 113</sup>.

Concentrating on the chelating aspect of the pterin ligand towards molybdenum, the Mo-N(5) bond plays a pivotal role here [Scheme (III – 1) indicates the O(4), N(5) etc, numbering system] and their bond distances show a fair agreement between the computed and experimental data <sup>3, 5, 20(a-c), 27, 29, 114, 115, 116</sup>; the calculated Mo-O(4) bond distance is slightly shorter than the available X – ray structural data, but this value is close to the Mo – O<sub>b</sub> bond distance (1.88 – 1.97  $\text{\AA}$ ) of Mo – O<sub>b</sub> – Mo bridges ( of binuclear complex ) and is much longer than the terminal Mo=O<sub>t</sub> bond distance (1.66 – 1.67  $\text{\AA}$ )<sup>3, 5, 20(a-c), 27, 29, 114, 115, 116</sup>.

Fig.(III –12) represents the most stable CHEM3D form (Steric energy = 10.006  $\text{Kcal mol}^{-1}$ ) of (1). In this form, the pterin ligand contains the C(9)-substituent part (with the thiosemicarbazide residue) on the O(11), N(7)- side, as is present in the most stable CHEM3D representation of the metal complexes. The CHEM3D form which contains C(9)- substituent part on the N(6), N(10) side, possesses highest amount of energy among all the probable forms of (1) and not considered here.

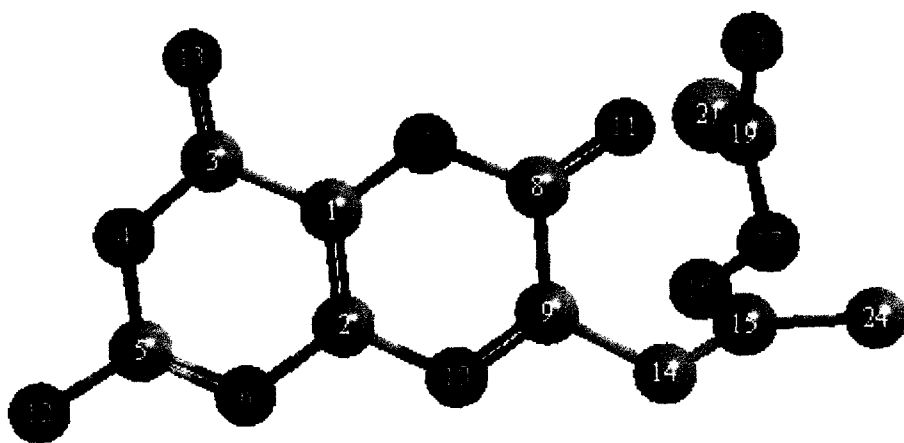


**Fig.(III-12):** The optimized geometry (CHEM3D model obtained through MM2 calculations) of (1) with a steric energy of 1.61 Kcal mol<sup>-1</sup>. Its numbering system is set by the software used<sup>87</sup> and is different from that in Scheme (III - 1).

**Table (III - 8):** Comparison of selected optimized bond lengths (Å) and bond angles (deg.) in the free ligand (1) and its molybdenum complex (2)

Atoms	Bond Distances(Å) <sup>†</sup>	Atoms	Bond Distances(Å) <sup>†</sup>
C(1)-C(3)	1.47 [1.45]	C(19)-S(21)	1.58 [1.83]
C(1)-C(2)	1.37 [1.38]	N(4)-C(5)	1.35 [1.42]
C(1)-N(7)	1.35 [1.40]	C(5)-N(12)	1.37 [1.30]
C(9)-N(10)	1.28 [1.29]	C(3)-N(4)	1.36 [1.30]
C(19)-N(20)	1.37 [1.46]	C(9)-C(14)	1.50 [1.51]
C(14)-C(15)	1.50 [1.51]	C(2)-N(10)	1.41 [1.41]
C(8)-C(9)	1.49 [1.49]	C(19)-N(17)	1.37 [1.28]
C(15)-C(24)	1.49 [1.49]	C(5)-N(6)	1.31 [1.41]
N(16)-N(17)	1.36 [1.38]	C(15)-N(16)	1.26 [1.27]
C(3)-O(13)	1.23 [1.38]	N(7)-C(8)	1.36 [1.38]
C(8)-O(11)	1.22 [1.23]	C(2)-N(6)	1.41 [1.38]

Angle Atoms	Bond Angle(deg.) <sup>†</sup>	Angle Atoms	Bond Angle(deg.) <sup>†</sup>
N(10)-C(9)-C(8)	123.5 [122.9]	C(1)-C(3)-N(4)	114.9 [120.5]
C(9)-C(8)-N(7)	114.7 [114.9]	C(1)-C(2)-N(10)	120.5 [119.0]
C(5)-N(4)-C(3)	124.8 [117.6]	C(1)-C(2)-N(6)	121.3 [114.2]
N(4)-C(5)-N(6)	121.0 [121.5]	C(3)-C(1)-C(2)	118.4 [124.1]
C(9)-N(10)-C(2)	118.4 [118.8]	C(2)-C(1)-N(7)	120.5 [122.1]
C(1)-N(7)-C(8)	122.4 [118.1]	C(2)-N(6)-C(5)	119.6 [121.8]

<sup>†</sup>From the respective optimized geometries (MM2 calculations)<sup>87</sup>. Atom numbering system corresponds to Fig.(III –12). Free ligand data are mentioned outside third bracket and the data derived from its molybdenum complex, (2), are mentioned within third bracket.

Tables (III – 8) shows the bond lengths and bond angles of the free ligand, H<sub>3</sub>(pte<sub>2</sub>-tsc), and that of the pterin ligand residue in one of the complex of this series e.g., complex (2). Comparing these two sets of data it is clear that both bond lengths and bond angles of the ligand residue have undergone a visible change in it's complex suggesting definite complexation of the H<sub>3</sub>(pte<sub>2</sub>-tsc) ligand with molybdenum metal. In comparison to the free ligand (1), the following bond lengths are increased in the complex: C(1) – N(7) from 1.35 Å to 1.40 Å, C(3) – O(13) from 1.23 Å to 1.38 Å and C(19) – S(21) from 1.58 Å to 1.83 Å. This observation is consistent with the N(7), O(13) and S(21) [Fig.(III –12)] atoms' bonding with the molybdenum atom [compare with Fig.(III –13)] leading to depletion of electron density from the bonds immediate to the bonds between the metal and these atoms (i.e., the bonds mentioned above) and hence the observed increase in bond lengths in the complex. The C(5) – N(12) bond length has undergone a decrease from 1.37 Å to 1.30 Å on complexation indicating the N(12) [N(2) as per Scheme – (III-1)] lone pairs' participation in metal coordination via the pterin rings. Some other bond lengths, such as, N(4) – C(5), C(19) – N(20), C(19) – N(17) etc. have also suffered visible change due to redistribution of overall electron density on metal coordination.

This observation is reflected in different physical data, such as, UV-VIS,  $^1\text{H}$  NMR, fluorescence, IR spectra etc. of the free ligand (1) and its molybdenum complexes discussed later. All these data support increased electron density in the pterin rings of the ligand part in almost all the molybdenum complexes of (1).

Fig.(III -13) shows the lowest energy (Steric energy = 13.68 Kcal mol $^{-1}$ ) CHEM3D model of (2) containing slightly distorted trigonal bi-pyramidal (TBP) geometry around the Mo $^{\text{IV}}$ -centre. The O(13), N(7) & S - atom of [(pte $_2$ -tsc)] $^{3-}$  ligand residue occupy three coordination sites; and the methoxy group (CH $_3$ O) and CH $_3$ OH molecule complete the coordination geometry. The case of CH $_3$ O- coordination is an X-ray crystallographically established one and reported by several authors <sup>7(a),18(a)</sup>.

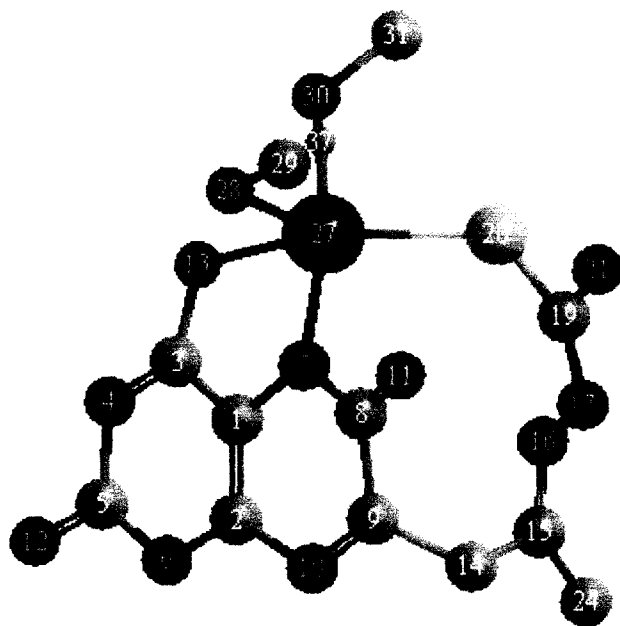


**Fig.(III-13):** The optimized geometry (CHEM3D model obtained through MM2 calculations) of (2) with a steric energy of 13.68 Kcal mol $^{-1}$ . Its numbering system is set by the software used<sup>87</sup> and is different from that in Schemes (III - 1).

**Table (III-9):** Comparison of selected computed bond lengths(Å) and bond angles (deg.) involving Mo – atom in (2) from the optimized geometry [Fig.(III –13), MM2 calculations] with the available literature data (in parenthesis) from X-ray structural studies\*

Atoms	Bond Distances(Å) <sup>+</sup>	Atoms	Bond Distances(Å) <sup>+</sup>
O(13)-Mo(27)	1.96(2.23) <sup>3(c)</sup>	O(30)-Mo(27)	2.07(2.32) <sup>109</sup>
S(20)-Mo(27)	2.33(2.37) <sup>109, 110</sup>	O(28)-Mo(27)	1.95
N(7)-Mo(27)	1.99(2.02) <sup>3(c)</sup>		

Angle Atoms	Bond Angle(deg.) <sup>+</sup>	Angle Atoms	Bond Angle(deg.) <sup>+</sup>
O(13)-Mo(27)-S(20)	153.9	S(20)-Mo(27)-N(7)	96.0
O(13)-Mo(27)-N(7)	81.4	O(28)-Mo(27)-N(7)	86.4
O(28)-Mo(27)-O(30)	87.6	O(13)-Mo(27)-O(30)	90.2
S(20)-Mo(27)-O(28)	126.8		

<sup>+</sup> Here O(13) and N(7) correspond to O(4) and N(5) donor atoms respectively of the pterin ring as per Scheme (III – 1), while N(16), N(17) and N(21) correspond to N(α), N(β) and N(γ) respectively of the same scheme.

\* X-ray structural data have been collected from the references mentioned as superscript on the data within parenthesis.

Table (III – 9) shows few relevant bond length and bond angle data of (2), together with the X-ray structural data on molybdenum complexes of pterin ligand obtained from the literature<sup>3(c), 109, 110</sup>. This approach of rationalizing optimized structural data, is in line with the recent trends in structure (and property) elucidation<sup>48, 86, 108, 179</sup>. The agreement between the computed bond lengths and the literature X-ray structural data is fair, especially for S(20) – Mo(27) and N(7) – Mo(27) [Table (III – 9)]. Of the different donor atoms from the pterin ligand, O(4) and N(5) atoms [this numbering system corresponds to Scheme (III – 1)] play a major role in the metal-ligand bonding process; incidentally in molybdenum–pterin complexes the pivotal role of the Mo-N(5) bond has been verified through X-ray crystallography<sup>20(a,d), 27, 114, 115, 116</sup>. From chemical and X-ray structural studies on 6-substituted pterins, it has been inferred that sufficiently

greater basicity / nucleophilicity resides at N(5) than at N(8) of the pterin ring, thereby influencing its above-mentioned coordinating ability<sup>88(a), 119</sup>. Another important factor in this direction is the close tally of Mo(27) – S(20) bond length from CHEM3D data with available X-ray data.. Considering the length of 7-sulphur chain [numbering as per Scheme (III – 1)] of the ligand, the S(20)-atom may be compared with that of a S – donor from peptide chain in oxomolybdoenzymes<sup>2</sup>.

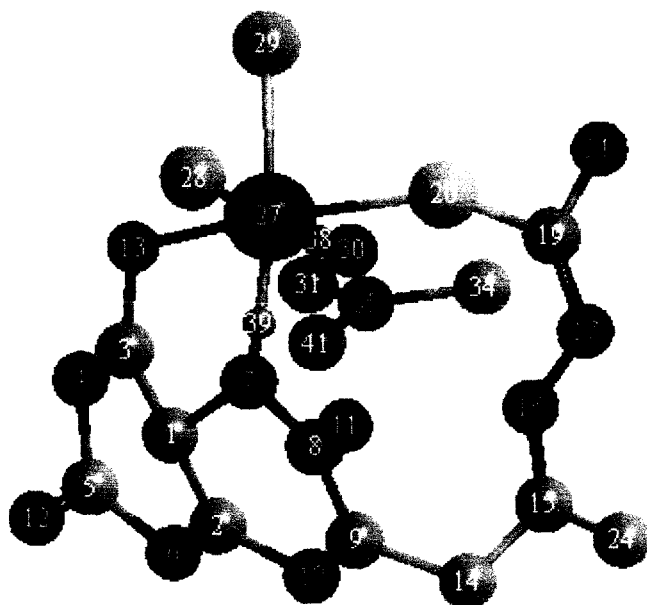


**Fig.(III-14):** The optimized geometry (CHEM3D model obtained through MM2 calculations) of (3) with a steric energy of 14.29 Kcal mol<sup>-1</sup>. Its numbering system is set by the software used<sup>87</sup> and is different from that in Scheme (III- 1).

**Table (III-10):** Comparison of selected computed bond lengths(Å) and bond angles (deg.) involving the Mo – atom in (3) from the optimized geometry [Fig.(III –14), MM2 method] with the available literature data (in parenthesis) from X-ray structural studies\*

Atoms	Bond Distances(Å) <sup>+</sup>	Atoms	Bond Distances(Å) <sup>+</sup>
S(20)-Mo(27)	2.34(2.37) <sup>109,110</sup>	Mo(27)-Cl(29)	2.31(2.38) <sup>3(c)</sup>
Cl(28)-Mo(27)	2.30(2.38) <sup>3(c)</sup>	N(7)-Mo(27)	2.14(2.02) <sup>3(c)</sup>
O(30)-Mo(27)	2.16(2.32) <sup>109</sup>	O(13)-Mo(27)	1.97(2.23) <sup>3(c)</sup>

Angle Atoms	Bond Angle(deg.) <sup>+</sup>	Angle Atoms	Bond Angle(deg.) <sup>+</sup>
S(20)-Mo(27)-Cl(29)	91.6	Cl(28)-Mo(27)-N(7)	88.8
Cl(28)-Mo(27)-O(30)	179.8	S(20)-Mo(27)-N(7)	96.7
Cl(28)-Mo(27)-O(13)	95.2	S(20)-Mo(27)-O(30)	89.5
N(7)-Mo(27)-O(30)	91.3	N(7)-Mo(27)-O(13)	80.2(74.1) <sup>3(c)</sup>
Cl(29)-Mo(27)-Cl(28)	93.7	O(30)-Mo(27)-O(13)	85.1
Cl(29)-Mo(27)-N(7)	171.4	C(3)-O(13)-Mo(27)	112.6(112.1) <sup>3(c)</sup>
Cl(29)-Mo(27)-O(30)	86.2	Mo(27)-N(7)-C(1)	117.5(119.3) <sup>3(c)</sup>
Cl(29)-Mo(27)-O(13)	91.3		

<sup>+</sup> Here O(13) and N(7) correspond to O(4) and N(5) donor atoms respectively, of the pterin ring as per Scheme (III – 1), while N(16), N(17) and N(21) correspond to N( $\alpha$ ), N( $\beta$ ) and N( $\gamma$ ) respectively.

<sup>\*</sup> X-ray structural data have been collected from references mentioned as superscript on the data within parenthesis.

The most stable (Steric energy = 14.29 Kcal mol<sup>-1</sup>) CHEM3D representation of **(3)** shows a distorted octahedral geometry around the Mo<sup>IV</sup>-atom [Fig.(III –14)]. The O(4), N(5) & S – atom of [H(pte<sub>2</sub>-tsc)]<sup>2-</sup> ligand residue [Scheme(III–2)] have occupied three positions of the octahedron and other three positions are occupied by two Cl atoms and one DMF molecule. Here, N(5), and O- atom of the DMF molecule are bonded to the Mo –atom through co-ordinate bonds (pink colour) but the other four are covalent bonds.

Similar to the case of **(2)** above, there is a good matching between the computed and X-ray structural bond length and bond angle data of **(3)**, especially for S(20)-Mo(27), N(7)-Mo(27), Mo(27)-Cl(28/29) [Table (III–10)]. This reflects the structural stability of **(3)** as presented in Fig.(III-14) above and supports the arguments / statements made for **(2)** in support of its correlation with oxomolybdoenzymes.

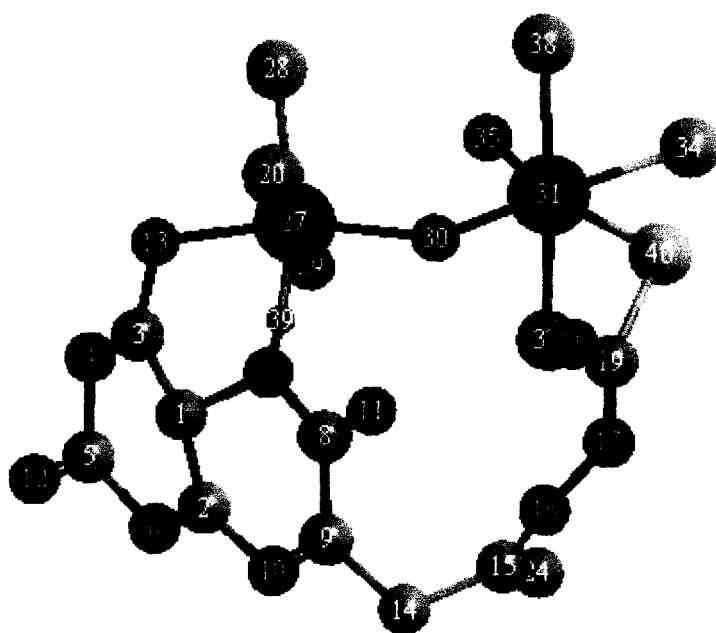


**Fig.(III-15):** The optimized geometry (CHEM3D model obtained through MM2 calculations) of (4) with a steric energy of 27.06 Kcal mol<sup>-1</sup>. Its numbering system is set by the software used<sup>87</sup> and is different from that in Scheme (III - 1).

**Table (III-11):** Comparison of selected computed bond lengths(Å) and bond angles (deg.) involving the Mo - atom in (4) from the optimized geometry [Fig.(III-15), MM2 method] with the available literature data (in parenthesis) from X-ray structural studies\*

Atoms	Bond Distances(Å) <sup>+</sup>	Atoms	Bond Distances(Å) <sup>+</sup>
S(40)-Mo(31)	2.35(2.37) <sup>109, 110</sup>	Mo(31)-Cl(34)	2.32(2.38) <sup>3(c)</sup>
N(7)-Mo(27)	2.16(2.02) <sup>3(c)</sup>	Mo(31)-Cl(38)	2.31(2.38) <sup>3(c)</sup>
Cl(28)-Mo(27)	2.31(2.38) <sup>3(c)</sup>	Mo(27)-Cl(20)	2.30(2.38) <sup>3(c)</sup>
Mo(31)-Cl(37)	2.31(2.38) <sup>3(c)</sup>	Mo(31)-O(35)	1.96(1.70) <sup>108</sup>
O(30)-Mo(31)	1.97(1.93) <sup>19</sup>	Mo(27)-O(29)	1.96(1.70) <sup>108</sup>
O(13)-Mo(27)	1.98(2.23) <sup>3(c)</sup>	Mo(27)-O(30)	1.97

Angle Atoms	Bond Angle(deg.) <sup>+</sup>	Angle Atoms	Bond Angle(deg.) <sup>+</sup>
Cl(38)-Mo(31)-O(30)	89.7(89.6) <sup>108</sup>	Cl(38)-Mo(31)-Cl(34)	90.0(91.9) <sup>108</sup>
N(7)-Mo(27)-O(13)	79.5(74.1) <sup>3(c)</sup>	C(3)-O(13)-Mo(27)	111.4(112.1) <sup>3(c)</sup>
C(1)-N(7)-Mo(27)	117.8(119.3) <sup>3(c)</sup>	O(29)-Mo(27)-O(13)	80.1
S(40)-Mo(31)-Cl(38)	91.6	O(30)-Mo(27)-N(7)	87.4
Cl(28)-Mo(27)-Cl(20)	95.0	Mo(27)-O(30)-Mo(31)	123.8
O(30)-Mo(27)-O(29)	96.2	O(35)-Mo(31)-O(30)	105.2
S(40)-Mo(31)-O(30)	89.4	O(30)-Mo(27)-O(13)	166.4
S(40)-Mo(31)-Cl(34)	86.1	Cl(28)-Mo(27)-O(13)	85.3
Cl(28)-Mo(27)-O(29)	86.0		

<sup>+</sup> Here O(13) and N(7) correspond to O(4) and N(5) donor atoms respectively, of the pterin ring as per Scheme (III – 1), while N(16), N(17) and N(21) correspond to N( $\alpha$ ), N( $\beta$ ) and N( $\gamma$ ) respectively.

<sup>\*</sup> X-ray structural data have been collected from references mentioned as superscript on the data within parenthesis.

Fig.(III –15) exhibits distorted octahedral geometry around each of the Mo<sup>VI</sup> – atoms bonded through a bridging O- atom in its (Mo<sup>VI</sup><sub>2</sub>O<sub>3</sub>) core in the lowest energy (Steric energy = 27.06 Kcal mol<sup>-1</sup>) structural form of (4). The O(4) & N(5) of [H(pte<sub>2</sub>-tsc)]<sup>2-</sup> ligand residue [Scheme (III – 2)] make covalent and co-ordinate (pink colour) bonds respectively to one of the two Mo-atoms. The S – atom of the C(7)-substituent is coordinated to another molybdenum atom. All the other bonds to the metal atoms are covalent in nature. Two (Mo = O<sub>i</sub>) bands of the (Mo<sup>VI</sup><sub>2</sub>O<sub>3</sub>) core are essentially cis in nature here, as revealed from different bond angles data in Table (III–11). Actually X-ray structural data on different pteridine system indicate non-planarity corresponding to the most stable thermodynamic form<sup>88</sup>.

The close tally of Mo(31)–S(40) bond length from CHEM3D data with available X-ray data is significant. Considering the length of 7-sulphur chain [numbering as per Scheme (III – 1)] of the ligand, the S(40)-atom may be compared with that of a S–donor from peptide chain in oxomolybdoenzymes <sup>2</sup>. The close agreements in other cases namely, N(7)-Mo(27), Mo(27/31)-Cl(20/28/34/37/38) etc. bond lengths and Cl(38)-Mo(31)-O(30), Cl(38)-Mo(31)-Cl(34), C(3)-O(13)-Mo(27), C(1)-N(7)-Mo(27) etc. bond angles supports the CHEM3D data discussions already made above in case of (2).

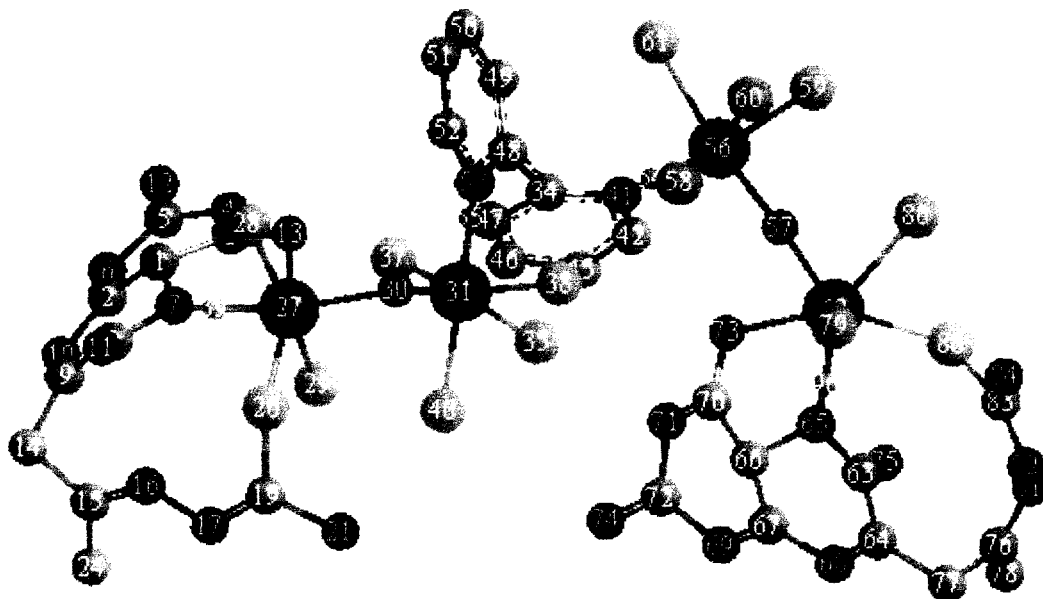


**Fig.(III–16):** The optimized geometry (CHEM3D model obtained through MM2 calculations) of (5) with a steric energy of 57.23 Kcal mol<sup>-1</sup>. Its numbering system is set by the software used <sup>87</sup> and is different from that in Scheme (III – 1).

**Table (III–12):** Comparison of selected computed bond lengths(Å) and bond angles (deg.) involving the Mo – atom in (5) from the optimized geometry [Fig.(III –16), MM2 method] with the available literature data (in parenthesis) from X-ray structural studies\*

Atoms	Bond Distances(Å) <sup>†</sup>	Atoms	Bond Distances(Å) <sup>†</sup>
N(41)-Mo(56)	2.13(2.02) <sup>3(c)</sup>	Mo(27)-Cl(29)	2.31(2.30) <sup>3(c)</sup>
S(20)-Mo(27)	2.34(2.37) <sup>109, 110</sup>	N(53)-Mo(31)	2.12(2.18) <sup>109</sup>
N(7)-Mo(27)	2.17(2.02) <sup>3(c)</sup>	Mo(31)-Cl(40)	2.32(2.30) <sup>3(c)</sup>

Mo(56)-Cl(58)	2.31(2.30) <sup>3(c)</sup>	O(73)-Mo(62)	2.00(2.229) <sup>3(c)</sup>
Mo(56)-Cl(60)	2.32(2.30) <sup>3(c)</sup>	Mo(31)-Cl(38)	2.32(2.30) <sup>3(c)</sup>
O(30)-Mo(31)	1.98(2.30) <sup>3(c)</sup>	S(86)-Mo(62)	2.37(2.37) <sup>109, 110</sup>
Mo(56)-Cl(61)	2.32(2.30) <sup>3(c)</sup>	O(13)-Mo(27)	1.98(2.23) <sup>3(c)</sup>
N(65)-Mo(62)	2.24(2.02) <sup>3(c)</sup>	Mo(62)-Cl(80)	2.34(2.30) <sup>3(c)</sup>
Mo(31)-Cl(35)	2.31(2.30) <sup>3(c)</sup>	Mo(27)-O(30)	1.97(1.93) <sup>19</sup>

<b>Angle Atoms</b>	<b>Bond Angle(deg.)<sup>+</sup></b>	<b>Angle Atoms</b>	<b>Bond Angle(deg.)<sup>+</sup></b>
N(65)-Mo(62)-O(73)	74.1(74.1) <sup>3(c)</sup>	Cl(38)-Mo(31)-Cl(35)	90.8(91.1) <sup>108</sup>
C(3)-O(13)-Mo(27)	114.7(112.1) <sup>3(c)</sup>	C(1)-N(7)-Mo(27)	118.02(119.3) <sup>3(c)</sup>
N(53)-Mo(31)-Cl(40)	179.8	O(57)-Mo(62)-O(73)	76.0
Cl(37)-Mo(31)-Cl(40)	86.6	Cl(37)-Mo(31)-Cl(38)	82.7
Cl(37)-Mo(31)-Cl(35)	169.3	N(7)-Mo(27)-S(20)	87.9
N(65)-Mo(62)-S(86)	74.5	O(30)-Mo(31)-Cl(38)	165.6
O(30)-Mo(31)-Cl(35)	78.8	Cl(40)-Mo(31)-Cl(38)	88.6
O(73)-Mo(62)-S(86)	148.1	Mo(31)-O(30)-Mo(27)	126.7
N(7)-Mo(27)-O(13)	81.0	N(53)-Mo(31)-Cl(37)	93.6
N(7)-Mo(27)-O(30)	164.1	S(20)-Mo(27)-O(30)	107.7
N(41)-Mo(56)-O(57)	91.1	S(20)-Mo(27)-O(13)	167.6

<sup>+</sup> Here O(13/73) and N(7/65) correspond to O(4) and N(5) donor atoms respectively, of the pterin ring as per Scheme (III – 1), while N(16/81), N(17/82) and N(21/84) correspond to N( $\alpha$ ), N( $\beta$ ) and N( $\gamma$ ) respectively.

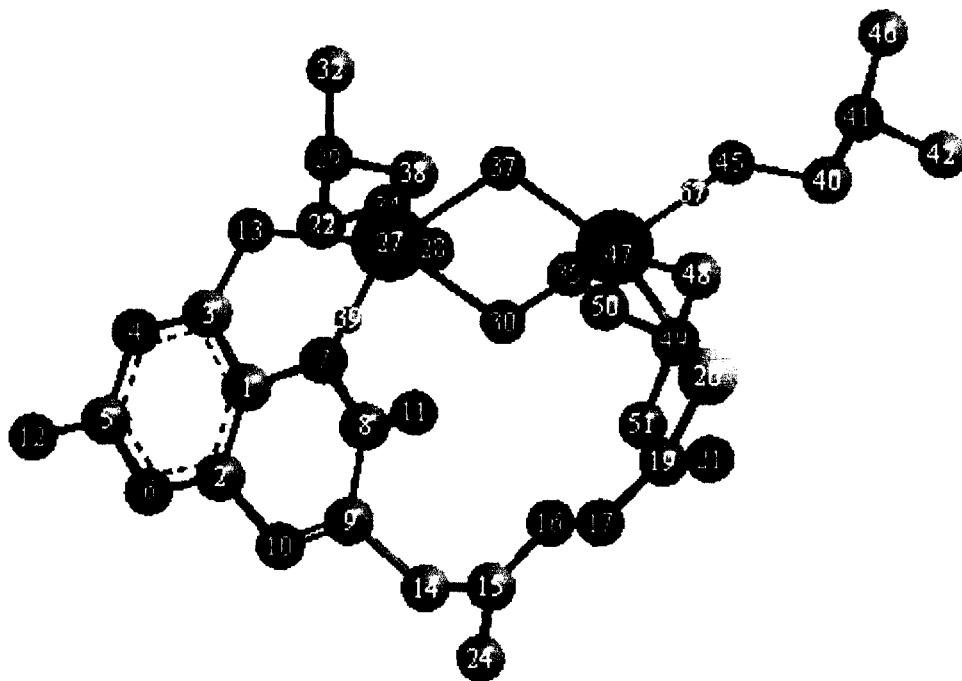
<sup>\*</sup> X-ray structural data have been collected from references mentioned as superscript on the data within parenthesis.

Fig.(III –12) represents the lowest energy (Steric energy = 57.23 Kcal mol<sup>-1</sup>) CHEM3D model geometry of (5). Here, again the aromatic or planner nature of the pterin ligand residue hinders its needed puckering in this bulky molecule and lowers its stability. The geometry around each Mo<sup>V</sup> – atom is distorted octahedral. Here, O(4) & S – atom of [H(pte<sub>2</sub>-tsc)]<sup>2-</sup> ligand residue [Scheme (III – 2)] and all the Cl – atoms make covalent bonds with the metal atoms, while N(5) of pterin ring and the N – atoms of ‘bipy’ are bonded to the Mo<sup>V</sup> – atom through co-ordinate bonds (pink colour). Air stability (low hygroscopic nature) of this tetra-nuclear species indicates that the Mo<sup>V</sup> – atoms are saturated with respect to both electronegativity as well as co-ordination number. Interesting aspect of synthesis of this compound is that the original starting material, [Mo<sup>V</sup>OCl<sub>3</sub>(bipy)], contained 3Cl atoms per Mo atom and the product (5), also maintains the same ratio, Mo : Cl = 1 : 3. Some of the ‘bipy’ ligands are lost and the vacant co-ordination positions are taken up by the [H(pte<sub>2</sub>-tsc)]<sup>2-</sup> ligand residue as well as by the bridging O – atoms.

The ESIMS peak of (5) at m/z = 894.3, [M/2 – Cl – 3H]<sup>+</sup>, can also be interpreted in the light of CHEM3D optimized geometry of the complex [Fig.(III –16)]. Origination of this peak corresponds to the breakage of the actual tetra-nuclear molecule into two binuclear species, followed by loss of one chlorine and three hydrogen atoms from each, where ‘M’ is the molecular formula of the complex (F.W.=1865.76.)<sup>7(a), 14, 15</sup>. This symmetric cleavage is possible by breaking of C(34) – C(48) bond of the bipyridyl residue in the molecular structure of (5).

Some specific data such as, Mo(27/62)– S(20/86), Mo(27/31/56/62)– N(7/53/41/65) etc. bond lengths and N(65)-Mo(62)-O(73), Cl(38)-Mo(31)-Cl(35) etc bond angles show close tally with the X-ray structural data and this is consistent with the above CHEM3D data interpretation for (2).

The lowest energy CHEM3D model geometry (Steric energy = 58.49 Kcal mol<sup>-1</sup>) of (6) is represented in Fig.(III-17). It has a distorted octahedral geometry around both the Mo<sup>V</sup> – atoms, O(4) & S –atom of [H(pte<sub>2</sub>-tsc)]<sup>2-</sup> ligand residue [numbering system as per Scheme (III – 2)] are bonded to the Mo – atoms through covalent bonds, whereas, N(5) and O –atoms from the DMF molecules are bonded to the metal atom via the formation of co-ordinate bond (pink colour). Pterin ring's O(4) & N(5) – atoms are bonded to one Mo – atom and the C(7)-substituent's S – atom along with two DMSO molecules are bonded to another Mo – atom of the (Mo<sup>V</sup><sub>2</sub>O<sub>4</sub>)<sup>2+</sup> core. From the bond angle data [Table (III-13)] of O(37)-Mo(27)-O(28) (= 77.7630) and O(30)-Mo(31)-O(35) (= 72.5074) involving the two terminal oxygen atoms, it can be inferred that the (Mo<sup>V</sup><sub>2</sub>O<sub>4</sub>)<sup>2+</sup> core in (6) is essentially trans in nature [Fig.(III-17)]. Its cis isomer was found to be comparatively less stable.



**Fig.(III-17):** The optimized geometry (CHEM3D model obtained through MM2 calculations) of (6) with a steric energy of 58.49 Kcal mol<sup>-1</sup>. Its numbering system is set by the software used<sup>87</sup> and is different from that in Scheme (III – 1).

**Table (III–13):** Comparison of selected computed bond lengths(Å) and bond angles (deg.) involving the Mo-atom in (6) from the optimized geometry [Fig.(III–17), MM2 method] with the available literature data (in parenthesis) from X-ray structural studies\*

Atoms	Bond Distances(Å) <sup>+</sup>	Atoms	Bond Distances(Å) <sup>+</sup>
S(20)-Mo(31)	2.33(2.37) <sup>109, 110</sup>	N(7)-Mo(27)	2.16(2.02) <sup>3(c)</sup>
O(34)-Mo(27)	2.09(2.01) <sup>109</sup>	O(47)-Mo(31)	2.11(2.01) <sup>109</sup>
O(13)-Mo(27)	2.02(2.23) <sup>3(c)</sup>	O(28)-Mo(27)	1.94(1.70) <sup>109</sup>
Mo(31)-O(35)	1.96(1.70) <sup>109</sup>	O(30)-Mo(31)	1.97(1.93) <sup>19</sup>
Mo(27)-O(30)	2.01		

Angle Atoms	Bond Angle(deg.) <sup>+</sup>	Angle Atoms	Bond Angle(deg.) <sup>+</sup>
N(7)-Mo(27)-O(13)	74.4(74.1) <sup>3(c)</sup>	Mo(27)-O(13)-C(3)	111.5(112.1) <sup>3(c)</sup>
Mo(27)-N(7)-C(1)	114.6(119.3) <sup>3(c)</sup>	O(45)-Mo(31)-O(35)	107.0(105.9) <sup>109</sup>
S(20)-Mo(31)-O(37)	160.2(153.0) <sup>109</sup>	S(20)-Mo(31)-O(35)	93.8(97.7) <sup>109</sup>
O(37)-Mo(27)-O(28)	77.8	O(30)-Mo(31)-S(20)	90.2
O(30)-Mo(31)-O(35)	72.5	O(37)-Mo(27)-O(30)	69.4
O(47)-Mo(31)-O(37)	91.2		

<sup>+</sup> Here O(13) and N(7) correspond to O(4) and N(5) donor atoms respectively, of the pterin ring as per Scheme (III – 1), while N(16), N(17) and N(21) correspond to N(α), N(β) and N(γ) respectively.

\* X-ray structural data have been collected from references mentioned as superscript on the data within parenthesis.

Almost all the bond lengths especially S(20)-Mo(31), O(34)-Mo(27), O(47)-Mo(31), N(7)-Mo(27) etc., show good matching between the computed and single crystal X-ray structural data supporting the interpretation presented above for (2) regarding bond length / bond angle data.

Fig.(III-18) reflects slightly distorted octahedral geometry of the new complex (7), in the lowest energy form (Steric energy = 29.22 Kcal mol<sup>-1</sup>), in which the Mo<sup>VI</sup> – centers have slightly distorted octahedral geometry. Here, the ligand residue, [H(pte<sub>2</sub>-tsc)]<sup>2-</sup>, acts as a binegative O(4), N(5), S – donor [numbering system as per Scheme (III-2)], in which the O(4) & S – atoms co-ordinated by covalent bond formation and N(5) & methanolic O – atoms are bonded to the Mo – centers through co-ordinate bond formation (pink colour). Here, (Mo<sup>VI</sup><sub>2</sub>S<sub>5</sub>)<sup>2+</sup> core is essentially in trans form, as supported by the magnitude of S(28)-Mo(31)-S(30) and S(32)-Mo(27)-S(30) bond angles [Table (III-14)]. The unique nature of (Mo<sup>VI</sup><sub>2</sub>S<sub>5</sub>)<sup>2+</sup> core is verified through elemental analysis, ESIMS data and CHEM3D optimized structural matching with the available X-ray structural data. This optimized geometry contains non – aromatic pterin ligand residue which gave the most stable, lowest energy form.

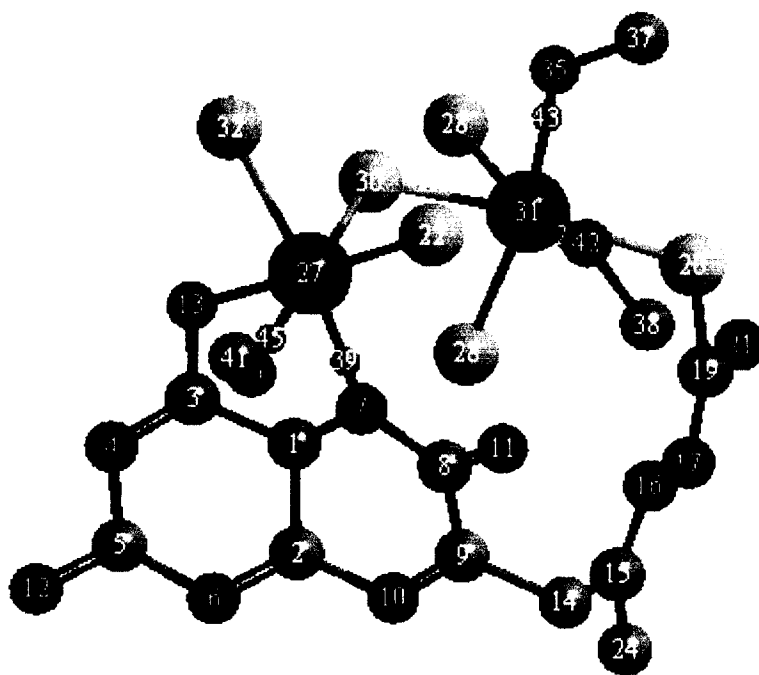


**Fig.(III-18):** The optimized geometry (CHEM3D model obtained through MM2 calculations) of (7) with a steric energy of 29.22 Kcal mol<sup>-1</sup>. Its numbering system is set by the software used<sup>87</sup> and is different from that in Scheme (III – 1).

**Table (III-14):** Comparison of selected computed bond lengths(Å) and bond angles (deg.) involving the Mo – atom in (7) from the optimized geometry [Fig.(III –18), MM2 method] with the available literature data (in parenthesis) from X-ray structural studies\*

<b>Atoms</b>	<b>Bond Distances(Å)<sup>+</sup></b>	<b>Atoms</b>	<b>Bond Distances(Å)<sup>+</sup></b>
S(20)-Mo(31)	2.34(2.37) <sup>109, 110</sup>	N(7)-Mo(27)	2.15(2.02) <sup>3(c)</sup>
O(13)-Mo(27)	1.97(2.23) <sup>3(c)</sup>	O(42)-Mo(31)	2.10 (2.32) <sup>109</sup>
O(40)-Mo(27)	2.08(2.32) <sup>109</sup>	Mo(27)-S(22)	2.34
S(30)-Mo(31)	2.35(2.30) <sup>19</sup>	Mo(31)-S(28)	2.35

<b>Angle Atoms</b>	<b>Bond Angle(deg.)<sup>+</sup></b>	<b>Angle Atoms</b>	<b>Bond Angle(deg.)<sup>+</sup></b>
Mo(27)-O(13)-C(3)	114.7(112.1) <sup>3(c)</sup>	C(1)-N(7)-Mo(27)	116.0(119.3) <sup>3(c)</sup>
N(7)-Mo(27)-O(13)	81.5(74.1) <sup>3(c)</sup>	O(42)-Mo(31)-S(28)	162.8(153.0) <sup>109</sup>
O(40)-Mo(27)-N(7)	81.7	S(28)-Mo(31)-S(20)	87.8
O(40)-Mo(27)-O(13)	88.4	O(40)-Mo(27)-S(32)	99.2
S(28)-Mo(31)-S(30)	91.4	S(32)-Mo(27)-S(30)	86.4
O(13)-Mo(27)-S(30)	86.3	Mo(31)-S(20)-C(19)	117.7
Mo(31)-S(30)-Mo(27)	122.6	O(40)-Mo(27)-S(22)	85.4

<sup>+</sup> Here O(13) and N(7) correspond to O(4) and N(5) donor atoms respectively, of the pterin ring as per Scheme (III-1), while N(16), N(17)and N(21) correspond to N(α), N(β) and N(γ) respectively.

\* X-ray structural data have been collected from references mentioned as superscript on the data within parenthesis.

Similar to the cases of other compounds discussed above, almost all the computed bond lengths and bond angles show good agreement with the available single crystal X-ray data. Some noteworthy cases are, S(20)-Mo(31), N(7)-Mo(27) etc., bond lengths which corroborate the arguments / statements made above regarding CHEM3D data interpretation of (2).

The above discussion on the geometrical aspect of optimized computational model (MM2) of the new complex compounds, having agreement with available X-ray structural data (e.g., bond length, bond angle and overall geometry) provides the frame work for discussion on their spectroscopic, reactivity and other relevant aspects <sup>108, 113</sup>. All the molybdenum complexes discussed in this Chapter, show essentially four types of computed bond angles ( $70^\circ - 86^\circ$ ,  $88^\circ - 100^\circ$ ,  $105^\circ - 130^\circ$  and  $138^\circ - 179^\circ$ ), which are in complete agreement with the X-ray structural studies on different molybdenum – pterin systems with the respective geometries around the Mo – atoms (both mono and binuclear types) <sup>3, 5, 20(a-c), 27, 114, 115, 116</sup>.

Some important observations are made from the comparative study of UV-VIS absorption spectroscopy of the ligand (1) and that of its molybdenum complexes. Three bands of (1) at 310 nm, 355.5 nm and 408 nm are completely modified in the metal complexes and appear at lower wave lengths and with larger intensity, except in (6), where 408 nm ligand peak is missing. A sharp increase in intensity of the UV-VIS absorption bands in the metal complexes can be accounted for <sup>34</sup> electronic drift from –NH<sub>2</sub>(2) group [Scheme (III-2)] towards metal – ligand bonding site via the pterin ring enhancing electron density (essentially  $\pi$ ) in the ligand part and hence the increased intensity in the absorption bands of (2) to (7) <sup>3, 20(a)</sup>. The phenomenon of NH<sub>2</sub>(2) lone pair's participate in metal coordination via the pterin rings is verified by the shortening of N(2)-C(2) [Scheme (III-2)] bond length on coordination with molybdenum atom, as discussed above regarding the interpretation of CHEM3D optimized geometry data of compounds (2) to (7). That metal – pterin coordination leads to greater electron flow resulting higher electron density around the coordination site and other parts of the molecule, are also substantiated by <sup>1</sup>H NMR and fluorescence study [Fig.(III-28)].

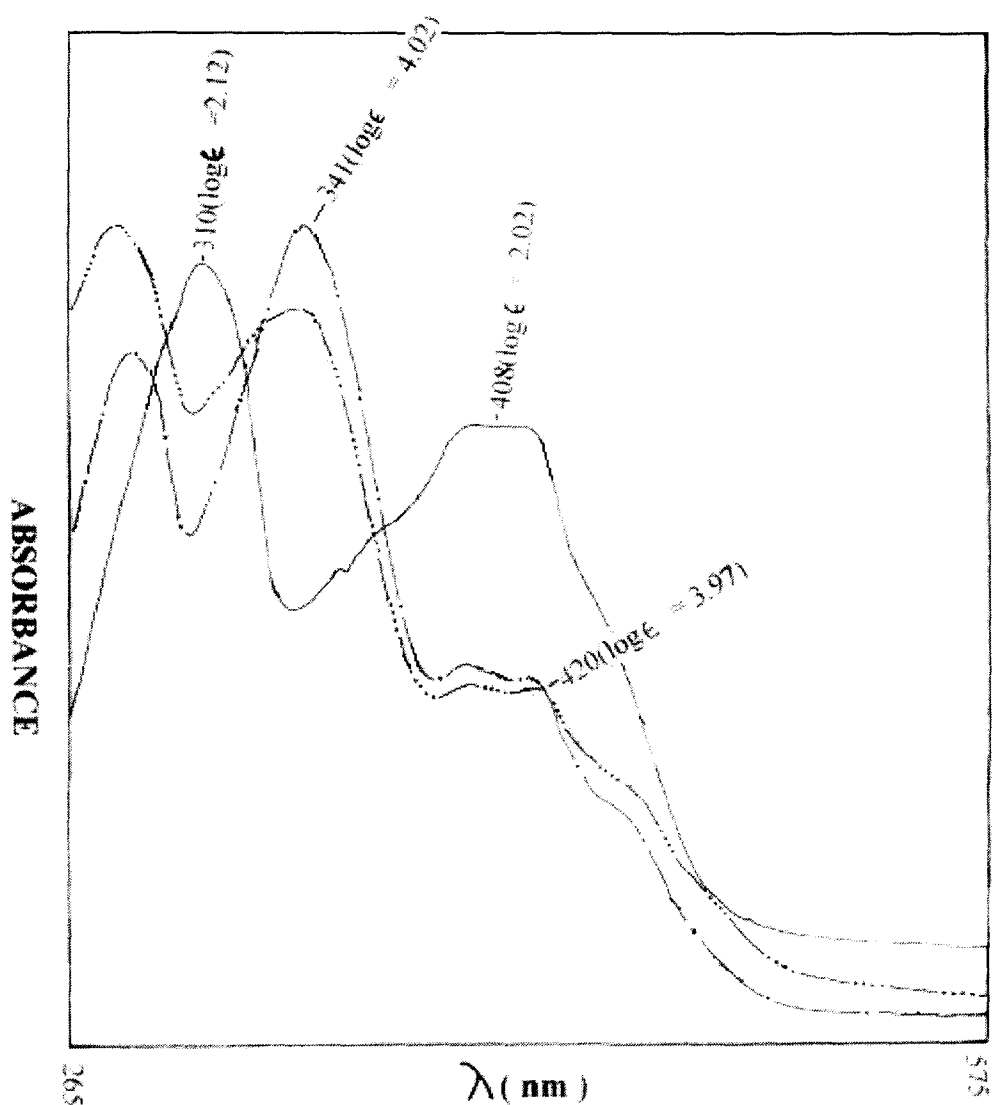


**Fig.(III-19) :** UV-VIS absorption spectra of (1) [—], (2) [- · - · -] and (7) [- · · · -] in DMF.

Another interesting phenomenon observed is the appearance of UV-VIS absorption bands at wave-lengths higher than 400 nm in these complexes [Fig.(III-19)]. One such band is observed at about 420 nm and another at 453 nm. These bands are essentially metal to ligand charge transfer (CT) bands <sup>8(a,b)</sup>; which are absent in the case of the ligand (1). Another high wave length CT band is observed at 491 nm (3.84) in case of (5) and at 486 nm (3.49) for (6).

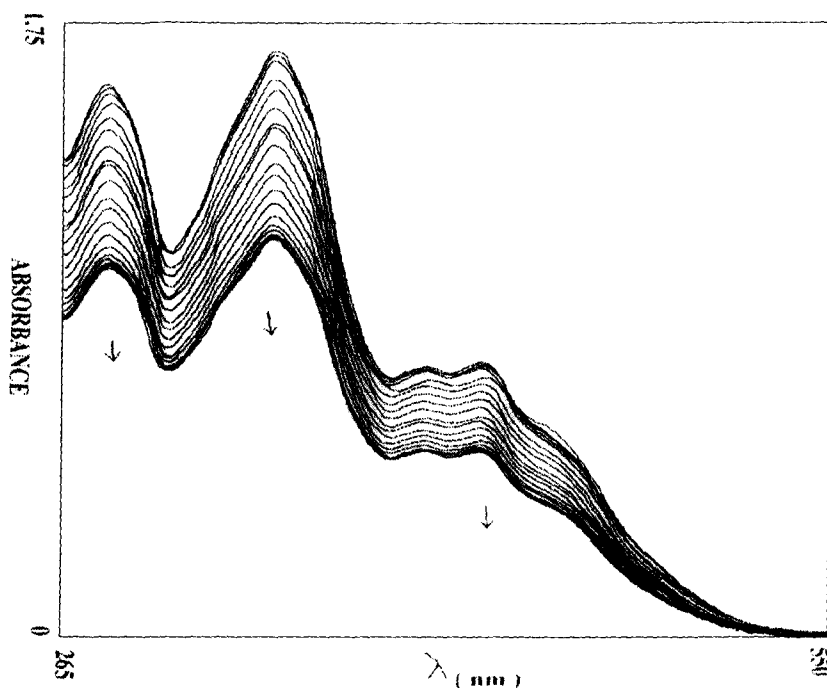


**Fig.(III-20):** UV-VIS absorption spectral changes recorded every 15 min. during the reaction of (2) [ $1.0 \times 10^{-4}$ (M)] with PyN $\rightarrow$ O [ $1.7 \times 10^{-3}$ (M)] in DMF at 301K.

All the present complexes (2-7) proved to be susceptible to oxygen atom transfer (OAT) reactions, along with coupled electron proton transfer (CEPT) reactions in some cases. Compounds (2), (3), (5) & (6) having metal centre (Mo - atom) in lower oxidation states (IV or V) show reactivity with potent oxygen donor species (typical enzyme substrate), like pyridine N - oxide (PyN $\rightarrow$ O), trimethyl amine N-oxide (Me<sub>3</sub>N $\rightarrow$ O) [Fig.s (III-20), (III-22), (III-26) & (III-29)], whereas, they do not react with oxygen abstractor, e.g., triphenyl phosphine (PPh<sub>3</sub>). The oxygen donor species, oxidize compounds (2), (3), (5) & (6) to some higher oxidation state and itself getting reduced to pyridine (PyN) or trimethyl amine (Me<sub>3</sub>N). This indicates that these complexes are in the reduced state. Spectrophotometric study of these reactions in an overlay mode

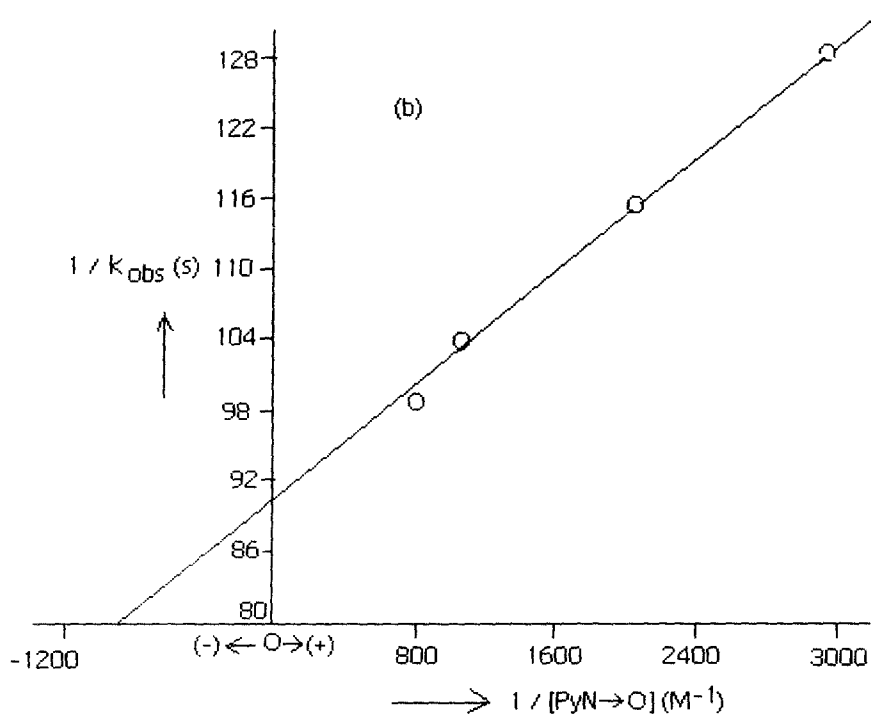
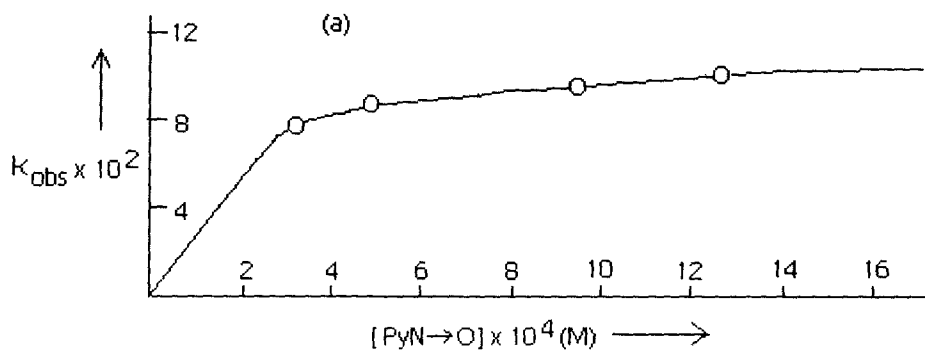


**Fig.(III-21):** (a) Dependence of the rate of reaction of (2) [ $2.9 \times 10^{-5} \text{ (M)}$ ] with  $\text{PyN} \rightarrow \text{O}$  in DMF at 301 K; (b) the corresponding double reciprocal plot.

clearly shows UV-VIS absorption change in the metal – centred charge transfer region as well as intra ligand transition [Fig.s (III-20), (III-22), (III-26) & (III-29) respectively]. So, it is the Mo-atom in these complexes which is the site of oxygen atom transfer reaction.

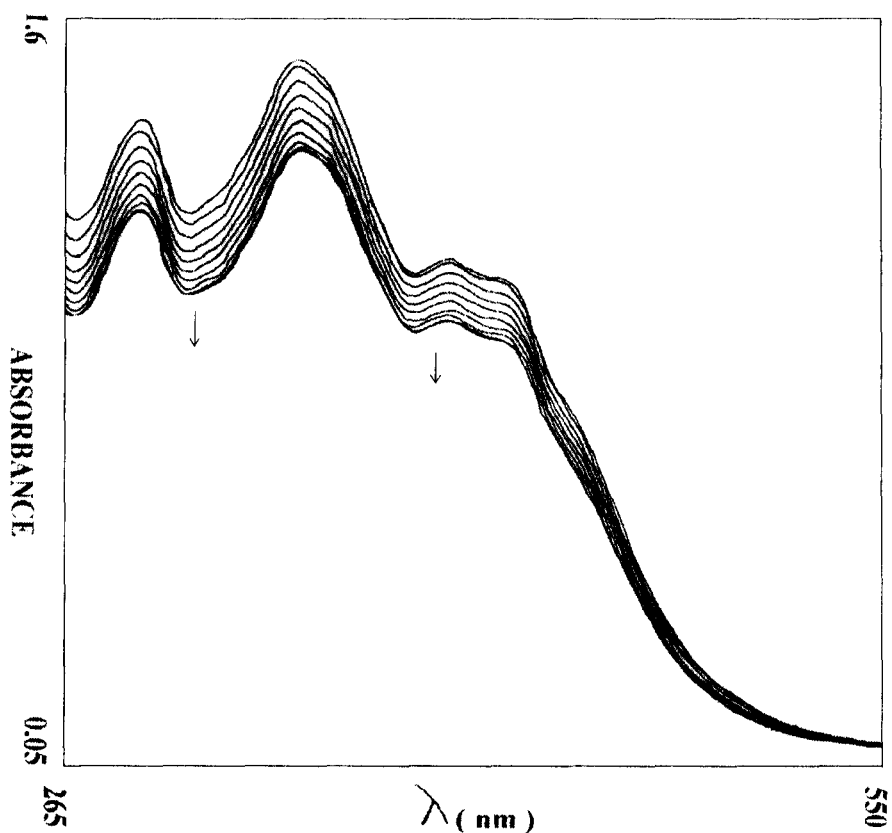


**Fig.(III – 22):** UV–VIS absorption spectral changes recorded every 13 min. during the reaction of (3) [ $6.76 \times 10^{-5}(\text{M})$ ] with  $\text{Me}_3\text{N} \rightarrow \text{O}$  [ $2.2 \times 10^{-3}(\text{M})$ ] in DMF at 301K.

But these molybdenum – pterin complexes have been synthesized from molybdenum starting materials (having V or VI metal oxidation states) and are reduced [except (5)] to some lower oxidation state ( $\text{Mo}^{\text{V}}$  or  $\text{Mo}^{\text{IV}}$ ) during their synthesis. So, the ligand here acts as a reducing agent. In case of (5), as the starting material was already in reduced state ( $\text{Mo}^{\text{V}}$ ), probably for this reason it did not undergo any further reduction by the ligand. Compounds (4) & (7) undergo reaction with a typical oxygen abstractor like  $\text{PPh}_3$  and UV-VIS spectrophotometric monitoring of such reactions have been recorded [Fig.s (III–24) & (III–32) respectively]. This indicates that the Mo – atoms in these compounds are in the higher oxidation state(e.g.,VI). This further corroborates the presence of oxomolybdenum and thiomolybdenum core in (4) & (7) respectively, as shown in their molecular formulas<sup>36</sup> and established by elemental analysis and ESIMS

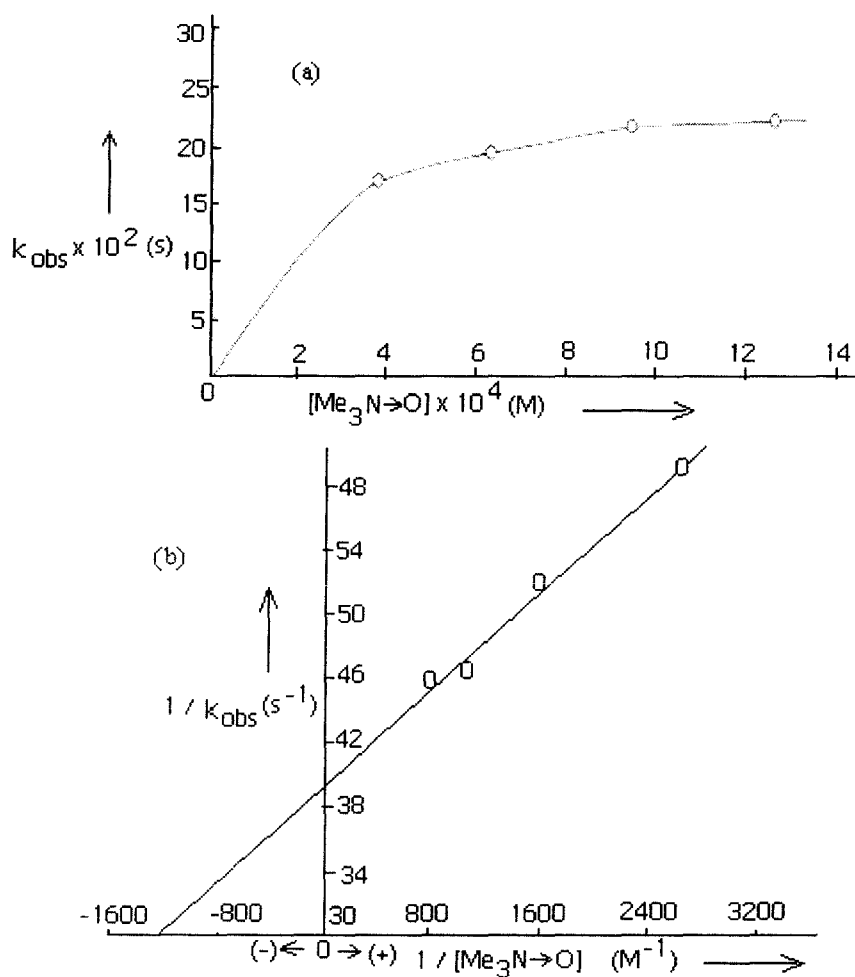
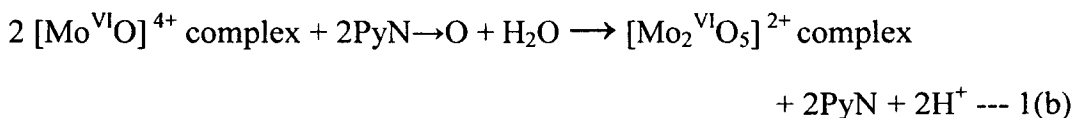


**Fig.(III-23):**(a)Dependence of the rate of reaction of (3) [ $3.46 \times 10^{-5} \text{ (M)}$ ] with  $\text{Me}_3\text{N}=\text{O}$  in DMF at 301 K; (b) the corresponding double reciprocal plot.

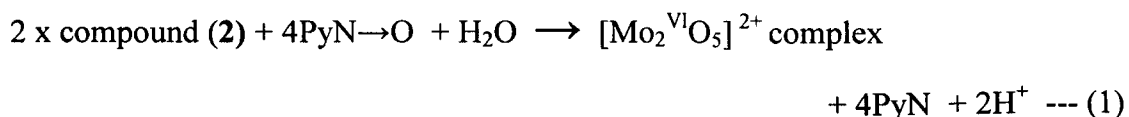
data. In case of (4), existence of  $\text{Mo}^{\text{VI}}$  - centre is likely as it was prepared from (3) (a  $\text{Mo}^{\text{IV}}$  compound) by prolong aerial oxidation. Exceptional nature of (7) with a  $\text{Mo}^{\text{VI}}$  - centre (i.e., the Mo - centre not undergoing reduction during complex synthesis), can be correlated with oxidizing property of the  $(\text{MoS}_4)^{2-}$  starting material; formation of  $(\text{Mo}^{\text{VI}}_2\text{S}_5)^{2-}$  core is also in line with the unique behavior of the Mo - S duo<sup>41</sup> in nature as well as in synthetic system.

Oxidation / reduction of these complexes by  $\text{Me}_3\text{N}\rightarrow\text{O}$ ,  $\text{PyN}\rightarrow\text{O}$  /  $\text{PPh}_3$  is also substantiated through fluorescence study of these molybdenum – pterin complexes and of their oxidized / reduced products. The oxidized product shows ca. one-third fluorescence intensity than that for the original complex [Fig.(III – 28)(a)]. Similarly, the reduced product has 2 – 3 times more intensity in its fluorescence spectrum compared to that of the original complex [Fig.(III – 28(b))]. This observation can be correlated with the electronic structure of the complexes on the basis of higher electron density generated in the complex due to its reduction by  $\text{PPh}_3$  and similarly decrease of electron density after oxidation by  $\text{Me}_3\text{N}\rightarrow\text{O}$  /  $\text{PyN}\rightarrow\text{O}$ . Hence, fluorescence spectral study can be a valuable probe for studying the changes in electronic structure during their reaction.

In few cases, quantitative aspects of these oxygen atom transfer reactions have been established by studying reaction stoichiometry for assigning oxidation state of the metal centers. A known weight of (2) was reacted with its ten equivalent of  $\text{PyN}\rightarrow\text{O}$  in DMF (100 ml) (328K, 50h,  $\text{N}_2$ - atm., darkness) and the amount of pyridine released was estimated gravimetrically as the known compound  $[\text{Zn}(\text{C}_5\text{H}_5\text{N})_2](\text{SCN})_2$  from the petroleum ether extract of the reaction medium<sup>25</sup>. About two moles of pyridine was recovered per mole of (2) added as per the following equations [1(a) and 1(b) are different steps leading to overall reaction (1)]:



**The overall reaction :**



The relevant oxidation product was isolated by evaporation in rotary evaporator, followed by treatment of the residue with methanol, filtration and washing with ether. Physico-chemical studies indicate the composition  $[(\text{Mo}^{\text{VI}}_2\text{O}_5)\{\text{H}(\text{pte-tsc})\}(\text{DMF})_3]$ . The  $\nu(\text{Mo}=\text{O})$  and  $\nu(\text{Mo}-\text{O}-\text{Mo})$  modes characteristic of the  $[\text{Mo}_2^{\text{VI}}\text{O}_5]^{2+}$  core are observed at  $925\text{ cm}^{-1}$ ,  $888\text{ cm}^{-1}$  and  $825\text{ cm}^{-1}$  respectively<sup>20</sup>.  $\text{H}_2\text{O}$  used in Equation 1(b), most probably came from moisture in the solvent and took part in the hydrolysis of  $[\text{Mo}^{\text{VI}}\text{O}]^{4+}$  core followed by oxo-dimerization to give  $[\text{Mo}_2^{\text{VI}}\text{O}_5]^{2+}$  species (Equation 1)<sup>19, 20(c,d)</sup>.

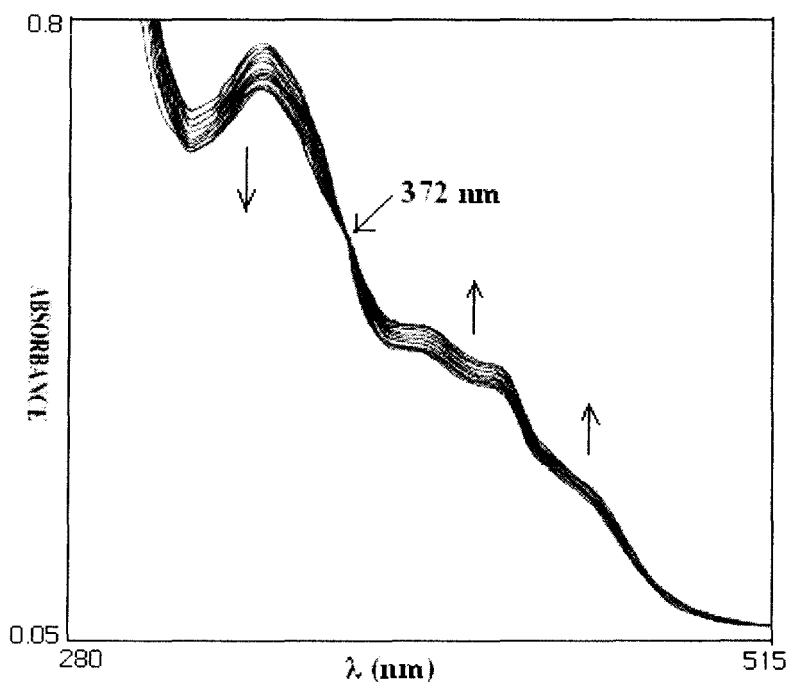


**Fig.(III-24):** UV-VIS absorption spectral changes recorded every 20 min. during the reaction of (4)  $[3.5 \times 10^{-5}(\text{M})]$  with  $\text{PPh}_3$   $[2.86 \times 10^{-4}(\text{M})]$  in DMF at 301K.

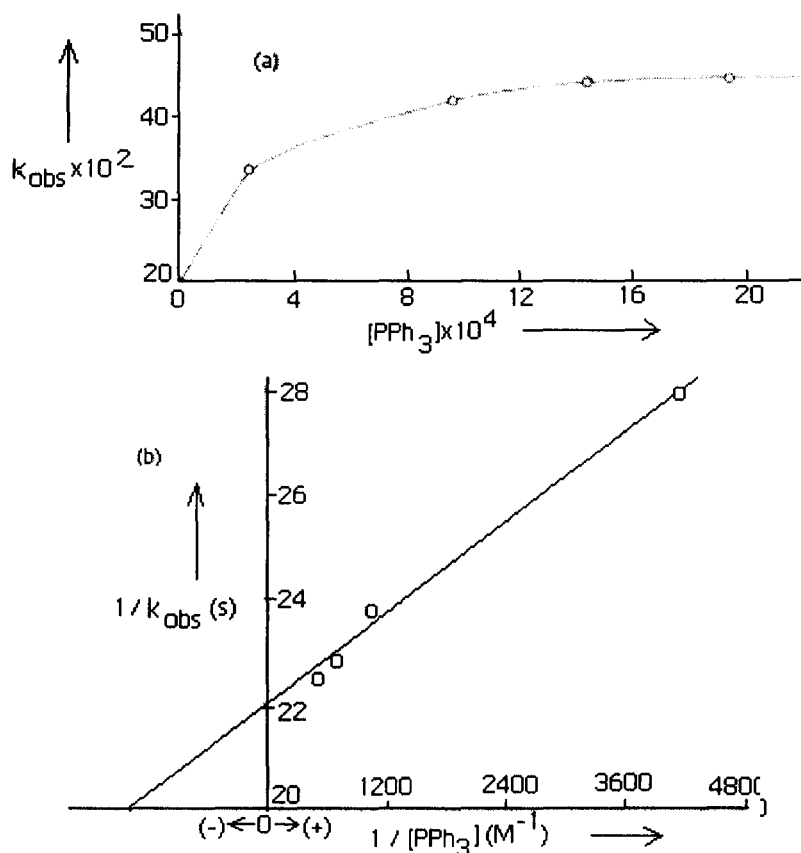
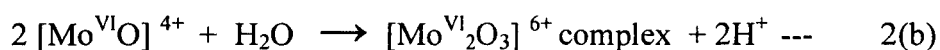
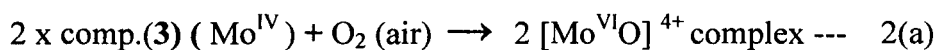
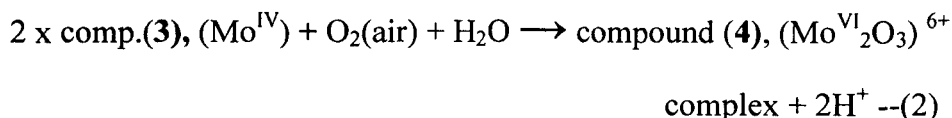


**Fig.(III - 25):**(a)Dependence of the rate of reaction of (4) [ $3.5 \times 10^{-5}$ (M)] with  $\text{PPh}_3$  in DMF at 301 K; (b) the corresponding double reciprocal plot.

Compound (3) undergoes aerial oxidation to give (4), which has been isolated in the solid state and well characterized through different physico-chemical means, as discussed above. Formation of (4) indicates the following reaction stoichiometry [steps 2(a) and 2(b) leading to overall reaction, as shown in (2)] as well as Scheme (III-3).

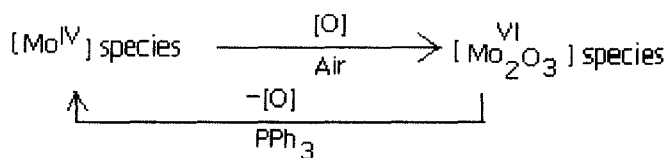


**The overall reaction :**



Similar to oxidation of (2) above (equation 1), moisture from atmosphere takes part in the second step oxidation of  $[\text{Mo}^{\text{VI}}\text{O}]^{4+}$  core to  $[\text{Mo}^{\text{VI}}_2\text{O}_3]^{6+}$  core<sup>19, 20(c,d)</sup>, leading to the formation of compound (4)<sup>36</sup> [Equation (2)].

To complete the redox cycle, (4), so isolated above, was treated with slight excess of  $\text{PPh}_3$ , an oxygen abstractor, whereby the  $\text{Mo}^{\text{VI}}$  - atom in (4) undergoes reduction to the lower oxidation state ( $\text{Mo}^{\text{IV}}$ ) as is present in (3) [Scheme (III - 3)].



[Scheme (III - 3)]

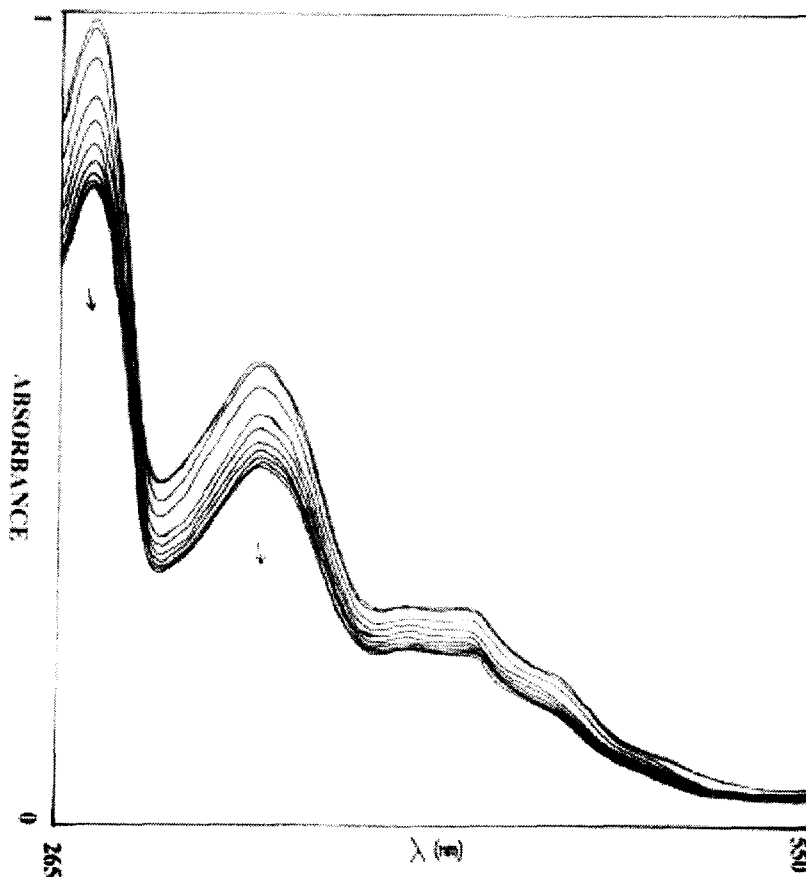


**Fig. (III-26):** UV-VIS absorption spectral changes recorded every 15 min. during the reaction of (5)  $[2.05 \times 10^{-5}(\text{M})]$  with  $\text{Me}_3\text{N} \rightarrow \text{O}$   $[2.40 \times 10^{-3}(\text{M})]$  in DMF at 301K.

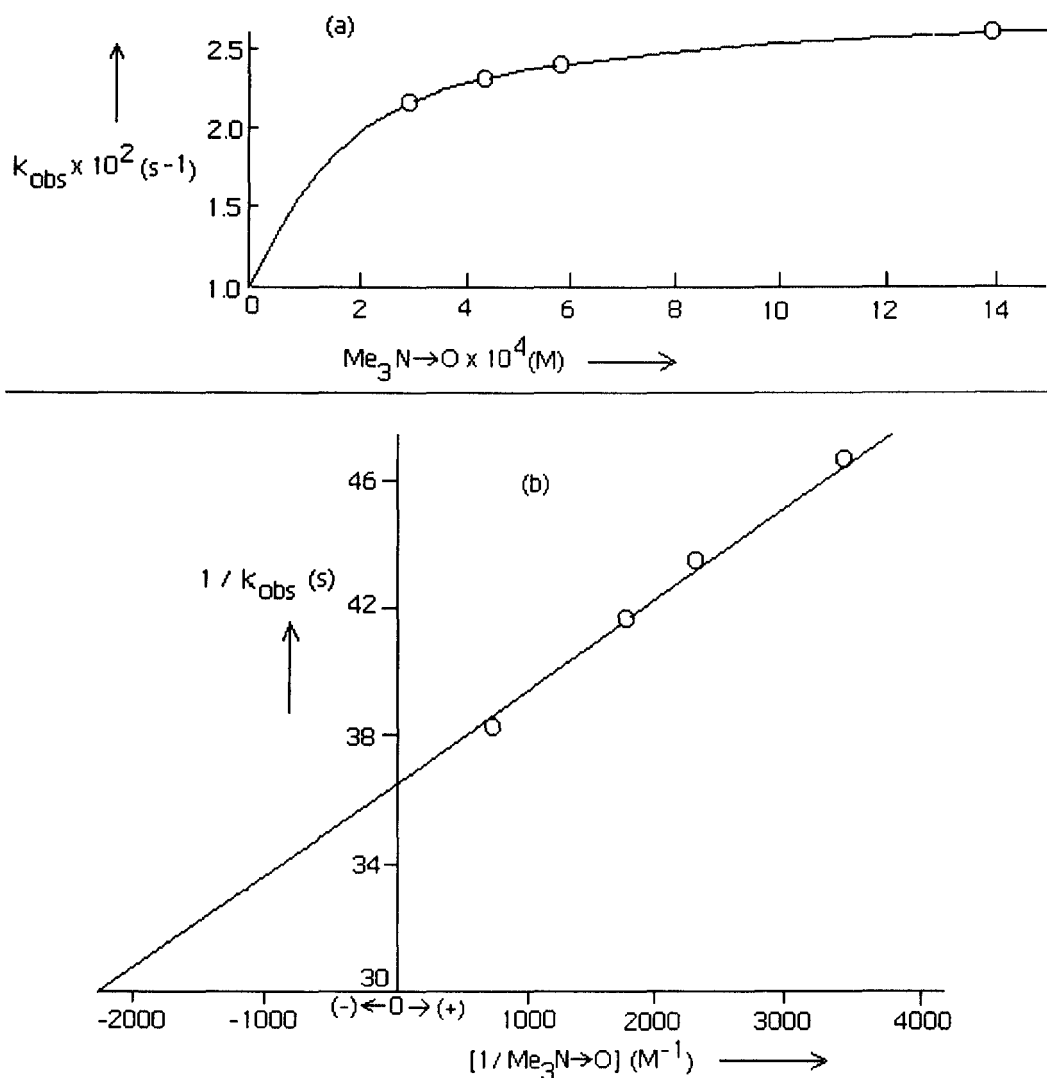


**Fig.(III - 27):**(a)Dependence of the rate of reaction of (5) [ $1.96 \times 10^{-5} \text{ (M)}$ ] with  $\text{Me}_3\text{N}\rightarrow\text{O}$  in DMF at 301 K; (b) the corresponding double reciprocal plot

Here one thing should be noted that both (3) & (4) are quite stable under atmospheric condition although they contain different oxidation states of molybdenum. This stability of the molybdenum complexes in different oxidation states is due to the unique chelating effect of  $\text{H}_3(\text{pte}_2\text{-tsc})$  ligand. The overlay UV-VIS spectral change for the reaction of (4) with  $\text{PPh}_3$  shows an isobestic point at 372 nm [Fig.(III-24)] suggesting a definite course of this conversion.

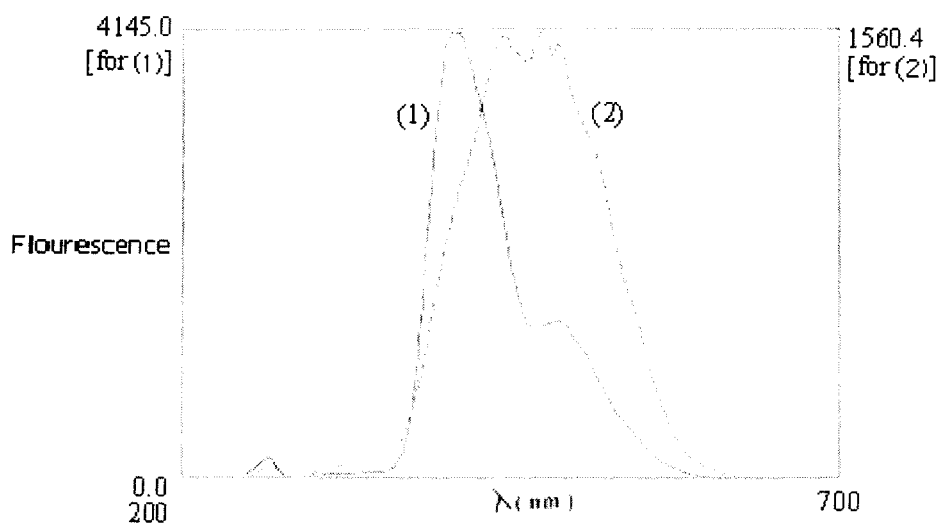


**Fig.[III-28(a)]:**Fluorescence spectra in DMF of (5)[  $1.0 \times 10^{-4}$ (M)], curve (1) for the complex & curve (2) for its oxidized product after reaction with  $\text{Me}_3\text{N} \rightarrow \text{O}$  in DMF.

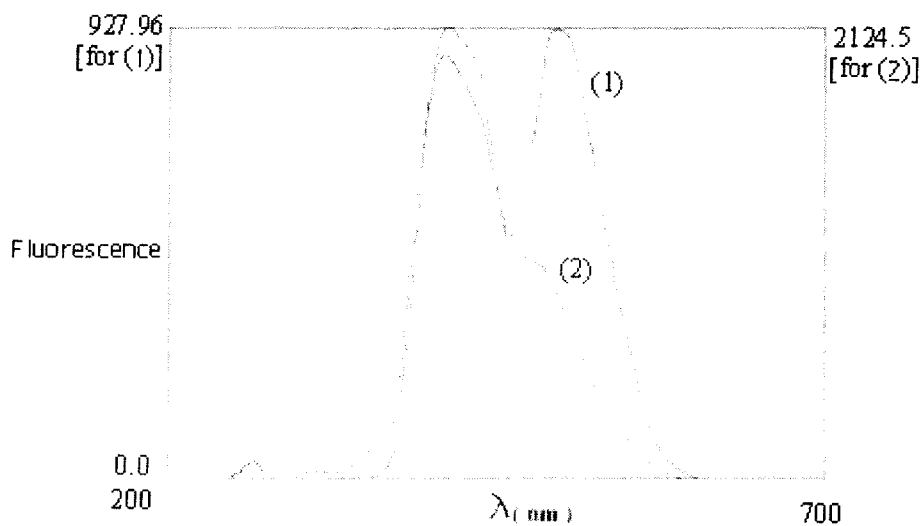
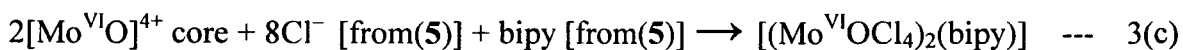
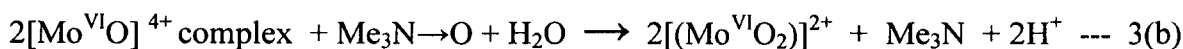
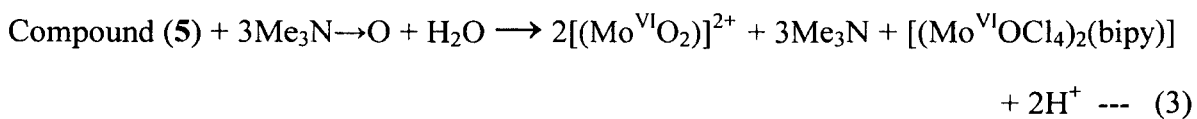


**Fig.[III-28(b)]:** Fluorescence spectra in DMF of (7) [ $1.0 \times 10^{-4}$ (M)], curve (1) for the complex & curve (2) for its reduced product after reaction with  $\text{PPh}_3$  in DMF.

To establish reaction stoichiometry of the reaction between **(5)** and Me<sub>3</sub>N→O, a DMF solution (60 ml) of **(5)** (1.87 g, 1 mmol) was allowed to react with Me<sub>3</sub>N→O (0.75 g, 10 mmol) in the dark under a slow flow of N<sub>2</sub> gas, at 298 K for the first 24 h and then at 333 K for the next 24 h. The emerging gas carrying Me<sub>3</sub>N (b.p. 275.9 K) was passed into a flask containing a measured excess of standard perchloric acid dissolved in glacial acetic acid and then the gas was released to the atmosphere through a silicone oil bubbler. Finally, the residual perchloric acid in the flask was back titrated potentiometrically using a standard sodium acetate solution<sup>47</sup> and the amount of perchloric acid consumed by Me<sub>3</sub>N was estimated. About 3.2 mol of Me<sub>3</sub>N was recovered per mol of **(5)** added, indicating a reaction represented by equation (3), below and supported by kinetic data.

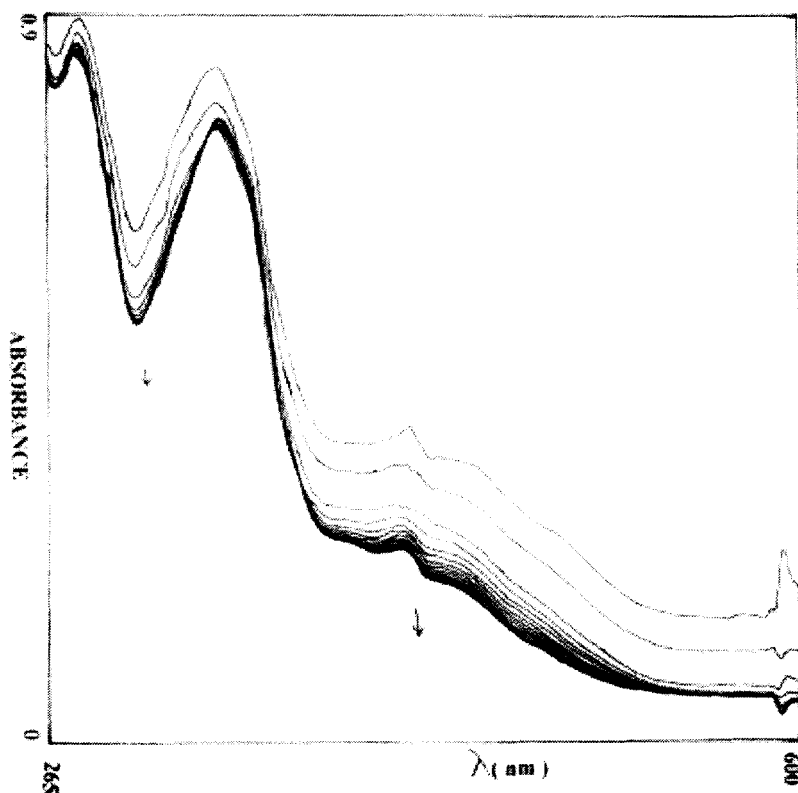


**The overall reaction :**

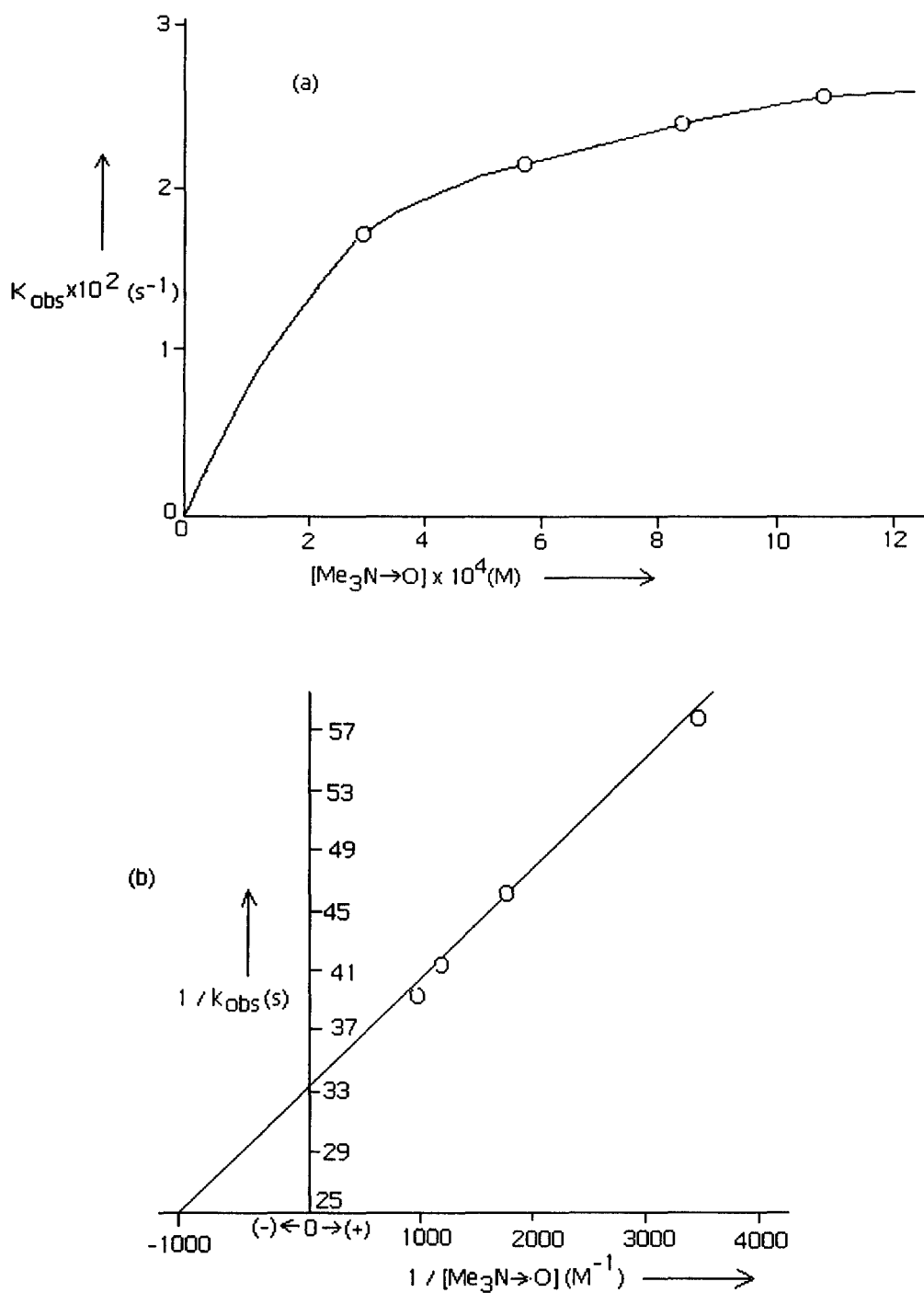


H<sub>2</sub>O used in equation 3(b) most probably came from moisture in the solvent and took part in the hydrolysis of [Mo<sup>VI</sup>O]<sup>4+</sup> core<sup>19, 20(c,d)</sup>.

The solution in the reaction flask was concentrated to dryness in rotary evaporator and the material so obtained was purified by flash chromatography; Et<sub>2</sub>O was used for removing the excess of Me<sub>3</sub>N→O and the oxidized complex was eluted in DMF – CH<sub>3</sub>OH (9 : 1, v/v). The product, [(Mo<sup>VI</sup>O<sub>2</sub>){H(pte<sub>2</sub>-tsc)}CH<sub>3</sub>OH], was characterized through elemental analysis, ESIMS and other physico-chemical studies. Its IR spectrum contains ν(Mo=O) band at 945.1 cm<sup>-1</sup>, characteristic of terminal (Mo=O<sub>t</sub>) frequency<sup>20</sup>. There is no band corresponding to bridging (Mo – O<sub>b</sub> – Mo) frequency. The inserted oxygen atoms are utilized in converting [(Mo<sup>V</sup>O<sub>2</sub>)<sub>2</sub>]<sup>16+</sup> core to 2(Mo<sup>VI</sup>O<sub>2</sub>)<sup>2+</sup> core along with the formation of [(Mo<sup>VI</sup>OCl<sub>4</sub>)<sub>2</sub>(bipy)] [as per Fig.(III-16), most likely the Mo-atoms bonded to the Schiff base ligands gave the (Mo<sup>VI</sup>O<sub>2</sub>)<sup>2+</sup> core and Schiff base containing product; while the other two Mo-atoms bonded to the bipyridyl molecule gave [(Mo<sup>VI</sup>OCl<sub>4</sub>)<sub>2</sub>(bipy)] as a side product] accompanied by one unit oxidation of each Mo<sup>V</sup> atom [equation (3)].



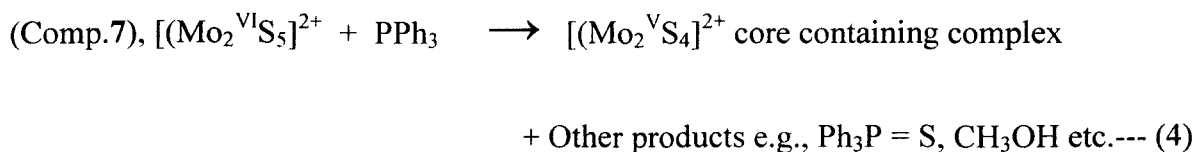
**Fig.(III-29):** UV-VIS absorption spectral changes recorded every 1 min. during the reaction of (6) [ $3.40 \times 10^{-5}$ (M)] with Me<sub>3</sub>N→O [ $1.87 \times 10^{-3}$ (M)] in DMF at 301K.



**Fig.(III-30):** (a)Dependence of the rate of reaction of (6)  $[3.14 \times 10^{-5} \text{ (M)}]$  with  $\text{Me}_3\text{N}\rightarrow\text{O}$  in DMF at 301 K; (b) the corresponding double reciprocal plot.

To establish reaction stoichiometry of (7) with PPh<sub>3</sub>, a DMF solution (60 ml) of (7) (0.786 g, 1 mmol) was allowed to react with PPh<sub>3</sub> (2.62 g, 10 mmol) in the dark under a slow but steady flow of N<sub>2</sub> gas, at 298 K for the first 24 h and then at 333 K for the next 24 h. The solution in the flask was concentrated to dryness in rotary evaporator and the material so obtained was purified by flash chromatography; Et<sub>2</sub>O was used to remove the excess PPh<sub>3</sub>. The oxidized product Ph<sub>3</sub>P = S, produced during the reaction was eluted in a mixture of CH<sub>2</sub>Cl<sub>2</sub> – CH<sub>3</sub>OH (1:1 v/v) (the metal complex is insoluble in this solvent mixture), evaporated to dryness and extracted in Et<sub>2</sub>O to get 0.85 mol of Ph<sub>3</sub>P = S per mol of (7) added<sup>90</sup>, supporting the reaction represented by equation (4), below and substantiated by kinetic data.

The reduced Mo-complex [equation (4)] was eluted in DMF - CH<sub>3</sub>OH solvent mixture (2 :3 v/v); and characterized through elemental analysis, ESIMS and other physico-chemical studies. Its composition was found to be [(Mo<sub>2</sub><sup>V</sup>S<sub>4</sub>){H(pte<sub>2</sub>-tsc)}(CH<sub>3</sub>OH)<sub>3</sub>].CH<sub>3</sub>OH. The oxygen atom containing counterparts of the [Mo<sub>2</sub><sup>VI</sup>S<sub>5</sub>]<sup>2+</sup> and [Mo<sub>2</sub><sup>V</sup>S<sub>4</sub>]<sup>2+</sup> core are well known, e.g., [Mo<sub>2</sub><sup>VI</sup>O<sub>5</sub>]<sup>2+</sup> and [Mo<sub>2</sub><sup>V</sup>O<sub>4</sub>]<sup>2+</sup> cores<sup>2, 19</sup>. Compound (7) has formula weight of 787, whereas, ESIMS spectrum of this reduced complex shows peak at m/z = 754 [Fig.(III-31e)] giving a difference of 33 mass unit (787 – 754 = 33) corresponding to the loss of one S atom from (7) by PPh<sub>3</sub> accompanied by the release of one H atom<sup>85, 107</sup>. This peak is simulated by using the IPC computer program<sup>46</sup> at m/z = 754 [Fig.(III-31f)]. [Fig.(III-31a)] represents the ESIMS peaks of (7) at m/z = 760, [M – CO + H]<sup>+</sup> and its computer simulation result [Fig.(III-31b)]; [Fig.(III-31c)] represents the experimentally found peaks in the reduced product, at m/z = 728, [M – (CO + S) + H]<sup>+</sup> corresponding to the loss of one S atom from that in Fig.(III-31a) [760 – 728 = 32 mass unit].



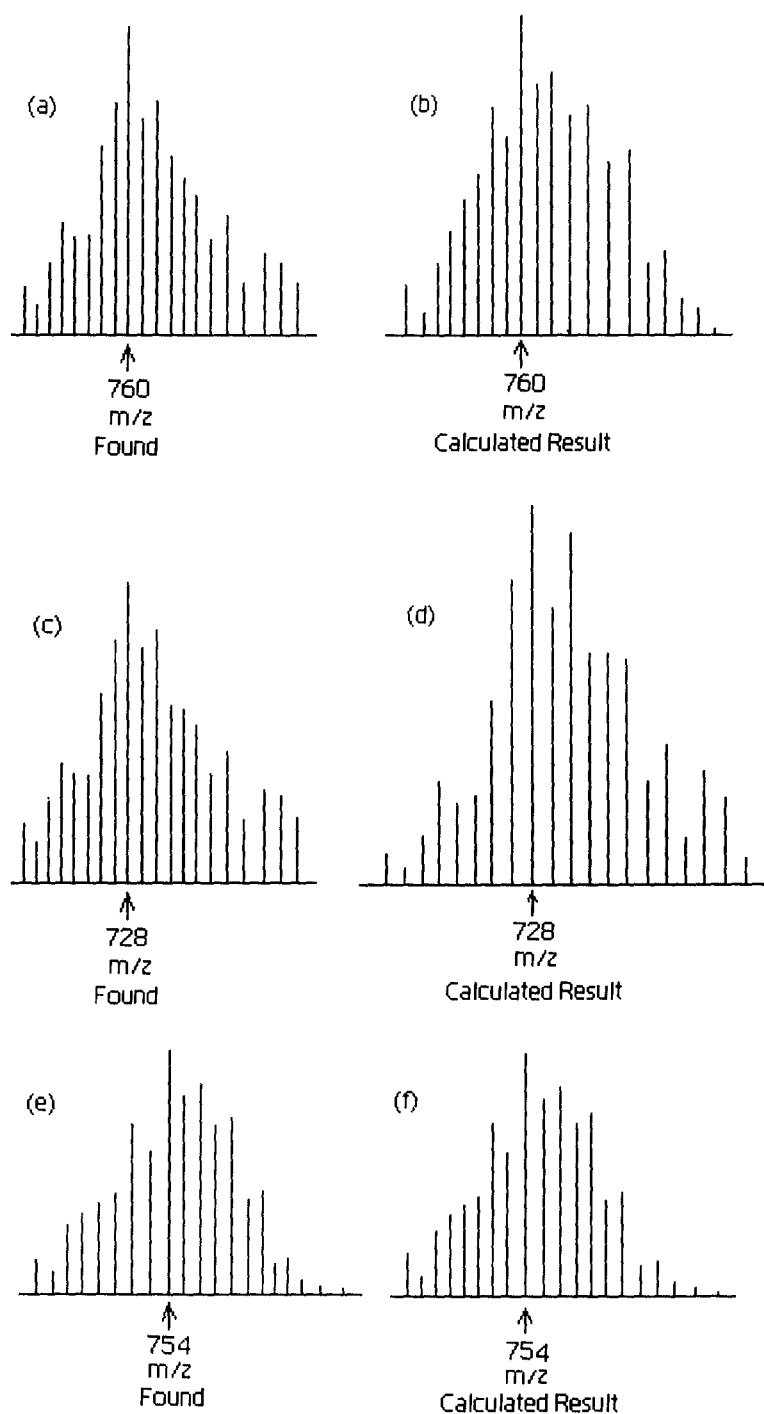


**Fig.(III-31):** (a) Experimentally found and (b) computer simulation peaks of (7) corresponding to  $m/z = 760, [M - CO + H]^+$ , formula-  $C_{13}H_{28}N_8O_5Mo_2S_6$ ; (c) experimentally found and (d) computer simulation peaks of the product obtained after reduction of (7) by  $PPh_3$ , corresponding to  $m/z = 728, [M - (CO + S) + H]^+$ , formula-  $C_{13}H_{28}N_8O_5Mo_2S_5$ ; (e) experimentally found and (f) computer simulation peaks of the product obtained after reduction of (7) by  $PPh_3$ , corresponding to  $m/z = 754, [M - S - H]^+$ , formula-  $C_{14}H_{26}N_8O_6S_5Mo_2$ .

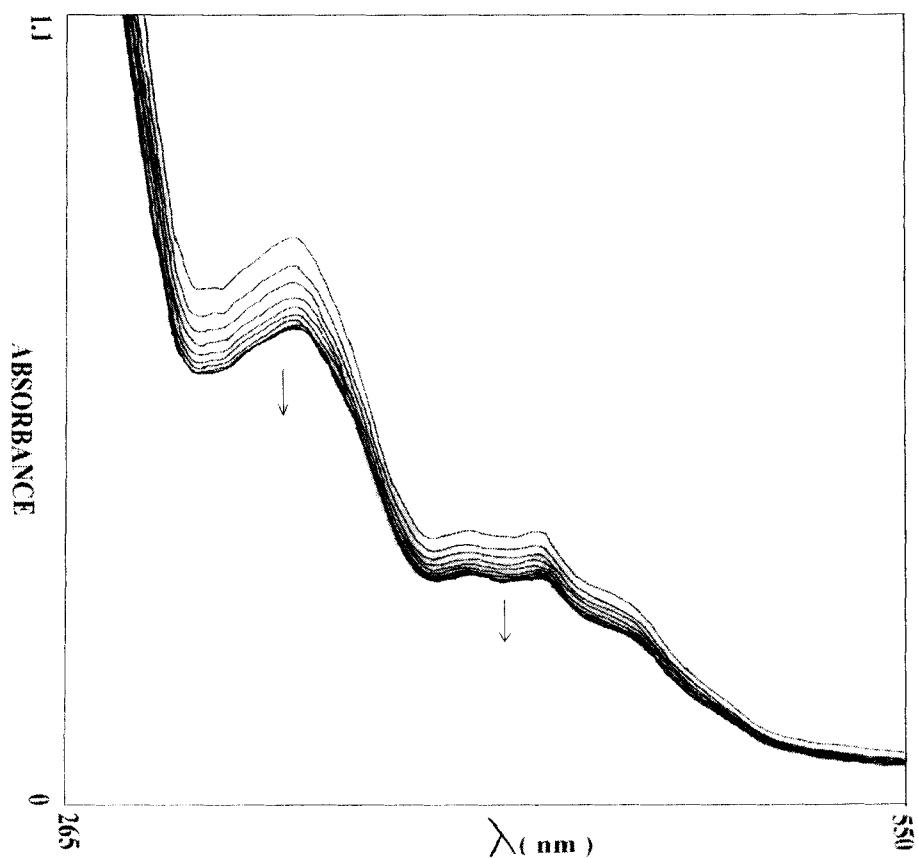


**Fig.(III-32):** UV-VIS absorption spectral changes recorded every 12 min. during the reaction of (7) [ $1.1 \times 10^{-5}$ (M)] with  $\text{PPh}_3$  [ $1.46 \times 10^{-3}$ (M)] in DMF at 301K.

As these compounds (2-7) undergo oxygen atom transfer reaction with  $\text{PyN} \rightarrow \text{O}$ ,  $\text{Me}_3\text{N} \rightarrow \text{O}$  /  $\text{PPh}_3$  ; kinetics of these reactions were followed spectrophotometrically at 400 nm for (2), 420 nm for (3), and at 415 nm for compounds (4 - 6) and in case of (7), kinetics studied at 510 nm. Rate constants were measured at room temperature as well as at three different higher temperatures by applying least square method and plotting  $\log(A_t - A_\infty)$  or  $\log(A_\infty - A_t)$  vs time for the decay or growth kinetics for (2, 3, 5, 6) and (4 & 7) respectively. At room temperature the  $k_{\text{obs}}$  ( $\text{s}^{-1}$ ) values were measured at different complex : substrate ratio and when plotted as a function of substrate concentrations, substrate saturation plots were obtained [Fig.s (III-21a), (III-23a), (III-25a), (III-27a), (III-30a) & (III-33a)]. Double reciprocal plots were obtained from the substrate saturation kinetic data by plotting  $1/k_{\text{obs}}$  vs.  $1/[\text{substrate}]$  for

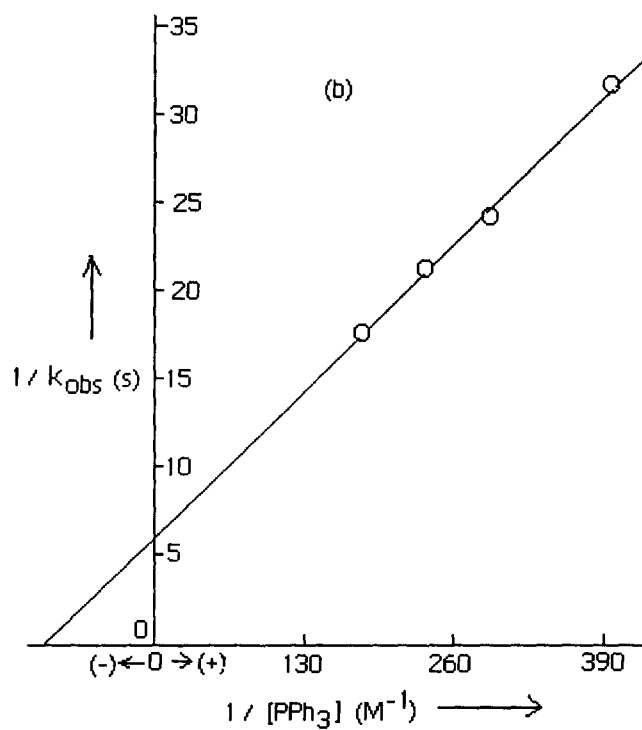
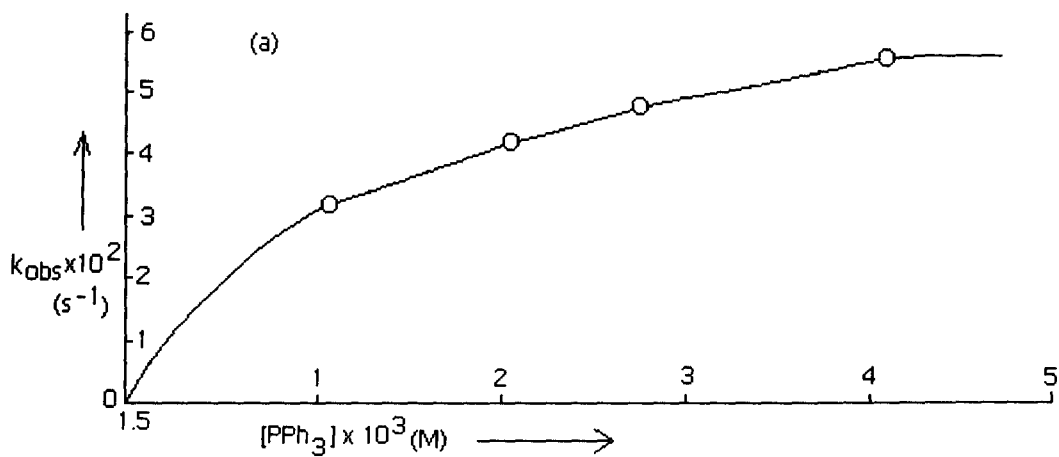


**Fig.(III-33):** (a)Dependence of the rate of reaction of (7)  $[2.28 \times 10^{-4} \text{ (M)}]$  with  $\text{PPh}_3$  in DMF at 301 K; (b) the corresponding double reciprocal plot.

each complex [Fig.s (III-21b), (III -23b), (III-25b), (III-27b), (III-30b) & (III-33b)].  $K_M$  and  $k_2$ -values [Table (III - 15)] were calculated from the slopes and intercepts of these straight line plots respectively.

Now, for measuring activation parameters, four different  $k_{obs}$  ( $s^{-1}$ ) values corresponding to four different reaction temperatures were measured for each complex, at the pseudo – first order substrate saturation composition (substrate concentration, 35–70 times excess to that of the complex)<sup>8(a,c), 17, 23</sup>. Arrhenius and Eyring plots were obtained from the temperature dependent rate constant values, by plotting  $\ln(k_{obs})$  vs.  $(1/T) \times 10^3$  and  $\ln(k_{obs}/T)$  vs.  $(1/T) \times 10^3$  respectively. From the slope of Arrhenius plots activation energy ( $E_a$ -value) is calculated [Table (III-15)]. Other activation parameters,  $\Delta H^\ddagger$  and  $\Delta S^\ddagger$  - values are obtained from slope and intercept of the Eyring plots respectively.  $\Delta G^\ddagger$ - values are calculated from the Gibb's-Helmholtz equation,  $\Delta G^\ddagger = \Delta H^\ddagger - T\Delta S^\ddagger$  [Table (III-15)].

The overlay scan during spectrophotometric monitoring of the oxygen atom transfer reactions of (2), (3), (5) and (6) with  $PyN \rightarrow O$  or  $Me_3N \rightarrow O$  show decay kinetics (i.e., lowering of OD value with time), whereas the reverse is true (growth kinetics) for the reaction of (4) with  $PPh_3$ . That is metal – centered oxidation is associated with decay kinetics and the reduction process shows a growth kinetics. The only exception to this general observation is compound (7), where sulphur atom abstraction (by  $PPh_3$ ) takes place instead of oxygen atom transfer reaction. Most likely greater polarisability of the thiomolybdate core is responsible for this decay kinetics observed here; the same factor may be responsible for the failure of the  $H_3(pte_2-tsc)$  ligand to reduce the metal centre (to V or IV state) during the synthesis of (7).

Table (III – 15)

Comp-ound No.s	Substrate used (in DMF)	T (K)	$k_{obs}$ ( $s^{-1}$ ) $\times 10^3$	$k_2$ ( $s^{-1}$ ) $\times 10^3$	$K_M$ (M) $\times 10^5$	$E_a$ (KJ, $mol^{-1}$ )	$\Delta H^\ddagger$ (KJ, $mol^{-1}$ )	$\Delta S^\ddagger$ (J, $mol^{-1}$ , $deg^{-1}$ )	$\Delta G^\ddagger$ (KJ, $mol^{-1}$ )
(2)	PyN $\rightarrow$ O	298 304 307.5 312	3.82 7.16 10.12 15.10	9.97	11.9	75.99	74.40	-208.29	137.73
(3)	Me <sub>3</sub> N $\rightarrow$ O	300.5 307 311.5 315	21.70 26.00 29.00 32.00	25.4	19.9	21.30	17.92	-202.40	78.75
(4)	PPh <sub>3</sub>	307 312 316 318	44.50 58.40 73.00 80.00	45.6	6.57	43.11	41.88	-205.00	104.83
(5)	Me <sub>3</sub> N $\rightarrow$ O	302 305.5 314 318	26.10 27.40 31.70 33.60	27.4	8.0	12.76	10.21	-200.4	70.64
(6)	Me <sub>3</sub> N $\rightarrow$ O	302 308.5 313 318	25.50 26.80 27.60 28.60	30.3	21.5	5.78	3.18	-198.63	63.12
(7)	PPh <sub>3</sub>	291 295.5 302.5 308.5	56.60 59.50 65.40 71.00	171.4	1100	9.95	7.09	-200.40	67.72

$$k_{obs} = k_2[S]/(K_M + [S]) \quad \text{---- (5)}$$

$$\text{Where, } K_M = (k_2 + k_{-1})/k_1,$$

Or,

$$1/k_{obs} = 1/k_2 + K_M/k_2[S] \quad \text{---- (6)}$$

Plots of  $k_{obs}$  vs.  $[S]$  indicates substrate saturation kinetics [Fig.s (III–21a), (III–23a), (III–25a), (III–27a), (III–30a) & (III –33a)] as per equation (5) above and plots of  $1/k_{obs}$  vs  $1/[S]$  gave straight lines, named as double reciprocal plots [Fig.s (III –21b), (III –23b), (III –25b), (III –27b), (III –30b) & (III –33b)] as per equation (6); with slope equal to  $K_M/k_2$  and intercept equal to  $1/k_2$ . The kinetic parameters for the above reactions along with  $k_{obs}$ ,  $k_2$  &  $K_M$  values are presented in Table (III – 15) and they found to be in good agreement with the available literature on molybdenum complex mediated oxygen atom transfer kinetics data <sup>8, 17, 23</sup>.

One interesting observation from the kinetic measurement [Table(III–15)] is that the entropy of activation ( $\Delta S^\ddagger$ ) value is found to be negative for all the reactions studied here. This is in conformity with the associative type of reaction mechanism, alike to enzyme – substrate type reaction mechanism <sup>24, 34</sup>. The variation in the magnitude of the kinetic parameters in Table-(III–15) can be understood in terms of several factors, e.g., the steric energy of the foregoing CHEM3D representations, metal atom oxidation states, steric crowding around the metal centre etc. High  $k_{obs}$  values are obtained in cases involving oxygen or sulphur abstraction by  $PPh_3$ . As a substrate,  $Me_3N \rightarrow O$  provides higher  $k_{obs}$  values than  $PyN \rightarrow O$ . Higher  $E_a$  (activation energy) value is observed for (2) where the ligand coordination around the  $Mo^{IV}$  centre is most compact, with lowest steric energy (for CHEM3D representations). Reactivity of compound (6) can also be viewed in the same light. Compounds with high steric energy usually show low  $E_a$  values with a few exceptions, indicating the responsibility of other factors stated above in the reactivity process.

Cyclic voltammetry (CV) data, (a) from  $-1.85$  to  $1.0$  V is shown in one figure along with expansion of the region (b)  $-0.2$  to  $0.9$  V of the free ligand,  $H_3(pte_2-tsc)$  (**1**). This shows a quasi-reversible couple in the region  $-0.85$  V (reduction) and  $-0.68$  V (oxidation).  $\Delta E_p$  ( $E_{pc} - E_{pa} = 170$  mV) value can be correlated essentially with a two-electron transfer process, taking into account the Nernst equation as well as the  $iR$  drop during the recording process. Presence of the 1,4-diazine residue in the pterin ligand in conjunction with the 7-substituted side chain containing the thiosemicarbazide residue, imparts a degree of structural stability and availability of suitable orbitals makes this ligand stable enough during this 2-electron redox process without undergoing chemical decomposition on the CV time scale. These factors are responsible for the observed quasi-reversible behaviour in Fig.(III-34a) <sup>4</sup>. Two irreversible oxidation peaks at  $-0.20$  V and  $+0.74$  V characterize the rest part of this CV data [Fig.(III-34)].

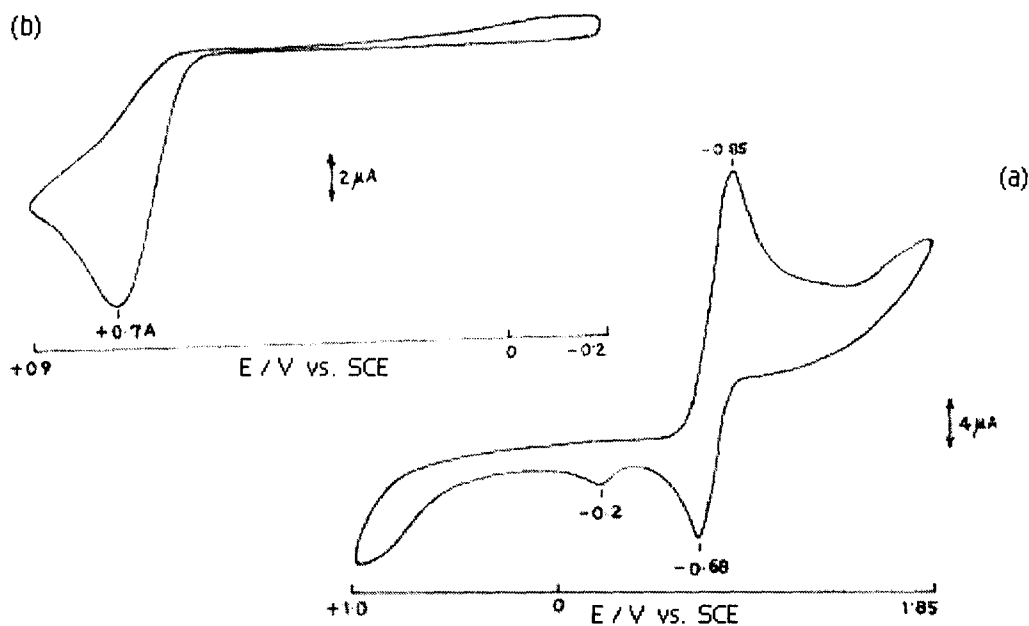


**Fig.(III-34):** CV scans of compound (**1**) [ $1.0 \times 10^{-3}$ (M)],  $Bu_4NClO_4$  [ $0.1$  (M)] in DMF, (a)  $-1.85$  to  $+1.0$  V, (b)  $-0.2$  to  $+0.9$  V. Scan rate  $50$  mVs $^{-1}$ .

Fig. (III -35) shows the CV data of compound (2) which is characterized by the aforesaid quasi - reversible peak as well as additional peaks on (b) for the metal centre; at  $-0.105$  V a reduction of the metal - centre ( $\text{Mo}^{\text{IV}} \rightarrow \text{Mo}^{\text{III}}$ ) takes place followed by chemical attack of the solvent leading to its partial decomposition. The quasi-reversible peak system in Fig.(III-35a) is essentially related to ligand redox process. A weak signal at  $+0.45$  V characterizes the reoxidation process of the metal - centre.

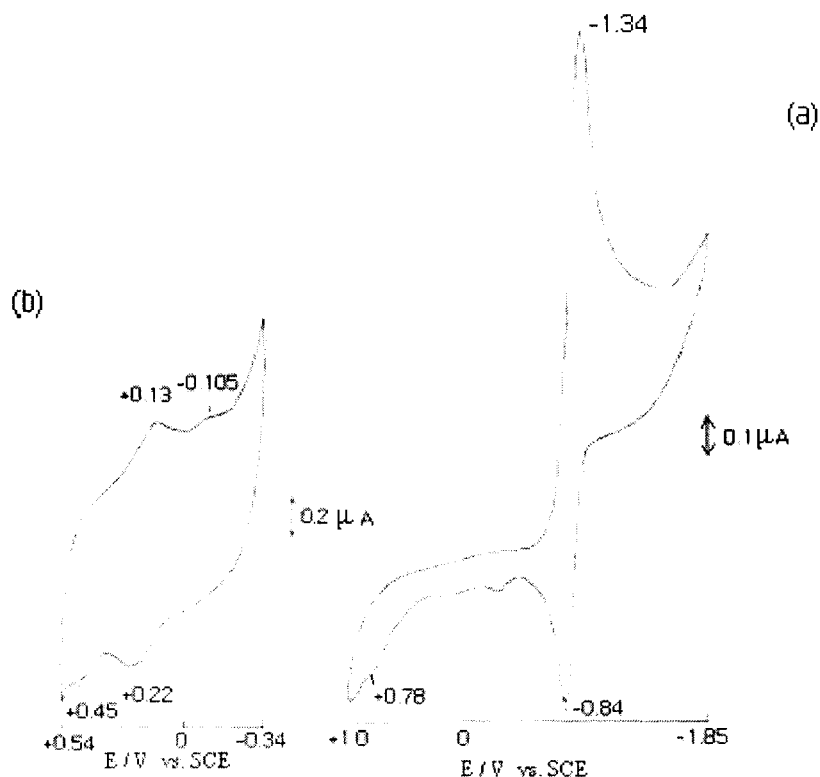


**Fig.(III-35):** CV scans of compound (2) [ $1.0 \times 10^{-3}$  (M)],  $\text{Bu}_4\text{NClO}_4$  [0.1 (M)] in DMF, (a)  $-1.85$  to  $-1.0$  V, (b)  $-0.34$  to  $+0.54$  V. Scan rate  $50 \text{ mVs}^{-1}$ .

In case of (3), in addition to the above mentioned common features the metal irreversible reduction peak ( $\text{Mo}^{\text{IV}} \rightarrow \text{Mo}^{\text{III}}$ ) is observed at  $-0.43$  V and the subsequent reoxidation step at  $+0.53$  V. In case of complex (4), the metal - centers undergo reduction ( $\text{Mo}^{\text{VI}} \rightarrow \text{Mo}^{\text{V}}$ ) at  $+0.15$  V and subsequent reoxidation occurs at  $+0.24$  V. The  $\Delta E_p$  value for the ligand reduction peak corresponds to essentially one electron transfer (taking into account the iR drop aspect). One additional irreversible ligand reduction peak appears at  $-1.34$  V. CV data of compound (5) is characterized

essentially by similar features as above with the metal reduction ( $\text{Mo}^{\text{V}} \rightarrow \text{Mo}^{\text{IV}}$ ) peak appearing at +0.16 V and the subsequent reoxidations occurring at - 0.17 V, + 0.22 V & + 0.49 V respectively. For compound (6) the metal reduction ( $\text{Mo}^{\text{V}} \rightarrow \text{Mo}^{\text{IV}}$ ) peak is observed at +0.13 V and the subsequent reoxidation occurs at + 0.47 V. In case of (7), [Fig.(III-36)], the metal reduction ( $\text{Mo}^{\text{VI}} \rightarrow \text{Mo}^{\text{V}}$ ) takes place at - 0.26V. Besides this the ligand part is characterized by essentially an irreversible system as opposed to quasi-reversible behavior here; possibly the highly polarizable thiomolybdate residue of this complex is responsible for this behavior.

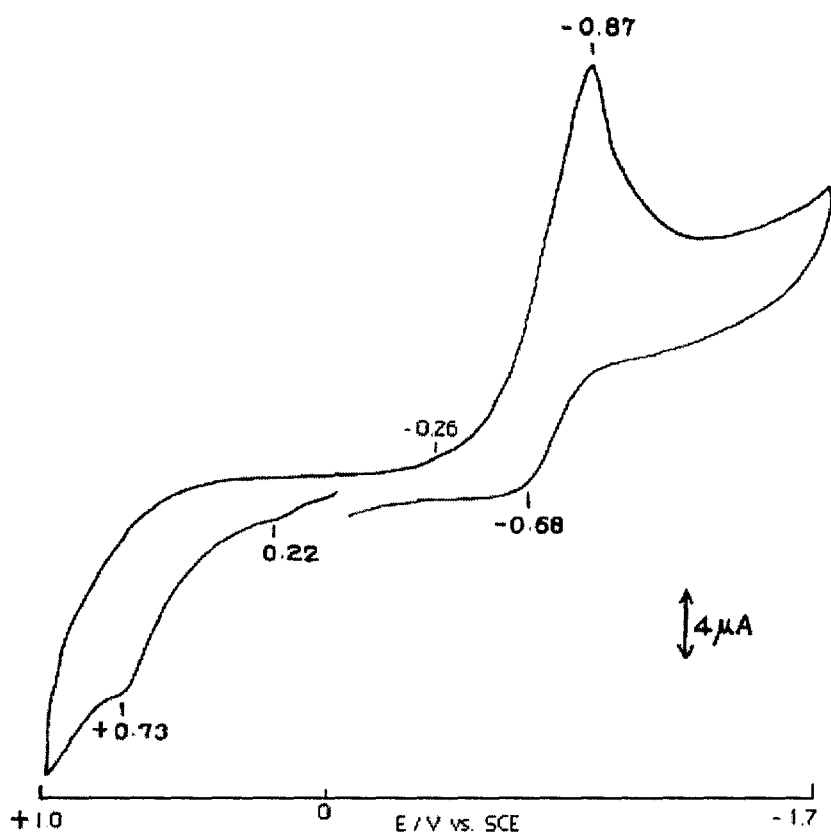


**Fig.(III- 36):** CV scans of compound (7) [ $1.0 \times 10^{-3}$  (M)],  $\text{Bu}_4\text{NClO}_4$  [0.1 (M)] in DMF. Scan rate  $50 \text{ mVs}^{-1}$ .

It may be summarized that both the ligand residue as well as the metal centre take part in the overall redox activity of these complexes.

## Conclusion

Here the synthesis and characterization of a new Schiff base ligand are described along with its six new complex compounds of molybdenum in different oxidation states. In most cases the pterin ligand acts as a reducing agent during synthesis and oxidation state of the metal centre in the final product depends on the reaction condition used as well as the nature of the molybdenum starting material. ESIMS data in conjunction with elemental analysis data and supported by IR and  $^1\text{H}$  NMR spectral studies, verify their **formulations / chemical compositions**. Molecular modeling studies [CHEM3D models obtained through MM2 calculations] provide with their optimized molecular geometry as well as bond length and bond angle data. The later type of parameters are in agreement with the published X-ray structural data on different molybdenum – pterin coordination compounds in related systems. This aspect verifies their **molecular structures**. Reactivities of these compounds towards oxygen donors ( $\text{Me}_3\text{N}\rightarrow\text{O}$  /  $\text{PyN}\rightarrow\text{O}$ ) or oxygen abstractor ( $\text{PPh}_3$ ) throw light on the **oxidation state of the metal centre** in these compounds. The  $k_{\text{obs}}$  ( $\text{s}^{-1}$ ) values are within the range of oxygen atom transfer reactions of related published synthetic  $\text{Mo}^{\text{IV} / \text{VI}}$  – systems. Nature of such group transfer reactions has been substantiated by **reaction stoichiometry studies** in several cases as well as ESIMS data in one case. Almost all these cases conform to **substrate saturation type kinetics** with **negative entropy of activation** value ( $\Delta S^\ddagger = -198$  to  $-208 \text{ J mol}^{-1}\text{deg}^{-1}$ ).

CV data as well as fluorescence spectral data throw light on the **changes in electronic structure during different redox steps** described in this chapter. It is evident that the ligand centred as well as the metal centred redox systems supplement each other in the present new molybdenum compounds, giving them unique oxygen atom transfer reactivity towards typical enzyme substrates of oxomolybdoenzymes. In this sense, they can be considered as **functional model systems**. UV-VIS as well as **fluorescence spectra** have proved to be **valuable probes for studying this aspect**.

## **CHAPTER IV**

### **SECTION – I**

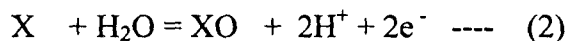
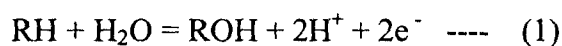
Synthesis, characterization and reactivity studies on mixed ligand molybdenum (IV,V,VI) complexes with 6-acetyl-isoanthopterin [ $H_2(pte_1)$ ] and a sulphur containing ligand (cysteine or 2 – amino thiophenol or dihapto disulphide).

## Abstract

Six new molybdenum (IV,V,VI) compounds with the biologically relevant ligand 6-acetyl-isoxanthopterin [ $H_2(pte_1)$ ] have been synthesized in presence of an ancillary ligand like cysteine ( $H_2cys$ ) or 2-amino thiophenol ( $H_2atp$ ) or dihapto disulphide. During the synthetic step the pterin ligand reduced the molybdenum (VI) starting materials to a lower oxidation state [e.g., Mo(V) or Mo(IV)]. In one case dimethyl sulphoxide used as a solvent constituent, reoxidized the intermediate molybdenum complex back to a Mo(VI) product. The compounds have been characterized by elemental analysis,  $\Lambda_M$  data, ESIMS, UV-VIS, IR,  $^1H$  NMR, fluorescence spectra and CV data ; the structural inferences have been supported by CHEM3D representations (MM2 method). Reactivity of these complexes towards  $PPh_3$  /  $Me_3N \rightarrow O$  have been followed spectrophotometrically; the rate constants data ( $k_{obs} s^{-1}$ ) for these OAT reactions exhibiting substrate saturation kinetics, bear consistency with the existing literature values. For a couple of cases isobestic points appear in the overlay scans, indicating uncomplicated pathway for these reactions. The large negative entropy of activation ( $\Delta S^\ddagger$ ) values suggest an associative type of pathway for these reaction. Fluorescence spectra throw light on the changes in electronic structures of the relevant complexes during such reactions. Their cyclic voltammograms provide with information regarding oxidation states of the metal centres and their cathodic reduction behaviour.

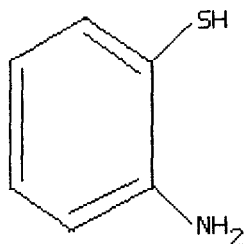
## Introduction

Molybdenum is associated (except in nitrogenase) with a pterin derivative through a cis – dithiolene group to form the Mo – centred functional unit (McFU) [Scheme (I –1)], common to several oxotransferases<sup>1</sup>. An intriguing aspect of the properties of McFU is the extent to which the molybdenum and the pterin in presence of sulphur ligands participate in the redox changes at the metal centre. The McFU enzymes have an additional coordinated protein ligand e.g., a serine, a cysteine or a selenocysteine residue as the case may be, to tune the reactivity of the metal site<sup>1, 2</sup>. Such enzymes catalyse formal hydroxylation (equation 1) and neat OAT (oxygen atom transfer) reaction, to and from a variety of biologically important substrates and the oxygen atom is ultimately derived from water<sup>1</sup>.

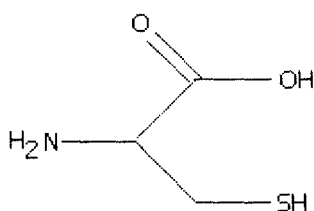


Equations (1) and (2) may also be regarded as CEPT (coupled electron proton transfer) reactions. Due to low resolution of X-ray crystal structure data of oxomolybdoenzymes, it is impossible to assign unambiguously oxo, hydroxo or water ligands and hence the uncertainty in assigning the correct oxidation state of the metal centre, pyrazine ring of the pterin moiety or that of the sulphur bearing side chain<sup>4, 143, 196</sup>. So, it is important to complement the crystallographic results with spectroscopic data<sup>1</sup>. In this regard the role of synthetic molybdenum – pterin complexes specially containing a S – bonded molybdenum centre, is vital for recording bench-mark data. Development of such coordination Chemistry will also enable accomplishment of chemical and electrochemical studies that are relevant and complementary for the study of the functional aspects of the relevant enzyme catalytic cycles<sup>1(b,c)</sup>. McFU [Scheme (I –1)] contains a 6-substituted pterin cyclised to form a pyran ring. The new ligand H<sub>2</sub>(pte<sub>1</sub>) [Scheme (II – 1)] also contain a 6 – acetyl part attached to the 1,4 – diazine ring, whose 7 – oxo group corresponds to the pyran ring oxygen atom in McFU, keeping in mind the difference in oxidation states of the two types of oxygen atoms ( that is, the pyran ring

oxygen atom and the 7 – oxo group of the present ligand)<sup>4, 143, 196</sup>. Considering the above aspects of the synthetic molybdenum – pterin complexes, especially those containing a sulphur bearing secondary ligand, this chapter embodies the work of synthesis, characterization, electrochemical reactivity and kinetic studies of six new complexes of molybdenum (IV,V,VI) with H<sub>2</sub>(pte<sub>1</sub>) and a secondary ligand. The secondary ligands used here are shown below.



2 – amino thiophenol [H<sub>2</sub>(atp), C<sub>6</sub>H<sub>7</sub>NS ; FW 125.19]



Cysteine [H<sub>2</sub>(cys), C<sub>3</sub>H<sub>7</sub>NO<sub>2</sub>S ; FW 121.16]



dihapto disulphide anion [S<sup>2-</sup>]

### Scheme (IV-1)

To study the chemical compositions of these complexes ESIMS data were recorded, molecular structures have been established through CHEM3D model study (MM2 method). IR spectral study provided information about the bonding sites and the electronic structure was supported by UV – VIS, fluorescence, CV and <sup>1</sup>H NMR data. Reactivity aspects of these complexes were studied through CV and OAT reaction kinetic data with typical enzyme substrates e.g., Me<sub>3</sub>N→O and PPh<sub>3</sub>. So, this chapter not only aimed to establish the structural resemblance of the synthetic molybdenum complexes with that of McFU, it also presents the reactivity aspects of these complexes and hence tried to establish the model role (especially reactivity model) of these newly synthesized molybdenum complexes to that of McFU.

## Experimental

**Materials:** Reagent grade chemicals were used as received. Solvents were purified before use following literature procedures<sup>9</sup>. Kinetic and electro-chemical studies were performed in spectroscopy grade DMF (SRL, Mumbai); Bu<sub>4</sub>NClO<sub>4</sub> (TBAP) were obtained from published methods<sup>11</sup>. Me<sub>3</sub>N→O were obtained from Sigma Aldrich, Mumbai. Na<sub>2</sub>MoO<sub>4</sub>.2H<sub>2</sub>O, H<sub>2</sub>MoO<sub>4</sub>.H<sub>2</sub>O, L- cysteine [H<sub>2</sub>(cys)] and 2 – aminothiophenol [H<sub>2</sub>(atp)] were obtained from BDH, E.Merck, Mumbai and Lancaster, England respectively. PPh<sub>3</sub> was obtained from SRL Mumbai. (Et<sub>4</sub>N)<sub>2</sub>[MoS<sub>4</sub>] and (Et<sub>4</sub>N)<sub>2</sub>[MoO<sub>2</sub>S<sub>2</sub>] were prepared as per the published methods<sup>40</sup>. DMSO used during the synthesis was obtained from SRL, Mumbai. H<sub>2</sub>(pte<sub>1</sub>) was prepared by modifying its original method of synthesis in the light of subsequent developments (e.g., darkness, dinitrogen atmosphere, pH 6.8)<sup>6</sup> and characterized through different physico-chemical methods including elemental analysis, ESIMS, IR, UV – VIS, and <sup>1</sup>H NMR data<sup>12</sup>

**Method :** Dinitrogen atmosphere was maintained by applying Schlenk technique during the preparation, evaporation in rotary evaporator and filtration steps. Most of the physico-chemical methods of characterization were the same as that discussed in Chapter II, Section – I. IR spectra (KBr) were recorded on a Shimadzu FTIR 8300. Kinetics of the reactions of (1) with PPh<sub>3</sub> and that of (2), (3), (4), (5) & (6) with Me<sub>3</sub>N→O respectively in DMF medium at RT (301 K) were followed at 500 nm, 452 nm, 422 nm, 400 nm, 401 nm and 445 nm respectively and at four different temperatures, under pseudo-first order condition (maintaining 50 – 100 times excess of the substrate). Magnetic susceptibilities were checked with a Gouy balance using Hg[Co(SCN)<sub>4</sub>] as the calibrant.

## Synthesis of the complexes

### **$[(\text{Mo}^{\text{VI}}_2\text{O}_5)(\text{Kpte}_1)(\text{Hcys})(\text{CH}_3\text{OH})] \cdot 2\text{CH}_3\text{OH}$ (1)**

$\text{H}_2(\text{cys})$  (0.121 g, 1 mmol) dissolved in methanolic KOH (5 ml, 0.056 g, 1 mmol) was added under stirring to a solution of  $\text{Na}_2\text{MoO}_4 \cdot 2\text{H}_2\text{O}$  (0.242 g, 1 mmol) in water (10 ml) taken in a three necked flask ; pH was adjusted to 4.75 (HAc). A white precipitate appeared, bulk of which was redissolved through addition of DMSO (5 ml). A suspension of  $\text{H}_2(\text{pte}_1) \cdot 0.5\text{H}_2\text{O}$  (0.244 g, 1 mmol) in methanol (100 ml) was added to the reaction mixture and stirring was continued for 16 h at room temperature (301 K) under dinitrogen atmosphere and darkness. The resulting cream coloured compound was filtered using a sintered glass crucible, washed with solvents e.g., water, methanol, ether purged by dinitrogen and dried in vacuo over silica-gel. Yield : 75 %. Solubility ca. 5 % in DMF. Its purity was checked through TLC (silica-gel GF<sub>254</sub> ; UV lamp) using DMSO solution (diluted with 100 times  $\text{CHCl}_3$ ) and  $\text{CH}_2\text{Cl}_2$  – benzene (1 : 1 v/v) as the eluant.  $R_f$  : 0.7. Found : C, 23.60; H, 3.75; N, 11.42; S, 4.24; Mo, 25.4 %. Calc. for  $\text{KMo}_2\text{C}_{15}\text{H}_{26}\text{N}_6\text{O}_{13}\text{S}$  : C, 23.65; H, 3.42; N, 11.05; S, 4.20; Mo, 25.2 %. UV – VIS absorption bands [DMF,  $\lambda_{\text{max}}^{\text{nm}}(\text{log}\epsilon)$ ]: 292.4 (3.91) ; 324.5 sh (3.96) ; 340 (3.99) ; 398 (3.76) ; 417.4 (3.75) and 453 sh (3.54). Magnetic susceptibility measurement suggests the diamagnetic nature of this compound.

### **$[\text{Mo}^{\text{IV}}(\text{pte}_1)(\text{atp})(\text{CH}_3\text{OH})]$ (2)**

To a well stirred suspension of  $\text{H}_2(\text{pte}_1) \cdot 0.5\text{H}_2\text{O}$  (0.244 g, 1 mmol) in 100 ml  $\text{CH}_3\text{OH} - \text{H}_2\text{O}$  mixture (7 : 3, v/v), an aqueous solution (20 ml) of  $\text{H}_2\text{MoO}_4 \cdot \text{H}_2\text{O}$  (0.179 g, 1 mmol) and a methanolic solution (10 ml) of  $\text{H}_2\text{atp}$  (0.125 g, 1 mmol) were added simultaneously at room temperature (301 K), under dinitrogen atmosphere and darkness. The pH adjusted to 4.65 with acetic acid and stirring was continued for 2 h. The resulting dark – green compound was filtered under dinitrogen using a fritte, washed with purged (by dinitrogen) solvents [ $\text{CH}_3\text{OH} - \text{H}_2\text{O}$  mixture (1 : 1, v/v),  $\text{CH}_3\text{OH}$ ,  $\text{Et}_2\text{O}$ ], and dried in vacuo over silica – gel. Yield : 70 %. Solubility ca. 5 % in DMF. Its purity was checked through TLC (silica-gel GF<sub>254</sub>; UV lamp) using  $\text{CH}_2\text{Cl}_2 - \text{CH}_3\text{OH}$  (3 : 2, v/v) solution and eluted with  $\text{CH}_2\text{Cl}_2 - \text{benzene}$  (1 : 1, v/v).  $R_f$  : 0.8. Found : C, 39.19 ; H, 3.71 ; N,

17.49; S, 6.63; Mo, 20.0 %. Calc. for  $\text{MoC}_{16}\text{H}_{16}\text{N}_6\text{O}_4\text{S}$  : C, 39.67 ; H, 3.31 ; N, 17.36; S, 6.61; Mo, 19.8 %. UV-VIS absorption bands [DMF,  $\lambda_{\text{max}}^{\text{nm}}(\text{log}\epsilon)$ ]: 291 (3.93) ; 324.5 sh (4.0); 339 (4.02) ; 396 (3.76) ; 417.4 sh (3.73) ; 453 (3.5). Magnetic susceptibility value suggests the diamagnetic nature of this compound.

### **[Mo<sup>IV</sup>(pte<sub>1</sub>)(cys)]. 2CH<sub>3</sub>OH (3)**

This yellow compound was obtained in a similar way as (2) above, using a methanolic KOH solution (5 ml) of H<sub>2</sub>(cys) (0.121 g, 1 mmol dissolved in 0.056 g, 1 mmol of KOH) instead of H<sub>2</sub>(atp). Yield : 70 %. Solubility ca. 5 % in DMF. Its purity was checked through TLC (silica-gel GF<sub>254</sub> ; UV lamp), using DMSO solution (diluted with 150 times CHCl<sub>3</sub>) and CH<sub>2</sub>Cl<sub>2</sub> – benzene (1 : 1, v/v) as eluant. R<sub>f</sub> : 0.75. Found : C, 34.69 ; H, 4.15 ; N, 17.35; S, 6.30; Mo, 18.9 %. Calc. for  $\text{MoC}_{14}\text{H}_{20}\text{N}_6\text{O}_7\text{S}$  : C, 32.82 ; H, 3.91 ; N, 16.41; S, 6.25; Mo, 18.8 %. UV – VIS absorption bands [DMF,  $\lambda_{\text{max}}^{\text{nm}}(\text{log}\epsilon)$ ]: 291 (3.97) ; 341 (4.11) ; 400 (3.84) ; 420 (3.84) ; 455.5 (3.66). This compound was found to be diamagnetic in nature.

### **(Et<sub>4</sub>N)[(Mo<sup>V</sup>O<sub>3</sub>)(Hpte<sub>1</sub>)(Hcys)Cl<sub>3</sub>]. CH<sub>3</sub>OH (4)**

To a DMF solution (20 ml) of (Et<sub>4</sub>N)<sub>2</sub>[MoOCl<sub>5</sub>] (0.549 g, 1 mmol) in a three necked flask, H<sub>2</sub>(cys) (0.121 g, 1 mmol) dissolved in CH<sub>3</sub>OH (10 ml) containing Et<sub>4</sub>NOH (0.147 g, 1 mmol) was charged through an addition funnel. After 2 – 3 minutes, H<sub>2</sub>(pte<sub>1</sub>).0.5H<sub>2</sub>O (0.244 g, 1 mmol) in DMF (100 ml) was allowed to mix with the above reaction mixture at 301 K, through an another addition funnel. The pink–red colour of the solution slowly changed to yellowish – red on pterin ligand addition; heating and stirring in oilbath at 343K in darkness was continued for 2 h, during which the colour slowly changed to red. The solvent was removed in rotary evaporator at 343 K to get a red oil which on trituration with CH<sub>3</sub>OH (5 ml) gave a green precipitate which after standing for 1 h was filtered in a glass-fritte, washed with CH<sub>3</sub>OH, Et<sub>2</sub>O and dried over silica-gel vacuum desiccator. All the above operations were performed under dinitrogen atmosphere and darkness. Yield : 55 %. Solubility ca. 4.5 % in DMF. Purity of the product was checked through TLC (silica-gel GF<sub>254</sub> ; UV lamp) using DMSO solution (diluted with 100 times CH<sub>3</sub>OH), developed in CH<sub>2</sub>Cl<sub>2</sub> – CHCl<sub>3</sub> (2 : 1 v/v) mixture. R<sub>f</sub> : 0.33. Found : C, 29.23 ;

H, 5.19 ; N, 11.70 ; S, 3.40; Mo, 12.7 %. Calc. for  $\text{Mo}_2\text{C}_{21}\text{H}_{38}\text{N}_7\text{O}_9\text{SCl}_3$  : C, 29.22 ; H, 4.41 ; N, 11.4 ; S, 3.7; Mo, 12.5 %. UV – VIS absorption bands [DMF,  $\lambda_{\text{max}}^{\text{nm}}(\log\epsilon)$ ]: 289 (4.14); 341 (4.22); 396 (3.93); 417 (3.89); 452 sh (3.63). Magnetic susceptibility measurement indicated the diamagnetic nature of this compound.

**$[\text{Mo}^{\text{IV}}_2(\mu - \text{S})(\mu - \text{pte}_1)_2(\text{Hpte}_1)_2]. \text{CH}_3\text{OH}$  (5)**

A suspension of  $\text{H}_2(\text{pte}_1).0.5\text{H}_2\text{O}$  (0.244 g, 1 mmol) in  $\text{CH}_3\text{OH}$  (100 ml) was treated with a methanolic solution (70 ml) of  $(\text{Et}_4\text{N})_2[\text{Mo}^{\text{VI}}\text{O}_2\text{S}_2]$  (0.452 g, 1 mmol) in a Schlenk flask under stirring and pH was adjusted to 4.8 by HAc. The reaction mixture was subjected to stirring for 16 h at 301 K under dinitrogen atmosphere and darkness. A cream coloured precipitate appeared which was filtered using a sintered glass crucible, washed with  $\text{CH}_3\text{OH}$ ,  $\text{Et}_2\text{O}$  and dried in vacuo over silica-gel. Yield : 45 %. Solubility ca.4% in DMF. Purity of the product was checked through TLC (silica-gel GF<sub>254</sub> ; UV lamp) using DMSO solution (diluted with 50 times  $\text{CH}_3\text{OH}$ ) and  $\text{CH}_2\text{Cl}_2$  – benzene (1 : 1, v/v) mixture as eluant.  $R_f$  : 0.4. Found : C, 38.51; H, 4.02; N, 23.55; S, 3.0; Mo, 16.2%. Calc. for  $\text{Mo}_2\text{C}_{37}\text{H}_{34}\text{N}_{20}\text{O}_{13}\text{S}$  : C, 37.31; H, 2.86; N, 23.53; S, 2.70; Mo, 16.1%. UV – VIS absorption bands [DMF,  $\lambda_{\text{max}}^{\text{nm}}(\log\epsilon)$ ]: 291 (4.40); 341 (4.54); 398 (4.22); 418.6 (4.20); 453 (3.94). Magnetic susceptibility measurement suggests the diamagnetic nature of this compound.

**$[\text{Mo}^{\text{IV}}(\text{S}_2^{2-})(\text{pte}_1)(\text{CH}_3\text{OH})]. 3\text{CH}_3\text{OH}$  (6)**

A methanolic solution (30 ml) of  $(\text{Et}_4\text{N})_2[\text{Mo}^{\text{VI}}\text{S}_4]$  (0.484 g, 1 mmol) was treated with a suspension of  $\text{H}_2(\text{pte}_1).0.5\text{H}_2\text{O}$  (0.244 g, 1 mmol) in  $\text{CH}_3\text{OH}$  (100 ml), pH of the reaction mixture was adjusted to 4.8 using HAc, and subsequently stirring was continued at 301 K under dinitrogen atmosphere and darkness for 16 h. A dark – brown precipitate appeared which was recovered by filtration in sintered glass crucible, washed with solvents like  $\text{CH}_3\text{OH}$ ,  $\text{Et}_2\text{O}$  purged by dinitrogen and dried in vacuo over silica-gel. Yield : 60 %. Solubility ca. 4.5% in DMF. Its purity was checked through TLC (silica-gel GF<sub>254</sub> ; UV – chamber) using diluted (with 50 times  $\text{CH}_3\text{OH}$ ) DMSO solution and  $\text{CH}_2\text{Cl}_2$  – benzene (1 : 1 v/v) mixture as eluant.  $R_f$  : 0.7. Found : C, 28.81; H, 3.77; N, 12.80; S, 13.20; Mo, 18.6 %. Calc. for  $\text{MoC}_{13}\text{H}_{23}\text{N}_5\text{O}_7\text{S}_2$  : C, 29.90; H, 4.40; N, 13.40; S, 12.30; Mo, 18.4 %.

UV-VIS absorption bands [DMF,  $\lambda_{\max}^{\text{nm}}(\log\epsilon)$ ]: 291 (3.69); 341 (3.78); 398 (3.43); 419.8 (3.41); 455.5 (3.15). This compound was diamagnetic in nature.

## Results and Discussion

ESIMS spectrum of (1) shows a number of peaks corresponding to the different fragments e.g., the important peaks are assigned in the following ways:  $m/z = 745.2$ ,  $[M - O]^+$ ;  $m/z = 683.1$ ,  $[M - 2CH_3O - O]^+$ .

In case of (2), the molecular ion peak appeared at  $m/z = 484$ ,  $[M]^+$ , where 'M' is the molecular formula of (2) (F.W. = 483.94)<sup>7(a), 14, 15</sup>. The molecular ion peak, at  $m/z = 484$ , appeared with its characteristic isotopic distribution patterns and a good match with its simulated counterpart is obtained through the computer program<sup>46</sup> [Fig.(IV-1)]. Appearance of a total of nine distinct peaks suggests the mononuclear nature of the complex<sup>14</sup>.

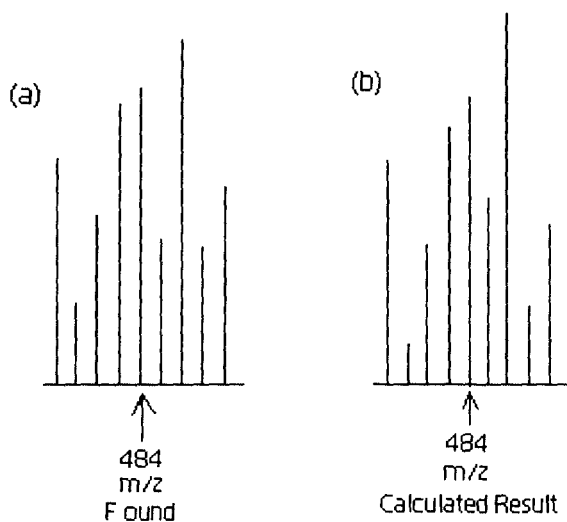


**Fig.(IV-1):** (a) ESIMS data of (2) at  $m/z (= 484)$  region corresponding to  $[M]^+$ ; (b) the calculated isotope pattern<sup>46</sup>. Formula :  $C_{16}H_{16}N_6O_4SMo$ .

ESIMS data of compound (3) gave the molecular ion peak at  $m/z = 512$ ,  $[M]^+$  which was simulated through the IPC program<sup>46</sup>, matching well with the experimental one [Fig. (IV- 2)], reflecting the mononuclear nature of the complex<sup>14</sup>.

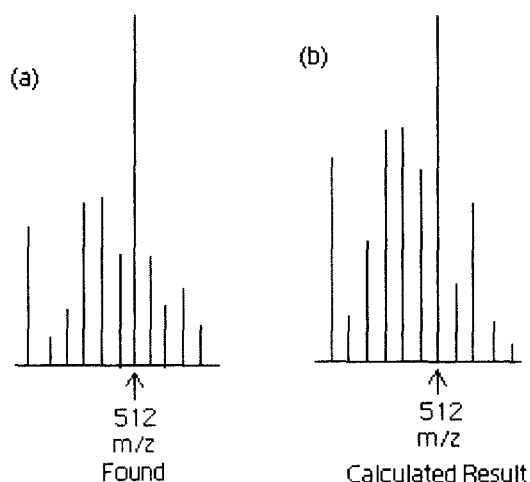


**Fig.(IV-2):** (a) ESIMS data of (3) at  $m/z$  (= 512) region corresponding to  $[M]^+$  ;  
 (b) the calculated isotope pattern <sup>46</sup>. Formula :  $C_{14}H_{20}N_6O_7SMo$ .

ESIMS spectrum of (4) contains a definite fragment obtained from molecular ion peak at  $m/z = 835$ ,  $[M - Et + 2H]^+$ ; where 'M' is the molecular formula of (4) (F.W. = 862.38)<sup>7(a), 14, 15</sup>. The peak at  $m/z = 835$  was simulated with the help of IPC computer program<sup>46</sup> and found to be in good agreement with the above experimental data [Fig.(IV-3)]. The multiplicity of peaks suggests the binuclear nature of the complex<sup>14</sup>.

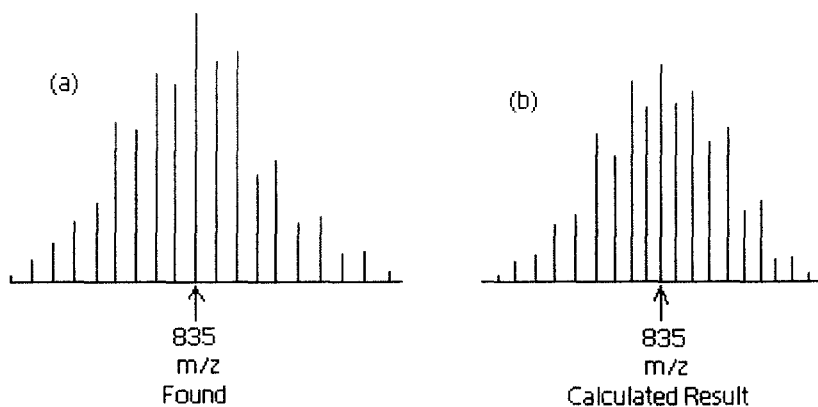


**Fig.(IV-3):** (a) ESIMS data of (4) at  $m/z$  (= 835) region corresponding to  $[M - Et + 2H]^+$  ;  
 (b) the calculated isotope pattern <sup>46</sup>. Formula :  $C_{20}H_{38}N_7O_8SCl_3Mo_2$ .

The ESIMS data of (5) are able to distinguish the bridging pattern ligands from the other two pterin ligand residues. For examples, the ESIMS peak at  $m/z = 693$  corresponds to the loss of two pterin ligand residues from (5) along with the solvent of crystallization, e.g.,  $m/z = 693$ ,  $[M + H - (CH_3OH + 2 pte_1)]^+$ . This peak is simulated

with IPC program <sup>46</sup> which is in good agreement with the experimental data [Fig.(IV-4)] <sup>195</sup>. Multiplicity of this peak (that is, the isotope distribution pattern) supports the binuclear nature of this complex <sup>14</sup>. Loss of a definite fragment, e.g., one or two ligand residues from a complex molecule, during the mass spectral process is well – established <sup>195</sup>.

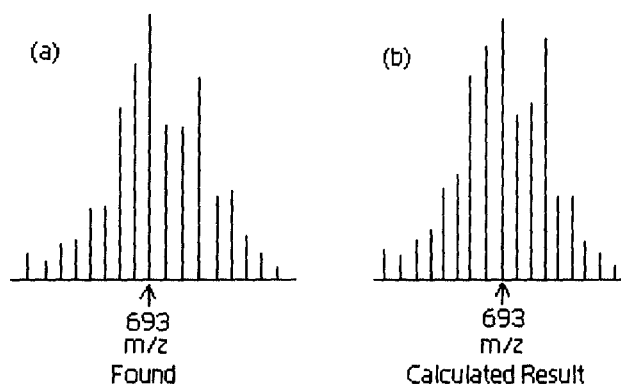


**Fig.(IV-4):**(a) ESIMS data of (5) at m/z (= 693) region corresponding to  $[M - CH_3OH - 2pte + H]^+$ ; (b) the calculated isotope pattern <sup>46</sup>. Formula :  $C_{18}H_{17}N_{10}O_6SMo_2$ .

In case of (6), the peak obtained from the molecular ion, appeared in the region of  $m/z = 525.0$ ,  $[M + 2H]^+$ , with its characteristic isotopic distribution pattern of Mo – atom along with the isotopic peaks of two S and other atoms for this mononuclear complex <sup>14</sup>; where ‘M’ is the molecular formula of (6) (F.W. = 520.94) <sup>7(a), 15</sup>. This peak is simulated with the help of IPC program <sup>46</sup> and the simulation result is in consistence with the experimentally found one [Fig.(IV-5)]. This validates the molecular formula of (6).

Some interesting observations can be inferred from the ESIMS spectral analysis of these complexes. ESIMS method involving a soft ionization technique provides with peaks having m/z values corresponding to either the molecular ion or

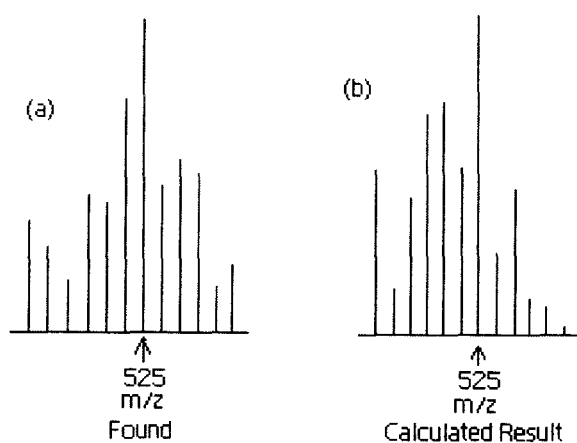


**Fig.(IV- 5):** (a) ESIMS data of (6) at  $m/z$  (= 525) region corresponding to  $[M + 2H]^+$ ; (b) the calculated isotope pattern<sup>46</sup>. Formula :  $C_{13}H_{27}N_5O_7S_2Mo$ .

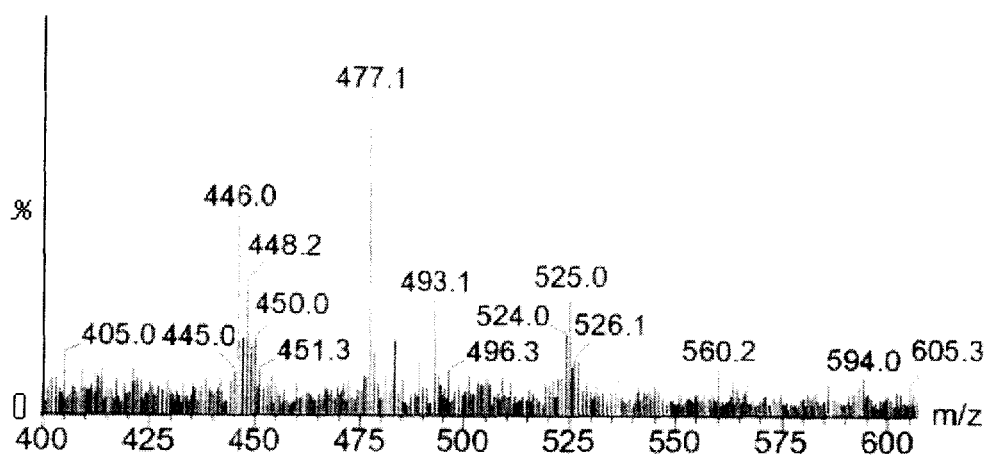
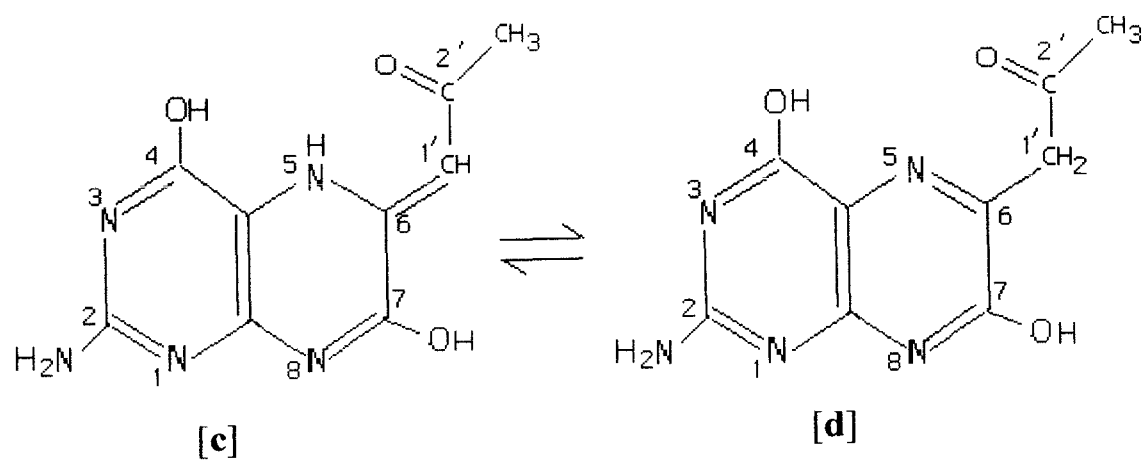
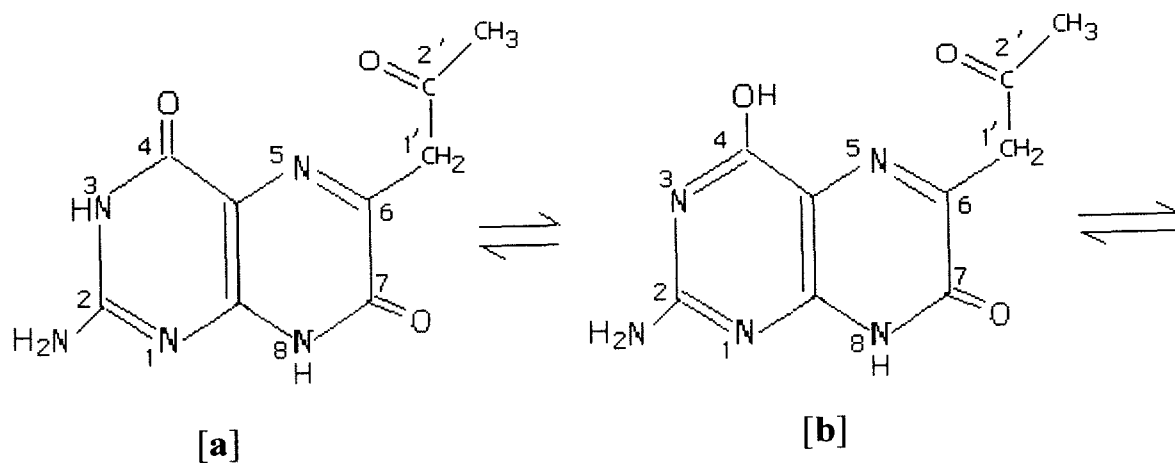


**Fig.(IV-6):** ESIMS spectrum of (6) in  $CH_3OH$

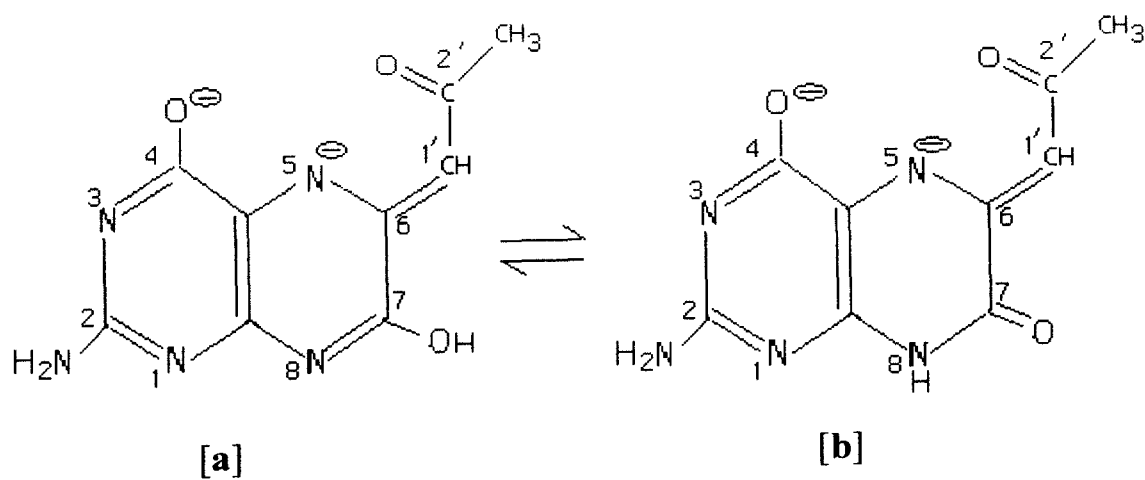
species obtained through loss of definite fragments from the molecular ion. Computer simulation of the isotope distribution pattern in each case verified the chemical composition of the original complex molecule; elemental analysis (carbon – hydrogen – nitrogen) data and different physico – chemical and spectroscopic data support this inference regarding chemical composition as well as presence of different functional groups in the complex molecule. Different authors have pointed out that compounds where both the X – ray crystal structure data and ESIMS data are available, they are in good agreement. In this sense, ESIMS method is a valuable tool for characterizing complex compounds without recourse to X – ray crystallography<sup>48, 179, 180</sup>.

$\Lambda_M$  [(6 – 11.5)  $\text{ohm}^{-1} \text{cm}^2 \text{mol}^{-1}$ , 301K,  $\text{CH}_3\text{OH}$ ] values of **(1)**, **(2)**, **(3)**, **(5)** & **(6)** are consistent with the non-electrolytic formulation of these complexes<sup>43</sup>. On the other hand  $\Lambda_M$  (84.6  $\text{ohm}^{-1} \text{cm}^2 \text{mol}^{-1}$ , 301K,  $\text{CH}_3\text{OH}$ ) value of **(4)** suggests a 1 : 1 electrolytic nature<sup>43</sup> of this complex as proposed in its molecular formula.

A comparative study of IR spectrum of  $\text{H}_2(\text{pte}_1)$  and that of its complexes is helpful in drawing useful inferences regarding ligand donor sites involved in metal – ligand interactions.  $\text{H}_2(\text{pte}_1)$  [Fig.(IV – 7)] shows intense peaks in the region 1695 – 1630  $\text{cm}^{-1}$  corresponding to the different types of  $\nu(\text{C} = \text{O})$  modes as per Scheme (IV-2); the ligand bands in the region 1614 – 1450  $\text{cm}^{-1}$  reflect the  $\nu(\text{C} = \text{C})$  and  $\nu(\text{C} = \text{N})$  modes of the pterin ring. The free ligand IR bands at 1361  $\text{cm}^{-1}$  (associated with shoulders) and 1248  $\text{cm}^{-1}$  (relatively broad) due to  $\delta(\text{OH})$  and  $\nu(\text{C} - \text{O}) + \delta(\text{OH})$  vibrations, respectively of  $\text{OH}(4)$ , undergo distinct modifications in the corresponding complexes, e.g., **(2)** and a new relatively sharp band appears at 1255  $\text{cm}^{-1}$  assignable to  $\nu(\text{C} - \text{O})$  (4) mode of the corresponding phenoxide group<sup>69, 70</sup>. Most of the aforesaid IR bands also undergo modifications during the complex formation process, due to the changes in electronic structure during the ligand anion formation process, as evident from a comparison of Schemes (IV-2) and (IV-3). The amide functions in position 3, 4 and the vinylogous amide in position 5 including the side – chain (6 – substituent) are involved in the pterin ligand dianion ( $\text{pte}_1^{2-}$ ) formation. The pterin ligand residue ( $\text{pte}_1^{2-}$ ) is bonded to the Mo(IV) atom [e.g., in **(2)**] through the O(4) and N(5) atoms with the Mo – N(5) bond playing a pivotal role, as established through X – ray crystallographic studies on several molybdenum – pterin complexes<sup>3, 5, 20, 127</sup>. Considering proximity of the O(2') atom to the above chelating site, it can be inferred that ( $\text{pte}_1^{2-}$ ) can function as a tridentate O(4), N(5), O(2') donor in suitable cases, e.g., **(2)**, as verified through CHEM3D modeling (discussed later)<sup>113</sup>. Joule and coworkers concluded from both chemical and X – ray structural studies that sufficiently greater basicity / nucleophilicity resides at N(5) than at N(8), thereby supporting such coordination property<sup>88(a)</sup>.



**Scheme (IV-2)**



**Scheme (IV-3)**

For (3) two additional bands could be identified at  $1489\text{ cm}^{-1}$  and  $1405\text{ cm}^{-1}$ , assignable to  $\nu_{as}$  and  $\nu_s$  modes of the  $\text{CO}_2^-$  group (cysteine residue) respectively<sup>69</sup>.

As far as the IR spectral region  $1000 - 750\text{ cm}^{-1}$  is concerned, for (1) the  $\nu(\text{Mo}=\text{O})$  and  $\nu(\text{Mo}-\text{O}-\text{Mo})$  bands appear at  $921\text{ cm}^{-1}$ ,  $895\text{ cm}^{-1}$  and  $844\text{ cm}^{-1}$  respectively; the corresponding bands of (4) appear at  $953\text{ cm}^{-1}$ ,  $921\text{ cm}^{-1}$  and  $795\text{ cm}^{-1}$  respectively<sup>19, 55</sup>.

For (5), a relatively weak band at  $490\text{ cm}^{-1}$  corresponds to the  $\nu(\text{Mo}-\text{S}-\text{Mo})$  mode; in case of (6), the  $\nu(\text{Mo}-\text{S})$  mode appears at  $470\text{ cm}^{-1}$ <sup>19, 40, 55</sup>.

The elemental analysis, ESIMS and IR data are in conformity with the chemical compositions of (1) to (6) formulated here;  $^1\text{H}$  NMR data and CHEM3D representations (discussed later) support this view, with the latter throwing light on the molecular structures. Their reactivity aspects as delineated here towards  $\text{Me}_3\text{N}\rightarrow\text{O}$  point out the existence of the molybdenum atom in a lower oxidation state [e.g., Mo(IV)] in (2), (3), (5) and (6); for (4) IR bands characteristic of the  $[\text{Mo}^{\text{V}}_2\text{O}_3]^{4+}$  core are commensurate with the presence of a Mo(V) atom here<sup>19, 55</sup>. The ability of (1) to react with  $\text{PPh}_3$  can be correlated with the presence of a Mo(VI) atom in this case. The pterin ligand  $[\text{H}_2(\text{pte}_1)]$  acts as a reducing agent during the complex formation process in most of these cases; (1) is an exception, as the DMSO used during its synthesis for solubility reasons, oxidized the intermediate product<sup>34(b)</sup>, leading ultimately to the  $[\text{Mo}^{\text{VI}}_2\text{O}_5]^{2+}$  core. This observation is in conformity with the studies in Chapter II, Section – I that the relevant Mo(V) – pterin complex can reduce DMSO through OAT reaction, giving a  $[\text{Mo}^{\text{VI}}_2\text{O}_5]^{2+}$  species. Maintenance of dinitrogen atmosphere and darkness during synthesis of these complexes is vital for getting pure products; otherwise, intractable products are obtained. Controlled heating in a paraffin oil bath ensures both the purity and the appropriate yield for (4).

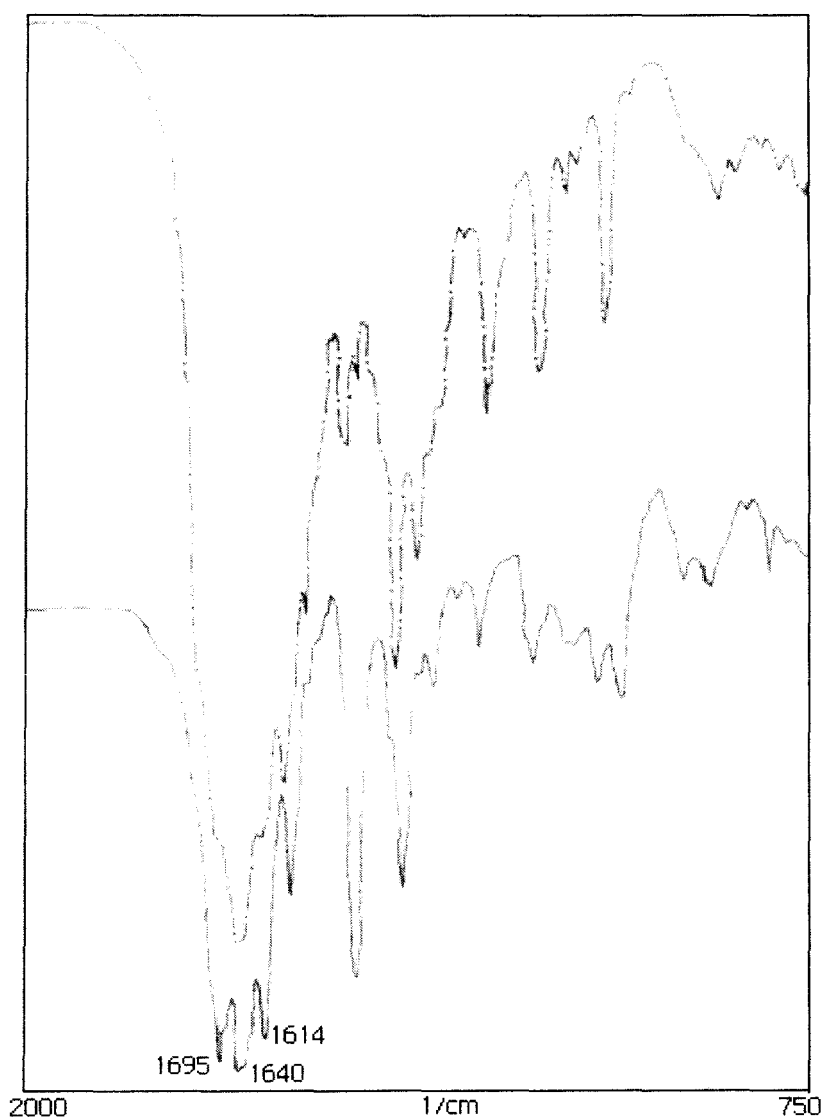
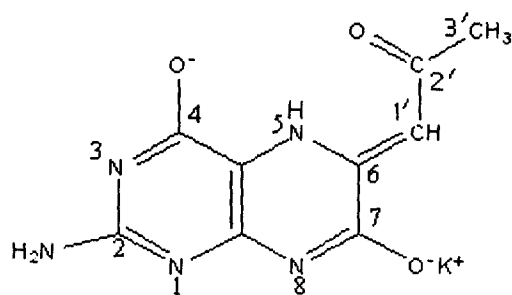


**Fig.(IV-7):** IR spectra of  $H_2(pte_1)$  [—] and of (2) [—•—•—]

All the complexes reported here are diamagnetic and exhibit good  $^1H$  NMR spectra. (1) is a  $d^0$  [Mo(VI)] system, (5) contains a  $[Mo^V_2O_3]^{4+}$  core, that is, an oxygen bridged binuclear species with two  $d^1$  [Mo(V)] centres ; well – characterized cases are mostly diamagnetic with cis – or trans – disposition of the two  $Mo = O$  bonds about the bridging oxygen atom<sup>19, 55</sup>. The  $d^2$  [Mo(IV)] systems [complexes (2), (3), (5) and (6)] present with interesting examples of diamagnetism<sup>26</sup>. As discussed in Chapter III, there is possibility of spin pairing of the two  $d$  – electrons in the  $d_{xy}(b_2)$  orbital in a low symmetry environment as well as strong antiferro-magnetic coupling with the delocalized electrons of the pterin ring<sup>19, 20(a), 55</sup>.

The possible existence of the pterin ligand [H<sub>2</sub>(pte<sub>1</sub>)] or its anion (pte<sub>1</sub><sup>2-</sup>) in several tautomeric forms as shown in Schemes (IV-2) and (IV-3), is in conformity with the discussion by different authors<sup>3, 20, 40, 89</sup>. <sup>1</sup>H NMR data of these complexes have been interpreted on the basis of appropriate tautomeric forms (indicated by the appropriate Scheme number in Table (IV-1) along with the corresponding data). Presence of sulphur containing ancillary ligands [Scheme (IV-1)] in most of these cases as well as the reaction conditions help to manifest the appropriate / required tautomeric form in each case. It is interesting to note that change from nonaromatic to aromatic state of the pyridine ring of the pterin moiety or conversion of its 7 – oxo group to OH(7) group [Schemes (IV-2) and (IV-3)], involve changes in oxidation state of the pterin ring<sup>4, 143</sup>, which is transmitted via the delocalized electron system of the pterin ring, upto the metal centre<sup>20(a)</sup>; this is coupled with the reactivity at the metal centre, e.g., reduction of Me<sub>3</sub>N→O or oxidation of PPh<sub>3</sub> as determined by the relevant case<sup>1, 2, 26</sup>. This redox ‘non – innocent’ behaviour of the pterin ring justifies its role as the essential component of several types of redox enzymes, e.g., oxomolybdoenzymes, tungstopterin enzymes, phenylalanine hydroxylases, etc.

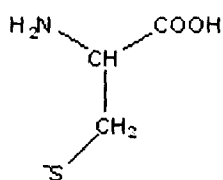


**Scheme (IV – 4) ; (KHpte<sub>1</sub><sup>-</sup> residue)**

In (1) the <sup>1</sup>H NMR signals of CH and CH<sub>2</sub> parts of (Hcys<sup>-1</sup>) residue [Scheme (IV – 5a)] appears at δ, 1.03 (t) and 2.04 (d) respectively. The NH<sub>2</sub> proton signal of (Hcys<sup>-1</sup>) residue appears at δ, 6.65 (bd) indicating coupling with the adjacent CH- proton. The presence of –COOH proton signal of (Hcys<sup>-1</sup>) (δ, 13.60 ,bs), indicates that the –COOH group is not deprotonated and is not involved in coordination with the metal

**Table (IV-1):**  $^1\text{H}$  NMR data of the pertinent complexes in  $\text{DMSO} - d_6$  ( $\delta$ , ppm versus TMS).

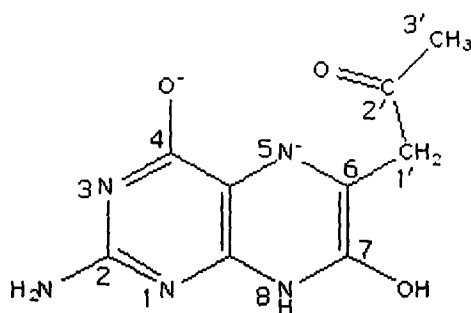
Compound [Scheme]	Signals
(1) [Schemes IV-4 and IV-5]	$\text{CH}_3(3')$ ( $\delta$ 2.16, d) $\text{CH}(1')$ ( $\delta$ 6.08, s); $\text{NH}_2(2)$ ( $\delta$ 6.98, bs); $\text{NH}_2(\text{HCys}^-)$ ( $\delta$ 6.65, bd); $\text{CH}(\text{HCys}^-)$ ( $\delta$ 1.03, t); $\text{CH}_2(\text{HCys}^-)$ ( $\delta$ 2.04, d); $-\text{CO}_2\text{H}(\text{HCys}^-)$ ( $\delta$ 13.6, bs); $\text{OH}(\text{CH}_3\text{OH})$ ( $\delta$ 13.40, bs); $\text{CH}_3(\text{CH}_3\text{OH})$ ( $\delta$ 3.77, s).
(2) [Schemes IV-6 and IV-7]	$\text{CH}_3(3')$ ( $\delta$ 2.05, t); $\text{CH}_2(1')$ ( $\delta$ 1.22 q); $\text{NH}_2(2)$ ( $\delta$ 5.96, bd); $\text{NH}(8)$ ( $\delta$ 11.08, bt); $\text{OH}(7)$ ( $\delta$ 13.62, bs); $\text{NH}(\text{atp}^{2-})$ ( $\delta$ 12.32, bt); aromatic protons ( $\text{atp}^{2-}$ ) ( $\delta$ 6.72, m); $\text{OH}(\text{CH}_3\text{OH})$ ( $\delta$ 14.25, bs); $\text{CH}_3(\text{CH}_3\text{OH})$ ( $\delta$ 3.72, s).
(3) [Schemes IV-6 and IV-5(b)]	$\text{CH}_3(3')$ ( $\delta$ 2.17, t); $\text{CH}_2(1')$ ( $\delta$ 1.08, q); $\text{NH}_2(2)$ ( $\delta$ 7.0, bs); $\text{NH}(8)$ ( $\delta$ 12.4, bs); $\text{OH}(7)$ ( $\delta$ 13.20, bs); $\text{NH}_2(\text{Cys}^{2-})$ ( $\delta$ 6.65, d); $\text{CH}(\text{Cys}^{2-})$ ( $\delta$ 1.12, t); $\text{CH}_2(\text{Cys}^{2-})$ ( $\delta$ 2.06, d).
(5) [Schemes IV-8 and IV-9]	$\text{CH}_3(3' - \text{pte}_1^{2-})$ ( $\delta$ 2.18, d); $\text{CH}(1' - \text{pte}_1^{2-})$ ( $\delta$ 5.80, s); $\text{NH}_2(2 - \text{pte}_1^{2-} / \text{Hpte}_1^-)$ ( $\delta$ 7.01, bs); $\text{NH}(8 - \text{pte}_1^{2-})$ ( $\delta$ 12.35, bs); $\text{CH}_3(3' - \text{Hpte}_1^-)$ ( $\delta$ 3.74, s); $\text{CH}_2(1' - \text{Hpte}_1^-)$ ( $\delta$ 1.00, q); $\text{NH}(8 - \text{Hpte}_1^-)$ ( $\delta$ 10.97, bs).
(6) [Schemes IV-6 (form a) and IV-9 (form b)]	$\text{CH}_3(3' - \text{form a})$ ( $\delta$ 2.19, t); $\text{CH}_2(1' - \text{form a})$ ( $\delta$ 3.20, q); $\text{NH}_2(2 - \text{forms a,b})$ ( $\delta$ 6.75, bs); $\text{NH}(8 - \text{form a})$ ( $\delta$ 11.12, bt); $\text{OH}(7 - \text{form a})$ ( $\delta$ 10.98, bs); $\text{CH}_3(3' - \text{form b})$ ( $\delta$ 1.15, d); $\text{CH}(1' - \text{form b})$ ( $\delta$ 5.84, s); $\text{NH}(8 - \text{form b})$ ( $\delta$ 12.35, t); $\text{OH}(\text{CH}_3\text{OH})$ ( $\delta$ 13.65, bs); $\text{CH}_3(\text{CH}_3\text{OH})$ ( $\delta$ 3.74, s).



**Scheme (IV – 5a)** ; (Hcys<sup>-1</sup> residue)

**Scheme (IV – 5b)** ; (cys<sup>2-</sup> residue)

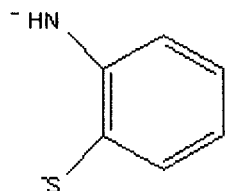
centre; the (Hcys<sup>-1</sup>) ligand residue here acts as a S, N – donor bidentate ligand<sup>30</sup> [Scheme (IV – 5a)]. The CH(1') [Scheme (IV – 4)] proton signal appears at  $\delta$ , 6.08 (s) supporting the olefinic nature of this carbon atom<sup>85,90</sup>. The pterin ligand residue here acts as a uninegative tridentate O, N, O – donor monopotassium salt [Scheme (IV – 4)], with the Mo – N(5) bond playing the pivotal role in the metal pterin bonding process as discussed earlier. The protonic integration values of the CH signal of (Hcys<sup>-1</sup>) residue and CH<sub>3</sub> (3') signal of (KHpte<sub>1</sub><sup>-1</sup>) residue indicate a 1 : 1 ratio of (Hcys<sup>-1</sup>) : (KHpte<sub>1</sub><sup>-1</sup>) moiety in (1) as indicated in its molecular formula. The OH signal (of coordinated CH<sub>3</sub>OH molecule) is strongly deshielded and appears at  $\delta$  13.40; the same trend is observed (in the range  $\delta$  13.65 – 14.25) for (2) and (6). The OH signal of CH<sub>3</sub>OH molecule of crystallization in all these complexes (1 – 6) could not be assigned with certainty.



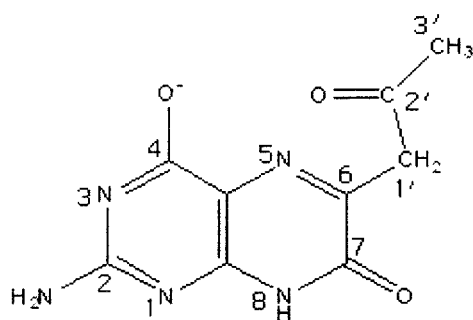
**Scheme (IV – 6)** ; (pte<sub>1</sub><sup>2-</sup> residue)

In case of (2), the CH<sub>2</sub>(1') proton signal appears at  $\delta$ , 1.22 (q) suggesting coupling with the CH<sub>3</sub>(3') protons<sup>34</sup> which appears at  $\delta$  2.05 (t). The OH (7) proton signal appears at  $\delta$  13.62 (bs). So, the pterin residue in (2) behaves as a binegative tridentate O, N, O – donor [Scheme (IV – 6)]. NH<sub>2</sub> proton signal is generally observed at ca.  $\delta$ , 7.0; in (2) the NH proton signal of the (atp<sup>2-</sup>) residue appears at  $\delta$ , 12.32 (bt);

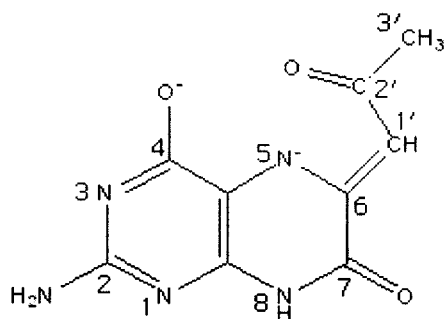
this deshielding is due to coordination of the  $\text{NH}_2$  group of ( $\text{H}_2\text{atp}$ ) through deprotonation [Scheme (IV – 7)] with the ( $\text{atp}^{2-}$ ) residue acting here as a binegative bidentate S, N – donor ligand <sup>31</sup>. Deprotonation of the  $\text{NH}_2$  group of 2 – aminothiophenol and its coordination property as a dianionic [ $\text{atp}^{2-}$ , Scheme IV – 7)] N, S – donor ligand in a Mo(V) complex, [ $\text{Mo}^{\text{V}}(\text{SC}_6\text{H}_4\text{NH})_2(\text{dedtc})$ ] has been established through X – ray crystallography <sup>31</sup>.



**Scheme (IV – 7)** ; ( $\text{atp}^{2-}$  residue)



**Scheme (IV – 8)** ; ( $\text{Hpte}_1^-$  residue)



**Scheme (IV – 9)** ; ( $\text{pte}_1^{2-}$  residue)

The proton NMR data of (3) [Table (IV – 1)] suggest the presence of a similar type of pterin ligand residue ( $\text{pte}_1^{2-}$ ) as in (2) [Scheme (IV – 6)]. But contrary to (1), in this case there is no  $^1\text{H}$  signal due to  $-\text{COOH}$  group of  $\text{H}_2(\text{cys})$ . So, it can be inferred that  $-\text{COOH}$  group is ionized in this complex to satisfy the charge balance on the  $\text{Mo}^{\text{IV}}$  centre and hence the cysteine ligand here acts as a binegative tridentate one <sup>32</sup> [Scheme (IV – 5b)].

The presence of two types of pterin ligand residues ( $\text{Hpte}_1^{-1}$  &  $\text{pte}_1^{2-}$ ) [Schemes (IV – 8) & (IV – 9)] in (5) as proposed in its molecular formula is supported by the  $^1\text{H}$  NMR data [Table (IV – 1)]. Here, the pterin ligand residues act as mono and binegative ones respectively and use the O(4), N(5) and C(2') – O centers to form a bridge between two  $\text{Mo}^{\text{IV}}$ - atoms in (5) <sup>3(b), 5, 19, 27, 39</sup> [Fig.(IV – 12)]. The NH(8) proton signal is observed at  $\delta$ , 10.97 and 12.35, that is, an appreciable amount of deshielding from the usual NH proton signal region (ca.  $\delta$  7.0). Absence of OH(7) proton signal suggests the presence of 7 – oxo groups as proposed in Schemes (IV – 8) & (IV – 9), maintaining overall charge balance of the complex.

The  $^1\text{H}$  NMR data of (6) [Table (IV – 1)] support the presence of two tautomeric forms of pterin ligand residue [Scheme (IV – 6) (form a) and Scheme (IV – 9) (form b)] in its molecule. The NH(8) proton signal appeared at  $\delta$ , 11.12 (bt) and at  $\delta$ , 12.35 (t) corresponding to form a and form b respectively. The peak at  $\delta$ , 5.84 (s) due to olephinic CH proton (form b) and at  $\delta$ , 3.20 (q) due to  $\text{CH}_2(1')$  protons (form a), substantiate the above inference regarding two tautomeric forms of the ligand <sup>89</sup>. Other  $^1\text{H}$  NMR signals appear at their expected positions [Table (IV – 1)].

A comparison of the Schemes (IV-2), (IV-3), (IV-4), (IV-6), (IV-8) & (IV-9) shows the basic change over in electronic structure of the pterin ligand during its coordination process, as evident from IR and  $^1\text{H}$  NMR spectral data, including attainment of aromatic character for the pyrimidine ring system of  $\text{H}_2(\text{pte}_1)$ . The lone pairs of the different types of N – atoms as well as the electron density of the double bonds, impart a reducing character to the ligand, leading to the reduction of the molybdenum (VI / V) starting materials during complex formation process. This change in electronic structure involving the entire ligand molecule is responsible for the above mentioned shielding

process of the CH<sub>2</sub>(1') and CH<sub>3</sub>(3') protons in most of the cases. In most cases NH<sub>2</sub>(2) protonic signals experience some amount of deshielding which can be accounted for by the strong intermolecular hydrogen bonding interaction with suitable functional groups of other molecules / CH<sub>3</sub>OH molecule. Although the –OH signal of CH<sub>3</sub>OH usually appears around  $\delta$  5.0 ; in complexes (1), (2) and (6), it appears at  $\delta$ , 13.40 – 14.25 (bs) indicating strong coordination of the – OH group of CH<sub>3</sub>OH to the Mo – atom. Coordination of the CH<sub>3</sub>OH molecule to the molybdenum atom in different types of compounds, sometimes leading to deprotonation / methoxide coordination, has been proposed by various workers and has been characterized by X-ray crystallographic data<sup>3, 18, 20, 27</sup>.

The above information helped in building up the schematic structures of complexes (1) to (6) which were optimized by molecular mechanics calculations (MM2), giving the lowest steric energy (Kcal/mol) CHEM3D models [e.g., Fig.(IV – 8) to Fig.(IV – 13)], and throwing light on both stability and geometry of these compounds<sup>86, 87</sup>. The atom numbering system of these optimized structures was set by the computer program used here<sup>87</sup>.

The molecular modelling force fields in use for molecular systems can be interpreted in terms of the four key contributions, e.g., bond stretching, angle bending, torsional terms and non-bonded interactions<sup>86, 111, 112</sup>; apart from the lowest steric energies of the molecules, two basic parameters were evaluated, e.g., bond distances (Å) and bond angles (deg.), the most relevant of which are shown in Table (IV – 2) to Table (IV – 8), together with the literature data obtained through X-ray structural studies on molybdenum complexes with different pterin ligands and other relevant compounds<sup>3, 5, 9, 20, 55, 109, 110, 128-140, 142</sup>; this is in conformity with the recent trends of structure elucidation using optimized computational models<sup>108, 113, 135</sup>. In Table (IV – 3) to (IV – 8) all the selected computed bond lengths are supported by literature X – ray structural data (in parenthesis); most of the computed bond angles centred around the molybdenum atom / atoms are shown here for indicating the coordination geometry around the metal atom, but few of them could be supported by literature X – ray data for the paucity of comparable types of mixed ligand molybdenum – pterin complexes.

Concentrating on the chelating aspect of the pterin ligand towards molybdenum, the Mo-N(5) bond plays a pivotal role here [Scheme (IV – 4), (IV – 6), (IV – 8) & (IV –9) indicates the O(4), N(5) etc, numbering system] and for this very bond distance, a fair agreement is observed between the computed and experimental data<sup>3, 5, 9, 20, 55, 109, 110, 128-140, 142</sup>; the calculated Mo-O(4) bond distance is slightly shorter than the available X – ray structural data, but this value is close to the Mo – O<sub>b</sub> bond distance (1.88 – 1.97 Å) of Mo – O<sub>b</sub> – Mo bridges ( of binuclear complex ) and is much longer than the terminal Mo=O<sub>t</sub> bond distance (1.66 – 1.67 Å). For the other bond lengths data (Å) shown in Table (IV – 3) to (IV – 8), good agreement is observed between the computed and literature X – ray structural data as well.

In this CHEM3D calculation program<sup>86, 87, 111, 112</sup> all the possible arrangements / orientations of the groups, atoms, side-chains of each complex, molecule were considered and consequently all the probable molecular structures (CHEM3D) were drawn ; but only one out of these CHEM3D structures possessed minimum steric energy and hence showed maximum stability. For the sake of brevity, only the thermodynamically most stable form, out of several probable molecular structures, is presented here along with the relevant bond length, bond angle information table<sup>180</sup>.

**Table (IV – 2):** Comparison of selected optimized bond lengths (Å) and bond angles (deg.) in the free ligand [H<sub>2</sub>(pte<sub>1</sub>)] [Fig. (II-8)] and its molybdenum complex (2) [Fig.(IV-9)].

Bond	Bond Distance(Å) <sup>+</sup>	Bond	Bond Distance(Å) <sup>+</sup>
C(1)-N(7)	1.41 [1.43]	C(1)-C(3)	1.48 [1.38]
C(3)-O(11)	1.22 (1.21–1.23) [1.37]	C(1)-C(2)	1.37 [1.41]
C(9)-O(13)	1.22 (1.24) [1.36]	C(3)-N(4)	1.37 (1.39 – 1.40) [1.36]
C(2)-N(6)	1.40 [1.35]	C(9)-N(10)	1.36 (1.30 – 1.44) [1.43]
C(15)-C(16)	1.51 [1.50]	C(5)-N(12)	1.37 [1.38]
C(2)-N(10)	1.35 [1.38]	C(8)-C(14)	1.50 (1.51) [1.52]
N(7)-C(8)	1.28 (1.36–1.47)[1.47]	C(14)-C(15)	1.51 [1.50]
C(8)-C(9)	1.49 (1.47–1.54)	N(4)-C(5)	1.35 [1.36]
C(15)-O(17)	1.21 [1.21]		

<b>Angle Atoms</b>	<b>Bond Angle(deg.)<sup>+</sup></b>	<b>Angle Atoms</b>	<b>Bond Angle(deg.)<sup>+</sup></b>
C(1)-N(7)-C(8)	118.7 [116.3]	C(3)-C(1)-C(2)	118.2 [120.5]
C(3)-N(4)-C(5)	124.8 [118.9]	C(1)-C(3)-N(4)	114.8 [120.0]
N(6)-C(2)-C(1)	121.6 [118.3]	N(10)-C(2)-C(1)	119.8 [114.5]
C(2)-N(10)-C(9)	122.7 [123.4]	N(7)-C(1)-C(2)	121.0 [125.5]

<sup>+</sup> Free ligand data are mentioned outside the bracket and the data derived from its molybdenum complex (2), are mentioned within third bracket. Available X – ray structural data are shown within first bracket. Atom numbering system as shown in Fig.(II-8).

Tables (IV – 2) shows the bond lengths and bond angles of the free ligand, H<sub>2</sub>(pte<sub>1</sub>), and that of the pterin ligand residue in one of the mononuclear complexes in this series e.g., complex (2). Comparing these two sets of data it is clear that both bond lengths and bond angles of the ligand residue have undergone a distinct change during the complex formation process, thereby providing justification for Schemes (IV-2), (IV-3), (IV-6), (IV-8).

The C(3)-O(11) and N(7)-C(8) bond lengths are increased from 1.22Å to 1.37 Å and from 1.28 Å to 1.47 Å respectively, corroborating to the fact that electron density is withdrawn from these bonds due to molybdenum centre coordination through O(11) and N(7) atoms. Other bond lengths and bond angles also have undergone changes due to redistribution of overall electron density on metal coordination.

This change in electron density in the pterin ligand residue on complexation with molybdenum atom is reflected in different physical data, such as, UV–VIS, <sup>1</sup>H NMR, fluorescence, IR spectra etc., discussed later. These data support increased electron density in the pterin ligand residue in almost all the molybdenum – pterin complexes.

Fig.(IV-8) reflects the most stable (steric energy = 19.9 Kcal mol<sup>-1</sup>) form, that is slightly distorted octahedral geometry around both the Mo<sup>VI</sup> centers in the new complex (1). This structure contains a nonaromatic pterin moiety specially its 1,4-diazine ring, which permits some amount of puckering in the ligand system and also has a skew disposition of the (Mo<sup>VI</sup><sub>2</sub>O<sub>5</sub>)<sup>2+</sup> core; O(4), N(5) and O(2) of (KHpte<sup>-1</sup>) ligand residue [Scheme (IV- 4)] are coordinated to one of the Mo<sup>VI</sup> - atom; other three coordination positions are occupied by the three oxygen atoms ( two terminal & one bridging) of (Mo<sup>VI</sup><sub>2</sub>O<sub>5</sub>)<sup>2+</sup> core. Coordination positions of the other Mo<sup>VI</sup> -centre is satisfied by N & S - atoms of (Hcys<sup>-1</sup>) [Schemes (IV - 5)], methanolic O - atom and three O - atoms of the (Mo<sup>VI</sup><sub>2</sub>O<sub>5</sub>)<sup>2+</sup> core. This agreement between computed bond length data (Å) and experimental data on related systems is fair [Table (IV-3)]. This structure indicates realistic nature of the Schemes (IV-4) & (IV-5).

Stiefel has pointed out in his comprehensive review that the Mo -O<sub>b</sub> - Mo bridge in the binuclear complexes with (Mo<sup>VI</sup><sub>2</sub>O<sub>5</sub>)<sup>2+</sup> core, may be linear or nonlinear depending on the other ligands in the coordination sphere of the two Mo(VI) centres<sup>19</sup>. In case of (1) [Fig.(IV-8)] presence of a non linear Mo -O<sub>b</sub> - Mo is indicated, which affords its maximum thermodynamic stability. A molybdenum - pterin complex possessing a (Mo<sup>VI</sup><sub>2</sub>O<sub>5</sub>)<sup>2+</sup> core with bent (Mo<sup>VI</sup><sub>2</sub>O<sub>5</sub>)<sup>2+</sup> bridge has been characterized by X - ray crystallography<sup>27</sup>.

Table (IV-3) shows computed bond angles, in fair agreement with the different types of bond angles found from X-ray structural studies on different molybdenum - pterin systems with distorted octahedral geometry around the Mo - atoms (both mono and binuclear types)<sup>3, 5, 20(a-c), 27, 114, 115, 116</sup> as well as a molybdenum - cysteine complex where the cysteine ligand acts as a N, S - donor<sup>131</sup>. The fair agreement in Mo(22)-S(23), N(7)-Mo(20) and O(21)-Mo(22) bond lengths is noteworthy.

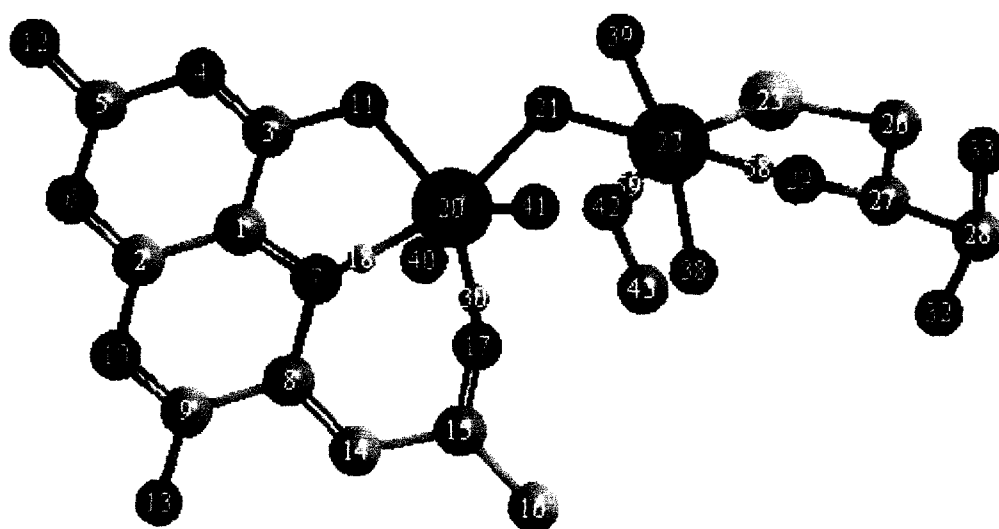


**Fig.(IV- 8):** The optimized geometry (CHEM 3D model obtained through MM2 calculations) of (1) with a steric energy of 19.9 Kcal mol<sup>-1</sup>. Its numbering system is set by the software used<sup>87</sup> and is different from that in Scheme (IV - 4).

**Table (IV-3):** Comparison of selected computed bond lengths(Å) and bond angles (deg.) involving Mo - atom in (1) from the optimized geometry [Fig.(IV -8), MM2 calculations] with the available literature data (in parenthesis) from X-ray structural studies\*

Bond	Bond Distance(Å) <sup>+</sup>	Bond	Bond Distance(Å) <sup>+</sup>
Mo(22)-S(23)	2.35(2.37) <sup>131</sup>	N(7)-Mo(20)	2.12(2.02) <sup>3</sup>
O(21)-Mo(22)	1.97(1.93) <sup>131</sup>	Mo(20)-O(40)	1.96(1.70) <sup>109</sup>
O(17)-Mo(20)	2.03(2.01) <sup>109</sup>	N(29)-Mo(22)	2.00(2.18) <sup>109, 131</sup>
(11)-Mo(20)	1.97(2.23) <sup>3</sup>	O(42)-Mo(22)	2.09(2.32) <sup>109</sup>
Angle Atoms	Bond Angle(deg.) <sup>+</sup>	Angle Atoms	Bond Angle(deg.) <sup>+</sup>
S(23)-Mo(22)-O(39)	115.2 (115.9) <sup>109</sup>	C(3)-O(11)-Mo(20)	113.1 (112.1) <sup>3</sup>
Mo(20)-N(7)-C(1)	120.1 (119.3) <sup>3</sup>	N(29)-Mo(22)-O(39)	107.0 (103.3) <sup>109</sup>
O(11)-Mo(20)-N(7)	81.1 (74.1) <sup>3</sup>	N(29)-Mo(22)-S(23)	80.4 (77.5) <sup>109, 131</sup>
O(21)-Mo(20)-O(17)	125.4 (105.9) <sup>109</sup>	O(21)-Mo(20)-N(7)	160.6 (158 - 169)
O(17)-Mo(20)-O(11)	154.3 (146.7)	O(17)-Mo(20)-N(7)	73.3 (72 - 74)
O(21)-Mo(22)-O(39)	78.3	O(39)-Mo(22)-O(38)	164.1
O(21)-Mo(22)-S(23)	92.8		

<sup>+</sup> Here O(11), N(7) and O(17) correspond to O(4), N(5) and O(2') donor atoms respectively, of the pterin ring as per Scheme (IV – 4), while N(12) and N(6) correspond to the 2-substituent NH<sub>2</sub> and N(1) respectively.

<sup>\*</sup> X-ray structural data have been collected from references mentioned as superscript on the data within parenthesis and / or 3,5,19,20,55,109,110,129-134.

Here, O(4) of (KHpte<sub>1</sub><sup>-1</sup>) [Scheme (IV-4)] and S of (Hcys<sup>-1</sup>) [Scheme (IV-5)] formed covalent bonds, while N(5), O(2') and N of (Hcys<sup>-1</sup>) formed coordinate bonds (pink colour) with the metal centers; the CH<sub>3</sub>OH molecule is coordinated through O(42)<sup>109</sup>.

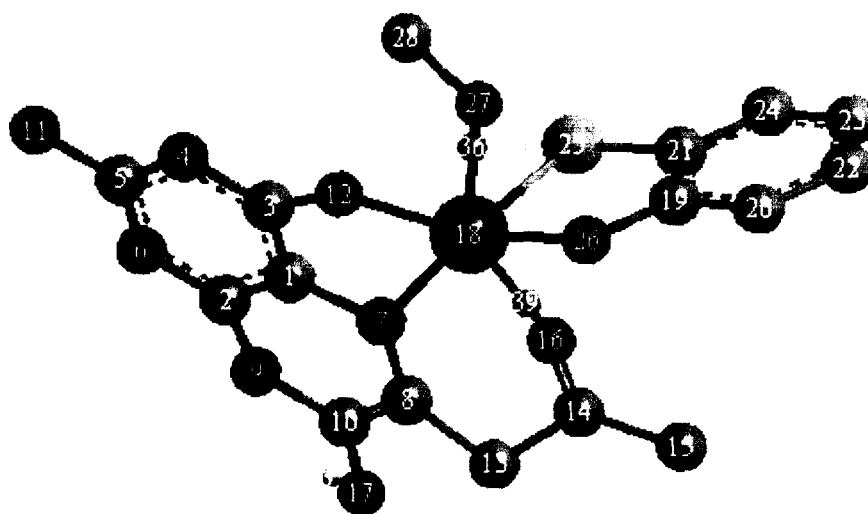


**Fig.(IV-9):** The optimized geometry (CHEM 3D model obtained through MM2 calculations) of (2) with a steric energy of 24.9 Kcal mol<sup>-1</sup>. Its numbering system is set by the software used<sup>87</sup> and is different from that in Scheme (IV – 6).

**Table (IV-4):** Comparison of selected computed bond lengths(Å) and bond angles (deg.) involving Mo – atom in (2) from the optimized geometry [Fig.(IV –9), MM2 calculations] with the available literature data (in parenthesis) from X-ray structural studies<sup>\*</sup>

Bond	Bond Distance(Å) <sup>+</sup>	Bond	Bond Distance(Å) <sup>+</sup>
S(25)-Mo(18)	2.36(2.37) <sup>109, 110</sup>	O(27)-Mo(18)	2.14(2.32) <sup>109</sup>
N(7)-Mo(18)	2.05(2.02) <sup>3</sup>	N(26)-Mo(18)	2.02(2.18) <sup>109</sup>
O(16)-Mo(18)	2.04(2.01) <sup>109</sup>	O(12)-Mo(18)	1.97(2.23) <sup>3</sup>

Angle Atoms	Bond Angle(deg.) <sup>+</sup>	Angle Atoms	Bond Angle(deg.) <sup>+</sup>
N(7)-Mo(18)-O(12)	76.3(74.1) <sup>3(c)</sup>	C(3)-O(12)-Mo(18)	115.6(112.1) <sup>3(c)</sup>
S(25)-Mo(18)-N(26)	83.0(77.5) <sup>109, 130</sup>	S(25)-Mo(18)-O(12)	124.1(115.0) <sup>109</sup>
Mo(18)-N(7)-C(1)	110.3(119.3) <sup>3(c)</sup>	N(7)-Mo(18)-O(16)	73.9(73.1) <sup>89</sup>
O(16)-Mo(18)-O(12)	147.6(146.7) <sup>89</sup>	N(7)-Mo(18)-S(25)	112.8
O(16)-Mo(18)-S(25)	79.7	N(26)-Mo(18)-O(12)	126.7
O(16)-Mo(18)-N(26)	72.9		

<sup>+</sup> Here O(12), N(7) and O(16) correspond to O(4), N(5) and O(2') donor atoms respectively, of the pterin ring as per Scheme (IV – 6), while N(11) and N(6) correspond to the 2-substituent NH<sub>2</sub> and N(1) respectively.

<sup>\*</sup> X-ray structural data have been collected from references mentioned as superscript on the data within parenthesis.

The most stable CHEM3D model [Fig. (IV-9)] of (**2**) exhibits distorted octahedral geometry around the Mo<sup>IV</sup> – atom. Its three coordination positions are occupied by the O(4), N(5) & O(2') donor atoms of (pte<sub>1</sub><sup>-2</sup>) ligand residue; N & S – atoms of (atp<sup>2-</sup>) satisfy other two coordination sites and the remaining sixth coordination position is occupied by a CH<sub>3</sub>OH molecule through O – coordination. The bonding pattern in this structure is in conformity with Schemes (IV – 6) & (IV – 7), which are proposed in consistence with all the characterization data of (**2**). The relevant computed bond lengths data (Å) are in agreement with literature X – ray data [Table (IV- 4)] ; this Table also shows computed bond angles, within the range of different types of bond angles found from X-ray structural studies on different molybdenum – pterin systems with distorted octahedral geometry around the Mo – atoms<sup>3, 5, 20(a-c), 27, 114, 115, 116</sup> as well as a molybdenum complex of 2 – aminothiophenol<sup>130</sup>. Significant are the cases of S(25)-Mo(18), N(7)-Mo(18) and O(16)-Mo(18) bond lengths matching.

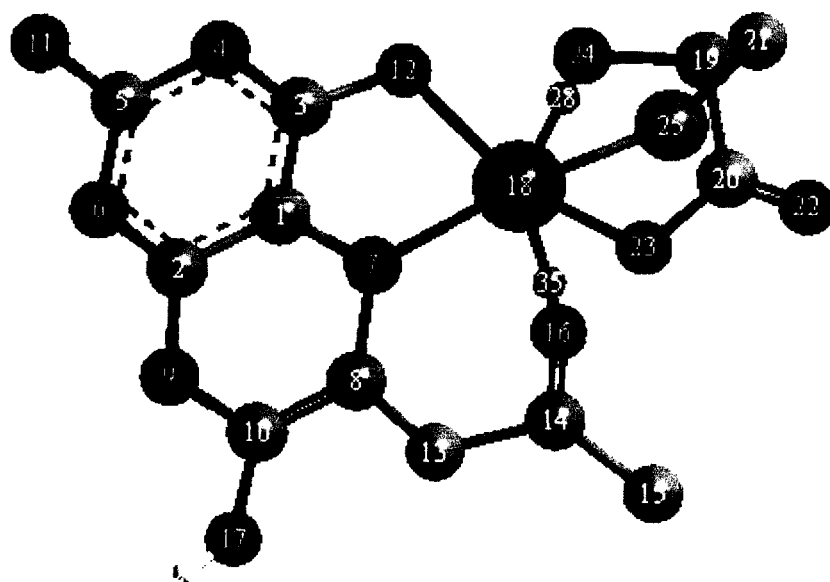


**Fig.(IV-10):** The optimized geometry (CHEM3D model obtained through MM2 calculations) of (3) with a steric energy of 24.1 Kcal mol<sup>-1</sup>. Its numbering system is set by the software used<sup>87</sup> and is different from that in Scheme (IV - 6).

**Table (IV-5):** Comparison of selected computed bond lengths(Å) and bond angles (deg.) involving Mo – atom in (3) from the optimized geometry [Fig.(IV -10), MM2 calculations] with the available literature data (in parenthesis) from X-ray structural studies<sup>88</sup>.

Bond	Bond Distance(Å) <sup>+</sup>	Bond	Bond Distance(Å) <sup>+</sup>
N(24)-Mo(18)	2.02(2.18) <sup>109</sup>	S(25)-Mo(18)	2.37(2.37) <sup>109, 110</sup>
O(12)-Mo(18)	1.98(2.23) <sup>3</sup>	Mo(18)-O(16)	2.02(2.01) <sup>109</sup>
N(7)-Mo(18)	2.05(2.02) <sup>3</sup>	O(23)-Mo(18)	1.99(1.93) <sup>109</sup>
Angle Atoms	Bond Angle(deg.) <sup>+</sup>	Angle Atoms	Bond Angle(deg.) <sup>+</sup>
O(12)-Mo(18)-N(7)	76.1(74.1) <sup>3(c)</sup>	N(24)-Mo(18)-S(25)	75.8(80.7) <sup>128</sup>
C(3)-O(12)-Mo(18)	115.3(112.1) <sup>3(c)</sup>	Mo(18)-N(7)-C(1)	110.0(119.3) <sup>3(c)</sup>
O(12)-Mo(18)-S(25)	111.6(115.9) <sup>109</sup>	N(7)-Mo(18)-O(16)	74.1(73.1) <sup>114</sup>
S(25)-Mo(18)-O(23)	82.1(78.3) <sup>128</sup>	N(24)-Mo(18)-O(23)	74.7(70.3) <sup>128</sup>
O(12)-Mo(18)-O(16)	147.6 (146.7) <sup>114</sup>		

Here O(12), N(7) and O(16) correspond to O(4), N(5) and O(2') donor atoms respectively, of the pterin ring as per Scheme (IV – 6), while N(11) and N(6) correspond to the 2-substituent NH<sub>2</sub> and N(1) respectively.

<sup>†</sup> X-ray structural data have been collected from references mentioned as superscript on the data within parenthesis.

Fig.(IV–10) reflects the most stable CHEM3D model with distorted octahedral geometry (steric energy = 24.1 Kcal mol<sup>-1</sup>) of (3). An interesting observation is that the CHEM3D structure which contains aromatic ring in (pte<sub>1</sub><sup>2-</sup>) [Scheme(IV-6)] is more stable than the other form which contains a nonaromatic pterin ring in its structure. The coordination around the Mo(IV) atom in (3) are fulfilled by O(4), N(5), O(2') of the (pte<sub>1</sub><sup>2-</sup>) ring and O, S and N atoms of (cys<sup>2-</sup>) ligand residue [Scheme(IV- 5b)].

The relevant computed bond angles data in Table (IV – 5), are in the range of X-ray structural studies on different molybdenum – pterin systems with distorted octahedral geometry around the Mo – atom<sup>125, 126, 127, 134, 135, 136</sup> as well as a binuclear molybdenum (V) – cysteine complex where each cysteine residue acts as a tridentate O, N, S – donor<sup>128</sup>. Good matching is observed for S(25)-Mo(18), Mo(18)-O(16) and N(7)-Mo(18) bond lengths.

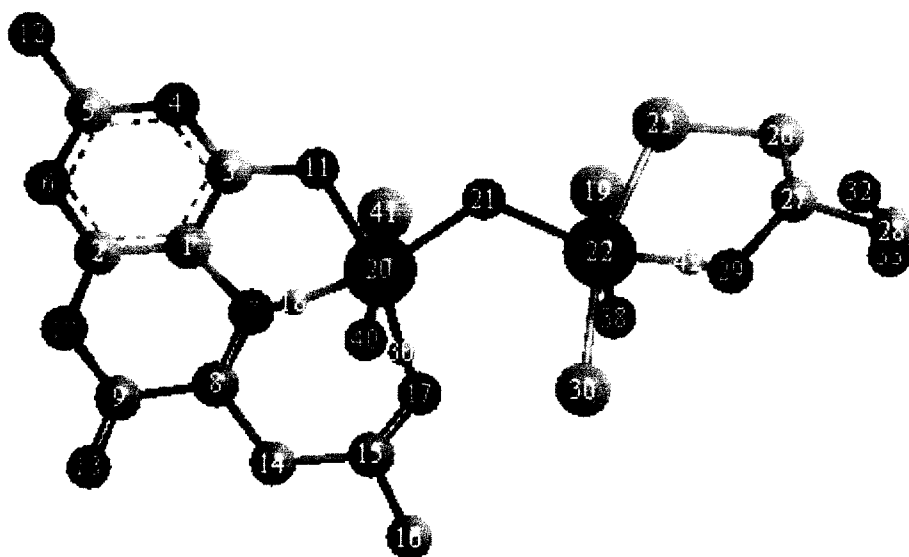


**Fig.(IV–11):** The optimized geometry (CHEM3D model obtained through MM2 calculations) of (4) with a steric energy of 24.6 Kcal mol<sup>-1</sup>. Its numbering system is set by the software used<sup>87</sup> and is different from that in Scheme (IV – 8).

**Table (IV-6):** Comparison of selected computed bond lengths(Å) and bond angles (deg.) involving Mo – atom in (4) from the optimized geometry [Fig.(IV –11), MM2 calculations] with the available literature data (in parenthesis) from X-ray structural studies\*.

<b>Bond</b>	<b>Bond Distance(Å)<sup>+</sup></b>	<b>Bond</b>	<b>Bond Distance(Å)<sup>+</sup></b>
Mo(22)-S(23)	2.35(2.37) <sup>109, 110</sup>	O(17)-Mo(20)	2.15(2.01) <sup>109</sup>
O(21)-Mo(22)	1.96 (1.93) <sup>128</sup>	N(29)-Mo(22)	2.01(2.18) <sup>109</sup>
Mo(22)-Cl(19)	2.29(2.38) <sup>3(c)</sup>	Mo(20)-Cl(41)	2.31(2.38) <sup>3(c)</sup>
N(7)-Mo(20)	2.07(2.02) <sup>3(c)</sup>	O(11)-Mo(20)	1.97(2.23) <sup>3(c)</sup>
Mo(22)-O(38)	1.95(1.80) <sup>109</sup>	Mo(22)-Cl(30)	2.31(2.38) <sup>3(c)</sup>
Mo(20)-O(40)	1.95(1.70) <sup>55</sup>	Mo(20)-Cl(41)	2.31(2.38) <sup>3(c)</sup>
Mo(20)-O(21)	1.95(1.95) <sup>128</sup>		

<b>Angle Atoms</b>	<b>Bond Angle(deg.)<sup>+</sup></b>	<b>Angle Atoms</b>	<b>Bond Angle(deg.)<sup>+</sup></b>
S(23)-Mo(22)-N(29)	78.2(77.5) <sup>109, 131</sup>	Cl(19)-Mo(22)-Cl(30)	91.6(91.9) <sup>108</sup>
N(7)-Mo(20)-O(11)	83.2(74.1) <sup>3(c)</sup>	Cl(19)-Mo(22)-O(21)	90.0(89.6) <sup>108</sup>
S(23)-Mo(22)-O(38)	94.1(97.7) <sup>109</sup>	C(3)-O(11)-Mo(20)	113.5(112.1) <sup>3(c)</sup>
Mo(20)-N(7)-C(1)	118.0(119.3) <sup>3(c)</sup>	O(17)-Mo(20)-O(21)	112.3(105.9) <sup>109</sup>
N(7)-Mo(20)-O(17)	82.2(73.1) <sup>114</sup>	N(29)-Mo(22)-Cl(30)	85.6
O(40)-Mo(20)-O(17)	80.1	Mo(22)-O(21)-Mo(20)	120.8

\* Here O(11), N(7) and O(17) correspond to O(4), N(5) and O(2') donor atoms respectively, of the pterin ring as per Scheme (IV – 8), while N(12) and N(6) correspond to the 2-substituent NH<sub>2</sub> and N(1) respectively.

\* X-ray structural data have been collected from references mentioned as superscript on the data within parenthesis.

Fig.(IV-11) shows the most stable CHEM3D model of (4) (steric energy = 24.6 Kcal mol<sup>-1</sup>) containing a slight distorted octahedral environment around each Mo<sup>V</sup> – center of the (Mo<sup>V</sup><sub>2</sub>O<sub>3</sub>)<sup>4+</sup> core. The bonding pattern is, O(4) of Hpte<sub>1</sub><sup>-</sup> and one Cl - atom formed covalents with one Mo atom of the (Mo<sup>V</sup><sub>2</sub>O<sub>3</sub>)<sup>4+</sup> core. Other two coordination positions are occupied by N(5) and O(2') of the Hpte<sub>1</sub><sup>-</sup> ring through coordinate bonding. The S – of Hcys<sup>-</sup> and two Cl – atoms formed covalent bonds with another Mo<sup>V</sup> – center of the (Mo<sup>V</sup><sub>2</sub>O<sub>3</sub>)<sup>4+</sup> core and the N – of Hcys<sup>-</sup> [Scheme (IV-5a)] made coordinate bond (pink colour) with that Mo atom. Rest of the coordination positions are occupied by the terminal and bridging oxygen atoms. This lowest energy structure possesses a skew disposition of the terminal O – atoms for its (Mo<sup>V</sup><sub>2</sub>O<sub>3</sub>)<sup>4+</sup> core and aromatic pyrimidine of pterin ring residue. On the other hand, the cis dioxomolybdenum core [(Mo<sup>V</sup><sub>2</sub>O<sub>3</sub>)<sup>4+</sup>] containing CHEM3D structure possesses slightly higher amount of energy and is not shown here.

The Mo(22)-S(23), O(21)-Mo(22), N(7)-Mo(20), Mo(20)-Cl(41) etc. bond lengths in Table (IV-6), show fair matching between the computed and experimental data. The computed bond angles are in agreement with the different types of bond angles found from X-ray structural studies on different molybdenum – pterin systems with distorted octahedral geometry around the Mo – atoms (both mono and binuclear types)<sup>3, 5, 20(a-c), 27, 114, 115, 116</sup> as well as a binuclear Mo(V) complex with cysteine ligand where it acts as a bidentate N, S – donor<sup>131</sup>.

The most stable CHEM3D model of (5) is shown in Fig.(IV-12) (steric energy = 65.2 Kcal mol<sup>-1</sup>), exhibits distorted octahedral geometry around each metal center. This structural representation is in consistency with Schemes (IV – 8) & (IV – 9) drawn above as per the characterization data of the complex. In this triply bridged complex, both the Mo<sup>IV</sup> –centers have symmetrical environment ; O(4) & N(5) atoms of two pterin ligand residues coordinate to each molybdenum atom; rest of the coordination positions are occupied by O(4), N(5) and O(2) atoms of the two (μ – pte<sub>1</sub>)<sup>2-</sup> residues and by the bridging sulphur ligand.

Table (IV-7) shows Mo(18)-S(19), N(7)-Mo(18), O(52)-Mo(18) etc. bond lengths having fair agreement with the experimental data. The table also reflects different types of computed bond angles of (5), which are in agreement with the bond angles found

from X-ray structural studies on different molybdenum – pterin systems with distorted octahedral geometry around the Mo – atoms (both mono and binuclear types)<sup>3, 5, 20(a-c), 27, 114, 115, 116</sup>. X – ray structural data exists on triply bridged binuclear molybdenum complexes with pterin<sup>27</sup> and other ligands<sup>136-138</sup> as well as sulphur bridged complexes<sup>139, 140</sup>.

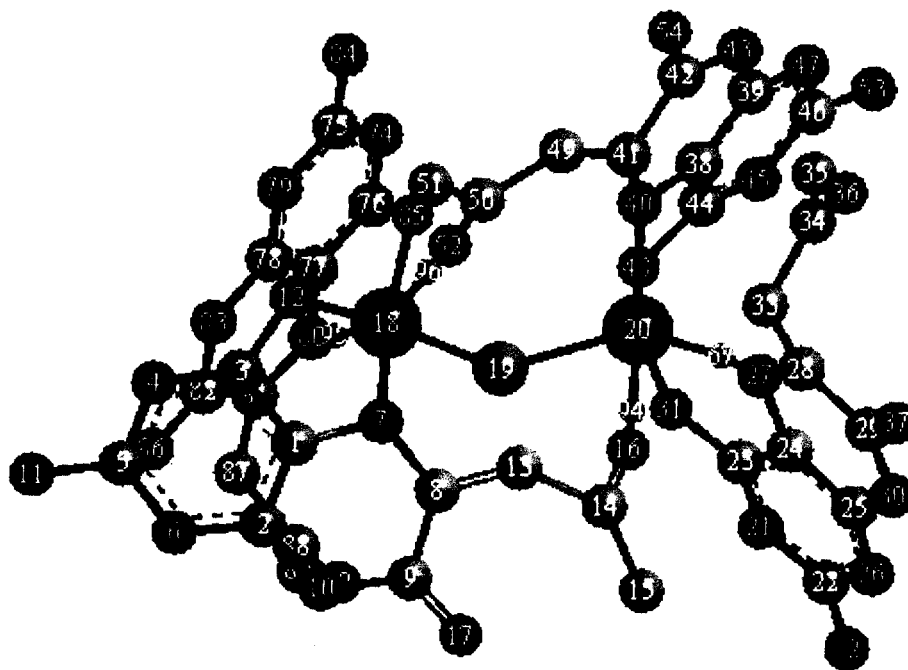


**Fig.(IV– 12):** The optimized geometry (CHEM3D model obtained through MM2 calculations) of (5) with a steric energy of 65.2 Kcal mol<sup>-1</sup>. Its numbering system is set by the software used<sup>87</sup> and is different from that in Scheme (IV – 8)/(IV – 9).

**Table (IV–7):** Comparison of selected computed bond lengths(Å) and bond angles (deg.) involving Mo – atom in (5) from the optimized geometry [Fig.(IV –12), MM2 calculations] with the available literature data (in parenthesis) from X-ray structural studies\*.

Bond	Bond Distance(Å) <sup>+</sup>	Bond	Bond Distance(Å) <sup>+</sup>
Mo(18)-S(19)	2.33(2.37) <sup>109, 110</sup>	N(7)-Mo(18)	2.06(2.01) <sup>20(b)</sup>
O(12)-Mo(18)	1.95(2.29) <sup>20(b)</sup>	N(27)-Mo(20)	2.12(2.03) <sup>20(b)</sup>
N(80)-Mo(18)	2.14(2.03) <sup>20(b)</sup>	O(48)-Mo(20)	1.96(2.29) <sup>20(b)</sup>
O(52)-Mo(18)	2.01(2.01) <sup>109</sup>	S(19)-Mo(20)	2.35(2.37) <sup>109, 110</sup>
O(85)-Mo(18)	2.03(2.29) <sup>20(b)</sup>	O(16)-Mo(20)	2.09(2.01) <sup>109</sup>
N(14)-Mo(20)	2.06(2.03) <sup>20(b)</sup>	O(31)-Mo(20)	2.01(2.29) <sup>20(b)</sup>

Angle Atoms	Bond Angle(deg.) <sup>†</sup>	Angle Atoms	Bond Angle(deg.) <sup>†</sup>
O(48)-Mo(20)-N(40)	74.4(74.1) <sup>3(c)</sup>	O(12)-Mo(18)-N(7)	72.5(74.1) <sup>3(c)</sup>
S(19)-Mo(18)-N(80)	84.0(77.5) <sup>109</sup>	O(12)-Mo(18)-O(52)	80.7(78.1) <sup>109</sup>
Mo(18)-O(12)-C(3)	109.3(112.1) <sup>3(c)</sup>	O(85)-Mo(18)-N(80)	78.4(74.1) <sup>3(c)</sup>
O(12)-Mo(18)-N(80)	98.6(103.3) <sup>109</sup>	C(1)-N(7)-Mo(18)	110.5(119.3) <sup>3(c)</sup>
O(52)-Mo(18)-S(19)	100.3(115.9) <sup>109</sup>	S(19)-Mo(20)-O(16)	80.98(84.8) <sup>27</sup>
O(12)-Mo(18)-O(85)	107.8	(48)-Mo(20)-O(31)	70.8
S(19)-Mo(20)-N(40)	110.7	O(52)-Mo(18)-N(7)	93.5
O(16)-Mo(20)-N(27)	69.6	O(85)-Mo(18)-S(19)	79.2
S(19)-Mo(20)-O(31)	78.9		

<sup>†</sup> Here O(12/31/48/85), N(7/27/40/80) and O(16/52) correspond to O(4), N(5) and O(2') donor atoms respectively, of the pterin ring as per Scheme (IV – 8)/(IV – 9).

\* X-ray structural data have been collected from references mentioned as superscript on the data within parenthesis.

Out of several probable CHEM3D representations of (6), the most stable one (steric energy = 119.7 Kcal mol<sup>-1</sup>) is presented in Fig.(IV–13). This distorted octahedral geometry contains the pterin ligand residue (pte<sub>1</sub><sup>2-</sup>) as depicted in Scheme (IV – 9) above. Here again O(4), N(5) and O(2') atoms of the (pte<sub>1</sub><sup>2-</sup>) residue coordinate to the Mo<sup>IV</sup> atom; (S<sub>2</sub>)<sup>2-</sup> acts as a dihapto disulphide chelating ligand; the sixth coordination position is occupied by a CH<sub>3</sub>OH molecule through O – coordination. Literature X – ray structural data are available on molybdenum and tungsten complexes with different types of ligands containing coordinated dihapto disulphide or methanol molecule<sup>40, 109</sup>.

Mo(18)-N(7), Mo(18)-O(15), S(20)-Mo(18) etc. bond lengths in Table (IV–8) reflects good matching between the computed and experimental data. The computed bond angles of (6) are in agreement with the bond angles found from X-ray structural studies on different molybdenum – pterin systems with distorted octahedral geometry around the Mo – atoms (both mono and binuclear types)<sup>3, 5, 20(a-c), 27, 114, 115, 116</sup>.

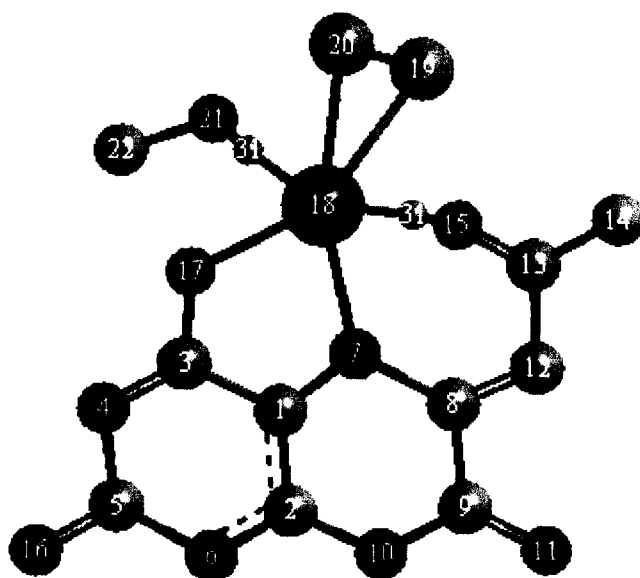


**Fig.(IV-13):** The optimized geometry (CHEM 3D model obtained through MM2 calculations) of (6) with a steric energy of 119.7 Kcal mol<sup>-1</sup>. Its numbering system is set by the software used<sup>87</sup> and is different from that in Scheme (IV - 6)/(IV - 9).

**Table (IV-8):** Comparison of selected computed bond lengths(Å) and bond angles (deg.) involving Mo - atom in (6) from the optimized geometry [Fig.(IV-13), MM2 calculations] with the available literature data (in parenthesis) from X-ray structural studies<sup>88</sup>.

Atoms	Bond Distances(Å) <sup>+</sup>	Atoms	Bond Distances(Å) <sup>+</sup>
Mo(18)-N(7)	2.06(2.02) <sup>20(b)</sup>	Mo(18)-O(15)	2.02(2.01) <sup>109</sup>
O(21)-Mo(18)	2.12(2.32) <sup>109</sup>	Mo(18)-S(19)	2.48(2.39-2.42) <sup>89</sup>
S(20)-Mo(18)	2.47(2.39-2.42) <sup>89</sup>	O(17)-Mo(18)	1.97(2.23) <sup>3(c), 20(b)</sup>
S(19)-S(20)	2.43(2.032) <sup>89</sup>		

Angle Atoms	Bond Angle(deg.) <sup>+</sup>	Angle Atoms	Bond Angle(deg.) <sup>+</sup>
N(7)-Mo(18)-O(17)	75.3(74.1) <sup>3(c)</sup>	C(3)-O(17)-Mo(18)	114.9(112.1) <sup>3(c)</sup>
C(1)-N(7)-Mo(18)	112.4(119.3) <sup>3(c)</sup>	S(19)-Mo(18)-O(17)	147.6(153.0) <sup>109</sup>
O(15)-Mo(18)-N(7)	72.7(73.1) <sup>114</sup>	O(15)-Mo(18)-O(17)	135.8(146.7) <sup>114</sup>
S(19)-Mo(18)-O(21)	78.1	O(15)-Mo(18)-S(20)	79.4
S(19)-Mo(18)-O(15)	76.4	O(21)-Mo(18)-S(20)	78.0
S(19)-Mo(18)-S(20)	58.8	N(7)-Mo(18)-S(20)	145.0

<sup>†</sup> Here O(17), N(7) and O(15) correspond to O(4), N(5) and O(2') donor atoms respectively, of the pterin ring as per Scheme (IV – 6), while N(16) and N(6) correspond to the 2-substituent NH<sub>2</sub> and N(1) respectively.

<sup>\*</sup> X-ray structural data have been collected from references mentioned as superscript on the data within parenthesis.

The above discussions on the geometrical aspects of optimized computational model (MM2) of the new complex compounds, having agreement with available X-ray structural data (e.g., bond length, bond angle and overall geometry) verifies the applicability of such an approach to molybdenum – pterin systems and provides the frame work for discussion on their spectroscopic, reactivity and other relevant aspects<sup>108, 113</sup>.

From a perusal of the above CHEM3D representations of the present complex compounds, it can be inferred that they are compatible with the schemes (IV –4 to IV – 9) utilized for interpreting the <sup>1</sup>H NMR spectral data in Table (IV – 1), except for a case, (6), where different energy factors in solution (e.g., salvation energy, hydrogen bonding interactions, etc) may convert one tautomeric form of the pterin ligand anion to a more stable one<sup>127, 141</sup>.

Analysis of UV-VIS absorption spectra of the present complex compounds side by side of that of their common pterin ligand, provide information regarding the nature of metal- ligand bonding. UV-VIS spectra of (1 to 6) contain all characteristic peaks of H<sub>2</sub>(pte<sub>1</sub>) but are slightly shifted towards the lower wavelength region due to coordination. A shoulder at 324.5 in (1) & (2) is due to the presence of secondary ligand (Hcys<sup>-1</sup> & atp<sup>-2</sup> respectively). There is a considerable increase in intensity (log $\epsilon$  – values) of the ligand bands in the complexes (essentially  $\pi \rightarrow \pi^*$  type). This can be accounted for by the NH<sub>2</sub>(2) lone pair electronic drift through the pterin ring towards the metal- centre coordination site and justifies the reduction capability of the metal-centres in (2) – (6). This increased  $\pi$  – electron density also comes from deprotonation of H<sub>2</sub>(pte<sub>1</sub>) prior to complexation with the Mo – atom to form (Hpte<sub>1</sub>)<sup>-1</sup> or (pte<sub>1</sub>)<sup>-2</sup> with aromatic character. These observations are substantiated by the NMR studies discussed above. An interesting observation regarding the log $\epsilon$  – values of all the six complexes (1 – 6) is

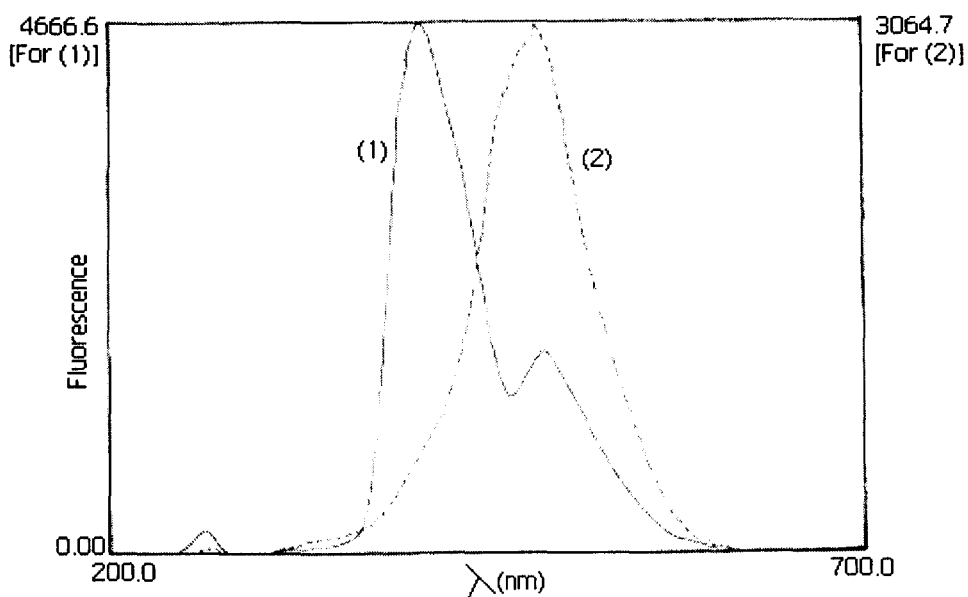


**Fig.(IV-14):**Fluorescence spectra of (2) [ $1.05 \times 10^{-4}$ (M)] in DMF, curve (1) for the complex & curve (2) that of its oxidized product [ $1.05 \times 10^{-4}$ (M)] after reaction with  $\text{Me}_3\text{N} \rightarrow \text{O}$  in DMF.

that the UV - VIS spectrum of (5) shows the highest  $\log \epsilon$  values indicating highest  $\pi$  - electron density in it among all the six complexes here. This is due to the presence of four pterin ring residues in the complex, which are deprotonated during complexation and hence contain high  $\pi$  - electron density. Ligand to metal charge transfer (LMCT) transitions in the 380 - 450 nm region, account for the colours (dark green, dark brown, pink-red, etc) of these complexes; presence of sulphur donor ligands allow them to retain sufficient absorption beyond 550 nm<sup>19, 20(a), 55</sup>. This finding is also supported by <sup>1</sup>H NMR, CHEM3D studies as well as fluorescence [Fig.(IV -14)] of (2).

As far as the fluorescence spectral property is concerned, the pterin ligand [ $\text{H}_2(\text{pte}_1)$ ] itself is essentially nonfluorescent, indicating dominance of its nonaromatic tautomer [Scheme (IV-2)(a)] in methanol. The fluorescence spectral property of (2) [curve (1) of Figure (IV - 14)] can be ascribed to a couple of factors<sup>144</sup>, e.g., aromatic character of the pyrimidine ring of its pterin residue [Scheme (IV-3)]. Again the chelation process makes the entire complex molecule rigid [Figure (IV- 9)]. As a result, dissipation of excitation energy in ways other than by the emission of fluorescent light is prevented. During reaction of this complex with  $\text{Me}_3\text{N} \rightarrow \text{O}$ , there is loss of electron density from this

complex molecule, resulting in a product [Fig.(IV -27)] with lower fluorescence intensity and the fluorescence emission maximum ( $\lambda_{\text{max}}$ ) appearing at a larger wavelength [curve (2) in Fig.(IV-14)]. This change in fluorescence property with subtle change in electronic structure of a complex, makes it a valuable probe for studying the molybdenum – cofactor (of oxomolybdoenzymes) after oxidative degradation <sup>145</sup>.

All the compounds undergo OAT reaction and in some cases CEPT reaction with suitable oxygen atom donor or oxygen atom abstractor. The spectrophotometric course of the reaction between (1) and PPh<sub>3</sub> in DMF medium is shown in Fig.(IV-15). Here, PPh<sub>3</sub> being a good oxygen abstractor, abstracts O – atom from the (Mo<sup>VI</sup><sub>2</sub>O<sub>5</sub>)<sup>2+</sup> core of the complex i.e., the reaction is a metal – centered OAT

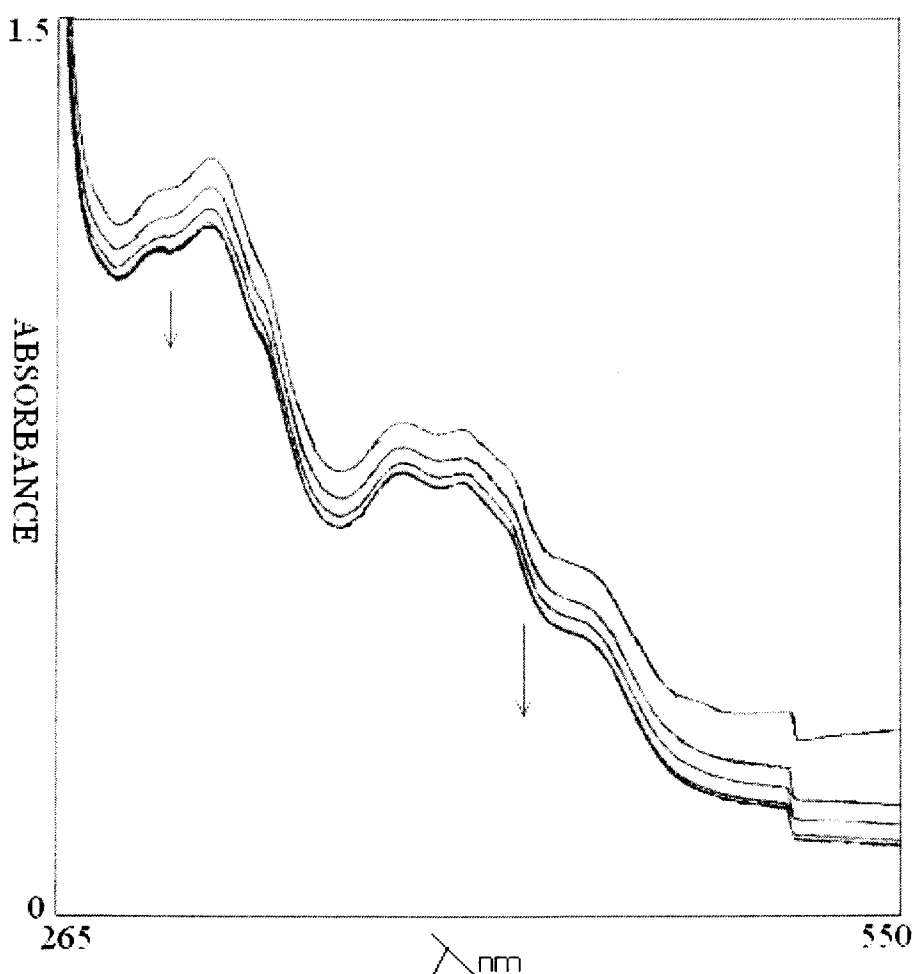


**Fig.(IV – 15):** UV–VIS absorption spectral changes recorded every 1 min. during the reaction of (1) [ $1.03 \times 10^{-4}$ (M)] with PPh<sub>3</sub> [ $1.02 \times 10^{-3}$ (M)] in DMF at 301K.

one which is substantiated by UV-VIS spectrometric absorption overlay change in the metal-centered CT region. On the other hand, this compound does not react with any oxygen donor substrate like,  $\text{Me}_3\text{N}\rightarrow\text{O}$  or  $\text{PyN}\rightarrow\text{O}$  etc. This suggests the presence of highest oxidation state of the metal centre (e.g.,  $\text{Mo}^{\text{VI}}$ )<sup>26</sup> in (1). Other five complexes (2 to 6) react with  $\text{Me}_3\text{N}\rightarrow\text{O}$ , a typical enzyme substrate, in DMF medium. The spectrophotometric study of these reactions are followed in overlay mode in a UV-VIS

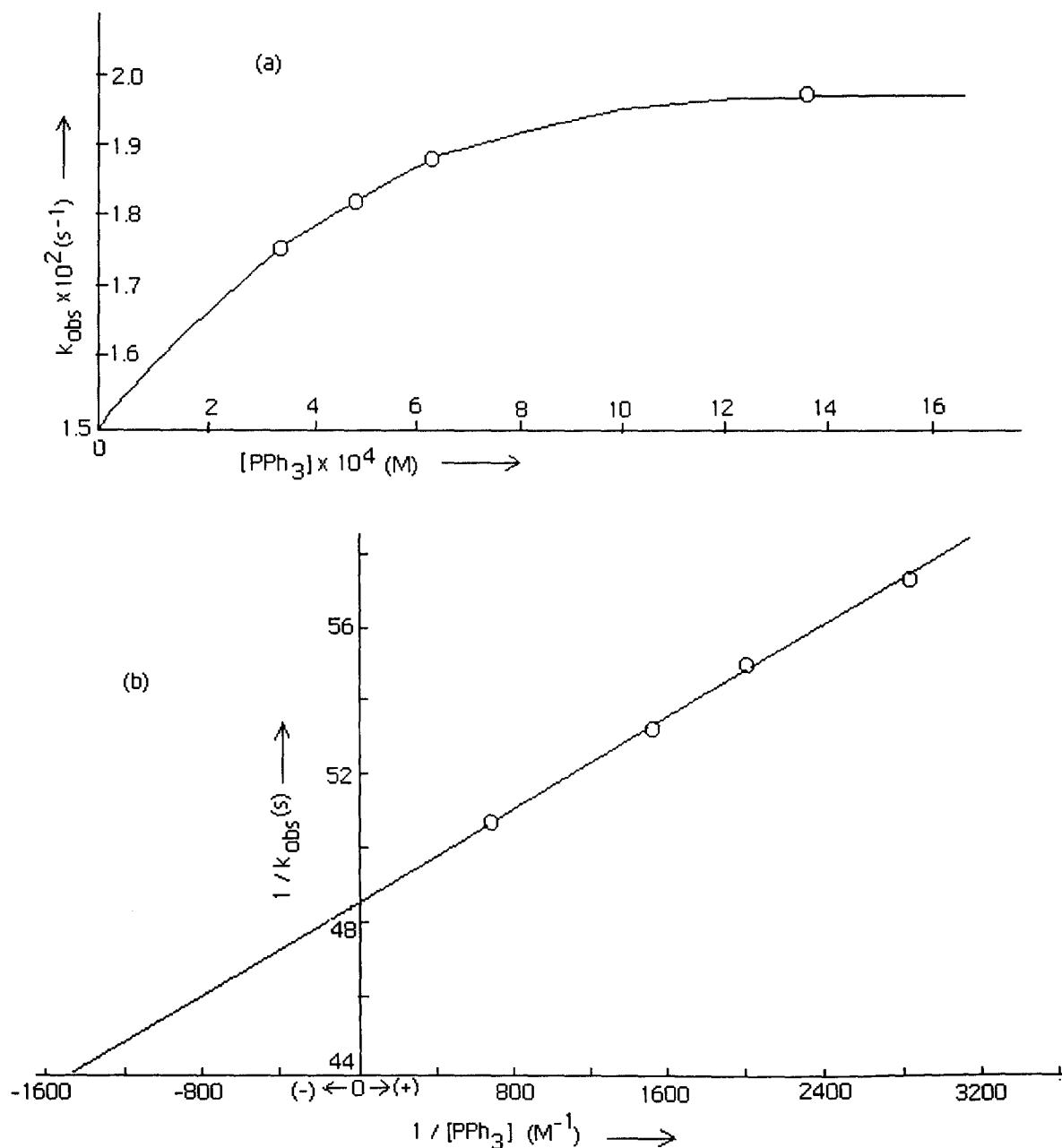


**Fig.(IV-16):** (a)Dependence of the rate of reaction of (1)  $[2.27 \times 10^{-5} \text{ (M)}]$  with  $\text{PPh}_3$  in DMF at 301 K; (b) the corresponding double reciprocal plot.

spectrophotometer at a definite time interval. In each case there is appreciable change in intensity in the metal-centered charge transfer region [Fig.(IV – 17), (IV – 19), (IV – 21), (IV – 23) & (IV – 25)] indicating metal-centered nature of these OAT reactions. This confirms the presence of a lower oxidation state (IV or V) of the Mo- atoms in these complexes. The overlay scans between  $\text{Me}_3\text{N}\rightarrow\text{O}$  and (4) contains two isosbestic points at 354 nm and 387 nm [Fig.(IV-21)]. This indicates a definite course of the reaction mechanism<sup>24</sup> at least for its initial phase.

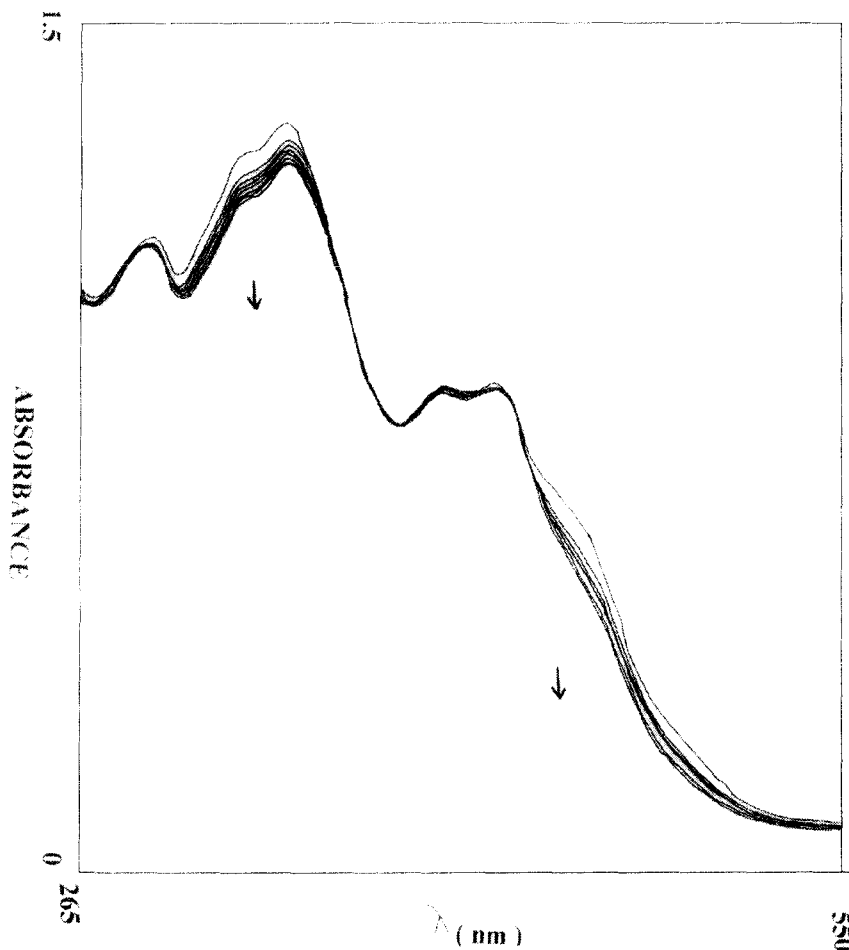


**Fig.(IV-17):** UV-VIS absorption spectral changes recorded every 12 min. during the reaction of (2) [ $1.33 \times 10^{-4}(\text{M})$ ] with  $\text{Me}_3\text{N}\rightarrow\text{O}$  [ $2.0 \times 10^{-3}(\text{M})$ ] in DMF at 301K.

Figure (IV-17) also shows two such isosbestic points at 364 nm and 432 nm for the reaction between  $\text{Me}_3\text{N}\rightarrow\text{O}$  and (2). As evident from isolation and characterization of the reaction product in this case, initial product of this reaction [eq. 3(a), below] is ultimately converted to a  $(\text{Mo}^{\text{VI}}_2\text{O}_5)^{2+}$  species [eq. 3(b), below] by the excess of  $\text{Me}_3\text{N}\rightarrow\text{O}$  and traces of  $\text{H}_2\text{O}$  present in the solvent. Kinetics of the reaction

between (1) and  $\text{PPh}_3$  was followed at 500 nm. The reactions of  $\text{Me}_3\text{N}\rightarrow\text{O}$  with (2), (3), (4), (5) & (6) were followed at 452 nm, 422 nm, 400 nm, 401 nm, and 445 nm

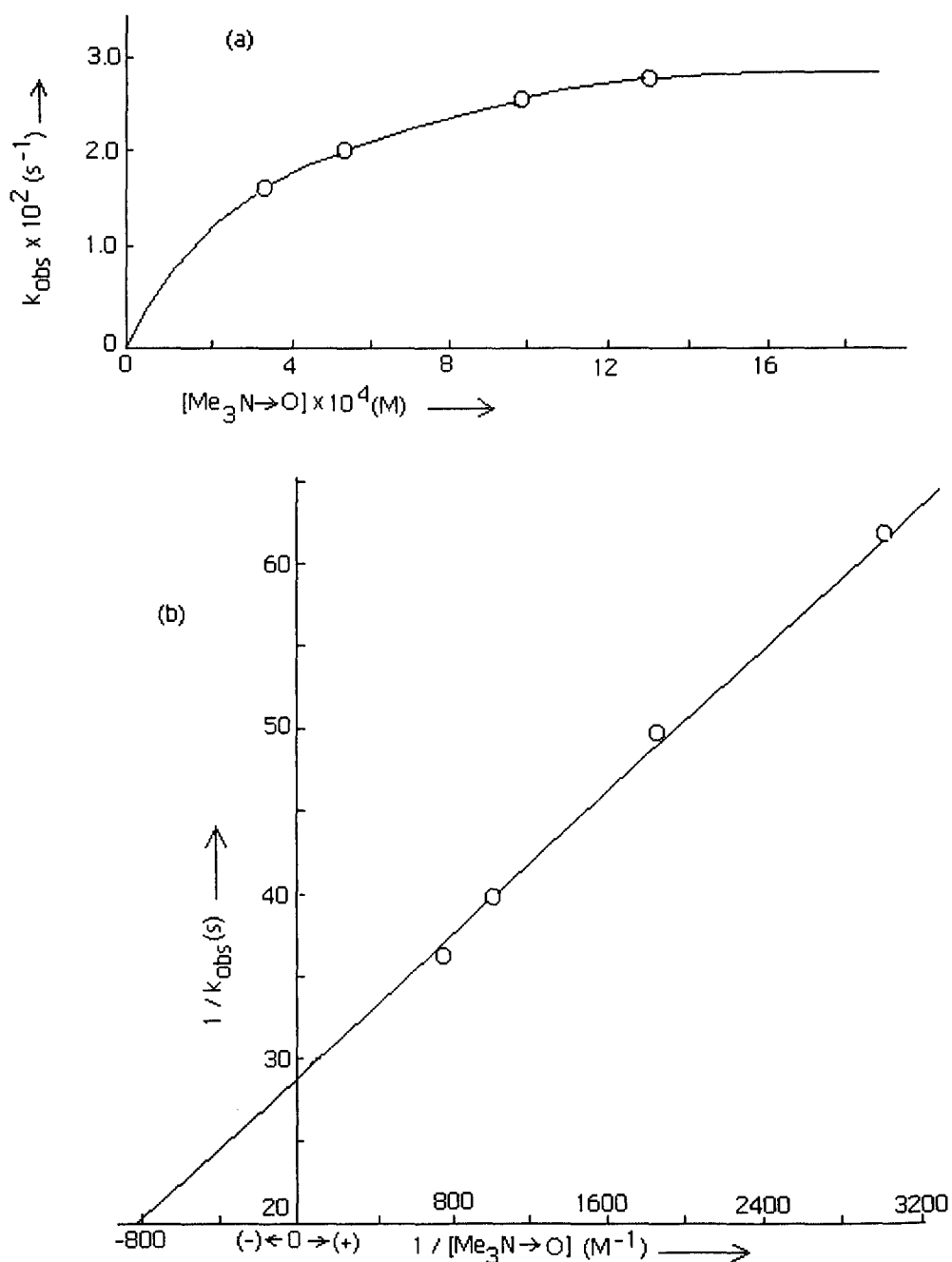


**Fig.(IV-18):** (a)Dependence of the rate of reaction of (2) [ $1.28 \times 10^{-5} \text{ (M)}$ ] with  $\text{Me}_3\text{N}\rightarrow\text{O}$  in DMF at 301 K; (b) the corresponding double reciprocal plot.

respectively. All the six compounds gave pseudo - first order reaction kinetics at sufficiently high substrate concentration and they gave substrate saturation plots [Fig.(IV-16a), (IV-18a), (IV-20a), (IV-22a), (IV-24a) & (IV-26a)]. Their rate



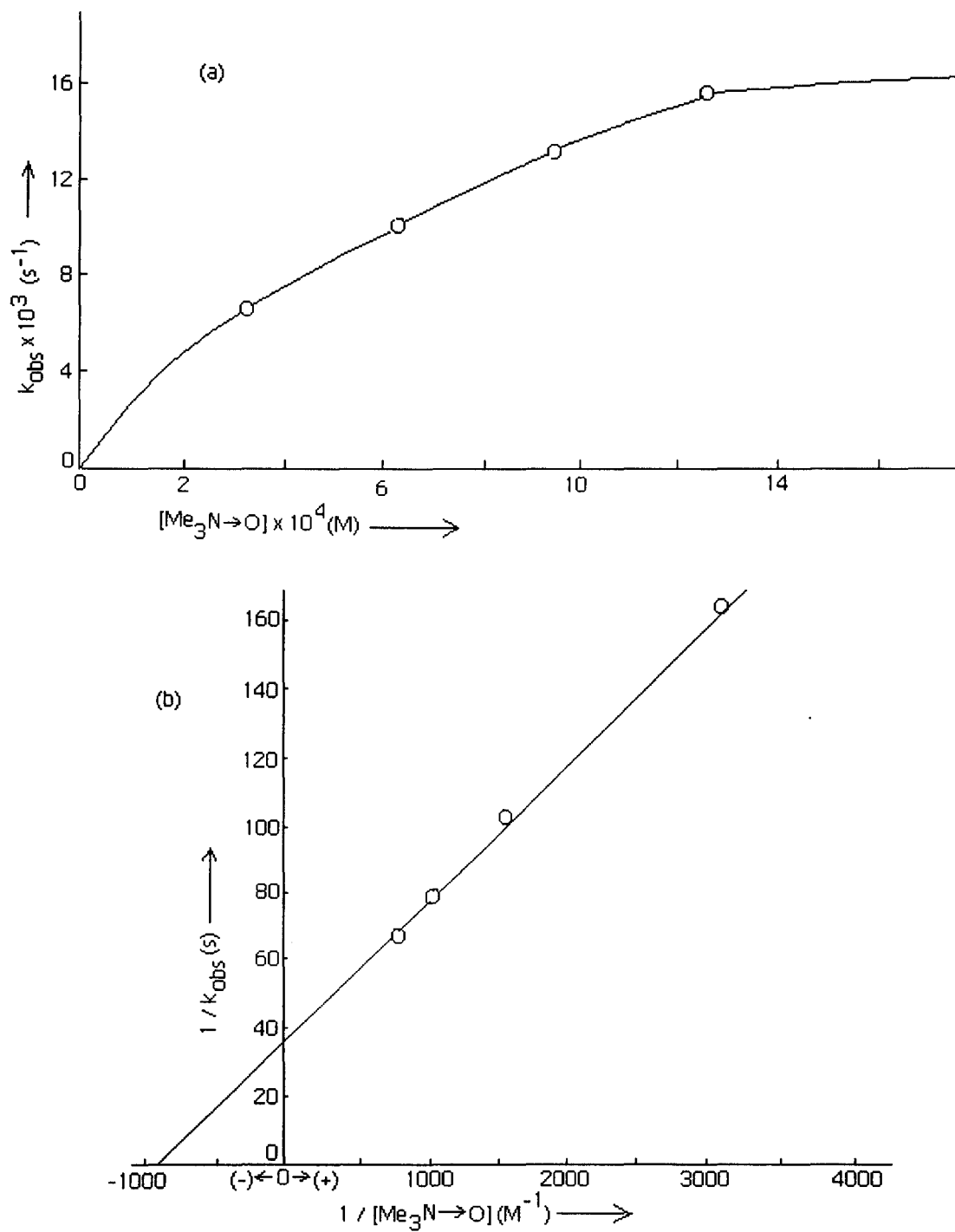


**Fig.(IV-20):** (a)Dependence of the rate of reaction of (3)  $[2.1 \times 10^{-5}(\text{M})]$  with  $\text{Me}_3\text{N}\rightarrow\text{O}$  in DMF at 301 K; (b) the corresponding double reciprocal plot.



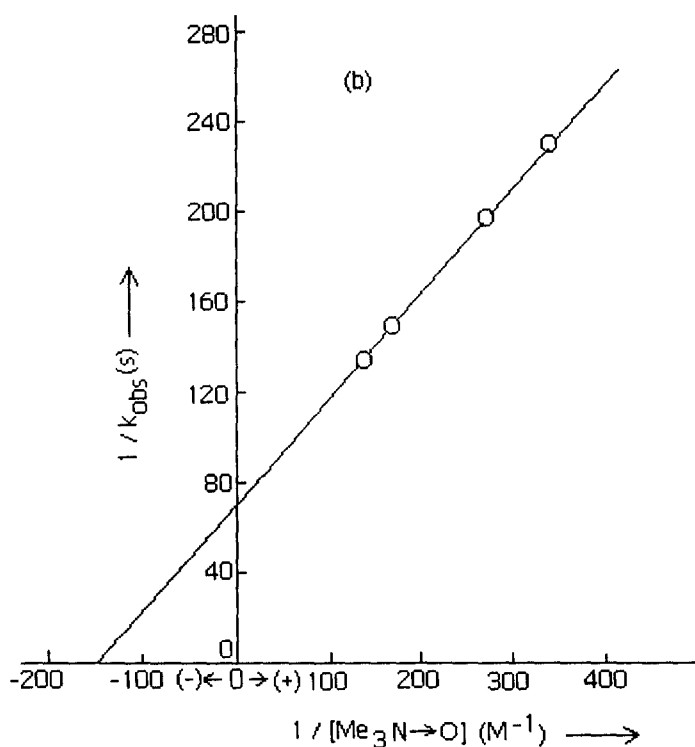
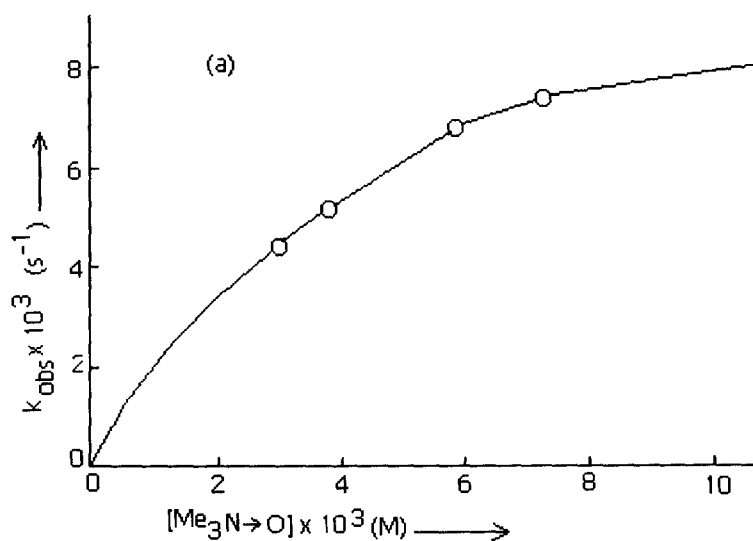


**Fig.(IV- 22):** (a)Dependence of the rate of reaction of (4)[ $1.33 \times 10^{-4} \text{ (M)}$ ] with  $\text{Me}_3\text{N} \rightarrow \text{O}$  in DMF at 301 K; (b) the corresponding double reciprocal plot.

In Schemes (IV-10 & IV- 11) above, the reactions leading to the formation of reduced or oxidized Mo - complexes as products, are initiated through reversible substrate [S] i.e.,  $\text{PPh}_3$  or  $\text{Me}_3\text{N} \rightarrow \text{O}$  binding followed by oxo-transfer (along with CEPT in some cases) reaction with rate constant  $k_2$ .

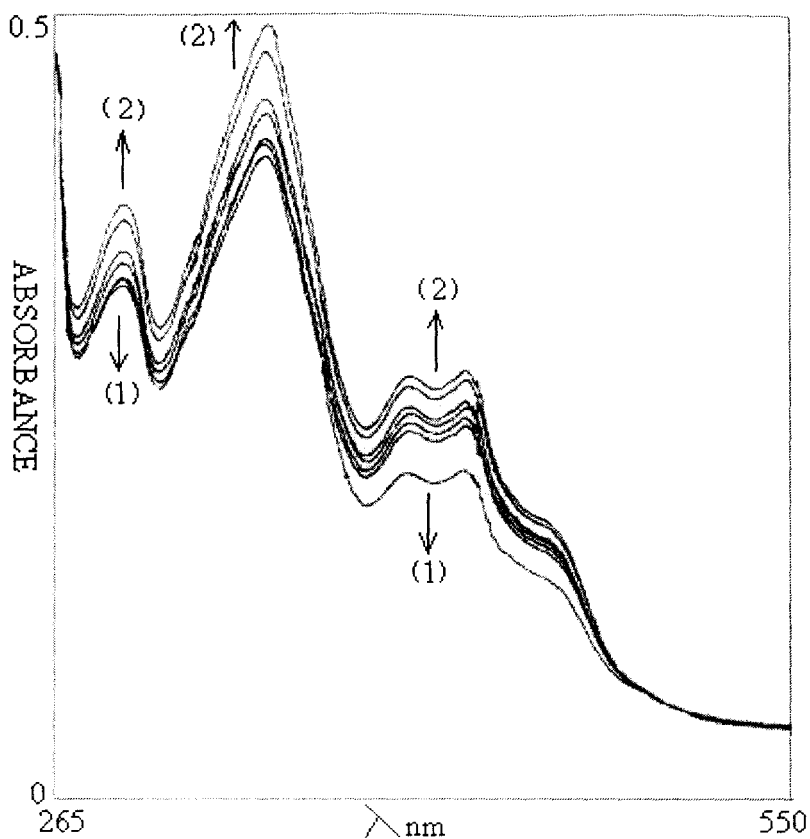
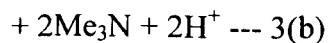
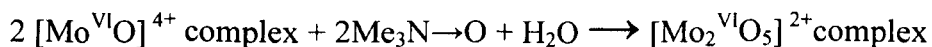
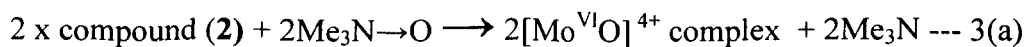


**Fig.(IV-23):** UV-VIS absorption spectral changes recorded every 10 min. during the reaction of (5) [ $1.05 \times 10^{-4}$  (M)] with  $\text{Me}_3\text{N} \rightarrow \text{O}$  [ $2.60 \times 10^{-3}$  (M)] in DMF at 301K. (1) indicates initial decrease and (2) indicates final rise in absorption.

For establishing reaction stoichiometry of the reaction between (2) and  $\text{Me}_3\text{N} \rightarrow \text{O}$ , a DMF solution (60 ml) of (2) (0.726 g, 1.5 mmol) was allowed to react with  $\text{Me}_3\text{N} \rightarrow \text{O}$  (0.75 g, 10 mmol) in the dark under slow but steady flow of dinitrogen gas, at 298 K for the first 24 h and then at 333 K for the next 24 h. The emerging gas carrying  $\text{Me}_3\text{N}$  (b.p. 275.9 K) was passed into a flask containing a measured excess of standard perchloric acid dissolved in glacial acetic acid and then the gas was released to atmosphere through a silicone oil bubbler. Finally, the residual perchloric acid in the flask was back titrated using a standard sodium acetate solution<sup>47</sup> and the amount of perchloric acid consumed by  $\text{Me}_3\text{N}$  was estimated. 2.05 mol of  $\text{Me}_3\text{N}$  was recovered per mol of (2) added, indicating a reaction represented by Equation (3) and supported by the kinetic data.



**The overall reaction :**

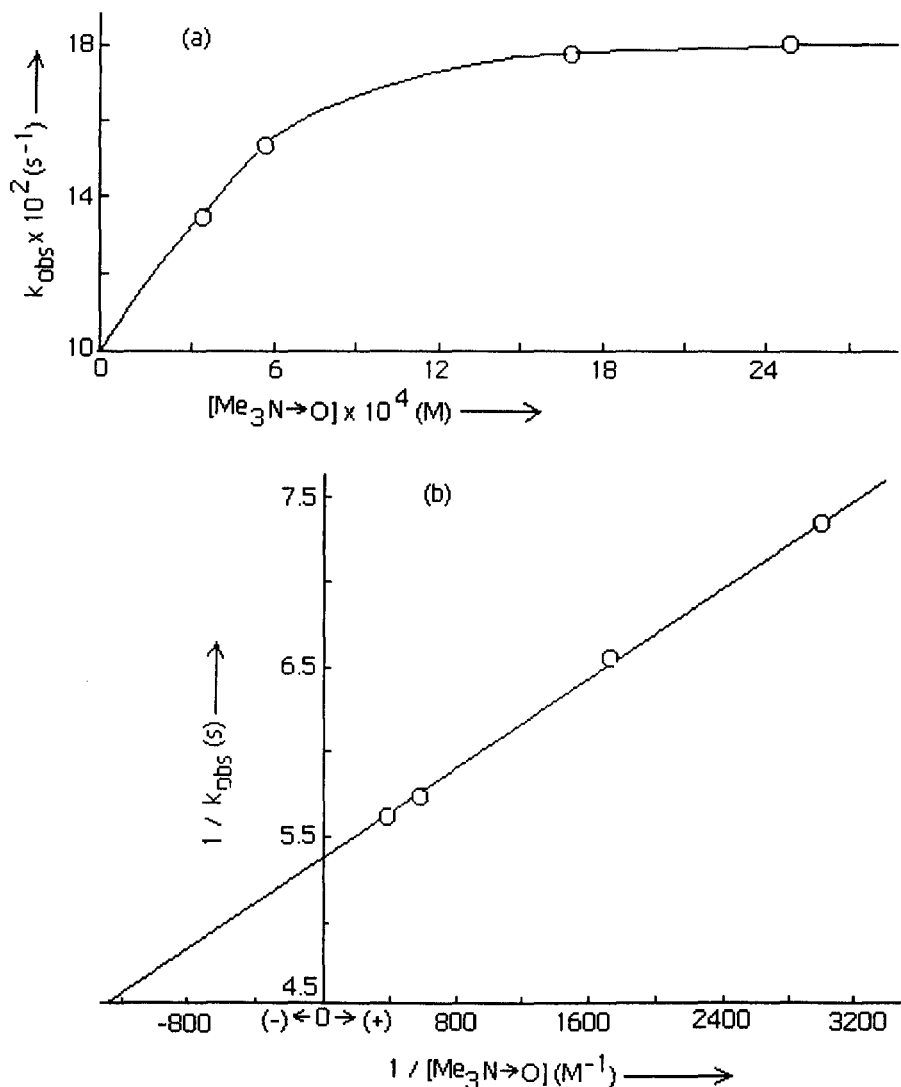
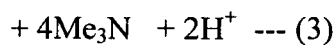
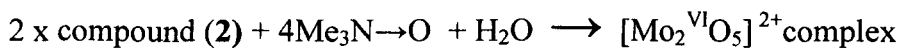


**Fig.(IV-24):** (a)Dependence of the rate of reaction of (5) [ $3.02 \times 10^{-5} \text{ (M)}$ ] with  $\text{Me}_3\text{N}\rightarrow\text{O}$  in DMF at 301 K; (b) the corresponding double reciprocal plot.

The solution in the reaction flask was evaporated to dryness in rotary evaporator and the compound so obtained was purified by flash chromatography ; Et<sub>2</sub>O was used for removing the excess of Me<sub>3</sub>N→O and the oxidized complex was eluted in DMF. Elemental analysis, ESIMS and other physico-chemical studies indicated its composition to be [(Mo<sup>VI</sup><sub>2</sub>O<sub>5</sub>)(Hpte<sub>1</sub>)(Hatp)(CH<sub>3</sub>OH)(Me<sub>3</sub>N→O)]. Its IR spectrum contains ν(Mo=O) and ν(Mo – O – Mo) bands characteristic of (Mo<sup>VI</sup><sub>2</sub>O<sub>5</sub>)<sup>2+</sup> core. Its ESIMS data show one peak corresponding to m/z = 675, [M – (Me<sub>3</sub>N + 3H)]<sup>+</sup>, where, 'M' is the molecular formula of the oxidation product of (2) (F.W. = 737)<sup>7(a), 14, 15</sup>, it was simulated by the IPC program<sup>46</sup> and found to be in good agreement with the experimentally obtained one [Fig.(IV-27)]. This isotope distribution pattern is consistent with the binuclear nature of this oxidation product<sup>14</sup>.

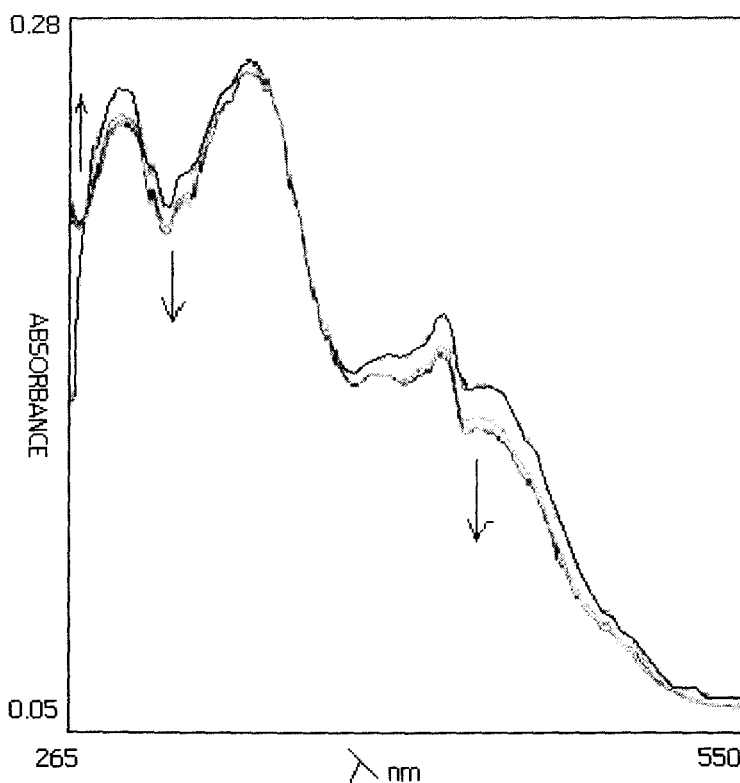


**Fig.(IV-25):** UV-VIS absorption spectral changes recorded every 3 min. during the reaction of (6) [ $6.86 \times 10^{-5}$  (M)] with Me<sub>3</sub>N→O [ $1.00 \times 10^{-3}$  (M)] in DMF at 301K.

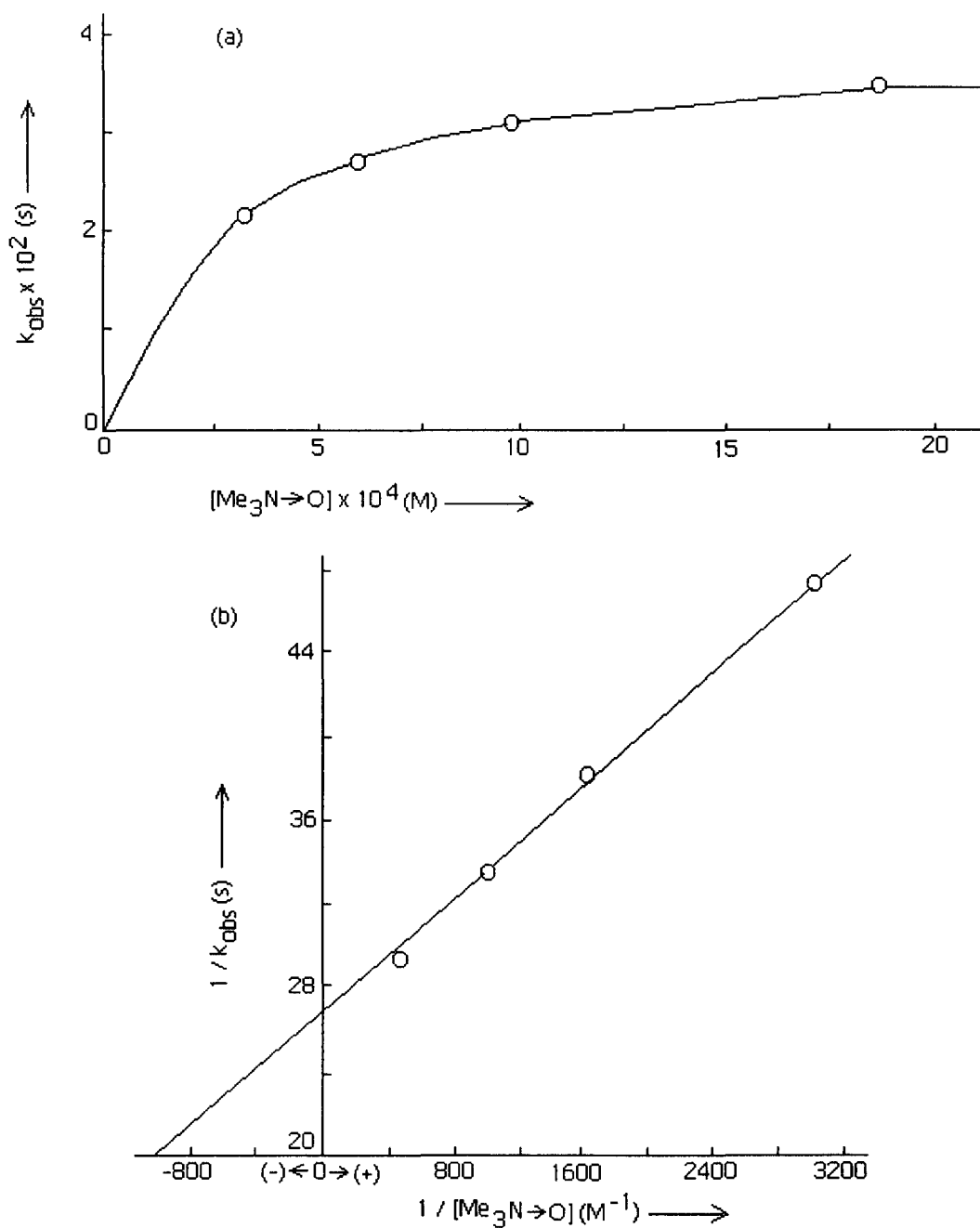


**Fig.(IV-26):** (a)Dependence of the rate of reaction of (6) [ $4.04 \times 10^{-5} \text{ (M)}$ ] with  $\text{Me}_3\text{N}\rightarrow\text{O}$  in DMF at 301 K; (b) the corresponding double reciprocal plot.

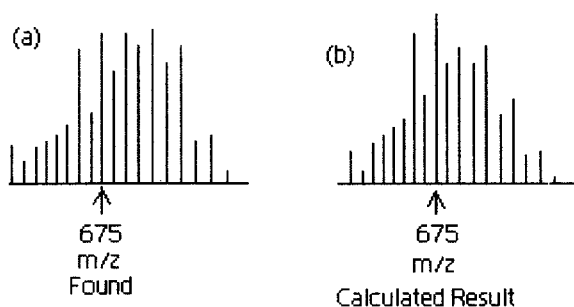


**Fig.(IV-27):** (a) ESIMS data of the oxidized product of (2) at  $m/z$  (= 675) region corresponding to  $[M-3H + O]^+$ ; (b) the calculated isotope pattern <sup>46</sup>. Formula:  $C_{16}H_{15}N_6O_{10}Mo_2S$ .

From the schematic representation of the above oxo-transfer reaction the  $k_{obs}$  values can be represented as follows <sup>22, 34</sup> :

$$k_{obs} = k_2[S]/(K_M + [S]) \quad \text{---- (4)}$$

$$\text{Where, } K_M = (k_2 + k_{-1})/k_1,$$

Or,

$$1/k_{obs} = 1/k_2 + K_M/k_2[S] \quad \text{---- (5)}$$

Plots of ( $k_{obs}$ ) vs. substrate concentration, e.g.,  $[PPh_3]$  or  $[Me_3N \rightarrow O]$  gave substrate saturation plots [Fig.(IV - 16a), (IV - 18a), (IV - 20a), (IV - 22a), (IV - 24a) & (IV - 26a)] according to equation (4). Straight line plots obtained by plotting  $1/k_{obs}$  vs.  $1/[PPh_3]$  or  $1/[Me_3N \rightarrow O]$  with slope equal to  $K_M/k_2$  and intercept equal to  $1/k_2$  according to equation (5). From these double reciprocal plots  $k_2$  and  $K_M$  values were calculated. The double reciprocal plot as per equation (5) is similar to the lineweaver - Burk plot obtained for a real enzyme <sup>22</sup>. These  $k_{obs}$  [Table (IV-9)] values are found to be in agreement with the literature data on molybdenum mediated oxygen atom transfer reactions with a variety of enzyme substrates <sup>8, 17, 23</sup>. The small  $K_M$  value [Table (IV-9)] signifies strong complex - substrate bonding in each case and this is in agreement with the corresponding large negative  $\Delta S^\ddagger$  value <sup>22</sup>. Activation parameters ( $E_a$ ,  $\Delta H^\ddagger$ ,  $\Delta G^\ddagger$ ,  $\Delta S^\ddagger$ ) were obtained from the Arrhenius and Eyring plots of temperature dependency of  $k_{obs}$  ( $s^{-1}$ ) at four different temperatures under pseudo-first order condition using large excess (60 - 100 fold) of  $[PPh_3]$  or  $[Me_3N \rightarrow O]$  for (1) and other complexes respectively. In each

case the negative  $\Delta S^\ddagger$ -value [Table (IV-9)] suggests associative type reaction mechanism as shown in Schemes (IV -10 & IV - 11), alike the enzyme – substrate type reaction mechanism<sup>24, 34</sup>. For throwing light on factors responsible controlling the reactivity aspects,  $k_{\text{obs}}$  ( $\text{s}^{-1}$ ) values at 301 K are compared in Table (IV-10).

Table (IV – 9)

Compound No.	Substrate used (in DMF)	Temperature (K)	$k_{\text{obs}}(\text{s}^{-1})$	$k_2 (\text{s}^{-1})$	$K_M$ (M)	$E_a$ (KJ, $\text{mol}^{-1}$ )	$\Delta H^\ddagger$ (KJ, $\text{mol}^{-1}$ )	$\Delta S^\ddagger$ (J, $\text{mol}^{-1}$ , $\text{deg}^{-1}$ )	$\Delta G^\ddagger$ (KJ, $\text{mol}^{-1}$ )
(1)	$\text{PPh}_3$	301	$1.97 \times 10^{-2}$						
		312	$2.80 \times 10^{-2}$	$2.06 \times 10^{-2}$	$6.26 \times 10^{-5}$	38.85	36.66	-206.1	99.4
		315.5	$3.40 \times 10^{-2}$						
		318	$3.80 \times 10^{-2}$						
(2)	$\text{Me}_3\text{N} \rightarrow \text{O}$	301	$2.76 \times 10^{-2}$						
		305.5	$2.93 \times 10^{-2}$	$3.49 \times 10^{-2}$	$3.66 \times 10^{-4}$	12.34	8.35	-200.0	68.55
		311	$3.23 \times 10^{-2}$						
		317	$3.55 \times 10^{-2}$						
(3)	$\text{Me}_3\text{N} \rightarrow \text{O}$	301	$1.54 \times 10^{-2}$						
		307.5	$1.78 \times 10^{-2}$	$2.86 \times 10^{-2}$	$3.03 \times 10^{-2}$	33.26	31.18	-204.7	93.42
		310	$1.99 \times 10^{-2}$						
(4)	$\text{Me}_3\text{N} \rightarrow \text{O}$	292	$7.4 \times 10^{-3}$						
		299.5	$7.8 \times 10^{-3}$	$1.43 \times 10^{-2}$	$6.70 \times 10^{-3}$	4.93	2.42	-199.0	62.99
		301	$8.0 \times 10^{-3}$						
		306	$8.2 \times 10^{-3}$						

<b>(5)</b>	Me <sub>3</sub> N→O	301	1.80 x 10 <sup>-1</sup>	1.87 x 10 <sup>-1</sup>	1.30 x 10 <sup>-4</sup>	30.04	27.53	-204.4	88.87
		306.5	2.33 x 10 <sup>-1</sup>						
		310	2.57 x 10 <sup>-1</sup>						
<b>(6)</b>	Me <sub>3</sub> N→O	301	3.41 x 10 <sup>-2</sup>	3.76 x 10 <sup>-2</sup>	2.50 x 10 <sup>-4</sup>	12.12	9.93	-200.4	70.22
		307	3.80 x 10 <sup>-2</sup>						
		310	3.92 x 10 <sup>-2</sup>						
		317	4.36 x 10 <sup>-2</sup>						

**Table (IV – 10)**

Comparison of  $k_{\text{obs}}$  (s<sup>-1</sup>) values of (1) to (6) at 301 K along with a few relevant kinetic parameters :

Complex (No.), substrate used (in DMF)	$k_{\text{obs}}$ (s <sup>-1</sup> )	$K_M$ (M)	$\Delta S^\ddagger$ (J, mol <sup>-1</sup> , deg <sup>-1</sup> )	Steric energy of CHEM3D model (Kcal, mol <sup>-1</sup> )
(1), PPh <sub>3</sub>	1.97 x 10 <sup>-2</sup>	6.26 x 10 <sup>-5</sup>	- 206.1	19.9
(2), Me <sub>3</sub> N→O	2.76 x 10 <sup>-2</sup>	3.66 x 10 <sup>-4</sup>	- 200.0	24.9
(3), Me <sub>3</sub> N→O	1.54 x 10 <sup>-2</sup>	3.03 x 10 <sup>-2</sup>	- 204.7	24.1
(4), Me <sub>3</sub> N→O	0.8 x 10 <sup>-2</sup>	6.70 x 10 <sup>-3</sup>	- 199.0	24.6
(5), Me <sub>3</sub> N→O	1.80 x 10 <sup>-1</sup>	1.30 x 10 <sup>-4</sup>	- 204.4	65.2
(6), Me <sub>3</sub> N→O	3.41 x 10 <sup>-2</sup>	2.50 x 10 <sup>-4</sup>	- 200.4	119.7 *

\* This high steric energy value for (6) is probably due to the presence of a three membered ring here involving the dihapto disulphide ligand and the Mo – atom.

Table (IV – 10) shows the pseudo – first order rate constants ( $k_{\text{obs}}$ ,  $\text{s}^{-1}$ ) data at 301 K of these complexes along with some of their pertinent data. Here the negative  $\Delta S^\ddagger$  values are consistent with the associative type pathway, with small  $K_M$  values indicating strong complex – substrate binding in these cases<sup>22</sup>. In terms of  $k_{\text{obs}}$ , ( $\text{s}^{-1}$ ) values, (5) is the most reactive species of this series [(6) is an exceptional case with a three membered ring involving the dihapto disulphide ligand and the Mo – atom]. Its CHEM3D model [Fig. (IV-12)] possesses highest steric energy with maximum steric crowding, thereby providing the driving force for its reactivity towards the oxo-transfer reagent ( $\text{Me}_3\text{N}\rightarrow\text{O}$ ), leading to a thermodynamically stable product. For other complexes [(1) to (4) and (6)] of this series, variation of  $k_{\text{obs}}$ , ( $\text{s}^{-1}$ ) values within a certain limit parallels that of their steric energy values (of CHEM3D models). They represent on the whole similar steric situation around the molybdenum atom in each case and the associated oxidation states of the molybdenum atoms (VI, V, IV) are easily interconvertible (through oxygen atom transfer or coupled proton – electron transfer)<sup>26</sup>. The  $E_a$  and  $\Delta H^\ddagger$  values [Table (IV-9)] are quite comparable and vary similarly, apparently providing with little guidelines regarding the reaction pathway. The stability of complex (4) with the lowest  $k_{\text{obs}}$  ( $\text{s}^{-1}$ ) value can be correlated with that of its  $(\text{Mo}^{\text{V}}_2\text{O}_3)^{4+}$  core.

The oxygen atom transfer activity of molybdenum complexes with different ligands towards enzyme substrates or substrate analogues (like  $\text{NO}_3^-$ ,  $\text{PPh}_3$  etc) have been analyzed in the light of HOMO – LUMO approach; such ideas can be extended to explain the reactivity of molybdenum – pterin complexes<sup>55</sup>.

The pterin ligand [ $\text{H}_2(\text{pte}_1)$ ] undergoes cathodic reduction beyond – 1.80V ( $E_{\text{pc}}$ ) in DMF medium and it is reoxidized at the anode at + 0.94V ( $E_{\text{pa}}$ ); cyclic voltammetric behaviour of the new complexes (1 – 6) could be well – studied within this potential window. Facile redox behaviour of molybdenum compounds including binuclear ones in common oxidation states (VI / V / IV) has received considerable attention<sup>55</sup>. The CV diagram of (1) [Fig.(IV-28)] shows two irreversible reduction peaks

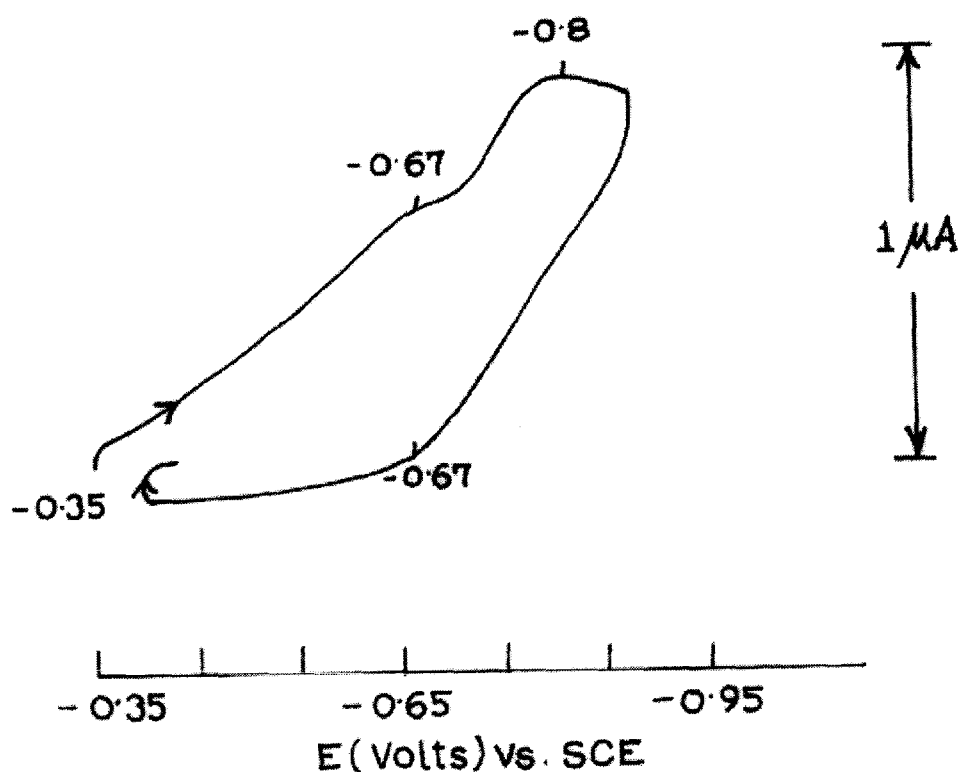


**Fig.(IV-28):** CV scans of compound (1) [ $1.0 \times 10^{-3}$ (M),  $\text{Bu}_4\text{NClO}_4$  [0.1 (M)] in DMF. . Data were recorded using a Pt working Electrode and scan rate was  $50 \text{ mVs}^{-1}$ .

( $E_{pc}$ ) at  $-0.67\text{V}$  and  $-0.80\text{V}$  corresponding to the two one – electron reductions  $\text{Mo}^{\text{VI}} \rightarrow \text{Mo}^{\text{V}}$  and  $\text{Mo}^{\text{V}} \rightarrow \text{Mo}^{\text{IV}}$  respectively ; solvent attack finally decomposes the reduced species. The reduced product is partly oxidized at  $-0.67\text{V}$ . The CV data of (2) shows that the metal centre undergoes reduction ( $\text{Mo}^{\text{IV}} \rightarrow \text{Mo}^{\text{III}}$ ) at  $-0.75\text{V}$  ( $E_{pc}$ ) and the solvent (DMF) interacts with the reduced species, resulting in an overall irreversible CV response. For (3) the corresponding irreversible reduction peak ( $\text{Mo}^{\text{IV}} \rightarrow \text{Mo}^{\text{III}}$ ) appears at  $-0.76\text{V}$  ( $E_{pc}$ ). CV data of (4) reflect two irreversible reduction peaks at  $-0.83\text{V}$  and  $-1.41\text{V}$  corresponding to the reductions ( $\text{Mo}^{\text{V}} \rightarrow \text{Mo}^{\text{IV}}$ ) and ( $\text{Mo}^{\text{IV}} \rightarrow \text{Mo}^{\text{III}}$ ) respectively, and ultimately chemical attack by DMF decomposes the electrochemical reduction

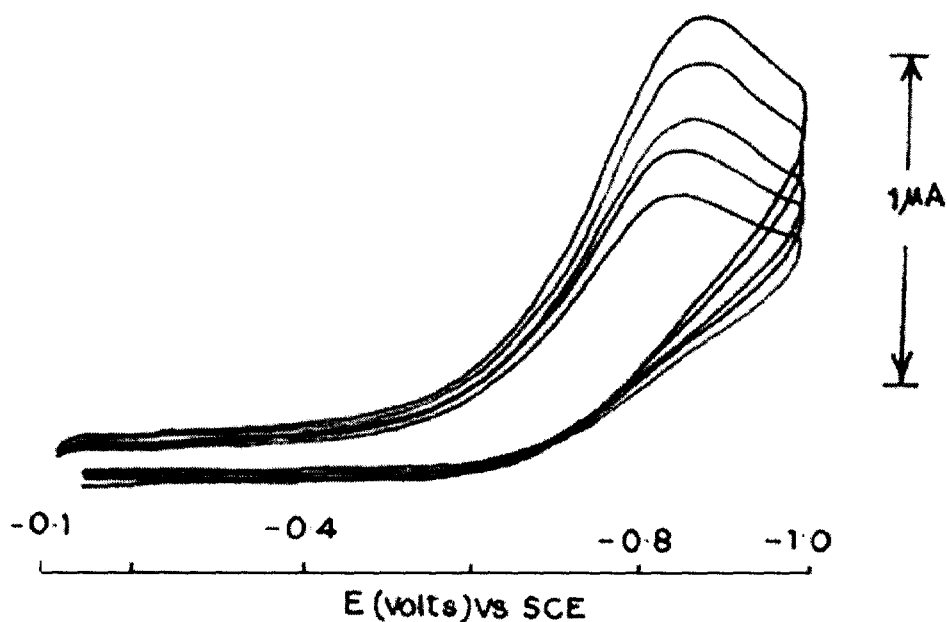


**Fig.(IV-29):** CV scans of compound (6) [ $1.0 \times 10^{-3}$ (M),  $\text{Bu}_4\text{NClO}_4$  [0.1 (M)] in DMF. Data were recorded at 5 min. intervals using a Pt working Electrode and scan rate was  $50 \text{ mVs}^{-1}$ .

product. CV data of (5) indicate two irreversible reduction peaks ( $E_{pc}$ ) at  $-0.72\text{V}$  and  $-0.90\text{V}$ , corresponding to reductions of the two  $\text{Mo(IV)}$  centres respectively, reflecting difference in their overall electronic environments. For (6), reduction of the  $\text{Mo}^{\text{IV}}$  centre is characterized by an irreversible reduction peak ( $E_{pc}$ ) at  $-0.83\text{V}$ . For the complexes (2, 3, 5, 6) with  $\text{Mo}^{\text{IV}}$  centres, the  $E_{pc}$  values vary over a limited range, and this is comparable to their variation of  $k_{obs}$  ( $\text{s}^{-1}$ ) values [Table (IV-10)] within a certain limit. Apparently, electronic structural similarity (or available electron density) of the metal centres here, is responsible for their comparable response with respect to electron transfer (e.g., cathodic reduction) as well as oxygen atom transfer activity.

## Conclusion

Physicochemical studies discussed above point towards the redox “non-innocent” behaviour of the pterin ligand [ $\text{H}_2(\text{pte}_1)$ ]. The ESIMS data and CHEM3D models (MM2 method) help to develop reliable **molecular structures** of the new complexes (**1 – 6**) and provide with suitable basis for discussion on their spectroscopic data and reactivity aspects. During synthesis of these complexes a redox reaction occurs involving the  $\text{Mo}^{\text{VI}}$  starting materials, with the pterin ligand acting as a reducing agent. Ability of complexes (**2**), (**3**), (**5**) and (**6**) to react with a typical enzyme substrate like  $\text{Me}_3\text{N}\rightarrow\text{O}$ , indicates the presence of the **metal centre** in a lower **oxidation state** (e.g.,  $\text{Mo}^{\text{IV}}$ ). During synthesis of (**4**), the mononuclear  $\text{Mo}^{\text{V}}$ - starting material is converted to a binuclear  $(\text{Mo}^{\text{V}}_2\text{O}_3)^{4+}$  species. In case of (**1**), DMSO used during its synthesis oxidized the intermediate  $\text{Mo}^{\text{IV}}$  complex to higher oxidation state [with  $(\text{Mo}^{\text{VI}}_2\text{O}_5)^{2+}$  case], its reactivity towards  $\text{PPh}_3$  verifies the assignment of oxidation state (e.g., VI). The solvent (e.g.,  $\text{CH}_3\text{OH}$ ) used during synthesis of these complexes also played an important role, as evident from its incorporation in the coordination sphere in several cases. The negative activation entropy ( $\Delta S^\ddagger$ ) of the above oxygen atom transfer reactions (with  $\text{Me}_3\text{N}\rightarrow\text{O}$  or  $\text{PPh}_3$ ) indicate **associative type reactions** and the  $k_{\text{obs}}$  ( $\text{s}^{-1}$ ) values are comparable with the literature data. The sulphur containing secondary ligands help to manifest different tautomeric forms of the pterin ligand residue in these complexes in solution, as evident from NMR spectral data ; besides this, electron flow from the  $-\text{NH}_2$  (2) group of the pterin ligand residue towards the  $\text{Mo}^{\text{IV}}$  centre, facilitates reactivity towards  $\text{Me}_3\text{N}\rightarrow\text{O}$ . Fluorescence spectral data help to follow changes in **electronic structures** during this reaction. Cyclic voltammetric data illuminate **electrochemical property** of these complexes. The flexibility of pterin ligand residue with respect to electron flow confers such reactivity property on these complexes. Probably such property has propped Nature to select pterin as the essential component of oxomolybdoenzymes.

## CHAPTER IV

### SECTION – II

Kinetics of oxygen atom transfer reactions of pyridine N – oxide substrate with mono  $\mu$  – oxo – bridged molybdenum(V) complexes of aldimine derivatives of L-/D-amino acids :  
Conformational control of reactivity.

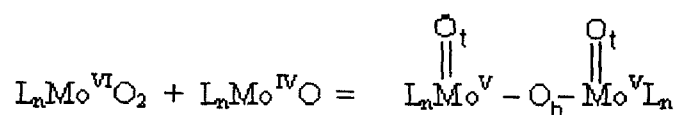
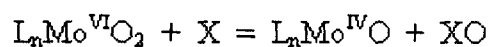
## Abstract

Both the kinetic and stoichiometric aspects of the oxygen atom transfer reactions of three  $\mu$  - oxo binuclear molybdenum(V) complexes [possessing the  $(\text{Mo}^{\text{V}}_2\text{O}_3)^{4+}$  core] with pyridine N - oxide (a typical oxomolybdoenzyme substrate analogue) were studied in DMF solutions. These reactions are characterized by Michaelis - Menten type behaviour ; the negative  $\Delta S^\ddagger$  values are consistent with associative type pathway for such cases. From the corresponding double reciprocal plots [ that is, Lineweaver - Burk type plot of  $1/k_{\text{obs}}$  versus  $1/[\text{S}]$  ] the  $k_2$  ( $\text{s}^{-1}$ ) and  $K_M$  ( $\text{mol}^{-1}$ ) values were obtained. The range of  $k_2$  values is comparable in magnitude to the literature data of metal - mediated oxygen atom transfer reactions using suitable substrates. Chemical compositions of these complexes (earlier established on the basis of elemental analysis, physicochemical and spectroscopic data) have been further verified through computer simulation of mass spectral data. Molecular mechanics method (MM2) provided with their molecular structures (i.e., optimized geometries with lowest steric energies) ; the optimized bond lengths and bond angles data tally with the literature X - ray structural data. These optimized geometries are able to explain not only their physical properties but also their reactivities in terms of conformational control [i.e., different arrangements of the two  $\text{Mo} = \text{O}_t$  bonds about the  $\text{Mo} - \text{O}_b - \text{Mo}$  axis of the  $(\text{Mo}^{\text{V}}_2\text{O}_3)^{4+}$  core].

## Introduction

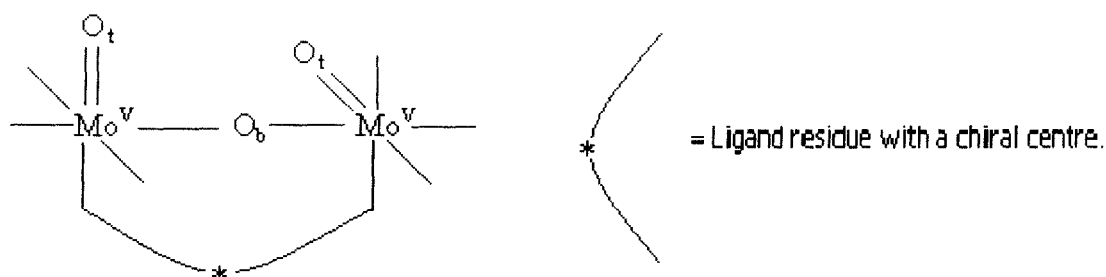
As discussed at the outset in Chapter I the oxomolybdoenzymes possess one or two mononuclear molybdenum sites and in all such cases the molybdenum atom shares a non-protein organic ligand called molybdopterin which is a 6-substituted [ene-dithiolate / dithiolene] pterin. In addition, such enzymes possess a coordinated protein ligand ; they probably use the protein ligand to tune the reactivity of the metal site, much in the way that hemoproteins use the extra ligand trans to the O<sub>2</sub> binding site to adjust the reactivity of heme towards dioxygen ; in hemoglobin a histidine in the position trans to the O<sub>2</sub> binding site facilitates the reversible binding of O<sub>2</sub> , whereas in cytochrome P-450, a cysteine thiolate in this position helps to achieve oxygen activation. Thus the iron-porphyrin unit can be intricately manipulated by its host protein to perform the varied Chemistry required by drastically different metalloprotein / metalloenzyme. Oxomolybdoenzymes act on a variety of substrates involved in carbon - / nitrogen – sulphur – metabolism and in such cases required activity of the molybdenum – molybdopterin complex (i.e., the molybdenum cofactor, Mo – co) is controlled to a large extent by the coordinated protein ligand <sup>2</sup>. Amino acid analysis of the molybdenum cofactor from xanthine oxidase and sulphite oxidase indicate the presence of histidine and arginine residues, among other amino acids <sup>52</sup>.

For the molybdenum – cofactor (Mo-co) both the pterin component as well as the anchoring peptide are vital for the oxygen atom transfer (or oxo-transfer) activity of these enzymes. While the pterin group is involved in electron transfer with the molybdenum centre during turnover, the peptide chain is likely to create steric constraint around the molybdenum atom, for preventing the irreversible oxo dimerization reaction during the oxo-transfer cycle.



Critical studies indicate that the role of oxo-bridged Mo(V) complexes in oxygen atom transfer reactions of systems designed to model enzyme behaviour cannot necessarily be ignored<sup>7, 8, 29, 41, 163</sup>.

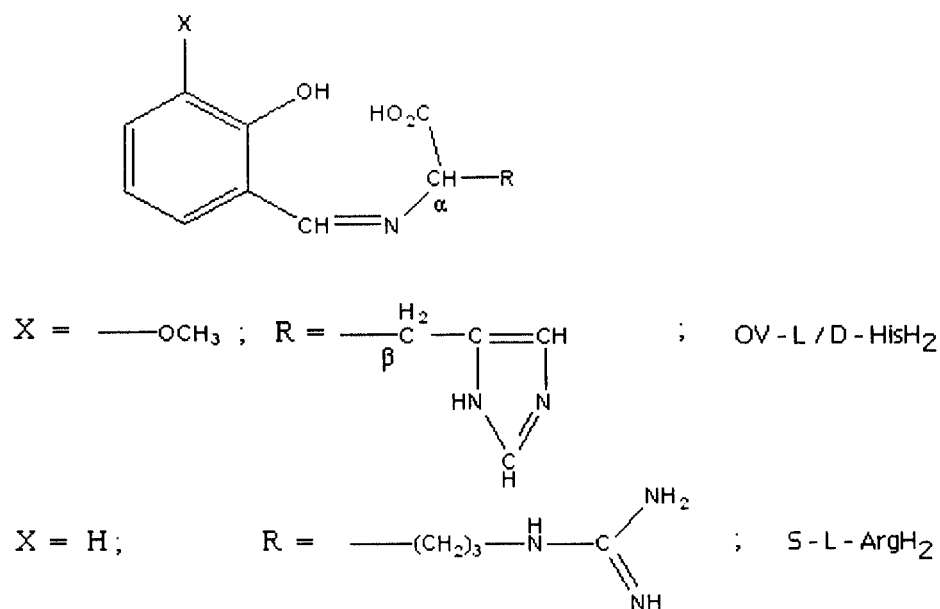
There are different possibilities of Mo = O distortional isomers of  $(\text{Mo}^{\text{V}}_2\text{O}_3)^{4+}$  core by rotations around the Mo –O<sub>b</sub> – Mo bridge ; X – ray crystal structure data of  $(\text{Mo}^{\text{V}}_2\text{O}_3)^{4+}$  compounds isolated so far, indicate cis – or trans – disposition of the terminal oxygens (O<sub>t</sub>) and they are diamagnetic due to coupling of the two Mo(V) d<sup>1</sup> electrons through the Mo –O<sub>b</sub> – Mo three – centre bond<sup>7, 19, 62, 76</sup>. For a skew arrangement of the two Mo = O<sub>t</sub> bonds these two ‘d’ electrons are unlikely to overlap significantly, leading to a triplet (S = 1) ground state. It is worthwhile to explore the possibility of isolating a paramagnetic complex containing the structurally atypical skew -  $(\text{Mo}^{\text{V}}_2\text{O}_3)^{4+}$  core with a chiral ligand, as such a system will bear an analogy to the oxomolybdoenzymes with two independent mononuclear molybdenum centres [Scheme (IV-12)].



**Scheme (IV-12):** Two oxomolybdenum(V) centres (d<sup>1</sup>) in a chiral ligand environment – hypothesis for a CD model.

Physicochemical and reactivity studies on this and related complexes containing different Mo = O<sub>t</sub> distortional isomers, will throw light on the influence of conformational (about the Mo –O<sub>b</sub> – Mo bond) factors on their characteristic properties as well as reactivities<sup>106</sup>. Interpretation of mass spectral data using computer simulation method and getting the optimized molecular structures through molecular mechanics method (MM2), give this study a new dimension. Possible correlation of oxygen atom transfer activity of these complexes towards an enzyme substrate analogue (PyN→O) with optimized molecular structures will be interesting.

Preformed ligands isolated as either free acids or monopotassium salts, containing histidine or arginine residues, have been used in this study [Scheme (IV-13)].



**Scheme (IV-13):** Schematic structures of aldimine ligands.

As stated above, choice of the amino acid residues is in conformity with the composition of the relevant peptides<sup>52</sup>. For synthetic purpose a Mo(V) starting material [MoOCl<sub>3</sub>(bipy)] (green) has been utilized<sup>67</sup>.

## Experimental

**Materials and Methods:** Orthovanillin (Fluka AG), salicylaldehyde (Kemphasol), L – histidine monohydrochloride monohydrate (E. Merck, Germany), D – histidine monohydrochloride monohydrate (Sigma, USA), L – arginine monohydrochloride (Fluka AG), 2,2' – bipyridyl (BDH), molybdenum trioxide (E. Merck, Germany), hydriodic acid (E. Merck, Germany) and tetra – n – butylammonium hydroxide (SISCO, Bombay) were used as such. [MoOCl<sub>3</sub>(bipy)] (green) (bipy = 2,2' – bipyridyl) was synthesized by a known method<sup>67</sup>.

The reactions were carried out in distilled solvents under dry dinitrogen atmosphere using Schlenk method, including the workup step<sup>11, 164</sup>.

Most of the details regarding instrumental measurements have been described in earlier chapters. X-band EPR spectra were recorded in a varian E-112 EPR spectrometer (9.51 GHz) using TCNE as the marker ( $g = 2.00277$ ). Magnetic susceptibility measurements at room temperature were made on a Gouy balance using  $\text{Hg}[\text{Co}(\text{SCN})_4]$  as the calibrant. Molybdenum was estimated gravimetrically by using 8-hydroxyquinoline as the precipitant<sup>25</sup>.

## Preparation of ligands

Monopotassium salts of N-(orthovanillidene)-L-histidine (OV-L-HisHK.2H<sub>2</sub>O) (**1**) and N-(orthovanillidene)-D-histidine (OV-D-HisHK.2H<sub>2</sub>O) (**2**) were prepared from L-histidine / D-histidine monohydrochloride monohydrate, following published procedure [Scheme (IV-13)]<sup>155</sup>. N-(salicylidene)-L-arginine (S-L-ArgH<sub>2</sub>) (**3**) was synthesized by reacting L-arginine monohydrochloride, KOH and salicylaldehyde in 2 : 2 : 2.05 molar ratio in methanol – water (4 : 1 v/v) medium<sup>146</sup>.

Purity of these compounds was checked through TLC, elemental analysis and matching of IR spectral data with the original ones. For TLC purpose methanolic solution of the compounds were used ; the TLC plates (Silica-gel G) were eluted with  $\text{CH}_3\text{OH} - \text{CH}_2\text{Cl}_2$  (1 : 1 v/v) and the spots were visualized in an iodine chamber.

## Synthesis of the Complexes

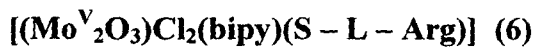
The following three complexes were synthesized using methods described by S. Panchanan<sup>146</sup>. Their purity was checked through TLC, elemental analysis, mass spectral data ; their magnetic susceptibility data ( $\mu_{\text{eff}}$  B.M.), IR and UV-VIS spectra were also recorded and compared with the original data<sup>146</sup>. These freshly prepared complexes were utilized for kinetic studies with pyridine N-oxide (PyN $\rightarrow$ O), in spectroscopy grade DMF (SRL, Mumbai).



Colour : snuff ;  $\mu_{\text{eff}}$  (295 K) : 1.05 B.M.

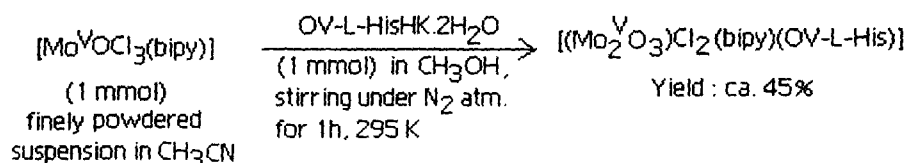


Colour : brown ;  $\mu_{\text{eff}}$  (295 K) : diamagnetic.



Colour : pink - brown ;  $\mu_{\text{eff}}$  (295 K) : 0.50 B.M.

An outline regarding the synthetic route of these complexes is shown in Scheme (IV-14); for complex (6) the time of stirring was restricted to 30 min. In each case the reaction mixture was allowed to settle for 15 min., filtered and washed under dinitrogen atmosphere with degassed  $\text{CH}_3\text{CN} - \text{CH}_3\text{OH}$  (1 : 1, v/v),  $\text{CH}_3\text{OH}$  and dried over anhy.  $\text{CaCl}_2$  in vacuo for 48h. Purity of each complex was checked through TLC [Silica-gel GF<sub>254</sub>, UV - chamber] using DMF solution (diluted with 100 times  $\text{CH}_3\text{OH}$ ) and  $\text{C}_6\text{H}_6 - \text{CHCl}_3$  (3 : 1 v/v) as eluant.



**Scheme (IV-14)** : Synthesis of complex (4); for complexes (5) and (6), OV-D-HisHK.2H<sub>2</sub>O and S-L-ArgH<sub>2</sub> were used respectively.

---

The  $\Lambda_{\text{M}}$  values [20-22  $\text{ohm}^{-1} \text{cm}^2 \text{mol}^{-1}$  in DMF, 301 K] of complexes (4), (5) and (6) are consistent with their non - electrolytic formulations<sup>13</sup>.

## Results and Discussion

The FAB mass spectra of complexes (4) and (6) are shown in Figures (IV-30) and (IV-31) respectively. The FAB mass spectrum of complex (4) shows the characteristic isotope pattern in the region  $m/z = 751$  [Figure (IV-32)] corresponding to the fragment  $[\text{M} - 3\text{H}]^+$  or  $[\text{C}_{24}\text{H}_{18}\text{N}_5\text{O}_7\text{Cl}_2\text{Mo}_2]^+$  (where M is the formula weight, 754.24). Here the  $m/z$  value (most abundant isotopic mass and the isotope distribution profile agreed with the corresponding theoretical value<sup>46</sup>, thereby supporting the

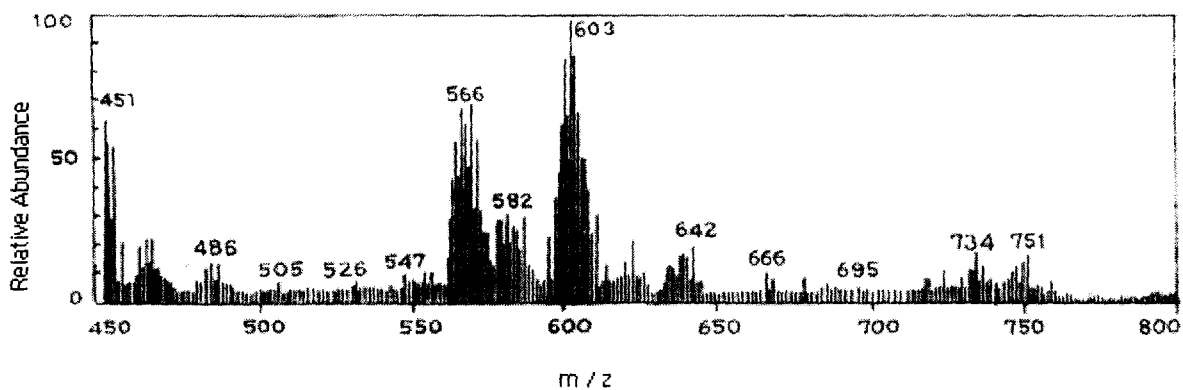


**Fig.(IV – 30):** FAB Mass Spectrum of (4) (relative abundance versus m/z)

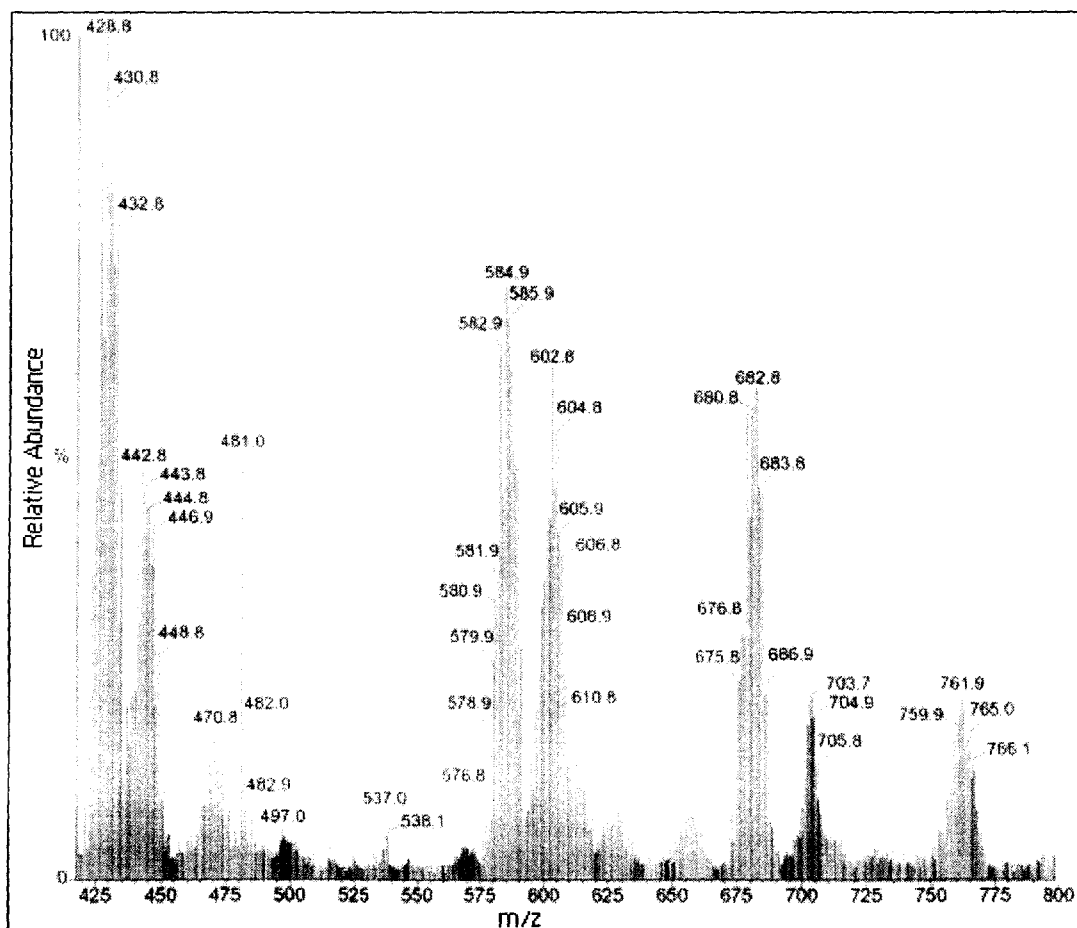


**Fig.(IV – 31):** FAB Mass Spectrum of (6) (relative abundance versus m/z)

chemical composition of complex (4), together with the elemental analysis and different physicochemical data. The number of isotope peaks in Figure (IV-32) verifies the binuclear nature of complex (4)<sup>14</sup>.

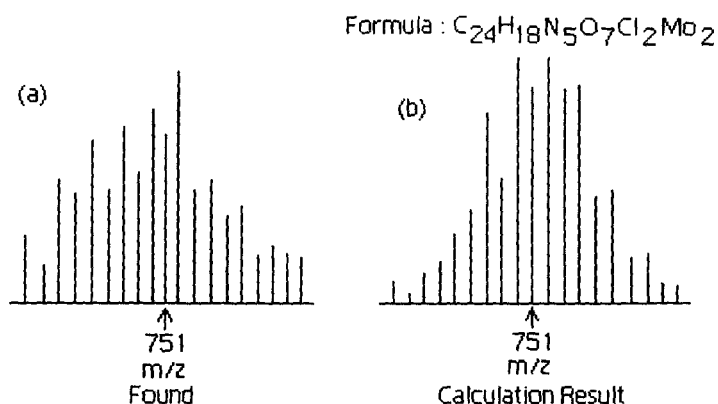


**Fig.(IV-32):** (a) FAB mass data of (4) at  $m/z$  ( $= 751$ ) region corresponding to  $[M - 3H]^+$  or  $[C_{24}H_{18}N_5O_7Cl_2Mo_2]^+$ ; (b) the calculated isotope pattern <sup>14, 46</sup>.

For complex (6) Figure (IV-33) shows the characteristic isotope pattern in the region  $m/z = 703.7$  corresponding to the fragment  $[M - C(NH)NH_2 + 2H]^+$  or  $[C_{22}H_{24}N_4O_6Cl_2Mo_2]^+$  (where M is the formula weight, 743). The released portion  $[C(NH)NH_2]$  shown above corresponds to the amidine group of the arginine residue [Scheme (IV-13)]. The  $m/z$  value (most abundant isotopic mass) and the isotope distribution profile agreed with the corresponding theoretical value <sup>46</sup>, thereby supporting the chemical composition of (6), including its binuclear nature <sup>14</sup>. These mass spectral studies indicate the overall architectural stability of these binuclear Mo(V) complexes.

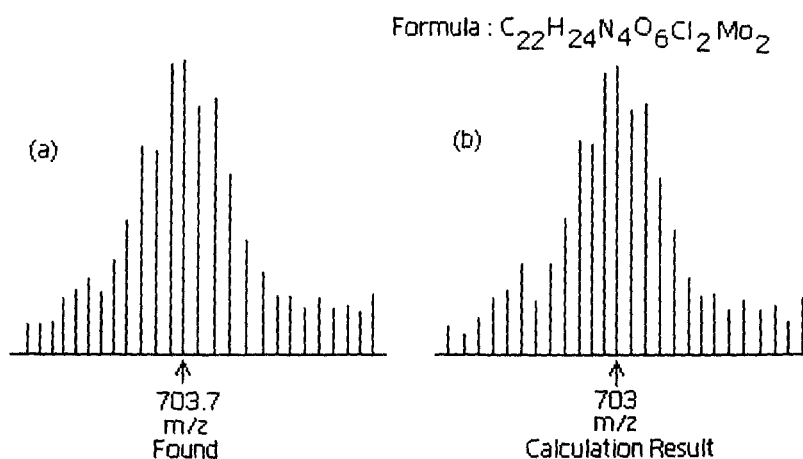


**Fig.(IV-33):** (a) FAB mass data of (6) at  $m/z$  ( $= 703.7$ ) region corresponding to  $[M - C(NH)NH_2 + 2H]^+$  or  $[C_{22}H_{24}N_4O_6Cl_2Mo_2]^+$ ; (b) the calculated isotope pattern <sup>14, 46</sup>.

From considerations of elemental analysis, FABMS data and different physicochemical studies, the chemical compositions of these binuclear complexes [(4), (5) and (6)] were established <sup>146</sup> and checked once again.

In the present study, this aspect has been strengthened through computer simulation of isotope distribution patterns of characteristic mass spectral fragments <sup>46</sup>. Further developments were achieved here by optimizing the possible schematic structures of (4), (5), (6), using molecular mechanics calculations (MM2), giving the lowest steric energy (Kcal/mol) CHEM3D models [Figures (IV-34) to (IV-36)]; this throws light on their stabilities as well as optimized molecular structures. The numbering system of these Figures is set by the software used <sup>87</sup>. For obtaining the CHEM3D model [Fig.(IV-35)] of complex (5) with OV-D-His<sup>2-</sup> ligand anion containing the D – histidine residue, positions of the two substituents (e.g., the imidazole group and the hydrogen atom, not shown here explicitly) of the chiral centre [C(12)] were interchanged, as compared to those in case of complex (4) with OV- L-His<sup>2-</sup> ligand anion [Figure (IV-34)]. This operation inverts the configuration about the chiral centre [C(12)] <sup>152</sup>. The two resulting CHEM3D models (MM2 method) are able to interpret the physicochemical and spectroscopic data of complexes (4) and (5) nicely (vide infra).

**Table (IV-11):** Comparison of computed bond lengths (Å) and angles (deg.) of the dianion (OV-L-His)<sup>2-</sup> with its chelated form in its molybdenum complex (4), shown in the parenthesis ; the data have been obtained from the respective optimized geometries (MM2 method).

Atoms	Bond Distances(Å) <sup>+</sup>	Atoms	Bond Distances(Å) <sup>+</sup>
C(3)-O(7)	1.37 [1.36]	C(22)-N(20)	1.27 [1.32]
C(1)-O(9)	1.36 [1.37]	C(4)-C(5)	1.42 [1.39]
C(14)-C(15)	1.50 [1.49]	N(11)-C(12)	1.47 [1.49]
C(2)-C(10)	1.51 [1.48]	C(2)-C(6)	1.42 [1.40]
C(10)-N(11)	1.26 [1.29]	C(3)-C(4)	1.43 [1.40]
C(12)-C(13)	1.52 [1.53]	C(13)-O(17)	1.21 [1.21]
C(1)-C(2)	1.43 [1.40]	C(5)-C(6)	1.42 [1.39]
C(19)-N(20)	1.47 [1.37]	C(15)-C(19)	1.34 [1.38]
C(12)-C(14)	1.53 [1.52]	C(15)-N(21)	1.47 [1.42]
C(22)-N(21)	1.47 [1.39]	C(1)-C(3)	1.43 [1.41]
C(13)-O(16)	1.35 [1.36]		

Angle Atoms	Bond Angle(deg.) <sup>†</sup>	Angle Atoms	Bond Angle(deg.) <sup>†</sup>
N(20)-C(22)-N(21)	110.8 [113.1]	C(22)-N(20)-C(19)	108.1 [106.7]
C(15)-N(21)-C(22)	104.8 [102.9]	C(15)-C(19)-N(20)	110.4 [109.5]
C(19)-C(15)-N(21)	105.9 [107.8]	C(2)-C(6)-C(5)	119.8 [117.9]
C(4)-C(5)-C(6)	118.7 [118.9]	C(3)-O(7)-C(8)	113.5 [113.5]
C(3)-C(4)-C(5)	122.5 [123.2]	C(4)-C(3)-C(1)	118.3 [118.1]
C(1)-C(2)-C(6)	121.3 [123.8]	C(2)-C(1)-C(3)	119.3 [117.8]

<sup>†</sup> Free ligand data are mentioned outside third bracket and the data derived from its molybdenum complex, (4), are mentioned within third bracket.

The molecular modeling force field in use for molecular systems can be interpreted in terms of the four key contributions, e.g., bond stretching, angle bending, torsional terms and non-bonded interactions<sup>86</sup>; in addition to the lowest steric energy, two other basic parameters were evaluated, e.g., bond distances (Å) and angles (deg)<sup>87</sup>. Tables (IV-12) to (IV-14) show some of the relevant data, together with the comparable X – ray data (given in the parenthesis) on mono  $\mu$  – oxo – bridged molybdenum (V) complexes [i.e., with the (Mo<sup>V</sup><sub>2</sub>O<sub>3</sub>)<sup>4+</sup> core] with Schiff base and other ligands obtained from the literature<sup>7, 19, 55, 62, 147, 151</sup>. The agreement between the computed bond distances and the literature X – ray structural data is fair in most cases showing the realistic nature of the CHEM3D models [Fig.(IV-34) to (IV-36)] obtained by MM2 method<sup>86, 87</sup>. This approach of rationalizing optimized structural data, is in line with the recent trends in structure (and property) elucidation<sup>148-150</sup>. As far as the computed bond angles data are concerned [Table (IV-12) to (IV-14)], they can be classified into four types (69<sup>o</sup> – 83<sup>o</sup>, 87<sup>o</sup> – 100<sup>o</sup>, 116<sup>o</sup> – 143<sup>o</sup> and 148<sup>o</sup> – 171<sup>o</sup>), in agreement with literature X – ray structural data on (Mo<sup>V</sup><sub>2</sub>O<sub>3</sub>)<sup>4+</sup> – type complexes with different types of ligands, where each molybdenum(V) atom is characterized by distorted octahedral geometry<sup>7, 55, 62, 147, 151</sup>. However, when the attention is focused here [complexes (4), (5), (6)] on specific computed bond angles around the Mo(V) atoms, they are found to depend considerably on the identity of the aldimine ligand involved in the particular complex; a comparative study [Table (IV-15)] of several relevant bond angles data bear this out.

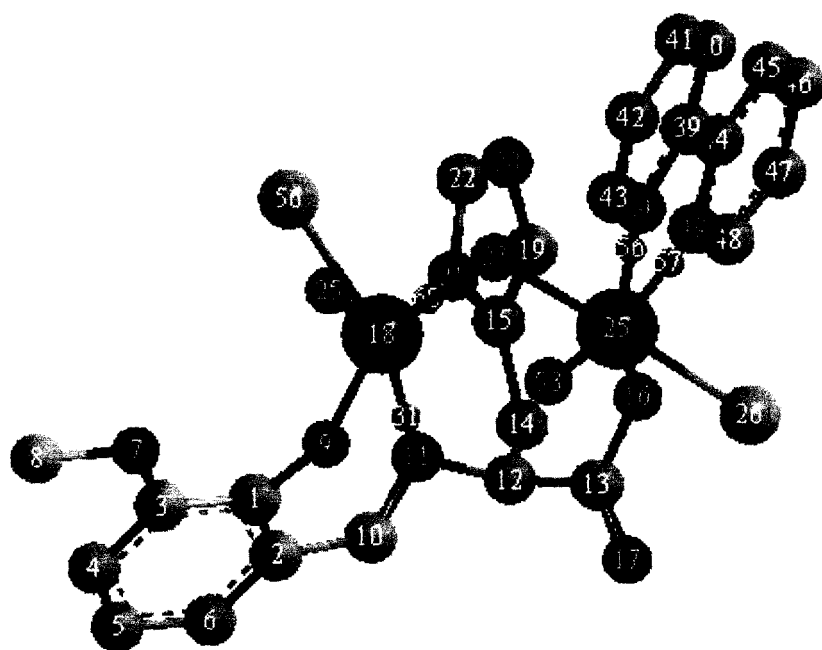


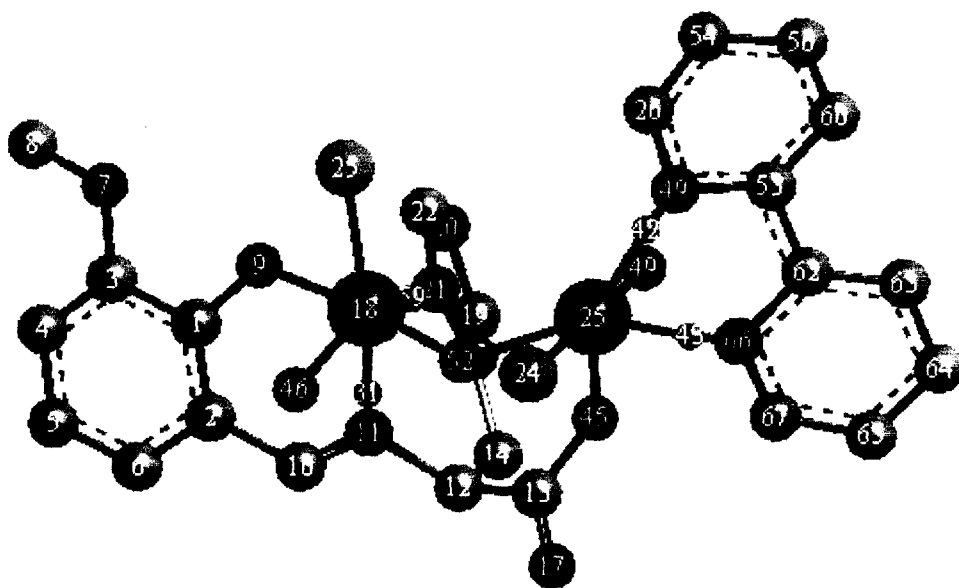
Fig.(IV- 34): The optimized geometry (CHEM3D model obtained through MM2 calculations) of (4) with a steric energy of 48.3 Kcal mol<sup>-1</sup>. Its numbering system is set by the software used<sup>87</sup>.

Table (IV-12): Comparison of selected computed bond lengths(Å) and bond angles (deg.) of complex (4) from the optimized geometry [Fig.(IV-34), MM2 method] with the available literature data (in parenthesis) from X-ray structural studies\*.

Atoms	Bond Distances(Å)	Atoms	Bond Distances(Å)
O(9)-Mo(18)	1.98(2.034) <sup>7</sup>	N(11)-Mo(18)	2.09(2.164) <sup>7</sup>
Mo(18)-Cl(56)	2.32(2.334) <sup>62</sup>	Mo(18)-O(25)	1.98(1.707) <sup>55</sup>
O(23)-Mo(25)	1.97(1.885) <sup>7</sup>	Mo(25)-O(53)	1.96(1.707) <sup>55</sup>
Mo(18)-O(23)	1.97(1.885) <sup>7</sup>	N(21)-Mo(18)	2.21(2.21) <sup>147</sup>
O(16)-Mo(25)	1.97(2.09) <sup>55</sup>	N(24)-Mo(25)	2.10(2.208) <sup>7</sup>
N(49)-Mo(25)	2.10(2.08) <sup>7</sup>	Mo(25)-Cl(26)	2.30(2.334) <sup>62</sup>
Angle Atoms	Bond Angle(deg.)	Angle Atoms	Bond Angle(deg.)
N(49)-Mo(25)-O(53)	160.0(162.7) <sup>7</sup>	N(24)-Mo(25)-O(53)	82.6(82.88) <sup>109</sup>
N(49)-Mo(25)-O(23)	88.0(93.3) <sup>62</sup>	N(21)-Mo(18)-O(9)	148.8(155.8) <sup>7</sup>
N(11)-Mo(18)-O(9)	74.2(80.6) <sup>7</sup>	N(49)-Mo(25)-N(24)	77.4(70.8) <sup>7</sup>
O(53)-Mo(25)-Cl(26)	83.6(89.6) <sup>108</sup>	N(21)-Mo(18)-Cl(56)	78.5(88.3) <sup>62</sup>
O(23)-Mo(25)-O(16)	100.2(105.9) <sup>109</sup>	N(49)-Mo(25)-Cl(26)	99.0(89.8) <sup>62</sup>
N(21)-Mo(18)-N(11)	75.0	Cl(56)-Mo(18)-O(23)	92.9
N(49)-Mo(25)-O(16)	74.7	Cl(26)-Mo(25)-O(16)	87.0
Mo(25)-O(23)-Mo(18)	116.3	N(11)-Mo(18)-O(23)	116.1
N(24)-Mo(25)-O(23)	81.0	Cl(26)-Mo(25)-O(23)	171.1

\* X-ray structural data have been collected from references mentioned as superscript on the data within parenthesis.

Participation of potential donor groups of the amino acid residues (e.g., imidazole and amidine nitrogen atoms) of the aldimine ligands [Scheme (IV-13)] in the coordination process to the Mo(18) atom here, is most likely responsible for this observation ; even the change of configuration about the chiral centre [C(12)] controls this aspect as evident from the bond angles data [Table (IV-15)] of complexes (4) and (5) with OV- L-His<sup>2</sup> and OV- D-His<sup>2</sup> residues respectively. Most interesting aspects of this study is the ability of the chiral ligands (L - / D - ) in giving rise to (Mo<sup>V</sup><sub>2</sub>O<sub>3</sub>)<sup>4+</sup> - complexes with different dispositions (trans - / skew - / near approach to cis - ) of the two Mo = O<sub>t</sub> bands about the Mo - O<sub>b</sub> - Mo axis (vide infra).



**Fig.(IV-35):** The optimized geometry (CHEM3D model obtained through MM2 calculations) of (5) with a steric energy of 46.6 Kcal mol<sup>-1</sup>. Its numbering system is set by the software used<sup>87</sup>.

**Table (IV-13):** Comparison of selected computed bond lengths(Å) and bond angles (deg.) in (5) from the optimized geometry [Fig.(IV-35), MM2 method] with the available literature data (in parenthesis) from X-ray structural studies<sup>\*</sup>

Atoms	Bond Distances(Å)	Atoms	Bond Distances(Å)
Mo(18)-O(46)	1.96(1.702) <sup>55</sup>	N(11)-Mo(18)	2.05(2.164) <sup>7</sup>
O(52)-Mo(25)	1.98(1.885) <sup>7</sup>	Mo(18)-Cl(25)	2.30(2.334) <sup>62</sup>
Mo(25)-Cl(24)	2.39(2.334) <sup>62</sup>	Mo(25)-O(45)	1.98(2.09) <sup>55</sup>
N(21)-Mo(18)	2.18(2.21) <sup>147</sup>	O(9)-Mo(18)	1.94(2.034) <sup>7</sup>
Mo(18)-O(52)	1.94(1.885) <sup>7</sup>	Mo(25)-O(49)	1.94(1.707) <sup>55</sup>
N(49)-Mo(25)	2.22(2.208) <sup>7</sup>	N(66)-Mo(25)	2.18(2.208) <sup>7</sup>

Angle Atoms	Bond Angle(deg.)	Angle Atoms	Bond Distances(Å)
Cl(25)-Mo(18)-O(9)	80.7(81.7) <sup>3(c)</sup>	N(11)-Mo(18)-O(9)	92.9(80.6) <sup>7</sup>
N(21)-Mo(18)-O(9)	81.6(83.2) <sup>108</sup>	Cl(25)-Mo(18)-N(11)	173.4(171.2) <sup>108</sup>
O(52)-Mo(18)-N(21)	104.0(103.3) <sup>109</sup>	O(46)-Mo(18)-Cl(25)	101.1(104.9) <sup>3(c)</sup>
O(52)-Mo(18)-N(11)	85.7(82.88) <sup>109</sup>	O(46)-Mo(18)-N(21)	148.0(158.8) <sup>109</sup>
Mo(25)-O(52)-Mo(18)	126.2	N(49)-Mo(25)-N(66)	74.6
O(52)-Mo(25)-N(49)	139.4	O(46)-Mo(18)-N(11)	77.5
O(52)-Mo(25)-O(45)	74.0	N(11)-Mo(18)-N(21)	70.6
O(52)-Mo(25)-O(49)	113.3	N(66)-Mo(25)-Cl(24)	123.1
O(52)-Mo(18)-Cl(25)	100.2	Cl(25)-Mo(18)-N(21)	110.1

X-ray structural data have been collected from references mentioned as superscript on the data within parenthesis.

Lowest steric energy of complexes (4), (5) and (6) are 48.3 Kcal/mol, 46.6 Kcal/mol and 44.7 Kcal/mol respectively ; these data indicate good deal of stability considering the binuclear nature of these complexes.

Table (IV-11) compares the computed (MM2 method) bond distances (Å) and bond angles (deg) data of OV- L-His<sup>2-</sup> with those (shown in parenthesis) of the corresponding chelated ligand dianion, in complex (4). Distinct changes in some of these data, resulting from electronic redistribution during the coordination process, indicate the

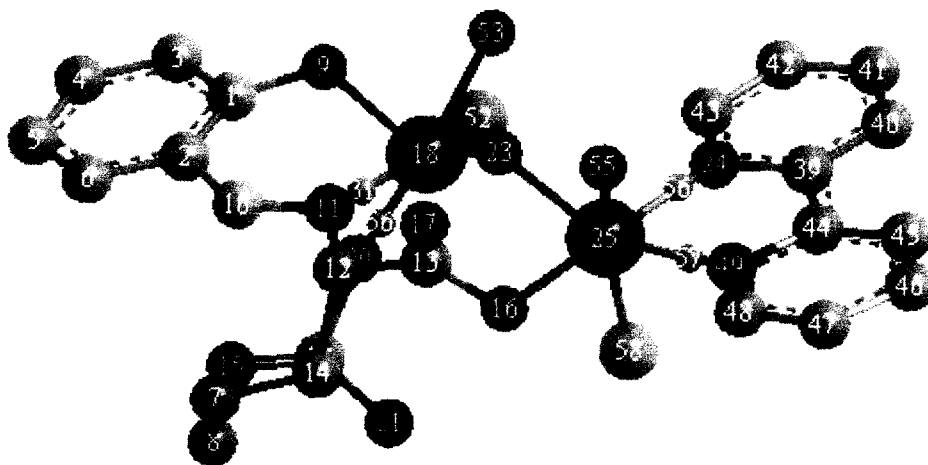


**Fig.(IV-36):** The optimized geometry (CHEM3D model obtained through MM2 calculations) of (6) with a steric energy of 44.7 Kcal mol<sup>-1</sup>. Its numbering system is set by the software used<sup>87</sup>.

**Table (IV-14):** Comparison of selected computed bond lengths(Å) and bond angles (deg.) of complex (6) from the optimized geometry [Fig. (IV-36), MM2 method] with the available literature data (in parenthesis) from X-ray structural studies\*

Atoms	Bond Distances(Å)	Atoms	Bond Distances(Å)
Mo(18)-Cl(52)	2.32(2.334) <sup>62</sup>	O(16)-Mo(25)	1.97(2.09) <sup>55</sup>
O(23)-Mo(25)	1.95(1.885) <sup>7</sup>	N(49)-Mo(25)	2.10(2.208) <sup>7</sup>
N(11)-Mo(18)	2.12(2.164) <sup>7</sup>	Mo(25)-Cl(58)	2.30(2.334) <sup>62</sup>
Mo(25)-O(55)	1.97(1.707) <sup>55</sup>	O(9)-Mo(18)	1.97(2.034) <sup>7</sup>
Mo(18)-O(53)	1.98(1.707) <sup>55</sup>	N(24)-Mo(25)	2.09(2.208) <sup>7</sup>
N(20)-Mo(18)	2.09(2.21) <sup>147</sup>	Mo(18)-O(23)	1.97(1.885) <sup>7</sup>

Angle Atoms	Bond Angle(deg.)	Angle Atoms	Bond Angle(deg.)
N(11)-Mo(18)-O(9)	86.3(83.2) <sup>108</sup>	O(16)-Mo(25)-N(49)	102.0(103.3) <sup>109</sup>
Cl(52)-Mo(18)-O(9)	82.4(89.6) <sup>108</sup>	N(49)-Mo(25)-O(23)	147.4(158.81) <sup>109</sup>
N(11)-Mo(18)-O(53)	121.8	Mo(18)-O(23)-Mo(25)	123.09
N(11)-Mo(18)-O(23)	73.9	O(55)-Mo(25)-O(23)	79.6
N(11)-Mo(18)-N(20)	78.7	O(9)-Mo(18)-N(20)	90.3
N(24)-Mo(25)-N(49)	78.3	O(53)-Mo(18)-N(20)	155.2
N(24)-Mo(25)-Cl(58)	84.9	N(24)-Mo(25)-O(55)	99.9

\* X-ray structural data have been collected from references mentioned as superscript on the data within parenthesis.

**Table (IV-15) :** Comparison of several specific computed bond angles (deg) data of the present complexes from their optimized geometries

Bond Angles	Complex (4)	Complex (5)	Complex (6)
O(9)-Mo(18)-N(11)	74.2 <sup>0</sup>	92.9 <sup>0</sup>	86.3 <sup>0</sup>
Cl(56)-Mo(18)-O(9)	120.5 <sup>0</sup>	80.7 <sup>0</sup>	82.3 <sup>0</sup>
N(11)-Mo(18)-N(21)	75.0 <sup>0</sup>	70.6 <sup>0</sup>	78.7 <sup>0</sup>
O(16)-Mo(25)-Cl(26)	87.0 <sup>0</sup>	178.0 <sup>0</sup>	95.0 <sup>0</sup>
Cl(26)-Mo(25)-N(49)	99.0 <sup>0</sup>	109.9 <sup>0</sup>	84.9 <sup>0</sup>

relevant ligand donor atoms involved in the metal coordination process [Fig.(IV-34) to (IV-36)]. Changes in IR spectral data of the ligands [(1), (2) and (3)] during the complex formulation process as discussed later, support the above inference drawn from Table (IV-11).

On scrutinizing the CHEM3D models of complexes (4), (5) and (6) [Figures (IV-34) to (IV-36)] the following important aspects are revealed, which are consistent with their physicochemical and spectroscopic data (vide infra); **earlier such data were interpreted only on the basis of their schematic structures**<sup>146</sup>. This approach also helps to rationalize the oxygen atom transfer activity of the present study.

**1. Coordination status around each molybdenum (V) atom of these binuclear (Mo<sup>V</sup><sub>2</sub>O<sub>3</sub>)<sup>4+</sup> – complexes :**

In each case the Mo(18) atom is coordinated by three donor atoms of the aldimine ligand residue ; for example in complex (4) with OV- L-His<sup>2-</sup> residue, the phenoxide oxygen atom [O(9)], the azomethine nitrogen atom [N(11)] and the histidine nitrogen atom [N(21)] perform this task ; the chlorine atom [Cl(56)], the terminal oxygen atom [O(25)] and the bridging oxygen atom [O(23)] satisfy the six coordination positions of the Mo(18) atom. A similar coordination situation exists around Mo(18) in complex (5) with OV- D-His<sup>2-</sup> residue. For complex (6) with S-L-Arg<sup>2-</sup> residue [Scheme (IV-13)], apart from the phenoxide oxygen atom [O(9)] and the azomethine nitrogen atom [N(11)], the arginine amidine nitrogen atom [N(20)] coordinates to Mo(18). The computed bond length data [from the optimized geometry of complex (6)] for the C(19) – N(20) and C(19) – N(21) bonds are 1.59Å and 1.38Å respectively ; evidently the nitrogen atom [N(20)] and not the other nitrogen atom [N(21)] is involved in coordination to the Mo(18) atom.

For each of these three complexes [(4) to (6)], the potential donor atom (imidazole or amidine nitrogen) from the amino acid moiety of the aldimine ligand is involved in coordination to Mo(18). In this respect, it is a novel situation as compared to various well – characterized molybdenum complexes with Schiff base ligands without amino acid residues<sup>7</sup>.

The six coordination positions around the other molybdenum(V) atom [i.e., Mo(25) in Figures (IV-34) to (IV-36)] of these binuclear complexes, are satisfied by the two nitrogen atoms of the 2,2' - bipyridyl ligand, the chlorine atom, the terminal and the bridging oxygen atoms and the carboxylate oxygen atom of the particular aldimine ligand residue.

As evident from the computed bond angles data in Tables (IV-12) to (IV-14) each molybdenum (V) atom [either Mo(18) or Mo(25)] is characterized by distorted octahedral geometry, in agreement with literature X – ray structural data on (Mo<sup>V</sup><sub>2</sub>O<sub>3</sub>)<sup>4+</sup> – complexes<sup>7, 19, 55, 62, 151</sup>.

## 2. The disposition of the two Mo = O<sub>t</sub> bonds about the Mo(18) – O<sub>b</sub> – Mo(25) axis :

An inspection of the CHEM3D model [Fig.(IV-34)] reveals that disposition of the two Mo = O<sub>t</sub> bonds about the Mo – O<sub>b</sub> – Mo axis is essentially skew (i.e., the two Mo = O<sub>t</sub> bonds are at almost 90° to each other). In case of complex (5) [Fig.(IV-35)], a close approach to trans – disposition of the two Mo = O<sub>t</sub> bonds about Mo – O<sub>b</sub> – Mo axis is observed. For complex (6) [Fig.(IV-36)] disposition of the two Mo = O<sub>t</sub> bonds about the Mo – O<sub>b</sub> – Mo axis deviates from a perfectly cis – arrangement, but the deviation is not large enough like the skew – disposition of the two Mo = O<sub>t</sub> bonds ; for complex (4) here the angle between the two Mo = O<sub>t</sub> bonds represents an intermediate situation between their cis – and skew – dispositions.

Both the trans – directed and cis – directed (nearly eclipsed) terminal oxygens have been characterized X – ray crystallographically in different (Mo<sup>V</sup><sub>2</sub>O<sub>3</sub>)<sup>4+</sup> – complexes, depending on the ligand present <sup>7, 19, 55, 62, 151</sup>. The former case has a crystallographically required centre of inversion, whereas the latter one has an approximate two – fold axis. The skew – arrangement of terminal oxygens possesses none of these two attributes. **Till date examples of well – characterized skew (Mo<sup>V</sup><sub>2</sub>O<sub>3</sub>)<sup>4+</sup> – complex is rare.** The above – mentioned symmetry aspects casts its influence on the IR spectral data [especially the ν (Mo = O<sub>t</sub>) bands, as indicated in Figure (IV-37) of complexes (4) to (6). CD spectral data of complex (4) could also be analyzed from the symmetry view point.

Besides this, either the cis – or trans -, but not the skew – orientation of the Mo = O<sub>t</sub> bonds favours three – centre π – bonding across the Mo – O<sub>b</sub> – Mo bridge and pairing of spins on the two Mo<sup>V</sup>(d<sup>1</sup>) atoms leading to diamagnetism, which has been verified experimentally <sup>19</sup>. For a possible skew – orientation of the two Mo = O<sub>t</sub> bonds, formation of the three – centre π – bond together with spin pairing of the two d<sup>1</sup> electrons is prevented, leading to a paramagnetic dimer with skew - (Mo<sup>V</sup><sub>2</sub>O<sub>3</sub>)<sup>4+</sup> core <sup>19</sup>. This aspect has been discussed here, on the basis of magnetic moment (μ<sub>eff</sub>, B.M.) values and EPR spectra.

Last but not the least, the different possibilities (cis- / trans- / skew-) of the (Mo<sup>V</sup><sub>2</sub>O<sub>3</sub>)<sup>4+</sup> core giving rise to different sets of MO levels, control the oxygen atom

transfer as well as electron transfer capabilities of complexes (4), (5) and (6). The kinetic studies involving pyridine N – oxide and the cyclic voltammetric data bear out this aspect.

**3. Utilization of the four donor atoms of the present aldimine ligands for coordination purpose and unique carboxylato – bridged  $(\text{Mo}^{\text{V}}_2\text{O}_3)^{4+}$  core :**

A perusal of the CHEM3D models of complexes (4), (5) and (6) [Fig. (IV-34) to (IV-36)] reveals a couple of interesting features about utilization of the four potential donor sites of the aldimine ligands [(1), (2), (3) ; Scheme (IV-13)] by the two molybdenum (V) atoms of the  $(\text{Mo}^{\text{V}}_2\text{O}_3)^{4+}$  core of complexes (4), (5) and (6). Deprotonation occurs from the phenolic – OH group and the carboxylic acid group leading to the formation of the dianions  $\text{OV} - \text{L} - \text{His}^{2-}$ ,  $\text{OV} - \text{D} - \text{His}^{2-}$  and  $\text{S} - \text{L} - \text{Arg}^{2-}$  respectively [Scheme (IV-15)]. In each case the phenoxide oxygen atom [O(9)], the azomethine nitrogen atom [N(11)] and the nitrogen atom [N(21) or N(20)] from the amino acid part (histidine or arginine) of the aldimine ligand, coordinate to one [Mo(18)] of the Mo(V) atoms ; the carboxylate oxygen atom [O(16) / O(45)] coordinates to the other Mo(V) atom [Mo(25)], thereby forming a carboxylato – bridge between the two Mo(V) atoms, in addition to the  $\mu$  – oxo bridge between them. In that sense the pertinent complexes are mono –  $\mu$  – oxo –  $\mu$  – carboxylato core containing binuclear Mo(V) systems. X – ray structurally characterized different types of binuclear molybdenum complexes are known which contain both bridging oxygen atom and bridging carboxylate group<sup>39, 136</sup>. However, all known  $(\text{Mo}^{\text{V}}_2\text{O}_3)^{4+}$  core containing complexes characterized through X – ray crystallography, contain only a linear (or nearly so) mono -  $\mu$  – oxo bridge between the two Mo (V) atoms<sup>7, 19, 55, 62, 128, 151</sup>. Linear or near – linear Mo –  $\text{O}_b$  – Mo linkage is also observed in case of the singly bridged  $(\text{Mo}^{\text{V}}_2\text{O}_5)^{2+}$  core containing systems<sup>153, 154</sup>.

Now a brief attention may be given to the bond angles associated with the bridging atom (s) between the two molybdenum atoms of well – characterized doubly bridged binuclear complexes<sup>39, 128, 131, 136, 140, 147</sup>. In all cases the Mo –  $\text{X}_b$  – Mo bridge is bent, e.g., for complexes with  $(\text{Mo}^{\text{V}}_2\text{O}_4)^{2+}$  and  $(\text{Mo}^{\text{V}}_2\text{S}_2\text{O}_2)^{2+}$  cores, the Mo –  $\text{O}_b$  – Mo and Mo –  $\text{S}_b$  – Mo bond angles are  $81.7^\circ - 83.4^\circ$  and  $75^\circ - 75.5^\circ$  respectively. In conformity with these structural information, the CHEM3D models (MM2 method) of the

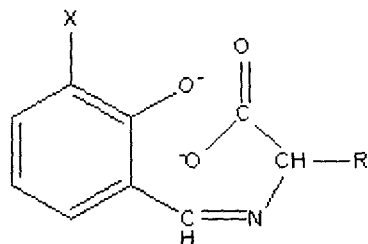
present doubly bridged complexes exhibit bent bridges with the Mo(18) – O<sub>b</sub> – Mo(25) bond angle varying in the range 116.3<sup>o</sup> – 126.2<sup>o</sup> [Tables (IV-12) to (IV-14)]. Here the Mo – O<sub>b</sub> – Mo bond angle is intermediate between those of the (Mo<sup>V</sup><sub>2</sub>O<sub>3</sub>)<sup>4+</sup> core (180<sup>o</sup> or nearly so) and the (Mo<sup>V</sup><sub>2</sub>O<sub>4</sub>)<sup>2+</sup> core (81.7<sup>o</sup> – 83.4<sup>o</sup>), because of the greater span of the μ – carboxylato group as compared to that of a μ – oxo group.

Complexes (4) and (5) have identical chemical composition ; so far as their aldimine ligand residues are concerned, only difference lies in the absolute configuration about the chiral centre [C(12)] related to the switching of positions of two of its substituents (e.g., the imidazole group and the hydrogen atom) <sup>152</sup>. In terms of chemical composition, complex (6) differs from the earlier two with respect to the aldimine ligand residue S – L – Arg<sup>2-</sup> ; here the methoxy (– OCH<sub>3</sub>) group of the aldehyde part and the imidazole group of the R part [Scheme (IV-13)] of OV – L – His<sup>2-</sup> or OV – D – His<sup>2-</sup> are replaced by a hydrogen atom and an amidine group respectively. In spite of all these similarities in composition, these complexes exhibit considerable structural differences as pointed out above along with possible reasons, e.g., the different arrangements of the Mo = O<sub>t</sub> bonds about the Mo – O<sub>b</sub> – Mo axis, the differences in bond angles as per Table (IV-15) and related aspects.

Now the experimental data of these complexes may be analyzed in a stepwise manner, within the framework of the above [Fig.(IV-34) to (IV-36)] CHEM3D models (MM2 method) and the associated structural inferences.

The prominent broad ligand [OV – L – HisHK.2H<sub>2</sub>O (1) and S – L – ArgH<sub>2</sub> (3)] IR bands belonging to the phenolic – OH group at 1360 – 1355 cm<sup>-1</sup> [δ (OH) mode] and 1231 – 1205 cm<sup>-1</sup> [δ (OH) + ν (C – O) mode] are absent in the IR spectra of the corresponding complexes (4), (5) and (6) ; the relevant ν (C – O) mode (phenoxide group) appears around 1165 – 1160 cm<sup>-1</sup> <sup>85</sup>. The ν (C=N) vibration of the free ligands appearing around 1635 – 1530 cm<sup>-1</sup> is lowered (by 20 - 25 cm<sup>-1</sup>) on coordination in all these cases <sup>85, 155</sup>. The ν<sub>as</sub> and ν<sub>s</sub> absorptions of the carboxylate (CO<sub>2</sub><sup>-</sup>) group appear around 1590 cm<sup>-1</sup> and 1415 cm<sup>-1</sup> respectively for these complexes <sup>85</sup> ; the Δν value (175 cm<sup>-1</sup>) indicates the presence of a unidentate carboxylate group <sup>72</sup>. It can be inferred that dianionic forms of the aldimine ligand residues utilize the phenoxide oxygen, azomethine nitrogen and one of the carboxylate oxygen atoms for coordination purpose [Scheme (IV-

15)] ; besides this, as per the CHEM3D models [Fig.(IV-34) to (IV-36)], the imidazole or amidine nitrogen atoms are also involved in coordination to one of the molybdenum (V) atoms. EPR simulation experiments as discussed later, support the participation of the nitrogen atoms of the later type.



**Scheme (IV-15):** Nature of the R group possessing nitrogen donor atom is shown in Scheme (IV-13).

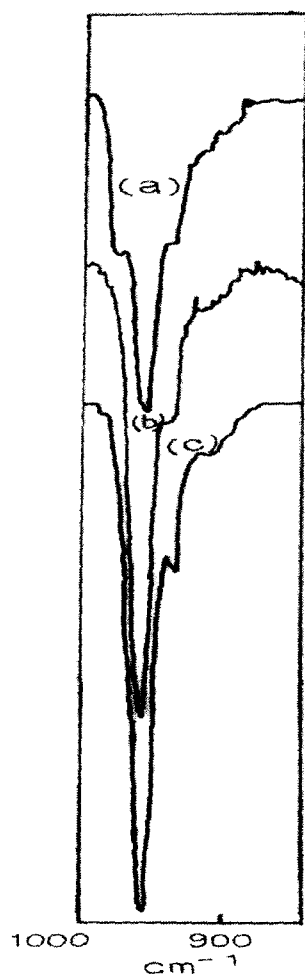
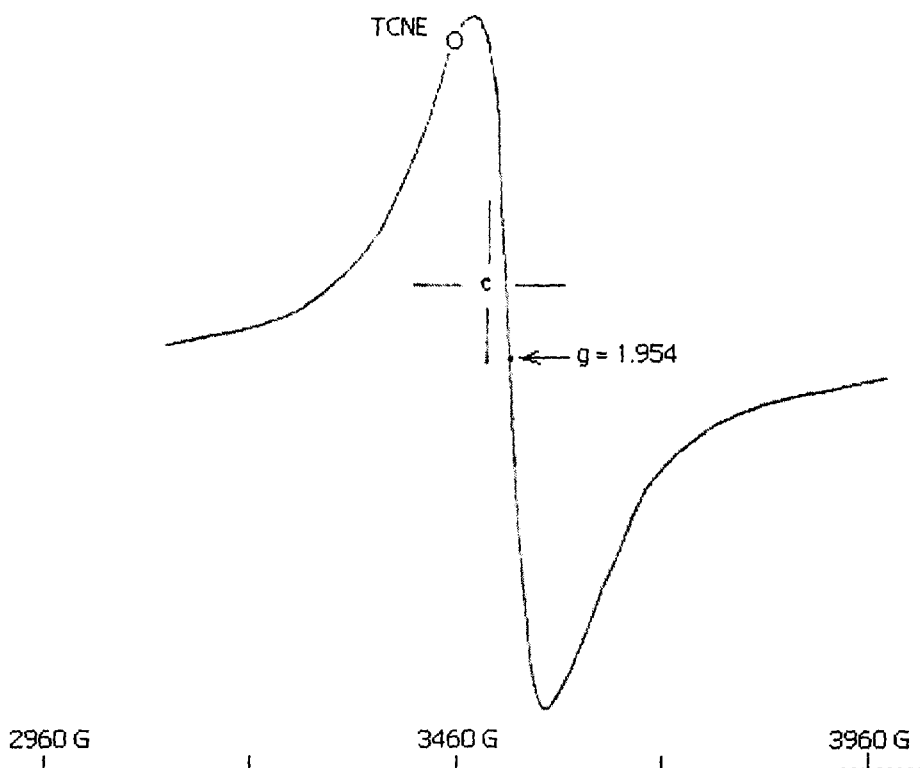


Figure (IV-37) shows the characteristic  $\nu(\text{Mo}=\text{O}_t)$  vibration of the  $(\text{Mo}^{\text{V}}_2\text{O}_3)^{4+}$  core of complexes (4), (5) and (6) at  $952 - 955 \text{ cm}^{-1}$  associated with fine structures (shoulders). This fine structure of the  $\nu(\text{Mo}=\text{O}_t)$  bands can be correlated with the arrangements (that is symmetry) of the two  $\text{Mo}=\text{O}_t$  bonds about the  $\text{Mo}-\text{O}_b-\text{Mo}$  axis of the  $(\text{Mo}^{\text{V}}_2\text{O}_3)^{4+}$  core in the light of the CHEM3D models [Fig.(IV-34) to (IV-36)]. Complex (4) with essentially skew – disposition of the two  $\text{Mo}=\text{O}_t$  bonds shows the most prominent fine structures for the  $\nu(\text{Mo}=\text{O}_t)$  bands ; complex (5) with essentially trans – disposition of the  $\text{Mo}=\text{O}_t$  bonds, possesses a  $\nu(\text{Mo}=\text{O}_t)$  band with lesser number of shoulder ; for the  $\nu(\text{Mo}=\text{O}_t)$  band of complex (6) a prominent shoulder is observed on the lower frequency side and the relevant CHEM3D model shows a moderate departure from a cis – disposition of  $\nu(\text{Mo}=\text{O}_t)$  bands. In short, lowering of symmetry of the  $(\text{Mo}^{\text{V}}_2\text{O}_3)^{4+}$  core results in greater fine

**Fig.(IV-37):** IR spectra of (4), (5) and (6) indicating characteristic  $\nu(\text{Mo}=\text{O}_t)$  stretching vibration of the  $(\text{Mo}^{\text{V}}_2\text{O}_3)^{4+}$  core<sup>19, 55</sup>; (a) → complex (4); (b) → complex (5); (c) → complex (6).

structure of the  $\nu(\text{Mo} = \text{O}_t)$  band of these complexes. This aspect is further substantiated by their magnetic susceptibility data, EPR and CD spectra, viewed in the light of MO theory<sup>19,55</sup>. It may be stated in this connection that the mononuclear starting material  $[\text{MoOCl}_3(\text{bipy})]$  with the  $(\text{Mo}^{\text{V}}\text{O})^{3+}$  core, used here for synthesizing the complexes under consideration possesses an intense structureless band at  $968 \text{ cm}^{-1}$  for the  $\nu(\text{Mo} = \text{O}_t)$  mode.

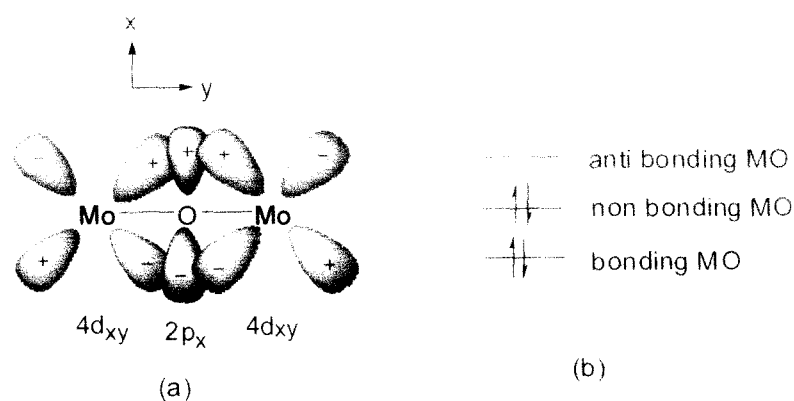
A medium intensity band in the region  $740 - 745 \text{ cm}^{-1}$  characterizes the  $\nu(\text{Mo}-\text{O}_b-\text{Mo})$  vibration of the  $(\text{Mo}^{\text{V}}_2\text{O}_3)^{4+}$  core in these cases<sup>19, 55</sup>. From room-temperature (295 K) magnetic susceptibility measurements it was observed that the  $\mu_{\text{eff}}$  (B.M.) values for complexes (4) and (6) are 1.05 and 0.50 respectively, while complex (5) is diamagnetic; out of them complex (4) is the only room-temperature (295 K) EPR active species. Although the observed  $\mu_{\text{eff}}$  value (1.05 B.M.) of complex (4) is much less than that expected for two unpaired electrons (that is, 2.83 B.M.), its room - temperature (295 K) EPR spectrum could be recorded both in the solid state as well as in DMSO solution [Fig.(IV-38) and (IV-39)]. As the melting point of DMSO is ca. 291 - 293 K, the



**Fig.(IV-38):** EPR spectrum of (4) in the solid state (295K); 9.528 GHz.

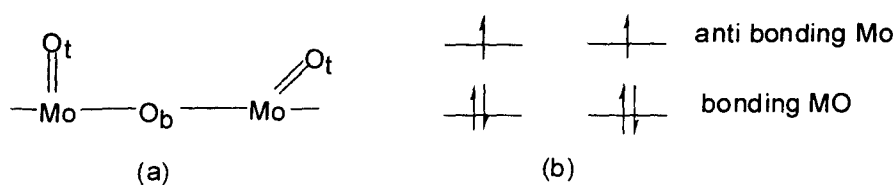
latter spectrum may be regarded as a close approach to a frozen solution data. Figure (IV-40) and (IV-41) represent the EPR spectra in DMSO at 77 K of complexes (4) and (6) respectively, indicating considerable increase in intensity of the EPR spectral lines (associated with broadening) at the liquid nitrogen temperature. Quantitation of the EPR signal intensity at 77 K of complex (4) corresponds to almost two unpaired electrons ( $S = 1$  ground state) supporting skew nature of its  $(\text{Mo}^{\text{V}}_2\text{O}_3)^+$  core ; for complex (6) the EPR signal intensity at 77 K corresponds to 1.10 electrons. Complex (5) is EPR silent ( $S = 0$ ) at both 295 K and 77 K, giving further support in favour of its trans -  $(\text{Mo}^{\text{V}}_2\text{O}_3)^+$  core. It may be mentioned here that only complex (4) is able to exhibit CD spectrum [Fig.(IV-42)] over the range 300 - 600 nm ; it gives additional evidence in favour of its skew -  $(\text{Mo}^{\text{V}}_2\text{O}_3)^+$  core, lacking the centre of symmetry.

The correlation of magnetic properties with the nature (cis - / trans - / skew - ) of the  $(\text{Mo}^{\text{V}}_2\text{O}_3)^+$  core can be elucidated in the light of MO theory. The cis - and trans - structures maximize  $\pi$  - bonding between each molybdenum and the bridging oxygen atom [Scheme (IV-16)], leading to a three - centre delocalized  $\pi$  - bond over the Mo - O<sub>b</sub> - Mo linkage. As per Scheme (IV-16), the four electrons [two from the bridging oxygen atom ( $2p_x$ ) and two from the two metal  $4d_{xy}$  orbitals<sup>19, 55</sup>, with each Mo(V) atom being a  $d^1$  system] fill up the bonding and non bonding levels, thereby producing a delocalized three centre  $\pi$  - bond over the Mo - O<sub>b</sub> - Mo linkage. This scheme predicts a



**Scheme (IV-16):** (a) Overlap of orbitals in the three - centre bonding MO of the Mo - O<sub>b</sub> - Mo bond for a cis - or trans -  $(\text{Mo}^{\text{V}}_2\text{O}_3)^+$  core<sup>19</sup> ; (b) the corresponding energy level diagram for the MOs involved in the three - centre bonding shown in (a), indicating the distribution of four electrons in them (details are given in the text).

bond order of 1.5 for each Mo – O<sub>b</sub> bond [the bonding level electron pair of Scheme (IV-16 b) provides with a π – bond order of 1 for the entire Mo – O<sub>b</sub> – Mo system, that is, 0.5 bond order for each Mo – O<sub>b</sub> π – bond and counting the Mo – O<sub>b</sub> σ – bond, the total bond order comes out to be 1.5]. This scheme indicates a singlet (S = 0) ground state with diamagnetic behaviour<sup>156</sup> and this is confirmed experimentally in case of complex (5). However, for a skew (Mo<sup>V</sup><sub>2</sub>O<sub>3</sub>)<sup>4+</sup> core (that is, the two Mo = O<sub>t</sub> bonds are at 90° to each other), the above – mentioned three – centre π – bond cannot be formed ; here individual π – bonds are formed between each Mo(V) 4d<sub>xy</sub> orbital and different O<sub>b</sub> (pπ) orbitals [Scheme (IV-17)]. For this case, each of the degenerate antibonding level contains one unpaired electron producing individual Mo – O<sub>b</sub> π – bond order of 0.5 and an overall bond order of 1.5 for this bond, counting the σ – contribution. Thus for the skew - (Mo<sup>V</sup><sub>2</sub>O<sub>3</sub>)<sup>4+</sup> core, although the Mo – O<sub>b</sub> bond is substantially of the same strength as for



**Scheme (IV-17):** (a) Skew - (Mo<sup>V</sup><sub>2</sub>O<sub>3</sub>)<sup>4+</sup> core ; (b) formation of two separate sets of MOs involving each molybdenum 4d<sub>xy</sub> orbital and the appropriate pπ orbital of the bridging oxygen atom, that is, either the 2p<sub>x</sub> or 2p<sub>y</sub> orbital, with a contribution of three electrons (one from the 4d<sub>xy</sub> orbital and two from the 2pπ orbital) to each set of Mo.

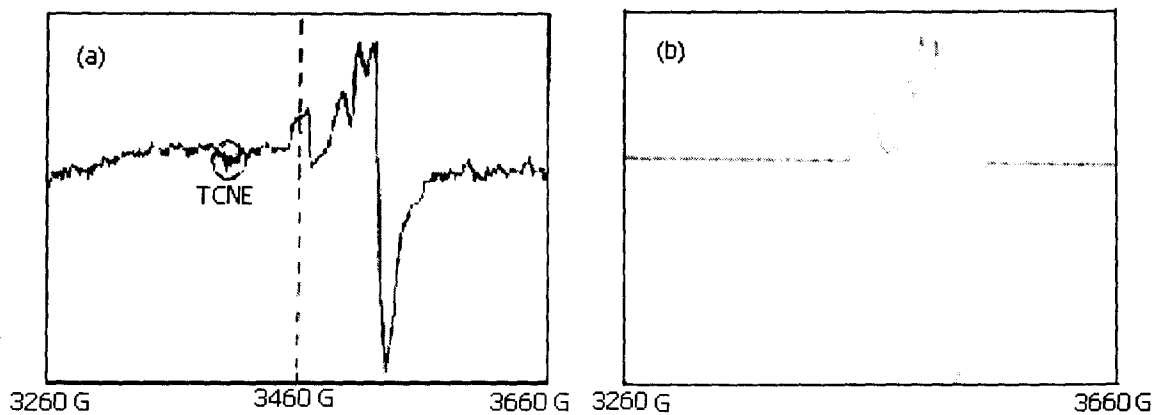


**Fig.(IV-39):** (a) EPR spectrum of (4) in DMSO at 295K at 9.528 G Hz.; (b) the simulated EPR spectrum of (4) with 75 % contribution of the Mo(18) centre and 25 % contribution of the Mo(25) centre ; it is the normalized spectrum of the two individual centres in the above ratio and the CHEM3D model in Fig(IV-34) indicates the donor atoms around each Mo(V) centre.

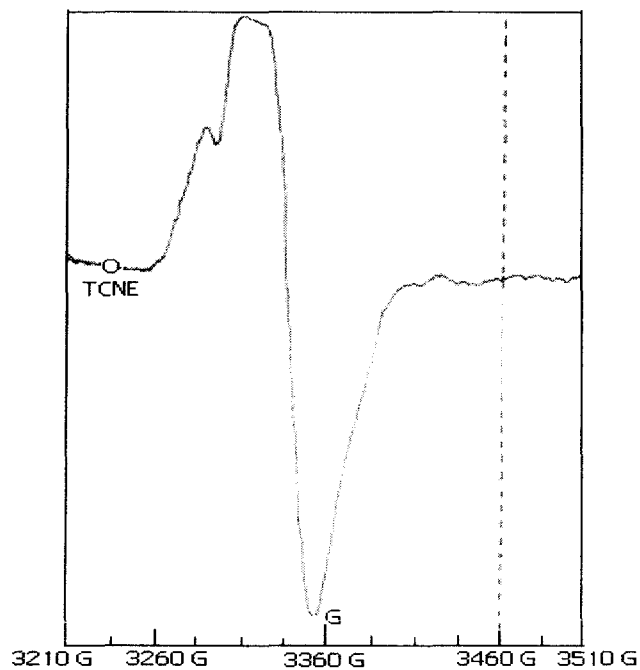


**Fig.(IV-40):** EPR spectrum of complex (4) in DMSO at 77 K ; 9.045 GHz.

complex (4) indicates the donor atoms around each Mo(V) atom ; out of them the azomethine hydrogen atom [Scheme (IV-13)] ( $I = 1/2$ ), the different types of nitrogen atoms ( $I = 1$ ) and the chlorine atoms ( $I = 3/2$ ) take part in hyperfine splitting of the EPR

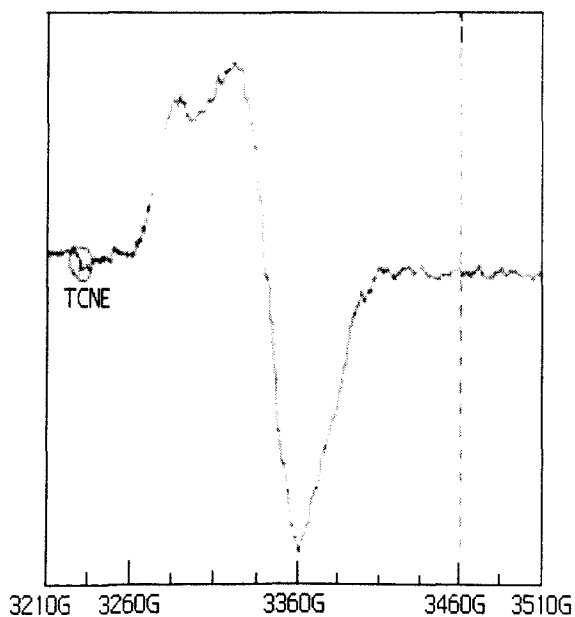


**Fig.(IV-41):** EPR spectrum of complex (6) in DMSO at 77 K ; 9.045 GHz. It is EPR silent at 295K ; 9.045 G Hz.

the cis – or trans -  $(\text{Mo}^{\text{V}}_2\text{O}_3)^{4+}$  core, a paramagnetic species with  $S = 1$  ground state would result <sup>19</sup>.

Skew nature of the  $(\text{Mo}^{\text{V}}_2\text{O}_3)^{4+}$  core for complex (4) is verified through EPR spectral simulation studies [Fig.(IV-39 b)] where spin contributions of both the Mo(V) centres [Scheme (IV-17)] have to be considered for matching the experimental EPR spectrum [Fig.(IV-39 (a))] <sup>157</sup>. The CHEM3D model of

signals of unpaired electrons of the two Mo(V) atoms (each a  $d^1$  system). The EPR spectra of the two Mo(V) atoms [Mo(18) and Mo(25)] were simulated separately taking into account their different coordination environments. To the overall simulated EPR spectrum [Fig.(IV-39 b)] the Mo(18) and Mo(25) centres contribute 75 % and 25 % respectively ; the resultant simulated EPR spectrum [Fig.(IV-39b)] is the normalized spectrum of the two individual centres in the above ratio.

Room-temperature (295K) magnetic susceptibility data in the solid state substantiate the above view. Complex (5) is diamagnetic and confirms to the three - centre MO formation [Scheme (IV-16)] with essentially trans -  $(\text{Mo}^{\text{V}}_2\text{O}_3)^{4+}$  core [Fig.(IV-35)]. Paramagnetism of complex (4) [with skew -  $(\text{Mo}^{\text{V}}_2\text{O}_3)^{4+}$  core as per Fig.(IV-34)] can be viewed in terms of Scheme (IV-17). Complex (6) with a low magnetic moment (0.50 B.M.) indicates an essentially intermediate situation, with moderate departure from a cis -  $(\text{Mo}^{\text{V}}_2\text{O}_3)^{4+}$  core [Fig.(IV-36)].

The electronic spectra [Figures (IV-43), (IV-45) and (IV-47)] of these complexes are characterized by similar spectral features, indicating their similarity in overall electronic structure, in spite of some differences in several physico-chemical properties. For Mo(V) system ( $d^1$ ) the 4d - orbital ordering appears to be  $d_{xy} < d_{xz}, d_{yz} < d_{x^2-y^2} < d_{z^2}$ ;  $d_{xz}, yz$  and  $d_{z^2}$  correspond to the  $\text{Mo} = \text{O}_t \pi^*$  and  $\sigma^*$  orbitals respectively<sup>19, 55</sup>. Thus the different d - d transitions [ $d_{xy}^1 \rightarrow (d_{xz}, yz)^1$ ;  $d_{xy}^1 \rightarrow (d_{x^2-y^2})^1$ ;  $d_{xy}^1 \rightarrow d_{z^2}^1$ ], ligand - to - metal charge transfer bands and  $\pi \rightarrow \pi^*$  transitions of ligands (aldimine / 2,2'

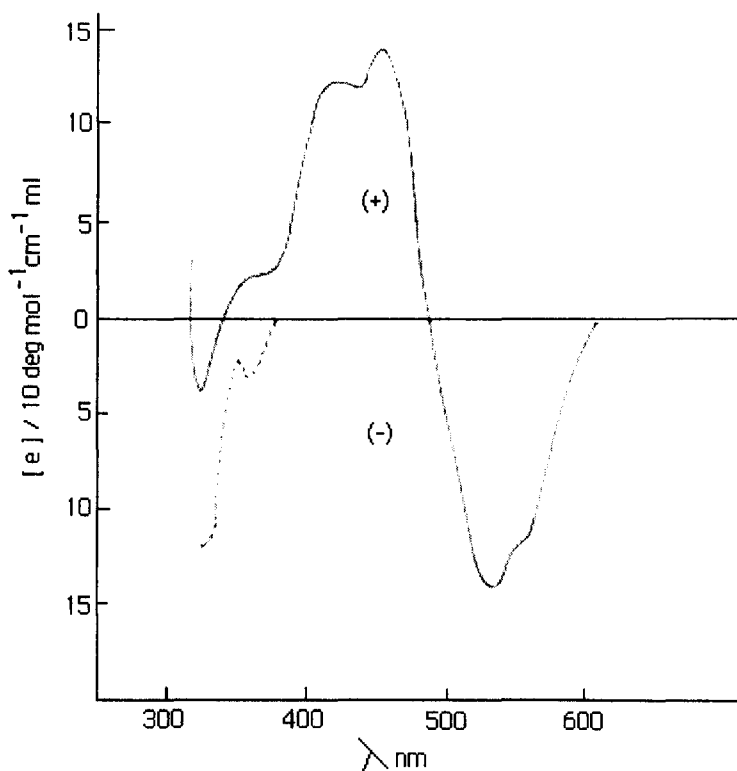


Fig.(IV-42): CD spectra in DMSO of complex (4) [—]  
<sup>146</sup>  
 and complex (5) [----].

- bipyridyl) are to be considered for the interpretation of electronic spectral data. The above - mentioned spectra can be divided into three parts : (a) 265 - 300 nm region which is characterized by an intense peak at 283 nm ( $\log \epsilon : 4.61 - 4.46$ ) due to an intraligand ( $\pi \rightarrow \pi^*$ ) transition ; (b) 300 - 335 nm region where a prominent shoulder appears at 310 ( $\log \epsilon : 4.23 - 4.33$ ) due to ligand - to - metal charge transfer transition ; (c)

335 – 500 nm region where two shoulders are observed at 350 – 360 nm ( $\log \epsilon : 3.37 - 3.52$ ) and 425 – 430 nm ( $\log \epsilon : 2.97 - 3.09$ ) due to  $d_{xy} \rightarrow d_{z^2}$  and  $d_{xy} \rightarrow d_{xz}, d_{yz}$  transitions respectively <sup>19,55</sup>. Their considerable molar extinction coefficient values are ascribed to intensity stealing from the (b) type charge transfer bonds. Transition of type (b) and (c) are responsible for the deep colours (snuff, brown and pink – brown) of these complexes. These transitions are better resolved in the corresponding CD spectrum [Fig.(IV-42)] along with the appearance of a new band at 533 nm ; the last transition is argued to be a characteristic feature of the  $(Mo^V_2O_3)^{4+}$  core <sup>19,55</sup>. Large  $\log \epsilon$  values of the above electronic spectral bands, derived from the charge transfer transitions involving the aldimine / 2,2' - bipyridyl ligands, cover the last type transition (533 nm) in the electronic spectra [Fig.(IV-43), (IV-45), (IV-47)]. In that sense CD data is a nice tool for resolving this type of electronic transition. The above CD spectrum [Fig.(IV-42)] bears remarkable similarity to that of the oxidized form of xanthine oxidase (a typical oxomolybdoenzyme with two mononuclear molybdenum centres) over the entire range 330 – 600 nm <sup>158</sup>.

Three distinct optically active transitions could be identified / assigned in the CD spectrum of complex (4).

1. A negative Cotton effect at 323 nm involving the ligand (aldimine) – to – metal charge transfer band and it is related to the aldimine ligand chiral centre.
2. A positive Cotton effect at 450 nm associated with shoulders due to different d – d transitions of the Mo(V) centre ( $d^1$ ), as delineated above.
3. A negative Cotton effect is observed at 533 nm along with a shoulder at 560 nm and this CD band extends upto ca. 600 nm. This corresponds to an electric dipole forbidden but magnetically allowed transition within the oxometal entity with the transition terminating in the antibonding component of the MO levels shown in Scheme (IV-17) <sup>19,55</sup>. The corresponding electronic spectrum [Fig.(IV-43)] of complex (4) hardly shows any absorption band beyond 500 nm due to the electric dipole forbidden nature of the transition responsible for the 533 nm CD band [Fig.(IV-42)]. <sup>146</sup>

The CD transitions of type 2 and 3 are influenced by the nature of the oxometal entity and become optically active due to low symmetry of the skew -  $(Mo^V_2O_3)^{4+}$  core in complex (4). This inference is further supported by the fact that

complex (5) with a trans -  $(\text{Mo}^{\text{V}}_2\text{O}_3)^{4+}$  core hardly shows any CD spectral response over the entire range 370 – 600 nm ; its weak CD signal at ca. 355 nm is influenced by the aldimine ligand chiral centre ; the CD spectrum of complex (6) is essentially similar to that of (5) [Fig.(IV-42)].

The above discussion on the electronic and CD spectral data lead to conclusion that the different d – d absorption bands including these characteristic of the  $(\text{Mo}^{\text{V}}_2\text{O}_3)^{4+}$  core, become optically active in complex (4) due to low symmetry of its skew -  $(\text{Mo}^{\text{V}}_2\text{O}_3)^{4+}$  core ; the chiral aldimine ligand can influence only the electronic transitions below ca. 360 nm, as evident from the CD spectrum of complex (5) [Fig.(IV-42)], where the transitions above 400 nm are not optically active due to high symmetry of its trans -  $(\text{Mo}^{\text{V}}_2\text{O}_3)^{4+}$  core.

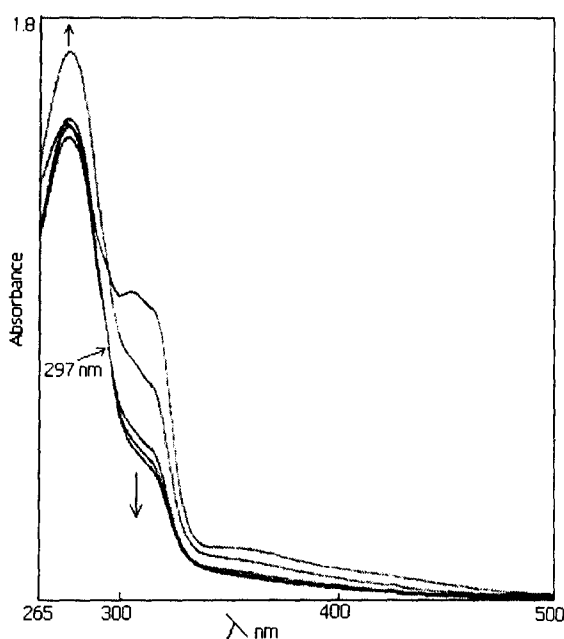
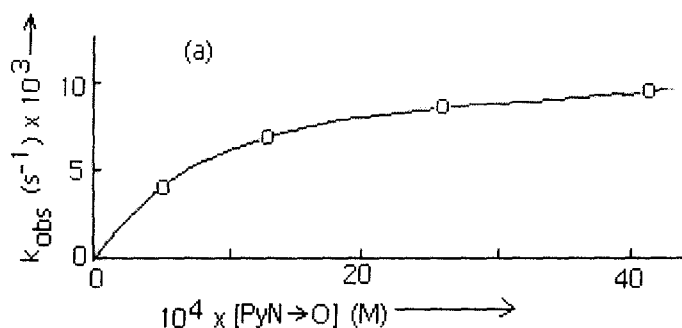


**Fig.(IV-43):** UV-VIS absorption spectral changes recorded every 5 min. interval during the reaction of (4)  $[4.2 \times 10^{-4} \text{ (M)}]$  with  $\text{PyN} \rightarrow \text{O}$   $[4.32 \times 10^{-4} \text{ (M)}]$  in DMF at 301K.

These complexes obey Beer's law in DMF solutions over the concentration range from  $4 \times 10^{-5} \text{ (M)}$  to  $4.5 \times 10^{-4} \text{ (M)}$ , indicating suitability of this medium for kinetic studies. Blank run (overlay mode) using a solution of the complex in DMF (purged) was recorded and it showed no change ; the same result was obtained using a solution of  $\text{PyN} \rightarrow \text{O}$  in DMF (purged). Figure (IV-43)] shows the spectrophotometric

monitoring of the reaction of complex (4) with PyN→O in DMF at 301 K ; continuous increase in optical density with time is observed at 283 nm, whereas the reverse is true at 310 nm and 360 nm. Comparable absorption spectral changes are observed for the molybdenum fragment of several oxomolybdoenzymes, usually in the longer wavelength region <sup>21, 160, 161</sup>. The pivotal point of the overlay spectral scans [Fig.(IV-43)] appears to be the region around 310 nm where ligand-to-metal charge transfer transition occurs. After initial several spectral scans an isosbestic point appears at 297 nm for the later scans. Complexes (5) and (6) exhibit similar UV – VIS spectral changes with time during the reaction with PyN→O [Fig.(IV-45) and Fig.(IV-47)] in DMF solution, with an isosbestic point at 297 nm in each case. For all the three complexes, the most interesting aspect is the spectral change observed around 310 nm. Maximum spectral change is observed for complex (4) with skew - (Mo<sup>V</sup><sub>2</sub>O<sub>3</sub>)<sup>4+</sup> core ; complex (5) with a trans - (Mo<sup>V</sup><sub>2</sub>O<sub>3</sub>)<sup>4+</sup> core shows only a moderate change in this region. The extent of this particular spectral change is intermediate for complex (6) with a slightly distorted (Mo<sup>V</sup><sub>2</sub>O<sub>3</sub>)<sup>4+</sup> core. As evident from Figure (IV-43), after a few spectral scans, the spectral

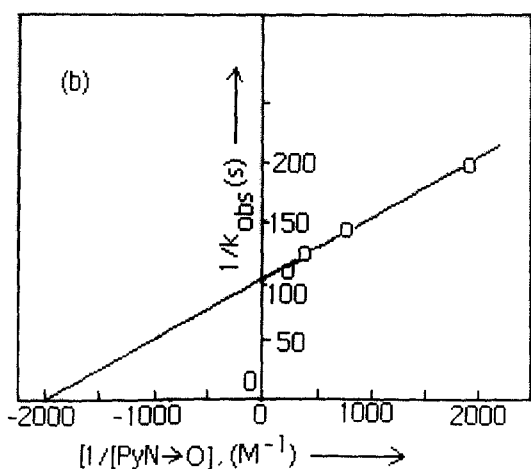


changes around 310 nm become comparable to those in Figure (IV-45) and (IV-47). Kinetics of this reaction was monitored at 310 nm under pseudo- first - order conditions (maintaining 3 – 100 times excess of PyN→O) in DMF. For an excess of the oxo transfer reagent, the kinetics could be described by single exponential as per the following equation :

$$(A - A_0) / (A_\infty - A_0) = e^{-k_{\text{obs}} t}$$

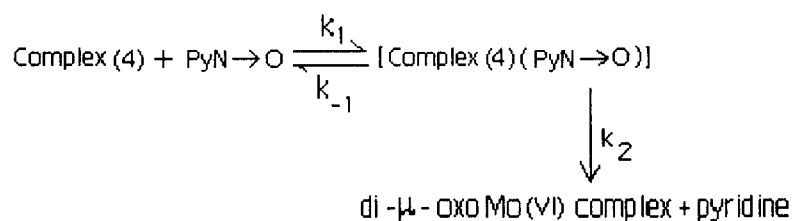
Where 'A' represents absorbance.

**Fig.(IV-44):** (a) Dependence of rate of reaction of (4) [ $4.17 \times 10^{-5}$  (M)] with PyN→O in DMF at 301K ;



(b) the corresponding double reciprocal plot in DMF.

Pseudo – first – order rate constants ( $k_{\text{obs}}$ ,  $\text{s}^{-1}$ ) were determined by least square method from the plots of  $\log (A_t - A_\infty)$  versus time, which were linear for more than two half lives. Figure (IV-44 a) shows the dependence of  $k_{\text{obs}}$ , ( $\text{s}^{-1}$ ) values on increasing substrate concentration and it confers to substrate saturation kinetics at high PyN→O concentration. Activation parameters [ $\Delta S^\ddagger$  and  $\Delta H^\ddagger$  values, Table (IV-16)] were obtained from the Eyring plot [ $\ln (k / T)$  versus  $1 / T$ ] using pseudo – first – order rate constants data determined (keeping a 100 – fold excess of PyN→O) at four different temperatures. The negative  $\Delta S^\ddagger$  values support the formation of an intermediate here as outlined in Scheme (IV-18). Activation energy values [ $E_a$ , Table (IV-16)] were obtained from the corresponding Arrhenius plot. Scheme (IV-18) represents the possible course of the reaction between complex (4) and PyN→O [substrate [S]] in DMF, which involves the reversible formation of an intermediate involving the two reactants, followed by its transformation to the products.




---

**Scheme (IV-18)**

---

In view of the above, the  $k_{\text{obs}}$ , ( $\text{s}^{-1}$ ) can be represented as follows <sup>7, 8, 17, 22, 23</sup>.

$$k_{\text{obs}} = k_2 [S] / (K_M + [S])$$

Where,  $K_M = (k_2 + k_{-1}) / k_1$

Or,

$$1/k_{\text{obs}} = 1/k_2 + K_M / k_2[S]$$

The plot of  $1/k_{\text{obs}}$  versus  $[1/\text{PyN} \rightarrow \text{O}]$  should give a straight line (analogous to the Lineweaver – Burk plot for an enzyme) with  $1/k_2$  as the intercept and  $K_M / k_2$  as the slope. The x – axis intercept equals  $1/K_M$ . From the double reciprocal plot of  $1/k_{\text{obs}}$  versus  $[1/\text{PyN} \rightarrow \text{O}]$  [Fig.(IV- 44 b)],  $k_2$  and  $K_M$  were calculated as  $10.0 \times 10^{-3} \text{ s}^{-1}$  and  $5.1 \times 10^{-4} \text{ mol}^{-1}$  respectively at 310.5 K [Table (IV-16)]. The value of  $k_2$  is comparable in

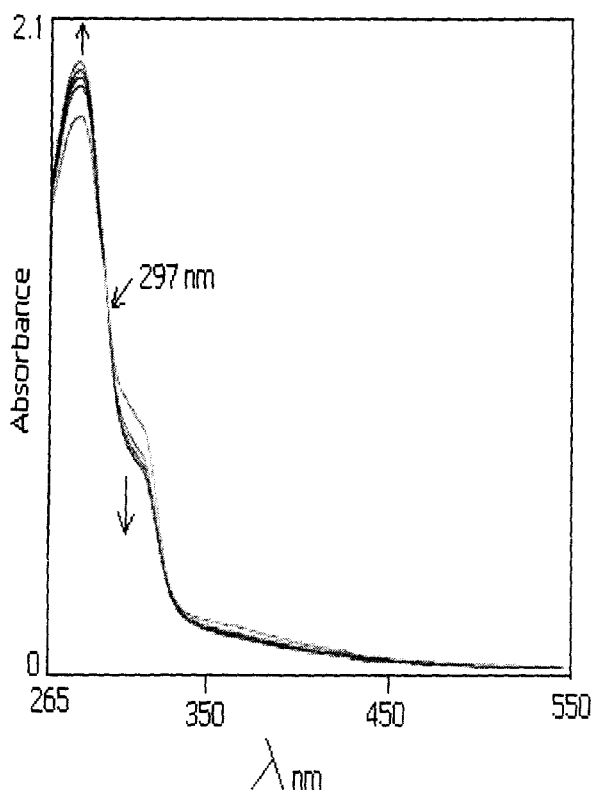


**Fig.(IV-45):** UV – VIS absorption spectral changes recorded every 5 min interval during the reaction of complex (5) [ $3.0 \times 10^{-4}$ (M)] with PyN→O [ $2.9 \times 10^{-4}$ (M)] in DMF at 301 K.

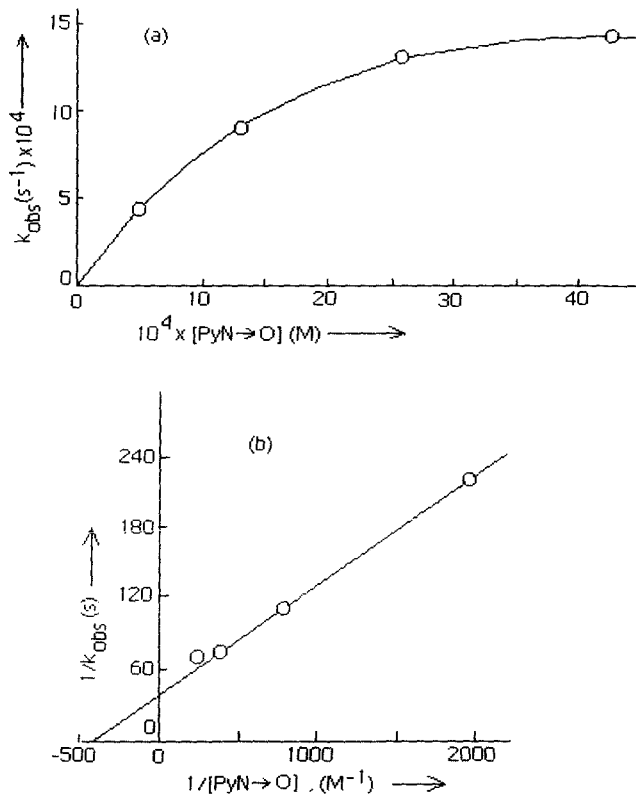


**Fig.(IV-46):**(a) Dependence of rate of reaction of (5) [ $4.17 \times 10^{-5}$  (M)] with PyN→O in DMF at 301K; (b) the corresponding double reciprocal plot.

magnitude to those of metal-mediated oxygen atom transfer reaction observed by different authors using suitable substrates<sup>7, 8, 17, 159</sup>. Figures (IV-46) and (IV-48) represent the substrate saturation kinetics and the corresponding double reciprocal plots for complexes (5) and (6) respectively ; the relevant data are grouped together in Table (IV-16).

The reaction stoichiometry was established by estimating the amount of pyridine released through reaction (328 K, 50h, dinitrogen atmosphere, darkness) of a known weight of complex (4) with 10 equivalents of PyN→O ; in DMF solution ; the

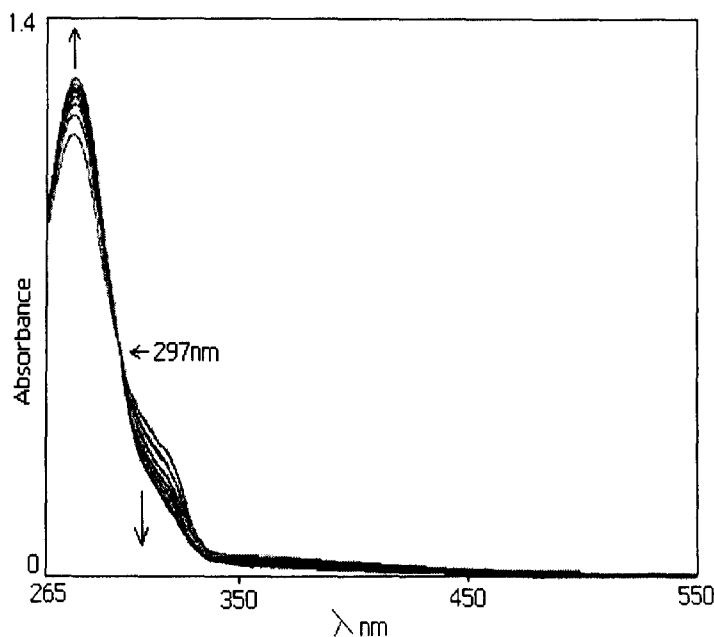
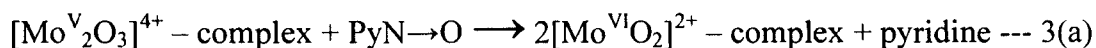
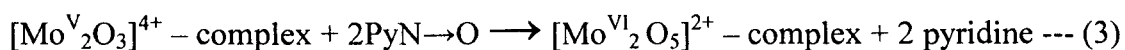


**Fig.(IV-47):** UV-VIS absorption spectral change recorded every 5 min interval (6) [ $2.34 \times 10^{-4}$  (M)] with PyN $\rightarrow$ O [ $3.01 \times 10^{-4}$ (M)] in DMF at 301K.

released pyridine was estimated gravimetrically as the known compound  $[\text{Zn}(\text{C}_5\text{H}_5\text{N})_2(\text{SCN})_2]$  from the petroleum ether extract of the reaction medium <sup>25, 34(a)</sup>. Nearly two moles of pyridine were recovered per mole of compound (4) used as per equation (3) [with equations 3(a) and 3(b) showing the intermediate steps].



**The overall reaction :**



The final di- $\mu$ -oxo binuclear Mo (VI) complex was isolated, characterized by physicochemical methods and was found to have the molecular formula  $[(\text{Mo}^{\text{VI}}_2\text{O}_5)(\text{O}^{\text{V}}\text{-L-His})(\text{bipy})] \cdot \text{DMF}$  thereby supporting Scheme (IV-18) and equation (3). Reaction stoichiometry [as per equation (3)] was established for complexes (5) and (6) ; in each case approximately 2 moles of pyridine were recovered per mole of the carticular complex used. A perusal of the kinetic and activation parameters [Table (IV-16)] reveals several interesting features. Although the steric energy values ( $44.7 - 48.3 \text{ kcal mol}^{-1}$ ,

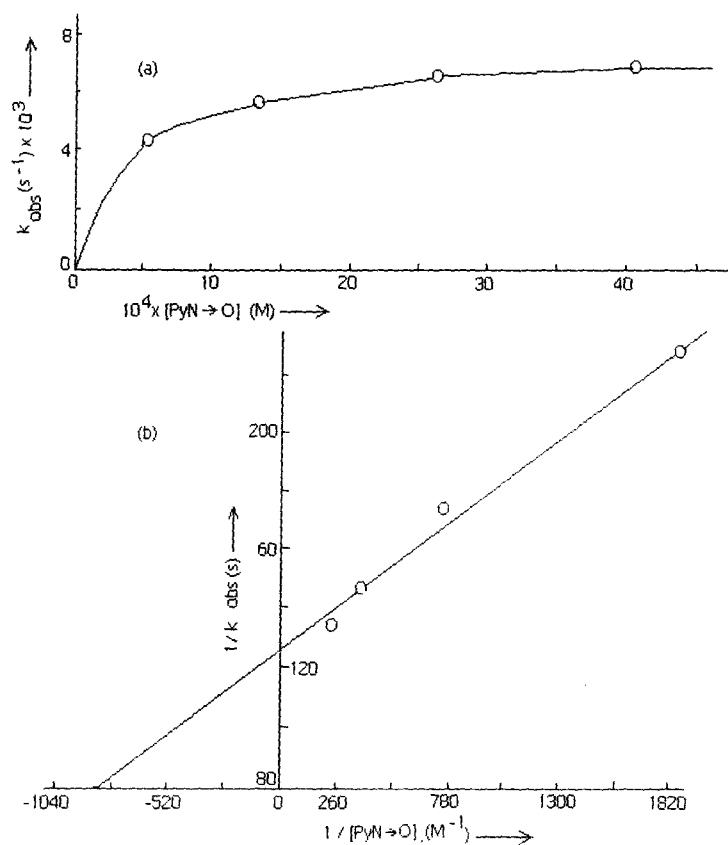


**Fig.(IV-48):**(a)Dependence of rate of reaction of complex (6) [ $4.2 \times 10^{-5}$  (M)] in DMF at 301K; (b) the corresponding double reciprocal plot.

CHEM3D models, MM2 method) and entropies of activation ( $\Delta S^\ddagger$ ,  $-199.4$  to  $-213.0$   $\text{J mol}^{-1} \text{ deg}^{-1}$ ) very over a short range, magnitudes of all other parameters are different from the three  $(\text{Mo}^{\text{V}}\text{O}_3)^{4+}$ -type complexes under consideration here. Comparison of data at a particular temperature (e.g., 310.5 K) shows considerable spread of

**Table (IV - 16)**

Compound No.	T (K)	$k_{\text{obs}} \times 10^3$ ( $\text{s}^{-1}$ )	$\Delta H^\ddagger$ <sup>a</sup> (KJ mol <sup>-1</sup> )	$\Delta S^\ddagger$ <sup>a</sup> (J mol <sup>-1</sup> deg <sup>-1</sup> )	$\Delta G^\ddagger$ <sup>b</sup> (KJ mol <sup>-1</sup> )	$E_a$ <sup>c</sup> (KJ mol <sup>-1</sup> )	$k_2^d \times 10^3$ ( $\text{s}^{-1}$ )	$K_M^d \times 10^4$ ( $\text{s}^{-1}$ )
(4)	306.5	9.2	64.3	-208.6	128.9	52.7	10.0	5.1
	310.5	12.8						
	315	18.2						
	317	22.3						
(5)	306.5	14.4	3.7	-199.4	65.6	6.2	24.7	23.0
	310.5	14.9						
	315	15.4						
	317	15.6						
(6)	306.5	7.4	103.7	-213.0	169.4	103.4	7.9	4.2
	310.5	13.2						
	315	23.0						
	317	28.1						

<sup>a</sup> values obtained from the Eyring plots; <sup>b</sup> values obtained from:  $\Delta G^\ddagger = \Delta H^\ddagger - T\Delta S^\ddagger$ , at 310.5 K; <sup>c</sup> values obtained from the Arrhenius plots; <sup>d</sup> values obtained from the plots of  $1/k_{\text{obs}}$  vs.  $1/[PyN \rightarrow O]$  at 306.5 K. <sup>a, b & c</sup> values were taken at [sample] =  $0.042 \text{ mmol dm}^{-3}$  and  $[PyN \rightarrow O] = 4.2 \text{ mmol dm}^{-3}$ .

$\Delta H^\ddagger$ ,  $\Delta G^\ddagger$  and  $E_a$  data ; moderate variation of  $k_2$  and  $K_M$  values are also observed. Lowest  $k_{obs}$  value is observed for complex (4). Variation in nature of the  $(Mo^V_2O_3)^{4+}$  core as discussed in terms of CHEM3D models, is the most probable factor responsible for the above observations. The above inferences regarding oxygen atom transfer reactivity is further supported by electron transfer behaviour of these complexes in terms of a temporal method like cyclic voltammetry [Fig.(IV-49)]<sup>146</sup>. Better understanding of the CV data is achieved in this study in terms of the CHEM3D models, supported by the MO pictures [Scheme (IV-16) and (IV-17)]. The two Mo(V) centres of complex (4) undergo

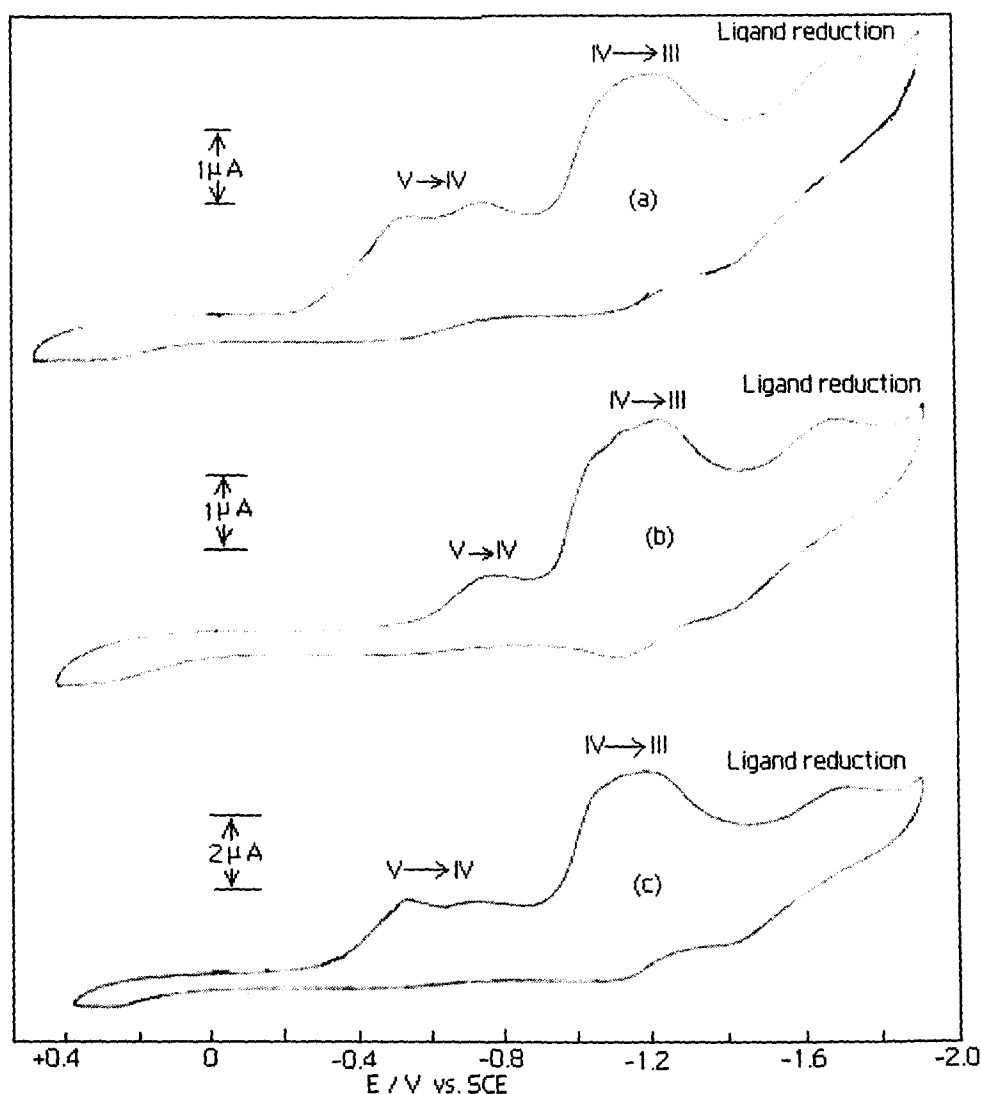


**Fig.(IV-49):** Cyclic Voltammograms in DMSO, 0.1M  $N[Bu_4]ClO_4$ , platinum electrode, scan rate =  $0.05 \text{ Vs}^{-1}$ . (a) complex (4) ( $1.00 \times 10^{-3} \text{ M}$ ); (b) complex (5) ( $1.03 \times 10^{-3} \text{ M}$ ) and (c) complex (6) ( $1.76 \times 10^{-3} \text{ M}$ ).<sup>146</sup>

reduction [Mo(V) → Mo(IV)] at – 0.50 V and – 0.71 V respectively, reflecting electron filling in the two separate antibonding MO levels [Scheme (IV-17)] originating from the skew nature of the (Mo<sup>V</sup><sub>2</sub>O<sub>3</sub>)<sup>4+</sup> core ; further reduction [Mo(IV) → Mo(III)] of the two metal centres occur at – 1.09 V and – 1.19 V respectively, followed by a chemical change through solvation. A ligand reduction peak appears at – 1.72 V ; for complexes (5) and (6), this particular reduction occurs at – 1.68 V and – 1.71 V respectively. For complex (5) the two Mo(V) centres undergo reduction [Mo(V) → Mo(IV)] at the same potential ( – 0.74 V ) as the two metal centres of the trans – (Mo<sup>V</sup><sub>2</sub>O<sub>3</sub>)<sup>4+</sup> core are covered by a three – centre MO, with the electrons entering into the same antibonding MO level [Scheme (IV-16)]. However, in the next stage of reduction [i.e., Mo(IV) → Mo(III)], the two metal centres became nonequivalent on the CV time scale, undergoing reductions at – 1.095 V and – 1.21 V respectively. Complex (6) with a slightly distorted (from a cis – arrangement) (Mo<sup>V</sup><sub>2</sub>O<sub>3</sub>)<sup>4+</sup> core, shows an intermediate CV behaviour for the reduction of its two Mo(V) centres at – 0.53 V and – 0.72 V respectively ; the former reduction is characterized by a well – defined CV peak, whereas only a broad – band corresponds to the latter one. Just like the two above cases, for the next stage of reduction [Mo(IV) → Mo(III)] two reduction peaks are observed at – 1.10 V and – 1.19 V respectively. In terms of HOMO – LUMO approach of explaining reactivity, the nature of the (Mo<sup>V</sup><sub>2</sub>O<sub>3</sub>)<sup>4+</sup> core of these complexes can be correlated with the number and nature of CV peaks [Fig.(IV-49)] in the region – 0.50 V to – 0.74V.

For confirming the proposed electron transfer stoichiometry in the above experiments, controlled – potential coulometric reduction were carried out on complex (5) at – 0.85 V and – 1.35 V respectively ; they correspond to the transfer (‘n’ value) of 2.14e<sup>–</sup> / molecule and 4.06e<sup>–</sup> / molecule respectively. These data verify the two stage reductions [Mo(V) → Mo(IV) and Mo(IV) → Mo(III)] of the two molybdenum (V) centres of these complexes [Fig.(IV-49)].

Thus both the oxygen atom transfer and the electron transfer reactivity aspects of these complexes are controlled by the nature of their (Mo<sup>V</sup><sub>2</sub>O<sub>3</sub>)<sup>4+</sup> cores, i.e., the conformations of the two Mo=O<sub>t</sub> bonds about the Mo – O<sub>b</sub> – Mo axis.

## Conclusion

In accordance with the aims and objectives of the work of this section, three  $(\text{Mo}^{\text{V}}_2\text{O}_3)^{4+}$  type complexes with chiral aldimine ligands have been synthesized, freshly characterized by ESIMS data and their physicochemical properties interpreted to a reasonable extent in the light of their CHEM3D models (MM2 method). The different arrangements of the two  $\text{Mo}=\text{O}_t$  bonds about the  $\text{Mo} - \text{O}_b - \text{Mo}$  axis of the  $(\text{Mo}^{\text{V}}_2\text{O}_3)^{4+}$  core have two implications : (i) presence or absence of a centre of inversion about the bridging oxygen atom ( $\text{O}_b$ ) ; (ii) cis - / trans - arrangement of the two  $\text{Mo}=\text{O}_t$  bonds giving rise to a three - centre MO with a diamagnetic ( $S = 0$ )  $(\text{Mo}^{\text{V}}_2\text{O}_3)^{4+}$  core ; the skew disposition of the two  $\text{Mo}=\text{O}_t$  bonds will lead to two sets of MO levels with a paramagnetic ground state ( $S = 1$ ). Presence of the chiral ligand backbone coupled with the above factors, adds a new dimension to this study as evident from the close similarity of the EPR and CD spectra of complex (4) with those of a typical oxomolybdoenzyme like xanthine oxidase, possessing two mononuclear molybdenum centres per protein unit<sup>161, 162</sup>. These chiroptical data will be of value in understanding the CD properties of oxomolybdoenzymes, containing two molybdenum atoms per protein molecule. The chiral ligand backbone as well as the symmetry of the  $(\text{Mo}^{\text{V}}_2\text{O}_3)^{4+}$  core cast their influence on the relevant EPR and CD spectra, associated with electronic transitions of the oxometal entity and the ligand - to - metal charge transfers. Of the three present complexes, complex (4) and (5) have identical chemical composition and their only difference lies in the absolute configuration of the chiral centre of the amino acid residue (histidine). Complex (6) has identical donor atoms for the  $(\text{Mo}^{\text{V}}_2\text{O}_3)^{4+}$  core as for complexes (4) and (5), the only difference being the replacement of the L-histidine residue by a L-arginine residue and the methoxy group ( $-\text{CH}_3$ ) of the aldehyde part by a hydrogen atom respectively. In spite of the above similarities and apparently small differences, these complexes possess different physicochemical and spectroscopic properties (e.g.,  $\mu_{\text{eff}}$  values, IR, EPR and CD spectral responses) ; they also differ with respect to their oxygen atom transfer and electron transfer reactivities as well. Much of these differences can be traced to their differences of the  $(\text{Mo}^{\text{V}}_2\text{O}_3)^{4+}$  core, viewed in the

light of their CHEM3D models (MM2 method). The specific steric demands of the aldimine ligands can lead to different types of  $\mu$  – oxo binuclear Mo(V) complexes, which in turn suggest intriguing chemical and structural transformations. Different factors have been enlisted for explaining the substrate selection aspects and reactivity of oxomolybdoenzymes possessing the pterin unit (i.e., molybdopterin) <sup>1, 2</sup>. The conformational control of reactivity as investigated here (supported by EPR and CD data) may prove vital in this respect, not withstanding the modeling / explaining their physicochemical and spectral behaviour.

---

## CHAPTER V

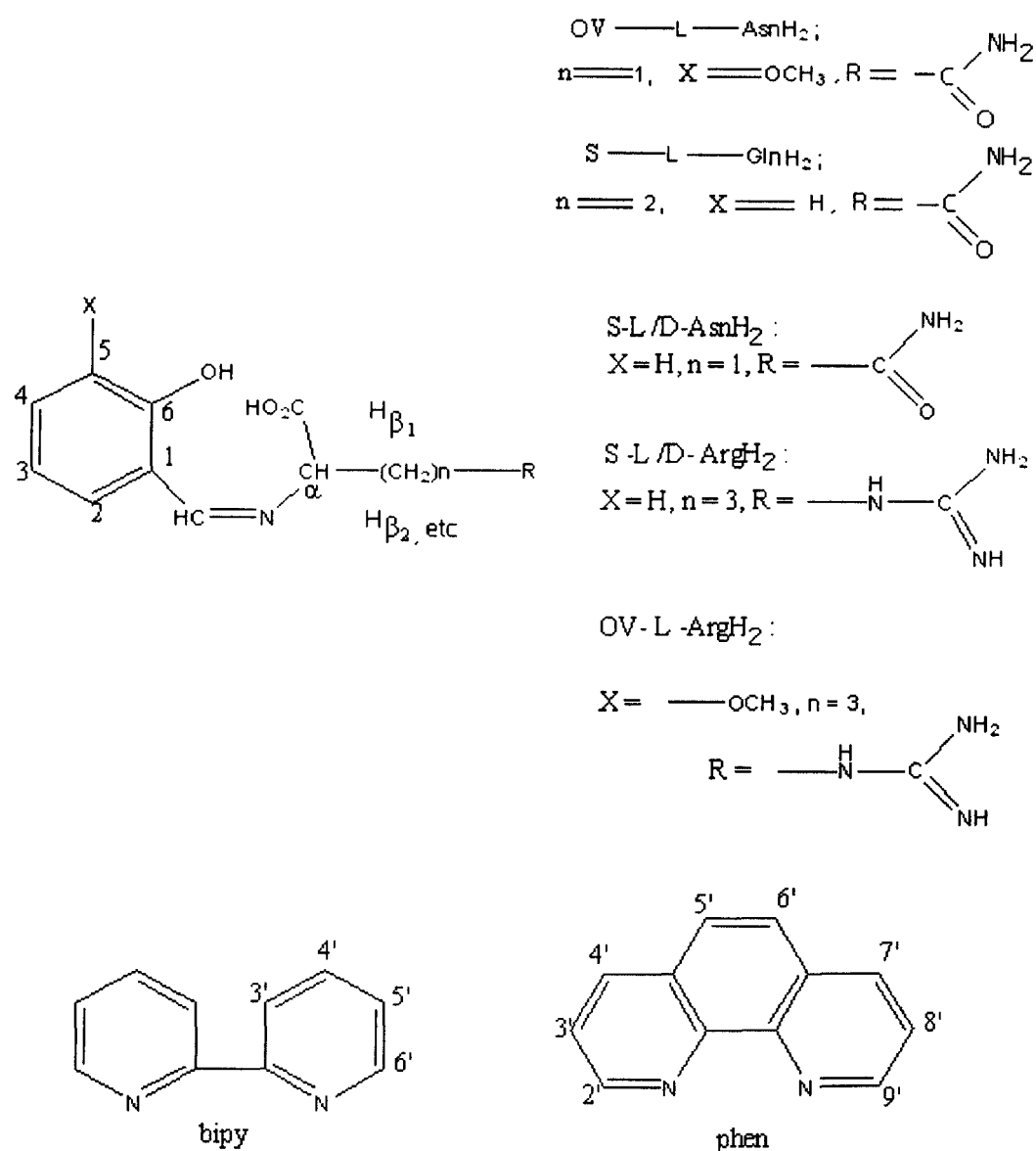
Kinetic studies on redox reactions between  $\text{Na}_2\text{SO}_3$  and dioxouranium (VI) complexes with chiral aldimine ligands derived from L-/ D - asparagine, arginine and glutamine; crystal structure of (2,2' - bipyridyl) dioxo (N - salicylidene - L - asparaginato) uranium (VI) - methanol (1/1).

## Abstract

Kinetic data of redox reactions between  $\text{Na}_2\text{SO}_3$  and several well-characterized dioxouranium (VI) / uranyl complexes with chiral aldimine ligands, possessing L – and D – asparagine, arginine and glutamine, have been recorded spectrophotometrically.  $[\text{UO}_2(\text{S-L-Asn})(\text{bipy})]$ .  $\text{CH}_3\text{OH}$  [compound (2)] crystallizes in the orthorhombic space group  $P 2_1 2_1 2_1$  with  $a = 7.179(3) \text{ \AA}$ ,  $b = 13.437(5) \text{ \AA}$ ,  $c = 23.812(8) \text{ \AA}$  and  $z = 4$ . The essentially linear  $\text{UO}_2^{2+}$  entity [ $\text{O}(1) - \text{U}(1) - \text{O}(2) = 176.0(3)^\circ$ ] achieves an equatorial coordination number of five involving the tridentate aldimine ligand anion ( $\text{S-L-Asn}^{2-}$ ) and the neutral bidentate donor (bipy). Chemical compositions of other complexes have been verified through simulation of mass spectral data. The above reactions follow second – order rate law in  $\text{DMSO} - \text{H}_2\text{O}$  (3 : 2 v/v) at 290 K. For complex (3) at 288 K the one – electron reduction product, that is, the  $\text{UO}_2^+$  entity could be identified in the available time – scale and this view is supported by electrochemical data (e.g., cyclic voltammetry and controlled – potential coulometry). A comparative study of the kinetic data reveals the dependence of  $k_{\text{obs}}$  ( $\text{s}^{-1}$ ) values on the chemical composition of the complexes, especially the nature of R group of amino acid residue and the associated stereochemistry around the  $\text{C}_\alpha$  atom (that is, relative positions of the  $\text{H}_\alpha$  atom and the R group as evident from chiroptical studies).

## Introduction

In this Chapter, the attention is focussed on the reactivity of chiral coordination compounds of  $UO_2^{2+}$  entity with aldimine ligands [Scheme (V-1)], towards a suitable reducing agent like  $Na_2SO_3$  and analyzing the kinetic data on the basis of different characteristic aspects of the chiral aldimine ligands and the  $M \rightarrow L \pi$  - bonding ability of the secondary ligands (2,2' - bipyridyl / 1,10 - phenanthroline).



**Scheme (V – 1):** Schematic formulae of aldimine ligands.

In the earlier Chapters coordination Chemistry of molybdenum in the oxidation states VI, V and IV has been discussed ; some of them contain the characteristic attribute of an oxometal entity, that is, the multiply bonded oxygen atom stabilizing the high charge on the metal atom. As pointed out in Chapter I, molybdenum in its higher oxidation states (VI, V, IV) can form a wide variety of oxometal entities, many of which have been characterized structurally<sup>55</sup>. This ability can be correlated with the fact that molybdenum is not as “oxophilic” as the early transition metals of groups IV and V. Its strong tendency to bind an oxo group ( = O) is balanced by a capacity to lose a single oxygen atom easily ; this is accompanied by changes in oxidation states (VI, V, IV) of the molybdenum atom<sup>41</sup>.

However, for the dioxouranium (VI) / uranyl ( $\text{UO}_2^{2+}$ ) ion, the situation is quite different. The linear  $\text{UO}_2^{2+}$  ion is remarkably stable with respect to the strength of the U – O bond and it can persist through a variety of chemical changes and behaves like a cation with properties intermediate between those of  $\text{M}^+$  and  $\text{M}^{2+}$  ions of similar size but greater charge<sup>141, 165</sup>. The  $\text{UO}_2^{2+}$  ion readily adds 4 – 6 donor atoms in its equatorial plane to give structures which range from octahedral to hexagonal bipyramidal, through pentagonal bipyramidal with overall coordination number of 6 – 8 for the central U(VI) atom ; the number of known complexes is vast involving oxygen, nitrogen and even sulphur donor ligands<sup>141</sup>. In spite of all these developments, specific areas of Chemistry of the  $\text{UO}_2^{2+}$  ion still continues to arouse avid interest as stated below. Both experimental and theoretical methods have been used to study  $\text{UO}_2^{2+}$  compounds in terms of their structural, electronic, spectroscopic and thermochemical properties<sup>166 – 169</sup>.

The rich coordination Chemistry of the  $\text{UO}_2^{2+}$  ion shows continued growth in specific directions<sup>105, 170 – 173</sup>.

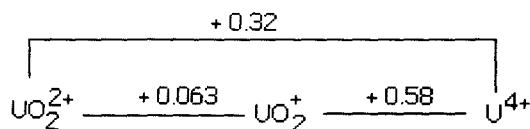
Here several coordination compounds of the  $\text{UO}_2^{2+}$  entity with aldimine ligands, possessing L – and D – arginine / asparagine / glutamine residues [Scheme (V-1)] have been found to be excellent candidates for kinetic studies with a suitable reducing agent, e.g.,  $\text{Na}_2\text{SO}_3$  in DMSO –  $\text{H}_2\text{O}$  (3 : 2 v/v) medium. Although they have been available from a previous synthesis<sup>146</sup>, one of them have been further characterized

structurally through X – ray crystallographically in this work ; in other cases, the assignments of chemical compositions have been verified through mass spectrometry. Importance of the aldimine ligands containing amino acid residues is well – known <sup>74, 93</sup>. The objectives of this study involving the  $\text{UO}_2^{2+}$  ion is outlined below.

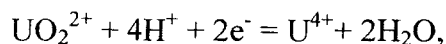
The U – O bonding (of  $\text{UO}_2^{2+}$  ion) can be formulated with a scheme in which appropriate d and f orbitals can be combined into MOs to give one  $\sigma$  plus two  $\pi$  bonds <sup>103, 168</sup>. The MOs are filled at  $\text{UO}_2^{2+}$  and succeeding electrons are fed into non – bonding orbitals ; the MO scheme is helpful for interpretation of spectroscopic and other data. For example, the reduction  $\text{UO}_2^{2+} \rightarrow \text{UO}_2^+$  involves feeding one electron into either of the uranium – centred nonbonding  $1 \delta_u$  or  $1 \emptyset_u$  orbitals which have pure atomic 5f character <sup>103, 168</sup> ; this process involves elongation of the U – O bond and it destabilizes the  $\text{UO}_2^+$  ion considerably <sup>168</sup>. As a result, aqueous Chemistry of the  $\text{UO}_2^+$  ion could be studied only by special techniques ( e. g., stopped – flow method) ; in DMSO it is more stable, both thermodynamically and kinetically <sup>141, 165</sup>. Besides this, involvement of the  $\text{UO}_2^+$  intermediate has been indicated in  $\text{UO}_2^{2+}$  catalysed photooxidation of either hydrocarbons with molecular oxygen or aromatic hydrocarbons by  $\text{H}_2\text{O}_2$  <sup>176, 177</sup>. The decay of the excited uranyl ion in water in presence of halide ions has been studied by laser flash kinetic spectrophotometry<sup>178</sup>; the proposed mechanism for effective quenching of the green luminescence of uranyl ion by halides involves the intermediate formation of the short – lived  $\text{UO}_2^+$  ion.

On the other hand, U(IV) ion has greater stability and it can be obtained by the reduction of the  $\text{UO}_2^{2+}$  ion with a strong reducing agent like a silver reductor or by  $\text{Cr}^{2+}$  <sup>25</sup>.

It will be interesting to follow the redox Chemistry of the present uranyl complexes with aldimine ligands, involving stepwise conversion of the  $\text{UO}_2^{2+}$  species to  $\text{UO}_2^+$  and finally to U(IV) state, which are related by the following redox couples (formal reduction potential in volts are shown) <sup>165</sup> :

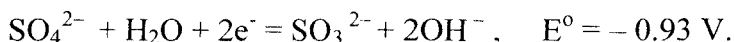


Here,  $\text{UO}_2^{2+}$  ion is the most stable species, whereas  $\text{UO}_2^+$  ion is the least stable one. The redox couple involving oxygen atom transfer, e.g.,

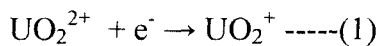


is irreversible, whereas a couple like  $\text{UO}_2^{2+} + \text{e}^- = \text{UO}_2^+$  should be reversible, at least for a brief time scale, as permitted by the life – time of the  $\text{UO}_2^+$  ion. The aim of this study is to utilize a milder reducing agent (than silver reductor or  $\text{Cr}^{2+}$ ) like  $\text{Na}_2\text{SO}_3$  in  $\text{DMSO} - \text{H}_2\text{O}$  medium towards the present uranyl – aldimine complexes, to explore whether the short – lived  $\text{UO}_2^+$  intermediate could be formed at least for a time duration for recording the kinetic data in the time - scale of a conventional recording UV – VIS spectrophotometer.

The reducing character of  $\text{SO}_3^{2-}$  ion is expressed quantitatively as follows <sup>165</sup> :



In aqueous medium the oxidation of  $\text{SO}_3^{2-}$  to  $\text{SO}_4^{2-}$  can be carried out by both one – electron and two – electron oxidants like  $\text{Fe}^{3+}$  ion and  $\text{Cl}_2$  respectively <sup>165</sup>. In view of the above, both the  $\text{UO}_2^+$  and  $\text{U(IV)}$  states should be attainable through stepwise reduction of  $\text{UO}_2^{2+}$  ion by  $\text{SO}_3^{2-}$ . The final requirement is the presence of a compact ligand donor set on the equatorial plane of the linear  $\text{UO}_2^{2+}$  entity with  $\text{M} \rightarrow \text{L} \pi$  bonding ability <sup>155</sup>, so that increased size of the  $\text{UO}_2^+$  entity accompanying the electron transfer step :



could be partly counter balanced, for a time duration needed for the pertinent measurements. The kinetic data recorded here throw light on the interesting aspects of this study. Reaction stoichiometry measurement (as stated here) indicated the following overall reaction :



## Experimental

**Materials and Methods :** Ortho –Vanilline (Fluka), salicylaldehyde (Kemphasol), L – asparagine monohydrate (BDH, England), L – glutamine (BDH, England), L – and D – arginine monohydrochloride (Fluka), 2,2' – bipyridyl (BDH), 1,10 – phenanthroline monohydrochloride (BDH) and uranyl nitrate hexahydrate GR (Loba, Bombay) were used as such.  $\text{Bu}_4\text{NClO}_4$  was prepared from  $\text{Bu}_4\text{NOH}$  (SRL, Mumbai) following published method <sup>11</sup>. The solvents were purified by literature procedures <sup>9</sup>.

Elemental analysis (C, H, N data), FAB mass spectra, ESIMS data, IR, UV – VIS, <sup>1</sup>H NMR, CD spectra and cyclic voltammetry data were recorded as described in earlier chapters. Uranium was estimated titrimetrically <sup>175</sup>. Kinetic measurement in DMSO – H<sub>2</sub>O (3 : 2 v/v) were carried out on a Shimadzu 160A UV – VIS spectrophotometer.

### X – ray data collection and reduction :

A brick-red coloured orthorhombic crystal of  $[\text{UO}_2(\text{S} - \text{L} - \text{Asn})(\text{bipy})].\text{CH}_3\text{OH}$  [compound (2)] was used for single crystal X – ray diffraction study at the Department of Chemistry, University of Helsinki, Finland, in collaboration with Prof. R. Hämäläinen. SHELXTL PC programs were used for this purpose. Structural refinement was done by using SHELXL – 93 programs. The basic conditions are stated in Table (V–1). The ORTEP diagram of the molecule is shown in Fig.(V–1) and the unit cell structure is shown in Fig.(V – 2). Bond lengths (Å) and bond angles (deg) data for compound (2) along with other X – ray crystallographic information are presented in Tables (V – 2) to (V – 5).

**Table (V – 1):** Crystal data and structure refinement for **(2)** :

---

Empirical formula	C <sub>22</sub> H <sub>22</sub> N <sub>4</sub> O <sub>7</sub> U
Formula weight (M)	692.47
Crystal system	Orthorhombic
Space group	P2 <sub>1</sub> 2 <sub>1</sub> 2 <sub>1</sub>
Unit cell dimensions	a = 7.179(3) Å. b = 13.437(5) Å. c = 23.812(8) Å.
Volume	2297.0(15) Å <sup>3</sup>
z	4
D <sub>m</sub> , D <sub>c</sub> / Mg m <sup>-3</sup>	2.03, 2.00
F(000)	1320
Diffractometer	Rigaku AFC – 7S
Monochromator	Graphite
Crystal size (mm)	0.25 x 0.15 x 0.05
Radiation	Mo/ Kα (λ 0.71069 Å)
μ (Mo / Kα) mm <sup>-1</sup>	7.12
Orientation reflections	25
T / °C	– 80
Scan method, speed / ° min <sup>-1</sup>	ω , 5
h,k,l ranges	0 > h > - 9, 0 > k > -16, 0 > l > -29
Measured 2θ range / °	3.0 --53.0
Check reflections, variation (%)	3,3
No. measured reflections	2622
R (for 2619 data)	0.035
wR [w = 1/ σ <sup>2</sup> (F) + 0.0024(F <sup>2</sup> )]	0.046
Maximum Δ/σ	0.007
Maximum, minimum ρ in ΔF map/e Å <sup>-3</sup>	1.12 – 1.43.

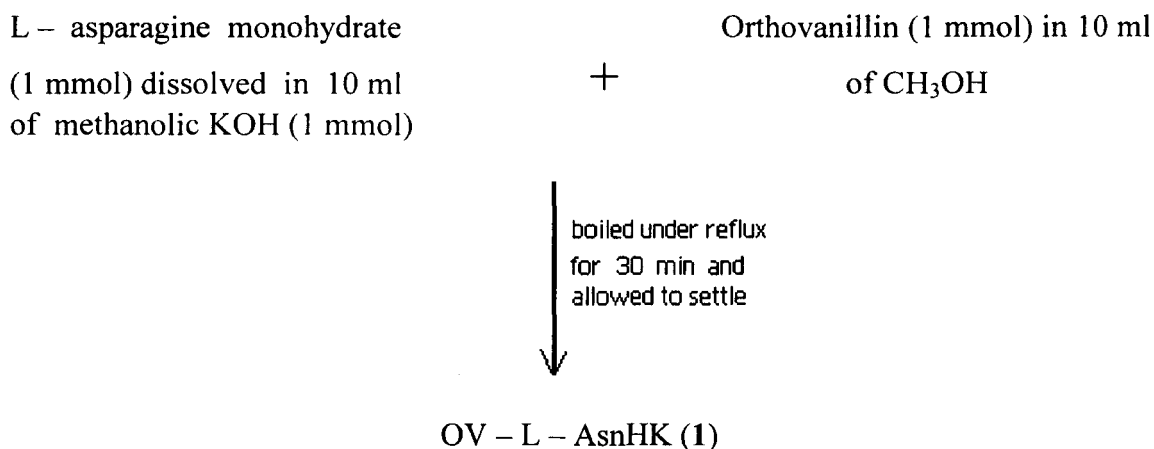
---

## Synthesis

The uranyl complexes of aldimine ligands [(2) – (6)] involved in the present study were synthesized by standard procedures <sup>146</sup>. In most cases the aldimine ligands were obtained in – situ during the complex formation process ; however, in one case, e.g., complex (6), the monopotassium salt of N – (orthovanillidene) – L – asparagine (OV – L – AsnHK) (1) was isolated in the solid state and used for the synthesis giving better results.

Purity of the freshly synthesized ligand (1) and the complexes (2 – 6) was checked through TLC, elemental analysis, FABMS / ESIMS data and matching of the UV – VIS as well as IR spectral data with the original ones. For TLC purposes, the compounds were dissolved in CH<sub>3</sub>OH for spotting the plates ( silica gel G with iodine chamber for detection) and absolute ethanol was used as the eluant. Outlines of the synthetic procedures are stated below <sup>146</sup>.

### Monopotassium salt of N – (orthovanillidene)– L – asparagine (OV–L–AsnHK) (1)



Orange – yellow crystals were washed thoroughly with CH<sub>3</sub>OH, diethyl ether and dried in vacuo over anhy. CaCl<sub>2</sub> ; yield : 50 %.

The other free ligands like S – L – AsnHK. H<sub>2</sub>O, S – L – ArgH<sub>2</sub> and OV – L – ArgHK could be synthesized by similar methods ; the purified products have been utilized for recording their <sup>1</sup>H NMR spectral data [Table (V – 6)].

**[UO<sub>2</sub>(S – L – Asn)(bipy)].CH<sub>3</sub>OH (2)**

A solution of L – asparagine monohydrate (1 mmol) and KOH (1.5 ml) in 15 ml of CH<sub>3</sub>OH – H<sub>2</sub>O (2 : 1 v/v)

+

A solution of salicylaldehyde (1 mmol) in CH<sub>3</sub>OH (10 ml)



To this in-situ ligand solution, the following reagents were added consecutively under stirring at 333 K.

UO<sub>2</sub>(NO<sub>3</sub>)<sub>2</sub>.6H<sub>2</sub>O (1 mmol) in 10 ml of CH<sub>3</sub>OH – H<sub>2</sub>O (1 : 1 v/v), followed by 2,2' – bipyridyl (1 mmol) in 10 ml of CH<sub>3</sub>OH. Final pH was 4.0. The brick – red compound was washed with CH<sub>3</sub>OH – H<sub>2</sub>O (1 : 1 v/v), CH<sub>3</sub>OH, diethyl ether and dried in vacuo over anhy. CaCl<sub>2</sub>. Yield : 30 % (after recrystallization from CH<sub>3</sub>OH).

X – ray quality crystals were obtained by recrystallizing the compound twice from CH<sub>3</sub>OH water (4 : 1 v/v).

The following compounds could be synthesized by a similar procedure as above, using the appropriate amino acid and 1,10 – phenanthroline instead of 2,2' – bipyridyl.

**[UO<sub>2</sub>(S – L – Arg)(phen)].2H<sub>2</sub>O (3)**

(light rose – red coloured compound)

**[UO<sub>2</sub>(S – D – Arg)(phen)].H<sub>2</sub>O (3')**

(rose – red coloured compound)

**[UO<sub>2</sub>(S – L – Gln)(phen)].H<sub>2</sub>O (5)**

(rosy – red coloured compound)

Schematic outlines of synthesis of complexes (4) and (6) are shown below <sup>146</sup>.

**K [UO<sub>2</sub>(OV – L – Arg) (OV – L – ArgH)]. 4H<sub>2</sub>O (4)**

L – arginine monohydrochloride (2 mmol)                      Orthovanilline (2 mmol) in 10 ml  
dissolved in KOH (2 mmol) in 20 ml                      +                      CH<sub>3</sub>OH  
CH<sub>3</sub>OH – H<sub>2</sub>O (1 : 1 v/v)

↓ addition of a solution of UO<sub>2</sub>(NO<sub>3</sub>)<sub>2</sub>·6H<sub>2</sub>O  
(1 mmol) in 5 ml H<sub>2</sub>O under stirring at  
343 K, final pH 4.3.

The dark – red compound separated on standing for 3h ; it was washed with CH<sub>3</sub>OH – H<sub>2</sub>O (1 : 1 v/v), CH<sub>3</sub>OH, diethyl ether and dried in vacuo over anhy. CaCl<sub>2</sub>. Yield : 45 %.

**[(UO<sub>2</sub>)<sub>2</sub>(OV – L – Asn)<sub>2</sub>(bipy)(H<sub>2</sub>O)<sub>2</sub> (6)**

To a solution of OV – L – AsnHK (1 mmol) in 15 ml CH<sub>3</sub>OH, the following solutions were added consecutively under stirring at 333 K

↓  
a solution of UO<sub>2</sub>(NO<sub>3</sub>)<sub>2</sub>·6H<sub>2</sub>O (1 mmol) in 5 ml H<sub>2</sub>O, followed by a solution of 2,2' – bipyridyl (1 mmol) in 5 ml CH<sub>3</sub>OH. The final pH was 4.5.

↓  
The brown compound was obtained on allowing the reaction mixture to settle and it was worked up through the aforesaid sequence of manipulations. Yield : 55 %.

## Results and Discussion

The molecular structure of (2) as shown in Figure (V – 1), is based on a mononuclear seven – coordinate uranium atom in pentagonal bipyramidal geometry. The tridentate coordination of the aldimine ligand is achieved by the phenoxide oxygen, imine nitrogen and one of the carbonyl oxygen atom ; the two nitrogen atoms of 2,2' – bipyridyl occupy the remaining two corners of the equatorial coordination pentagon. The two apical oxygen atoms of the  $\text{UO}_2^{2+}$  entity complete the pentagonal bipyramid. The O – U – O axis shows a  $4^\circ$  deviation from linearity ; the two nitrogen atoms of

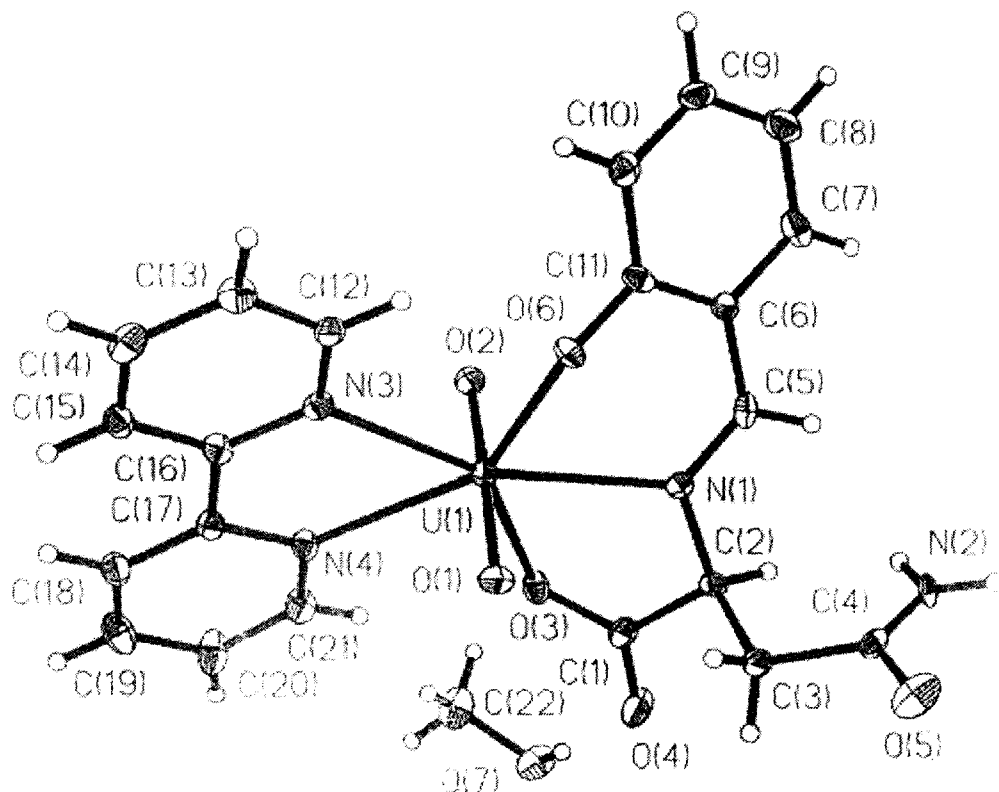


**Fig.(V – 1):** An ORTEP diagram of  $[\text{UO}_2(\text{S-L-Asn})(\text{bipy})] \cdot \text{CH}_3\text{OH}$  (2) showing the atom – numbering scheme. Thermal ellipsoids represent 50 % probability.

2,2' – bipyridyl have different U – N bond lengths. The bond angles data in Table (V – 2) throw light on the puckering of the equatorial chelate rings. The  $\text{CH}_3\text{OH}$  molecule forms a hydrogen bond with the carboxylate oxygen, O (4), where the O(7) to O(4) distance is 2.713 Å. Another interesting aspect is that the amide nitrogen atom, N(2) is not involved in coordination with the metal centre.

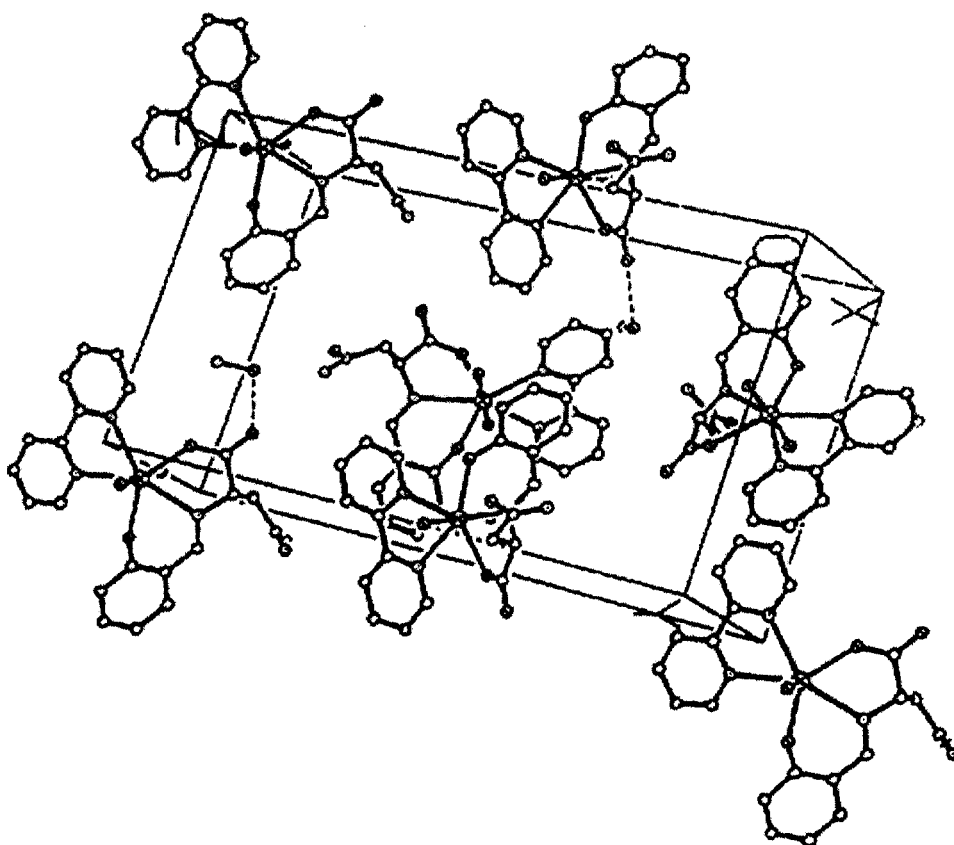


**Fig.(V – 2):** The unit cell structure of  $[\text{UO}_2(\text{S-L-Asn})(\text{bipy})] \cdot \text{CH}_3\text{OH}$  (2) crystal.

**Table (V – 2):** Bond lengths [ $\text{\AA}$ ] and bond angles [deg.] for compound (2)

U1 --- O1	1.772(7)	C10 --- C11	1.423 (14)
U1 --- O2	1.764 (7)	C12 --- C13	1.380 (15)
U1 --- O3	2.369 (7)	C13 --- C14	1.371 (15)
U1 --- O6	2.214 (6)	C14 --- C15	1.388 (15)
U1 --- N1	2.505 (7)	C15 --- C16	1.405 (14)
U1 --- N3	2.563 (8)	C16 --- C17	1.496 (13)
U1 --- N4	2.577 (8)	C17 --- C18	1.391 (13)
O3 --- C1	1.287 (12)	C18 --- C19	1.373 (15)
O4 --- C1	1.230 (13)	C19 --- C20	1.376 (17)
O5 --- C4	1.349 (12)	C20 --- C21	1.382 (16)
O6 --- C11	1.330 (11)		
O7 --- C22	1.390 (17)	O1---U1---O2	176.0 (3)
N1 --- C2	1.468 (12)	O1---U1---O3	88.9 (3)
N1 --- C5	1.300 (12)	O2---U1---O3	88.1 (3)
N2 --- C4	1.232 (12)	O1---U1---O6	94.4 (3)

N3 --- C12	1.346 (12)	O2---U1---O6	89.5 (3)
N3 --- C16	1.344 (13)	O3---U1---O6	135.0 (2)
N4 --- C17	1.344 (12)	O1---U1---N1	89.2 (3)
N4 --- C21	1.352 (13)	O2---U1---N1	92.0 (3)
C1 --- C2	1.531 (13)	O3---U1---N1	64.3 (3)
C2 --- C3	1.536 (13)	O6---U1---N1	70.8 (3)
C3 --- C4	1.508 (14)	O6---U1---N3	81.2 (3)
C5 --- C6	1.430 (13)	O1---U1---N3	87.1 (3)
C6 --- C7	1.416 (14)	O2---U1---N3	93.7 (3)
C7 --- C8	1.406 (15)	O3---U1---N3	143.8 (2)
C8 --- C9	1.371 (18)	N1---U1---N3	151.4 (2)
C9 --- C10	1.379 (15)	O1---U1---N4	88.5 (3)
C6 --- C11	1.394 (14)	O2---U1---N4	88.4 (3)
O3---U1---N4	81.2 (2)	N3---C16---C17	116.6 (8)
O6---U1---N4	143.6 (3)	N4---C17---C16	115.4 (8)
N1---U1---N4	145.5 (2)	N4---C17---C18	121.7 (8)
N3---U1---N4	62.8 (2)	N4---C21---C20	123.7 (10)
U1---O3---C1	123.9 (6)	C1---C2---C3	109.2 (7)
U1---O6---C11	128.4 (6)	C2---C3---C4	113.0 (8)
U1---N1---C2	115.3 (5)	C2---N1---C5	118.1 (8)
U1---N1---C5	126.0 (6)	C5---C6---C7	116.9 (9)
U1---N3---C12	119.4 (6)	C6---C7---C8	119.9 (10)
U1---N3---C16	122.1 (6)	C6---C11---C10	118.9 (9)
U1---N4---C17	122.4 (6)	C7---C8---C9	119.3 (11)
U1---N4---C21	120.2 (6)	C8---C9---C10	122.0 (10)
O3---C1---O4	123.8 (9)	C11---C6---C5	123.1 (8)
O3---C1---C2	116.4 (8)	C11---C6---C7	120.0 (9)
O4---C1---C2	119.8 (9)	C11---C10---C9	119.8 (10)
O5---C4---N2	122.1 (9)	C12---N3---C16	117.9 (8)
O5---C4---C3	115.9 (8)	C12---C13---14	119.1 (9)
O6---C11---C6	121.5(8)	C13---C14---C15	119.4 (10)
O6---C11---C10	119.5 (9)	C14---C15---C16	118.4 (9)
N1---C2---C1	109.2 (8)	C15---C16---C17	121.2 (9)
N1---C2---C3	111.7 (8)	C16---C17---C18	122.8 (8)
N1---C5---C6	125.1 (8)	C17---N4---C21	117.4 (8)
N2---C4---C3	122.0 (9)	C17---C18---C19	119.8 (10)
N3---C12---C13	123.1 (9)	C18---C19---C20	119.3 (11)
N3---C16---C15	122.1 (9)	C19---C20---C21	118.0 (11)

**Table (V – 3): Atomic coordinates for compound (2)**

Atom	x / a	y / b	z / c
U1	0.8547(1)	0.5636(1)	0.5556(0)
O1	0.6311(10)	0.5138(5)	0.5414(3)
O2	1.0830(10)	0.6047(5)	0.5701(3)
O3	0.8940(9)	0.4413(5)	0.6262(3)
O4	0.7688(14)	0.3569(6)	0.6970(4)
O5	0.1771(12)	0.5811(7)	0.7096(4)
O6	0.7595(9)	0.7203(4)	0.5543(3)
O7	1.0116(12)	0.2029(6)	0.7054(4)
N1	0.7446(10)	0.6115(5)	0.6517(3)
N2	0.4321(11)	0.6227(5)	0.7600(3)
N3	0.8831(11)	0.5966(6)	0.4499(3)
N4	0.9958(11)	0.4242(6)	0.4947(3)
C1	0.7897(13)	0.4341(7)	0.6700(4)
C2	0.6849(13)	0.5284(6)	0.6875(4)
C3	0.4743(13)	0.5098(7)	0.6829(5)
C4	0.3612(13)	0.5766(6)	0.7207(4)
C5	0.7579(14)	0.6993(7)	0.6743(4)
C6	0.8124(12)	0.7878(6)	0.6452(4)
C7	0.8599(16)	0.8711(7)	0.6786(5)
C8	0.9157(17)	0.9604(8)	0.6528(6)
C9	0.9183(16)	0.9663(8)	0.5954(5)
C10	0.8672(14)	0.8872(7)	0.5618(5)
C11	0.8145(12)	0.7953(7)	0.5868(4)
C12	0.8214(13)	0.6835(7)	0.4288(4)
C13	0.8114(14)	0.7026(7)	0.3719(4)
C14	0.8651(16)	0.6301(8)	0.3348(5)
C15	0.9298(15)	0.5397(8)	0.3551(4)
C16	0.9361(15)	0.5255(7)	0.4136(4)
C17	1.0037(13)	0.4298(7)	0.4384(4)
C18	1.0704(16)	0.3515(7)	0.4060(7)
C19	1.1314(19)	0.2659(8)	0.4315(5)
C20	1.1232(19)	0.2586(9)	0.4891(15)
C21	1.0612(17)	0.3402(7)	0.5190(5)
C22	1.1566(21)	0.2162(10)	0.6675(6)

**Table (V – 4):** Hydrogen Atom coordinates for compound (2). Isotropic temperature parameters (U) are fixed at 0.08 Å<sup>2</sup>.

H2	0.713	0.545	0.726
H2A	0.464	0.593	0.795
H2B	0.498	0.684	0.756
H3A	0.437	0.521	0.645
H3B	0.450	0.442	0.693
H5	0.729	0.705	0.713
H7	0.856	0.867	0.719
H7A	0.926	0.258	0.702
H8	0.951	1.017	0.675
H9	0.957	1.027	0.578
H10	0.867	0.894	0.522
H12	0.783	0.735	0.454
H13	0.767	0.766	0.359
H14	0.858	0.642	0.295
H15	0.969	0.488	0.330
H18	1.074	0.357	0.366
H19	1.179	0.212	0.410
H20	1.159	0.198	0.508
H21	1.065	0.337	0.559
H22	1.242	0.162	0.670
H23	1.220	0.277	0.676
H24	1.107	0.219	0.630

**Table (V – 5):** Anisotropic temperature factors for compound (2) (Å<sup>2</sup> x 10<sup>3</sup>).

	U11	U22	U33	U23	U13	U12
U1	19(1)	21(1)	18(1)	-2(1)	1(1)	1(1)
O1	23(3)	23(3)	37(4)	1(2)	-1(3)	-1(3)
O2	25(3)	29(3)	27(4)	-2(3)	3(3)	-5(3)
O3	32(4)	26(3)	24(3)	-1(3)	1(3)	12(3)
O4	49(5)	38(4)	46(5)	8(4)	22(4)	11(4)
O5	34(4)	63(5)	48(5)	9(4)	5(4)	-4(4)
O6	29(3)	20(3)	32(3)	-7(3)	2(3)	7(3)
O7	33(4)	45(4)	55(5)	15(4)	4(4)	4(4)
N1	17(4)	20(3)	22(4)	1(3)	-2(3)	-2(3)
N2	18(3)	25(4)	18(3)	-6(3)	-4(3)	5(3)
N3	23(4)	27(3)	19(4)	4(3)	-3(3)	-3(3)
N4	24(4)	26(4)	22(4)	-2(3)	4(3)	10(3)
C1	18(4)	31(4)	28(5)	2(4)	3(4)	1(4)
C2	23(5)	19(4)	21(4)	1(3)	-3(4)	-2(3)
C3	19(5)	26(5)	41(6)	-3(4)	10(4)	-2(4)
C4	12(3)	26(4)	28(4)	1(3)	2(4)	6(4)
C5	26(5)	35(5)	15(4)	-6(4)	-4(4)	7(4)

C6	17(5)	20(4)	30(5)	-2(3)	5(4)	2(3)
C7	19(4)	33(5)	46(6)	-17(4)	-2(5)	1(4)
C8	30(5)	32(6)	57(7)	-6(5)	2(5)	-6(4)
C9	24(5)	28(5)	47(6)	2(4)	6(5)	-6(4)
C10	20(4)	30(4)	39(6)	3(4)	8(5)	10(4)
C11	19(5)	21(4)	32(5)	-3(3)	-2(4)	1(3)
C12	21(5)	21(4)	37(5)	1(4)	9(4)	-1(4)
C13	35(6)	27(4)	29(5)	9(4)	-6(4)	11(4)
C14	27(5)	46(6)	28(5)	11(4)	-5(5)	-5(5)
C15	16(4)	38(5)	30(5)	-12(4)	5(4)	-2(4)
C16	17(4)	22(4)	29(5)	-4(4)	1(4)	5(4)
C17	19(4)	28(4)	19(4)	-2(4)	-2(3)	2(4)
C18	32(5)	32(5)	23(5)	-6(4)	3(4)	2(4)
C19	46(7)	31(5)	49(7)	-13(5)	4(6)	19(5)
C20	61(8)	41(5)	28(6)	5(5)	11(6)	30(6)
C21	35(5)	26(4)	39(6)	5(4)	5(5)	14(4)
C22	45(7)	64(7)	47(7)	9(6)	13(7)	6(7)

The FAB mass spectra as well as ESI mass spectra of these complexes have proved to be valuable tools in assigning their molecular formulae (or definite fragments resulting from them) by the experimental value of  $m/z$  (most abundant isotopic mass) as well as matching between the experimental and simulated (calculated) isotopic distribution profile; the simulated isotopic distribution profile has been obtained by a computer program developed by Prof. Y. Yan<sup>46</sup>. The FAB mass spectrum of (3) shows

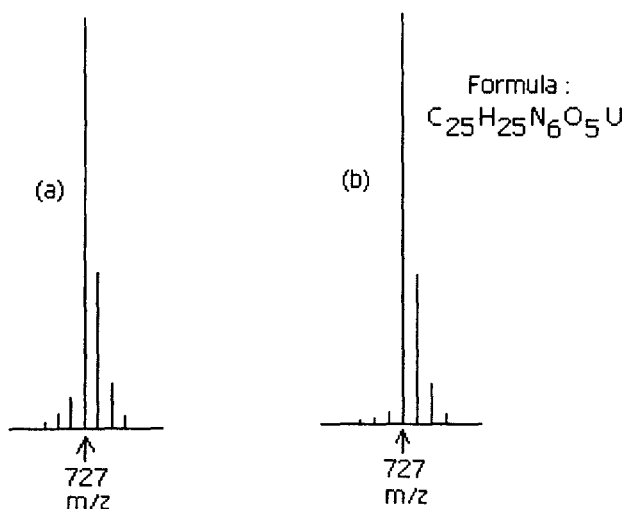


**Fig.(V- 3):**(a) FABMS data of (3) at the  $m/z$  (= 727) region corresponding to  $[M-2H_2O+ H]^+$ ; (b) the calculated isotope pattern<sup>46</sup>.

the characteristic isotopic distribution pattern in the region  $m/z = 727$  [Figure (V - 3a)] corresponding essentially to the desolvated species  $[M + H - 2H_2O]^+$  or  $[UC_{25}H_{25}N_6O_5]^+$ , where 'M' is the molecular formula of (3) (F.W. = 762). These data agreed with the corresponding theoretical value [Figure (V-3b)] thereby supporting the chemical composition of (3), along with its elemental analysis and other physicochemical data ; the same is true in other cases as well. In case of complex (4), the essentially intact molecular ion peak,  $[M+3H]^+$  is observed at  $m/z = 997$ , and this assignment is verified through matching with the calculated data [Figure (V - 4)] ; here 'M' is the molecular formula of (4) (F.W. = 994). The noble aspect is that none of the extraspheric water molecules are lost during the mass spectral process, indicating their strong hydrogen bonding most likely with the amidine nitrogen atoms of the amino acid residue [Scheme (V - 1)]. In case of complex (5), the FAB mass spectrum shows the essentially intact desolvated species  $[M+H-H_2O]^+$  at  $m/z = 699$ , where 'M' is the molecular formula of (5) (F.W.= 716). A good matching is observed with the corresponding simulated isotopic distribution

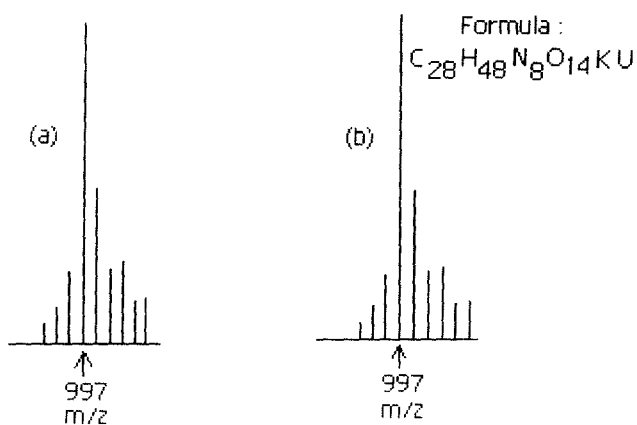


**Fig.(V- 4):** (a) FABMS data of (4) at the  $m/z$  (= 997) region corresponding to  $[M + 3H]^+$ ; (b) the calculated isotope pattern<sup>46</sup>.

pattern in this case as well [Scheme (V – 5)]. For complex (6) almost intact molecular ion peak,  $[M+3H]^+$  is observed at  $m/z = 1263$ , where ‘M’ is the molecular formula of (6) (F.W.=1260). In Figure (V – 6) a tally between the experimental and calculated isotopic distribution pattern around  $m/z = 1263$ , is shown.

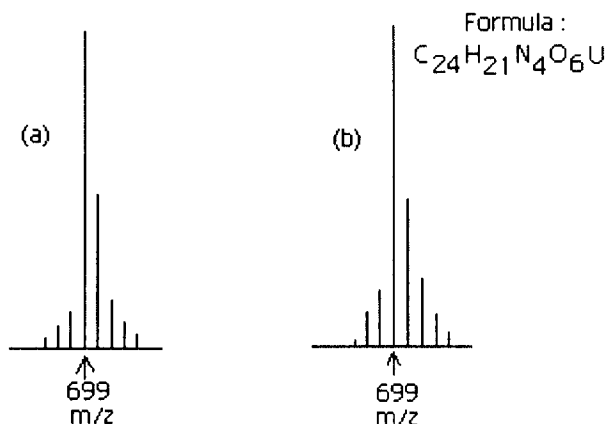


**Fig.(V – 5):** (a)FABMS data of (5) at the  $m/z$  (= 699) region corresponding to  $[M-H_2O + H]^+$ ; (b) the calculated isotope pattern<sup>46</sup>.

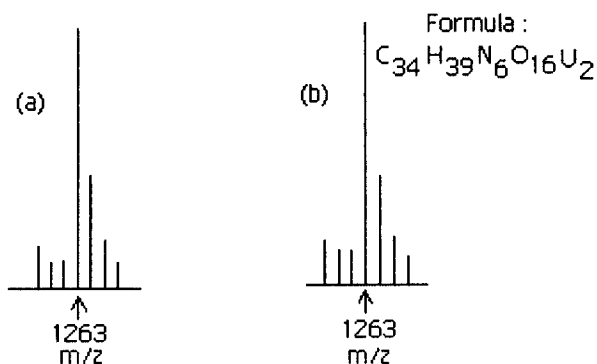


**Fig.(V – 6):** (a)ESIMS data of (6) at the  $m/z$  (= 1263) region corresponding to  $[M + 3H]^+$ ; (b) the calculated isotope pattern<sup>46</sup>.

The above- mentioned mass spectral data consistently indicate architectural stability of the present uranyl – aldimine ligand complexes where characterization is possible either for the essentially intact desolvated species in two cases or for the

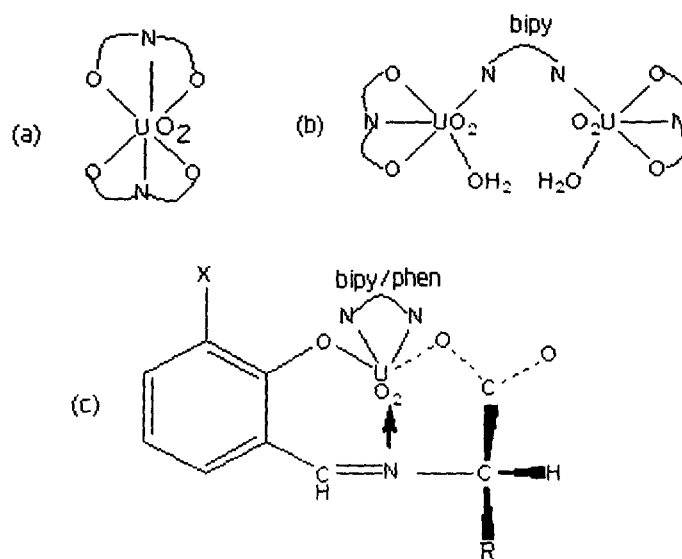
complexes along with their extraspheric or intraspheric water molecules in other two cases. Their ability to retain this identity indicates stable nature of the  $\text{UO}_2^{2+}$  - aldimine ligand coordination ; this property is vital for the present kinetic studies where the size increase accompanying the electron transfer step  $\text{UO}_2^{2+} \rightarrow \text{UO}_2^+$  is to be counterbalanced for a short duration for recording the relevant data.

The  $\Lambda_M$  [13.0 – 25  $\text{ohm}^{-1} \text{mol}^{-1} \text{cm}^2$ , 301K,  $\text{CH}_3\text{OH}$ ] values for complexes (2), (3), (5) & (6) are consistent with their non-electrolytic formulation<sup>43</sup>. In case of compounds (1) and (4),  $\Lambda_M$  (91.0 & 86.0  $\text{ohm}^{-1} \text{mol}^{-1} \text{cm}^2$ , 301K,  $\text{CH}_3\text{OH}$ ) values indicate their 1:1 electrolytic nature<sup>43</sup>.

The IR spectrum of the free ligand [e.g., (1)] exhibits the  $\nu$  (CH=N) band at  $1635 \text{ cm}^{-1}$  and it undergoes a red shift (by  $20 \text{ cm}^{-1}$ ) in the corresponding complex (6)<sup>85</sup>; for other complexes [(2), (3), (4), (5)] of this series, this  $\nu$  (CH=N) band is located in the region  $1620 - 1615 \text{ cm}^{-1}$ . For the free ligand [e.g., (1)], the  $\delta$  (OH) and  $\nu(\text{C} - \text{O}) + \delta(\text{OH})$  modes of the phenolic – OH group appear at  $1370 \text{ cm}^{-1}$  and  $1200 \text{ cm}^{-1}$  respectively ; such bands disappear on chelation and the corresponding  $\nu(\text{C} - \text{O})$  mode of the phenoxide group is observed around  $1210 \text{ cm}^{-1}$ <sup>155</sup>. For this compound [OV – L – AsnHK (1)], the  $\nu_{\text{as}}$  and  $\nu_{\text{s}}$  modes of the carboxylate group are observed at  $1615 \text{ cm}^{-1}$  and  $1410 \text{ cm}^{-1}$  respectively ; these two bands appear at ca.  $1600 \text{ cm}^{-1}$  and ca.  $1400 \text{ cm}^{-1}$  respectively, for the present complexes with the  $\Delta\nu$  value ( $\nu_{\text{as}} - \nu_{\text{s}} = 200 \text{ cm}^{-1}$ ) being in the range for unidentate carboxylate coordination<sup>72</sup>. The above data are in agreement with the X – ray structural data of (2) [Figure (V – 1)] regarding tridentate aldimine ligand coordination (involving the deprotonated phenolic – OH group, the azomethine nitrogen atom and are of the carboxylate oxygen atoms) for the present complexes.

The asymmetric stretching frequency ( $\nu_3$ ) of the  $\text{UO}_2^{2+}$  entity appears as a prominent band in the range  $915 - 900 \text{ cm}^{-1}$ , sometimes accompanied by a shoulder on the lower frequency side in all these cases<sup>103</sup>.

On the basis of the above discussions, the schematic structural formulas of these complexes, as per Scheme (V – 2), may be adopted for further discussion.



**Scheme (V-2):** Schematic structural formulas of the complexes; (a) complex (4); (b) complex (6) and (c) complexes (2), (3) & (5).

Now, the attention is focussed on the stereochemical aspect (both configurational and conformational factors) of these complexes on the basis of their chiroptical data, i.e., CD spectral data supported / substantiated by UV – VIS and  $^1\text{H}$  NMR spectral data. Some of these data are reproduced here from reference 146 for lucid discussion ; such data together with the present X – ray structural, mass spectral and kinetic data will be published together comprehensively, as continued interest of this laboratory on chiral system <sup>174</sup>. This will help to rationalize their reactivity data (as discussed later). In the first stage we discuss the  $^1\text{H}$  NMR spectral data of the ligand S – L – ArgH<sub>2</sub>, its corresponding complex (3), the related complex (4) as well as that of complex (3'), [UO<sub>2</sub> (S – D – Arg)(phen)]. H<sub>2</sub>O ; the last one contains the D – arginine

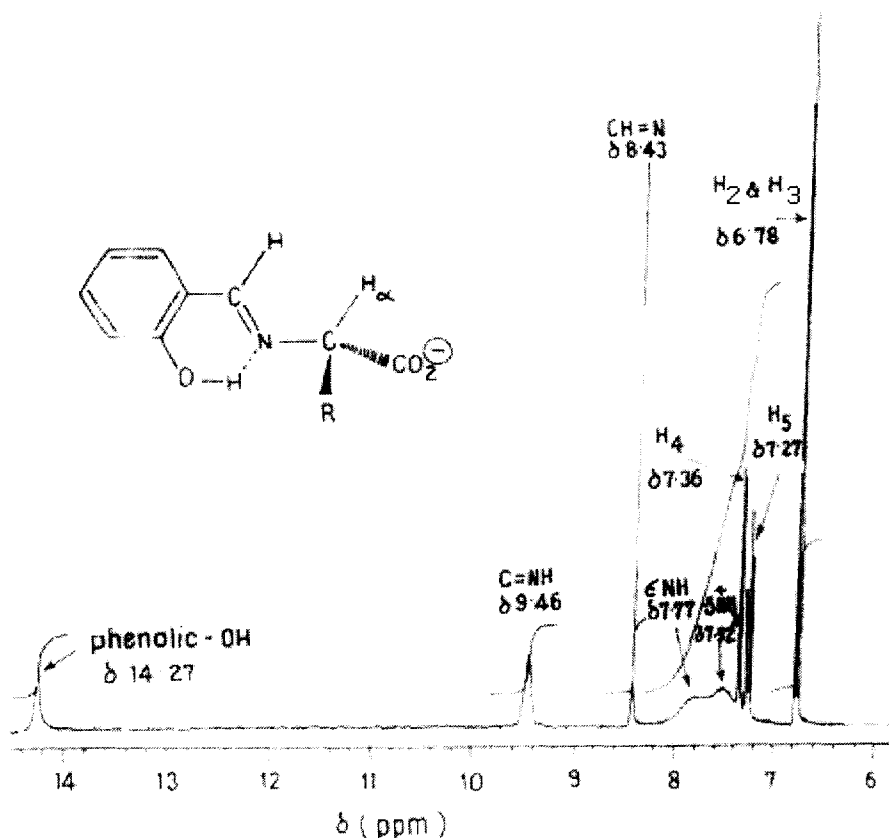


**Fig.(V - 7):**  $^1\text{H}$  NMR spectrum of (S - L - ArgH<sub>2</sub>) in DMSO - d<sub>6</sub>. The schematic formula in the inset represents positive chirality, consistent with CD data <sup>146</sup>.

residue and it is the quasi - enantiomer of (3) as evident from CD spectral data [Fig.(V - 12)] <sup>146</sup>. Some of the  $^1\text{H}$  NMR spectral data have been recorded afresh to substantiate the data recorded earlier <sup>146</sup>; their interpretation have been checked here once again. The assignments of different  $^1\text{H}$  NMR signals have been done on the basis of spin - decoupling experiments as well as 2D NMR data ( $^1\text{H}$  -  $^1\text{H}$  cosy experiments). Scheme (V - 1) indicates the different proton designations of the ligand S - L - ArgH<sub>2</sub> in Figure (V - 7) which shows its  $^1\text{H}$  NMR spectrum in DMSO - d<sub>6</sub> over the region  $\delta$  14.40 to  $\delta$  3.60 ppm and the data for the lower ppm range are summarized in Table (V - 6).

**Table(V-6):**Chemical shift ( $\delta$ , ppm) values of major conformers of the ligands protons and those of the corresponding dioxouranium (VI) complexes along with the  $\Delta$  ( $= \delta_{\text{complex}} - \delta_{\text{ligand}}$ ) ppm values for the latter<sup>146</sup>.

Free ligands / Compl -exes		Amino acid residue						Aldehyde residue					bipy, phen parts <sup>c</sup>								
		H <sub><math>\alpha</math></sub>	H <sub><math>\beta_1</math></sub>	H <sub><math>\beta_2</math></sub>	H <sub><math>\gamma</math></sub>	H <sub><math>\delta</math></sub>	-NH <sub>2</sub>	C <sub>5</sub>	CH=N	OCH <sub>3</sub> /H <sub>5</sub>	H <sub>4</sub>	H <sub>2</sub>	H <sub>3</sub>	H <sub>6'</sub>	H <sub>5'</sub>	H <sub>4'</sub>	H <sub>3'</sub>	H <sub>2' &amp; 9'</sub>	H <sub>3' &amp; 8'</sub>	H <sub>4' &amp; 7'</sub>	H <sub>5' &amp; 6'</sub>
OV-L-AsnHK <sub>b</sub>		4.47	2.68	3.02 <sup>d</sup>	-	-	- <sup>e</sup>	8.30	3.82	7.04	6.96	6.63	-	-	-	-	-	-	-	-	-
S-L-AsnHK · H <sub>2</sub> O <sup>b</sup>		4.41	3.02	2.62 <sup>d</sup>	-	-	- <sup>e</sup>	8.36	(7.64-7.24) <sup>h</sup>	(7.0-6.7) <sup>f</sup>			-	-	-	-	-	-	-	-	
S-L-ArgH <sub>2</sub> <sup>a, n</sup>		3.78	1.75	1.92	1.49	3.10	7.77-7.52 <sup>l</sup>	8.43	7.27	7.36	6.78 <sup>f</sup>			-	-	-	-	-	-	-	
OV-L-ArgHK <sup>a, o</sup>		3.87	1.77	1.90	1.49	3.11	7.74 <sup>m</sup>	8.38	3.73	6.88 <sup>g</sup>	6.53			-	-	-	-	-	-	-	
(3) <sup>a</sup>	$\Delta$	4.90	1.93	1.67	3.10			9.27	7.58 <sup>h</sup>	7.00 <sup>j</sup>	6.71			9.13	7.79	8.52	8.03				
		1.12	0.015	0.18	0.00			0.84	0.26					0.03	0.08	0.06	0.05				
(3) <sup>a</sup>	$\Delta^k$	4.87	1.78	2.05	1.58	3.07		9.25	7.57	6.98	6.70			9.10	7.78	8.50	8.00				
		1.09	0.03	0.13	0.09	-0.03		0.82	0.25					0.00	0.07	0.04	0.03				
(4) <sup>a</sup>	$\Delta$	4.87	1.90	2.12	1.67	3.12		9.12	3.99	7.14 <sup>g</sup>	6.55			-	-	-	-				
		1.00	0.13	0.22	0.18	0.01		0.74	0.26	0.26	0.02										
(5) <sup>a</sup>	$\Delta^i$	4.83	1.94	2.30	2.22	-	7.33 & 6.72	9.22	7.56 <sup>h</sup>	6.98	6.7			9.11	7.78	8.5	8.0				
		0.42						0.86						0.11	0.07	0.04	0.03				
(6) <sup>a</sup>	$\Delta$	5.29	2.56	2.78	-	7.23 & 6.87		9.22	3.94	7.13	6.59			7.22	8.69	7.46	7.95	8.39			
		0.82						0.92	0.12	0.17	-0.04			0.18	0.06	0.11	0.10	0.08			

<sup>a</sup> In DMSO - d<sub>6</sub> ; <sup>b</sup> In D<sub>2</sub>O ; <sup>c</sup>  $\delta$  ppm values for free bipy and phen protons have been obtained from references 99 and 100 ; <sup>d</sup> signals could not be resolved due to low solubility and their range is only given here ; <sup>e</sup> the -NH<sub>2</sub> protons have undergone exchange in D<sub>2</sub>O ; <sup>f</sup> H<sub>2</sub> & H<sub>3</sub> signals are appearing together ; <sup>g</sup> H<sub>2</sub> & H<sub>4</sub> signals are appearing together ; <sup>h</sup> H<sub>4</sub> & H<sub>5</sub> signals are appearing together ; <sup>i</sup>  $\Delta$  values for the S - L - GlnH<sub>2</sub> compound is calculated using the corresponding  $\delta$  ligand values of S - L - AsnHK.H<sub>2</sub>O ; <sup>j</sup> H<sub>2</sub> & C=NH proton signals appear together ; <sup>k</sup>  $\Delta$  values are calculated on the basis of the corresponding L- ligand (S-L-ArgH<sub>2</sub>) data ; <sup>l</sup>  $\epsilon$ NH( $\delta$ 7.77) &  $\xi$ NH<sub>3</sub><sup>+</sup> ( $\delta$ 7.52) signals ; <sup>m</sup>  $\epsilon$ NH &  $\xi$ NH<sub>3</sub><sup>+</sup> signals appear together ; <sup>n</sup>  $\xi$  >C=NH signal appears at  $\delta$  9.96 ; <sup>o</sup>  $\xi$  >C=NH signal appears at  $\delta$  9.23 ; provide Scheme (V - 1) for different proton designations.

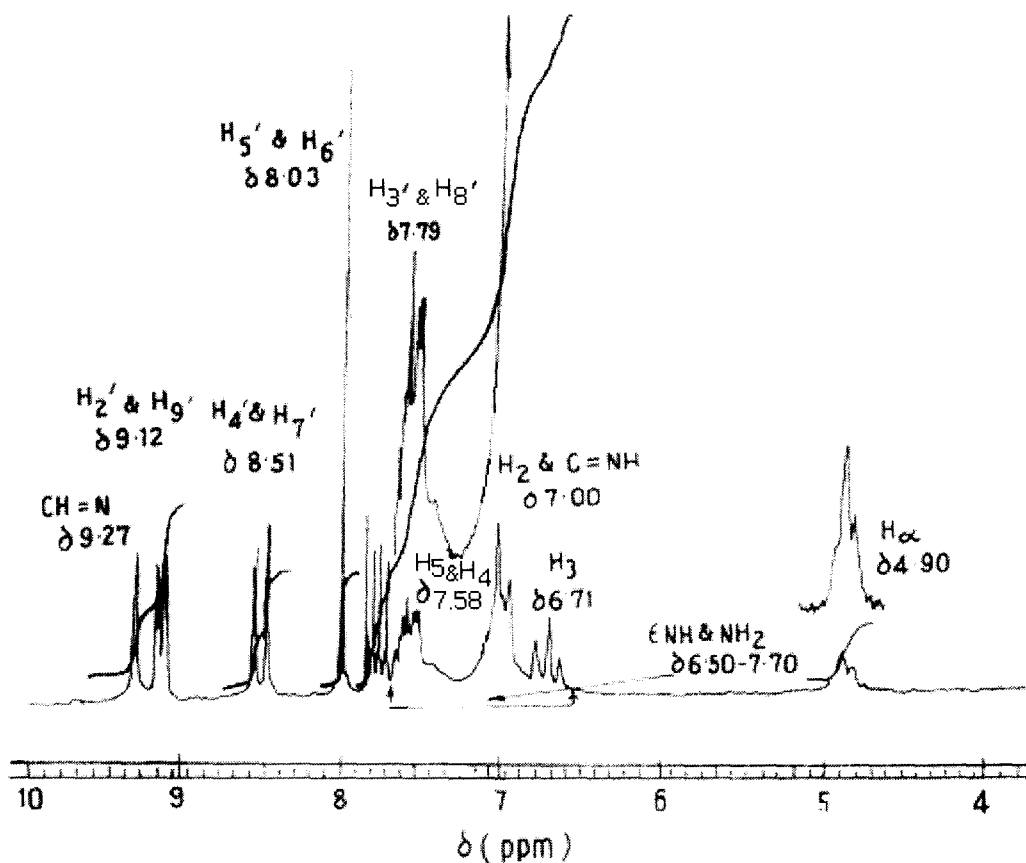
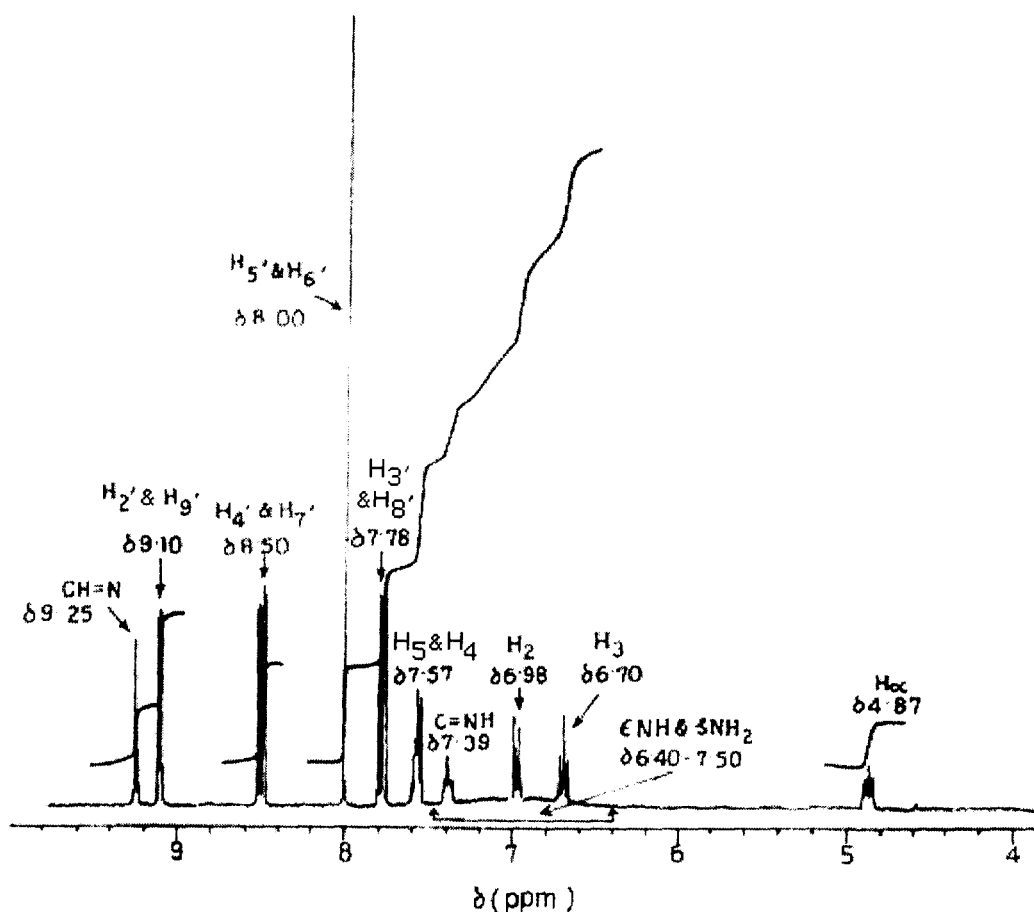


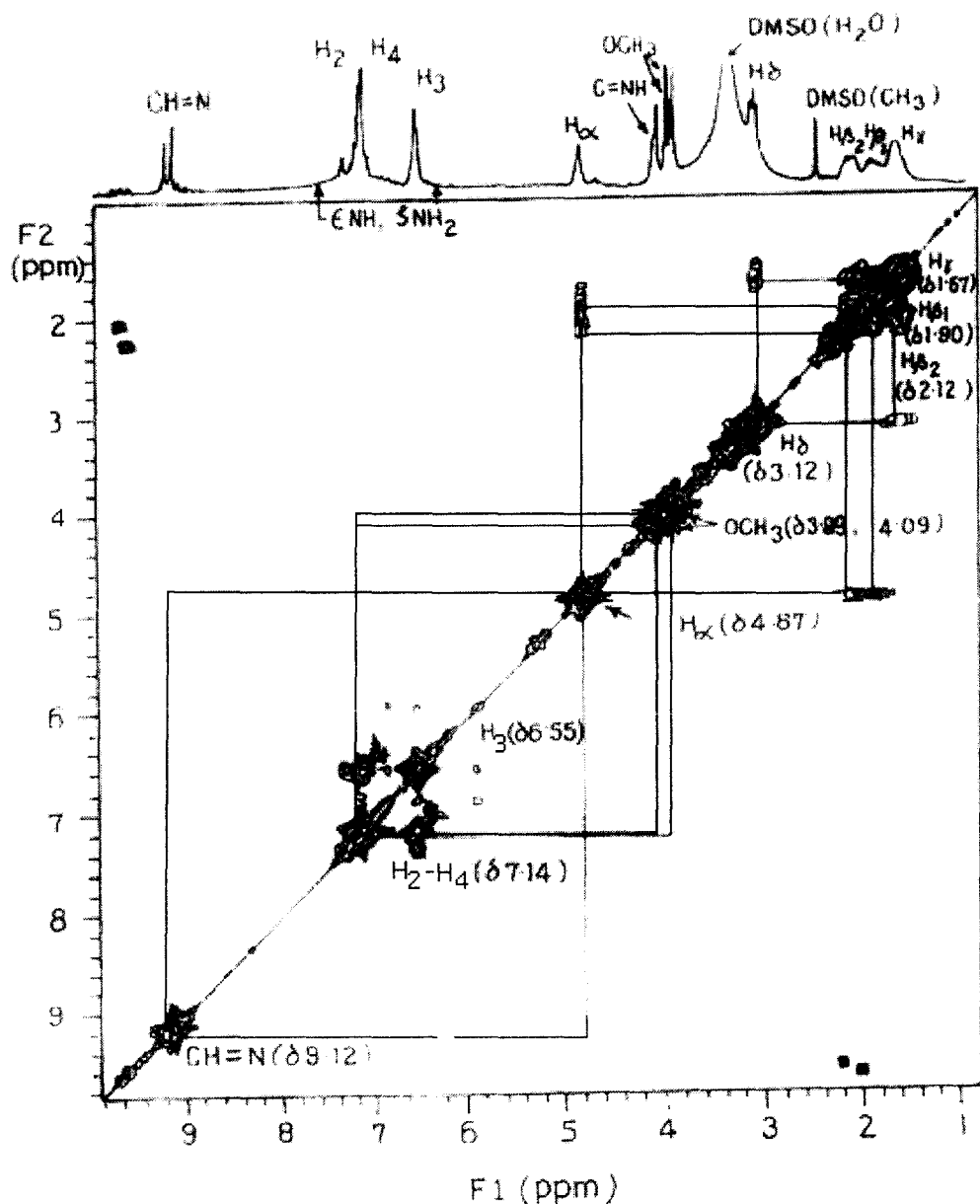
Fig.(V – 8):  $^1\text{H}$  NMR spectrum of compound (3) in  $\text{DMSO} - d_6^{146}$ .

Figure (V – 8) shows the  $^1\text{H}$  NMR spectrum of the corresponding complex (3), over the range  $\delta$  10.0 to  $\delta$  5.8 ppm, with the data for the lower ppm range being shown in Table (V – 6). A comparison of Figures (V – 7) and (V – 8) along with the  $\Delta$  values ( $= \delta_{\text{complex}} - \delta_{\text{ligand}}$ ) for the different proton signals in Table (V – 6), reveals several interesting features. In contrast to the strong deshielding effect (of  $\delta$  1.12 –  $\delta$  0.74 ppm) observed for the aldimine ligand protons situated around the immediate coordination zone [e.g.,  $\text{H}_\alpha$  and  $\text{CH} = \text{N}$ , Scheme (V – 1)], the ‘phen’ ring protons [Scheme (V–1) depicts the numbering system of different protons of the 1,10 – phenanthroline ligand] hardly undergo any deshielding effect [Table (V – 6)], although this bidentate nitrogen donor ligand is quite strongly coordinated to the  $\text{UO}_2^{2+}$  entity. The X – ray structural data of compound (2) [Figure (V – 1) and Table (V – 2)] illustrate this point involving the other bidentate nitrogen donor ligand (e.g., 2,2’ – bipyridyl) utilized in



**Fig.(V - 9):**  $^1\text{H}$  NMR spectrum of compound (3') in  $\text{DMSO} - d_6$  <sup>146</sup>.

this study. Similar trend of low  $\Delta$  values is observed for the 'bipy' ring protons in case of compound (6) as well [Table (V - 6)]. The strong deshielding of  $H_\alpha$  and  $\text{CH} = \text{N}$  protons on coordination to the  $\text{UO}_2^{2+}$  entity, depends on several factors, e.g., drainage of electron density from the ligand through  $\text{L} \rightarrow \text{M}$   $\sigma$  bonding as well as magnetic anisotropy of the  $\text{UO}_2^{2+}$  entity <sup>96</sup>. On the other hand, extensive  $\text{L} \rightarrow \text{M}$   $\pi$  bonding occurs involving suitably disposed uranium orbitals and  $\pi^*$  orbitals of 1,10 - phenanthroline, thereby counterbalancing the deshielding effect through  $\text{L} \rightarrow \text{M}$   $\sigma$  bonding, leading to little change in  $\Delta$  values of the 'phen' ring proton signals [Table (V - 6)]. The same is true for the  $\Delta$  values of the 'bipy' ring protons of complex (6) {Table (V - 6)}. This electron withdrawing  $\pi$  - bonding influence is beneficial for studying the electron transfer process  $\text{UO}_2^{2+} \rightarrow \text{UO}_2^+$  here, as it provides with a small time lag for recording the relevant absorption spectral data [Figure (V - 14b)] as stated later.



**Fig.(V - 10):**  $^1\text{H} - ^1\text{H}$  COSY spectrum (symmetrized) of compound (4) in  $\text{DMSO} - d_6^{146}$ .

Another interesting aspect is revealed by comparing the  $^1\text{H}$  NMR spectra of compounds (3) and (3') in Figures (V - 8) and (V - 9) respectively. Although these two compounds have essentially identical chemical compositions, they differ in the absolute configuration about the  $\text{C}_\alpha$  atom [Scheme (V - 1)]. A closer look at the two above-mentioned  $^1\text{H}$  NMR spectra reveals that for similar types of proton signals, small but distinct differences could be identified with respect to both their positions ( $\delta$  ppm values) and multiplicities. This is mainly due to conformational differences of the 'R' part of the

amino acid residue in each case with respect to the chelate ring [conformer (b) in Scheme (V – 3) as shown later]. This is substantiated by their CD spectral data [Figure (V – 12)] where the two CD curves (briefly interpreted later) are almost mirror images to each other with respect to positions of CD maxima due to opposite configurations about the  $C_\alpha$  atom [Scheme (V-1)], but intensity difference [ $(\theta)_M$  values] exist due to the above – mentioned conformational differences.

Figure (V – 10) shows the 2D NMR spectrum of complex (4); it represents the procedure adopted here for assigning the different proton signals as well as the different spin – spin interactions existing here responsible for the observed multiplicities of the  $^1H$  NMR signals, e.g., the long – range spin – spin interaction between the  $H_\alpha$  and the azomethine ( $CH = N$ ) protons<sup>85, 107</sup>.

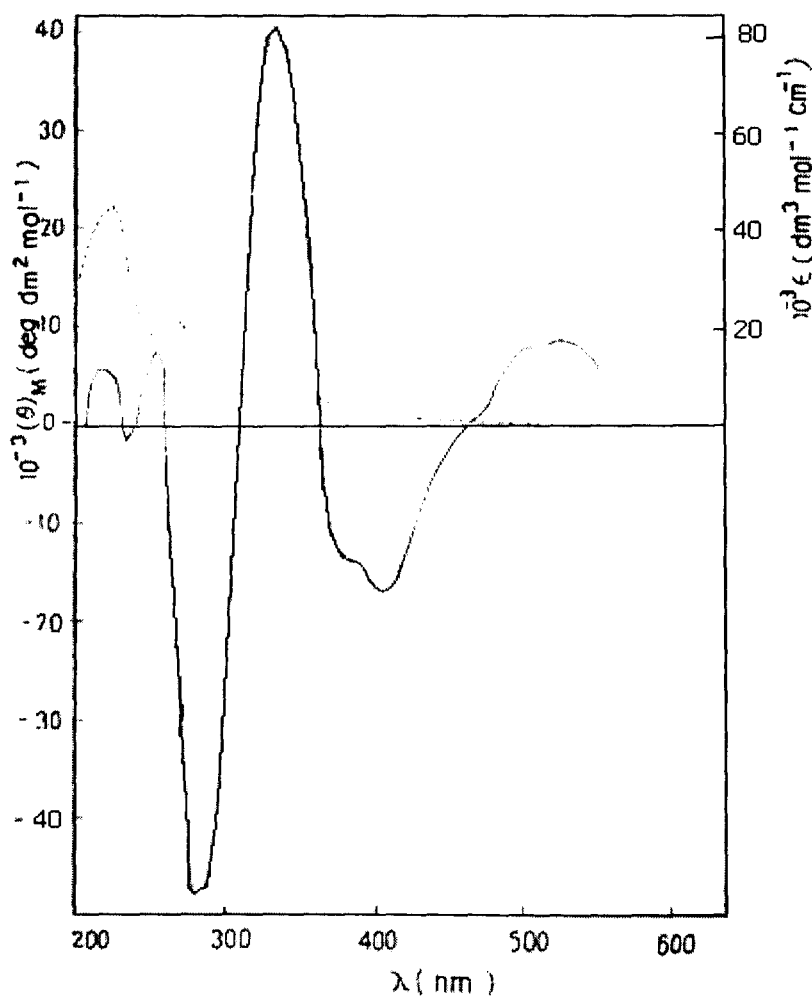


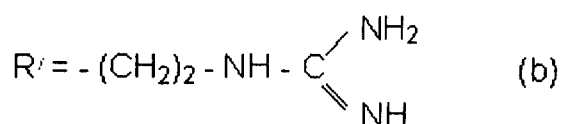
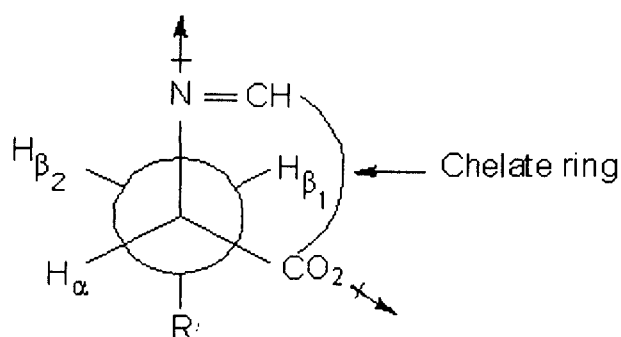
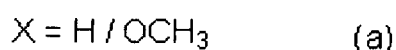
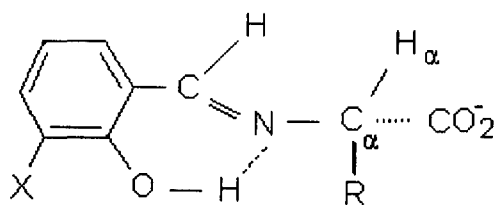
**Fig.(V – 11):** Electronic [ - - - - ] and CD [ — ] spectra of compound (4) in  $CH_3OH$ <sup>146</sup>.

Presently, some of the relevant electronic absorption and CD spectral data [Figure (V – 11), (V – 12)] may be viewed in the light of existing guidelines for assigning absolute configuration / conformation of the pertinent ligands / complexes <sup>79</sup>. The quasi – enantiomeric nature of the CD curves of complexes (3) and (3') in Figure (V–12) indicates the importance of absolute configuration of the amino acid residue in determining the overall chirality here <sup>79</sup>.

In Figure (V – 11) the characteristic electronic spectral bands of complex (4) around 227 nm and 332 nm (sh) are assigned to  $\pi \rightarrow \pi^*$  transitions of the O – vanillideneamino chromophore [Scheme (V – 3)] <sup>79</sup>. The band at 262 nm is due to a  $n \rightarrow \pi^*$  transition of the azomethine group <sup>79</sup>. Another band extending from 355 nm to longer wavelength with diminishing intensity is assigned to charge transfer transition from the equatorial ligand  $p\pi$  orbitals to the 5f / 6d orbitals of the uranium atom [Figure (V – 11)]. The relatively weaker apical oxygen  $p\pi \rightarrow 5f$  transition within the  $UO_2^{2+}$  entity is observed by the aforesaid strong absorption occurring in the range 350 – 550 nm <sup>96, 102, 203, 155</sup>. However, the corresponding CD spectrum of complex (4) [Fig. (V– 11)] is helpful in resolving the two above electronic transitions by giving rise to two separate CD bands, e.g., a negative Cotton effect around 405 nm corresponding to the former equatorial ligand L  $\rightarrow$  M charge transfer transition, while a positive Cotton effect around 530 nm characterizes the magnetically allowed intra oxometal transition <sup>102, 155</sup>.

The typical couplet (S – shaped) CD band centred around 306 nm (with negative and positive maxima at 281 nm and 333nm respectively [Fig. (V – 12)]) justifies the use of a coupled oscillator model [e.g., the salicylideneamino (SA) chirality rule <sup>79</sup>], for assigning the absolute configuration / conformation of the pertinent complexes. According to the SA chirality rule, for the N – salicylidene / orthovanillidene derivatives of aliphatic  $\alpha$  – amino acids, this couplet CD band arises by transition moment dipole coupling of the carboxylate group (its  $\pi \rightarrow \pi^*$  transition appears below 210 nm) with that of the aldimine chromophore [Scheme (V – 3)] and the positive Cotton effect (for L – type ligand system) around 320 – 330 nm is used here as the decisive one for chiroptical studies, as it usually undergoes only partial modification on coordination to a metal ion ; for the ligand S – L – ArgH<sub>2</sub> this positive CD band appears at 316 nm. According to the

above chirality rule, the sign of this 320 – 330 nm band can be predicted from the preferred chirality that the attachment band of the  $\text{CO}_2^-$  group has with the phenyl group methane carbon in the salicylidene / orthovanillidene chromophore. Positive chirality indicated by the 320 – 330 nm CD maximum can be represented by either conformer (a) or conformer (b), as per Scheme (V – 3).



**Scheme (V–3):** Dominant conformers of aldimine ligands / complexes giving rise to positive chirality.

In case of conformer (a), the observer is looking along the  $\text{C}_\alpha - \text{N}$  bond, with the  $\text{CO}_2^-$  group located on the right hand side ; the resultant of the two electric vectors (e.g., the  $\text{CO}_2^-$  group and the aldimine chromophore) is on the right – hand side of the observer which is correlated with positive CD maximum at 320 – 330 nm<sup>79</sup>. For conformer (b), contributions of the two above – mentioned electric vectors (indicated by arrows) give rise to a right – handed resultant, leading to the positive CD band at 320 – 330 nm. In case of aliphatic amino acids (including arginine), the contribution from the electric vector of R or R' group [Scheme (V – 3)], is smaller than the two above – mentioned chromophores<sup>79</sup>. On the other hand, a left – handed  $\text{CO}_2^-$  group [Scheme

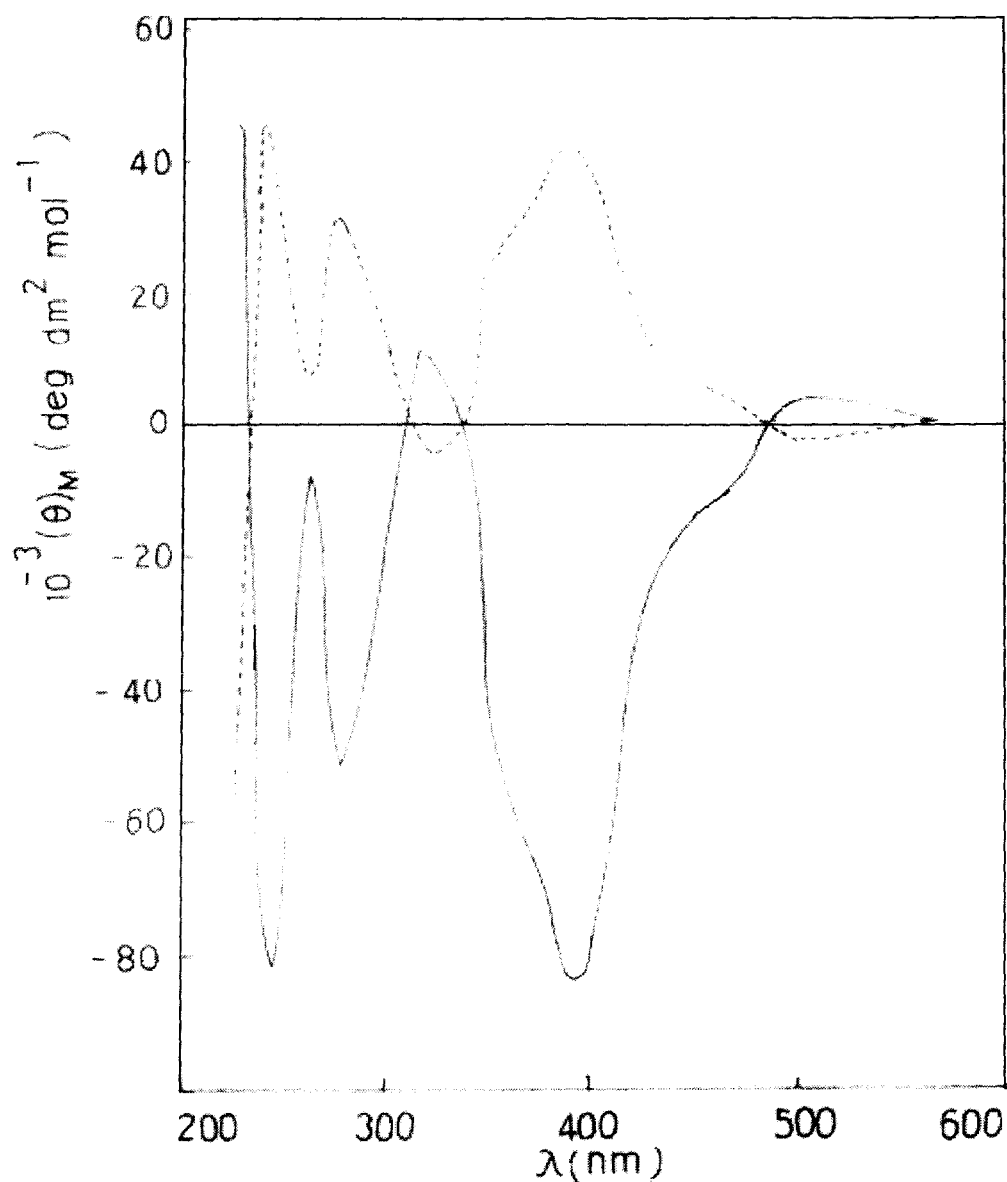
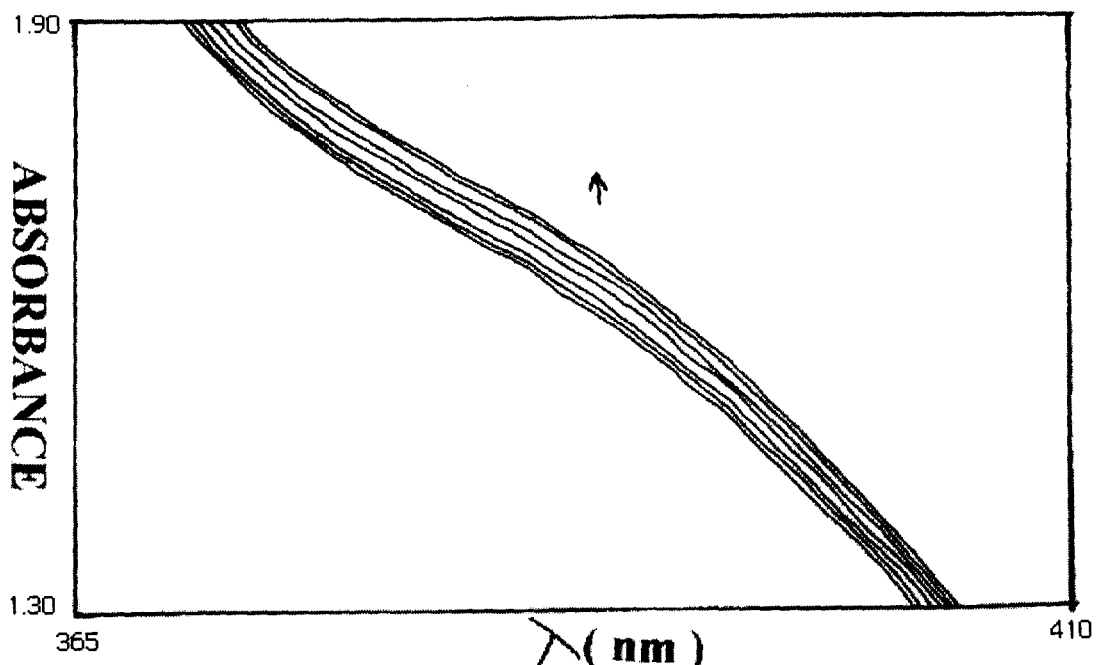


Fig.(V – 12): CD spectra of compounds (3) [—] and (3') [-----] in CH<sub>3</sub>OH <sup>146</sup>.

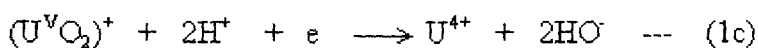
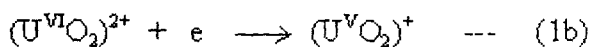
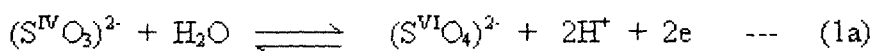
(V-3)] would have given rise to negative chirality with negative sign for the 320 – 333 nm CD band. Now viewing the two CD spectra in Figure (V– 12) in the above light, in case of complex (3) the positive CD maximum at 320 nm can be correlated with the configuration ( $C_\alpha$ ) of L – arginine residue, whereas for complex (3') with D – arginine residue (possessing opposite configuration at  $C_\alpha$ ), a negative CD maximum is observed at 325 nm. However, the reduced intensity of these two CD bands [as compared to the 333 nm CD band in Figure (V – 11)] is due to the opposite electric vector contribution from the  $\pi \rightarrow \pi^*$  transition of the neutral donor ligand (1,10 – phenanthroline) <sup>155</sup>.

As stated earlier, the essentially mirror image nature of the two CD curves in Figure (V – 12) with respect to band positions arise from opposite configurations of the two amino acid residues of the two complexes [(3) and (3')] as well as stereospecific nature of the chelation process of the  $\text{UO}_2^{2+}$  entity with each aldimine ligand residue, leading to retention of configuration in each case. However, the difference in intensity between the two CD curves in terms of  $(\theta)_M$  values in Figure (V – 12) can be traced to the conformational differences between the 'R' part of each amino acid residue. A comparison (proton signal by proton signal with respect to position and fine structure) of the two relevant  $^1\text{H}$  NMR spectra [Figure (V – 8) and (V – 9)] support this view.

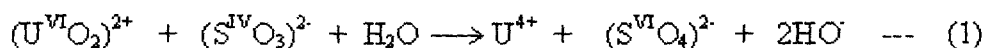
As evident from  $^1\text{H}$  NMR spectra the extensive  $\text{M} \rightarrow \text{L} \pi$  bonding occurs here in appropriate cases, involving suitably disposed uranium orbitals and  $\pi^*$  orbitals of the 'phen' ligand. This partial removal of electron density from the uranium orbitals as well as the compact donor set of ligands on the equatorial plane (as evident from X – ray structural data) can give the  $\text{UO}_2^+$  entity some stability to be studied on both the spectrophotometric and the cyclic voltammetric time scale [equation (1b)]. Reaction stoichiometry study (discussed later) indicate the overall reaction as per equation (1).



**Fig.(V-13):** UV-VIS absorption spectral changes recorded every 20 seconds during the reaction of compound (2) [ $1.12 \times 10^{-3}(\text{M})$ ] with  $\text{Na}_2\text{SO}_3$  [ $2.95 \times 10^{-5}(\text{M})$ ] in  $\text{DMSO-H}_2\text{O}$  (3 : 2, v/v) at 290 K.



**The overall reaction :**



Reactivity of the present uranyl complexes towards  $Na_2SO_3$  was studied in DMSO –  $H_2O$  (3 : 2 v/v) medium (purged with dinitrogen) spectrophotometrically [that is, recording of absorbance versus  $\lambda_{(nm)}$  data every 20 seconds at 290 K, Figure (V-13)]. Distinct changes of absorbance with time occurred over the range 370 – 405 nm for complex (2) and other uranyl complexes of this series. From these data, the wavelength 383 nm was chosen for recording the time scan data (that is, for following the change of absorbance with time in order to calculate the rate constant data). At 290 K the change of absorbance with time [Figure (V – 14a)] during reaction with  $Na_2SO_3$ , is characterized by a single reduction step for complex (3). Interestingly, at a slightly lower temperature (288 K), the corresponding data [Figure (V – 14b)] represents a two – step reduction process, that is, a short – lived (ca. 65 seconds) intermediate could be detected in the first stage of reduction using the present conventional recording UV – VIS spectrophotometer. Most likely, Figure (V-14a) represents the overall two – electron reduction process as per equation (1), whereas Figure (V-14b) is able to distinguish between the two one – electron reduction steps ( $UO_2^{2+} \rightarrow UO_2^+ \rightarrow U^{4+}$ ) with the  $UO_2^+$  entity appearing as a short – lived intermediate as per equation (1b). Cyclic voltammetry and coulometry data of this complex (3) in DMSO medium [Figure (V-17) and (V-18)], support this inference<sup>146</sup>. This in agreement with the literature report on both thermodynamic and kinetic stability of the  $UO_2^+$  species in DMSO medium<sup>141, 165</sup>. Using this single step absorbance change versus time data as in Figure (V – 14a), the observed rate constant ( $k_{obs}, s^{-1}$ ) were determined by least square method from the plots of  $\log (A_a - A_t)$  versus

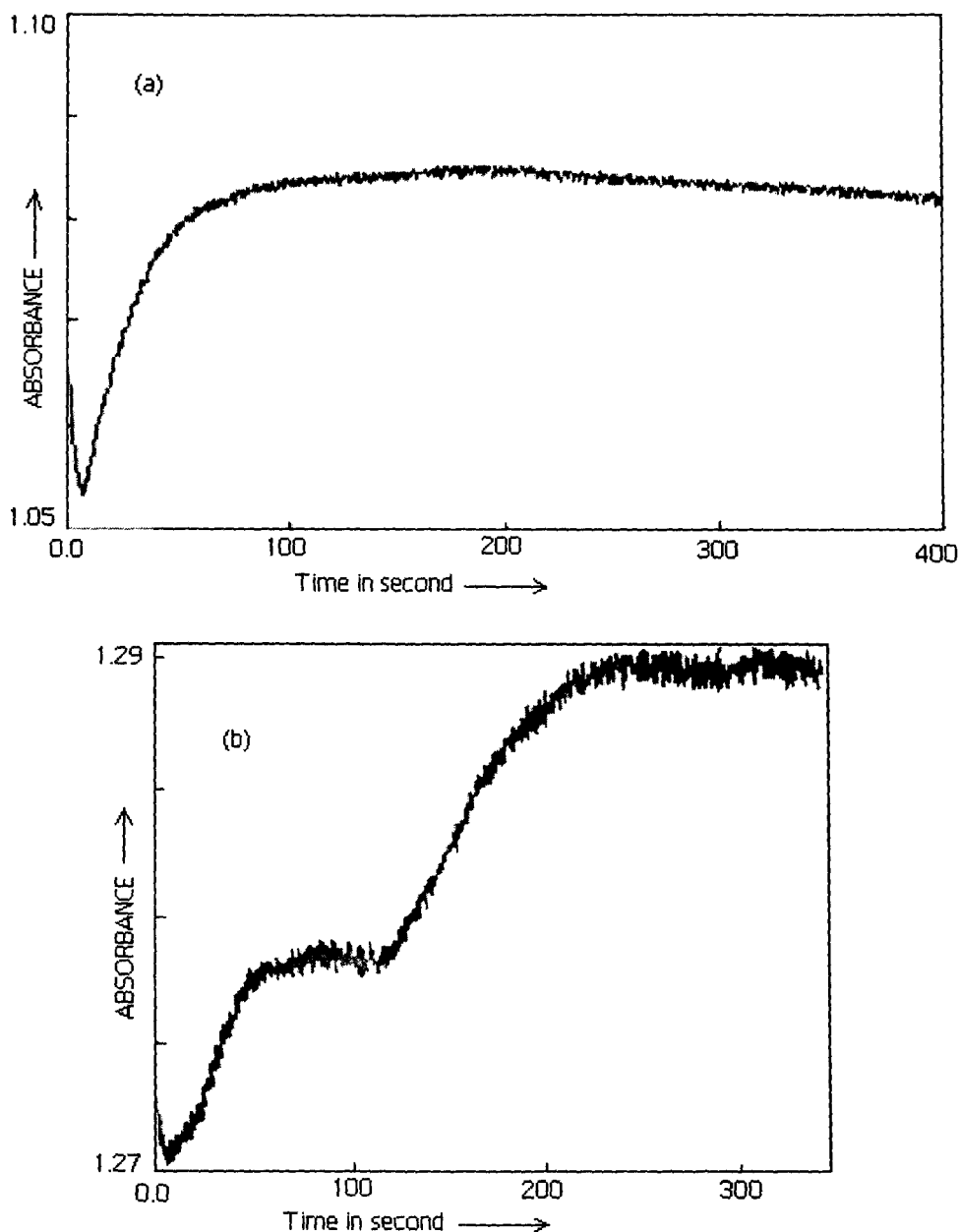


**Fig.(V – 14):** Monitoring of the change of absorption with respect to time (Time scan) for the reaction:- (a) between compound (3) [ $8.75 \times 10^{-4}$  (M)] and  $\text{Na}_2\text{SO}_3$  [ $1.75 \times 10^{-5}$  (M)] in DMSO –  $\text{H}_2\text{O}$  (3 : 2, v/v) at 290 K and at  $\lambda = 383$  nm ; (b) between compound (3) [ $8.75 \times 10^{-4}$  (M)] and  $\text{Na}_2\text{SO}_3$  [ $2.76 \times 10^{-5}$  (M)] in DMSO –  $\text{H}_2\text{O}$  (3 : 2, v/v) at 288 K and at  $\lambda = 383$  nm.

time, which were linear for nearly three half – lives. In the next stage, variation of the  $k_{\text{obs}}$  ( $\text{s}^{-1}$ ) values was followed at a fixed  $\text{Na}_2\text{SO}_3$  concentration with increasing concentration of each complex and from the linear plots [Figures (V–15), (V–16) showing some of them] of  $k_{\text{obs}}$  ( $\text{s}^{-1}$ ) values versus complex concentration (M), the second order rate constants ( $k_2 \text{ M}^{-1} \text{ s}^{-1}$ ) were obtained [Table (V–7)].

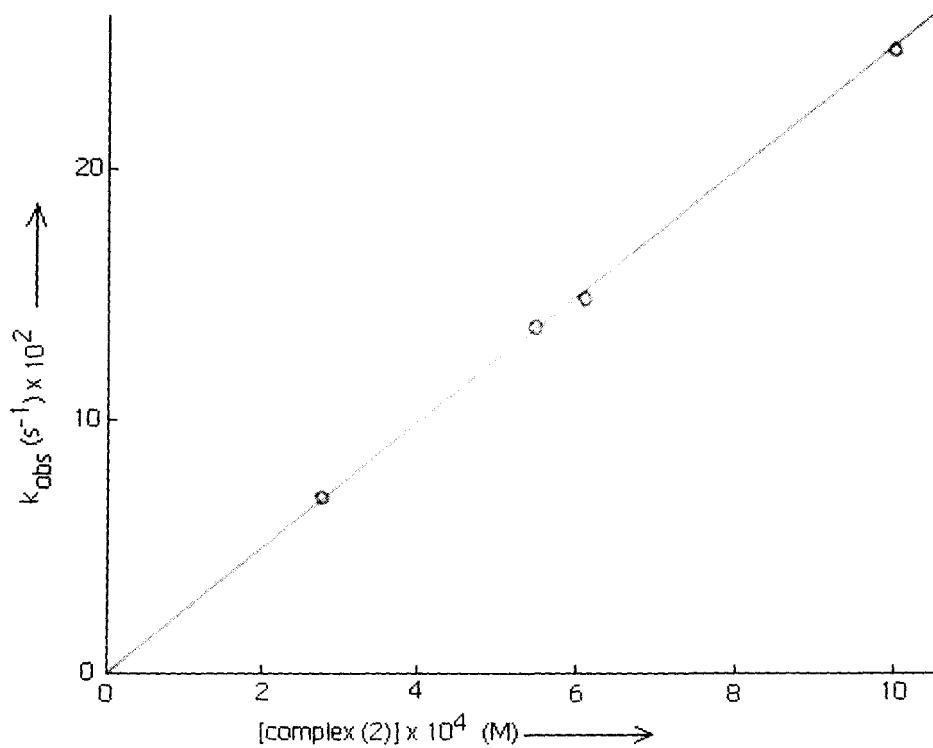


**Fig.(V-15):** Dependence of the rate of reaction on the concentration of (2) with Na<sub>2</sub>SO<sub>3</sub> [1x10<sup>-5</sup> (M)] in DMSO - H<sub>2</sub>O (3 : 2, v/v) at 290 K.

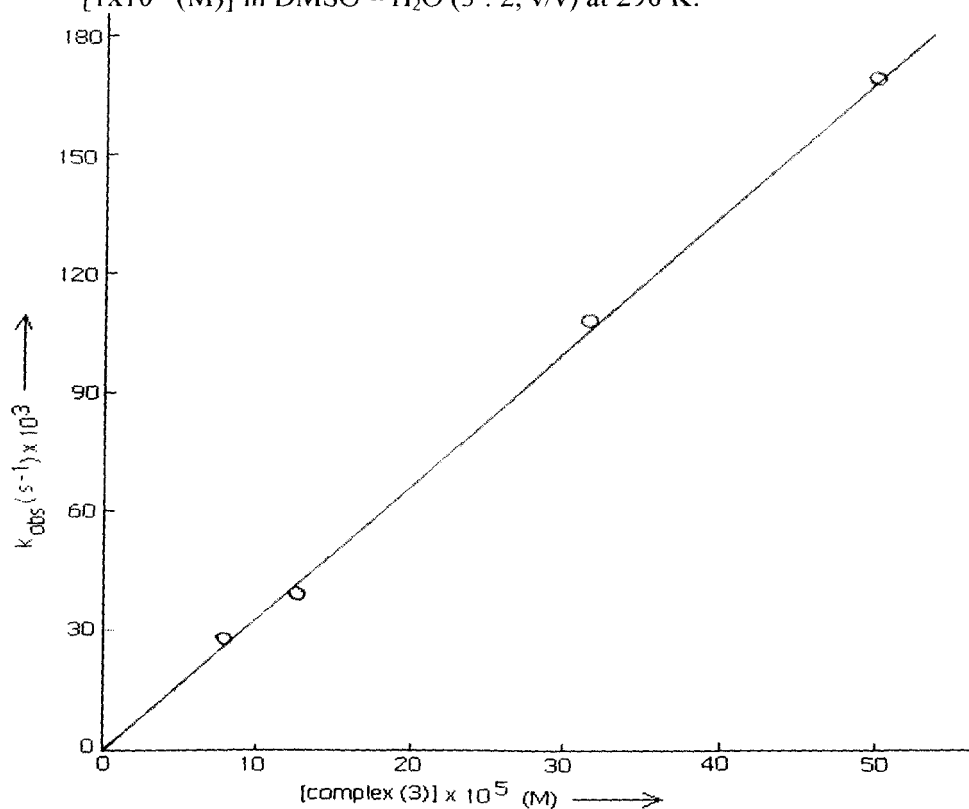


**Fig.(V-16):** Dependence of the rate of reaction on the concentration of compound (3) with Na<sub>2</sub>SO<sub>3</sub> [1.0x10<sup>-5</sup> (M)] in DMSO - H<sub>2</sub>O (3 : 2, v/v) at 290 K.

**Table (V-7):** Kinetic data for the present uranyl complexes for the reaction with Na<sub>2</sub>SO<sub>3</sub> [1.0 x 10<sup>-5</sup> (M)] in DMSO – H<sub>2</sub>O (3 : 2, v/v) at 290 K.

Complex No.	[Complex] (M) x 10 <sup>-4</sup>	k <sub>obs</sub> (s <sup>-1</sup> ) x 10 <sup>-2</sup>	k <sub>2</sub> (M <sup>-1</sup> , s <sup>-1</sup> ) <sup>*</sup> x 10 <sup>3</sup>
(2)	2.76	7.10	1.75
	5.50	13.70	
	6.10	14.90	
	10.0	24.70	
(3)	0.78	2.80	0.33
	1.27	3.90	
	3.17	10.80	
	5.0	16.90	
(3')	1.55	88.50	1.86
	3.62	50.20	
	4.65	29.70	
	5.85	8.00	
(4)	0.50	10.00	1.80
	0.69	11.80	
	1.13	17.90	
	1.58	32.20	
(5)	0.06	2.81	5.45
	0.11	5.50	
	0.16	8.80	
	0.58	32.50	
(6)	0.30	2.70	1.12
	2.01	22.90	
	3.35	38.80	

\* Derived rate constants from the plots of k<sub>obs</sub> (s<sup>-1</sup>) versus complex concentration [e.g., Figures (V-15), (V-16)].

Some important observations regarding these kinetic data are summarized below.

1. For evaluating the second order rate constants (k<sub>2</sub> M<sup>-1</sup> s<sup>-1</sup>) data, the concentration of the reducing agent (e.g., Na<sub>2</sub>SO<sub>3</sub>) was kept constant and the concentration of each complex was gradually increased over a range [e.g., Figures (V – 15), (V – 16)]. The alternative pathway, that is, increasing the concentration of Na<sub>2</sub>SO<sub>3</sub> and keeping the

complex concentration fixed, could not be adopted here as the reactions become too fast at higher Na<sub>2</sub>SO<sub>3</sub> concentration, to be followed by a conventional spectrophotometer.

2. For reactions between NaHSO<sub>3</sub> and [Bu<sub>4</sub>N] [Mo<sup>VI</sup>O<sub>2</sub> (mnt)<sub>2</sub>] in CH<sub>3</sub>CN – H<sub>2</sub>O medium, saturation kinetics was observed for the dependence of k<sub>obs</sub> (s<sup>-1</sup>) values on [HSO<sub>3</sub><sup>-</sup>] <sup>197</sup>, unlike the second – order kinetic behaviour in the present case.

In spite of the above difference in overall kinetic behaviour of the two systems (e.g., UO<sub>2</sub><sup>2+</sup> and MoO<sub>2</sub><sup>2+</sup>), the k<sub>obs</sub> (s<sup>-1</sup>) values for the present uranyl complexes are comparable in magnitude with those of [Bu<sub>4</sub>N] [MoO<sub>2</sub> (mnt)<sub>2</sub>] <sup>89, 104, 197</sup>. Most likely, the closely related end products (that is, SO<sub>4</sub><sup>2-</sup> or HSO<sub>4</sub><sup>-</sup>) of these two reaction systems, decide the issue.

3. For the two – step reduction process at 288 K [Figure (V – 14b)], the k<sub>obs</sub> (s<sup>-1</sup>) values were calculated to be 26.1 x 10<sup>-2</sup> s<sup>-1</sup> and 12.7 x 10<sup>-2</sup> s<sup>-1</sup> for the first and second steps respectively.

The initial electron transfer step UO<sub>2</sub><sup>2+</sup> → UO<sub>2</sub><sup>+</sup> is followed by the relatively slower coupled electron and group transfer step UO<sub>2</sub><sup>+</sup> → U<sup>4+</sup>. Evidently, the overall two electron transfer coupled with oxygen atom transfer (SO<sub>3</sub><sup>2-</sup> + [O] → SO<sub>4</sub><sup>2-</sup>), involves a short – lived UO<sub>2</sub><sup>+</sup> intermediate and could be detected here. This is in conformity with the ability of SO<sub>3</sub><sup>2-</sup> ion to react with both one – electron and two – electron oxidants like Fe<sup>3+</sup> and Cl<sub>2</sub> respectively <sup>141, 165</sup>.

4. The second – order rate constants data of these complexes vary over a range [k<sub>2</sub> = 0.33 – 5.45 M<sup>-1</sup> s<sup>-1</sup>, Table (V – 7)] reflecting their dependence on chemical compositions of the complexes, especially the donor atoms on the equatorial plane around the UO<sub>2</sub><sup>2+</sup> entity as well as nature of the R groups of the amino acid residues. This is consistent with the inner – sphere nature of the overall electron transfer process [equation (1)] .

5. Another notable aspect is the kinetic behaviour of complex (3') where the  $k_{\text{obs}}$  ( $\text{s}^{-1}$ ) values measured as usual at a fixed  $\text{Na}_2\text{SO}_3$  concentration, decrease with increasing complex concentration, unlike other complexes of this series [Table (V - 7)]. As per Scheme (V - 1), arrangement of the two substituents of  $\text{C}_\alpha$  atom ( that is the hydrogen atom,  $\text{H}_\alpha$  and the R group) are interchanged for the D - arginine residue of complex (3') as compared to that of the L - arginine residue of complex (3). The present inner - sphere electron transfer reaction [equation (1)] depend on the orientation of the R group around  $\text{C}_\alpha$  [Scheme (V - 1)] in complexes (3) and (3') as evident from the kinetic data in Table (V - 7) ; most likely electron transfer from the reducing agent ( $\text{SO}_3^{2-}$ ) to the suitable orbital (HOMO) of the  $\text{UO}_2^{2+}$  entity in complex (3') is hindered by the orientation of the R group, indicating configurational / conformational control of the electron transfer process <sup>106, 155</sup>.

6. To establish reaction stoichiometry, a solution of complex (2) (0.08 g, 0.115 mmol) in 20 ml  $\text{DMSO} - \text{H}_2\text{O}$  (3 : 2 v/v) was treated with a solution of anhydrous  $\text{Na}_2\text{SO}_3$  (0.38 g, 2.99 mmol) in 80 ml of the same solvent mixture, after thorough purging with dinitrogen. The reaction mixture was stirred under dinitrogen atmosphere at 301 K for 20 h. The organic part was extracted with  $\text{CH}_2\text{Cl}_2$  and the sulphate ( $\text{SO}_4^{2-}$ ) formed through the relevant reaction [equation (1)] was estimated as  $\text{BaSO}_4$ , giving 0.66 g (2.83 mmol) of  $\text{BaSO}_4$  <sup>89, 104</sup>. As sulphite ( $\text{SO}_3^{2-}$ ) oxidizes fairly rapidly in air, performing a blank experiment is essential for getting the reliable data about the amount of sulphate ( $\text{SO}_4^{2-}$ ) formed in the pertinent reactions of the uranyl complexes <sup>89, 104</sup>. A blank experiment was performed under similar conditions, using the same amount (0.38 g, 2.99 mmol) of anhydrous  $\text{Na}_2\text{SO}_3$  dissolved in same volume (100 ml) of the above solvent mixture ; 0.634 g (2.72 mmol) of  $\text{BaSO}_4$  was obtained from the blank experiment. The difference between the two results, that is, 0.026 g (0.114 mmol) is the actual amount of  $\text{BaSO}_4$  obtained, corresponding to the sulphate ( $\text{SO}_4^{2-}$ ) formed through the reaction between complex (2) and  $\text{Na}_2\text{SO}_3$ . Therefore, almost 0.99 mol of sulphate was formed per mol of complex (2), during its reaction with  $\text{Na}_2\text{SO}_3$  in accordance with equation (1).

Cyclic voltammetry and coulometry data in DMSO medium of a few of the present uranyl complexes are summarized here,<sup>146</sup> for complementing the above data on their redox activity towards  $\text{Na}_2\text{SO}_3$ , especially regarding the formation of the short-lived  $\text{UO}_2^+$  intermediate. In the entire potential range of 0.0 to  $-1.9$  V, the free ligands display a reduction ( $E_{pc}$ ) peak around  $-1.60$  V. For the present complexes the reductive response ( $E_{pc}$ ) in the range of  $-0.95$  V to  $-1.05$  V can be assigned to a metal-centred process, involving reduction of the  $\text{UO}_2^{2+}$  entity. For example, in case of complex (3) [Figure (V-17)] the catho-anodic peak system  $E_{pc} / E_{pa}$  is due to the one-electron transfer process [equation (1b & 1c)]. Controlled-potential coulometry [Figure (V-18)] of this complex at  $-1.15$  V versus SCE indicates a 'n' value (number of electrons

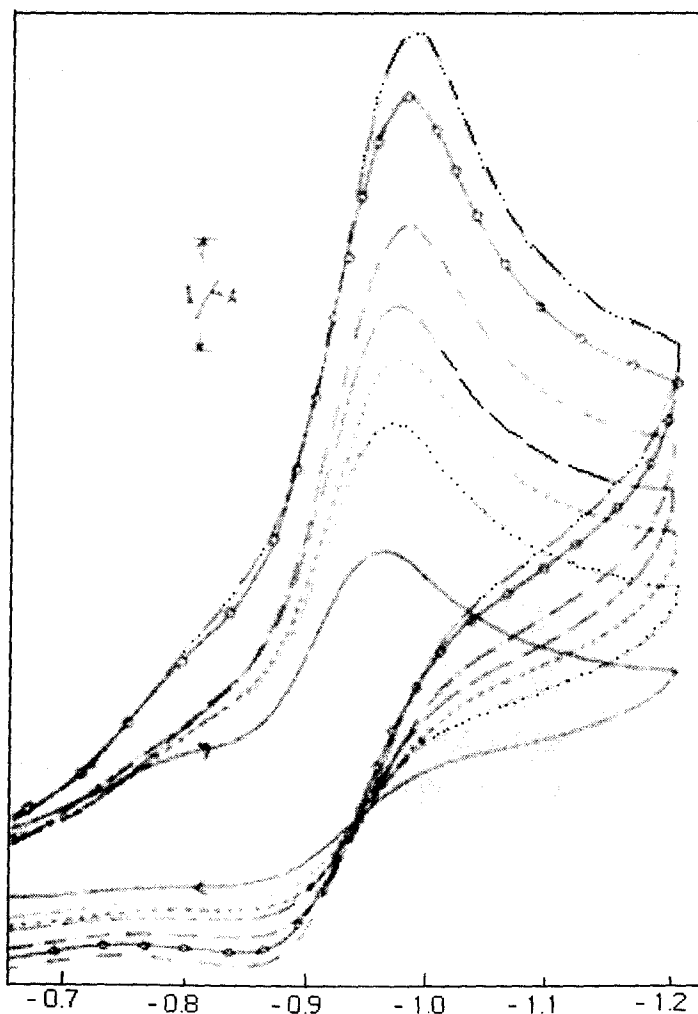


**Fig.(V-17):** Cyclic voltammogram of  $[\text{UO}_2(\text{S-L-Arg})(\text{phen})].2\text{H}_2\text{O}$  ( $2.90 \times 10^{-3}$  M) in DMSO with  $0.1$  M  $\text{Bu}_4\text{NClO}_4$ ; scan rates: (i)  $50$  (—), (ii)  $100$  (.....), (iii)  $150$  (---), (iv)  $200$  (- - -), (v)  $250$  (- - - -), (vi)  $300$  (-o-o-), (vii)  $350$  (- - - - -)  $\text{mVs}^{-1}$ . Platinum working electrode<sup>146</sup>.

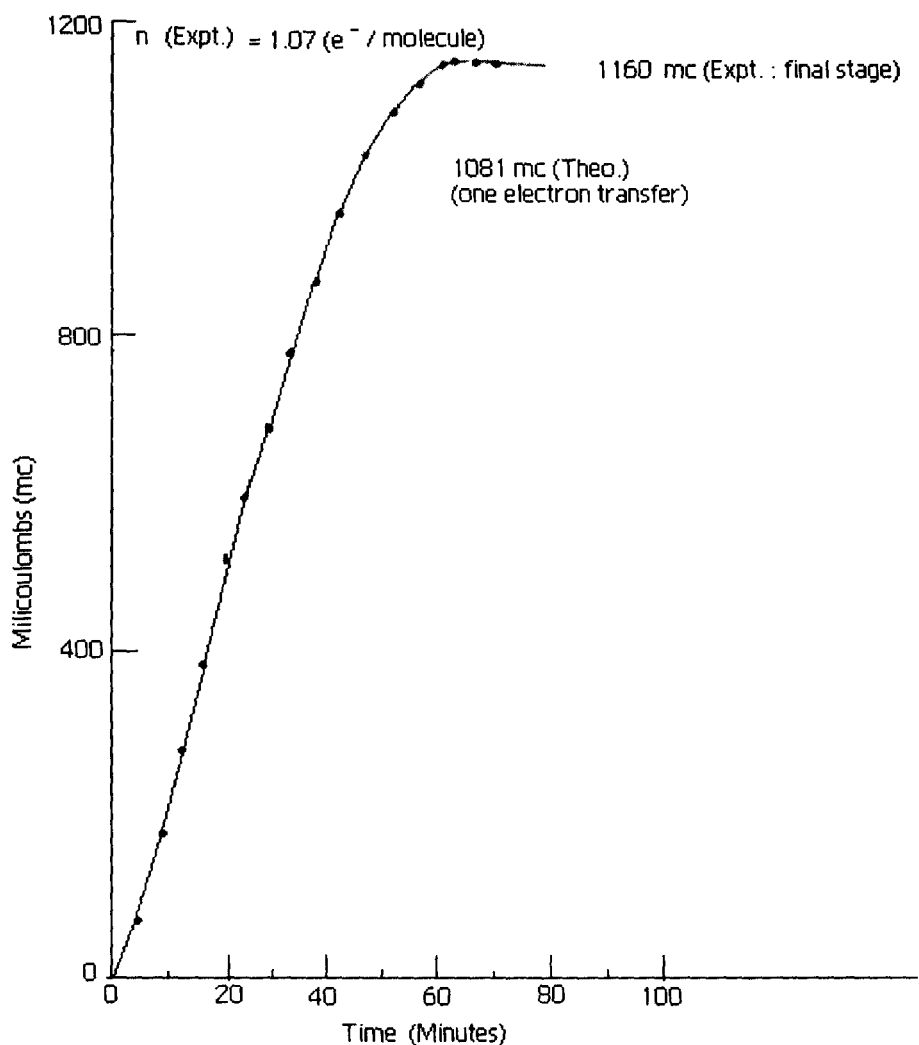


**Fig.(V-18):** Controlled – potential coulometry of  $[\text{UO}_2(\text{S-L-Arg})(\text{phen})].2\text{H}_2\text{O}$  in 0.05M  $\text{Bu}_4\text{NClO}_4$  / DMSO at a platinum plate electrode (4.2 cm x 2.2 cm) under  $\text{N}_2$  at room temperature; electrolysis at  $-1.15\text{V}$  vs SCE, using  $11.2 \mu\text{M}$  of the substance <sup>146</sup>.

transferred per molecule of complex) of 1.07, thereby confirming the formation of the  $\text{UO}_2^+$  ion on the cyclic voltammetry and coulometric timescales in DMSO medium. In the cyclic voltammetric experiment [Figure (V – 18)], the forward scan generates the  $\text{UO}_2^+$  species which undergoes solvation before start of the reverse scan and this is reflected by the departure of the peak – current ratio ( $i_{\text{pc}} / i_{\text{pa}}$ ) from unity. The broad anodic peak becomes more prominent at faster scan rates ;  $\Delta E_p$  value ( $E_{\text{pa}} - E_{\text{pc}}$ ) increases upto 130 mV at a scan rate of  $200 \text{ mVs}^{-1}$  and remains constant beyond that limit. The corresponding quasi – enantiomeric complex (**3'**) containing the ( $\text{S} - \text{D} - \text{Arg}^{2-}$ ) residue, exhibits different CD and  $^1\text{H}$  NMR spectral response, as compared to those of complex

(3), due to configurational / conformational differences, as stated earlier. These differences are also reflected in the cyclic voltammetric data ; such data recorded at a scan rate of  $50 \text{ mV s}^{-1}$  for complex (3) indicate  $\Delta E_p$  (mV) and ( $i_{pc} / i_{pa}$ ) values of 90 mV and 1.64 respectively, as compared to the corresponding values of 130 mV and 1.55 for complex (3'). However, such differences are magnified to a large extent during redox reaction with  $\text{Na}_2\text{SO}_3$ , as evident from the relevant data in Table (V – 7) for these two complexes ; this aspect stresses the importance of the present kinetic studies, as they supplement not only the earlier cyclic voltammetric data but also substantiate the inference regarding configurational / conformational control of electron transfer reactions, in the present system. The compact equatorial donor set of ligands of the  $\text{UO}_2^{2+}$  entity contributed by the aldimine ligands, in conjunction with the  $\text{M} \rightarrow \text{L} \pi$  bonding ability of the neutral bidentate donor (bipy / phen), provide some stability to the  $\text{UO}_2^+$  entity generated during the cyclic voltammetric process (cathodic reduction) and allow characterization of the one – electron process ( $\text{UO}_2^{2+} \rightarrow \text{UO}_2^+$ ) through coulometry [Figure (V–18)]<sup>146</sup>. In the absence of such compact donor set of ligands, e.g., for  $\text{UO}_2(\text{NO}_3)_2 \cdot 6\text{H}_2\text{O}$ , cyclic voltammetric data in DMSO displays a single irreversible reduction wave [ $E_{pc} = -0.52 \text{ V}$  at a scan rate of  $50 \text{ mVs}^{-1}$  with similar conditions as in Figure (V – 17)] ; that is, the  $\text{UO}_2^+$  entity generated during the forward scan is completely decomposed through the post – chemical process (e.g., solvation) before starting the reverse anodic scan.

Figure (V–17) can be treated as a representative of the cyclic voltammetric data in DMSO medium of the present uranyl complexes where both the cathodic reduction ( $E_{pc}$ ) and anodic oxidation ( $E_{pa}$ ) peaks could be identified, with the latter type of peak becoming more prominent at faster scan rates.

## Conclusion

Well – characterized uranyl complexes of aldimine ligands containing amino acid residues, have been utilized for studying their reactivities towards a suitable reducing agent like  $\text{Na}_2\text{SO}_3$ . Unlike the substrate saturation kinetics observed for the reaction of a  $\text{MoO}_2^{2+}$  - dithiolene ligand complex with  $\text{HSO}_3^-$  ion <sup>197</sup>, the present uranyl complexes show linear dependence of  $k_{\text{obs}}$  ( $\text{s}^{-1}$ ) values on complex concentration, i.e., they follow second – order kinetics [Figure (V–15), (V–16)]. The one – and two – electron reducing capability of  $\text{Na}_2\text{SO}_3$  is utilized here for reactions with the pertinent uranyl complexes leading ultimately to the  $\text{U}^{4+}$  state [equation (1)], as verified through reaction stoichiometric studies. However, in case of complex (3) in DMSO -  $\text{H}_2\text{O}$  (3 : 2 v/v) medium at 288 K, the intermediate  $\text{UO}_2^+$  state could be identified and  $k_{\text{obs}}$  ( $\text{s}^{-1}$ ) value for the one – electron reduction process ( $\text{UO}_2^{2+} \rightarrow \text{UO}_2^+$ ) could be calculated. These results are in agreement with the corresponding cyclic voltammetry and coulometry data [Figure (V – 17), (V – 18)]. The compact equatorial ligand donor set of ligands make it possible to resolve the overall 2 – electron transfer process into two one – electron reduction steps ( $\text{UO}_2^{2+} \rightarrow \text{UO}_2^+ \rightarrow \text{U}^{4+}$ ) [Figure (V–14)] and help to stabilize the short – lived  $\text{UO}_2^+$  intermediate for a time duration for its spectrophotometric characterization. Another interesting aspect is the difference in kinetic behaviour [Table (V–7)] between complexes (3) and (3') containing the (S – L –  $\text{Arg}^{2-}$ ) and (S – D –  $\text{Arg}^{2-}$ ) residues respectively ; these data reflect the subtle configurational / conformational control via the relevant HOMO – LUMOs of the corresponding electron transfer processes <sup>155</sup>.

The above data and inferences will surely substantiate the continued interest on the different facets of reactivity of the uranyl entity <sup>176 – 178</sup>.

**SUMMARY**  
**&**  
**CONCLUDING REMARKS**

Now, it is time for an assessment of the experimental findings of this thesis vis – a – vis the objectives stated in Chapter I.

The pterin ligands [H<sub>2</sub>(pte<sub>1</sub>)], [H<sub>2</sub>(pte<sub>2</sub>)] or [H<sub>3</sub>(pte<sub>2</sub> – tsc)] act here as reducing agents and reduce the molybdenum starting materials in the higher oxidation state to a lower one (Mo<sup>V</sup> / Mo<sup>IV</sup>) in the complex, which has been assignment using different physicochemical methods. Besides this, new oxomolybdenum cores are formed during such synthetic steps. For example, in Chapter IV, Section – I, the mononuclear Mo<sup>V</sup> – starting material used for the synthesis of (4) {(Et<sub>4</sub>N)[(Mo<sup>V</sup><sub>2</sub>O<sub>3</sub>)(Hpte<sub>1</sub>)(Hcys)Cl<sub>3</sub>]. CH<sub>3</sub>OH} was converted to a binuclear species (Mo<sup>V</sup><sub>2</sub>O<sub>3</sub>)<sup>4+</sup>. In case of (1) {[Mo<sup>VI</sup><sub>2</sub>O<sub>5</sub>](Kpte<sub>1</sub>)(Hcys)(CH<sub>3</sub>OH)]. 2CH<sub>3</sub>OH} DMSO used during its synthesis, oxidized the intermediate Mo<sup>IV</sup> complex to a higher oxidation state with (Mo<sup>VI</sup><sub>2</sub>O<sub>5</sub>)<sup>2+</sup> core ; its reactivity towards PPh<sub>3</sub> verified the assignment of higher oxidation state (e.g., VI).

The role of the solvent used for the preparative purpose (e.g., CH<sub>3</sub>OH) is to be assessed with respect to that of H<sub>2</sub>O in the catalytic cycle of oxomolybdoenzymes. Loss of an oxo group from the Mo<sup>VI</sup> species during enzyme turnover is made up by the H<sub>2</sub>O molecule giving Mo – OH<sub>2</sub> and undergoes facile deprotonation to Mo – OH or Mo = O species accompanied by changes in the oxidation state of the metal centre <sup>26</sup>. Incorporation of the solvent (e.g., CH<sub>3</sub>OH) in the coordination sphere of several complexes during their synthesis, points towards the important role played by it during the synthetic process.

Chemical compositions of the new complexes have been established with the help of elemental analysis, ESIMS, IR and <sup>1</sup>NMR data. Their optimized molecular geometries have been obtained by molecular modelling studies [CHEM3D models obtained through MM2 calculations] along with their bond lengths and bond angles data, which are in agreement with the published X-ray structural data on different molybdenum – pterin coordination compounds. Besides this, the molecular structure of the ligand [H<sub>2</sub>(pte<sub>2</sub>)] has been established by X-ray crystallography. The spectroscopic data are consistent with the frame work of the above molecular structures.

The present molybdenum – pterin complexes undergo oxygen atom transfer reaction with typical enzyme substrates like DMSO,  $\text{Me}_3\text{N} \rightarrow \text{O}$ ,  $\text{PyN} \rightarrow \text{O}$  or  $\text{PPh}_3$ , as per the oxidation state of the molybdenum centre. Complex (7)  $\{[(\text{Mo}_2^{\text{VI}}\text{S}_5) \{\text{H}(\text{pte}_2\text{-tsc})\} (\text{CH}_3\text{OH})_3].\text{CH}_3\text{OH}\}$  in Chapter III, contains a  $(\text{Mo}_2^{\text{VI}}\text{S}_5)^{2+}$  core and undergoes sulphur atom transfer reaction with  $\text{PPh}_3$ , indicating a higher oxidation state for the Mo – centre here. Most of the above reactions conform to substrate saturation type kinetics with negative entropy of activation values, indicating associative type reaction mechanism. The kinetic parameters of these reactions are comparable to the available literature data for similar type of reactions. Nature of such group transfer reactions has been substantiated by reaction stoichiometry studies as well as ESIMS data in a few cases. The sulphur containing secondary ligands (Chapter IV, Section – I) help to manifest different tautomeric forms of the pterin ligand residue in the relevant complexes in solution, which are evident from the  $^1\text{H}$  NMR spectral data. These data also indicate electron flow from the  $\text{NH}_2(2)$  group of the pterin ligand residue towards the molybdenum centre in the relevant complexes, thereby promoting the reactivity as mentioned above. Probably such property (that is, flexibility of the pterin ligand residue with respect to electron flow coupled with the possibility of different tautomeric forms) has promoted Nature to select pterin as the essential component of the molybdenum – containing enzymes (except nitrogenase).

The CV data as well as fluorescence spectral data throw light on the changes in electronic structures during different redox reactions involving these complexes. It is evident from the discussions (in the different chapters of this thesis) that the ligand – centred as well as the metal – centred redox systems supplement each other in the new molybdenum – pterin complexes, giving them unique oxygen atom transfer reactivity property towards typical enzyme substrates ; electronic as well as fluorescence spectra have proved to be valuable probes in this respect. In other words, at least a few of the above – mentioned new complexes can be considered as functional models of oxomolybdoenzymes.

In Chapter IV, Section – II fresh characterization and reactivity studies of  $(\text{Mo}^{\text{V}}_2\text{O}_3)^{4+}$  - aldimine ligand complexes are discussed. The possible skew disposition of the two  $\text{Mo} = \text{O}_t$  bonds about the  $\text{Mo} - \text{O}_b - \text{Mo}$  bond [of the  $(\text{Mo}^{\text{V}}_2\text{O}_3)^{4+}$  - core] leads to two sets of MO levels with a paramagnetic ground state ( $S = 1$ ). This aspect coupled with the chiral ligand backbone casts its influence on the relevant EPR and CD spectra, associated with electronic transitions of the oxometal entity and the  $L \rightarrow M$  charge transfers. Complexes (4), (5) and (6) possess almost similar type of chemical compositions, but different physicochemical and spectroscopic properties (e.g.,  $\mu_{\text{eff}}$  values, IR, EPR and CD spectral data); they also differ with respect to their oxygen atom transfer and electron transfer reactivities. Most of these differences can be attributed to the different arrangements of the  $(\text{Mo}^{\text{V}}_2\text{O}_3)^{4+}$  - core, viewed in the light of their CHEM3D models (MM2 method). This conformational control of reactivity / property may prove vital in understanding the behaviour of oxomolybdoenzymes or their model systems.

Chapter V deals with the fresh characterization (ESIMS data as well as X-ray structural study in one case) and reactivity studies on  $\text{UO}_2^{2+}$  - complexes with aldimine ligands. These complexes serve as excellent vehicle for correlating the  $^1\text{H}$  NMR and CD spectra of the aldimine ligands, using the diamagnetic  $\text{UO}_2^{2+}$  - entity as a chiroptical probe. The  $L \rightarrow M$   $\pi$  - bonding ability of the  $\text{UO}_2^{2+}$  - entity as evident from  $^1\text{H}$  NMR data, may be valuable for a search of  $\text{UO}_2^{2+}$  - complexes with purposefully modified chemical / physical behaviour. These uranyl complexes react with  $\text{Na}_2\text{SO}_3$ , undergoing reduction to the  $\text{U}^{\text{IV}}$  state with second order rate constants. The kinetic data are at par with the available literature data. The novelty of this work is the kinetic aspect where the two step reduction of the  $\text{UO}_2^{2+}$  - entity to the  $\text{U}^{\text{IV}}$  state, is distinctly presented.

Before closing the concluding remark, the author feels that the investigations presented in this thesis will be helpful to the researchers working in the field of molybdenum – pterin chemistry in particular and coordination chemistry of redox “non-innocent” ligands in general.

## **REFERENCES**

## References

- (a) McMaster J and Enemart JH 1998 *Curr. Opinion Chem. Biol.* **2** 201;  
(b) Enemark JH and Garner CD 1997 *J. Biol. Inorg. Chem* **2** 817;  
(c) Collision D, Garner CD and Joule JA 1996 *Chem. Soc. Rev.* **25** 25.
- Stiefel EI 1996 *Science* **272** 1599.
- (a) Fischer B, Schmale HW, Baumgartner MR and Viscontini M 1997 *Helv. Chim. Acta* **80** 103 ;  
(b) Fischer B, Schmale H, Dubler E, Schafer A and Viscontini M 1995 *Inorg. Chem.* **34** 5726 ;  
(c) Fischer B, Strahle J and Viscontini M 1991 *Helv. Chim. Acta* **74** 1544.
- Kaim W 1987 *Rev. Chem. Intermediates* **8** 247.
- (a) Perkinson J, Brodie S, Yoon K, Mosny K, Carroll PJ, Morgan TV and Burgmayer SJN 1991 *Inorg. Chem.* **30** 719 ;  
(b) Burgmayer SJN and Stiefel EI 1988 *Inorg. Chem.* **27** 4059.
- (a) Matsuura S, Nawa S, Kakizawa H and Hirata Y 1953 *J. Am. Chem. Soc.* **75** 4446 ;  
(b) Korte F and Wallace R 1964 *Pteridine Chemistry (eds) W Pfeleiderer and EC Taylor (Oxford : Pergamon) pp 75 – 86 ;*  
(c) Schircks B, Bieri JH and Viscontini M 1985 *Helv. Chim. Acta* **68** 1639 ;  
(d) Russell JR, Garner CD and Joule JA 1992 *Synlett.* 711.
- (a) Craig JA, Harlan EW, Snyder BS, Whitener MA and Holm RH 1989 *Inorg. Chem.* **28** 2082 ;  
(b) Rajan OA and Chakravorty A 1981 *Inorg. Chem.* **20** 660 ;
- (a) Holm RH 1990 *Coord. Chem. Rev.* **100** 183 ;  
(b) Craig JA and Holm RH 1989 *J. Am. Chem. Soc.* **111** 2111 ;  
(c) Schultz BE and Holm RH 1993 *Inorg. Chem.* **32** 4244 ;  
(d) Holm RH and Berg JM 1984 *Pure Appl. Chem.* **56** 1645.
- (a) Vogel AI 1978 *Textbook of Practical Organic Chemistry* 4<sup>th</sup> edn. (London : Longman / ELBS) Chap.2 ;  
(b) Perrin DD and Armarego WLF 1988 *Purification of Laboratory Chemicals* 3<sup>rd</sup> edn. (Oxford : Pergamon).
- (a) Bellas M and Suschitzky H 1963 *J. Chem. Soc.* 4007 ;  
(b) Carde RN, Hayes PC, Jones G and Cliff CJ 1981 *J. Chem. Soc., Perkin Trans.* **1** 1132.

11. Sawyer DT and Roberts JL Jr. 1974 *Experimental Electrochemistry for Chemists* (New York : Wiley) pp 212.
12. (a) Schafer A, Fisher B, Paul H, Paul R, Bosshard R, Hesse M and Viscontini M 1992 *Helv. Chim. Acta.* **75** 1955 ;  
(b) Feichtinger D and Plattner DA 1997 *Angew. Chem., Int. Ed. Engl.*, **36** 1718.
13. Geary WJ 1971 *Coord. Chem. Rev.* **7** 110.
14. Ebsworth EAV, Rankin DWH and Cradock S 1987 *Structural Methods in Inorganic Chemistry* (Oxford : Blackwell / ELBS) pp 349.
15. Young CG 1995 *J. Chem. Edu.* **72** 751.
16. (a) Soyka R, Pfeleiderer W and Prewo R 1990 *Helv. Chim. Acta* **73** 808 ;  
(b) Soyka R and Pfeleiderer W 1990 *Pteridines* **2** 63.
17. (a) Bhattacharjee S and Bhattacharyya RG 1992 *J. Chem. Soc., Dalton Trans.* 1357 ;  
(b) Bhattacharjee S and Bhattacharyya RG 1993 *J. Chem. Soc., Dalton Trans.* 1151.
18. (a) Gibson VC, Redshaw C, Walker GLP, Howard JAK, Hoy VJ, Cole JM, Kuzmina LG and De Silva DS 1999 *J. Chem. Soc., Dalton Trans.* 161 ;  
(b) Bazhenova TA, Bazhenova MA, Petrova GN, Shilova AK and Shilov AE 1998 *Russ. Chem. Bull.* **47** 861.
19. Stiefel EI 1977 *Prog. Inorg. Chem.* **22** 1 – 223.
20. (a) Burgmayer SJN, Arkin MR, Bostick L, Dempster S, Everett KM, Layton HL, Paul KE, Rogge C and Rheingold AL 1995 *J. Am. Chem. Soc.* **117** 5812 ;  
(b) Kaufmann HL, Sands LL, Rheingold AL and Burgmayer SJN 1999 *Inorg. Chem.* **38** 2592 ;  
(c) Kaufmann HL, Carroll PJ and Burgmayer SJN 1999 *Inorg. Chem.* **38** 2600 ;  
(d) Burgmayer SJN, Kaufmann HL, Fortunato G, Hug P and Fischer B 1999 *Inorg. Chem.* **38** 2607.
21. (a) Bastian NR, Kay CJ, Barber MJ and Rajagopalan KV 1991 *J. Biol. Chem.* **266** 45 ;  
(b) Wuebbens MM and Rajagopalan KV 1993 *J. Biol. Chem.* **268** 13493 ;  
(c) Kim JH and Hille R 1993 *J. Biol. Chem.* **268** 44.
22. (a) Ochiai EI 1977 *Bioinorganic Chemistry* (Boston : Allyn and Bacon) pp 27 ; 402 – 407.  
(b) Das SK, Chaudhury PK, Biswas D and Sarkar S 1994 *J. Am. Chem. Soc.* **116** 9061.

23. (a) Berg JM and Holm RH 1985 *J. Am. Chem. Soc.* **107** 917 – 925 ;  
 (b) Caredonna JP, Reddy PR and Holm RH 1988 *J. Am. Chem. Soc.* **110** 2139.
24. Wilkins RG 1991 *Kinetics and Mechanism of Reactions of Transition Metal Complexes 2-nd edn.* (Weinheim : VCH) pp 87, 105.
25. Vogel AI 1978 *Textbook of Quantitative Inorganic Analysis 4-th edn.* (England : Longman / ELBS) pp 378, 472, 489.
26. Enemark JH and Young CG 1993 *Adv. Inorg. Chem.* **40** 1.
27. Burgmayer SJN and Stiefel EI 1986 *J. Am. Chem. Soc.*, **108** 8310.
28. Pfeleiderer W, Katritzky AR and Rees CW 1984 *Comprehensive Heterocyclic Chemistry, Ed. Vol. 3*, Pergamon press, Oxford pp 276.
29. Holm RH 1987 *Chem. Rev.*, **87** 1401.
30. (a) Drew MGB and Kay A 1971 *J. Chem. Soc. (A)*, 1846 ;  
 (b) Kay A and Mitchell P.C.H. 1972 *J. Chem. Soc., Dalton Trans* 1388.
31. (a) Swedo KB and Enemark JH 1979 *J. Chem. Edu.*, **56** 70 ;  
 (b) Yamananchi K and Enemark JH 1978 *Inorg. Chem.*, **17** 1981.
32. Knox JR and Pront CK 1968 *Chem. Commun.*, 1227.
33. Malinak SM and Conconvanis 1996 *Inorg. Chem.*, **35** 4810.
34. (a) Ali Md. A and Roy Parag S 2001 *Proc. Indian Acad. Sci. (Chem. Sci.)*, **113** No.2, 77 – 87.  
 (b) Ali Md. A and Roy Parag S 2002 *Trans. Met. Chem.*, **27** 366 – 371.
35. Albelleira A, Galang RB and Clarke MJ 1999 *Inorg. Chem.* **29** 633.
36. Spiro TG 1985 *Molybdenum Enzymes*, pp 353, 451.
37. Xin X, Jin G, Wang B and Pope MT 1990 *Inorg. Chem.*, **29** 553.
38. Spivack B, Dori Z and Stiefel EI 1975 *Inorg. Nucl. Chem. Lett.*, **11** 501.
39. Glowiak T, Sabat M, Sabat H and Rudolf MF 1975 *J. C. S., Chem. Comm.*, 712.
40. (a) Chen GJJ, McDonald JW and Newton WE 1976 *Inorg. Chem.*, **15** 2612.  
 (b) Banerjee AK and Saha HK 1974 *Inorg. Synth.*, **15** 100.  
 (c) Saha HK and Halder MC 1971 *J. Inorg. Nucl. Chem.*, **33** 3719 ; 1972 **34** 3097.

- (d) McDonald JW, Friesen GD, Rosenhein LD and Newton WE 1983 *Inorg. Chim. Acta.*, **72** 205.
- (e) Fuchs J and Hartl H 1976 *Angew Chem. Int. Ed. Engl.*, **5** No.6, 375 – 376.
- (f) Young CG 1995 *J. Chem. Edu.*, **72** 751.
41. Burgmayer SJN and Stiefel EI 1985 *J. Chem. Edu.*, **62** 943.
42. Young CG 1997 *J. Biol. Inorg. Chem.*, **2** 810.
43. Geary WJ 1971 *Coord. Chem. Rev.*, **7** 81 – 122.
44. Richard L, Martin C, Wiest R and Weiss R 1975 *Inorg. Chem.*, **14** 2301.
45. Gatehouse BM, Nunn EK, Guerchains JE and Kergoat R 1976 *Inorg. Nucl. Chem., Lett.*, **12** 23.
46. Yan J 2001 *Isotope Pattern Calculator*, v 4.0.
47. Vogel AI 1987 *Elementary Practical Organic Chemistry part III, Quantitative Organic Analysis*, CBS Publishers & Distributers, New Delhi, pp 694.
48. Sen S and Roy PS 2005 *Trans. Met. Chem.*, **30** 797.
49. Johnson JL and Rajagopalan KV 1982 *Proc. Natl. Acad. Sci. USA*, **79** 6856.
50. Kramer SP, Johnson JL, Ribeiro AA, Millington DS and Rajagopalan KV 1987 *J. Biol. Chem.*, **262** 16357.
51. Johnson ME and Rajagopalan KV 1987 *J. Bacteriology* **169** 117.
52. (a) Johnson JL 1980 *Molybdenum and Molybdenum Containing Enzymes*, ed. Coughlan M.P., Pergamon Press Ltd., Oxford, Ch.10 and pp 371.
- (b) Pope MT, Still ER and Williams RJP 1980 *Molybdenum and Molybdenum Containing Enzymes*, Ed. Coughlan MP, Pergamon Press Ltd., Oxford, Ch.1.
53. Cramer SP and Stiefel EI 1985 *Molybdenum Enzymes*, ed. Spiro TG, Wiley John & Sons, New York, Ch.8.
54. Spence JT 1983 *Coord. Chem. Rev.*, **48** 59.
55. Garner CD and Bristow S 1985 *Molybdenum Enzymes*, ed. Spiro TG, Wiley John & sons, New York, Ch.7.
56. Bowden FL 1975 *Techniques and Topics in Bioinorganic Chemistry*, ed. McAuliffe CA ; The Macmillan Press Ltd., London, pp 205 – 267.

57. Wentworth RAD 1976 *Coord. Chem. Rev.* **18** 1.
58. Kaul BB, Enemark JH, Merbs SL and Spence JT 1985 *J. Am. Chem. Soc.*, **107** 2885.
59. Kay CJ, Barber MJ and Solomonson LP 1988 *Biochemistry*, **27** 6142.
60. Hille R and Massey V 1985 *Molybdenum Enzymes*, ed. Spiro TG, Wiley John & sons, New York, Ch. 9, pp 443.
61. Chang CSJ, Collison D, Mabbs FE and Enemark JH 1990 *Inorg. Chem.*, **29** 2261.
62. Lincoln S and Koch SA 1986 *Inorg. Chem.*, **25** 1594.
63. Blake AB, Cotton FA and Wood JS 1964 *J. Am. Chem. Soc.*, **86** 3024.
64. Andruchow W, Jr. and Archer RD 1972 *J. Am. Chem. Soc.*, **34** 3185.
65. Hare CR, Bernal I and Gray HB 1962 *Inorg. Chem.*, **1** 831.
66. Suzuki KZ, Sasaki Y, Ooi S and Saito K 1980 *Bull. Chem. Soc. Jpn.*, **53** 1288.
67. Saha HK and Halder MC 1971 *J. Inorg. Nucl. Chem.*, **33** 3719.
68. Ott VR, Swieter DS and Schultz FA 1977 *Inorg. Chem.*, **16** 2538.
69. Silverstein RM, Bassler GC and Morrill TC 1981 *Spectrometric Identification of Organic Compounds*, 4<sup>th</sup> edn., Wiley John & Sons, New York.
70. Bellamy LJ 1975 *The Infrared Spectra of Complex Molecules*, 3<sup>rd</sup> edn. Chapman and Hall, London.
71. Garner CD, Buchanan I, Collison D Mabbs FE, Porter TG and Wynn CH 1982 *Proceedings of the Fourth International Conference on Chemistry and Uses of Molybdenum*, ed. Mitchell PCH and Barry HF, Climax Molybdenum Co., Michigan, pp 163.
72. Deacon GB and Phillips RJ 1980 *Coord. Chem. Rev.*, **33** 227.
73. Bere A and Helene C 1979 *Biopolymers*, **18** 2659.
74. Holm RH 1973 *Inorganic Biochemistry*, vol. 1 and 2, ed. Eichhorn GL, Elsevier Scientific Publishing Co., New York, Ch. 31.
75. Hämäläinen R, Ahlgren M, Turpeinen U and Rantala M 1978 *Acta Chem. Scand.*, **A32** 235, 549.

76. Chen GJJ, McDonald JW, Bravard DC and Newton WE 1985 *Inorg. Chem.*, **24** 2327.
77. Barber MJ and Salerno JC 1980 *Molybdenum and Molybdenum Containing Enzymes*, ed. Coughlan MP, Pergamon Press Ltd., Oxford, Ch. 18.
78. Isbell AF, Jr., and Sawyer DT 1971 *Inorg. Chem.*, **10** 2449.
79. Smith HE 1983 *Chem. Rev.*, **83** 359.
80. Schultz BE and Holm RH 1993 *Inorg. Chem.*, **32** 4244.
81. (a) Chan MK, Mukund S, Kletzin A, Adams MWW and Rees DC 1995 *Science*, **267** 1463 ;  
(b) Johnson MK, Rees DC and Adams MWW 1996 *Chem. Rev.*, **96** 2817.
82. (a) Dix TA and Benkovic SJ 1988 *Acc. Chem. Res.*, **21** 101 ;  
(b) Ochiai EI 1997 *Bioinorganic Chemistry*, Allyn and Bacon, Inc., Boston, pp 211.
83. Burgmayer SJN, Baruch A, Kerr K and Yoon K 1989 *J. Am. Chem. Soc.*, **111** 4982.
84. (a) Mengel R, Pfeleiderer W and Knappe WR 1977 *Tetrahedron Lett.*, 2817 ;  
(b) Pfeleiderer W 1992 *J. Heterocycle Chem.*, **29** 583.
85. Silverstein RM, Webster FX 2005 *Spectroscopic Identification of Organic Compounds*, 6<sup>th</sup> Edn. John Wiley & Sons, New York.
86. (a) Leach R Andrew 2001 *Molecular Modelling Principles and Applications*, 2<sup>nd</sup> Edn. Pearson Education Ltd., Ch. 4;  
(b) Allinger NL 1977 *J. Am. Chem. Soc.*, **99** 8127 ;  
(c) Zimmer H 1995 *Chem. Rev.*, **95** 2629.
87. *Chem. Office 2004 & 2005, Chem3D Ultra, version 8.0 & higher*, Cambridge Soft Corporation, 100 Cambridge Park Drive, Cambridge, MA 02140 – 9802, USA.
88. (a) Beddoes RL, Russell JR, Garner CD and Joule JA 1993 *Acta Cryst.*, **C49** 1649 – 1652.  
(b) Soyka R, Pfeleiderer W and Prewo R 1990 *Helv. Chim. Acta*, **73** 808.
89. Samar KD, Biswas D, Maiti R and Sarkar S 1996 *J. Am. Chem. Soc.*, **118** 1387 – 1397.
90. (a) Iwanami Y 1971 *Bull. Chem. Soc. Japan*, **44** 1314 – 1316.  
(b) Iwanami Y 1972 *Bull. Chem. Soc. Japan*, **45** 2829 – 2834.

- (c) George GN, Garrett RM, Prince RC and Rajagopalan KV 1996 *J. Am. Chem. Soc.*, **118** 8588 – 8592.
91. Dyer JR 1987 *Application of Absorption Spectroscopy of Organic Compounds*, Prentice – Hall of India Pvt. Ltd., New Delhi, pp 114 – 122, 125.
92. Casellato U, Vidali M and Vigato PA 1976 *Inorg. Chim. Acta.*, **18** 77.
93. Tsai MD, Byrn SR, Chang C, Heinz GF and Weintraub HJR 1978 *Biochemistry*, **17** 3177.
94. Casellato U, Guerriero P, Tamburini S, Vigato PA and Graziani R 1990 *J. Chem. Soc., Dalton Trans.*, 1533.
95. Abraham RJ and Loftus P 1980 *Proton and Carbon NMR Spectroscopy*, Heyden and Son Ltd., London, pp 42 – 51.
96. Siddall TH and Prohaska CA 1965 *Inorg. Chem.*, **4** 783 ; Pedrosa JD and Gil VMS 1974 *J. Inorg. Nucl. Chem.*, **36** 1803 ; Kim BI, Miyake C and Imoto S 1974 *J. Inorg. Nucl. Chem.*, **36** 2015.
97. Baker BC and Sawyer DT 1968 *Anal. Chem.*, **40** 1945.
98. Cattalini L, Croatto U, Degetto S and Tondello E 1971 *Inorg. Chim. Acta. Rev.*, **5** 19.
99. Castellano S, Gunther H and Ebersole 1965 *J. Phys. Chem.*, **69** 4166.
100. Miller JD and Prince RH 1965 *J. Chem. Soc.*, 4706.
101. Hawkins CJ and Palmer JA 1982 *Coord. Chem. Rev.*, **44** 1.
102. Pasini A, Gullotti M and Cesarotti E 1972 *J. Inorg. Nucl. Chem.*, **34** 3821.
103. McGlynn SP, Smith JK and Neely WC 1961 *J. Chem. Phys.*, **35** 105; McGlynn SP and Smith JK 1961 *J. Mol. Spectrosc.*, **6** 164 ; Denning RG, Snellgrove TR and Woodwork DR 1979 *Mol. Phys.*, **37** 1109.
104. Das SK, Choudhury PK, Biswas D and Sarkar S 1994 *J. Am. Chem. Soc.*, **116** 9061.
105. Lintvedt RL, Lynch WE and Zehetmair JK 1990 *Inorg. Chem.*, **29** 3009 ; Zanello P, Cinquantini A, Guerriero P, Tamburini S and Vigato PA 1986 *Inorg. Chim. Acta.*, **117** 91.
106. Huber W and Müllen K 1986 *Acc. Chem. Res.*, **19** 300 ; Osvath P and Lappin

- AG 1986 *J. Chem. Soc., Chem. Commun.*, 1056 ; Bernardo MM, Schroeder RR and Rorabacher DB 1991 *Inorg. Chem.*, **30** 1241 ; Chang CSJ and Enemark JH 1991 *Inorg. Chem.*, **30** 683 ; Chang CSJ, Collison D, Mabbs FE and Enemark JH 1990 *Inorg. Chem.*, **29** 2261.
107. Kemp W 1991 *Organic Spectroscopy, Third Edition*; Palgrave, U. K. p. 293 – 299, pp 303 – 325.
108. Carrano CJ, Chohan BS, Hammes BS, Kail BW, Nemykin VN and Basu P 2003 *Inorg. Chem.*, **42** 5999 – 6007.
109. Dutta SK, McConville DB, Youngs WJ and Chaudhury M 1997 *Inorg. Chem.*, **36** 2517 – 2522.
110. Davices ES, Baddoes RL, Collison D, Dinsmore A and Garner CD 1997 *J. Chem. Soc., Dalton Trans.*, 3985 – 3995.
111. Allinger NL 1977 *J. Am. Chem. Soc.*, **99** 8127 – 8134.
112. Zimmer M 1995 *Chem. Rev.*, **95** 2629.
113. Peariso K, McNaughton RL and Kirk ML 2002 *J. Am. Chem. Soc.*, **124** 9006 – 9007.
114. Kohznma T, Masuda H and Yamanchi O 1989 *J. Am. Chem. Soc.*, **111** 3431.
115. Odani A, Masuda H, Inukai K and Yamanchi O 1992 *J. Am. Chem. Soc.*, **114** 6294.
116. Nasir MS, Karlin KD, Chem Q and Zubietta J 1992 *J. Am. Chem. Soc.*, **114** 2264.
117. Williams DH and Fleming I 1989 *Spectroscopic Methods in Organic Chemistry, 4<sup>th</sup> Edition*, McGraw – Hill International (U.K.).
118. Andraos J 1999 *J. Chem. Edu.*, **76** 258.
119. Burgmayer SJN 1998 *Structure and Bonding*, **92** 67.
120. Russell JR, Garner CD and Joule JA 1992 *J. Chem. Soc., Perkin Trans.*, **1** 1245 ; Dinsmore A, Birks JH, Garner CD and Joule JA 1997 *J. Chem. Soc., Perkin Trans.*, **1** 89,801.
121. Cotton R and Traeger JC 1992 *Inorg. Chim. Acta*, **201** 153 ; Curtis JM, Derrick PJ, Schnell A, Constantin E, Gallagher RT and Chapmen JR 1992 *Inorg. Chim. Acta*, **201** 197 ; Falaras P, Mitsopoulou CA, Argyropoulos D, Lyris E, Psaroudakis N, Vrachnon E and Kotakis D 1995 *Inorg. Chem.*, **34** 4536 ; Basu

- P, Nemykin VN and Sengar RS 2003 *Inorg. Chem.*, **42** 7489.
122. Boyd IW and Spence JT 1982 *Inorg. Chem.* **21** 1602.
123. Bieri JH, Hummel WP and Viscontini M 1976 *Helv. Chim. Acta*, **59** 2374.
124. Mandelli R and Merlini L 1966 *Tetrahedron*, **22** 3253.
125. Campbell MJM 1975 *Coord. Chem. Rev.*, **15** 279
126. McNamara JP, Joule JA, Hitler IH and Garner CD 2005 *Chem. Commun.* 177.
127. Crispini A, Pucci D, Bellusci A, Barberio G, Deba ML, Cataldi A and Ghedini M 2005 *Crystal Growth & Design*, **5** 1597 – 1601 ; Bieri JH, Hummel W and Viscontini M 1976 *Helv. Chem. Acta.*, **59** 2374 – 2382.
128. Knox JR, Pront CK 1969 *Acta Cryst.*, **B25** 1857.
129. Delbaere LTJ and Pront CK 1971 *Chem. Commun.*, 162.
130. Yamananchi K and Enemark JH 1978 *Inorg. Chem.*, **17** 1981.
131. Drew MGB and Kay A 1971 *J. Chem. Soc.*, (A), 1851.
132. Buchanan I, Minelli M, Ashby MT, King TJ, Enemark JH and Garner CD 1984 *Inorg. Chem.*, **23** 495.
133. Drew MGB and Kay A 1971 *J. Chem. Soc.*, (A), 1846
134. Gibson VC, Redshaw C, Walker GLP, Howard JAK, Hoy VJ, Cole JM, Kuzmina LG and De Silva CS 1999 *J. Chem. Soc., Dalton Tran.*, 161.
135. McNamara JP, Joule JA, Hillier IH and Garner CD 2005 *Chem. Commun.*, 177.
136. Kneale GG, Geddes AJ, Sasaki Y, Shibahara Tand Sykes AG 1975 *J. Chem. Soc., Chem. Commun.*, 356.
137. Kamenar B, Penavic M and Markovic B 1984 *Croat. Chem. Acta*, **57** 637 ; cited in R. Cotton, 1988 *Coord. Chem. Rev.*, **90** 29.
138. Garner CD, Nicholson JR and Clegg W 1984 *Angew. Chem. Int., Ed. Engl.*, **23** 972.
139. Stevenson DL and Dahl LF 1967 *J. Am. Chem. Soc.*, **89** 3721.

140. (a) Spivack B and Dori Z 1973 *J. Chem. Soc., Dalton Trans.*, 1173 ; (b) Spivack B and Dori Z 1975 *J. Chem. Soc., Dalton Trans.*, 1077.
141. Cotton FA and Wilkinson G 1988 *Advanced Inorganic Chemistry, 5<sup>th</sup> Ed.*, John Wiley & Sons, New York, pp 53 – 56, 987 – 1010.
142. (a) Cotton R 1988 *Coord. Chem. Rev.*, **90** 29 ; (b) Nixon DM 1994 *Coord. Chem. Rev.*, **134** 1 ; (c) Morris MJ 1995 *Coord. Chem. Rev.*, **138** 121 ; (d) Morris MJ 1995 *Coord. Chem. Rev.*, **146** 43 ; (e) Morris MJ 1997 *Coord. Chem. Rev.*, **164** 289 ; (f) Morris MJ 1998 *Coord. Chem. Rev.*, **172** 181.
143. (a) March J 2005 *Advanced Organic Chemistry, 4<sup>th</sup> Ed.*, John Wiley & Sons (Asia) Pvt. Ltd., Singapore, Ch. 19; (b) March J 1988 *Advanced Organic Chemistry, 3<sup>rd</sup> Ed.*, Wiley Eastern Ltd, New Delhi, Ch. 19 ; (c) March J 1968 *Advanced Organic Chemistry*, McGraw Hill Book Co., New York, Ch. 19.
- 144.(a) Sharma A and Schulman SG 1999 *Introduction to Fluorescence Spectroscopy*, John Wiley & Sons, Inc, New York, p. 55 – 57 ; (b) Willard HH, Merritt LL, Dean JA and Settle FA 1986 *Instrumental Methods of Analysis, 6<sup>th</sup> Ed.*, CBS Publishers, Delhi, 1986, Ch. 4 ; (c) Rohatgi – Mukherjee KK 1986 *Fundamentals of Photochemistry*, New Age International Pvt. Ltd., Publishers, New Delhi, pp140.
145. (a) Pitterle DM, Johnson JL and Rajagopalan KV 1993 *J. Biol. Chem.*, **268** 13506; (b) Bastian NR, Kay CJ, Barber MJ and Rajagopalan KV 1991 *J. Biol. Chem.*, **266** 45 ; (c) Gardlic S and Rajagopalan KV 1991 *J. Biol. Chem.*, **266** 4889.
146. Panchanan S 1994 “*Studies on coordination compounds of dioxouranium (VI) and molybdenum with ligands derived from amino acids [especially with imidazole amine and amide R groups]*”, Ph. D. thesis, University of North Bengal.
147. Delbaere LTJ and Prout CK 1971 *Chem. Commun.*, 162.
148. Carrano CJ, Chohan BS, Hammes BS, Kail BW, Nemykin VN and Basu P 2003 *Inorg. Chem.*, **42** 5999.
149. Peariso K, McNaughtan RL and Kirk ML 2002 *J. Am. Chem. Soc.*, **124** 9006.
150. McNamara JP, Joule JA, Hiller IH and Garner CD 2005 *Chem. Commun.*, 177, together with the supplementary information.
151. Baird DM, Rheingold AL, Croll SD and DiCenso AT 1986 *Inorg. Chem.*, **25** 3458.

152. Eliel EL 1962 "*Stereochemistry of carbon compounds*", McGraw – Hill Book Co. Inc, New York, pp 16 – 18.
153. Cotton FA, Morehouse SM and wood JS 1964 *Inorg. Chem.*, **3** 1603.
154. Wieghardt K, Backes – Dahmann G, Herrmann W and Weiss J 1984 *Angew Chem., Int, Ed, Engl.*, **23** 899.
155. Panchanan S, Hämäläinen R and Roy PS 1994 *J. Chem. Soc., Dalton Trans.*, 2381.
156. Dutta RL and Syamal A 1993 "*Elements of Magnetochemistry*" 2<sup>nd</sup> Ed., Affiliated East – West Press Pvt. Ltd., pp 241 – 242.
157. (a) The EPR spectra were simulated using EPPROW program originally developed by White LK and Belford RL and later modified by White LK and Chasteen ND.  
(b) White LK and Belford RL 1976 *J. Chem. Soc.*, **98** 4428 ; White LK and Chasteen ND 1979 *J. Phys. Chem.*, **83** 279.
158. Hille R and Massey V 1985 "*Molybdenum Enzymes*", ed. Spiro TG, John Wiley & Sons, New York, pp 451.
159. Caradonna JP, Reddy PR and Holm RH 1988 *J. Am. Chem. Soc.*, **110** 2139.
160. Meyer O 1982 *J. Biol. Chem.*, **257** 1333.
161. Coughlan MP 1980 "*Molybdenum and molybdenum – containing enzymes*", Pergamon Press, Oxford, pp 168, 371.
162. Hille R and Massey V 1985 "*Molybdenum Enzymes*", Ed. Spiro TG, John Wiley & Sons, New York, pp 451.
163. Baird DM, Falzone S and Haky JE 1989 *Inorg. Chem.*, **28** 4561.
164. Shriver DF and Drezdhan MA "*The manipulation of air – sensitive compounds*", 2<sup>nd</sup> ed., John Wiley & Sons, New York, 1986.
165. Cotton FA, Wilkinson G, Murillo CA and Bochman M 1999 "*Advanced Inorganic Chemistry*", 6<sup>th</sup> ed., John Wiley & Sons Inc, Ch. 20, pp 526 – 527.
166. "*Gmelin Handbook of Inorganic Chemistry*", 1992 U. suppl., Vol. A6, Springer, Berlin.
167. Denning RG 1992 *Structure and Bonding*, **79** 215.

168. Cornehl HH, Heinemann C, Marcalo J, Matos AP and Schwarz H 1996 *Angew. Chem., Int. Ed. Engl.*, **35** 891.
169. Buhl M and Kabrede H 2006 *Inorg. Chem.*, **45** 3834.
170. Kannan S, Moody MA, Barnes CL and Duval PB 2006 *Inorg. Chem.*, **45** 9206.
171. Bertke JA and Bunge SD 2007 *Dalton Trans.*, 4647.
172. Fenton DE and Vigato PA 1988 *Chem. Soc. Rev.*, **17** 69.
173. Burrell AK, Cyr MJ, Lynch V and Sessler JL 1991 *J. Chem. Soc., Chem. Commun.*, 1711.
174. Ali Md. A, Panchanan S, Hämäläinen R and Roy PS, a manuscript is being finalized for publication in a suitable journal.
175. Charlot G and Bezier D (transl. R. C. Murray) 1957 "*Quantitative Inorganic Analysis*", Methue, London, pp 309, 619.
176. Wang WD, Bakac A and Espenson JH 1995 *Inorg. Chem.*, **34** 6034.
177. Mao Y and Bakac A 1996 *Inorg. Chem.*, **35** 3925.
178. Burrows HD 1990 *Inorg. Chem.*, **29** 1549.
179. Sen S, Ghosh B and Roy PS 2007 *Trans. Met. Chem.*, **32** 737.
180. Ghosh B and Roy PS 2007 *Ind. J. Chem.*, **46A** 1585.
181. (a) Maurya RC, Chaurasia J and Sharma P 2007 *Ind. J. Chem.*, **46A** 1594  
(b) Maurya RC, Pandey A and Sutradhar D 2004 *Ind. J. Chem.*, **43A** 763.
182. Sessler JL, Gebaner A, Hoehner MC and Lynch V 1998 *Chem. Commun.*, 1835.
183. Hennig C, Panak PJ, Reich T, Roberg A, Raff J, Selenska - Pobell S, Matz W, Buchner JJ, Bernhard G and Nitsche H 2001 *Radiochimic Acta*, **89** 625.
184. Beira khov A, Orlova I, Ilin E, Gorbunova Y and Mikhailov Y 2007 *Russian Journal of Inorganic Chemistry*, **52** 34.
185. Bharara MS, Strawbridge K, Vilsek JZ, Brag TH and Gordan AEV 2007 *Inorg. Chem.*, **46** 8309.
186. Nockemann P, Servoes K, Deun RV, Hecke KV, Meervelt LV, Binnemans K

- and Gorller - walrand C 2007 *Inorg. Chem.*, **46** 11335.
187. Hille R 1996 *Chem. Rev.*, **96** 2757.
188. Manikandan P, Ellis P, Kuhn P, Choi EY, Hoffman B and Hille R 2002 *Ind. J. Chem.*, **41** 22.
189. Enemark JH, Cooney JJA, Wang JJ and Holm RH 2004 *Chem. Rev.*, **104** 1175.
190. Mendel RR 2005 *J. Chem. Soc., Dalton Trans.*, 3404.
191. Burgmayer SJN 2004 *Prog. Inorg. Chem.*, **52** 491.
192. McMaster J, Tunney JM and Garner CD 2004 *Prog. Inorg. Chem.*, **52** 539.
193. (a) Ferreira K, Iversan T, Maghlaoui K, Barber J and Iwata S 2004 *Science*, **303** 1831; (b) Robblee J, Cinco R and Yachandra V 2001 *Biochimica et Biophysica Acta*, **1503** 7 ; (c) Ananyev G, Zaltsman L, Vasko C and Dismukes G 2001 *Biochimica et Biophysica Acta*, **1503** 52.
194. Kappock TJ and Caradonna JP 1996 *Chem. Rev.*, **96** 2659.
195. Nemykin VN, Davie SR, Mondal S, Rubie N, Kirk ML, Somogyi A and Basu P 2002 *J. Am. Chem. Soc.*, **124** 756 – 757.
196. Brewster RQ and McEwen 1968 *Organic Chemistry*, 3<sup>rd</sup> Ed., Prentice Hall of India Pvt. Ltd., pp 36, 68, 157 – 159, 194 – 198, 223, 314.
197. Lorber C, Plutino MS, Elding LI and Nordlander E 1997 *J. Chem. Soc., Dalton Trans.*, 3997.
-

## Functional model of oxomolybdoenzymes: Synthesis and characterization of a molybdenum complex with sulphur and pterin ligands exhibiting saturation kinetics with pyridine N-oxide

MD AFSAR ALI and PARAG S ROY\*

Department of Chemistry, University of North Bengal, Dist. Darjeeling  
734 430, India  
e-mail: paragsroy@hotmail.com

MS received 30 September 2000

**Abstract.** Redox reaction between 6-acetylisoanthopterin ( $H_2pte$ ) and  $[Mo^{VI}O_2(ssp)]$  [ $ssp =$  anion of 2-(saliicylideneamino) benzenethiol] in  $CH_3OH-C_2H_5OH$  medium produces a new mixed ligand compound  $[Mo^{IV}(ssp)(Hpte)(OCH_3)]$  (**1**). It has been characterized by elemental analysis, ESMS data, UV-Vis, IR,  $^1H$  NMR (1D and 2D) spectroscopy and cyclic voltammetry. Kinetics of formation of this compound as well as that of its reaction with pyridine N-oxide have been followed spectrophotometrically. Both the reactions follow substrate saturation kinetics and involve metal-centred oxygen atom transfer process. Large negative values of entropy of activation indicate the operation of associative mechanism.

**Keywords.** Mixed ligand molybdenum (IV) compound with a 6-substituted pterin; model system of oxomolybdoenzymes; oxygen atom transfer reaction.

### 1. Introduction

Recent X-ray structural characterization of several oxomolybdoenzymes reveal that a special pyranopteria (molybdopterin, chart 1) is coordinated to the molybdenum atom through a dithiolene group<sup>1</sup>. It has been proposed that the  $Mo(O)$  (molybdopterin) moiety is the metal-centred functional unit for such enzymes and variations in properties of the metal centre occur with the binding of other ligands, e.g. a terminal oxo or sulphido group, OH and/or  $H_2O$  group(s), a second pterin, and/or a serine, a cysteine or selenocysteine group from the polypeptide backbone of the protein<sup>1,2</sup>. Such enzymes

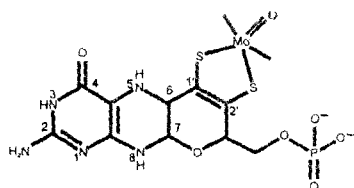


Chart 1.

\*For correspondence

catalyse formal hydroxylation, (1), and net oxygen atom transfer (OAT) reaction, (2), to and from a variety of biologically important substrates and the oxygen atom is ultimately derived from water<sup>1</sup>.



Alternatively, (1) and (2) may be regarded as coupled electron-proton transfer (CEPT) reactions. Intimate catalytic mechanisms proposed for (1) and (2) involve the coordination of water to the molybdenum atom to give Mo–OH<sub>2</sub>, Mo–OH or Mo=O species which cycle between the Mo(VI) and Mo(IV) oxidation states<sup>1(a)</sup>. The resolution of the X-ray crystal structures is insufficient for unambiguously resolving oxo, hydroxo and water ligands from one another, which leads to uncertainty in the oxidation state of the metal. Other limitations include uncertainty about the state of oxidation at the pyrazine ring carbon atoms, or at the side-chain sulphur-bearing carbon atoms. Hence the need for complementing the protein crystallographic results with spectroscopic data about the metal centres of these enzymes. In this context, the role of synthetic molybdenum-pterin compounds is vital for recording bench-mark data; development of such coordination chemistry will also enable accomplishment of chemical and electrochemical studies that are relevant and complementary for the study of the functional aspects of the enzyme catalytic centres<sup>1(b),1(c)</sup>. Besides these, considerable challenge lies ahead to achieve a clear description of how the nature of each of these metal centres changes during the operation of the enzyme's catalytic cycle as well as that of the corresponding molybdopterin moiety. For explaining the DMSO reduction capability of a synthetic Mo(IV)-pterin complex, Viscontini and co-workers<sup>3(b),4,5(a)</sup> proposed a model reaction cycle, which involves participation of the NH<sub>2</sub>(2) and NH(5) protons of the pterin ring (chart 1) associated with electronic redistribution in the latter as well as in the oxo groups attached to the molybdenum centre.

In view of the above perspectives, the present work embodies the redox reaction of 6-acetylisoxanthopterin<sup>6</sup> (H<sub>2</sub>pte, whose 7-oxo group corresponds to the pyran ring oxygen atom of molybdopterin, chart 2) with a well-established dioxomolybdenum (VI) compound<sup>7</sup>, [Mo<sup>VI</sup>O<sub>2</sub>(ssp)] [ssp = anion of 2-(salicylideneamino) benzenethiol], leading to the isolation of a new mixed ligand Mo(IV) compound in the solid state. Its reactivity towards pyridine N-oxide (a typical enzyme substrate) has also been studied for corroborating the assignment of oxidation state of the metal centre<sup>8</sup>.

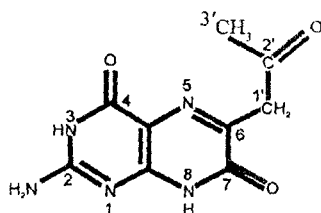


Chart 2.

## 2. Experimental

### 2.1 Materials

Reagent grade chemicals were used as received. Solvents were purified prior to use following the literature procedures<sup>9</sup>. Kinetic and electrochemical measurements were performed in spectroscopy grade DMF (SRL, Mumbai). 2-(Salicylideneamino) benzenethiol ( $H_2ssp$ ),  $[Mo^{VI}O_2(ssp)]$ , pyridine N-oxide ( $pyN \rightarrow O$ ) and tetrabutylammonium perchlorate (TBAP) were obtained by published methods<sup>7,10,11</sup>. 6-Acetylisoanthopterin ( $H_2pte$ ) was prepared by modifying its original method of synthesis in the light of subsequent developments (e.g. darkness,  $N_2$  atmosphere, pH 6.4)<sup>6</sup> and characterized through different physico-chemical methods including elemental analysis, ESMS data, 1D and 2D  $^1H$  NMR spectra<sup>12</sup>.

### 2.2 Synthesis of complex (1)

The complex (1),  $[Mo^{IV}(ssp)(Hpte)(OCH_3)]$  (chart 3) was synthesized as follows. 6-Acetylisoanthopterin (0.235 g, 1 mmol) in methanol (100 ml) was added to a suspension of  $[Mo^{VI}O_2(ssp)]$  (0.355 g, 1 mmol) in ethanol (50 ml), and stirred for 30 h at room temperature ( $\approx 301$  K), in darkness under dinitrogen atmosphere. The resulting chocolate-brown compound was filtered under dinitrogen using a fritte, washed with purged solvents (methanol, ether) and dried *in vacuo* over silica gel. Yield 50%. Its purity was checked through TLC (silica gel GF<sub>254</sub>; UV lamp) using diluted (with 50 times methanol) DMSO solution ( $\approx 0.5\%$ ) and benzene as eluant. Found: C, 47.10; H, 3.16; N, 14.52; S, 5.20%. Calc. for  $C_{23}H_{19}N_6O_5S$  Mo: C, 46.94; H, 3.23; N, 14.29; S, 5.44%. The  $\Lambda_M$  ( $20\text{ ohm}^{-1}\text{cm}^2\text{mol}^{-1}$ , 303 K, DMF) value is consistent with its nonelectrolyte nature<sup>13</sup>. ESMS data: the peak at  $m/z = 525.0$  (relative abundance = 100%), associated with the characteristic distribution of molybdenum isotopes (seven) for mononuclear species, corresponds to the fragment  $[M-CH_3OH-CH_3O$  (of 6-acetyl substituent)]<sup>+</sup>, where M is the molecular formula (M.W. 588)<sup>7(a),14,15</sup>. Its cyclic voltammogram is characterized by a single irreversible reduction peak  $[Mo(IV) - Mo(III)]$  at  $-0.82$  V ( $50\text{ mV s}^{-1}$ ); the pterin ligand ( $H_2pte$ ) itself undergoes reduction beyond  $-1.8$  V<sup>12</sup>. UV/Vis absorption bands [DMF,  $\lambda_{max}^{nm}$  ( $\log \epsilon$ ): 285 (4.23); 320 (4.16); 338 *sh* (4.13); 398 (3.85); 424 *sh* (3.70); 458 *sh* (3.46)].  $^1H$  NMR data [ $\delta$ ,  $d_5$ -DMSO, 300 MHz, tautomeric form of ( $Hpte'$ ) residue, scheme 2, involving =NH(2) and NH(1) protons]: 12.34 (1H, *s*, NH(8)), 10.96 (1H, *s*, NH(1)), 9.06 (1H, *s*, CH=N), 7.84–6.89 (8H, *m*, protons of ( $ssp^{2-}$ ) residue)<sup>12</sup>, 3.74 (2H, *s*,  $CH_2(1')$ ), 2.18 (3H, *s*,  $CH_3(3')$ ).

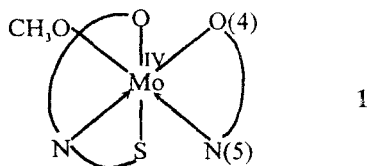
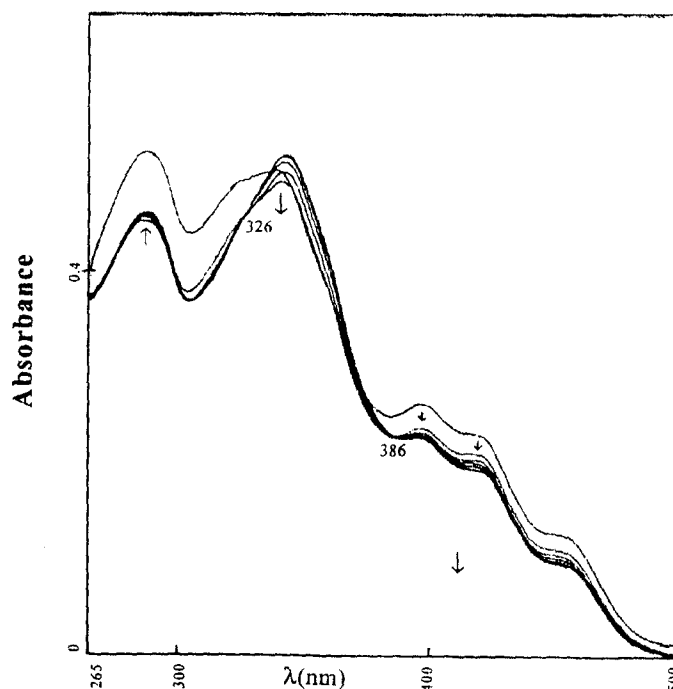


Chart 3.

### 2.3 Physical measurements and kinetic studies

Elemental analysis (C, H, N) data were obtained from the Indian Association for the Cultivation of Science, Kolkata, and sulphur was estimated by the Schöniger flask method.  $^1\text{H}$  NMR data in  $d_6$ -DMSO were obtained from IICB (Bruker, DPX, 300 MHz), Kolkata, RSIC (Bruker, DRX, 300 MHz), Lucknow and TIFR (Bruker, AMX, 500 MHz), Mumbai. The electrospray mass spectra in methanol were obtained from RSIC (Micromass Quattro II triple quadrupole mass spectrometer), Lucknow. IR spectra on nujol mull were recorded on a Philips Analytical SP3-300 spectrometer. Electrical conductivity in DMF ( $0.001 \text{ mol dm}^{-3}$ ) was measured using a digital conductivity meter (Systronics, model 304). Cyclic voltammetry data ( $1 \times 10^{-3} \text{ mol dm}^{-3}$  in DMF:  $0.1 \text{ mol dm}^{-3}$  TBAP, uncorrected for the junction contribution) were recorded under purified dinitrogen atmosphere on a BAS (CV-27), USA instrument using a BAS planar platinum-inlay working electrode, a platinum-wire auxiliary electrode and a saturated calomel electrode (SCE). Electronic spectra and kinetic data (under dinitrogen atmosphere) were recorded on a Shimadzu (UV-240) spectrophotometer, with thermostatic condition ( $\pm 0.5 \text{ K}$ ) being maintained using a Shimadzu (TB-85) thermostat. Figure 1 demonstrates the absorption spectral changes associated with the reaction of  $[\text{Mo}^{\text{VI}}\text{O}_2(\text{ssp})]$  with 6-acetylisoanthopterin in DMF medium at 309 K. Kinetics of this reaction was followed at 400 nm and four different temperatures in the range 299–324 K under pseudo-first-order conditions (maintaining  $\approx 9$ –109 times excess of the pterin



**Figure 1.** Absorption spectral changes recorded every 8 min during the reaction of  $[\text{Mo}^{\text{VI}}\text{O}_2(\text{ssp})]$  ( $3 \times 10^{-6} \text{ mol dm}^{-3}$ ) and 6-acetylisoanthopterin ( $7 \times 10^{-5} \text{ mol dm}^{-3}$ ) in DMF solution at 309 K.

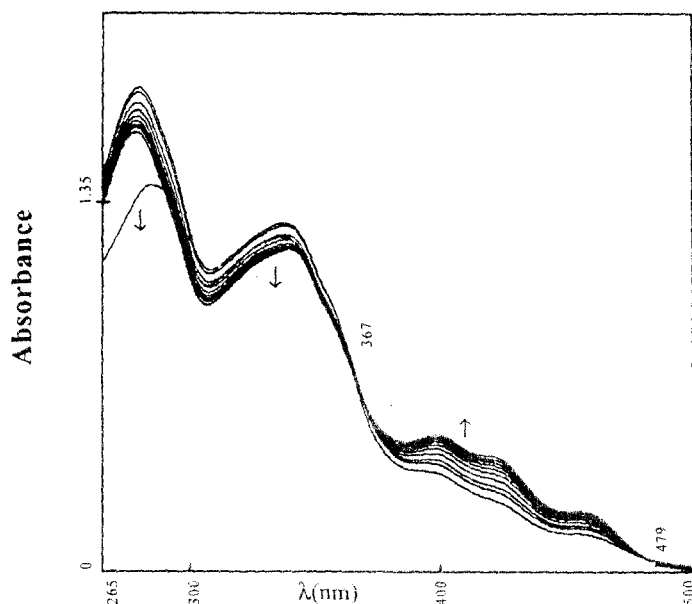


**Figure 2.** Absorption spectral changes recorded every 3 min in the reaction of **1** ( $3.4 \times 10^{-4}$  mol dm $^{-3}$ ) and pyridine N-oxide ( $2.5 \times 10^{-2}$  mol dm $^{-3}$ ) in DMF solution at 298 K.

ligand). Observed rate constants were determined by least squares method from the plots of  $\log (A_t - A_\infty)$  vs time, which were linear for at least 3 half-lives<sup>8</sup>. Figure 2 shows the course of the change in absorption spectra (DMF, 298 K) over time resulting from the reaction of **1** with a typical enzyme substrate like pyridine N-oxide<sup>8</sup>. This reaction was monitored under similar conditions as above (at 400 nm, keeping about 13–130 fold excess of pyridine N-oxide). As delineated later the two above-mentioned kinetic studies reflect molybdenum-centred oxygen atom transfer reactions involving two-unit reduction [Mo(VI)  $\rightarrow$  Mo(IV)] in the first case and subsequent reoxidation of the Mo(IV) species respectively.

### 3. Results and discussion

The  $^1\text{H}$  NMR data of **1** have been assigned on the basis of the expanded spectrum ( $\delta$  8.0–6.5), the corresponding  $^1\text{H}$ – $^1\text{H}$  COSY data, protonic integration values and  $^1\text{H}$  NMR data of 6-acetylisoalloxanthopterin<sup>12</sup>. A tautomeric form of (Hpte') residue involving protons of the N(1) and N(2) atoms (chart 2), is consistent with these data. The  $\text{CH}_3(3')$ ,  $\text{CH}_2(1')$ , NH(1) and NH(8) signals of the (Hpte') residue appear as singlets at  $\delta$  2.18,  $\delta$  3.74,  $\delta$  10.96 and  $\delta$  12.34 respectively<sup>16</sup>. The characteristic azomethine (CH=N) signal at  $\delta$  9.06 (singlet) of the ( $\text{ssp}^{2-}$ ) residue is consistent with the data observed for closely related chelated ligand residues (ONO/ONS donors) in well-characterized coordination compounds of molybdenum<sup>7(a),17</sup>. The protonic integration values of these signals (e.g., NH(8) and CH=N protons) indicate a 1:1 ratio of ( $\text{ssp}^{2-}$ ): (Hpte') in **1**. The proton signal of the methoxide ( $\text{OCH}_3$ ) residue is covered by the residual  $\text{H}_2\text{O}$  signal (of  $d_6$ -DMSO) at  $\delta$  3.35. The importance of the molybdenum-methoxide interaction has been pointed out by several authors and established through X-ray crystal structure determination in one

case<sup>18</sup>. For 6-acetylisoxanthopterin (in *d*<sub>6</sub>-DMSO), the CH<sub>3</sub>(3') and CH<sub>2</sub>(1') proton signals (singlets) appear at δ2.18 and δ3.74 respectively<sup>12</sup>; in **1** δ values of these proton signals for the (Hpte') residue remain essentially unchanged, thereby indicating that the O(2') atom of the 6-substituent (chart 2) remains uncoordinated. Besides this, the <sup>1</sup>H NMR data of 6-acetylisoxanthopterin also indicate that the NH<sub>2</sub>(2) group exists here as shown in chart 2, with its two protons appearing essentially as a broad signal at δ7.0. However, during the redox reaction of H<sub>2</sub>pte with [Mo<sup>VI</sup>O<sub>2</sub>(ssp)], a tautomeric change takes place and the NH(1) signal appears at δ10.96 in **1**; this supports the participation of the pterin ring during oxygen atom transfer reaction occurring at the molybdenum centre (chart 3)<sup>3(b)</sup>. The =NH(2) proton signal (**1**) lies hidden under proton signals of the (ssp<sup>2-</sup>) residue, as evident from protonic integration data of the expanded spectrum (δ8.0–6.5)<sup>12</sup>.

A comparative study of the IR spectra of **1** and the reactants responsible for its formation, throws light on the nature of the ligand (Hpte') donor atoms as well as on the molybdenum-centred oxygen atom transfers occurring during its formation. IR absorptions typical of terminal Mo=O (930 cm<sup>-1</sup>) and bridging Mo=O → Mo (780 cm<sup>-1</sup>) groups of [Mo<sup>VI</sup>O<sub>2</sub>(ssp)] are absent in case of **1**<sup>7(b),17</sup>, indicating removal of such molybdenum-oxygen entities through reaction with the redox noninnocent pterin ligand. The residual IR band at 780 cm<sup>-1</sup> of **1** can be correlated with the IR absorption of the (ssp<sup>2-</sup>) residue, as verified through recording of IR spectrum of H<sub>2</sub>ssp<sup>7(a)</sup>. The intense IR bands in the region 1700–1600 cm<sup>-1</sup> of H<sub>2</sub>pte are modified significantly on coordination to the molybdenum atom in **1**, reflecting enolisation of the 4-oxo group followed by coordination of the (Hpte') residue involving the O(4), N(5) atoms, where the Mo-N(5) bond plays a pivotal role<sup>3(b),5,19</sup>. The ν(C=O) modes of the 2' and 7-oxo groups appear together at 1625 cm<sup>-1</sup> as a strong broad band in **1**; the ν(CH=N) mode of the azomethine group (observed at 1598 cm<sup>-1</sup> in [Mo<sup>VI</sup>O<sub>2</sub>(ssp)]) and the ν(C=C), ν(C=N) vibrations of the pterin ring lie hidden under this band<sup>5</sup>. Now considering the tridentate ONS donating (ssp<sup>2-</sup>) residue and the (OCH<sub>3</sub>) group, a coordination number of 6 can be inferred for the Mo(IV) atom in **1** (chart 3)<sup>7(a),18(a)</sup>.

Reactivity (discussed later) of **1** towards pyridine N-oxide indicates that the molybdenum atom exists here in a lower oxidation state, e.g. +4. The relevant oxidation product was isolated by reacting (328 K, darkness, 5 h, DMF) **1** with pyridine N-oxide (in 1:3 molar ratio), followed by evaporation in a rotary evaporator, treatment of the residue with methanol, filtration and washing with ether; elemental analysis indicated the composition [Mo<sub>2</sub><sup>VI</sup>O<sub>5</sub>(Hssp)(Hpte)], 0.5 DMF. The ν(Mo=O) and ν(Mo–O–Mo) modes characteristic of the [Mo<sub>2</sub><sup>VI</sup>O<sub>5</sub><sup>2+</sup>] core are observed at 925, 888 cm<sup>-1</sup> and 825 cm<sup>-1</sup> respectively<sup>20</sup>. Most likely the initial product (e.g., possessing the [Mo<sup>VI</sup>O<sub>4</sub>]) core of pyridine N-oxide oxidation undergoes hydrolysis with the moisture present in the solvents and μ-oxo dimerization reaction, giving ultimately the Mo<sub>2</sub><sup>VI</sup>O<sub>5</sub><sup>2+</sup> species [5(a)–5(c)]<sup>19,20(c,d)</sup>.

Figures 1 and 2 represent the spectrophotometric monitoring of the reaction of [Mo<sup>VI</sup>O<sub>2</sub>(ssp)] with H<sub>2</sub>pte and that of **1** with pyridine N-oxide respectively<sup>21(a),21(b)</sup>. In figure 1 isobestic points are observed at 326 and 386 nm, while two isobestic points can be identified at 367 and 479 nm in figure 2. Both the reaction systems exhibit saturation kinetics at sufficiently high substrate concentration (figures 3 and 4)<sup>21</sup>. Under these conditions, the reactions are first order in [Mo<sup>VI</sup>O<sub>2</sub>(ssp)] and **1** respectively, as shown by linear plots of log (A<sub>t</sub>–A<sub>∞</sub>) vs time, from which the observed rate constants were obtained<sup>8(a),8(c),17,23</sup>.

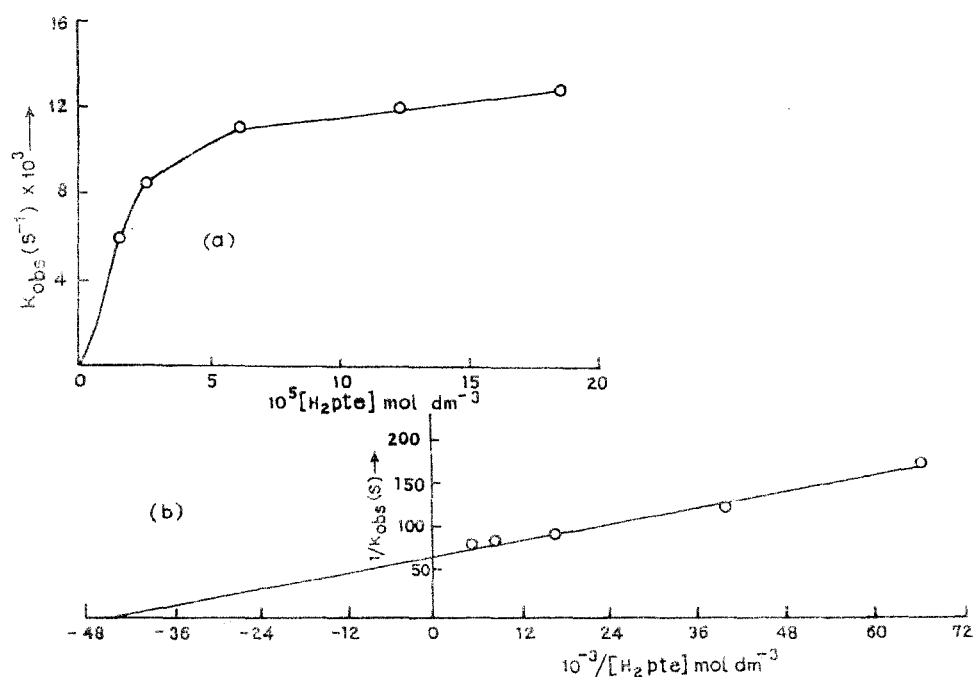


**Figure 3.** (a) Dependence of the rate of reaction of  $[\text{Mo}^{\text{VI}}\text{O}_2(\text{ssp})](1.7 \times 10^{-6} \text{ mol dm}^{-3})$  and 8.8–108.8 equivalent of  $\text{H}_2\text{pte}$  in DMF at 299 K on  $\text{H}_2\text{pte}$ ; (b) the corresponding double reciprocal plot.

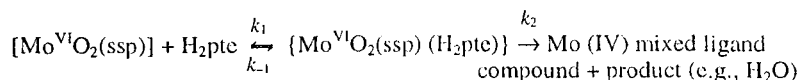
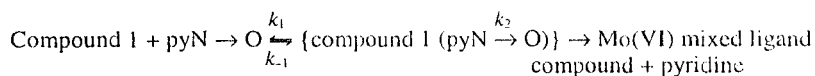
The reaction (scheme 1) leading to the formation of **1**, i.e. the Mo (IV) mixed ligand compound, is initiated through reversible substrate [S], i.e., ( $\text{H}_2\text{pte}$ ) binding, followed by oxo transfer (along with coupled  $\text{H}^+/\text{e}^-$  transfer) with rate constant  $k_2$ . During isolation of the product on preparative scale in presence of methanol, further reactions occur with loss of both the oxo groups of  $[\text{Mo}^{\text{VI}}\text{O}_2(\text{ssp})]$ , giving **1** as the ultimate product (vide §2). Loss of oxo ligands, during complex formation process involving  $\text{Mo}^{\text{VI}}\text{O}_2^{2+}$  starting materials, is rare with conventional ligands unless an oxo abstractor like  $\text{PPh}_3/\text{Ph}_2\text{MeP}$  is present<sup>7(a),(c),17,23(a)</sup>. In terms of scheme 1 the observed rate constant ( $k_{\text{obs}}$ ) can be represented as follows<sup>22</sup>:

$$k_{\text{obs}} = (k_2[\text{S}]/(K_m + [\text{S}])), \quad (3)$$

where  $K_m = (k_2 + k_{-1})/k_1$  or

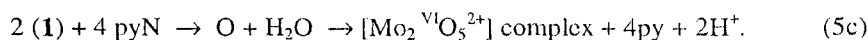
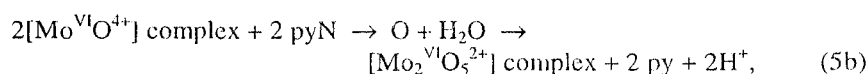
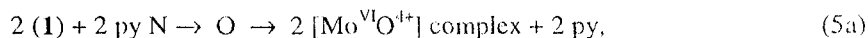
$$\frac{1}{k_{\text{obs}}} = \frac{1}{k_2} + \frac{K_m}{k_2[\text{S}]}. \quad (4)$$

A plot of the observed rate constant ( $k_{\text{obs}}$ ) vs  $[\text{H}_2\text{pte}]$  is shown in figure 3a. The plot of  $1/k_{\text{obs}}$  vs  $1/[\text{H}_2\text{pte}]$  should give a straight line with  $1/k_2$  as the intercept and  $K_m/k_2$  as the slope. The x-axis intercept equals  $1/K_m$ . From the double reciprocal plot of  $1/k_{\text{obs}}$  vs  $1/[\text{H}_2\text{pte}]$  (figure 3b),  $k_2$  and  $K_m$  were calculated as  $1.5 \times 10^{-2} \text{ s}^{-1}$  and  $2.2 \times 10^{-5} \text{ mol dm}^{-3}$

**Scheme 1.****Scheme 2.**

respectively at 299 K. The value of  $k_2$  is comparable in magnitude to those of molybdenum-mediated oxygen atom transfer reactions obtained using a wide variety of model compounds and substrates<sup>8,17,23</sup>. Activation parameters [ $\Delta H^\ddagger = 11.3 \text{ kJ mol}^{-1}$ ;  $\Delta S^\ddagger = -200.8 \text{ J K}^{-1} \text{ mol}^{-1}$ ] were obtained from the Eyring plot [ $\ln(k/T)$  vs  $1/T$ ] using pseudo-first-order rate constants data determined (keeping a 90-fold excess of  $\text{H}_2\text{pte}$ ) at different temperatures. The negative activation entropy is consistent with the proposed associative mechanism (scheme 1)<sup>24</sup>.

Scheme 2 represents the possible pathway of the reaction between **1** and pyridine N-oxide in DMF medium, which involves the reversible formation of an intermediate involving both the reactants, followed by its transformation to the products. Reaction stoichiometry was established by estimating the amount of pyridine released through the reaction (328 K, 50 h,  $\text{N}_2$  atm, darkness) of a known weight of **1** with 10 equivalents of  $\text{pyN} \rightarrow \text{O}$ ; pyridine was determined gravimetrically as the known compound  $[\text{Zn}(\text{C}_5\text{H}_5\text{N})_2](\text{SCN})_2$  from the petroleum ether extract of the reaction medium<sup>25</sup>. About 2 mols of pyridine were recovered per mol of **1** added as per the following equations.



The plot of observed rate constant ( $k_{\text{obs}}$ ) vs  $[\text{py N} \rightarrow \text{O}]$  is shown in figure 4a. Assuming the validity of (3) and (4) in this case as well, the double reciprocal plot of  $1/k_{\text{obs}}$  vs  $1/[\text{py N} \rightarrow \text{O}]$  (figure 4b) was utilized for the calculations of  $k_2 = 6.7 \times 10^{-2} \text{ s}^{-1}$  and  $K_m = 2.3 \times 10^{-3} \text{ mol dm}^{-3}$  at 299 K. Variable temperature pseudo-first-order rate constants data (determined using 80-fold excess of  $\text{pyN} \rightarrow \text{O}$ ) were used for calculating the activation parameters ( $\Delta H^\ddagger = 3.8 \text{ kJ mol}^{-1}$ ;  $\Delta S^\ddagger = -200.3 \text{ JK}^{-1} \text{ mol}^{-1}$ ) from the Eyring plot. The negative  $\Delta S^\ddagger$  value supports the formation of an intermediate in scheme 2. The  $k_2$  value is in line with the existing rate constants data for oxo transfer reactions of various Mo(IV) complexes with pyridine N-oxide and other similar substrates<sup>8(c),23(b)</sup>.

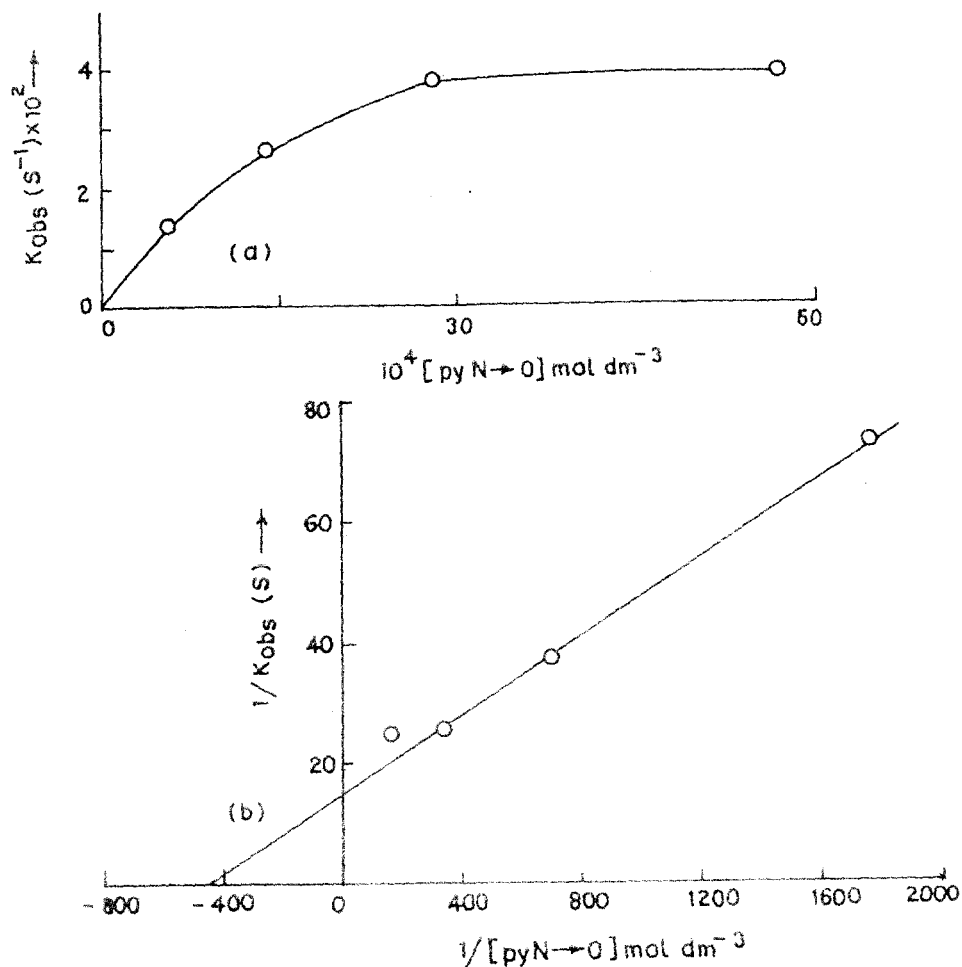


Figure 4. (a) Dependence of the rate of reaction of **1** ( $4.4 \times 10^{-5} \text{ mol dm}^{-3}$ ) and 12.9–129.2 equivalent of py N  $\rightarrow$  O in DMF at 299 K on pyN  $\rightarrow$  O; (b) the corresponding double reciprocal plot.

#### 4. Conclusions

$^1\text{H}$  NMR and IR spectral data point out that **1** exhibits redox noninnocent behaviour during its reaction with  $[\text{Mo}^{\text{VI}}\text{O}_2(\text{ssp})]$ ; the loss of oxygen atoms of the latter (leading to the formation of **1**) is accompanied by a tautomeric change involving the  $\text{NH}_2(2)$  group (chart 2) and related electronic redistribution in the pterin ring. The process is characterized by substrate saturation kinetics (figure 3) and may be regarded as a CEPT reaction. On the other hand, the reaction between **1** and pyridine N-oxide is essentially an OAT process, conforming to substrate saturation kinetics as well (figure 4) and throwing light on the oxidation state of the molybdenum atom in **1**. The final product in (5c) reflects the role of hydrolysis and  $\mu$ -oxo dimerization reaction. The reductive half

reaction of xanthine oxidase with substoichiometric amounts of xanthine exhibits substrate saturation kinetics with faster  $k_2$  values<sup>21(c)</sup>.

Finally, the role of the solvent used for the preparative purpose here (e.g., CH<sub>3</sub>OH) is to be assessed *vis-a-vis* that of H<sub>2</sub>O in the catalytic cycle of oxomolybdoenzymes. As pointed out in the introductory part, loss of an oxo group from the Mo(VI) species during enzyme turnover is made up by the H<sub>2</sub>O molecule giving Mo–OH<sub>2</sub> and undergoes facile deprotonation to Mo–OH or Mo=O species accompanied by changes in oxidation state of the metal centre<sup>1(a),26</sup>. During formation of **1**, loss of oxo groups from [Mo<sup>VI</sup>O<sub>2</sub> (ssp)] is made up partly by the pterin ligand residue (Hpte')<sup>20(a)</sup> and partly by the solvent molecule (CH<sub>3</sub>OH); charge balance is achieved through deprotonation leading to methoxide group formation<sup>18</sup>.

### Acknowledgements

The authors express their gratitude to the CSIR, New Delhi, for a research fellowship (to MAA), the Department of Science and Technology and University Grants Commission, New Delhi for financial support (to PSR), Indian Association for the Cultivation of Science, Kolkata for microanalytical data, RSIC, CDRI, Lucknow for ESMS and NMR spectra. Some of the NMR spectra were recorded by TIFR, Mumbai and IICB, Kolkata.

### References

1. (a) McMaster J and Enemark J H 1998 *Curr. Opin. Chem. Biol.* **2** 201; (b) Enemark J H and Garner C D 1997 *J. Biol. Inorg. Chem.* **2** 817; (c) Collison D, Garner C D and Joule J A 1996 *Chem. Soc. Rev.* **25** 25
2. Stiefel E I 1996 *Science* **272** 1599
3. (a) Fischer B, Schmalle H W, Baumgartner M R and Viscontini M 1997 *Helv. Chim. Acta* **80** 103; (b) Fischer B, Schmalle H, Dubler E, Schafer A and Viscontini M 1995 *Inorg. Chem.* **34** 5726; (c) Fischer B, Strahle J and Viscontini M 1991 *Helv. Chim. Acta* **74** 1544
4. Kaim W 1987 *Rev. Chem. Intermediates* **8** 247
5. (a) Perkinson J, Brodie S, Yoon K, Mosny K, Carroll P J, Morgan T V and Burgmayer S J N 1991 *Inorg. Chem.* **30** 719; (b) Burgmayer S J N and Stiefel E I 1988 *Inorg. Chem.* **27** 4059
6. (a) Matsuura S, Nawa S, Kakizawa H and Hirata Y 1953 *J. Am. Chem. Soc.* **75** 4446; (b) Korte F and Wallace R 1964 *Pteridine chemistry* (eds) W Pfeleiderer and E C Taylor (Oxford: Pergamon) pp. 75–86; (c) Schircks B, Bieri J H and Viscontini M 1985 *Helv. Chim. Acta* **68** 1639; (d) Russell J R, Garner C D and Joule J A 1992 *Synlett.* 711
7. (a) Craig J A, Harlan E W, Snyder B S, Whitener M A and Holm R H 1989 *Inorg. Chem.* **28** 2082; (b) Rajan O A and Chakravorty A 1981 *Inorg. Chem.* **20** 660; (c) Boyd I W and Spence J T 1982 *Inorg. Chem.* **21** 1602
8. (a) Holm R H 1990 *Coord. Chem. Rev.* **100** 183; (b) Craig J A and Holm R H 1989 *J. Am. Chem. Soc.* **111** 2111; (c) Schultz B E and Holm R H 1993 *Inorg. Chem.* **32** 4244; (c) Holm R H and Berg J M 1984 *Pure Appl. Chem.* **56** 1645
9. (a) Vogel A I 1978 *Textbook of practical organic chemistry* 4th edn (London: Longman/ELBS) chap 2; (b) Perrin D D and Armarego W L F 1988 *Purification of laboratory chemicals* 3rd edn (Oxford: Pergamon)
10. (a) Bellas M and Suschitzky H 1963 *J. Chem. Soc.* 4007; (b) Carde R N, Hayes P C, Jones G and Cliff C J 1981 *J. Chem. Soc., Perkin Trans. 1* 1132
11. Sawyer D T and Roberts J L Jr. 1974 *Experimental electrochemistry for chemists* (New York: Wiley) p. 212
12. Supplementary data available with the authors include ESMS, IR, <sup>1</sup>H NMR (1D and 2D) and CV data of H<sub>2</sub>p<sub>te</sub> and **1**; expanded NMR (1D and 2D) data identify each proton signal of (ssp<sup>2-</sup>) residue in **1**.

13. Geary W J 1971 *Coord. Chem. Rev.* **7** 110
14. Ebsworth E A V, Rankin D W H and Craddock S 1987 *Structural methods in inorganic chemistry* (Oxford: Blackwell/ELBS) p. 349
15. Young C G 1995 *J. Chem. Edu.* **72** 751, and the additional information folder available with the author
16. (a) Soyka R, Pfeleiderer W and Prewo R 1990 *Helv. Chim. Acta* **73** 808; (b) Soyka R and Pfeleiderer W 1990 *Pteridines* **2** 63
17. (a) Bhattacharjee S and Bhattacharyya R G 1992 *J. Chem. Soc., Dalton Trans.* 1357; (b) Bhattacharjee S and Bhattacharyya R G 1993 *J. Chem. Soc., Dalton Trans.* 1151
18. (a) Gibson V C, Redshaw C, Walker G L P, Howard J A K, Hoy V J, Cole J M, Kuzmina L G and De Silva D S 1999 *J. Chem. Soc., Dalton Trans.* 161; (b) Bazhenova T A, Bazhenova M A, Petrova G N, Shilova A K and Shilov A E 1998 *Russ. Chem. Bull.* **47** 861
19. Stiefel E I 1977 *Prog. Inorg. Chem.* **22** 1
20. (a) Burgmayer S J N, Arkin M R, Bostick L, Dempster S, Everett K M, Layton H L, Paul K E, Rogge C and Rheingold A L 1995 *J. Am. Chem. Soc.* **117** 5812; (b) Kaufmann H L, Sands L L, Rheingold A L and Burgmayer S J N 1999 *Inorg. Chem.* **38** 2592; (c) Kaufmann H L, Carroll P J and Burgmayer S J N 1999 *Inorg. Chem.* **38** 2600; (d) Burgmayer S J N, Kaufmann H L, Fortunato G, Hug P and Fischer B 1999 *Inorg. Chem.* **38** 2607
21. (a) Bastian N R, Kay C J, Barber M J and Rajagopalan K V 1991 *J. Biol. Chem.* **266** 45; (b) Wuebbens M M and Rajagopalan K V 1993 *J. Biol. Chem.* **268** 13493; (c) Kim J H and Hille R 1993 *J. Biol. Chem.* **268** 44
22. (a) Ochiai E I 1977 *Bioinorganic chemistry* (Boston: Allyn and Bacon) p. 27; (b) Das S K, Chaudhury P K, Biswas D and Sarkar S 1994 *J. Am. Chem. Soc.* **116** 9061
23. (a) Berg J M and Holm R H 1985 *J. Am. Chem. Soc.* **107** 917, 925; (b) Caredonna J P, Reddy P R and Holm R H, 1988 *J. Am. Chem. Soc.* **110** 2139; (c) Craig J A and Holm R H 1989 *J. Am. Chem. Soc.* **111** 2111
24. Wilkins R G 1991 *Kinetics and mechanism of reactions of transition metal complexes* 2nd edn (Weinheim: VCH) pp 87, 105
25. Vogel A I 1978 *Textbook of quantitative inorganic analysis* 4th edn (England: Longman/ELBS) p. 489
26. Enemark J H and Young C G 1993 *Adv. Inorg. Chem.* **40** 1

## A di- $\mu$ -oxomolybdenum(V) complex of 6-acetylisoanthopterin, undergoing oxygen atom transfer with dimethyl sulphoxide

Md Afsar Ali and Parag S. Roy\*

Department of Chemistry, University of North Bengal, Darjeeling – 734430, India

Received 15 March 2001; accepted 01 June 2001

### Abstract

The new compound,  $\text{Na}[(\text{Mo}_2^{\text{V}}\text{O}_4)(\text{pte})(\text{OMe})(\text{MeOH})_2]$  (pte = anion of 6-acetylisoanthopterin), has been prepared using the redox 'non-innocent' title ligand in  $\text{MeOH-H}_2\text{O}$ , and characterized by elemental analysis and physico-chemical methods including e.s.m.s., i.r., u.v.–vis. and  $^1\text{H-n.m.r.}$  spectra. Rate constants data ( $1.4 \times 10^{-3} \text{ s}^{-1}$  at 300 K) for its oxygen atom transfer with dimethyl sulphoxide tally with those of synthetic analogue systems reported earlier by different authors. The negative activation entropy ( $-206.3 \text{ J mol}^{-1} \text{ deg}^{-1}$ ) is consistent with an associative mechanism for this reaction.

### Introduction

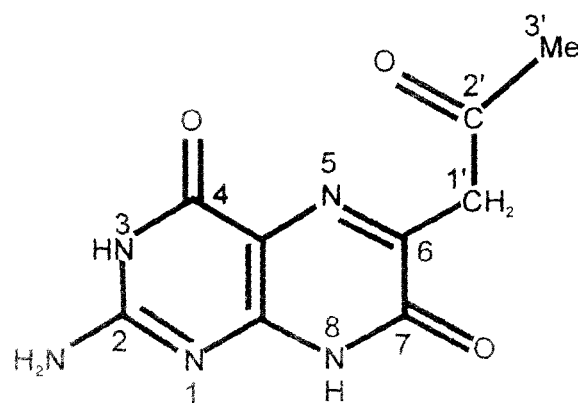
Pterin derivatives, especially those with different types of 6-substituent, have been found in many metalloenzymes, where the metal atom may be Mo for oxomolybdoenzymes, W for tungstopterin enzymes, and Fe or Cu for aromatic amino acid hydroxylases [1–3]. The well-known ability of the pterin ring to act as a redox partner in biological redox systems, is intimately connected with the ability of the pyrazine moiety (pterin ring) to exist in different oxidation states [4]. These facts have inspired symbiotic developments in the coordination chemistry of pterin ligands [5, 6]. In view of the multi-electron redox capability of both the molybdenum atom (VI, V, IV) and the pterin ligand, the redox aspect of molybdenum–pterin interaction and the reactivity of the resulting compounds still need careful study [6].

This paper is concerned with the synthesis, characterization and reactivity, towards  $\text{Me}_2\text{SO}$ , of a new dinuclear molybdenum(V) complex of 6-acetylisoanthopterin ( $\text{H}_2\text{pte}$ , Scheme 1), whose 7-oxo group corresponds to the pyran ring oxygen atom of Mo-cofactor (Mo-co) [1] (Scheme 1).

As delineated here,  $\text{H}_2\text{pte}$  acts as a reducing agent towards  $\text{Na}_2\text{MoO}_4$  in a  $\text{MeOH-H}_2\text{O}$  medium during the synthesis of the above-mentioned complex.

### Experimental

Reagent grade chemicals were used as received. Solvents were purified, prior to use, following literature procedures [7]. Kinetic and electrochemical measurements were performed in spectroscopic grade  $\text{Me}_2\text{SO}$  (SRL, Mumbai).  $\text{Bu}_4\text{NClO}_4$  (TBAP) for c.v. measurements was



Scheme 1.

obtained by published methods [8]. Elemental analysis (C, H, N) data were obtained from I.A.C.S., Calcutta. Molybdenum was determined by atomic absorption spectroscopy.  $^1\text{H-n.m.r.}$  data in  $d_6\text{-Me}_2\text{SO}$  were obtained from the I.I.S., Bangalore (Bruker, DRX 500), R.S.I.C., Lucknow (Bruker, DRX 300) and T.I.F.R., Mumbai (Bruker, AMX 500). The electrospray mass spectra in  $\text{MeOH}$  were obtained from R.S.I.C., Lucknow (Micromass Quattro II triple quadrupole mass spectrometer). I.r. spectra (nujol mull) were recorded on a Philips Analytical SP3-300 spectrometer. Electrical conductivity data in DMF and  $\text{Me}_2\text{SO}$  ( $0.8 \text{ mmol dm}^{-3}$  solution) were measured using a digital conductivity meter (Systronics, model 304). Cyclic voltammetry data (*versus* s.c.e., uncorrected for the junction contribution) were recorded under a  $\text{N}_2$  atmosphere on a BAS (CV-27), USA instrument. Electronic spectra and kinetic data (under a  $\text{N}_2$  atmosphere) were recorded on a Shimadzu (UV-240) spectrophotometer, with thermostatic conditions ( $\pm 0.5 \text{ K}$ ) being maintained using a Shimadzu (TB-85) thermostat. Figure 3 demonstrates the absorption

\* Author for correspondence

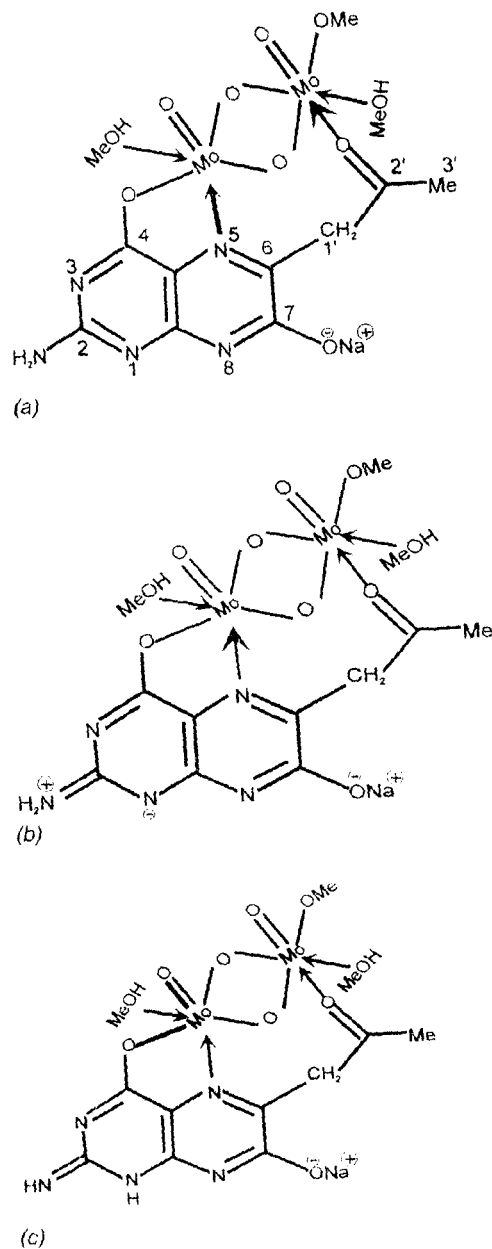
spectral changes associated with the reaction of  $\text{Na}[(\text{Mo}_2^{\text{V}}\text{O}_4)(\text{pte})(\text{OMe})(\text{MeOH})_2]$  (2) with  $\text{Me}_2\text{SO}$  at 299.5 K. The growth kinetics of the reaction was followed at 401 nm and at four temperatures in the 300–325 K range. Pseudo-first-order rate constants ( $k$ ,  $\text{s}^{-1}$ ) were determined by the least squares method from the plots of  $\log(A_\infty - A_t)$  versus time, which were linear for at least three half-lives. These rate constants were used to determine activation parameters by means of an Eyring plot ( $\ln k/T$  versus  $1/T$ ); relevant data are collected in Table 2.

#### 6-Acetylisoxanthopterin, $\text{H}_2\text{pte}$ (1)

The pterin ligand was prepared in 75% yield by modifying the original method of synthesis in the light of later developments (e.g., darkness,  $\text{N}_2$  atmosphere,  $\text{pH} = 6.4$ ) [9]. (Found: C, 44.0; H, 4.4; N, 28.4.  $\text{C}_9\text{H}_9\text{N}_5\text{O}_3 \cdot 0.5\text{H}_2\text{O}$  calcd.: C, 44.3; H, 4.1; N, 28.7%). T.l.c. [silica gel  $\text{GF}_{254}$ , u.v. lamp, using  $\text{MeOH}-\text{H}_2\text{O}$  (4:1 v/v) solution and  $\text{Me}_2\text{CO}-\text{Et}_2\text{O}$  (1:1 v/v) as eluant]. The product gives a positive 2,4-DNP test and decomposes without melting above 573 K. Electrospray mass spectrometry (e.s.m.s.): molecular ion peak without  $0.5\text{H}_2\text{O}$  was observed at  $m/z = 235.9$  (relative abundance = 63%). I.r. (nujol mull,  $\text{cm}^{-1}$ ): two intense bands with fine structure at 1690 and 1650 correspond to different types of  $\nu(\text{C}=\text{O})$  modes; the  $\nu(\text{C}=\text{C})$  and  $\nu(\text{C}=\text{N})$  vibrations of the pterin ring appear at  $1610\text{ cm}^{-1}$ . U.v.-vis. [DMF,  $\lambda_{\text{max}}/\text{nm}$  ( $\log \epsilon$ ): 293 (3.68), 341 (3.86), 400 (3.28), 422 (3.27), 456sh (3.00)]. C.v. study (1  $\text{mmol dm}^{-3}$  in  $\text{Me}_2\text{SO}$  with 0.1  $\text{mol dm}^{-3}$  TBAP, Pt electrode versus s.c.e., 50  $\text{mV s}^{-1}$ ) shows that (1) undergoes cathodic reduction beyond  $-1.8\text{ V}$  and anodic oxidation at 0.94 V.

#### $\text{Na}[(\text{Mo}_2^{\text{V}}\text{O}_4)(\text{pte})(\text{OMe})(\text{MeOH})_2]$ (2)

A purged ( $\text{N}_2$ ) aqueous solution (10  $\text{cm}^3$ ) of  $\text{Na}_2\text{MoO}_4 \cdot 2\text{H}_2\text{O}$  (0.242 g, 1 mmol) was treated with a stirred suspension of 6-acetylisoxanthopterin hemihydrate (0.244 g, 1 mmol) in  $\text{MeOH}$  (100  $\text{cm}^3$ ) under  $\text{N}_2$  in the dark, and the pH was adjusted to 4.8 ( $\text{AcOH}$ ); finally a  $\text{MeOH}$  solution (10  $\text{cm}^3$ ) of  $\text{Et}_4\text{NBr}$  (0.525 g, 2.5 mmol) was added and stirring was continued for 25 h (301 K). The light yellow compound was recovered by filtration (fritte) under  $\text{N}_2$  in the dark, washed with purged solvents [e.g.,  $\text{H}_2\text{O}-\text{MeOH}$  (1:1 v/v),  $\text{MeOH}-\text{Et}_2\text{O}$ ] dried *in vacuo* (silica gel); Yield: 60%. T.l.c. [using  $\text{Me}_2\text{SO}$  solution diluted with  $\text{MeOH}$  (50 times) and  $\text{CH}_2\text{Cl}_2-\text{C}_6\text{H}_6$  (1:1 v/v) as eluant]. (Found: C, 24.1; H, 3.1; N, 11.7; Mo, 31.9.  $\text{NaMo}_2\text{O}_{10}\text{C}_{12}\text{H}_{18}\text{N}_5$  calcd.: C, 23.7; H, 3.0; N, 11.5; Mo, 31.6%).  $A_M$  ( $\text{ohm}^{-1}\text{ cm}^2\text{ mol}^{-1}$ , 301 K) = 27 ( $\text{Me}_2\text{SO}$ ) and 73 (DMF) [10]. E.s.m.s. data: the  $[\text{M} + 2\text{H}]^+$  peak appears at  $m/z = 609.1$  (relative abundance = 38.1%) where M corresponds to the molecular formula; it is associated with the characteristic distribution of molybdenum isotopes [11, 12]. The ligand ( $\text{pte}^+$ ) peak is observed at  $m/$



Scheme 2.

$z = 235.9$  (relative abundance = 89.2%). Breaking up of (2) to some extent during recording of e.s.m.s. data along with cluster formation ( $m/z = 825.0$ , relative abundance = 16.2%) is indicated [13]. I.r. (nujol mull,  $\text{cm}^{-1}$ ):  $\nu(\text{C}=\text{O})$ , 1645 (vs, br);  $\nu(\text{Mo}=\text{O})$ , 955 (vs);  $\nu(\text{Mo}-\text{O}-\text{Mo})$ , 790 (vs) [14]. U.v.-vis. [DMF,  $\lambda_{\text{max}}/\text{nm}$  ( $\log \epsilon$ ): 291 (4.03), 342 (4.25), 400 (3.56), 422sh (3.53), 458sh (3.23)].<sup>1</sup>

#### Results and discussion

The  $A_M$  values of (2) are consistent with its formulation as a 1:1 electrolyte [10]. Comparison of the i.r. spectra of

<sup>1</sup> Supplementary information available with the authors include e.s.m.s., i.r., u.v.-vis., <sup>1</sup>H-n.m.r. spectra of (1) and (2) as well as kinetic data for (2).

(1) and (2), show that the three ligand bands in the 1600–1700  $\text{cm}^{-1}$  region undergo considerable modification due to deprotonation of NH(3) and NH(8) groups (Scheme 1) through enolisation involving the 4- and 7-oxo groups respectively, followed by coordination involving the O(4), N(5) atoms (Scheme 2) [5, 6, 15]. For (2) the  $\nu(\text{C}=\text{O})$  mode of the 2'-oxo group appears as a strong band at 1645  $\text{cm}^{-1}$ ; the  $\nu(\text{C}=\text{C})$ ,  $\nu(\text{C}=\text{N})$  vibrations of the pterin ring are associated with this band [5, 6, 15, 16]. The characteristic i.r. bands of the  $\text{Mo}_2\text{O}_4^{2+}$  core in (2) appear at their expected positions (Figure 1); as (2) has been obtained from a MeOH–H<sub>2</sub>O reaction medium (pH = 4.5), presence of a di- $\mu$ -oxo core here is quite likely [14].

For (1) (Table 1)  $^1\text{H}$ -n.m.r. signals of the  $\text{CH}_3(3')$  and  $\text{CH}_2(1')$  groups (Scheme 1) appear as singlets at  $\delta$  2.18 and  $\delta$  3.74 respectively; these spectral assignments have been carried out on the basis of  $^1\text{H}$ – $^1\text{H}$  COSY data, supported by proton integration values. In view of the oxo-transfer reaction of (2) with  $\text{Me}_2\text{SO}$  (*vide infra*), several of its high resolution  $^1\text{H}$ -n.m.r. spectra were recorded for unambiguous spectral assignments. One such spectrum (Figure 2) shows the  $\text{CH}_3(3')$  and

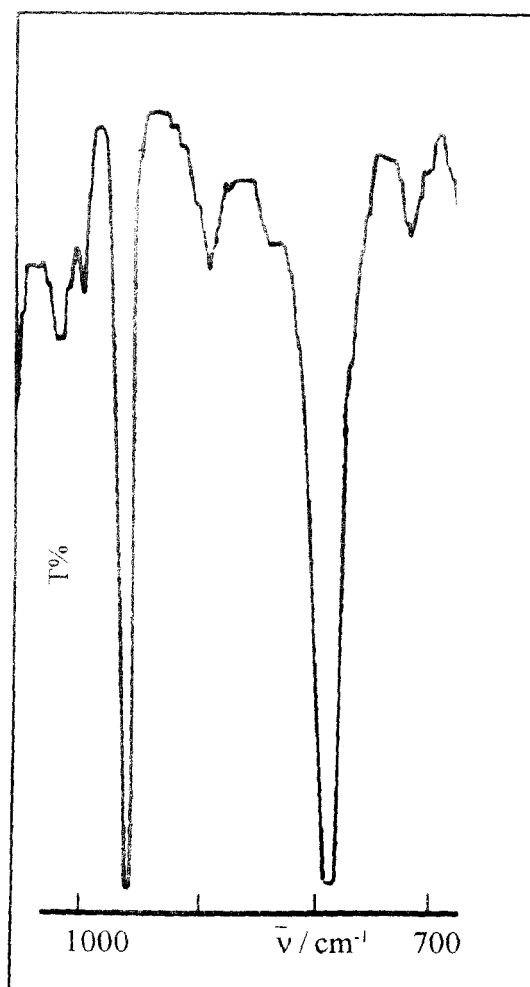


Fig. 1. I.r. spectrum (nujol) of (2),  $\text{Na}[(\text{Mo}_2\text{O}_4)(\text{pte})(\text{OMe})(\text{MeOH})_2]$ .

Table 1. Relevant  $^1\text{H}$ -n.m.r. signals in  $d_6$ - $\text{Me}_2\text{SO}$  ( $\delta$  ppm, internal TMS) of 6-acetyloxanthopterin (1), (2) and  $\Delta$  ( $=\delta_{\text{compound}} - \delta_{\text{ligand}}$ ) values

Compound <sup>a</sup>	$\text{CH}_3(3')$	$\text{CH}_2(1')$
(1) <sup>b</sup>	2.18(s)	3.74(s)
(2) <sup>c</sup>	1.16(t)	3.21(q)
$\Delta$	-1.02	-0.53

<sup>a</sup> *Vide* Scheme 1 for proton numbering system; <sup>b</sup> data at 500 MHz, 300 K; <sup>c</sup> Data at 300 MHz, 298 K.

$\text{CH}_2(1')$  signals at  $\delta$  1.16 and  $\delta$  3.21 respectively.  $^1\text{H}$ – $^1\text{H}$  COSY data (500 MHz, 280 K) help to identify the  $\text{CH}_3(3')$  ( $\delta$  1.18, triplet,  $J = 7.5$  Hz) and  $\text{CH}_2(1')$  ( $\delta$  3.22, quartet,  $J = 7.7$  Hz) signals; the  $J$  values were estimated from the corresponding 2D –  $J$  resolved spectrum. In Figure 2 the  $\text{CH}_3$  – signal of the two MeOH molecules and MeO – group appear together with the residual proton signal ( $\text{H}_2\text{O}$ ) at  $\delta$  3.38.

For (2), the  $-\text{NH}_2$  (2) signal (500 MHz, 280 K) consists of a broad prominent signal at  $\delta$  7.0, associated with two weaker ones at  $\delta$  6.75 and  $\delta$  6.50 due to the two additional forms  $=\text{N}^+\text{H}_2$  and  $=\text{NH}$  [Scheme 2(b) and (c)] respectively. The proton integration data for the two protons of the  $-\text{NH}_2(2)$  group (involving the three above-mentioned signals) tally with those of the two  $-\text{OH}$  signals of the two MeOH molecules, (2). As suggested by different authors, such transformations involving the  $-\text{NH}_2(2)$  group are quite likely and help the pterin ring to play an active part essential for enzyme reactions [6, 16, 17]. Although the OH signal of MeOH (neat) usually appears at *ca.*  $\delta$  5.0, in (2), the two MeOH molecules exhibit two separate  $-\text{OH}$  signals [due to the overall unsymmetrical nature of (2), Scheme 2] at  $\delta$  12.35 and  $\delta$  10.96 respectively. Depletion of electron

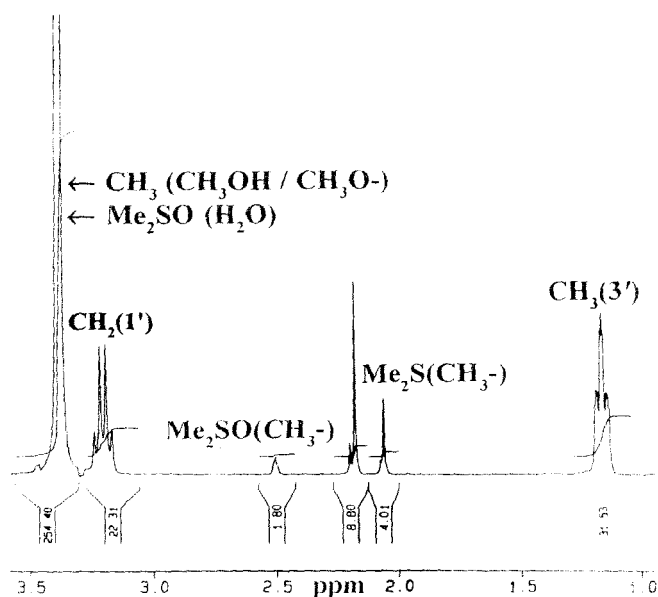


Fig. 2. 300 MHz (298 K)  $^1\text{H}$ -N.M.R. spectrum in  $d_6$ - $\text{Me}_2\text{SO}$  ( $\delta$ , ppm versus TMS) of (2),  $\text{Na}[(\text{Mo}_2\text{O}_4)(\text{pte})(\text{OMe})(\text{MeOH})_2]$ .

density associated with strong coordination to the molybdenum(V) atoms [14], is responsible for the substantial deshielding of these —OH signals, of MeOH in (2). Coordination of the MeOH molecule to the molybdenum atom in different types of compound, sometimes leading to deprotonation/methoxide coordination, has been proposed by various workers and has been characterized by X-ray crystallographic data [5, 6, 15, 18]. The electronic effects associated with the possible existence of the —NH<sub>2</sub>(2) group in two additional forms (Scheme 2) as stated above, are transmitted (via the pterin ring) even up to the two coordinated MeOH molecules in (2); this is evident from the fact that each major methanolic —OH signal is accompanied by two minor ones. A comparative study (Table 1) of the splitting patterns of the CH<sub>3</sub>(3') and CH<sub>2</sub>(1') signals in (1) and (2) also throws light on the above-mentioned electronic circulation effect. In (1), these two signals appear as singlets, whereas in (2) they are split into a triplet and a quartet respectively. Although <sup>1</sup>H–<sup>1</sup>H COSY data indicate spin–spin interaction between these two signals in both these cases, most likely the increased electronic circulation due to coordination (Scheme 2) in (2) is responsible for the observed splitting of the CH<sub>3</sub>(3'), CH<sub>2</sub>(1') signals in this case. Besides this, contrary to expectation the proton signals (Table 1) of (2) exhibit varying degree of shielding effects (negative  $\Delta$  values) [19]. The +2 charge on the Mo<sub>2</sub><sup>V</sup>O<sub>4</sub><sup>2+</sup> core is satisfied by the deprotonated O(4) atom and methoxide group; the additional electron density released through deprotonation of —NH(8) (Na<sup>+</sup> salt formation, consistent with  $A_M$  values) is transmitted via the redox 'non-innocent' pterin ligand to the region around the O(2') atom of the 6-substituent (Schemes 1 and 2), causing the observed shielding effect [4–6, 15]. This extra electron density around the Mo<sub>2</sub><sup>V</sup>O<sub>4</sub><sup>2+</sup> core in (2), makes it a good reducing agent towards a typical enzyme substrate like Me<sub>2</sub>SO, as revealed by the following kinetic data; this process also indicates an oxidation state less than VI for the molybdenum atoms in (2). The proposed schematic structure (Scheme 2) of (2) involving a bridging pterin ligand is consistent with different types of structurally characterized dinuclear molybdenum(V) complexes including triply bridged ones as well as structurally characterized metal–pterin complexes where the N(5) atom (pterin residue) plays a pivotal role [5, 6, 14–16, 20].

Kinetic data for Me<sub>2</sub>SO reduction (Figure 3) by (2) are summarized in Table 2. The large negative activation entropy is consistent with an associative mechanism. Rate constants for molybdenum-centred oxygen atom transfer reactions determined by different authors on a variety of analogue reaction systems, are in line with the present data [21]. To establish reaction stoichiometry, the reaction of (2) (0.3 mmol dm<sup>-3</sup>) with Me<sub>2</sub>SO was followed for 70 h (333 K, in the dark) under a continuous flow of N<sub>2</sub> and the emerging gas was passed into an aqueous solution of HgCl<sub>2</sub>; the resulting precipitate of the known compound (HgCl<sub>2</sub>)<sub>3</sub>(Me<sub>2</sub>S)<sub>2</sub> was estimated [22]. *Ca.* 0.9 mol of Me<sub>2</sub>S (b.p. 309–

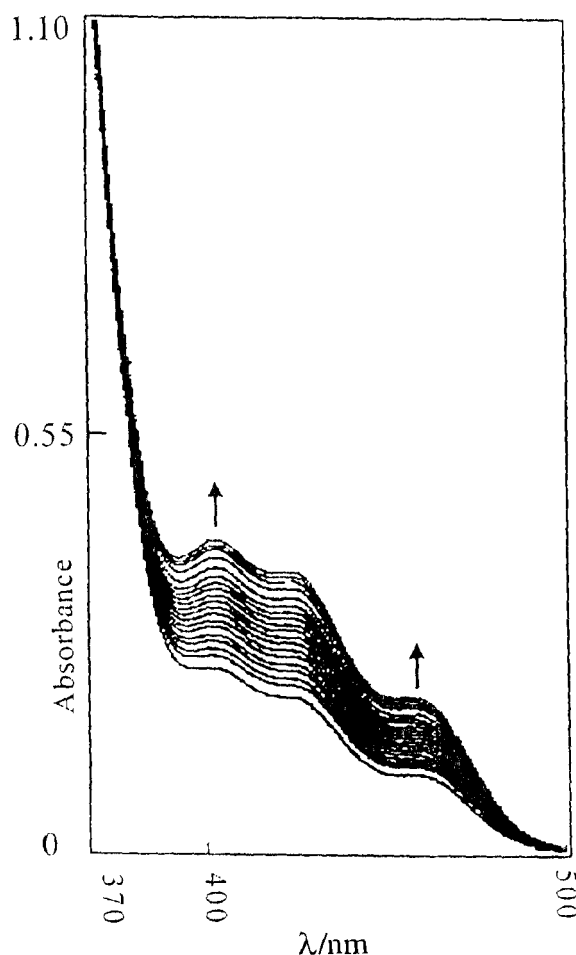


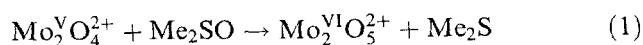
Fig. 3. Spectral changes in the reaction of (2) (0.8 mmol dm<sup>-3</sup>) and Me<sub>2</sub>SO at 299.5 K, recorded at 8 min intervals.

Table 2. Kinetic data for Me<sub>2</sub>SO reduction by (2) through oxygen atom transfer

T (K)	10 <sup>3</sup> k (s <sup>-1</sup> )	ΔH <sup>‡a</sup> (kJ mol <sup>-1</sup> )	ΔS <sup>‡a</sup> (J mol <sup>-1</sup> deg <sup>-1</sup> )	ΔG <sup>‡b</sup> (kJ mol <sup>-1</sup> )
300	1.4			
309	1.9	25.5	-206.3	
318	2.7			91.2
325	3.4			

<sup>a</sup>Values obtained from the Eyring plot; <sup>b</sup>value obtained from: ΔG<sup>‡</sup> = ΔH<sup>‡</sup> - TΔS<sup>‡</sup> at 318 K.

310 K) was recovered per mol of (2) added, according to the following equation:



The i.r. spectrum of the isolated oxidation product (Equation 1) shows two strong, broad bands at 936 and 902 cm<sup>-1</sup> and a weaker band at 833 cm<sup>-1</sup>, which can be correlated with the presence of a Mo<sub>2</sub><sup>VI</sup>O<sub>5</sub><sup>2+</sup> core in this case. Reactions of Mo<sub>2</sub><sup>V</sup>O<sub>4</sub><sup>2+</sup> species involving breaking of one or both of the bridges, even conversion to

mononuclear molybdenum(V) complexes could be achieved through careful choice of reagents/ligands [14].

Progress of the reaction between (2) and  $\text{Me}_2\text{SO}$  can also be monitored using cyclic voltammetry (Figure 4 shows three c.v. scans recorded at 5 min interval) indicating a gradual fall in concentration of the electroactive species. The cathodic reduction peak ( $E_{pc}$ ) at  $-0.84\text{ V}$  and the two shoulders at  $-0.74$  and  $-0.42\text{ V}$  reflect reduction of the two molybdenum atoms [molybdenum(V)  $\rightarrow$  molybdenum(IV)], associated with rearrangement.

A comparison of the electronic spectral data (*vide* characterization data stated earlier) of (1) with that of (2) indicates that there are considerable increases in intensity of the ligand bands (essentially  $\pi \rightarrow \pi^*$  type) through complex formation, although their positions remain almost unchanged. The characteristic transitions of pterins (positions and particularly intensities of the bands in the 220–500 nm region), depend to a large extent on the oxidation state and the tautomeric form of this ring system [5, 6, 15, 23]. The electronic spectral bands of (2) above 400 nm are essentially of metal-centred c.t. type (Figure 3) and their intensities grow with the progress of the oxygen atom transfer with  $\text{Me}_2\text{SO}$  [21]. Additional time-dependent spectral studies indicated that (1) did not react with  $\text{Me}_2\text{SO}$ . The reaction (Equation 1) is initiated through inner sphere electron transfer (*e.g.*, concomitant with breaking of one of the bridges of the  $\text{Mo}_2\text{O}_4^{2+}$  core), followed by

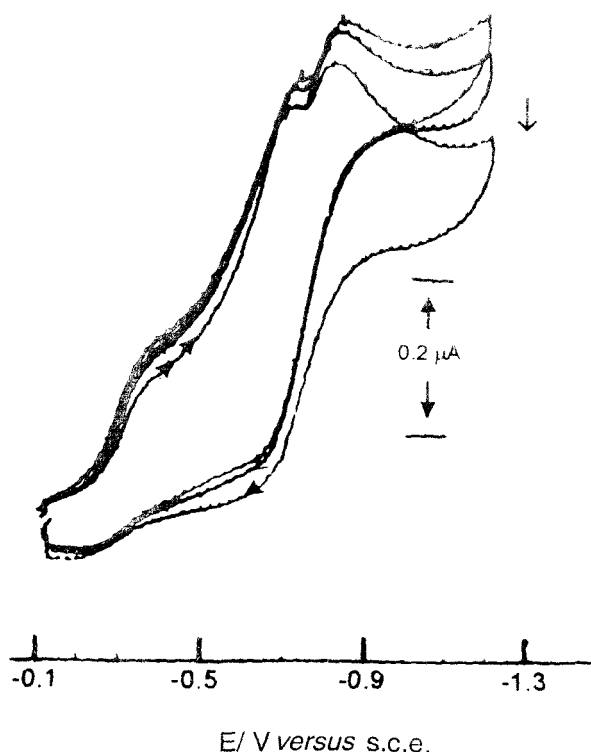


Fig. 4. Cyclic voltammograms during the progress of the reaction between (2) ( $0.8\text{ mmol dm}^{-3}$ ) and  $\text{Me}_2\text{SO}$ . Data were recorded at 5 min intervals using a Pt working electrode, TBAP ( $0.1\text{ mol dm}^{-3}$ ), scan rate,  $15\text{ mV s}^{-1}$ .

relatively slow oxygen atom transfer reaction from the substrate,  $\text{Me}_2\text{SO}$  [14].

### Acknowledgements

The authors wish to express their gratitude to the C.S.I.R., New Delhi, for a research fellowship (to M.A.A.), the D.S.T. and U.G.C., New Delhi for financial support (to P.S.R.), I.A.C.S., Calcutta for microanalytical data, R.S.I.C., C.D.R.I., Lucknow for e.s.m.s. and n.m.r. spectra. Some of the n.m.r. spectra were recorded by T.I.F.R., Mumbai and I.I.S., Bangalore. A.a.s data (molybdenum) were provided by Dr M.C. Saha, G.S.I., Calcutta.

### References

1. J. McMaster and J.H. Enemark, *Current Opinion in Chemical Biology*, **2**, 201 (1998); D. Collison, C.D. Garner and J.A. Joule, *Chem. Soc. Rev.*, **25**, 25 (1996); E.I. Stiefel, *Science*, **272**, 1599 (1996).
2. M.K. Chan, S. Mukund, A. Kletzin, M.W.W. Adams and D.C. Rees, *Science*, **267**, 1463 (1995); M.K. Johnson, D.C. Rees and M.W.W. Adams, *Chem. Rev.*, **96**, 2817 (1996).
3. T.A. Dix and S.J. Benkovic, *Acc. Chem. Res.*, **21**, 101 (1988); E.-I. Oehli, *Bioinorganic Chemistry*, Allyn and Bacon, Inc., Boston, 1997, p. 211.
4. W. Kaim, *Rev. Chem. Intermed.*, **8**, 247 (1987).
5. S.J.N. Burgmayer, H.L. Kaufmann, G. Fortunato, P. Hug and B. Fischer, *Inorg. Chem.*, **38**, 2607 (1999) and refs. 4–13 therein; S.J.N. Burgmayer, *Structure and Bonding*, **92**, 67 (1998).
6. B. Fischer, H. Schmalie, E. Dubler, A. Schafer and M. Viscontini, *Inorg. Chem.*, **34**, 5726 (1995); B. Fischer, H.W. Schmalie, M.R. Baumgartner and M. Viscontini, *Helv. Chim. Acta*, **80**, 103 (1997).
7. A.I. Vogel, *Text Book of Practical Organic Chemistry*, 4th edit., ELBS, Longman, England, 1978; D.D. Perrin and W.L.F. Armarego, *Purification of Laboratory Chemicals*, 3rd edit., Pergamon Press, Oxford, 1988.
8. D.T. Sawyer and J.L. Roberts Jr., *Experimental Electrochemistry for Chemists*, Wiley, New York, 1974, p. 212.
9. S. Matsuura, S. Nawa, H. Kakizawa and Y. Hirata, *J. Am. Chem. Soc.*, **75**, 4446 (1953); F. Korte and R. Wallace, in W. Pfeleiderer and E.C. Taylor (Eds.), *Pteridine Chemistry*, Pergamon Press, Oxford, 1964, pp. 75–86; B. Schircks, J.H. Bieri and M. Viscontini, *Helv. Chim. Acta*, **68**, 1639 (1985); J.R. Russell, C.D. Garner and J.A. Joule, *SYNLETT*, 711 (1992).
10. W.J. Geary, *Coord. Chem. Rev.*, **7**, 110 (1971).
11. E.A.V. Ebsworth, D.W.H. Rankin and S. Craddock, *Structural Methods in Inorganic Chemistry*, Blackwell Scientific Publications, Oxford, 1987, p. 349; C.G. Young, *J. Chem. Educ.*, **72**, 751 (1995) and associated information folder.
12. J.A. Craig, E.W. Harlan, B.S. Snyder, M.A. Whitener and R.H. Holm, *Inorg. Chem.*, **28**, 2082 (1989).
13. A. Schafer, B. Fischer, H. Paul, R. Bosshard, M. Hesse and M. Viscontini, *Helv. Chim. Acta*, **75**, 1955 (1992).
14. E.I. Stiefel, *Prog. Inorg. Chem.*, **22**, 1 (1977).
15. S.J.N. Burgmayer and E.I. Stiefel, *J. Am. Chem. Soc.*, **108**, 8310 (1986); S.J.N. Burgmayer, M.R. Arkin, L. Bostick, S. Dempster, K.M. Everett, H.L. Layton, K.E. Paul, C. Rogge and A.L. Rheingold, *J. Am. Chem. Soc.*, **117**, 5812 (1995).
16. S.J.N. Burgmayer and E.I. Stiefel, *Inorg. Chem.*, **27**, 4059 (1988); J. Perkinson, S. Brodie, K. Yoon, K. Mosny, P.J. Carroll, T.V. Morgan and S.J.N. Burgmayer, *Inorg. Chem.*, **30**, 719 (1991).
17. A. Abelleira, R.B. Galang and M.J. Clarke, *Inorg. Chem.*, **29**, 633 (1999).

18. V.C. Gibson, C. Redshaw, G.L.P. Walker, J.A.K. Howard, V.J. Hoy, J.M. Cole, L.G. Kuzmina and D.S. De Silva, *J. Chem. Soc., Dalton Trans.*, 161 (1999); T.A. Bazhenova, M.A. Bazhenova, G.N. Petrova, A.K. Shilova and A.E. Shilov, *Russ. Chem. Bull.*, **47**, 861 (1998).
19. S.J.N. Burgmayer, A. Baruch, K. Kerr and K. Yoon, *J. Am. Chem. Soc.*, **111**, 4982 (1989).
20. T. Głowiak, M. Sabat, H. Sabat and M.R. Rudolf, *J. Chem. Soc., Chem. Commun.*, 712 (1975).
21. R.H. Holm, *Coord. Chem. Rev.*, **100**, 183 (1990); J.A. Craig and R.H. Holm, *J. Am. Chem. Soc.*, **111**, 2111 (1989); B.E. Schultz and R.H. Holm, *Inorg. Chem.*, **32**, 4244 (1993).
22. R.H. Holm and J.M. Berg, *Pure Appl. Chem.*, **56**, 1645 (1984); H.E. Szmant and O. Cox, *J. Org. Chem.*, **31**, 1595 (1966).
23. R. Mengel, W. Pfeleiderer and W.R. Knappe, *Tetrahedron Lett.*, 2817 (1977); W. Pfeleiderer, *J. Heterocycl. Chem.*, **29**, 583 (1992).

TMCH 5057

Studies on coordination compounds of molybdenum  
with a new Schiff base ligand ( $H_3(pte_2 -tsc)$ ),  
synthesized by condensing 7-acetyl-xanthopterin  
[ $H_2(pte_2)$ ] with thiosemicarbazide ( $H(tsc)$ ): crystal  
structure of 2-pivaloylamino-7-acetyl-xanthopterin  
.water (1/1)

Md. A. Ali and P.S.Roy,\*

Department of Chemistry,  
University of North Bengal, Siliguri 734013  
E-mail: afsarali\_nbu@yahoo.co.in/paragsroy@hotmail.com

The pterin starting material of this study was characterized by X-ray structure determination of its 2-pivaloylamino derivative and other data. Six new Mo(IV,V,VI) complexes of the title Schiff base ligand have been synthesized and characterized by elemental analysis, ESIMS and different spectroscopic data, cyclic voltammetry and supported by optimized molecular structures (CHEM3D models, MM2 calculations). The Mo(IV,V) complexes show reactivity towards typical oxygen atom donors like  $Me_3N \rightarrow O$ ,  $PyN \rightarrow O$ ; the negatives  $\Delta S^\ddagger$  values indicate associative type pathway and the magnitudes of the  $k_{obs}(s^{-1})$  values are comparable with the literature data on molybdenum centred oxygen atom transfer reactions on related systems. CV data as well as fluorescence spectral data throw light on the changes in electronic structures during the different redox steps involved in this study [Ali, Md. A; Roy, P.S.; Proc.Indian Acad. Sci. (Chem. Sci.) **2001**, 113, 77; Ali, Md. A.; Roy, P.S. Transition Metal Chem. **2002**, 27, 366; Sen, S.; Roy, P.S. Transition Metal chem.. **2005**, 30, 797; Sen, S.; Ghosh, B; Roy, P.S. Transition Metal Chem. **2007**, 32, 737; Ghosh, B.; Roy, P.S. Indian. J. Chem. **2007**, 46A. 1585.]

